CRANFIELD UNIVERSITY

JENNIFER A ROBERTS

SATELLITE FORMATION FLYING FOR AN INTERFEROMETRY MISSION

College of Aeronautics

PhD THESIS

CRANFIELD UNIVERSITY

College of Aeronautics

PhD THESIS

2005

JENNIFER A ROBERTS

SATELLITE FORMATION FLYING FOR AN INTERFEROMETRY MISSION

Supervisor: Dr. S E Hobbs

Presented: October 2005

ABSTRACT

The autonomous formation flying of multiple spacecraft to replace a single large satellite will be an enabling technology for many future missions. In this research, the current status of formation flying missions and technologies is determined, and the Darwin nulling interferometry mission, which aims to detect and characterise extrasolar planets, is selected as the research focus. Darwin requires high precision formation flying of multiple telescopes near the Sun-Earth L2 point.

A comprehensive account of current research in astrobiology is presented which provides the motivation for a Darwin-type mission. Astrobiology is integral to the definition of formation manoeuvres and target identification. The system design issues associated with developing a higher resolution, Planet Imager mission are also explored through a preliminary mission design.

Relative dynamics models for satellite formation flying control in Low Earth Orbit (LEO) and L2 are developed and methods of incorporating the Earth oblateness perturbation (J_2) into the equations of relative motion to improve model fidelity are investigated. The linearised J_2 effect is included in the Hill equations in time averaged and time varying form. The models are verified against the Satellite Tool Kit (STK) numerical orbit propagator, and applied to optimal control system design and evaluation for formation keeping tasks.

The 'reference orbit' modelling approach applied in LEO is applied to the development of a new formation flying model at L2. In this case, linearised equations of motion of the mirror satellites relative to the hub are derived and performance evaluated for different initial conditions. These and other higher order models are compared to STK. The linearised model is applied to controller design for station keeping and formation manoeuvring tasks suitable for a Darwin-type mission, and the role of the model in developing controllers for a load levelling guidance system is explored.

The Galaxy Song

Just remember that you're standing on a planet that's evolving
And revolving at 900 miles an hour
That's orbiting at 19 miles a second, so it's reckoned
A sun that is the source of all our power
The sun and you and me, and all the stars that we can see
Are moving at a million miles a day
In an outer spiral arm, at 40,000 miles an hour
Of the galaxy, we call the Milky Way

Our galaxy itself contains 100 billion stars
It's 100,000 light-years side-to-side
It bulges in the middle, 16,000 light-years thick
But out by us it's just 3000 light-years wide
We're 30,000 light-years from galactic central point
We go round every 200 million years
And our galaxy is only one of millions of billions
In this amazing and expanding universe

The universe itself keeps on expanding and expanding
In all of the directions it can whiz
As fast as it can go, at the speed of light you know
Twelve million miles a minute and that's the fastest speed there is
So remember, when you're feeling very small and insecure
How amazingly unlikely is your birth
And pray that there's intelligent life somewhere up in space
Because there's b****r all down here on Earth

Monty Python, “The Meaning of Life” (1983)

ACKNOWLEDGEMENTS

Many thanks to Dr. Steve Hobbs, my supervisor, for his guidance and freedom in equal measure, and for piling on the pressure to finish this document.

Thanks must also go my wonderful husband for his love and support, to my dearest friend and colleague, Dr. Jenny Kingston, who has been very understanding! My pussy cats also deserve a mention for being a joyful distraction and good company during the long days of writing up.

Finally I wish to thank my parents who inspired me to do a PhD in the first place by setting the example in the family. I promise I will stop doing degrees now....

CONTENTS

1 INTRODUCTION

This thesis chronicles the investigation process and results of three years of research that began with a broad remit to study the field of satellite formation flying and sparse aperture techniques for a space science mission. Ideally the project would contribute to the Cranfield Space Research Centre's current range of skills and interests, including among other areas, image processing, formation flying mission design, and orbital dynamics and control, while developing wider knowledge of the field of satellite formation flying.

The early chapters of the thesis provide significant background that summarises the route taken to establish an appropriate area of research. Key interferometry mission design drivers are identified and applied to a satellite formation flying dynamics and control simulation study in the final part of the thesis. The following sections outline the motivation, aim, and objectives of the study and provide a more detailed thesis overview.

1.1 Motivation

The motivation for this research can be considered from two perspectives. The overall objective in taking this research position at Cranfield was to investigate dynamics and control aspects of satellite formation flying in a suitable systems context. However, the direction of the research has ultimately been governed by the author's personal interest in astronomy and the wider questions concerning the existence of life elsewhere in the Universe. These two aspects of motivation are described in separate sections below, although they are of course interrelated. The formation flying motivation in section 1.1.1 introduces the background to the development of the more specific research objectives in section 1.2, and the parallel motivation to contribute to the search for Earth-like planets and potentially extraterrestrial life, is outlined in section 1.1.2.

1.1.1 Formation Flying

The autonomous formation flying of multiple spacecraft to replace a single larger satellite will be an enabling technology for a number of future missions. Formations of satellites operating as synthetic apertures have a range of potential applications, for example, surveillance and high-resolution interferometry.

Future Civilian Commercial and Military Requirements:
Helvajian (1999) highlights a series of future requirements that can be best achieved through the application of distributed satellite systems. Civilian, commercial and military drivers for the developments of distributed satellite systems include:

- The expected increase in demand for communications facilities at any point on the Earth's surface

- The need for high accuracy navigation capability for the military, and for control of the increasingly cluttered civilian airspace
- The increasingly high volume of information transfer and future requirements for this capability
- The requirement for high resolution military Earth surveillance at different wavelengths.

In summary, the requirement for distributed satellite systems can be paralleled to the requirements that promoted the recent expansion of distributed computing facilities, where multiple platforms allow tasks to be completed which cannot be achieved by a single platform.

Future Scientific Requirements:

Scientific drivers for distributed satellite systems, and in particular for satellite formation flying, include the benefits of being able to make simultaneous widespread field measurements in the space environment, and the ability to make much higher resolution astronomical observations using a distributed aperture telescope system. Higher resolution Earth observations can also be performed by a similar, but Earth-pointing system. The demand by astronomers for the technology to observe objects further and further away, and at higher resolution is driving the demand for increasingly large telescope mirrors, although ultimately for space telescopes, these are limited by launcher capacity and mirror deployment technology. The technique of interferometry utilises a series of accurately positioned smaller telescopes with a beam combining hub, that together offer much higher imaging resolutions than those of the largest single mirror telescope.

It was intended that the author's research be targeted toward both a futuristic and realistic mission, which was at the very early planning stage within the space industrial and research organisations. Selected from a large number of potential missions and formation flying applications, the area of interest for this research was defined by the author to be the orbital analysis and formation flying control of a formation of telescopes performing optical interferometry. A number of cornerstone astronomical observatories and technology demonstrator missions performing optical interferometry had been proposed in the ESA Cosmic Vision 2020 (formerly Horizon 2000 and Horizons 2000) Programme and the NASA Origins Programme, although a number have been delayed or cancelled since the start of this research. Their main focus, however, remains the detection, characterisation (in terms of orbit, and atmospheric composition), and observation of extrasolar planets in the search for extraterrestrial life.

Initially, for this research, the NASA Planet Imager mission (launch beyond 2020) was identified as a suitable target mission. Planet Imager aims to take the first images of Earth-like planets, and is the natural successor to a number of nearer-term missions which will detect and observe suitable target extrasolar planets (Jackson, 2004).

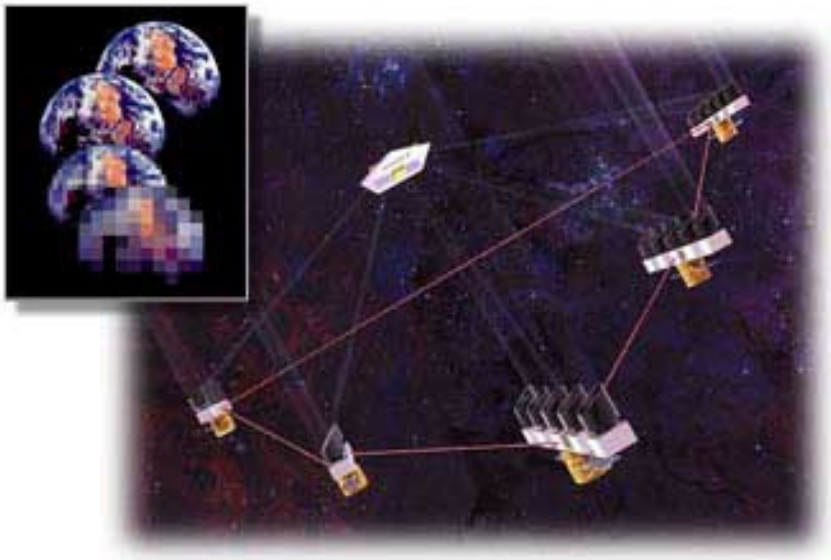

Figure 1-1: Planet Imager Mission (NASA Origins Website, 2000)

However, industrial feedback regarding the status of the Planet Imager mission revealed that very little work had been done to define the mission, and that potentially quite low resolution images of a distant planet were of much smaller significance than the acquisition and analysis of atmospheric data through spectral analysis, which was to be performed by the nearer term Darwin and Terrestrial Planet Finder (TPF) missions (ESA Report (2000), Coulter (2003)). Without sufficient specific mission information, the majority of the research work in this case would have focussed on a detailed, optimised mission design, and on the development of image reconstruction techniques. Some of the limitations of a Planet Imager-type mission have therefore been established through the preliminary mission design summarised as part of the research background. For the demonstration of the dynamics and control research in the last part of the thesis, information from the ESA Darwin mission specification (ESA Report, 2000) was used instead.

Having established a research focus at the mission and systems level, a review of the current status of dynamics modelling and control for satellite formations in both Low Earth Orbit (LEO) and around the L2 Lagrange point of the Sun-Earth system (Figure 1-2) was performed to support the definition of the more detailed aims and objectives. Most information was available for the LEO case, and there were no published relative dynamics models for formation flying in the vicinity of L2. Following an initial study on LEO formation flying in the presence of perturbations, based on work previously carried out at Cranfield and the development of an alternative dynamics model, a new dynamics model for formation flying in the three-body-problem in the vicinity of L2 was proposed.

At the outset, the ability of a control system to achieve the precision necessary for optical interferometry to be performed had also not been established in the public domain. Therefore, one of the original aims of the study was to combine the spatial formation keeping ability of the control system with optical path length control onboard the spacecraft. This may have achieved the nanometre relative position accuracy

required for observations. However, communications with ESA revealed that this was already under investigation within industry.

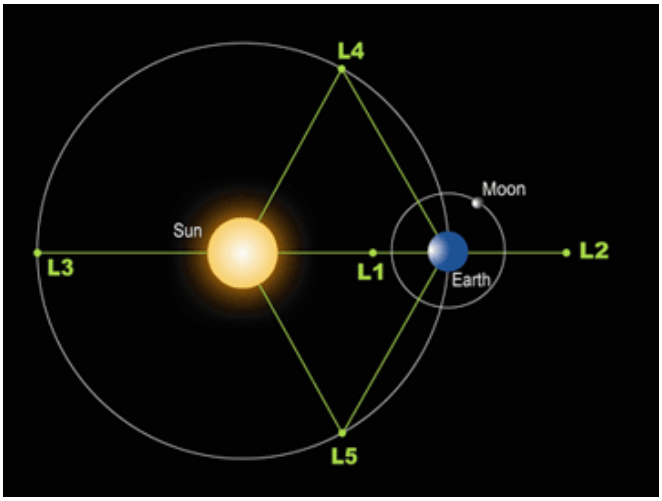

Figure 1-2: Location of the Lagrange Points in the Sun-Earth System (Office of Naval Research Website, 2005)

A second aim of the investigation was to assess the cost and precision of manoeuvres of the satellite formation within the simulated perturbed environment. These manoeuvres are required in practice to slew the formation to observe different objects in the sky, and to vary the size and shape of the interferometer while observing the same target object to improve the image quality. ESA suggested that the work could be complemented by the investigation of these types of manoeuvres under the constraint of fuel use balancing or 'load-levelling' across the formation. A summary of the final research objectives is provided in section 1.2.

1.1.2 The Search for Earth-Like Planets

A more fundamental motivation for this research is philosophical, and regards the natural human curiosity about the existence of extraterrestrial life in the Universe. The relatively new field of astrobiology encompasses, amongst others, a range of disciplines including biology, ecology, geology, planetary sciences, and astronomy. Recent findings in the subject continue both to fuel this curiosity and generate scientific questions that can only be answered by the appropriate design and implementation of space science missions.

Without any other examples, it is appropriate in the first instance to search for other Earth-like planets as we know this 'reference planet' can support life. In parallel to the engineering benefits of formation flying interferometry, some of the basic questions that must be addressed to provide the motivation for such a mission include:

- What are we looking for?
- Where are we looking for it?
- How shall we observe and identify it?

What Are We Looking For?
The answer to the first question appears to be relatively straightforward. Particularly with the earlier missions, we are initially trying to detect and identify the basic characteristics of other Earth-like planets orbiting Solar-type stars. These basic characteristics include planet size, shape, mass, rotation and orbit radius. We are also looking for evidence of life through the measurement of planet temperature and atmospheric composition.

Where Are We Looking For It?
Astrobiology researchers have defined a habitable zone within which a planet must lie in order to support water during some part of the local year (Leger, Labeque, Ollivier, Sekulic, and Valette, 2002). Although other requirements are placed on the definition of a habitable zone, liquid water is deemed essential to the existence of all life, and can only exist at certain planet temperatures, and therefore at a certain distance from the parent star. The discovery of extremophiles has meant that, although the Earth provides a suitable reference from which to begin observations, it is also important to investigate the characteristics of other extrasolar planets with more extreme environments. Therefore, a wide range of planetary systems in deep space should be targeted with any new high resolution observatory.

How Shall We Observe and Identify It?
The answer to this final question is much more complicated, and drives the detailed mission design for planet and life finding missions. These questions are briefly addressed within the thesis in the context of astrobiology and optical astronomy, and a more detailed study is due to be published in a separate report (Roberts, 2006). This background supports the justification for a mission comprising a formation of space-based telescopes, operating in the infrared wavelength regime and using nulling interferometry. Nulling interferometry uses the interference of light to 'null' the light from a bright object (star) and allow the light from a less bright object (planet) to be observed more easily.

1.2 Research Aim and Objectives

The motivation for the following research aim and objectives and the process by which they were derived were summarised above in section 1.1. The overall aim of this research project is:

To assess the feasibility of achieving high precision formation flying of a fleet of satellites in both the Low Earth Orbit and Lagrange point (L2) environments using a variety of dynamics models which can be compared and contrasted. Ultimately, the satellites need to operate autonomously and hold position sufficiently accurately to enable them to perform the appropriate formation manoeuvring and optical interferometry tasks associated with imaging a distant extrasolar planet from L2, in support of an ESA Darwin-type mission.

A number of objectives were defined within the stated aim, and these are summarised below:

- To develop, evaluate and validate analytical and time varying formation flying dynamics models for multiple spacecraft operating in different orbits (in LEO and within the three-body-problem, in particular near L2) so that their relative motion can be calculated when they are subject to a range external disturbances.
- To develop robust, stable and practical control laws which will enable precise relative position maintenance of the satellite formation in the presence of disturbances.
- To calculate the fuel required to maintain these orbits.
- To extend the guidance and control laws to meet more detailed mission requirements, including manoeuvring to perform specific imaging and spectroscopy tasks.
- To apply the L2 formation flying model to the problem of 'load-levelling'.
- To develop the necessary software to visualise multiple satellites interacting and formation flying in a 'real space' perturbed numerical orbit propagator environment.

1.3 Thesis Overview

The road map of Figure 1-3 illustrates the thesis structure. Chapter 2 describes the interferometry mission design background, and motivation for the research based on an extensive survey of the literature. The definition and role of satellite formation flying is presented, supplemented by a formation flying missions survey in appendix A. A target mission is selected with the purpose of detecting and characterising extrasolar planets, and the mission concept is justified from an optical, astronomical and astrobiological perspective. Example formation flying manoeuvres are derived for the demonstration of the dynamics and control research in chapter 7.

The remainder of the thesis focuses on satellite formation flying dynamics and control. The literature review in chapter 3 summarises and critically analyses research in this field for formations in both LEO and L2. The conclusions of this chapter feed directly into the subsequent dynamics model developments and verification, and control within chapters 4, 5, 6 and 7. Chapters 4 and 5 relate to the LEO formation flying dynamics research, where the perturbation due to J_2 is investigated in detail, and fuel estimates to maintain a satellite formation in its presence and in the presence of other perturbations are evaluated. Chapters 6 and 7 describe the derivation, verification and application of a new dynamics model for satellite formation flying in the vicinity of L2, drawing on the manoeuvre requirements derived in chapter 2. The development of a load-levelling guidance and control system is considered to equalise the ΔV across the formation.

In chapter 8, the main points within the summary sections of each chapter are gathered together. Conclusions are presented in concise format and further work is proposed. Appendices provide supporting material and are linked to the different chapters as illustrated in Figure 1-3.

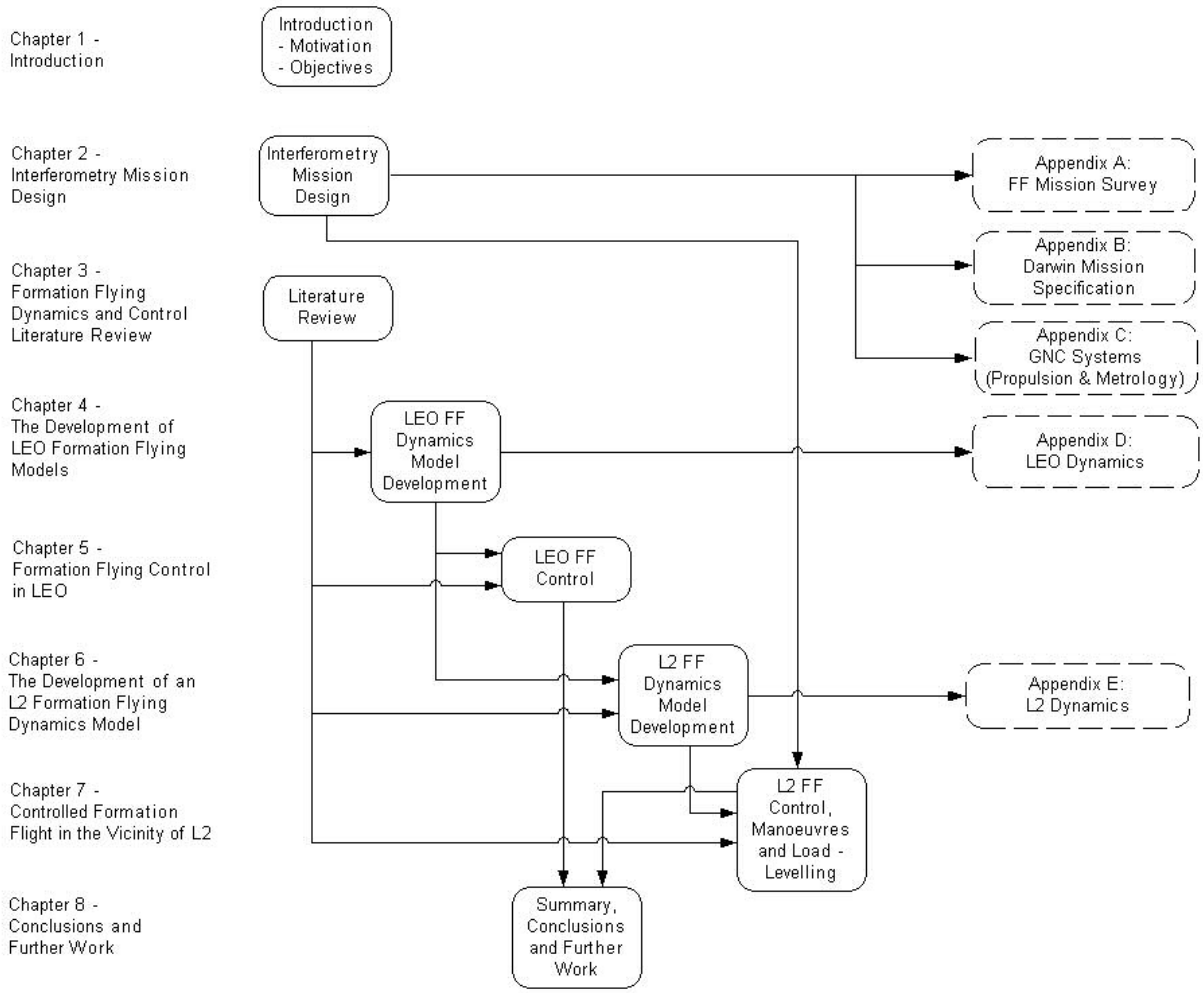

Figure 1-3: Road Map Illustrating Thesis Structure

2 INTERFEROMETRY MISSION DESIGN

This introductory chapter provides a summary of the significant background research performed prior to the satellite formation flying dynamics and control research presented in this thesis. Supporting material is due to be published in a separate report which has been referenced frequently throughout the chapter (Roberts, 2006). In section 2.1 the results of a thorough survey of current and planned formation flying missions are presented and in this context, satellite formation flying in its various forms is defined, and its purposes are established. From the many missions considered, an astronomical observatory interferometry mission is selected to be the focus for the research.

Following mission selection, key design drivers for this and a futuristic planet imager mission are identified from a detailed investigation into optical interferometry and astrobiology (Roberts, 2006), and the technical requirements and specifications for the ESA Darwin mission are summarised. Important guidance, navigation and control (GNC) systems design aspects are introduced as these support the interpretation of the simulation work performed in this research.

In section 2.3, the design drivers identified are applied to the derivation and specification of typical science manoeuvres that a Darwin-type formation would need to perform. These provide test cases which support the simulation work in chapters 6 and 7. The sensitivity of individual design parameters to telescope formation design is explored and demonstrated through a preliminary planet imager mission feasibility study.

2.1 Formation Flying Missions

Satellite formation flying is an important branch of the wider research and application-rich area of distributed satellite systems. According to Shaw et al. (1999) a ‘distributed satellite system’ refers to the coordinated operation of many satellites to perform a particular function. In section 2.1.1, a more precise definition of satellite formation flying is presented with reference to the definitions and terms encountered in the literature which are used to describe satellite formations.

The replacement of a single satellite with multiple smaller satellites is likely to be beneficial for some applications, but uneconomical for others. Many opinions exist, and some of the advantages and disadvantages of multiple-satellite systems are discussed in section 2.1.2. Section 2.1 concludes with a survey of current and future satellite formations and formation flying missions, and reveals the numerous applications of formation flying research that would contribute to scientific, military and communications mission operations.

2.1.1 Types of Formation

Formation flying can be defined as 'the on-orbit position maintenance of multiple spacecraft relative to measured separation errors' (Bauer, Bristow, Folta, Hartman, Quinn, and How, 1997). To be formation flying, several spacecraft must either maintain constant or time varying configurations (station keeping within a formation or manoeuvring from one formation to another), and formation flying in this context implies that there is at least a minimal level of collective autonomy.

A number of terms are used to describe different spacecraft formations. Those encountered during the literature survey are listed in Table 2-1. In this case, however, the existence of several spacecraft flying in similar or differing orbits as a type of formation for the purposes of the same mission does not necessarily mean that they are 'formation flying'. The formation types are illustrated in Figure 2-1.

Formation	Description
Constellation	Regularly spaced satellites with separation on a global scale
Cluster	Satellites operating interdependently and cooperatively
Leader-Follower	Satellites with a hierarchy of authority

Table 2-1: Types of Spacecraft Formation

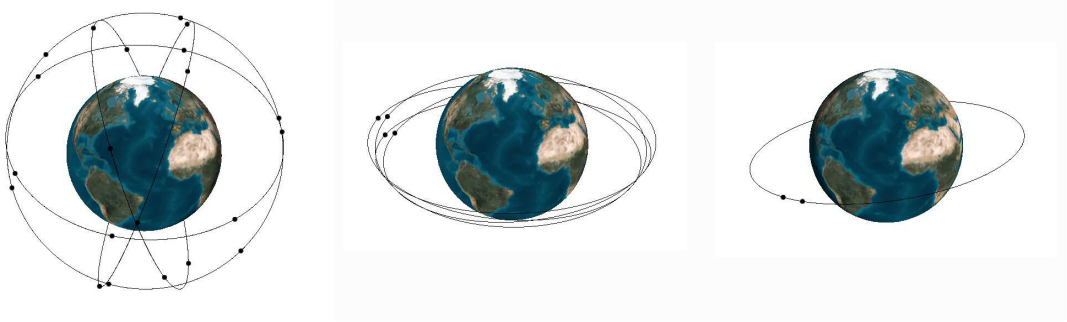

(a) **(b)** **(c)**

Figure 2-1: Types of Spacecraft Formation (a) Constellation (b) Cluster (c) Leader-Follower

'Constellations' refer to more than two spacecraft, operating at large separations, usually dispersed across different orbital planes, and often equally spaced around the globe. Examples include the constellation of 24 satellites in the NAVSTAR Global Positioning System (GPS), and communications constellations (for example, Iridium with 66 LEO satellites) that can simultaneously cover significant proportions of the Earth. Generally these types of constellation are not considered to be 'formation flying'.

A 'Cluster' includes any group of two or more spacecraft whose cooperation and knowledge of relative position is essential for completion of the mission. The term generally implies a level of spacecraft inter-dependency, but does not imply that precision formation keeping is required. While a cluster is not a constellation formation, it is not possible to specify an upper limit to spacecraft separation distance for this definition, although a cluster would usually operate in a closer formation than a constellation. Examples of cluster missions include the deep space X-ray observatory

mission, Constellation-X (Mattson, 2005), the optical interferometry mission, Darwin (ESA Report, 2000), and the former US proposal for a LEO Earth surveillance mission, TechSat21 (Cobb, Das, and Denoyer, 1999). A cluster can also be used to describe a 'swarm' of satellites. The proposed Magnetic Constellation Mission (NASA Science and Technology Definition Team, 2004) comprises a cluster or 'swarm' of around 50 nanosatellites to make simultaneous magnetic field measurements.

The term 'Leader-Follower' has clearest meaning when used to describe two spacecraft where one (the follower) is constrained to fly in formation with the leader. In some texts this term can also apply to multiple spacecraft where there is a specific hierarchical leader. Alternative terms to describe a leader-follower formation hierarchy are described in Table 2-2, and the final entry relates specifically to optical interferometry formations.

Leader	**Follower**
Reference	(Non-Reference)
Chief	Deputy
Master	Slave
Mother	Daughter
Primary	Secondary
Hub/Combiner	Telescopes/Mirrors

Table 2-2: Alternative Descriptions of Satellite Hierarchy

Regardless of the term applied, in this definition of formation flying, the follower spacecraft will follow a path defined by the leader's position, and not necessarily a natural orbit trajectory. For a cluster formation (of more than two spacecraft), the followers may require little onboard processing capability, but sufficient to obey the commands of the master spacecraft. Alternatively, a follower spacecraft may have the ability to operate without the intervention of the leader, controlling and maintaining a desired relative position, but remaining below in the hierarchy (Saenz-Otero, 2000). Although in the conventional sense, the leader-follower formation is specifically referring to one satellite following another in some relative orbit, the hierarchy concept of leader-follower formations means that both this description and the term 'cluster' may apply simultaneously to a formation. Of course, it may also be possible for a cluster of spacecraft to comprise a node within a global-scale constellation, to create a constellation of clusters. However, in any scenario, the definition of Bauer et al. (1997) is assumed to hold if a formation is 'formation flying'.

As it is not the focus of the research, the benefits in efficiency and functionality of different inter-satellite communications protocols and control hierarchies have not been investigated in depth or simulated. In this case, a leader-follower architecture has generally been implemented whereby the leader satellite follows a natural orbit trajectory, and controllers on-board the follower spacecraft act to maintain the formation based on relative position measurements. The nature of the communications between spacecraft is dependent on formation control hierarchy. For most applications anticipated, the transmitted data would be in the form of guidance functions from the leader to the follower spacecraft, for example, desired relative orbit trajectories and relative position measurements. Further information on the potential control hierarchy, automation, and communications protocols for distributed satellite systems can be found

in, for example, Mueller (2004), Mueller and Brito (2003), Megla et al., (2002), Bhasin and Hayden (2001), and Shaw et al. (1999).

2.1.2 Generic Advantages and Disadvantages of Formation Flying

Although many of the main drivers for satellite formation flying arise from the numerous potential benefits of replacing future large satellites with a number of smaller, less massive satellites, clusters and constellations can actually refer to satellites of any size. By flying in a formation, and spreading functionality across a cooperating and communicating cluster, significantly improved functionality beyond that of a much larger single spacecraft can be achieved. The cluster may be reconfigured on-orbit to perform alternative tasks in a mission, or even redeployed onto different missions. The addition of one or two members to the cluster may quickly and simply enhance the collective performance and multi-mission capability of the formation. Conversely, should a satellite in the formation fail, the mission can remain operational, perhaps exhibiting a 'graceful degradation of performance' (Sabol, Burns, and McLaughlin, 1999) rather than a full mission failure. Complete system redundancy for all subsystems can be distributed across a cluster of spacecraft, minimising the dependency on a single satellite. To continue operation in the event of a failure on a single complex satellite, redundancy is required at the sub-system level. However, on a cluster of satellites, sub-system redundancy on each spacecraft need not be incorporated as redundancy is held at the cluster level.

While each satellite requires a complete set of fundamental subsystems, for example, power generation, structure, communication system and a control system, the payloads can be distributed, reducing the design and development work that would have been required to ensure that the individual payload requirements on a larger spacecraft were not conflicting. For science missions in particular, a constellation or cluster of spacecraft could be beneficial for improved sampling rates using more sensors. Production costs could be reduced through the development of multiple similar spacecraft on a production line, compared to the production of a single complex satellite. The associated costs of design and development of this process would be reduced further once the initial investment had been made. A major advantage of using multiple satellites is launch flexibility which can significantly benefit cost control measures, ultimately reducing overall mission cost as satellites can be launched when the market demands (Shaw et al, 1999). However, these benefits of flexibility are less significant for science missions when it is likely that a specific number of satellites must be launched simultaneously into unique operational orbits.

Using a formation of satellites to replace a single larger satellite also has a number of potential disadvantages. Table 2-3 contains a summary of both the potential advantages and disadvantages of using constellations and clusters of satellites for a mission.

The total mass of the cluster is likely to be larger than that of the single spacecraft, thus increasing the cost of launch (on a cost per kilogram basis). However, the launch costs could be reduced if the smaller spacecraft were auxiliary payloads on larger mission launches. This would depend on the operational implications of not launching all the

satellites simultaneously and also the difficulty in establishing the formation accurately if the spacecraft are launched at different times. In general, launch costs do not scale linearly with payload mass, and a large-mass deployment of multiple satellites may be the most efficient approach.

Potential Advantages and Disadvantages of using Multiple Spacecraft
Advantages: • Multi-mission capability and design flexibility possible by (on-orbit) reconfiguring of the spatial relation within the formation. • Inherent adaptability afforded by the ability to add incrementally new or upgrade older elements of the formation. • Reduced design and development work that would have been required to ensure that the individual payload requirements on a larger spacecraft were not conflicting. • Distributed redundancy across the formation and improved fault tolerance. • Mission improvement through an increased range of opportunities to make measurements/observations e.g. more frequent sampling. • Opportunity to reduce size and complexity of satellites within the formation. • Lower individual launch mass and smaller spacecraft volume (reduced launch cost and increased launch flexibility). • Reduced manufacturing costs from mass production techniques/economies of scale. • Application specific benefits include – the opportunity to create synthetic apertures for interferometry or radar surveillance missions and to increase the scope of field measurements for survey missions.
Disadvantages: • Each cluster satellite requires its own core systems i.e. there is a minimum overhead associated with each small satellite which may in total be more than that of a single large spacecraft. • Initialisation and maintenance of formation (especially if component satellites are launched separately). • Misalignment of sensors may introduce additional measurement errors if they are mounted on different platforms (for example telescopes in an interferometry mission). • Increased complexity of ground system operations. • Small satellite development costs can be equally high compared to large satellites when they retain the complexity needed to achieve demanding scientific requirements. Complexity reduction and the use of commercial off the shelf (COTS) components may counter this. • Increased quantity of orbital debris, and the introduction of potentially complex decommissioning processes.

Table 2-3: Summary of the Potential Advantages and Disadvantages of Flying Multiple Spacecraft Rather than a Single Satellite for a Mission (based on information from Cobb et al. (1999), National Academy of Sciences (2000), O'Neil (1999), Tollefson (2001), Shaw et al. (1999))

Shaw et al. (1999) apply parametric cost models to assess the cost of distributed systems and find that distributed systems generally are more expensive than single satellites due to the requirements for additional hardware, the division of single-spacecraft functionality, and the development and integration of new technology. However, the cost models are limited due to their reliance on historical data relating to expensive missions, and do not take into account the more recent changes in approach to risk. Accepting more risk and managing failures can significantly reduce costs, particularly in the development of small satellites. Operations costs (which scale linearly with formation size in the absence of autonomy) must be offset against mass production savings, and for very large numbers of satellites operations costs are likely to drive the requirement for increasing levels of automation.

However, ultimately, by expanding the consideration of the use of multiple satellites beyond just the replacement of single larger satellites, a cluster of spacecraft could be extremely effective for many missions. Of particular interest for this research is the enhanced performance made available by the use of multiple telescopes in combination to improve the resolution of an astronomical observatory. A single aperture telescope would not be able to achieve the same resolution as a multi-satellite interferometer (with apertures separated by hundreds of metres) without being impractically large for precision mirror manufacture, launch, and on-orbit deployment or construction.

2.1.3 Formation Flying Missions Survey

The missions involving formations of satellites can be categorised into three primary application areas; communications, military and science. Table 2-4 lists a summary of the different missions in these categories according to formation type, including launch year, and the number of satellites in the formation. Those already in operational orbit, and those truly formation flying are highlighted. A more detailed review of each of the missions and the appropriate references for further mission information are included in appendix A, where acronyms are expanded either in each table or in section A.1.

	Constellation	Cluster	Leader-Follower
Science	***POES (1988-2015), 2***	***Cluster (2000), 4***	***Earth Orbiter-1 (2000) and LandSat7 (1999), 2***
	GOES (1995-2014), 2	*Magnetospheric Multiscale Mission (2010), 4*	***GRACE (2002), 2***
	The A-Train Constellation (2002-2005), 6	*SMART-3 (2010), 3*	*XEUS X-ray Evolving Universe Spectroscopy (2010+), 2*
	COSMIC (2005), 6	*Constellation-X (2011), 4*	
	Space Technology-5 (ST-5) (2005), 3	*GEC (Geospace Electrodynamic Connections) (2011), 4*	
	TWINS (2005), 2-3	*LISA (Laser Interferometer Space Antenna) (2012), 3*	
	GPM and EGPM (European) Global Precipitation Measurement Constellation (2007-2012), 5	*Darwin (2015), 4*	
	Magnetospheric Constellation Mission (2010), 50 (Swarm)	*TPF Terrestrial Planet Finder (2018), 5*	
		Generation-X (2020+), 6	
		Life Finder (2020+)	
		Planet Imager (2020+)	
Military	***GPS (1978-1994), 24***	***TechSat21 Flight Experiment (2003), 3***	
	GLONASS (1982-1998), 24	*TechSat21 (2004, cancelled)*	
	Galileo (2005-2008), 30		
	NPOESS (2008),5		
Comms	***Iridium/Globalstar****/Teledesic/* ***Skynet****/Odyssey*		
Demo		*University Nanosatellite Programme (cancelled)*	*SNAP-1/Tsinghua-1 (2000), 2*
		ORION, 6	*MUSTANG (2004), 2*

Table 2-4: Summary of Current and Planned Satellite Formations and Formation Flying Missions Detailing Launch Year and Number of Satellites (Key: Current Satellite Formation Missions, Current Formation Flying Missions) (Refer to Appendix A for further details)

The tables in appendix A describe current formation flying missions, current and future satellite formations (which do not perform formation flying), future formation flying missions, and recent university studies supporting formation flying missions. The missions are grouped by common objective in each table, and then listed in ascending date order within the group. In this case each mission is summarised in terms of mission programme, title, formation type, orbit, launch year, objectives and supporting organisations. The tables are revised from earlier work performed by the author in 2001-2002 (Perrins, 2002), and the revision process has highlighted the changes in mission objectives, technology readiness, and the down-selection process of missions within the space agencies. It should be noted that rendezvous can be considered as formation flying for only a small proportion of a mission, and although a wealth of literature exists, rendezvous missions and related studies have not been considered in detail.

2.1.3.1 Current Formation Flying Missions

The operational missions involving satellite formations are highlighted in Table 2-4. However, the only missions actually formation flying for at least part of their mission (excluding those performing any rendezvous manoeuvres) are the two-satellite leader-follower formations of GRACE (Mauldin, Bettadpur, and Fowler, 2004) and the Earth Orbiter-1/Landsat7 satellites (Folta and Hawkins, 2002). The US military TechSat21 flight experiment was proposed for launch in 2003, but no further information was found in the public domain to confirm whether this mission is underway. The missions are described further in Table A-1 of appendix A.

NASA's Earth-Orbiter-1 technology demonstrator satellite (EO-1) has flown autonomously in a leader-follower formation with Landsat7 to validate the 'Advanced Land Imager' instrument and demonstrate formation flying. The spacecraft are not maintaining precise relative position in orbit but are instead maintaining an accurate temporal separation along an Earth ground track. This allows the two satellites to observe the same ground location through similar atmospheric conditions for stereographic imaging. EO-1 has Enhanced Formation Flying (EFF) technology onboard (Folta and Hawkins, 2002). This onboard software plans and executes the required manoeuvres using fuzzy logic and closed-loop control. EO-1 maintains relative position by initially flying at an altitude 50m above the Landsat7, and due to the differences in drag to mass ratio for the two spacecraft, the EO-1 loses altitude more quickly and therefore moves towards Landsat7. When the spacecraft reach the specified separation limits, EO-1 operates autonomously to manoeuvre back to the higher altitude and the process repeats.

The two GRACE (Gravity Recovery and Climate Experiment) satellites are also loosely formation flying in an along-track leader-follower formation, separated by up to 220km (Mazanek, Kumar, Seywald, and Qu, 2000). The mission is performing accurate geodesy, oceanography and Earth science by making many measurements including inter-satellite range which is also used for ground controlled relative position maintenance. The variation in the strength of the Earth's gravity field is detected through minute changes in the on-orbit spacecraft separation. The satellites are not

autonomously formation flying, but do use relative position measurements for loose formation keeping.

2.1.3.2 Current and Future Satellite Formations

There are a number of current multi-satellite missions which are not formation flying (Table A-2, appendix A). However, these missions would benefit from the development of formation flying technologies. These could include the ability of the constellation to detect failures and automatically acquire a new formation to retain coverage levels, improvements in orbit maintenance, and a larger degree of autonomy to reduce the need for human involvement in the operations of the satellite. Examples include environmental, navigation, and communications satellites (including co-located GEO satellites) that are currently operating primarily as global constellations but are controlled and monitored from the ground.

Ten missions involving satellite formations for Earth sciences are listed in Table A-2. These involve atmospheric observation and magnetosphere measurements. GOES and POES (Peslen (2005a) and Peslen (2005b)) primarily provide national weather service operations. Satellites within the A-Train constellation will fly within 15 seconds of each other in an along-track formation, and will monitor the Earth atmosphere for various constituents, including for example, carbon dioxide, water and ozone (Vincent and Salcedo, 2004). However they are not formation flying and will be individually controlled to maintain their own positions within fairly restrictive pre-defined error boxes.

The Cluster multi-satellite mission highlights the benefits of using a cluster of small identical spacecraft to make simultaneous measurements in different parts of an environment. The four Cluster spacecraft, the first science platforms to be produced on a 'production line' by ESA, are enabling the observation of the effects of the solar wind on the Earth's magnetic field. By flying in almost identical orbits around the Earth, their proximity is being varied between hundreds and thousands of kilometres, depending on the scale of the structures to be studied in the magnetosphere. The spacecraft are all controlled from ground stations, and do not fly autonomously. Space Technology-5 (ST-5) is a three-satellite technology demonstrator mission developed in support of the future NASA Magnetospheric Constellation Mission which aims to characterise the Earth's magnetotail with its 50-satellite 'swarm' (launch ~2010). The ST-5 satellites will not be formation flying but will take measurements in the Earth magnetosphere autonomously and cooperatively.

The satellite formations comprising by far the most satellites are the navigation and communications constellations, with, for example, 24 GPS, 66 Iridium, and a proposed 30 Galileo satellites. The location of each of these satellites is determined from the ground, and must be maintained within predefined 'error boxes'.

Constellation design is an active research area motivated primarily by the desire to improve performance, for example communications range and capacity, or improved global positioning accuracy. Turner (2001) proposes a new Molniya orbit constellation

for continuous broadband connection between locations widely separated by longitude. Park, Wilkins and Mortari (2004) and Mortari et al. (2003) suggest that more than four satellites in view are necessary for more accurate navigation and propose improved constellation designs beyond those of GPS, GLONASS and Galileo (Table A-2). In their study, Flower Constellation theory is applied to global navigation system design. The satellite relative trajectories must be closed and periodic relative to the Earth-Centred Earth-Fixed (ECF) coordinate system, and the J_2 perturbation effect is also taken into account (orbit perturbations are described in chapters 3 and 4). However, although relative orbits are considered, the satellites are not formation flying.

2.1.3.3 Future Satellite Formation Flying Missions

Future formation flying missions, supported by industry and academia, in the ESA and NASA programmes are described in Table A-3 of appendix A. These are limited to science and observatory missions as the most prominent recent military surveillance mission, TechSat21 (Garnham, Wainwright, and Burns, 2001), was cancelled in early 2003. The missions are all scheduled for launch from 2010 onwards, the earliest being the SMART-3 technology demonstrator for the ESA Darwin mission (Beichman, 2004b). Other recent university studies involving formation flying, but with no planned launch date, are included in Table A-4 and discussed in section 2.1.3.4.

The missions are again categorised in terms of area of mission interest. For the future formation flying missions, these include the progressively more ambitious x-ray observatories (XEUS, Constellation-X and Generation-X), the Sun-Earth Connection programme missions (Magnetospheric Multiscale Mission, and GEC, Geospace Electrodynamic Connections), and the progressively higher resolution visible and infrared wavelength observatories (Darwin/Terrestrial Planet Finder, Life Finder and Planet Imager).

XEUS, the X-ray Evolving Universe Spectroscopy Mission has been recently redefined as a single mission operating at the L2 Lagrangian point (ESA Website, 2004). The mission aims to detect and study black holes by detecting the photons emitted from accretion discs associated with black holes, using one mirror spacecraft and one detector, separated by a telescope focal length of 50m and accurately formation flying to 1mm accuracy. This will improve the resolution of the observatory beyond that of the precursor missions, XMM-Newton and INTEGRAL. The NASA Constellation-X mission concept is being developed simultaneously, and will meet the same objectives using a four spacecraft formation at L2 (Grady and Gadwal, 2001). The more futuristic Generation-X mission aims to significantly increase the telescope aperture (to $15m^2$ across six spacecraft) for improved x-ray detection (Zhang and Newman, 2002).

The successors to Cluster (ST-5, MagCON), described in Table A-2, are complemented by two formation flying missions in the SEC programme. The Magnetospheric Multiscale mission and GEC will study the small-scale processes in the magnetosphere and ionosphere to complement the large-scale observations of MagCON.

Significant programme changes have occurred since 2000 for the ESA Darwin and NASA Terrestrial Planet Finder (TPF) missions which both aim to detect and characterise extrasolar planets using nulling interferometry techniques. The missions are likely to become a single joint mission, using technology demonstrated by SMART-3 (Caramagno, Araujo, Bastante, and Penin, 2005). Until very recently, four configurations were being considered for the TPF mission. These included two coronagraphs of different sizes, a formation flying interferometer, and an alternative interferometer comprising a series of interconnected telescopes (Beichman (2004a),(2004b)). Findings suggest that astronomical observations would be complementary at both visible and infrared wavelengths, and as a result two TPF missions have been defined. TPF-C (launch 2014) would be a visible light coronagraph comprising a single satellite, and TPF-I would be a formation of five spacecraft (four telescopes and a hub) performing infrared nulling interferometry (Figure 2-2a).

(a) **(b)**

Figure 2-2: a) TPF-C and TPF-I Formation (Jackson, 2004a) b) Early Darwin Mission Formation (Alcatel Space Industries (ESA Website, 2003))

The early Darwin mission formation, illustrated in Figure 2-2, comprised six telescopes, one beam combiner (hub), and a separate communications relay satellite. The telescopes and hub were to operate in a planar circular formation, and like TPF, would orbit around the Sun-Earth L2 point.

NASA has also proposed two additional formation flying missions within the Origins Programme. Building on the discoveries of TPF/Darwin, Life Finder aims to produce higher resolution infrared spectra of extrasolar planets to make more detailed observations of life signs and biosignatures (Jackson, 2004b). The most futuristic mission is the NASA Planet Imager (Figure 2-3) which will achieve sufficient resolution to take pictures of planets using a greater number of large-diameter telescopes operating across much larger baselines (NASA Origins Website, 2000). Only a very short NASA study was performed in 2000 in support of a Planet Imager, and work performed by Hyland et al. (2002) since then to overcome some of the problems associated with imaging over such extensive baselines is reviewed in Roberts (2006).

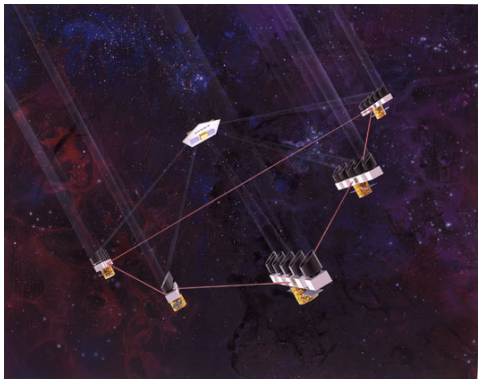

Figure 2-3: Planet Imager Mission (NASA Origins Website, 2000)

2.1.3.4 Recent University Formation Flying Mission Studies

The final section of the formation flying missions survey includes a selection of recent missions designed primarily as technology demonstrators within university environments, and further details can be obtained from Table A-4 in appendix A. These have been serious programmes with provisional launch dates, but also have been particularly susceptible to funding availability or programme cancellation. Of course there are many other multi-satellite missions that are also just at the paper study phase.

The former US University Nanosatellite Programme (UNP) aimed to develop and launch a number of nanosatellites to demonstrate formation flying and new miniature technologies (Agee, Janni, King, Witt, and Fender, 2001). A number of American universities participated in this Air Force Research Laboratory study which was designed to support the TechSat21 synthetic aperture radar mission. TechSat21 was a concept level formation flying mission being designed to perform high-resolution Earth surveillance using a series of microsatellite clusters in LEO (Cobb et al, 1999). In addition to technology demonstration, the fundamental research objective of the UNP was to investigate global ionospheric effects which affect the performance of space based radars, navigation and communication signals.

Initially proposed through the merging of microsatellite and carrier phase differential GPS (CDGPS) research at Stanford University in 1998, the 6-satellite Orion mission became the 3-spacecraft Orion-Emerald mission of the UNP. The main objective of Orion-Emerald mission was the demonstration of autonomous formation flying using Carrier Phase Differential GPS for real time relative navigation and formation flying control (Ferguson, Busse, Engberg, How, and Tillerson, 2001).

In the UK, SSTL (with links to Surrey University) has already flown a formation flying demonstrator, although rendezvous manoeuvres between SNAP-1 and Tsinghua-1 were ultimately unsuccessful due to the large inter-satellite separations (Underwood et al, 2001) and thruster limitations. MUSTANG was another British project which aimed to demonstrate microsystems technologies (MST) related to distributed systems and formation flying (Roberts, Bowling, and Hobbs, 2002). This technology demonstrator comprised two nanosatellites with the ability to fly autonomously in precise formation.

2.1.4 Mission Selection

Currently, the future formation flying missions in the ESA and NASA programmes are restricted to deep space science and observatory missions, and no LEO missions are formally proposed. Of particular interest for this research was the enhanced performance made available by the use of multiple telescopes and initially the futuristic Planet Imager mission was selected. However communications with NASA revealed that the mission definition had not been formally investigated in any detail, information about the mission was limited, and the technical hurdles to be able to achieve such a mission were extremely large. In fact, there already remained significant unknowns for the precursor missions of Darwin and TPF. It was therefore proposed that the research be refocused towards the nearer-term Darwin mission.

2.2 The Darwin Mission

Following the selection of a target mission for the research, this section highlights the mission objectives and primary design drivers for a Darwin-type mission. Design drivers are identified and the mission motivation is established using information drawn from a thorough survey of astrobiology and optical astronomy requirements (Roberts, 2006). The technical specifications for the ESA Darwin mission are summarised from the feasibility study carried out at ESA (ESA Report, 2000) and updated through reviews of recent literature, and in this context an overview of formation flying guidance, navigation and control (GNC) systems is presented. An appreciation of formation flying GNC systems is required in order to interpret the results of later dynamics and control analysis, and the use of analytical relative dynamics models for the analysis is proposed.

2.2.1 Darwin Mission Objectives

In the context of formation flying and planet detection, Darwin fits into the mission sequence and timeline illustrated in Figure 2-4. Further details regarding the sequence of precursor missions which will demonstrate both science and technology for Darwin are given in Roberts (2006). These precursor missions, for example, COROT, will each demonstrate one of a range of possible techniques for extrasolar planet detection. The planet detection techniques identified in Roberts (2006) include:

- *Indirect detection methods* (planet presence is inferred): Photometric transit, Electromagnetic radiation detection, Radial velocity, Astrometry, Microlensing.
- *Direct detection and observation methods* (planet is directly observed): Polarimetry, Coronagraphic methods, Nulling interferometry.

The questions that the Darwin mission aims to address can be posed in numerous ways, although fundamentally, the driving motivation is to discover whether we are alone in the Universe. Fridlund (2002) states the following primary objective for Darwin:

"To detect and study Earth-type planets and characterize them as possible abodes of life"

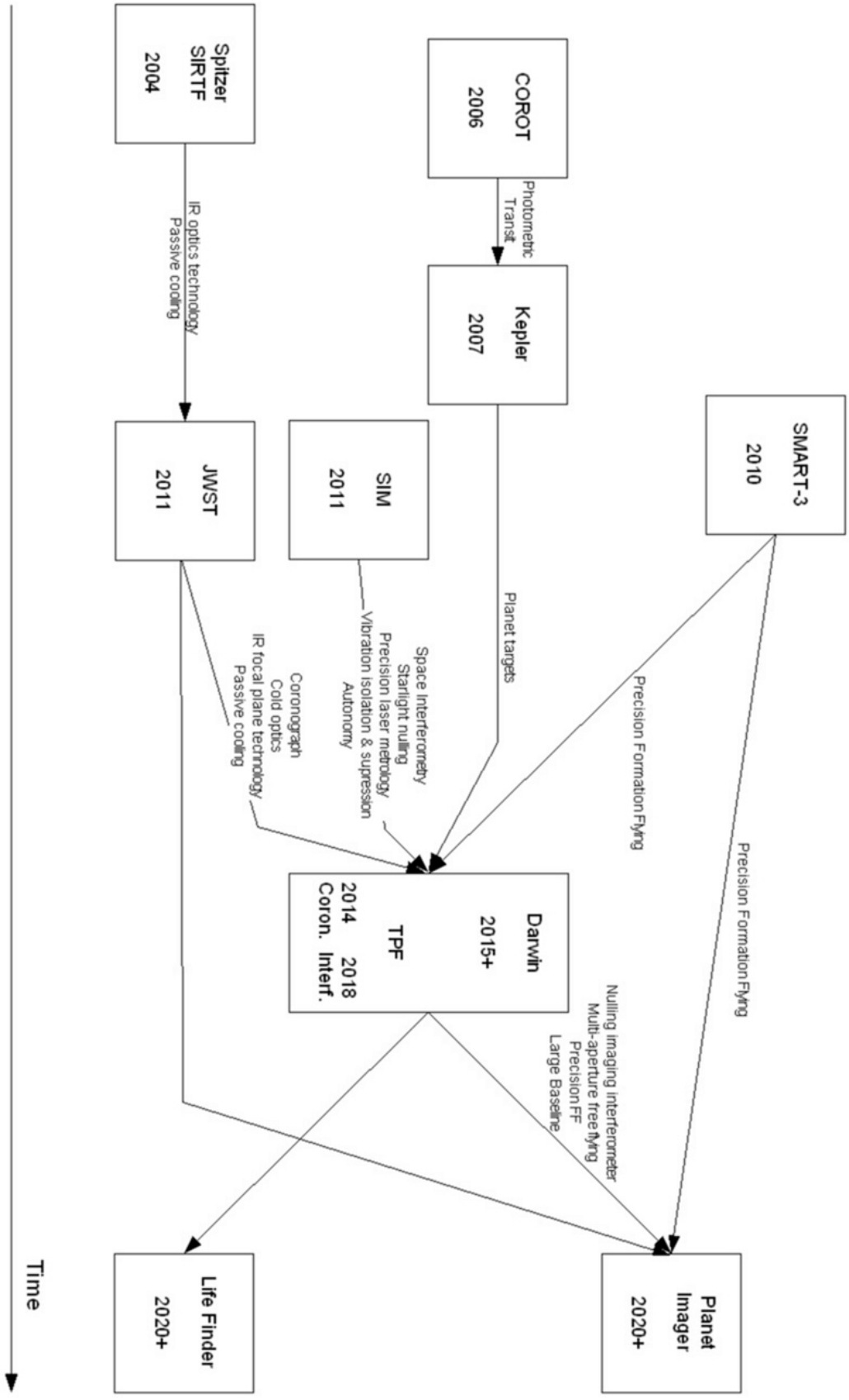

Figure 2-4: Mission and Technology Roadmap Towards Darwin and Planet Imager (Data from Roberts (2006) and Table A-3 (appendix A)

To simplify the investigation, Earth-like planets remain the focus of the mission as Earth represents our only example of life and its influence on the environment. By observing the characteristics of Earth, it is possible to design the mission systems that will enable these features to be detected and observed from great distances. Darwin will aim to:

- Detect planets within the Habitable Zone (HZ) of their parent star (where liquid water exists). Refer to section 2.2.2.2 for a definition of the HZ.
- Determine the mass of the planet, and orbital characteristics through repeat observations
- Observe the planet spectrum to determine temperature, albedo, and therefore planet size, and also of significant importance, determine the atmospheric composition of the planet.

Recently, the top-level mission requirements were revised and the following summary (from Fridlund (2004)) complements the earlier aims:

- The mission must be able to detect a large enough sample of Earth-like planets, preferably in different stages of evolution, and around as wide a range of stars as possible (in terms of spectral type, age, metallicity and evolutionary status) to enable useful conclusions to be drawn.
- The mission should be designed so that it could observe as much as possible about the result of different physical conditions in different star-planet systems with respect to the evolution of different bodies in these systems and to establish the conditions for the formation of life.
- The mission needs to be able to detect key signatures in the atmosphere indicating the possibility of habitability, and biomarkers which indicate the presence of biological activity, while remaining robust against false positives.

A second Darwin objective is defined by Fridlund (2001) and Selsis (2002) as:

"The imaging of astrophysical objects with unprecedented spatial resolution"

Darwin not only aims to observe Earth-like planets using nulling interferometry, but also aims to become a high resolution astronomical imaging facility for other observations in the infrared. Targets for the imaging phase include star forming regions, active galactic nuclei, super-massive black holes, and also, galaxy formation and evolution will be observed (Rottgering, D'Arcio, Eiroa, Labbe, and Rudnick, 2003). Darwin must, therefore, be able to perform both nulling and imaging interferometry. These techniques and their influence on formation manoeuvring and mission design are described in sections 2.2.3 and 2.3.

The mission concept was initially developed during the 1980s, and between 1997 and 2000, a feasibility study was performed by Alcatel (France) for ESA. Now an important part of the ESA Cosmic Vision 2020 program, Darwin is in a technological development phase, although more recently, ESA and NASA have signed a letter of agreement to 'jointly arrive at the mission architecture for Darwin/TPF before the end of 2006' (Fridlund, 2004).

2.2.2 Astrobiological Mission Design Drivers

Driven by the desire for knowledge as to whether we are alone in the Universe, the relatively new subject of astrobiology helps us to define what we should look for and where we should be looking for it. An overview of this field of research in the context of extrasolar planet detection and observation is given in Roberts (2006) where the likelihood and ubiquity of life in the Universe, and the methods by which life can be detected are described in detail. In particular, the following are considered:

- The creation of the Earth and its orbital characteristics
- The methods by which life might have arrived or arisen on Earth
- The ability of life to inhabit extreme environments
- The number of Earth-like planets that are likely to exist in the Universe.

To make a positive identification of life on an extrasolar Earth-like planet, a number of biosignatures must be detected. A biosignature is an 'object, substance and/or pattern whose origin specifically requires a biological agent' (NASA Astrobiology Roadmap, 2002). In this case, biosignatures have been defined by considering the historical aspect of the evolution of life on Earth and how it can be detected at the planet surface, and the life signs which can be detected over inter-stellar distances.

The first point focuses upon the chemical and environmental processes that have hypothetically stimulated the evolution of the earliest, single-cellular life into multi-cellular and larger fossil form. In this case, research suggests that the most relevant life indicators are water, organic matter and sources of energy (Westall, Nijman, Brack, Steele, and Toporski, 2001). The search for these features requires close observation of the surface of the planet, and ultimately, direct surface measurements to detect organic compounds. Atmospheric composition and characteristics must also be considered, and energy sources at the surface level such as hydrothermal vents and geothermal environments should be considered in addition to the energy source of the parent star.

In the second case, where life cannot be directly observed, it is the life-sustaining atmospheric environment which must first be detected. Better resolution may eventually enable surface observation for other life signs at the planetary surface. This is the objective of the futuristic NASA Planet Imager mission (NASA Origins Programme, 2004). Fridlund et al. (2002) suggest that the most reliable biosignatures would be oxygen (O_2) and ozone (O_3), present simultaneously with liquid water (H_2O) and carbon dioxide (CO_2). They also suggest that methane (CH_4) together with molecular oxygen could indicate biological activity on a planet, depending upon the degree of oxidation of the planet's crust.

The following subsections focus on the application of astrobiology to the design of Darwin or a future planet imaging mission. In particular the following are considered:

- Detection and spectral analysis of the planetary atmosphere and its effect on wavelength range of observation.
- The definition of a Habitable Zone and its effect on target selection, observation duration, and interferometer resolution.

These and other influences on mission design are considered further in the preliminary planet imager formation design, presented in section 2.3.

2.2.2.1 Atmospheric Composition and Observation Wavelength

Using Earth-like characteristics as a basis in the search for a habitable environment, it is important to consider the biosignatures of both the early and modern Earth atmosphere (Roberts, 2006). These include oxygen, ozone, carbon dioxide, water, and methane. Table 2-5 illustrates the current composition of Earth's atmosphere.

Constituent	Chemical Symbol	Mole Percent %
Nitrogen	N_2	78.084
Oxygen	O_2	20.947
Argon	Ar	0.934
Carbon dioxide	CO_2	0.035
Neon	Ne	0.00182
Helium	He	0.00052
Methane	CH_4	0.00017
Krypton	Kr	0.00011
Hydrogen	H_2	0.00005
Nitrous Oxide	N_2O	0.00003
Xenon	Xe	0.00001
Ozone	O_3	Trace to 0.00080
Water Vapour	H_2O	Trace to Few Percent

Table 2-5: Components of the Earth's Atmosphere (Samson, 2004)

Molecular oxygen (O_2) is essential for the life with which we are familiar. The increase in atmospheric oxygen, related to the beginnings of photosynthesis, caused some life forms to die out while others adapted to its presence (Mullen, 2002). In describing the work of Knauth, Mullen suggests that the 'Cambrian Explosion' occurred when oxygen quantities, produced by bacteria, had increased to a critically sufficient level, and that oxygen use is linked to the development of complex life forms. Prior to this, life was predominantly methane producing. Today it is unknown why oxygen levels lie steadily at 21%. However, if all life were removed from Earth, the molecular oxygen would disappear within 4 million years (Kaltenegger, Karlsson, and Hanslmeier, 2002). It should be noted that oxygen can only be detected in the visible range and therefore for infrared observations, ozone becomes the preferred indicator (Schneider, 2002).

Ozone (O_3) is a 'tracer' of oxygen, and is currently present in the Earth's atmosphere at between trace level and 0.0008% (Kaltenegger et al, 2002). The spectral absorption of ozone has a logarithmic dependence on the quantity of molecular oxygen in the atmosphere, and therefore serves as a useful indicator for the presence of certain amounts of oxygen, until saturation occurs. On Earth, the level of ozone is saturated and does not indicate the level of biological activity, therefore measurements of ozone alone on extrasolar planets cannot be used for this purpose. Ozone is created through reactions of nitrous oxide and hydrocarbons in sunlight, and in the stratosphere it absorbs harmful UV radiation.

Selsis (2002) considers the false positive and negative detection of life due to the discovery of ozone and therefore oxygen in spectroscopic results. Oxygen is present in

the atmospheres of all the Solar System planets, but its presence is not due to biological activity, and is instead due to the photodissociation of carbon dioxide and water. Through simulation of the reactions of oxygen and ozone in humid and dry carbon dioxide atmospheres, and water rich environments, Selsis was able to determine that the only robust biosignature for an ecosystem-sustained, oxygen-rich atmosphere was the simultaneous existence of ozone, carbon dioxide and water. The detection of ozone was found to be dependent on the partial pressure of carbon dioxide, for a given resolution and signal-to-noise (SNR) ratio of the observing equipment.

Carbon components are the building blocks of life and the balance of atmospheric carbon in the form of carbon dioxide is also affected by life with the burning of fossil fuels and forest, and by photosynthesis. Spectral analysis will also indicate the presence of water vapour (H_2O) in the atmosphere. Knowledge of the balance of other atmospheric constituents and their partial pressures would indicate remotely whether liquid water was likely at the planet surface. Close visual inspection of the planet surface would give the clearest indication for the presence of liquid water.

In conclusion, the triple biosignature O_3-H_2O-CO_2 is the best indicator for life on an extrasolar planet in the context of current conditions on Earth (Selsis, 2002). The spectral features of the CO_2, H_2O and O_3 biosignatures are visible in the 5-20μm infrared wavelength band, and due to the Earth atmospheric absorption spectrum, it is necessary to observe this regime from space.

2.2.2.2 The Habitable Zone

In addition to the definition of biosignatures and their associated effects on observatory design, astrobiology affects target selection, observation duration, and interferometer resolution through the characterisation of a ‘Habitable Zone’. The Habitable Zone (HZ) is defined as ‘the region around a star where water can remain liquid at least during some part of the local year, for long enough geological time, typically a few billion years’ (Leger, Labeque, Ollivier, Sekulic, and Valette, 2002). In this case ‘long enough geological time’ implies sufficient time for biological evolution to occur.

The HZ is characterised by the proximity of the planet to the star and also the behaviour of the star. Many other factors must also be considered, including planetary size, mass, temperature, albedo, and orbit. In addition to the atmospheric composition and its ability to support convection, the magnetosphere, planetary motion in terms of seasonal and diurnal characteristics, and the presence of planetary satellites or rings must be considered (Schneider, 2002). A higher resolution observation of an extrasolar planet would reveal other useful indicators of life, for example the presence of clouds, oceans, continents, and eventually the surface detail confirming the presence of liquid water.

Table 2-6 summarises the stellar characteristics that affect the location of the HZ, based primarily on the Sun-Earth relationship.

Stellar Feature	Description (in Solar Context where applicable)	Effect on the Habitable Zone
Lifetime	Duration of existence of parent star measured from the onset of core hydrogen burning to 'Terminal Age' at the Hertzsprung Gap.[a] The Sun is a main sequence star with a life expectancy of 10 billion years.	If stellar lifetime is of insufficient duration, the existence of extrasolar intelligent life is deemed unlikely. Duration of life on Earth is thought to be 3.8 billion years. Proposed minimum stellar lifetime for a HZ to exist for sufficient duration is 3 billion years.[a]
Mass	Stellar mass affects balance of gravitational force and internal pressure, and therefore internal temperature, density and magnetic properties. Luminosity varies linearly with mass for main sequence stars. Stellar lifetime depends on mass and rate of fuel use. Solar mass M_S=1.9891x10^{30}kg	High mass stars have faster evolution, and shorter lifetime (a short duration HZ for life to develop). Low mass star will bring HZ closer to provide sufficient heat for life, but the close proximity may have other extreme effects that limit the HZ e.g. 'tidal lock'. Define HZ around stars with mass close to that of the Sun and slightly smaller (F, G, K and possibly M type stars). Suggested range is 0.7 to 1.5 times Solar mass.[b] Suggested width of HZ for a given mass of star is from $0.1M_{star}/M_S$ AU to $4M_{star}/M_S$ AU.[c]
Age, (Indicated by Activity and Rotational Period)	Mean magnetic activity decreases and the rotational period increases with age. Mean activity is measured by observation of activity cycles over a long period of time (e.g. the 11yr sunspot cycle and 22yr magnetic cycle). Rotation of a charged body (e.g. Sun) induces a magnetic field. The gradual decrease in rotation rate is due to the loss of angular momentum through magnetically driven winds. Solar age is around 4.76 billion years[d]	Violent stellar activity may force the HZ to lie further from the star, depending upon the type of and variation in energy output from the star, and also a planet's ability to protect itself. Damaging UV (and X-ray) radiation from the Sun increases with sunspot activity, affecting Earth's upper atmosphere. Earth's magnetosphere provides protection from Solar activity (coronal mass ejections and Solar flares). There may be a link between low sunspot activity and a colder climate on Earth.[b] Slower rotation is related to reduced X-ray emission and chromospheric activity. Proposed HZ limit based on stellar rotation is vsini=10km/s corresponding to stellar age of 1 billion years.[a]
Luminosity	Total energy emitted from stellar surface. Luminosity varies linearly with mass for main sequence stars, and is also related to temperature (spectral class) and activity. Solar luminosity, L=384.6x$10^{24}$$Js^{-1}$ [e]	Fainter (M) stars have a closer narrower, HZ but it may last longer. The width of the HZ varies with $L^{0.5}$ due to the inverse-square fall-off in radiation. Habitable Zone for Earth is proposed to be 0.95AU to1.37AU (or 1.67AU for a 'maximum greenhouse limit')[f]

Luminosity Variation	Variation in energy emitted from stellar surface. For the Sun, variation in radiation at: Solar Maximum ~ +/-0.1% Solar Minimum ~ +/- 0.02% Maunder minimum = approx. -0.22 to -0.55%	Proposed stellar luminosity variation limit is 1%.[a] The effects of Solar luminosity variations on the Earth can be seen as changes in atmospheric circulation, weather, temperatures – climate change.
Metallicity	Proportion of star which is composed of heavy elements.	Metallicity may be linked to terrestrial planet formation, indicating the presence of sufficient mass in the system.
Multiplicity	Binary and multiple star systems.	Multiple star systems may offer multiple HZs in a given system (one around each star or around a number of stars).

Table 2-6: The Effects of Stellar Characteristics on the Habitable Zone ([a]Turnbull and Tarter (2002), [b]Wanner (1998), [c]von Bloh et al. (2002), [d]Watanabe (2004), [e] Williams (2004b), [f]Kasting et al. (1993))

The stellar features associated with the definition of a HZ are interrelated. The Sun appears to be a 'normal' star, and our understanding of its life cycle, magnetic activity and luminosity variations can therefore be applied to other stellar systems. To conclude:

- The lifetime (and age) of a main sequence parent star must be of sufficient duration for evolution to occur (3 billion years (Turnbull and Tarter, 2002)).
- Luminosity directly affects the HZ. The energy emitted by the star causes water to dissociate and hydrogen to be emitted to space at the inner limit, and CO_2 to condense at the outer limit (Kasting et al, 1993). The outer limit is defined in Turnbull et al. (2002) as 'the maximum distance from a star that a cloud-free CO_2 atmosphere can maintain a surface temperature of 273K'.
- Stars harbouring the first extrasolar planets discovered have been found to be more metal-rich than other stars nearby (Udry and Mayor, 2001).
- The number of HZs present in any multi-stellar system will depend on the stellar separations and mass ratios. There must be stable planetary orbits, and a suitable radiation and luminosity variation exposure to a planet within the HZ.

Table 2-7 summarises the important features of a habitable, terrestrial extrasolar planet and any limitations that would take the planet outside the HZ. The following conclusions can be drawn:

- Planetary mass is the most significant characteristic of a habitable planet. As detection methods improve, extrasolar planets of progressively smaller mass are being discovered. The aim is to find lower mass, rocky planets similar to the Earth and the inner planets of the Solar System. The lower limit allows the retention of an atmosphere, and beyond the upper radius limit, the planet is likely to be or to develop into a low density gas giant.
- The planetary orbit must permanently reside within the HZ.
- Multiple moons and rings may cause a planet to experience a different 'tidal' environment to that of the Earth or inner planets of the Solar System.

- According to Schneider (2002), the temperature of habitable extrasolar planets must be approximately 300K to allow primarily for the presence of liquid water (other suggested temperature ranges are given in Table 2-7). The black body temperature can be easily measured in the infrared.
- Infrared spectra with sufficient resolution may reveal properties of the planet surface. For example, large temperature differences between day and night may reveal significant atmospheric or oceanic circulation.
- Albedo measurements in the visible range indicate the nature of the planetary surface (continent and ocean), atmospheric motion (for example, clouds or dust circulation), and the diurnal and seasonal (axis tilt/eccentricity) characteristics of an extrasolar planet.
- The solid planets and moons in the Solar System have the same chemical composition. The iron core provides the protective magnetosphere, and volcanic activity and plate tectonics are essential in providing a circulation of the raw materials necessary for the development of life.

Planetary Feature	**Description**	**Characteristics of a Habitable Planet (in the Habitable Zone)**
Mass (Related to Radius and Density)	Planetary mass is the primary parameter obtained by indirect detection techniques. Mass (and size/density) determines the type of planet being observed: Gas giants (large, low density) Terrestrial planets (small, high density).	Mass of interest (for the Kepler mission) for a telluric planet in the HZ is 0.5 to 2 times Earth mass.[a] Mass of Earth $M_E = 5.9736 \times 10^{24}$ kg[b] Proposed planet radius is 0.8 to 3 Earth radii (Eddington Mission).[c] Radius of Earth (equatorial) = 6378.1km
Orbit	Planetary orbit depends on the HZ defined in terms of stellar characteristics i.e. Multiplicity, Luminosity, Age. Important orbital characteristics are inclination, eccentricity, and radius.	HZ requires planet to have a stable orbit where it is exposed to an even dose of stellar flux. Orbit eccentricity should maintain the planet within the HZ. Suggested maximum Earth eccentricity for habitability is between 0.3 and 0.7.[a] Earth e = 0.00335.[b]
Moons/Rings	Planetary satellites.	The terrestrial planets have maximum of 2 moons and no rings.
Planetary Neighbours (Giants)	Other planets in the stellar system (influence orbital stability in the HZ or may harbour habitable moons).	May provide protection from bombardment by other bodies. Influence orbital shape and dynamic stability of neighbouring planets. Minimum separation between habitable planet in the HZ and a giant planet is R_H (one Hill Radius).[d]
Magnetosphere	Region enclosed by all the lines of a planet's magnetic field.	A habitable planet needs a magnetosphere for protection from stellar activity. Size of magnetosphere depends on Stellar-planetary magnetic field interaction, but must lie sufficiently above the planet surface.

Temperature	Global temperature can be directly measured in thermal infrared, and also calculated in the visible if distance and albedo are known.[e] Surface temperature is higher than the black body temperature due to 'greenhouse effect'.	Black body (global) temperature of Earth is 254.3K. Surface temperature of Earth is 200-300K.[f] HZ is limited by requirement for a surface temperature range of 0 to 100°C (273.15K to 373.15K) for liquid water. HZ requirement for photosynthesis-based life at the surface is a temperature of 0°C to 60°C (273.15K to 333.15K).[g]
Albedo (Related to Seasonal and Diurnal cycles)	Albedo variation can indicate three features: 1. Short term variation indicating rate of planet rotation (duration of day/night) 2. Long term variation indicating seasonal effects (tilt of planetary axis or eccentricity of planet orbit) 3. Chaotic variation indicating cloud coverage.[e]	Earth albedo = 0.37 (on average)[f] Suggested HZ limits in terms of orbital period for an Earth-like extrasolar planet are 215 and 450 Earth days.[c]
Composition (Structural)	Main chemical components of the extrasolar planet, and its structure.	For a telluric planet in the HZ: Metal Core (Fe, some Ni, Co) Mantle Layer (O_2, Si, some Fe, Mg) Crust (62% O_2, 22% Si, 6.5% Al, some Fe, Ca, K, Na). Surface Ocean (H, O)
Atmosphere: Composition	Chemical components of the atmosphere.	HZ atmosphere is dominated by N_2, O_2, CO_2, H_2O, Ar. [h] The primary biosignature for the presence of life in the HZ is the triple signature of O_3-H_2O-CO_2.[i]
Pressure	Atmospheric pressure.	Varies on the terrestrial planets, and a wide range is tolerated by extremophiles. CO_2 partial pressure higher than 10^{-5} bar is required to allow photosynthesis.[g]
Circulation	Tidal, Surface winds, Convection	Provides heating, lessens temperature extremes, and creates many environmental balances which support life.

Table 2-7: Characteristics of a Habitable Planet for Land-Based Life (in the Habitable Zone) ([a]Sol Company (2004), [b]Williams (2004), [c]Deeg et al. (2002), [d]Turnbull et al. (2002), [e]Schneider (2002), [f]Snow (1991), [g]von Bloh et al. (2002), [h]Richmond (2004), [i]Selsis (2002))

In completing this overview of HZ, the interrelationships between all the varying stellar and planetary characteristics that create a habitable environment, have been highlighted. Where possible, definitions of HZ limits have been provided, but only based on current knowledge of Earth and the Solar System. If the full range of extreme habitable environments were considered, the HZ would be significantly extended. The characterisation of the HZ has been used to establish the Darwin mission objectives (section 2.2.1), and in particular, an understanding of the HZ enables the following mission design parameters to be defined:

- *Interferometer resolution*: Depends on the zone of orbit radii which could harbour a potentially habitable planet, for a given age of star. The interferometer must be able to resolve the distance between the planet and star.
- *Star/Planet Contrast*: This is critical to the ability of the interferometer to detect the light from an extrasolar planet and in conjunction with the detection of biosignatures, influences the selection of observation wavelength range. Relative brightness also affects the observation signal to noise ratio (SNR) and observation duration, thus affecting formation manoeuvres.
- *Planet Observation Frequency and Duration*: Analysis supporting the definition of the HZ has also influenced 'global' mission design by providing data on the likely frequency of existence and ultimately, frequency of detection of Earth-like planets (based on planet formation rates and stellar type). This influences formation manoeuvres (duration and distances between targets), and the size of the sphere of observation.

2.2.3 Optical Astronomy Mission Design Drivers

In this section an overview of the operation of an interferometer for planet detection, characterisation and astrophysical imaging is presented. An appreciation of the function of a nulling interferometer is essential for understanding the operation of the target Darwin mission. The function of the optical system is also directly related to formation design, and the design of spacecraft formation manoeuvres which are investigated as part of the dynamics and control analysis in chapter 7.

Extrasolar Planet Detection Using Nulling Interferometry

- Mission design for extrasolar planet detection and observation is governed by the capability of the optical payload, and its ability to achieve the mission objectives. Two classes of interferometer used for astronomical observations are illustrated below (Figure 2-5).

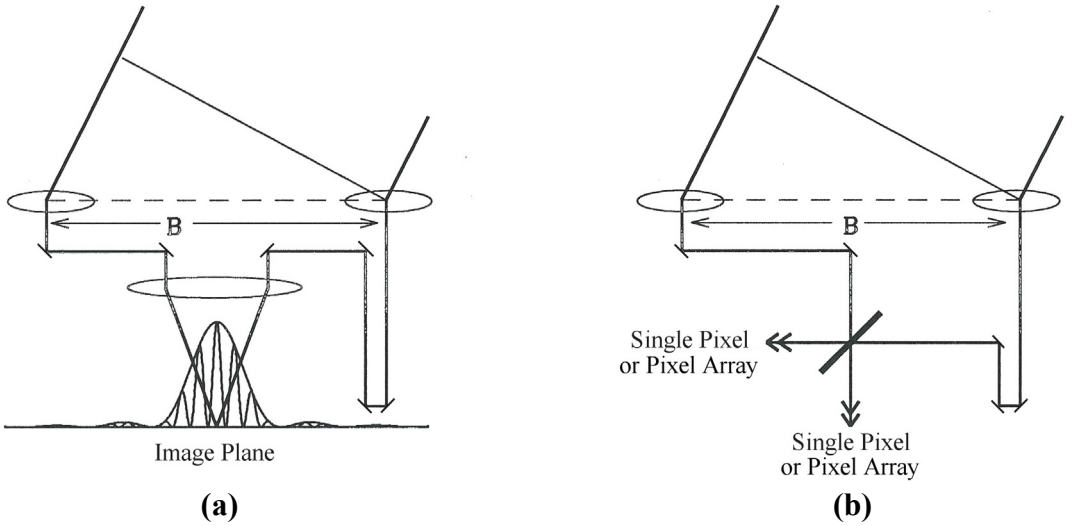

Figure 2-5: The Fizeau and Michelson Interferometers (edited from Traub, 2005)
(a) Fizeau (b) Michelson

These are the:

- *Fizeau Interferometer*: An image-plane interferometer that superposes light gathered at the aperture to create the fringes familiar from well known Young's slits experiment (Sears, Zemansky and Young, 1987).
- *Michelson Interferometer*: A pupil-plane interferometer that uses optical path length control to eliminate phase delay, and a beamsplitter to interfere light before it reaches the image plane.

Michelson devised a method of resolving the angular separation of distant celestial bodies using interferometry (Hecht, 1998). If two incoherent sources, for example two separate stars, at almost infinite distance from the interferometer are observed, with one star aligned with the formation pointing axis, two sets of interference fringes will be observed. Fringes centred on the image plane correspond to the on-axis star, and a separate set of fringes due to the interference of off-axis stellar light arriving at the different apertures will be offset from these. This offset is a measure of the phase difference between rays from the off-axis source arriving at the different apertures, and is a function of the angular separation of the sources. By adjusting the separation of the apertures (through formation baseline manoeuvring and internal mirror adjustment for precision control), the fringe patterns can be superimposed. When the fringes disappear (the phase difference between the two sets of fringes is π), the angular separation, θ, between the two incoherent objects can be measured using equation (2-1), where B is the separation between apertures and λ is the wavelength of observation.

$$B = \frac{\lambda}{2\theta} \tag{2-1}$$

In comparison, if two incoherent sources are viewed through a circular telescope aperture, two Airy discs will be produced. The resolution of a telescope can be described in terms of its ability to distinguish between the two sources, and the angular measure of theoretical maximum resolution for a telescope ($\Delta\theta_t$) can be determined from equation (2-2) (D is the mirror diameter).

$$\Delta\theta_t \approx 1.22\frac{\lambda}{D} \tag{2-2}$$

In terms of geometric optics, the Michelson interferometer baseline will be equivalent to a telescope of diameter equal to the separation of the apertures (B=D), but when diffraction effects are taken into account, the interferometer will achieve a higher resolution for a given baseline/diameter. The main difference between the telescope and interferometer when B=D is the amount of light collected by the system. This is significantly less for an interferometer which therefore requires a longer integration time to produce an image.

This type of interferometry can be applied to the direct detection and observation (including spectral analysis) of extrasolar planets. Under normal observation, the stellar light diffracted by the edges of any telescope aperture will obscure the light from a planet, however it is possible to overcome this by nulling the brightness of the parent star with interferometric techniques. The Michelson interferometer proposed for Darwin

is an amplitude-splitting device that uses a beam combiner to split and interfere the coherent light collected by the telescope mirrors (Figure 2-5b). Light is captured from the operational field-of-view either at two single-pixel detectors, or resolved into spectral bands across a linear detector array. Fringes are not formed at the image plane, and a direct image cannot be produced. Instead this must be reconstructed from time varying intensity measurements at the detectors. The Michelson interferometer is particularly appropriate for this application as a phase shift can be easily implemented within the beamsplitter optics.

Bracewell and MacPhie (1979) were the first to propose the use of a nulling interferometer for extrasolar planet detection (Figure 2-6). They considered just a two-element Michelson-type interferometer, and by introducing a phase difference of π in one of the interference channels, found it was possible to introduce a central dark fringe in the interference pattern. This could be placed directly over the star, allowing the much dimmer planet to be directly observed in the zones of constructive interference.

Without nulling, an interferometer would produce fringes of destructive interference on either side of a central constructive band, but these null regions will not suppress the starlight as they will move depending on wavelength. For sensitivity, it is necessary to observe over at least a small wavelength band, and therefore the null areas are diluted. Bracewell and MacPhie found that a central null, invariant to changes in wavelength could be achieved by incorporating a beam splitter into the optical path, and that this null covered a wider region than the central bright fringe obtained from the basic, non-nulling dual-aperture interference pattern.

The intensity recorded at the detector of a Michelson nulling (or Bracewell) interferometer contains light from both the star and planet. The fringe pattern can be considered to form according to basic interference theory, but must be visualised as though the apertures could project the interference pattern back onto the sky at infinity, instead of being focussed at the detector. The signal received by the interferometer is the convolution of this projected intensity pattern or 'transmission map' and the sources themselves (including the star, planet and background noise sources). The on-axis null will eliminate most of the starlight, but not all as the star has a finite diameter. In order to distinguish between the off-axis stellar and planetary light, it is necessary to spin the interferometer while retaining the pointing axis alignment with the star. The stellar flux would remain the same during the rotation, but the signal strength from a planet would vary due to its transition across successive fringes of constructive and destructive interference according to the transmission map. Two-aperture and six-aperture transmission maps are illustrated in Figure 2-7.

However, the thermal flux from the zodiacal background, primarily from extrasolar dust clouds may in some cases also produce a modulated signal. In addition to rotating the interferometer, internal modulation, or high frequency 'chopping' between the nulled outputs of different combinations of the apertures with additional phase shifts applied to their outputs can be performed to ensure that a planet signal has been detected (Velusamy and Beichman (2001), Kaltenegger, Karlsson and Hanslmeier (2002)).

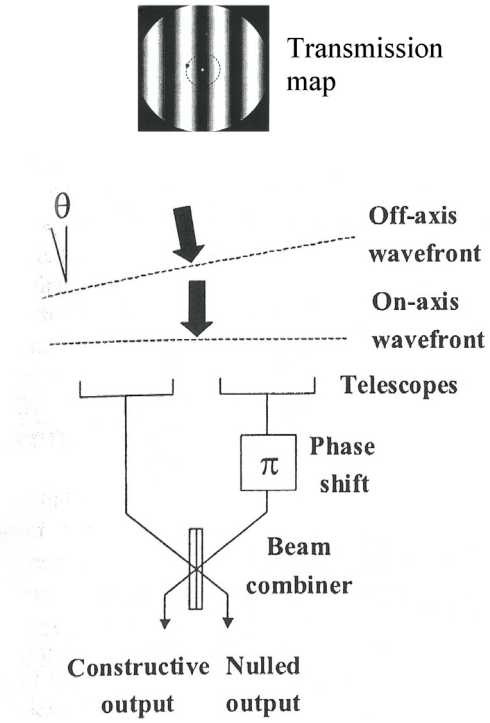

Figure 2-6: The Bracewell Nulling Interferometer and Resulting Intensity Pattern (D'Arcio and Karlsson, 2004)

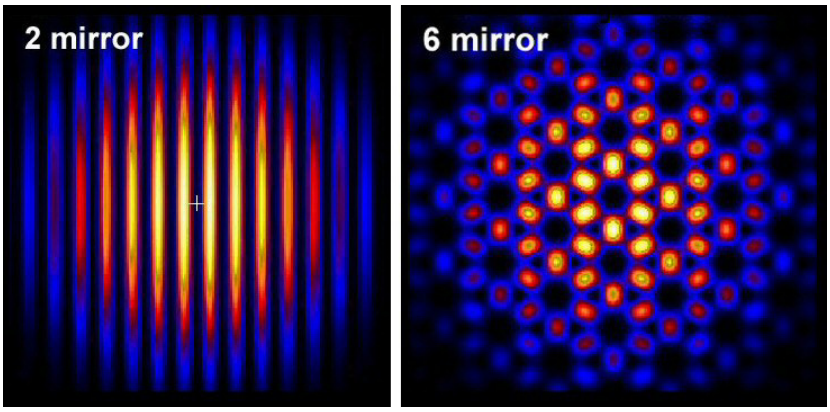

(a) **(b)**

Figure 2-7: Nulling Interferometer Fringe Intensity Patterns with Two and Six Apertures – Projected onto the Sky (Leitch, 1999)

Figure 2-7b illustrates the intensity pattern for a six-aperture (equally spaced axisymmetric) interferometer observing a point source. Increasing the number of apertures has the advantage of increasing the light gathering capacity of the system and providing a deeper null over a bright source for nulling interferometry. A complex interference pattern can be produced with multiple apertures according to imaging requirements and thus interferometer formation design. The use of additional apertures in this particular arrangement reduces the formation rotation and baseline variation requirements for image capture, and also provides greater flexibility in shaping and positioning areas of destructive interference over objects not required in the image.

For a planet to be detectable by a nulling interferometer, the integration time required to accumulate an adequate signal depends strongly on the planet brightness, the contrast between the planet and parent star, and the thermal zodiacal background radiation. The size of the stellar disc must also be sufficiently small relative to the fringe spacing to lie in a dark fringe, and the planet should be located in a bright fringe. The fringe width to maximise planet light detection is achieved by the selection of a suitable aperture baseline. The integration time depends on the total collecting area of the interferometer, and the sensitivity of the detecting equipment so that a sufficient signal-to-noise ratio can be achieved. If the integration time can be reduced, then the stringent station keeping requirements for imaging are also only required for shorter periods of time, and there is more time available to observe extra targets during a mission.

Interference fringes can only be attained if the light being combined is coherent. According to interference theory, this requires that the optical path length difference (OPD) between the radiation arriving at the image plane through each aperture is less than the coherence length (Figure 2-8). For visible light emitted by a Solar-type star, this is approximately 1μm (Lagadec, Lebas, and Ankersen, 2002), (Donges, 1998).

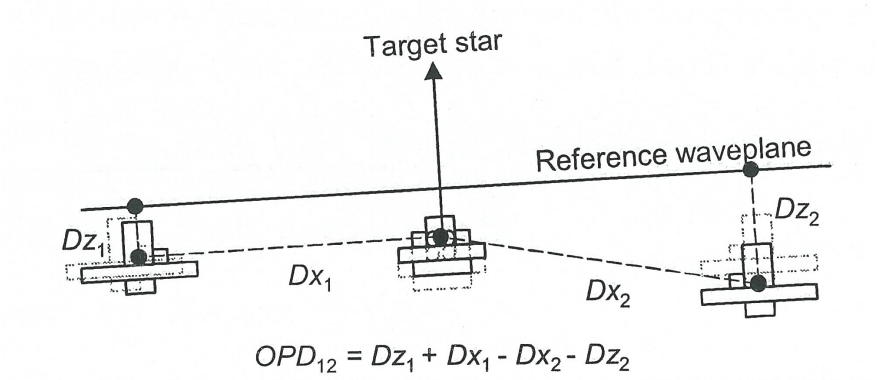

Figure 2-8: Optical Path Length Difference (Lagadec et al, 2002)

For a formation flying interferometer, the control of optical path difference can be achieved by precision formation flying of the apertures and even greater precision optical path length control using optical delay lines. For Darwin, a stable optical path length difference must be maintained below 5nm to ensure sufficient starlight rejection and sustained nulling throughout the integration time. This will be achieved using a high frequency control system and fringe tracker measurements which detect the interference fringes from the target star. (For interferometric imaging of extended objects, an alternative off-axis source outside the field-of-view must be used to control the optical path, as the target object is not bright enough).

As a direct planet detection technique, nulling interferometry enables the extrasolar planet light to be directly detected through modulation of the resulting intensity patterns. Images of the extrasolar system can be reconstructed from visibility measurements using suitable image processing techniques

Interferometric Imaging

In order to perform interferometric imaging and determine the intensity distribution at the image plane, it is necessary to sample complex visibility amplitude and phase

information of radiation arriving at a range of points across the u-v, or 'Fourier', plane. u and v are spatial frequencies, and each u-v location represents just one sample point in the spatial frequency power spectrum (the power spectrum is found by 'Fourier transforming of the autocorrelation of the source' (Hecht, 1998)). u-v plane coverage is achieved by altering the baseline between the apertures and rotating the formation. To improve coverage efficiency, simultaneous multi-baseline measurements can be achieved by using multiple (>2) apertures. The aperture diameter of the interferometer elements will be much smaller than the baseline, and therefore, the required manoeuvres can be considered as 'filling in' the areas between the apertures in order to cover the greater number of spatial frequencies that lie outside the catchments of the apertures at a particular instant in time. Ideally, these spatial frequencies will be sampled frequently and in a uniform manner for a high resolution image (Figure 2-9).

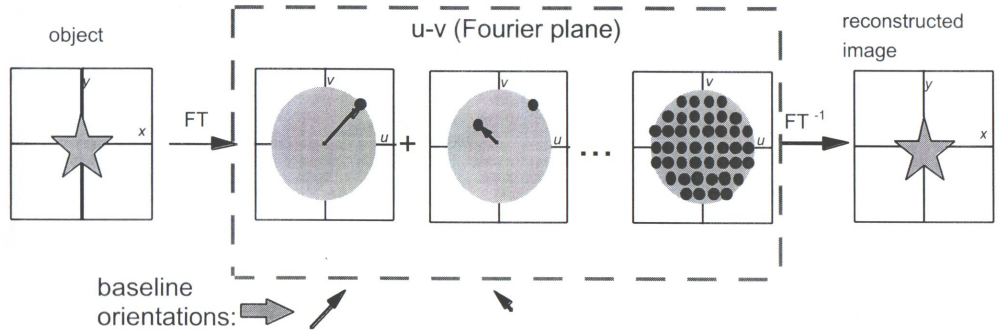

Figure 2-9: Image Processing and the u-v Fourier Plane (NASA Presentation, 1997)

Velusamy and Beichman (2001) state that certain types of interferometer will capture complex visibility which allows image reconstruction by simple Fourier transformation (especially in radio interferometry). However, only the fringe amplitude can be measured at each u-v point for nulling optical interferometers, and therefore other numerical correlation techniques must be applied to obtain the image. Velusamy and Beichman describe a Maximum Correlation Method (MCM) of image reconstruction by simulation to demonstrate this.

Optical Astronomy Mission Design Drivers

Roberts (2006) provides a detailed review and comparison of coronagraph and interferometric methods, and a survey of space and ground-based observatories for astronomy. The review highlights the main design drivers behind the selection of optical systems for an interferometry mission design. A number of these are summarised below, and support the justification for using a space-based infrared Michelson nulling interferometer for both the Darwin and the futuristic Planet Imager missions presented in section 2.3.

- The angular resolution of the interferometer is significantly larger than that of single-aperture diffraction-limited telescope with a mirror diameter equal to the separation (or baseline) between the interferometer mirrors.
- The baseline between apertures of an interferometer can be extended beyond the practical size limit of a single telescope aperture, thus providing increased resolution and flexibility in observations.

- The optical path length can be accurately controlled between the aperture and beamsplitter to ensure coherence and therefore the production of fringe intensity patterns.
- Pupil-plane nulling can be performed by introducing a π phase delay into one of the optical paths, which will enable extrasolar planet observation.
- Astrophysical imaging can also be performed using the same optical system, but without the nulling phase shift. This may not be optimal, but does give the Darwin mission two goals by which to measure the mission success.
- The apertures can be manoeuvred to collect sufficient information for correlation methods, and inverse Fourier transform techniques can be developed to reconstruct an image, so this is not a disadvantage compared to using a single telescope.
- Spectral analysis can still be performed using the light gathered by an interferometer.
- The observatory must operate in the infrared range (corresponding to maximum star-planet contrast and peak black body emissions for an Earth-like planet).
- The light gathered by space-based observatories does not experience atmospheric absorption and disturbances.

The formation and manoeuvre design drivers arising from optical payload considerations can be summarised from earlier discussions as follows.

- *Aperture Size/Integration Time/Equipment Sensitivity/SNR*: These parameters are interrelated and influence the duration of precision formation flying manoeuvres. Given a formation aperture area, the duration of observations performed by precision station-keeping must be sufficient to detect a planetary signal.
- *Aperture Number and Distribution*: This will determine the transmission map and null depth achieved by the interferometer. The number of multiple apertures will determine the number of simultaneous baselines that can be used for u-v plane coverage (interferometric imaging).
- *Baseline*: Manoeuvres are required to adjust formation baseline to achieve desired interferometer resolution and fringe width.
- *Formation Rotation and Signal Modulation*: Formation spin is necessary to distinguish the off-axis planet light from the brighter star. Additional internal signal modulation will further enable the detection of the planetary signal in the presence of noise.
- *Fourier (u-v) Plane Coverage for Imaging*: Image reconstruction requirements will determine the necessary u-v plane coverage by apertures of the interferometer, which will determine additional formation manoeuvres.
- *Optical Path Control Requirements*: Optical path control defines the formation flying manoeuvre precision requirements in the science modes.

2.2.4 Darwin Technical Requirements and Specifications

In this section, the technical requirements and specifications for the Darwin mission are described for the original six-telescope design (Figure 2-2b). Summary tables of

technical requirements are included in appendix B, and represent a snapshot of the 2002-2003 timeframe mission status. This information has been used to define the unknowns with regard to the formation manoeuvres, and used as a basis for their design (section 2.3). These are then implemented in the simulation study in chapter 7. Since this work was performed, a new four-spacecraft configuration for Darwin has been proposed by ESA.

2.2.4.1 Darwin Mission Requirements

In appendix B, tables B-1 and B-2 (section B.1) summarise the specific optical and astronomy requirements for each of the planet detection and spectroscopy, and astrophysical imaging phases of the Darwin mission. An overview of these requirements is given below.

Planet Detection and Observation Phase Requirements
To meet the primary objective, Darwin must have the capacity to observe an Earth-sized planet orbiting a Solar-type star up to 25 parsec (pc) away (approximately 81.6 light years). This requirement is driven by the need to ensure that a sufficient number of targets are detected and observed, and all must lie in a region centred on the anti-Sun direction for the elimination of as much scattered light as possible from the observation. The statistics relating to the frequency of extrasolar planets, and therefore the number of potential targets for observation are continually changing as more extrasolar planets of differing sizes and orbital characteristics are discovered in different stellar systems. Currently, the mission requires the observation of around 500 target star-planet systems. Of these, a minimum of 150 planets will be observed for spectral analysis during a second phase of the mission (Fridlund, 2004). The characteristic features of suitable extrasolar systems were identified in section 2.2.2. For all the planet detection and observation tasks, infrared nulling interferometry is performed, specifically operating in the 6-18μm range to enable the detection of biosignatures.

The desired observation distance and angular resolution of the interferometer are related to the distance between the parent star and the boundaries of the habitable zone (HZ). The HZ was introduced in section 2.2.2.2 and describes the region where a habitable planet could exist around a star. The maximum resolution required of the system would be that necessary for the detection and observation of a habitable planet orbiting a cool star at the upper distance extreme (25pc). The operating wavelength defined above was selected due to the benefits of star/planet contrast and its effect on null depth requirements, and for biosignature detection. Observation wavelength also restricts the level of signal from the targets and other noise sources detected at the aperture, and therefore influences integration time.

The planetary light received by the nulling interferometer is passed through a spectrometer. Selsis (2000) compares Earth emission spectra at resolutions R (where $R \equiv \lambda/\Delta\lambda$ with λ being the mean wavelength of the detected radiation and $\Delta\lambda$ being the smallest resolvable wavelength range) of 25 and 100 to investigate how the spectrometer will perform if observing an extrasolar Earth. At R=25, the triple-biosignature (O_3-H_2O-CO_2) can be detected, but there is a risk of false positive detection

of O_3 as the spectral line will be indicated by just one pixel against the background. At resolutions of 100 or more, not only is the triple-biosignature visible, but the ozone line now spans multiple pixels, thus reducing the chance of a false positive detection, and additional H_2O features can be seen at alternate ends of the observing spectrum. Such high resolution enables conclusions about the structure of the atmosphere (for example, the presence of clouds, and stratospheric warming) to be drawn. However, to observe at such a high resolution would require a much longer integration time to achieve a sufficient SNR. This requires extended periods of stability of the telescope formation, and will inevitably lead to fewer targets being observed. The minimum resolution of the spectrometer for the Darwin mission has been defined as 20, although Bowey and Yates (2000) agree with Selsis that a minimum resolution for the reliable detection of absorption lines without false positives would be 100-200.

Astrophysical Imaging Phase Requirements

Darwin will also use interferometry to image distant sources. The detail of the technique that will be eventually used is still undergoing research and development. However, the main contenders are:

- The Michelson nulling interferometer that was used for planet detection, but without the π-phase shift, and including a new focal plane detector for imaging.
- A Fizeau interferometer, although this would require the construction of an alternative hub (or optical system within the nulling hub).

The optical characteristics of these two types of interferometer were briefly introduced in section 2.2.3 (and are described in more detail in Roberts (2006)). Table B-2 in appendix B.1 describes the target parameters for the astrophysical imaging phase of the mission, which will ideally be achieved with the same optical system (Michelson) as that used for planet detection and observation. However, this has a very narrow coherent field-of-view (FOV) compared to a Fizeau interferometer where beam combining occurs at the image plane rather than at the pupil plane. Although it may be possible to combine multiple observations with the smaller FOV Michelson system, the integration of the two objectives of Darwin into the one mission remains a challenge.

2.2.4.2 Darwin Technical Specifications

The Darwin configuration, defined for the initial feasibility study (ESA Report, 2000), comprised six infrared telescopes, arranged in a hexagonal pattern, and equidistant from a central beam combiner (hub). The planar formation is illustrated in Figure 2-10.

(a) **(b)**

Figure 2-10: The Darwin Configuration (a) Planet Detection (formation is split into subgroups for signal modulation) (b) Imaging (edited from ESA Report (2000))

The factors influencing the Darwin configuration design included:

- *Thermal stability* – the formation must be planar to thermally decouple the telescopes (radiation).
- *Null depth* – increasing the number of apertures and interference pattern complexity produces a deeper null by increasing stellar rejection.
- *Sub-Aperture arrangements for planet signal modulation* – the configuration can be split into groups of smaller numbers of nulling systems enabling internal modulation of outputs to distinguish the planet signal.
- *Modulation efficiency* – the ability of the formation to isolate the planetary signal by rotation.

Table 2-8 summarises the spacecraft configuration design and formation flying requirements to meet the mission specifications. A brief overview of the Darwin subsystems is given in appendix B (Table B-3).

Configuration Characteristics	Current Design	Comments
Spacecraft[a,b,c]	- 6 of 1.5m diameter telescopes - 1 hub - 1 master (communications satellite)	The proposed 'Robin Laurance' Configuration has 6 telescopes arranged in a hexagon around the central hub. The formation has been reduced to 4 spacecraft in a recent ESA Mission Design review**.
Formation Configuration[d]	Planar	Good for thermal control – passive cooling
Formation Separation[e,f]	40-250m for nulling (planet detection). 50-500m for imaging.	Lower limit for collision avoidance. Baseline may extend up to 1km for imaging[f].
Orbit[a,g]	Sun-Earth L2, large Lissajous (unstable) orbit	Thermally and gravitationally stable environment.
Formation Flying Precision[h,i]	- Relative position maintenance to μm when targeting new object. - After fringe acquisition, relative position (baseline) is maintained to cm accuracy. - Optical path length control must be 5nm over a 500m baseline. - Telescope pointing accuracy ~1mas during fringe acquisition, increasing to 24mas for normal operation.	Precise relative position must be maintained until fringes are detected for the target star. Once fringes are acquired, relative position constraints can be slightly relaxed. Internal OPD control achieves nm accuracy for mission tasks.

Table 2-8: Darwin Specification: Formation Configuration, Orbit and Metrology ([a]Karlsson and Kaltenegger (2003), [b]Fridlund and Kaltenegger (2002), [c]Fridlund (2001), [d]Fridlund (2002), [e]D'Arcio and Karlsson (2004) [f]Rottgering et al. (2003), [g]Fridlund (2004), [h]Lagadec, Lebas and Ankersen (2002), [i]ESA Report (2000), [**]Karlsson, Kaltenegger et al. (2004))

Darwin will host a number of metrology systems capable of relative position and velocity measurement at different levels of precision. These systems are used individually and in combination, depending on the operational control mode (Table 2-9 and Table 2-10). As specified in section 2.2.3, during science modes the optical path

difference between light captured at each aperture must be controlled to nanometre precision before the beams are interfered to ensure coherence. This involves a combination of internal optical path control using a fringe tracker to track the interference fringes of the on-axis star, and external formation flying control of the satellite formation. To achieve the formation flying objectives to sufficient precision, the two main contenders for the micro-propulsion system are:

- FEEP (Field Emission Electric Propulsion - milli-Newton and micro-Newton)
- Miniature Cold Gas Thrusters

System	Accuracy	Application
Radar Ranging	<1cm interstallite <1m lateral position	Coarse metrology, Baseline maintenance
Laser Metrology	<<1mm	Out-of-Plane station keeping, Transverse manoeuvring, Formation rotation
Fringe Tracker	5nm	Optical Path Difference control
Wide Field Camera	1mas	Coarse pointing of array

Table 2-9: Darwin Metrology Systems (ESA Report (2000), Lagadec, Lebas and Ankersen (2002))

The modes already defined for Darwin by ESA and industry are summarised in Table 2-10. Formation deployment strategies on arrival at L2 using potential function theory are being investigated by McQuade et al. (2002). The breakdown of the mission into specific tasks and phases was not reported in the ESA study, and in section 2.3 a series of manoeuvre modes are therefore proposed. In some cases these are defined in more detail to meet the mission requirements of planet detection and astrophysical imaging for simulation in chapter 7, and future work.

Modes of Operation	Comment
• Deployment at L2	• Incorporates collision avoidance as satellites disperse from the transport vehicle into the initial formation.
• Baseline Control	• Formation station keeping (outer-loop control) and acquisition of laser metrology systems following deployment.
• Fringe Acquisition	• Mode is entered prior to any target observation: e.g. after initial deployment, or after slewing to a new target. • Precise formation flying to as close to μm level as possible is required for sufficient duration to acquire fringes by: - Using combinations of laser metrology and a fine pointing camera to maintain formation geometry - Compensate for formation drift using the OPD lines - Adjust the OPD lines at fractions of a coherence length to scan the uncertainty in this compensating OPD until fringes are detected. - Enable the fringe tracker sensor to take over OPD control.
• Normal Operational (Science Mode)	• Inner loop OPD control with respect to the fringe tracker measurements are combined with RF and laser metrology outer loop control of the satellite formation (cm accuracy required depending on OPD stroke length).

Table 2-10: Darwin Operational Modes (McQuade et al. (2002), ESA Report (2000), Lagadec, Lebas and Ankersen (2002))

Of the sub-system characteristics highlighted in this section, the metrology system accuracy, propulsion sensitivity, and thermal design are the most critical issues for the Darwin mission success (beyond achieving technology readiness with the payload optics). High precision metrology and propulsion is necessary to achieve the levels of control to perform imaging and planet detection at infrared wavelengths, and thermal control is required to ensure that the optical systems are sufficiently cool for the detection and recording of a planetary signal.

2.2.5 Guidance, Navigation and Control Systems Design

More generally, the accuracy with which a formation can be controlled is dependent on the quality of the sensed variables (sensor performance, bias and noise characteristics), and the sensitivity of the actuating (propulsion) system. In this section, an overview of essential GNC systems to support formation flying missions is presented to support the motivation and interpretation of the analysis and results described in later chapters. The role of simulation in GNC system design is considered and the use of analytical relative dynamics models for control system design and onboard relative trajectory generation is proposed. A number of aspects of formation control architecture design which must be considered for autonomous distributed satellite systems have also been identified. Launch, transfer, and end-of-life disposal are important phases of a formation flying mission, and the formation deployment phase is critical, however they have not been considered in this research.

2.2.5.1 Metrology and Propulsion

The appropriate sensors for the measurement of absolute and relative position and velocity, and therefore also the relative orbit elements of different satellites in a formation, are introduced in this section. The advantages, limitations and accuracy of each technique are summarised, and the review includes current technology and new technologies in the development phase. Relative attitude sensing systems are also briefly considered, however the optimal distribution of sensors across a multi-satellite system, and data fusion are not discussed.

Absolute and Relative Position and Velocity Measurement
Table C-1 in appendix C contains a summary of sensors that can be used to provide on-orbit absolute and relative position, velocity and attitude measurements.

GPS is proposed as a reliable and cheap option for primarily LEO navigation, however accuracy is limited. The accuracy of GPS also degrades significantly for satellite position and velocity measurement above the constellation altitude of 20200km (Table A-2, appendix A). However, although GPS signals are directed towards Earth, the wide beam width causes the signals to also transmit past the Earth, and this spill-over signal can be used by satellites in medium Earth orbit, above the GPS constellation. With increasing distance from the Earth, the poor distribution of the GPS satellites gives increasing dilution of precision. For formation flying, it may not be necessary to have accurate absolute knowledge of the formation position, and instead, relative position

and velocity measurements are sufficient. Lau et al. (1996) propose the use of GPS pseudolites to mimic a GPS signal, mounted on members of a formation to transmit and receive relative position data in deep space, thus overcoming this limitation.

CDGPS has been successfully developed in recent years to achieve centimetre (and in some cases sub-centimetre) relative position and centimetre/second relative velocity accuracy in real time using codes which do not require high-power computing facilities (Busse, Inalhan, and How, 2000). CDGPS measures relative carrier phase (rather than the transmitted code in standard GPS) and with a carrier wavelength of 20cm, sub-centimetre relative position can be measured, provided that a good estimate of the integer bias on the signal has been made. A Cross Link Transceiver, comprising GPS receiver with extended Kalman filter for relative (or absolute) navigation, operating simultaneously with a crosslink communications module, is introduced by Stadter et al. (2001) to enhance the operating range of CDGPS. By allowing pseudo-random noise codes to be transmitted and received between satellites on-orbit, CDGPS measurements can be resolved more rapidly.

Radio Frequency sensors for range, range rate and direction finding are common for aircraft navigations systems, and also particularly for satellite rendezvous and docking systems. Comprising a variety of antennae, receivers and transponders, these systems can successfully measure relative range and angular measurements between satellites in relatively close proximity. Compared to the optical sensors, RF metrology is deemed relatively coarse.

Optical sensors can be used for higher precision relative position and velocity measurements between satellites. These include laser range finders and cameras for visual navigation, and the techniques were developed for rendezvous and docking operations (Fehse, 2003). The Laser Ranging techniques are similar to those for RF sensors, but greater measurement accuracy can be achieved. Both signals depend on signal-to-noise ratio and transmitter power, and are performance limited at large separations or at very close proximity when sensor fields of view are compromised.

Image processing and reconstruction is continuously improving and promises to be an enabling technology for relative navigation. In order to measure range and line-of-sight angles between two spacecraft on-orbit, incident light is projected from the camera-mounted spacecraft to illuminate the target spacecraft over the camera field of view. The location of a minimum of three reflectors, strategically placed on the target spacecraft, are determined by the reflected light captured at the camera CCD, and relative parameters can be calculated. However, this technique is limited by the camera field of view, potential inflexibility of the distribution of reflectors, and the power of the reflected light. According to Fehse (2003), a suitable maximum operating range for a large reflector distribution would be approximately 200 metres, although accuracy improves with a reduction in range. A simpler strategy using LEDs for vision-based relative navigation has been proposed by Alonso, Crassidis and Junkins (2000).

Each of these sensor options offers benefits over different relative position and velocity regimes and formation locations for formation flying satellites. While certain

measurements may be achieved with improved accuracy, each system must also be evaluated in the context of their effects on, for example, mass and power budgets.

The relative position and velocity of satellites can also be expressed in terms of relative orbit elements. Ground based orbit determination techniques can be used to evaluate the classical orbit elements for both satellites, and these can be differenced to obtain the relative elements. Alternatively, the measurements made in the Cartesian frame, using the sensing techniques summarised in appendix C, can be converted into this alternative reference frame. The use of both frames for relative motion dynamics modelling for satellites in Earth orbit is discussed further in chapter 3.

A number of the sensing techniques summarised in appendix C are also able to determine relative attitude. A review of attitude determination and sensor technologies, including available hardware, for satellite formation flying was performed at Cranfield University by Carrel (2003). Absolute attitude sensors measure attitude in an inertial frame. Examples of sensor types include Sun sensors, Earth sensors, star trackers, and magnetometers. Three-axis attitude control can be applied to a satellite using different actuators, including thrusters, magnetorquers, reaction wheels, momentum wheels and Solar radiation pressure flaps. Relative attitude is the angular difference between the orientation of the body axes of one satellite with respect to the body axes of a second. This can be measured through line-of-sight measurements between three spacecraft, or through the use of combinations of the above sensors, depending on accuracy requirements.

Propulsion Systems

Significant literature is available regarding the range of propulsion systems suitable for formation flying, for example Larson and Wertz (1996), Stenmark and Eriksson (2002), Reichbach, Sedwick and Martinez-Sanchez (2001). In modelling and simulation work it is usually simply the acceleration that is calculated as a control input to a thruster system to execute a corrective or desired manoeuvre, whether it be station-keeping in the presence of disturbances, or reconfiguration of a satellite formation. Propulsion systems appropriate to formation flying include cold gas, liquid chemical, electrostatic (FEEP, Colloid), and electromagnetic (Pulsed Plasma) thrusters. These systems are described in Table C-2, appendix C.

2.2.5.2 Guidance and Control Architecture

The control system architecture for formation flying satellites can be broadly categorised into two types.

- *Centralised Control* describes a formation where a one satellite performs high-level control tasks, and is therefore aware of the status of all the ‘follower’ satellites. It also performs the formation decision-making, and if this is not autonomous, remains responsible for relaying commands to the fleet. This architecture has the advantage of minimising the inter-satellite communications complexity, but relies heavily on the functionality of the control satellite.
- *Decentralised Control* requires significant inter-satellite communication bandwidth. Each satellite has knowledge of the status of other satellites in the

fleet as necessary, and determines its own manoeuvre paths and control responses. This clearly improves system redundancy, but adds significant complexity to the GNC system of each satellite. A major problem with the lack of a hierarchy is fault identification and in that event, autonomous fault management. If a formation member malfunctions, a collective decision-making process would be required to, for example, reconfigure the remaining satellites to achieve the mission objectives.

There are many formation control architectures that could be implemented which lie between the extremes of centralised and decentralised control. For example, the reference satellite could be allowed to fly freely, with only absolute position being of importance for orbit maintenance. The follower satellites could then use a decentralised control approach to maintain their own position relative to the leader (and each other for collision avoidance). Alternatively, a reference satellite in a widely dispersed formation with a centralised control architecture could determine where individual satellites in the formation needed to be to complete a particular task, and the low-level control system onboard each individual satellite would determine the optimal collision-free trajectory to achieve the desired position. Individual satellites could determine their own position via a decentralised architecture, and control this to within an error box, without further reference to the location of the other satellites. Larger formations could be grouped into smaller clusters, each with a mid-level 'leader' that reports to an overall formation reference satellite, creating a true hierarchy. Ultimately, however, the most appropriate architecture is dependent on the mission, the number of satellites and their proximity within the formation, and the manoeuvres they are likely to perform. There are a number of references which describe the results of studies into satellite formation flying control topology, autonomy and communications protocols. Examples include Mandutianu, Hadaegh et al. (2001), Smith and Hadaegh (2002), and Mueller (2004).

A selection of classical orbit determination techniques which use various combinations of Earth-based observations to calculate a satellite orbit are described by Curtis (2005). However, the differencing of satellite absolute position data measured from the ground (usually by radar, telemetry, or optical telescopes) will not provide sufficiently accurate relative position information for formation flying, and it is therefore necessary to make on-orbit relative position measurements using the systems introduced in section 2.2.5.1. This more accurate data can be used to actively control the formation to a higher precision from onboard the spacecraft than if the data is to be relayed to Earth (although the necessary control reactions can be planned quite accurately using orbit propagators). This ability to respond to position errors with basic actuation requires a minimum level of autonomy for each spacecraft in a formation, and will be greatly facilitated by accurate on-board real time orbit determination.

Autonomy encompasses the (artificial) intelligent decision-making process as well as being a formation flying guidance and control problem, and Mueller (2004) defines three levels of autonomy in this context:

- *Low Autonomy* where the target state for each spacecraft is specifically defined (a desired position and velocity by a certain time, or a trajectory which must be accurately followed).

- *Medium Autonomy* where relative separations or relative orbital elements between spacecraft are specified to the formation. The guidance system will then generate the trajectories to the desired locations for each spacecraft in a formation-wide optimal manner.
- *High Autonomy* where a few formation sizing objectives are specified, for example, overall size and orientation of the formation, and the desired relative positions are deduced and target manoeuvre trajectories generated autonomously for each member of the formation in an optimal manner.

Although autonomy at high-level is very much in the research phase, and even at its basic low-level is costly to implement, the benefits of formation autonomy are potentially numerous. These include:

- Reduced operating costs due to the significant reduction in man-hours required for monitoring and control of the formation from the ground.
- Increased range of useful mission scenarios where autonomy can enable mission operations to continue during times of poor visibility or inaccessibility to ground stations.
- Improved accuracy even at the low autonomy level by path planning in the real environment (enabling unmodelled effects to be considered in on-board trajectory optimisation, for example, collision avoidance in the event of an unexpected obstacle).
- Ability to actively control position with rapid response to position errors, rather than waiting for commands from the ground.
- Rapid fault detection.
- Active fuel optimisation to reduce total consumption and balance fuel use across the formation to improve overall mission lifetime.

In order to operate autonomously, a satellite formation must accurately know where individual members of the formation are at least relative to a known point. They must also be able to predict where they will be in a given time in order to perform autonomous path planning and generate desired spacecraft trajectories. Both absolute and relative real time orbit determination can be performed on-orbit in LEO using, for example, the GPS or TDRS, but this is not completely autonomous, nor achievable to the required accuracy. However, even if the quality of the sensor information is good for relative position measurement, the orbit determination process must be able to autonomously smooth, filter and predict future navigation data (Vallado, 2001). Orbit propagation techniques are therefore required, although accuracy is generally limited due to the onboard computer memory capacity and computational time. The estimation process can use deterministic equations of motion (which assume an accurate system dynamics model), but for higher accuracy formation flying, a stochastic approach is favourable (this takes into account both the dynamics and model uncertainty). A selection of appropriate numerical techniques (differential correction), and the role of extended Kalman filters for orbit estimation are outlined in Vallado (2001).

The orbit determination problem for a formation flying mission at L2 is more complicated. Although relative metrology is equally effective, the absolute satellite positions would need to be obtained through, for example, measurements of the motion of Solar System bodies against background stars, powerful star tracker measurements

for variations in stellar parallax, and Earth-based range and range rate (Doppler) measurements, which would not be very accurate across the 1.5 million kilometre distance between the Earth and L2.

Currently, an onboard orbit propagator would project the absolute motion of a single satellite, regardless of whether this was operating within a formation. However, for precision formation flying, there would be many benefits in developing suitable high fidelity analytical models of relative motion which, given a set of initial conditions could predict relative motion in the short term, thus transferring the control objective from an absolute to a relative motion scenario. This would significantly simplify the computational overhead in individually propagating the orbits of several satellites. However, analytical models would need to be of sufficiently high fidelity to replace the generally more accurate numerical integration techniques for propagation. In the case of poor relative motion models, iterative procedures could be applied to improve the model dynamics on orbit.

Research supporting the design and implementation of formation flying missions has progressed through desktop simulation, laboratory testbed development, technology demonstrator design and flight, and ultimately spacecraft formation flying mission design. Simulation studies are relatively cheap to perform for a range of mission scenarios, and the effects of variables are easy to determine. Requirements on hardware and control system performance can be determined, and solutions for complex dynamics, control and mission analysis problems can be obtained to minimise risk and expense in the programme. Simulations can be performed using high fidelity mathematical models of relative motion dynamics, a range of controller design techniques, and numerical orbit propagators to simulate the 'real' space environment. Many simulation studies completed internationally within academia, industry, and the space agencies have been reviewed in the literature survey (chapter 3), and it is within this context that the research for this thesis has been performed.

2.3 Interferometer Formation Manoeuvres and Mission Design

In the final section of this chapter, the design drivers highlighted in sections 2.1 and 2.2 are evaluated and applied where appropriate to different aspects of interferometry mission design. Firstly a series of typical manoeuvres that a Darwin-type mission would need to perform to detect and characterise extrasolar planets is derived for implementation in the simulation studies in chapter 7, and secondly the effects of different mission design drivers are investigated through the preliminary design of a large-scale planet imaging formation flying mission. Further details are given in Roberts (2006).

2.3.1 Darwin Formation Flying Manoeuvres

The types of manoeuvres required for the successful performance of a Darwin-type mission for both nulling interferometry planet detection and astrophysical imaging were introduced in section 2.2.3. The manoeuvres already defined through industry studies

(Table 2-10) included initial formation deployment, and fringe acquisition, however, science manoeuvres were not specified. In this section a selection of sample manoeuvres, primarily associated with the planet detection and spectroscopy phase of the Darwin mission are derived, as other authors have investigated u-v plane coverage manoeuvres associated with image quality and trajectory optimisation for the imaging phase of an interferometry mission (Kong and Miller, 1998), (van der Avoort, D'Arcio, and den Herder, 2003). Table 2-11 summarises the appropriate types of manoeuvre for both planet detection and astrophysical imaging phases of the mission.

The 'nulling mission tasks' in Table 2-11 include separate rotation, translation slewing and station keeping tasks. The hub satellite is assumed to be a leader of the formation, receiving commands relayed from Earth through the master satellite. For the formation flying task, and application of the dynamics models derived chapter 6, the telescope manoeuvres are derived in terms of relative motion parameters. The relative position and velocity of each telescope with respect to the hub is expressed in terms of a set of Cartesian coordinates located at the hub.

Mission Task	Manoeuvre	Description
Nulling • Planet Detection	Rotation	Formation rotation enables planet signal modulation, although switching between sub-interferometers (without rotation) may provide sufficient modulation.
Nulling • Planet Detection	Station Keeping	Planet detection by internal signal modulation. Depends on integration time.
Nulling • Spectroscopy	Station Keeping (or very slow rotation)	Long-term continuous observation of a target. This depends on integration time.
Nulling • Spectroscopy	Slewing	Long-term continuous observation of a target may require a slew to maintain pointing as target moves out of narrow field-of-view.
Nulling Between Science Measurements. Fringe acquisition.	Translation	Baseline expansion and contraction while maintaining the hub at the formation centre and pointing at target. Changes resolution and fringe widths of the interferometer.
Nulling/Imaging Between Science Measurements	Slewing	Alter pointing direction within the design region of observation ($\pm 45^{o}$ cone in the anti-Sun direction) while maintaining planar formation. Repeat observation of targets to measure orbit characteristics.
Nulling/Imaging Between Science Measurements	Slewing/Translation	Simultaneous altering of pointing direction within the design region of observation, and adjustment of baseline for observation of a new target, while maintaining planar formation.
Imaging	Station Keeping	Long-term continuous observation of a target. This depends on integration time.
Imaging	Translation/Rotation	Simultaneous translation and rotation of formation to optimally cover the u-v plane. This must occur sufficiently slowly for 'snapshot' visibility measurements to be made.

Table 2-11: Summary of the Scientific Modes of Operation for Different Phases of a Darwin-Type Mission

2.3.1.1 Rotation and Translation Manoeuvres

If it is assumed that Darwin must rotate in order to modulate a planetary signal, a rotation rate must be selected that is achievable by the available propulsion systems. In addition, sufficient photons must be captured at each observation point during the rotation in order measure the fringe visibility. To take 'snapshot' images of the extrasolar planet system, the rotation must be extremely slow, however, to simply reorient the formation and then hold it stationary for a longer period, the initial manoeuvre can be quicker. Also, for a Darwin formation of six evenly spaced telescopes (Figure 2-10), a rotation of just 60^{o} would cause the formation to repeat, thus bringing no benefit in terms of spatial frequency information.

During a rotation, the hub and telescopes must remain planar and equally spaced for both thermal and optical control requirements. The telescopes must point at the same target star, and maintain this 'locked' attitude during the rotation. The relative precision should be maintained to centimetre accuracy once the optical delay line is responding to fringe tracker measurements, as required by the GNC specification for this mission phase. A rotation manoeuvre could be repeated a few times to verify detection results and identify orbit characteristics.

For the purposes of the simulation study, which could apply to any Darwin configuration with the same collecting area as the six-telescope design, the rotation rate was selected to be a full rotation divided by the integration time for planet detection (approximately 30 hours for an Earth-like planet at 1AU from a Solar-type star at 10pc –Table B-1, appendix B) to give an extremely slow 0.00333^{o}/s.

The translation requirements on the formation will involve varying the baseline between the minimum and maximum design values (40-250m) for planet detection as defined in the Darwin specifications. Fine manoeuvres will be required to ensure a planet is visible in the bright fringe of a projected interference pattern, and quicker manoeuvres may be required to alter the system resolution between target observations. The acceptable rate of translation will depend on fuel consumption (governed by the acceleration and deceleration cycles), and any overshoot in the response will depend on the guidance and control system requirements for collision avoidance. For imaging it is likely that combined rotation and baseline manoeuvres will be sought to optimise coverage of the u-v plane. This must occur a rate which prevents each sample point from being blurred by movement of the array. For a 1.5m diameter telescope, a 15cm movement is deemed acceptable for a 10 second astrophysical imaging exposure (Rottgering et al, 2003), and control by milli-Newton thrusters was proposed. Although an imaging requirement, rather than a planet detection requirement, this is incorporated into the first sample translation manoeuvre. A second translation manoeuvre involves a precision baseline adjustment associated with fringe acquisition.

These translation manoeuvres do not involve any simultaneous formation rotations, and in this case, the baseline expansion is coordinated so that all of the telescopes simultaneously manoeuvre away from the hub. Ideally, the formation maintains a stable orbit during the manoeuvres. These and the proposed rotation manoeuvre are summarised in Table 2-12. The baseline for the planar rotation manoeuvre was

subsequently fixed at 127.2m to enable the maximum velocity of each telescope relative to the hub to be 3.7mm/s at the selected rotation rate. (This maximum rate was defined following communications with the ESA Darwin team).

Relative Manoeuvre	Rate	Other Conditions	Duration of Manoeuvre	Out-of-Plane Precision	In-Plane Precision
Precision Rotation	0.00333^{o}/s	Fix baseline at 127.2m. Full 360^{o} rotation. Maintain pointing.	30 hours	Maintain planar configuration to 1cm	Hub-telescope separation 1cm
Translation (Imaging)	1.5cm/s average	Vary baseline between 40-250m. No rotation during translation. Maintain pointing. Apply mN thrust.	38.89hr	Maintain planar configuration to 1cm	Ensure no overshoot at short baseline limit (collision avoidance)
Precision Translation	3.7mm/s* maximum	Vary baseline by 50cm, from 100m to 100.5m. Apply μN thrust.	135.1sec	Maintain planar configuration to 1cm	Achieve desired baselines to 1cm accuracy.

Table 2-12: Proposed Science Manoeuvres for the Six-Telescope Darwin Configuration (*ESA Communication (May 2005) – the maximum rate was derived from optical requirements)

At this stage, these basic manoeuvres are being proposed in order to demonstrate the link between mission tasks and formation flying requirements. However, future analysis should include formation reconfiguration, and fuel optimisation strategies, particularly for the new Darwin formation. The concept of load-levelling or fuel balancing across the formation, and its effect on manoeuvres is considered in chapter 7.

2.3.1.2 Station Keeping for Spectroscopy

Once a planet has been detected, it is necessary to perform observations of much longer duration to detect a full range of biosignatures, although the integration time is dependent on many factors. A baseline appropriate to the location of the planet on a bright fringe of the transmission map, at an observation wavelength corresponding to one of the biosignature spectral lines was selected for the simulations in chapter 7. In this science mode, the centimetre-accurate precision formation flying requirements must hold in the presence of perturbations.

The Spectral Analysis test case for simulation was defined as follows:

- Station Keeping Spectroscopy (no rotation)
- Maintain formation position on orbit (L2 Lissajous (near-halo))
- Maintain all baselines and planar configuration to 1cm accuracy
- Wavelength of Observation: 9.6μm for Ozone
- Fixed baseline: 74.25m
- Task duration: 6 days

The final two parameters were selected as reasonable values for a spectral analysis scenario. The baseline according to calculations for ozone detection from a Sun-Earth

system, 25pc away would need to be a minimum of 25m (using a λ/θ relation). This places the planet in the bright fringe of the interference pattern. However, the Darwin specifications (Table 2-8) require a minimum formation baseline of 40m, primarily for collision avoidance, therefore the planet was placed in the second bright fringe which required a baseline of 74.25m. An appropriate scaling factor was applied to the 1-day planet detection requirement at low spectral resolution across the whole spectrum to define a duration for a typical spectral analysis task. A few days may be required to analyse a short waveband (containing the ozone signature) with a resolution of 20, although the spectroscopy integration time is also very dependent on the SNR. If the manoeuvre was much longer than a few days, and repeated, the target may not be suitable for observation in the design mission lifetime. Also, the duration for which Darwin can point at a particular location in the sky may be a consideration. This value is estimated below for the calculation of slewing manoeuvres.

2.3.1.3 Formation Slew Between Targets

In order to generate a sample manoeuvre for a realistic slew between target stars, it is necessary to consider the distribution of candidate systems within the Darwin observation field-of-view (FOV). The extrasolar planet catalogue is continually being updated as more planets are discovered and confirmed (Schneider, 2005), and the generation of a target list will ultimately depend on the success of the Kepler and SIM missions in providing candidate target statistics. In deriving slewing manoeuvres between targets, the following factors were considered:

- *Darwin*: The Darwin orbit and pointing requirements according to the feasibility study (ESA Report, 2000).
- *Kepler*: The population of potential targets within the patch of sky already selected for the precursor mission, Kepler.
- *Statistics*: The proportion and extent of different magnitude stars and the likelihood of them harbouring planets in the habitable zone in the region of observation.
- *SETI*: The SETI catalogue of candidate life-supporting stellar systems.
- *Current Status of Discoveries*: The current extrasolar planet catalogue.

Darwin will orbit around the L2 point, while this equilibrium point rotates with the Earth about the Sun. The Darwin observatory will continuously point at targets within a ±45 degree cone in the anti-Sun direction, and will therefore be able to observe targets within a band of sky 90 degrees wide and centred on the ecliptic plane. Figure 2-11 illustrates the observation area of the Darwin formation, although at any one time, the Darwin FOV is limited to 0.3arcsec (Table B-2, appendix B).

The precursor mission, Kepler, has a 10x10degrees FOV, and will spend the entire mission duration looking at one patch of the sky while on a heliocentric orbit. Borucki, Koch et al. (2004) suggest that this observation area should be centred on a galactic longitude and latitude of 70^{o} and $+6^{o}$ (Figure 2-11) as this area has a very rich star field with 450,000 stars brighter than 15^{th} magnitude, and will enable Sun avoidance. According to the ESA-ESO Working Group (2005), Kepler will detect 35 Earth-like planets through the observation of 100,000 stars. Borucki, Koch et al. (2003) also

suggest that the Kepler FOV is 'indistinguishable' from the Solar neighbourhood that Darwin will observe (although the regions do not overlap), and that the relationship between stellar type and frequency of accompanying extrasolar planets and their semi-major axes will provide the necessary parameters for a Darwin/TPF mission design.

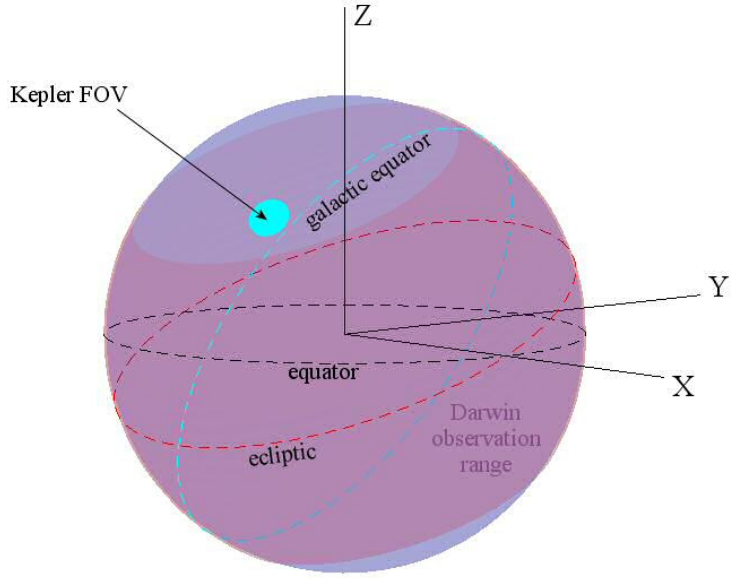

Figure 2-11: Celestial Sphere and Field-of-View Coverage for Kepler and Darwin

According to Eiroa et al. (2003) approximately 1000 F, G, K and M-type stars have been identified within the Darwin zone of observation out to 25pc (Figure 2-11). This is approximately twice as many observation targets than the most ambitious estimate set for the mission timeframe, and therefore the target list must be refined. This process has begun with the investigation of Solar-type G stars, of which there are 73 in the 25pc range (according to Hipparcos data), and another 35 so far identified between 25 and 50pc. Radial velocity methods have identified giant planets around nine of these stars (as of April 2003). Clearly the science return is potentially limited for such a technologically challenging and costly mission. However, the discovery of giant planets or stars with lower luminosity harbouring planets will still provide useful science data, particularly in the study of planet formation.

Proposed Slew Manoeuvres

Two types of slew manoeuvre are derived:

- *Retargeting Slew* - this may be simultaneously combined with a baseline adjustment, and must take place as quickly as possible to maximise science time.
- *Science Slew* – this is a precision manoeuvre relative to the L2 frame to maintain the target object in the interferometer FOV during extended observations (constant inertial pointing).

A preliminary estimate of target density for the purposes of a slew manoeuvre between targets was deduced by considering the analysis of Eiroa et al. (2003). The 73 G-type stars out to 25pc across the Darwin observation zone would on average have an angular

separation in terms of ecliptic latitude or longitude of 21^o, and therefore a typical retargeting manoeuvre would involve a relatively rapid 29^o diagonal slew.

In the science mode, the target must be continuously observed for extended periods. If the target is maintained at the centre of the FOV across the full 90^o cone of observation, the longest possible observation time will be 91.25days. During this period, the slew rate relative to the L2 frame to maintain the target would be 0.9863^o/day. While both slewing manoeuvres involve attitude control to alter the formation pointing, the manoeuvres in Table 2-13 are specified in terms of relative motion requirements and the formation must remain planar. The speed with which the retargeting manoeuvres can be performed is likely to be dependent on collision avoidance issues or thruster capacities.

Manoeuvre	Duration	Manoeuvre Conditions	Out-of-Plane Precision	In-Plane Precision
Retargeting Slew	Depends on thrusters.	Fix baseline at 127.2m.	Maintain planar configuration to a few cm.	1m using coarse lateral metrology.
Science Slew	6 days	Out-of-plane translation and pointing adjustment for slewing interferometer axis by 0.9863^o/day. Spectroscopy baseline 40m.	Maintain planar configuration to 1cm	Hub-telescope separation 1cm. Ensure no overshoot at short baseline limit (collision avoidance).
Slew/Resize	Depends on thrusters.	Alter baseline from 127.2m to 100m while slewing 29^o.	Maintain planar configuration to a few cm.	1m accuracy during manoeuvre. Acquire new baseline to few cm.

Table 2-13: Proposed Slewing Manoeuvres for a Darwin-Type Configuration

These manoeuvres can be used to generate guidance functions and to demonstrate formation control and load-levelling. The requirements are defined according to a balance between both optical and thruster limitations, and whether these manoeuvres can be performed within the maximum and minimum thrust range while within the specified integration time must be investigated.

2.3.2 Interferometry Mission Design for a Planet Imager

In this section, the design drivers founded in optical astronomy and astrobiology, introduced in section 2.2, have been evaluated. Following the selection of a nulling interferometry optical system, the effects of specific parameters on formation design are investigated through the preliminary design of an extrasolar planet imager. The technology challenges and limitations are then highlighted as the requirements are compared to those for a Darwin-type mission. Star/planet emission and contrast, observation wavelength and range (biosignatures, black body emission), photon capture at the aperture, number and sizing of apertures, resolution and baseline, CCD operation, starlight cancellation, and fringe patterns and image reconstruction are considered in the design.

Initially, a design point was defined, requiring the planet imager to be able to observe a 12x12 pixel image of an Earth-like planet orbiting a Solar-type star at 1AU, and at a distance of 25pc from the observation point. At this resolution the surface features, including continents, clouds and ocean, can be discerned (Figure 2-12). The number of pixels was defined to simplify the specification of integration time by restricting it to the time for a one-pixel area of the planet to move into the next (1 hour), assuming that the planet rotates at the same rate as the Earth. A design distance of 25pc also enables any Earth-like planets detected by Darwin to be revisited and imaged at a minimum 12-pixel resolution.

Figure 2-12: High-Resolution and 12x12 Pixelated Earth Images

Proposed Planet Imager Concept

Initially, the extension of the Darwin six-element nulling interferometer to achieve the spatial resolution necessary for a 12-pixel wide image of an Earth-size planet was considered. This was a single-stage nulling interferometer comprising six wide-aperture telescopes in the Darwin configuration, and a central nulling and beam combining hub (Figure 2-10). However, Velusamy and Beichman (2001) proposed the use of a multi-stage system of interferometers for a Darwin/TPF-scale planet detection mission. This system would enable the decoupling of the sub-aperture baseline, which determines the nulled fringe width (b), and the interferometer baseline (B), which governs spatial resolution of the system (Figure 2-13).

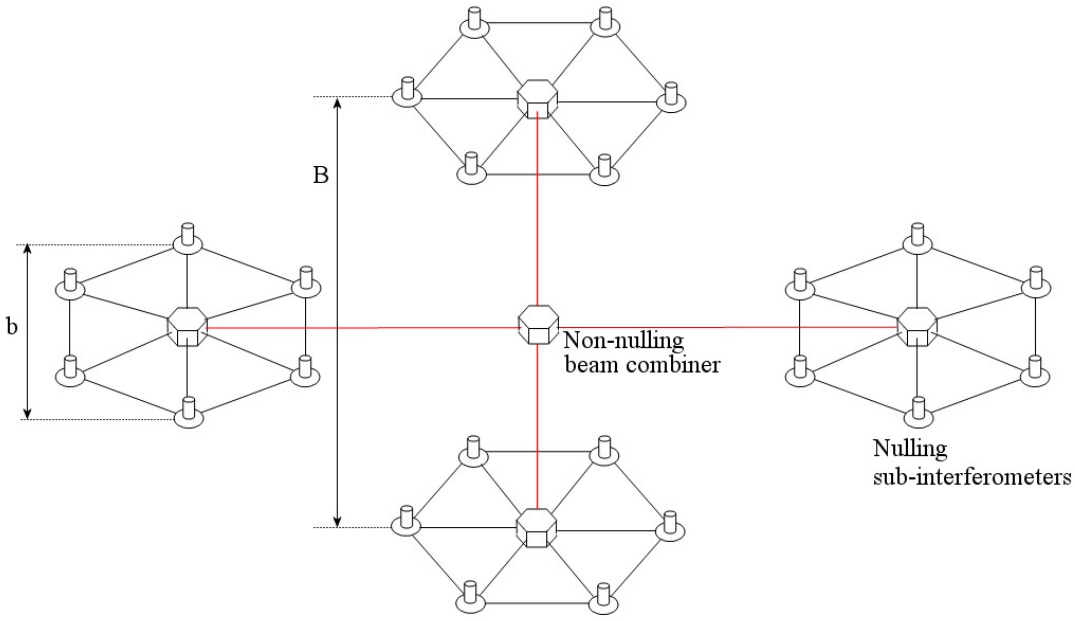

Figure 2-13: Planet Imager Concept
Note: b = *sub-aperture baseline,* B = *resolution baseline*

The concept is drawn from the original Michelson stellar interferometer where primary and secondary mirrors can be separately adjusted to alter resolution and fringe width on the image plane (Hecht, 1998). For the high spatial resolution requirements of a planet imager, extremely long baselines were envisaged, and therefore the latter approach was adopted for the preliminary mission design. Figure 2-13 illustrates the proposed multi-stage nulling interferometer. Each element of the interferometer formation, which is normally a single aperture, is now a smaller scale nulling sub-interferometer. The central beam combining hub behaves as a non-nulling Michelson interferometer (Figure 2-5b).

Overview of Design Calculations

Figure 2-14 summarises the calculation steps and assumptions made in the first iteration of planet imager mission design. Initially the star/planet contrast at the visible and infrared wavelengths was evaluated for an extrasolar Sun-Earth system at the design condition (a distance of 25pc and 1AU separation). This enabled contrast and a suitable observation wavelength range for the observatory to be determined, and also the number of photons arriving at the aperture to be quantified.

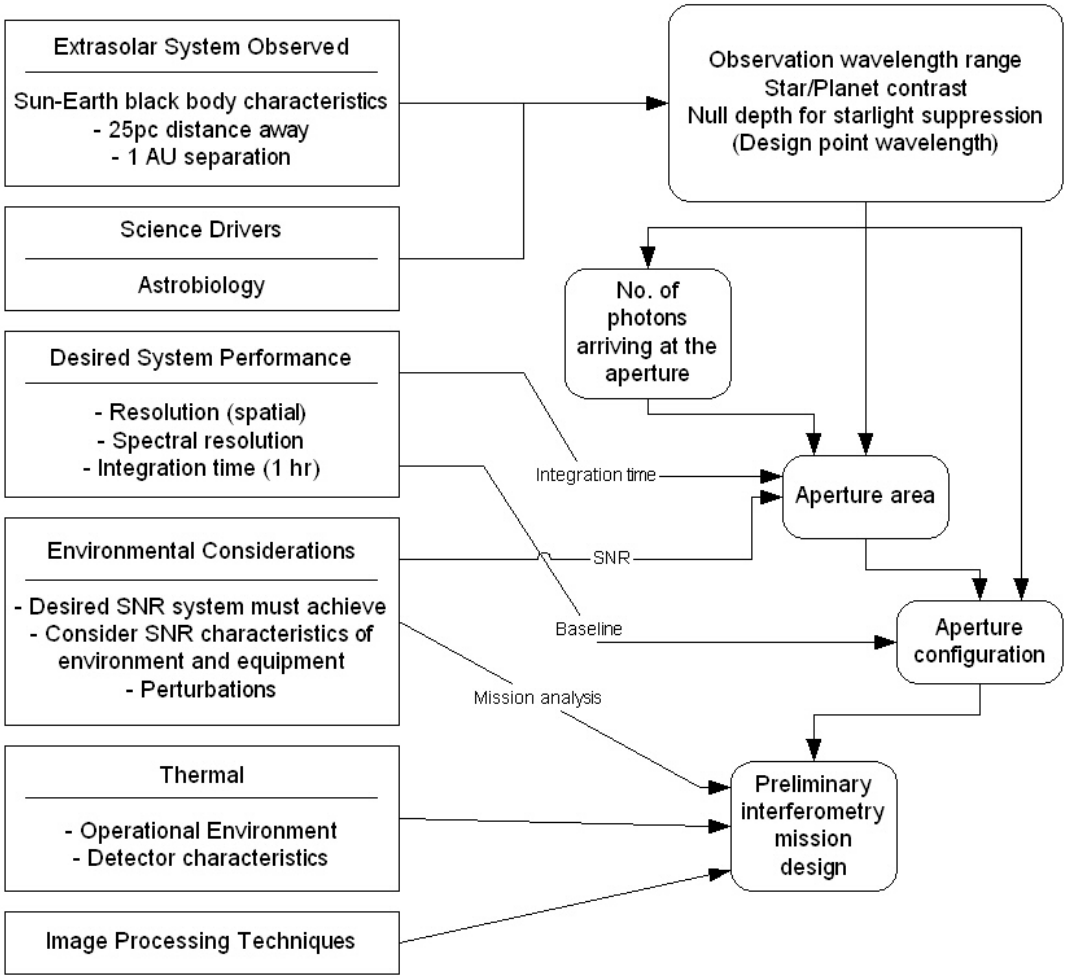

Figure 2-14: First Cycle of an Iterative Preliminary Design Process for a Planet Imager

In order to calculate the thermal contrast between an extrasolar Sun-like star and Earth-like planet, the total flux per unit wavelength ($W\lambda^{-1}$) emitted by each body was evaluated using a form of Planck's Radiation Law (equation (2-3)) which holds for a surface of uniform brightness. R is the radius of a black body, h is Planck's constant, k is Boltzmann's constant, c is the speed of light, T is temperature in Kelvin (K), and λ is the radiation wavelength.

$$F_{total} = \frac{8\pi^2 hc^2 R^2}{\lambda^5\left(e^{hc/\lambda kT} - 1\right)} \qquad (2\text{-}3)$$

However, to obtain a more accurate measure of star/planet contrast, the planetary light must also include an albedo component in the visible range. The reflected stellar flux arriving at a $1m^2$ aperture was therefore also evaluated by assuming that the flux radiated away from the bodies in a uniform sphere. A more detailed description of the analysis performed can be found in Roberts (2006). Figure 2-15 illustrates the total flux of an extrasolar Sun received at a $1m^2$ aperture, and the total thermal and reflected flux from an extrasolar Earth over 25pc.

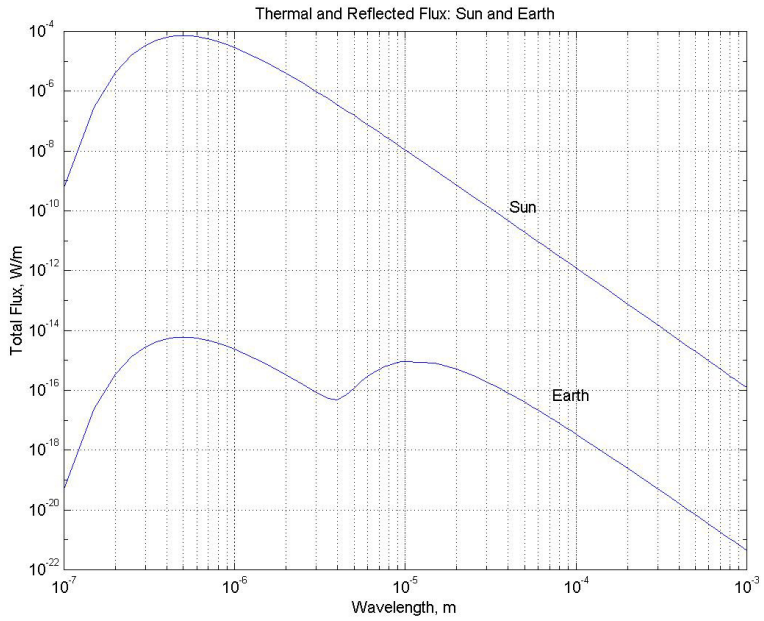

Figure 2-15: Stellar Flux and Total Thermal and Reflected Radiance from an Extrasolar Earth

Peaks in the Earth flux line correspond to the maximum of the black-body radiation curve for an Earth-like planet (infrared 10μm), and also the peak emission of a Solar-type star (visible albedo 500nm) due to the reflected light. The total star/planet contrast variation over visible and infrared wavelengths for an extrasolar Sun-Earth system is illustrated in Figure 2-16. A high value of contrast means that the stellar flux detected at the aperture is much greater than that of the extrasolar planet, and the planet is therefore harder to discern. An extremely gradual decrease in contrast continues into the radio wavelength range. It could be argued that observations should take place at radio

wavelengths for extrasolar planet detection due to improved contrast, and reduced formation flying relative position performance requirements, but it is necessary to consider the number of photons collected at the different wavelengths to determine whether this is practical.

The extrasolar Sun-Earth contrast at visible wavelengths is just over 10^{10}. A rapid drop in contrast begins at 3.5μm and at the peak emission wavelength (10μm), the contrast has reduced to 10^{7}. In the far infrared, this decreases further to approximately 10^{5}.

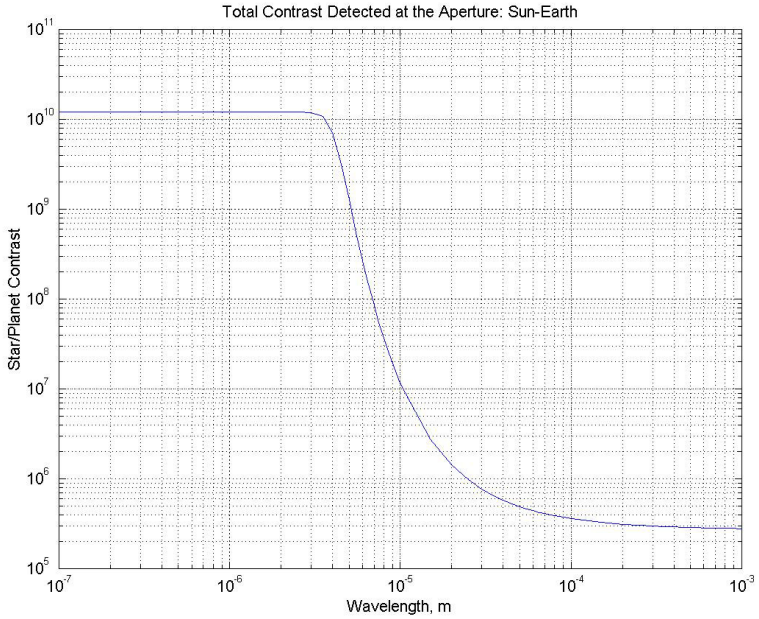

Figure 2-16: Total (Thermal and Reflected Light) Contrast for an Extrasolar Sun-Earth System

The number of photons arriving at the aperture per second is given by the flux divided by the energy of a photon at each wavelength. Figure 2-17 illustrates the resulting number of photons arriving per second at the aperture from the star and planet at different wavelengths. The maxima no longer lie exactly at the wavelengths of peak spectral radiance, and the number of photons from the planet decreases rapidly as wavelength increases beyond 20μm. The peak number of photons per second arriving from an Earth-like planet 25pc away is approximately 1 at 20μm.

It was proposed that observations between 9 and 30μm would balance the requirements of contrast (Figure 2-16), and photon collection, therefore limiting the integration time. A 20μm wide imaging band is larger than that proposed for the Darwin mission (currently 12μm), but observation distances will be consistently greater, and therefore fewer photons will be received in a given time. The lower wavelength limit was selected to capture the ozone spectral feature at 9.6μm. The carbon dioxide and water spectral features would be visible at 15 and 18-20μm respectively, enabling the planet imager to perform a more detailed analysis of a planetary atmosphere in the infrared wavelength range than that achievable with Darwin.

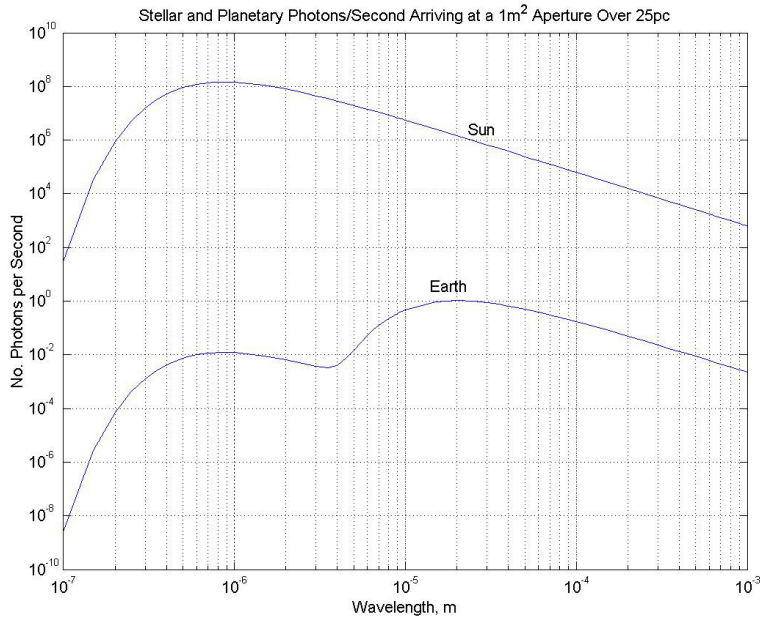

Figure 2-17: Stellar and Planetary Photons per Second Arriving at a 1m^2 Aperture Over 25parsec

In this preliminary design, the estimated SNR, desired integration time, and calculated photon capture rate design parameters were then used to size the aperture of the planet imager. The total number of photons per second arriving at 1m^2 aperture over the selected 9-30μm wavelength range was evaluated and for photons of average energy in this range, just 1.881 planetary photons are detected per second. The number of photons that must be accumulated in order to distinguish a planetary signal and produce an image will depend on the defined minimum SNR, and also the spectral resolution.

Observatory systems experience different types of additive and multiplicative noise (with respect to the desired signal). In this case, the capacity of the observatory to produce a sufficiently deep null to eliminate all stellar light is initially assumed in the evaluation of the SNR. In this first iteration of design, both signals and a range of noise characteristics were identified, and their contributions to the SNR quantified where possible. These included detector (CCD) quantum efficiency, planetary signal strength, stellar signal strength, thermal zodiacal and exo-zodiacal background noise, telescope thermal noise, and ultimately, the effect of noise characteristics on aperture area and aperture distribution. Further details and descriptions of these SNR contributions are given in Roberts (2006).

The aperture area was evaluated using equation (2-4), adapted from Angel (2003) where F_p is the planet flux, I_b the sky intensity, D_{eff} is the effective telescope aperture (circular), λ is the wavelength of observed radiation, q is system quantum efficiency, t_{eff} is the integration time, and $\Delta\lambda$ is the bandwidth.

$$D_{eff} \propto \sqrt{\frac{SNR\sqrt{I_b + I_T}\lambda}{F_P\sqrt{qt_{eff}\left(1/R_{spectral}\right)}}} \qquad (2\text{-}4)$$

In order to determine the required collecting aperture area, the design parameters summarised in Table 2-14 were specified.

Design Parameter	Value	Comment
Signal-to-Noise Ratio, SNR	10	Upper Darwin limit*
Observation Wavelength, λ	19.5μm	Mid-range value (9-30μm range)
Integration Time, τ	1 hour	For 12x12 pixel image
Spectral Resolution, $R_{spectral}$	100	Maximise to improve image quality for feature recognition
Quantum Efficiency, q	0.2	Includes detector quantum efficiency and other losses
Planet Flux, Fp	68.81nJy**	Calculated from Figure 2-17
Thermal Background Flux, I_b	6.3mJy/arcsec^2	Value obtained by extrapolation of data in ESA report (2000)
Telescope Optics Thermal Flux, $I_T=I_b$	6.3mJy/arcsec^2	Equal to the background flux

Table 2-14: Aperture Design Parameters (*Refer to appendix B, **1Jy=10^{-26}Wm^{-2}Hz^{-1}, Refer to Roberts (2006) for further details)

Using this approximation, the resulting values for the effective aperture diameter and total aperture area were evaluated: $\mathbf{D_{eff} = 112.5\ metres}$ and $\mathbf{A_{total} = 9945\ metres^2}$

A telescope mirror of diameter (D_{eff}) would clearly be impractically large for launch as either a pre-deployed or on-orbit deployable structure. However, the division of the total aperture area into a number of smaller apertures does not affect the overall SNR. In this case, the advantages of additional apertures include improved null depth, practical mirror diameters, and more simultaneous baselines for u-v plane coverage. In this case, aperture diameters equal to that of the James Webb Space Telescope (JWST) were selected. Each aperture has a primary mirror diameter of 6.5m, therefore requiring a total of 307 telescopes. The size of individual apertures is also governed by the interferometer field-of-view (FOV). This is related to both spectral resolution and angular resolution, and is relatively small for a Michelson inteferometer. In order to achieve sufficient FOV for the star and planet to be observed simultaneously, the effective aperture diameter of the interferometer must be increased.

The interferometer sub-apertures (Figure 2-13) could be six-telescope formations which may rotate about their hub, although internal modulation of the optical signal may be sufficient to extract planet light. The sub-apertures could be arranged around a circle of diameter equal to the resolution baseline to ensure they are equidistant from a central hub where the planet light is constructively interfered. However, this is unlikely to be practical for 52 sub-apertures, and tiers of beam combining satellites may replace a planar formation.

The requirement for a high resolution optical system depends on the desired quality of the planetary image (Figure 2-12). To create an extended image of the planet, the baseline must be increased beyond that necessary to simply distinguish between the star and planet (separated by semi-major axis). Equation (2-1) relates angular resolution (θ) to baseline (B) and observation wavelength (λ) for a Michelson-type interferometer. In this case, the average wavelength and angular resolution (equal to 1/12th Earth diameter

divided by the 25pc distance of the extrasolar system from the observatory) requires an extremely large baseline of 7,022km.

The sub-aperture baseline determines the fringe width of the interferometer, and is calculated to ensure that the central null will cover the star, while both the star and planet remain in the FOV. According to Bracewell and MacPhie (1979), the fringe baseline is given by equation (2-5), where Φ is the fringe spacing.

$$b = \frac{\lambda}{\Phi} \qquad (2\text{-}5)$$

For an Earth-like planet at the centre of a bright fringe at a distance of 1AU from the Solar-type star, for a system 25pc away, the baseline b must be 50m. The fringe width is 80mas, which covers the stellar diameter of 0.375mas (calculated using the photosphere radius in the NASA Sun Fact Sheet (Williams, 2004b)). For the large mirror diameters required (6.5m), this baseline would leave a 43.5m separation between the edges of each telescope mirror. For a Darwin-type telescope, Sun shields would be required thus effectively increasing the telescope diameter, and therefore this would be proposed as a minimum baseline, assuming that the system of free flyers has strict collision avoidance control.

In this case, the output of a pupil plane interferometer only requires a single pixel detector, or if spectrally resolved, an appropriate number of pixels in a linear array. The single pixel measures photons from the FOV of the interferometer, and for a linear detector array, the variation of intensity at different wavelength bands or 'spectral channels' over time is recorded (for example, as the formations are rotated for planet detection). These data, sampled at different outputs of the interferometer, depending on the number of apertures and the signal combination schemes, are used to reconstruct the image by post-processing. The baseline specification for Darwin is a linear array of Si:As detectors with a quantum efficiency of over 50% and low dark current. The detector must be cooled to between 6 and 8 Kelvin (D'Arcio and Karlsson, 2004). For this planet imager preliminary design operating with a spectral resolution of 100, a linear array of 100 pixels would be required.

Design Summary

Table 2-15 compares some of the Planet Imager design parameters to recent Darwin and Terrestrial Planet Finder (TPF) specifications, illustrating the increase in performance and scale of a futuristic mission. However, implementing and operating a planet imager on this scale would be prohibitively costly in terms of technology readiness and magnitude. It may be more appropriate to develop alternative optical techniques (Fizeau interferomtery and homothetic mapping) rather than increasing the scale of the Darwin nulling inteferometer. Alternative techniques are discussed further in Roberts (2006).

Interferometer Specifications	Planet Imager	Darwin	TPF
Wavelength, λ (μm) (for planet observations)	9-30	6-18	7-20
Maximum Baseline, B (km)	7022	0.5	1
Resolution, θ (μas)	0.286	2500 @6μm	750 @3μm
Field-of-View θ_{FOV} (mas) • $R_{spectral}$ = 100 • $R_{spectral}$ ~20 • $R_{spectral}$ = 75000	 0.053 42.96	 300	 250-1000
Total Aperture Area (m^2)	9945	10.6	38.48
Observation Distance, r (pc)	25	25	10
Apertures: Mirror Diameter (m) No. of mirrors No. Sub-Apertures Baseline, b (m) Fringe Width (mas) FOV (mas)	 6.5 370 52 50 80 8	 1.5 6 -- -- -- --	 3.5 4 -- -- -- --

Table 2-15: Comparison of Planet Imager Design Parameters with Darwin and TPF (Darwin data from Appendix B and Section 2.2.4, TPF data from Beichman (2000))

The main findings of this design study can be summarised as follows:

- A larger wavelength range than that selected for Darwin is required for a larger scale mission looking at more distant targets, as fewer photons are gathered per unit wavelength.
- Due to thermal noise, the optics payload of a planet imager is likely to be required to operate at an even colder temperature than the 40K specified for Darwin. In this case, the telescope temperature must be reduced well below 20K to operate successfully at 30μm.
- Given current estimates of noise contributions and the weak planet signal, an extremely large telescope collecting area is required in order to meet the short integration time.
- Integration time has a significant effect on most aspects of the mission design (including aperture size, formation complexity, formation manoeuvres and mission duration).
- An extremely large baseline of approximately 7000km is required in order to achieve sufficient resolution according to basic interferometry theory.
- According to the literature, the interferometer resolution and fringe width can be determined by two separate baseline measurements. It has been possible to specify these to enable a central null to be placed over the diameter of the on-axis star, while achieving sufficient resolution and field-of-view to image the planet (typically separated from the star by 1AU).
- The beam combination and formation flying precision requirements would be the same as those for Darwin in terms of interference at each sub-aperture nuller, and therefore L2 would be a suitable operating environment.

Some of the challenges associated with the design of a Planet Imager mission are summarised below (Table 2-16).

Design Limitation	Comments
Large Aperture Area or Integration Time (due to low photon counts) The aperture area must be reduced and therefore an increase in integration time is proposed. As progressively fainter objects are observed, the integration time required to form an image begins to conflict with the speed of the object being observed.	• Image processing techniques could be developed to examine the time history of photon accumulation, perhaps to subtract the rotation of the planet from the image thus enabling longer integration times and reduced aperture area. • Even greater aperture area may be required than that specified in this analysis if 'chopping' techniques are to be employed as only a few apertures would be operational at any instant in time. • Aperture shape should also be considered.
Optical Systems The nulling interferometer will still experience optical problems such as limited field-of-view.	• Novel optical systems architectures may be required to implement a large scale interferometer. • The difficulty of performing both high resolution imaging and nulling would have conflicting FOV requirements which could be overcome by using sub-interferometers. • A comparison of conceptual designs of both a nulling interferometer and a Fizeau-type interferometer (using homothetic mapping) would demonstrate advantages and disadvantages of each method for planet imaging. Note: Nulling interferometry and coronagraph techniques were compared in chapter 4 (section 4.2.3).
Metrology and Propulsion The sensor/actuator/optical path length control systems must enable the formation to achieve the level of control to perform planet imaging.	• Although operating as a nulling interferometer like Darwin, a planet imager will require precision metrology and optical path length control between spacecraft separated over thousands of kilometres rather than a few hundred metres. This may require impractically large optical delay lines.
Thermal Control Thermal control to temperatures below those required for Darwin will be necessary to ensure the detection and recording of a planetary signal.	• Thermal control for the Darwin detector is already challenging for current technology. Continued development of detector cooling systems and payload optics cooling strategies would be required to reduce noise and distortion of optical surfaces.
Formation Flying The complexity of formation flying operations is significantly greater.	• The frequency of launch of a large number of large-aperture spacecraft and deployment of the satellites into the formation becomes a substantial problem. • Novel solutions to the formation autonomy problem to enable formation flying of such a large formation following a command to observe a particular target will be required. • Complex data handling and image processing is likely to be required onboard the satellites prior to relaying data to Earth, driving the autonomy requirement. • It is difficult to envisage the formation manoeuvres without further knowledge of the optical system. Example manoeuvres (illustrating the complexity of the GNC systems) for the planet imager may include: - Slow, simultaneous rotation of each sub-interferometer to isolate the planetary signal before relaying this to a central beam combiner across the interferometer baseline. - Simultaneous variation of sub-interferometer and interferometer baselines. - Large scale slewing manoeuvres.

Table 2-16: Some of the Challenges Associated with the Design of a Planet Imager Mission

2.4 Summary

The material presented in this chapter provides a sound basis for the more focussed dynamics and control research presented in later chapters. As part of a wider literature review, formation flying has been defined and its applications determined. The guidance, navigation and control systems and technologies associated with formation flying have been identified, and following a formation flying missions survey, a target mission for the research has been selected. Subsequently, the operation of an infrared astronomical interferometry mission has been investigated, and the key design drivers governing mission performance, and formation flying requirements identified.

Satellite formation flying for the purposes of this research has been defined as the 'the on-orbit maintenance of multiple spacecraft relative to measured separation errors' (Bauer et al, 1997). The satellite separations can be fixed or time varying, but there must exist a level of autonomy in the formation. A survey of space missions revealed three major applications of formation flying:

- Simultaneous scientific field measurements
- Earth surveillance from LEO (by interferometry or aperture synthesis)
- Interferometry for astronomical observations

The Darwin mission was selected to be the focus for the formation flying dynamics and control research, although the role of LEO formation flying for interferometry applications is also considered in chapters 3, 4 and 5. Darwin has the primary objective "to detect and study Earth-type planets and characterize them as possible abodes of life" (Fridlund, 2002). The mission aims to detect Earth-like planets in the Habitable Zone, determine planetary characteristics, and analyse the planetary spectrum. A second mission objective also exists to perform astrophysical imaging.

The optical systems and operational modes of the Darwin interferometer were investigated in order to appreciate the current mission formation flying requirements. A number of additional formation manoeuvring modes were also identified (Table 2-11). Many of the key design parameters and design considerations essential for the proposal of a nulling interferometer mission to perform extrasolar planet detection or imaging have been highlighted throughout the chapter, and ultimately applied to interferometry mission design. Sample manoeuvres have been specified to provide test cases for the formation flying dynamics and control research presented in chapter 7.

3 FORMATION FLYING DYNAMICS AND CONTROL LITERATURE REVIEW

Satellite formation flying in its various forms was defined and its purposes established in chapter 2, where the use of nulling interferometry for a Darwin-type mission to detect and observe extrasolar planets was described. The focus of the remainder of the thesis is formation flying dynamics and control. In this chapter an overview of the formation flying dynamics modelling and control literature available in the public domain, and where possible, from industry is given to establish the context for the simulation work presented in the following chapters.

Following the summaries and descriptions in the previous chapter of different types of formation flying missions, the literature review focuses on many related areas associated with their design. These include mission drivers and preliminary scenario-specific studies performed by academia and industry. The majority of the preliminary and detailed mission design work is performed using simulation tools, and most formation flying literature relates to relative dynamics models and control system designs which enable fuel use estimates to be performed for a particular mission scenario. Reflecting the normal sequence of technology development, a number of sources describe the status of formation flying testbeds, LEO on-orbit experiments, and in limited cases, actual formation flying, for example the Earth Orbiter-1 and Landsat7, and GRACE mission satellites.

The review covers both the basic theory of and advanced research work in satellite formation flying in both Low Earth Orbit (LEO) and in 'Deep Space' outside the Earth's gravity well, usually at the Sun-Earth Lagrange points. A number of alternative modelling strategies and control techniques are also described. Formation flying in both regimes has been addressed as at the outset the literature relating to Lagrange point formation flying was relatively limited, and for a full understanding of the dynamics models and control techniques being explored, a more extensive body of LEO research was accessible through the literature. In addition, the formation flying work being performed within the Space Research Centre at Cranfield University focussed on the MUSTANG (Multi-University Space Technology Advanced Nanosatellite Group) project. MUSTANG was designed to demonstrate distributed systems using two nanosatellites formation flying in LEO.

Of course, research has been progressing quickly on an international scale throughout the period of this study in the field of formation flying. Since defining this programme of research at the outset in early 2002, it has become apparent that there are inevitable similarities between the studies performed here and in parallel elsewhere, although the work presented here was performed completely independently. In the discussion and summary subsections, the context and justification for aspects of the thesis work are described, based on the literature available at the time. Further justification is presented as appropriate in the introductory sections of chapters 4 to 7. Significant additional material produced by the space research community since proposal of the project is also summarised throughout the chapter.

The chapter concludes with a summary of the review, supporting the rationale behind the proposed research programme. This aims to develop new tools to ultimately control a Darwin-type formation of satellites near the Sun-Earth L2 point with sufficient station keeping precision and manoeuvring accuracy for planet observation while load-levelling.

3.1 Low Earth Orbit Formation Flying

The material reviewed in this section is restricted to the LEO environment, although in some cases there are similarities with deep space formation flying. The following sections comprise the detailed review, which is broken down into the primary formation flying subject areas identified in Table 3-1, before conclusions are drawn.

Research Area	Description
Relative Dynamics Models	A brief history of the main contributors in Astrodynamics to the field of formation flying and a description of the origins of the basic equations of motion in the local coordinate reference frame and in terms of orbit elements. This section also covers any model verification work.
Missions and Applications Overviews	A summary of mission-specific studies, highlighting the drivers behind LEO formation flying research and introducing the range of tasks a formation must perform e.g. interferometry, data gathering, astronomy, Earth imaging, in a dynamics and control context.
Natural Formation Dynamics and Formation Design	A summary of the studies performed into natural or 'bounded' solutions to the equations of motion which produce orbits that require minimal fuel to maintain. The application of these orbits and tools for their design are also reviewed.
Orbit Perturbations	A brief summary of LEO orbit perturbations, and the studies that have been performed to establish their effects on a formation of satellites. Perturbation modelling and the use of orbit perturbations to control a formation is considered. Although not strictly a 'perturbation', the effects of orbital eccentricity may be treated as a perturbing effect on the relative motion dynamics, and it is therefore included in this section. Techniques for fuel use evaluation to compensate for the perturbing effects are considered.
Formation Flying Control	This extensive area covers the application of relative dynamics models to a variety of controller designs, and their evaluation. Control strategies and techniques are considered.

Table 3-1: LEO Formation Flying Research Categories for Literature Review

The focus of research has been formation flying as defined in chapter 2, and does not relate to constellation design and maintenance, or swarm behaviour, although there are some areas of overlap in the research, especially in terms of formation design. The reader is referred to chapter 2 and appendix A for LEO formation flying mission details.

3.1.1 Relative Dynamics Models

In this section relative dynamics models are introduced, and the alternative methods of expressing relative motion are explained. Although elements of this subject are covered in much more detail in chapter 4, it is necessary to include an overview of relative motion dynamics models at this stage as they are fundamental to the subsequent elements of the literature review (Table 3-1). The approaches highlighted below utilise either a set of linearised equations based in a Cartesian LVLH (local vertical local horizontal) or curvilinear frame, translating and rotating around a circular orbit, or the classical orbital elements. Alternative relative dynamics models for satellites in eccentric orbits are considered in section 3.1.4. Literature relating to model transformations and their application to dynamics and control studies is reviewed in this section where the emphasis is on the derivation, role and implementation of the relative dynamics models. Their application to control system design is reviewed in section 3.1.5. This section concludes with a detailed summary of the advantages and disadvantages of each modelling approach for satellite formation flying in LEO.

3.1.1.1 Relative Motion in the Cartesian LVLH Frame

The mathematical modelling of relative motion in space is so fundamentally based in the theory of astrodynamics, that without referencing a great number of scientists and mathematicians it is impossible to describe the area of study from its earliest roots. Table 3-2 highlights just a few of the major contributors to the field of celestial mechanics. There are many other mathematicians of the period who produced fundamental algebraic and arithmetical theorems and techniques appropriate to the field of astrodynamics, for example, Gauss (1777-1855), Fourier (1768-1830), and Hamilton (1805-1865), and Poincare (1854-1912) who also addressed the three- body problem.

Many regard the first contribution to formation flying as the linearised equations of motion developed in Hill's 'Researches in the Lunar Theory' (1878). Hill derives expressions for the motion of the Moon relative to the Earth by placing a rectangular coordinate system at the centre of the Earth which translates and rotates as it orbits the Sun. Hill proposed that this new way of describing the motion of the Moon facilitated modelling and would ease the addition of perturbing forces in the equations. He also demonstrated that the use of second order differential equations rather than first order would reduce the number of variables and still enable solutions to be easily obtained.

Clohessy and Wiltshire (1960) proposed a system for satellite rendezvous. Guidance, command and control system architectures are introduced for rendezvous, and in the later stages of the scenario, a relative motion dynamics model based on the equations derived by Hill is applied. In the dynamics model, a 'control' or 'reference' satellite is assumed to be in a circular orbit around the Earth, and the equations are described in the 'Hill' frame, based at the moving reference. This translating and rotating reference frame, about which the relative motion of additional satellites can be described for formation flying, is analogous to the Cartesian axis frame used by Hill to describe Lunar motion with respect to the Earth on its circular orbit of the Sun. Clohessy and Wiltshire modified Hill's equations by including the effects of linearised gravitational force due

to a point mass central body in the equations (thus eliminating the nonlinear μ/r^3 term in the Hill equations). Figure 3-1 illustrates the Cartesian and curvilinear Hill coordinate frames on the circular orbit. The Clohessy-Wiltshire or, as they will continue to be referred to throughout the thesis, the 'Hill' equations of relative motion are given by equations (3-1), where x, y and z are relative positions in the radial, along-track and cross-track directions respectively, n is orbital rate, and terms in 'a' are perturbing relative accelerations. Further detail on the derivation of the equations is given in chapter 4 where they are applied to LEO formation flying scenarios.

Name	Dates	Field	Related Areas of Contribution
Copernicus	1473-1543	Astronomy	Heliocentric (Solar) System
Galileo	1564-1642	Astronomy, Philosophy	Telescopes Heliocentric (Solar) System
Kepler	1571-1630	Astronomy, Mathematics	Laws of Planetary Motion
Newton	1642-1727	Physics, Mechanics, Mathematics	Three Laws of Motion Particle/Wave Nature of Light Differential Calculus Gravitational Law
Euler	1707-1783	Mathematics	Three Body Problem Binomial Theorem
Lagrange	1736-1813	Analytical Mechanics	Differential Equations Solution of DEs by Variation of Parameters Calculus of Variations
Laplace	1749-1827	Mathematics, Physics	Libration of the Moon Gravitational Potential Solution of ODEs by Transforms
Jacobi	1804-1851	Mathematics	Jacobi Integral (in sidereal coordinate system) Reduction of the Quintic Equation Elliptic Functions
DeLaunay	1816-1872	Astronomy	Lunar Theory
Hill	1838-1914	Mathematics	Lunar Theory Three Body Problem

Table 3-2: Ten of the Main Contributors to the Field of Astrodynamics
(DE=Differential Equation, Table contents based on information from Weisstein (2005))

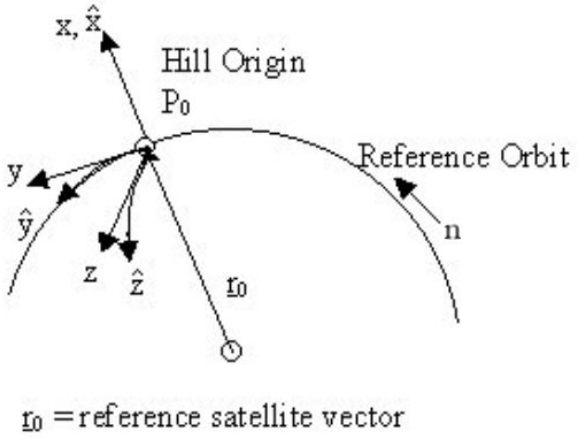

Figure 3-1: The Cartesian and Curvilinear Hill Frame

$$\ddot{x} - 2n\dot{y} - 3n^2 x = a_x$$
$$\ddot{y} + 2n\dot{x} = a_y \qquad (3\text{-}1)$$
$$\ddot{z} + n^2 z = a_z$$

In their rendezvous scenario, the 'rendezvous' satellite is assumed to have achieved the reference orbit altitude at apogee, and then further propulsive manoeuvres are made to place both satellites in the same orbit. Ideally the rendezvous satellite orbits ahead of the reference satellite. The equations of motion are based at the reference and used to predict relative motion, thus enabling timely thrust-vectored corrective manoeuvres to be performed by the rendezvous satellite to ensure docking.

The main assumptions inherent within the relative motion equations are that the reference orbit is circular, with a radius much larger than the separation between the satellites. Clohessy and Wiltshire (1960) suggest an upper limit on satellite separation of 200 miles for the equations to hold. The second satellite must therefore also have a near-circular orbit, both orbits must have similar radii and the satellites must have similar initial velocities. The Hill equations also assume that the separation variables can be linearised, and that the only force acting on the satellites is point mass gravity due to a perfectly spherical Earth. Rewritten in state space form, where A is the dynamics matrix, B is the control matrix and $\underline{x}$ is the state vector for the LVLH Hill frame,

$$\dot{\underline{x}} = A\underline{x} + B\underline{u} \qquad (3\text{-}2)$$

the equations of motion become, where n is orbital rate,

$$\begin{bmatrix} \ddot{x} \\ \ddot{y} \\ \ddot{z} \\ \dot{x} \\ \dot{y} \\ \dot{z} \end{bmatrix} = \begin{bmatrix} 0 & 2n & 0 & 3n^2 & 0 & 0 \\ -2n & 0 & 0 & 0 & 0 & 0 \\ 0 & 0 & 0 & 0 & 0 & -n^2 \\ 1 & 0 & 0 & 0 & 0 & 0 \\ 0 & 1 & 0 & 0 & 0 & 0 \\ 0 & 0 & 1 & 0 & 0 & 0 \end{bmatrix} \begin{bmatrix} \dot{x} \\ \dot{y} \\ \dot{z} \\ x \\ y \\ z \end{bmatrix} + \begin{bmatrix} 1 & 0 & 0 \\ 0 & 1 & 0 \\ 0 & 0 & 1 \\ 0 & 0 & 0 \\ 0 & 0 & 0 \\ 0 & 0 & 0 \end{bmatrix} \begin{bmatrix} a_x \\ a_y \\ a_z \end{bmatrix} \qquad (3\text{-}3)$$

Since the work of Clohessy and Wiltshire (1960), many authors have published further research into the LEO rendezvous problem. Carter (1998) references many authors and a significant number of his own publications on trajectory generation and fuel optimisation for rendezvous. In particular he surveys a range of linearised relative motion models for circular, near-circular, and elliptic orbits, and their limitations. It is apparent through rendezvous simulation work, for example, Hablani, Tapper and Dana-Bashian (2001), that the Hill equations are sufficiently accurate for the relatively short-term manoeuvres associated with satellite rendezvous (frequent thruster firings) where the satellites are briefly in close proximity prior to docking. However, a justification for the work in chapter 7 arises from the suggestions that the Hill model is too inaccurate to model the behaviour of satellites separated by a large distance (Clohessy and Wiltshire, 1960), or for the study of relative motion over an entire mission due to the growth of

modelling errors over time (Schweighart and Sedwick, 2002). Also, particularly in Carter's review, orbital perturbation effects are not considered.

Of course, the equations can be extended to nonlinear form while remaining based in the same Hill reference frame. Vaddi, Vadali and Alfriend (2002), (2003) extend the Hill equations to include eccentricity and nonlinear terms (limited to quadratic gravitational terms in x, y, z) to evaluate their effects. Perturbation analysis is used to solve the modified equations for a chosen formation which projects a circle onto the y-z plane, and approximate initial conditions are derived to eliminate secular growth from the perturbation variables. The new bounded motion initial conditions are compared to the conditions for the closed form solutions to the Hill equations. Both are evaluated in nonlinear simulations and the former are found to reduce significantly the secular drift in relative motion.

Recently, Richardson and Mitchell (2002) have extended the Hill equations by modelling the point mass gravitational effect of the primary body (Earth) as a third-body perturbation force in the Hill frame. They extend the Hill equations to include nonlinear terms, and produce a solution to the third order equations using a method of successive approximations. Sedwick, Miller and Kong (1999) also made a preliminary analysis of the errors introduced by linearising the equations of motion. The modelling improvements associated with including additional nonlinear terms are assessed in chapter 4.

The Hill equations and their solutions have been applied to LEO formation design, control and maintenance by many authors. In particular, researchers at MIT have concentrated on applying and developing the Hill equations, and the production of higher fidelity relative motion models. This programme of work is elaborated upon further in sections 3.1.3 and 3.1.4.

3.1.1.2 Relative Motion and Orbital Elements

An alternative method for modelling the relative motion of spacecraft in LEO is the orbit element approach. Keplerian motion of a single satellite can be described in terms of six classical orbit elements and these are listed in the first six rows of Table 3-3. The last two entries are also useful orbital parameters, but these are not required in order to fully define the location of a satellite in an orbit. Time or mean anomaly (related by Kepler's equation) must be known to specify the exact location of the satellite, where

$$M = nt \tag{3-4}$$

In this section, the roles of both the classical orbit elements and relative orbit elements in describing relative motion for formation flying are considered (Table 3-3). The relative orbit elements are simply the difference in classical orbit parameters of two satellites in different orbits. Relative orbit elements have an advantage over the Hill relative parameters ($\underline{x}$ from equations (3-2) and (3-3)) in that it is not necessary to solve differential equations to determine their variation over time.

Symbol	Orbit Elements	Relative Orbit Elements
a	Semi-major axis	δa
e	Eccentricity	δe
i	Inclination	δi
Ω	Longitude of the ascending node	δΩ
ω	Argument of periapsis	δω
M	Mean anomaly	δM
f=ω+θ	True latitude/Argument of latitude	δf
θ	True anomaly	δθ

Table 3-3: Classical Orbit Elements and Relative Orbit Elements for Formation Flying

For modelling satellite formation flying dynamics using a relative orbit elements approach, other parameters are often derived to replace some of the elements. Schaub and Junkins (2003) and Gim and Alfriend (2001) define q_1 and q_2 to replace eccentricity, e, and the argument of perigee, ω, in order to avoid singularities in the analysis in certain orbital conditions (near-circular or polar orbits). For relative orbit elements, δe and δω are replaced by δq_1 and δq_2 (equations (3-5)).

$$\begin{aligned} q_1 &= e\cos\omega \quad & \delta q_1 &= \cos\omega\delta e - e\sin\omega\delta\omega \\ q_2 &= e\sin\omega \quad & \delta q_2 &= \sin\omega\delta e + e\cos\omega\delta\omega \end{aligned} \tag{3-5}$$

A series of 'equinoctial variables' can be used to avoid singularities at zero orbit eccentricity or inclination, but although it is easy to transform between these and the classical elements, they are harder to visualise (Vallado, 2001), (Gim and Alfriend, 2002).

Another well-known set of orbit elements are the Delaunay elements (Brouwer, 1959), (Vallado, 2001). The first three terms in the element set (l,g,h,L,G,H) are equivalent to M, ω and Ω of the classical elements. The remaining variables are momenta variables which are functions of e, a and i. These have been extensively used for the design of relative orbits (Schaub and Alfriend, 1999), (Alfriend and Schaub, 2000).

In the presence of perturbations, the orbit elements and relative orbit elements will slowly vary with time, becoming 'osculating elements'. At any point in time, each element or relative element can be considered to have an instantaneous value which corresponds to an 'osculating orbit' or in the latter case, 'osculating relative orbit'. In the case of the single satellite, Roy (1988) uses the Variation of Parameters technique to derive the Lagrange Planetary Equations which express the rate of change of the orbital elements due to perturbing forces acting on an object in orbit. The perturbation accelerations are much smaller than those caused by the two-body gravitational potential (μ/r^2). Roy also presents methods for obtaining approximate solutions to the equations.

The perturbing accelerations acting on a single satellite can be resolved into the Cartesian LVLH frame, based at the orbiting satellite, and related to the orbit element rates via the Lagrange Planetary Equations in 'Gaussian' form (equations (3-6) to (3-11)) (Chobotov, 2002). These are expressed in a spherical coordinate system where $F_{x,y,z}$ are perturbing accelerations in the Hill frame (Figure 3-1), n is mean motion,

$x=\sqrt{(1-e^2)}$, and all other terms are listed in Table 3-3. These equations enable the effects of perturbing accelerations, due to for example, Solar radiation pressure, atmospheric drag, or the Earth's oblateness, to be visualised in terms of their effects on the orbit of a satellite, which may be of any eccentricity. They also provide insight into the location within an orbit where it is optimal to adjust a particular element of the orbit. Absolute values of the orbit elements can be obtained by substitution of the expressions for force in each direction, and integration of the expressions with respect to time. The effects of orbit perturbations on both individual and relative satellite motion are discussed further in section 3.1.4.

$$\frac{da}{dt} = \frac{2e\sin\theta}{nx}F_x + \frac{2ax}{nr}F_y \tag{3-6}$$

$$\frac{de}{dt} = \frac{x\sin\theta}{na}F_x + \frac{x}{na^2e}\left(\frac{a^2\left(1-e^2\right)}{r} - r\right)F_y \tag{3-7}$$

$$\frac{di}{dt} = \frac{r\cos f}{na^2x}F_z \tag{3-8}$$

$$\frac{d\Omega}{dt} = \frac{r\sin f}{na^2x\sin i}F_z \tag{3-9}$$

$$\frac{d\omega}{dt} = -\frac{x\cos\theta}{nae}F_x + \frac{a\left(1-e^2\right)}{e\sqrt{\mu a\left(1-e^2\right)}}\left[\sin\theta\left(1+\frac{1}{e\cos\theta}\right)\right]F_y - \frac{r\cot i\sin f}{na^2x}F_z \tag{3-10}$$

$$\frac{dM}{dt} = n - \frac{1}{na}\left(\frac{2r}{a} - \frac{\left(1-e^2\right)}{e}\cos\theta\right)F_x - \frac{\left(1-e^2\right)}{nae}\left(1+\frac{r}{a\left(1-e^2\right)}\right)\sin\theta F_y \tag{3-11}$$

In order to observe the secular growth of a parameter over time, rather than the smaller scale, short period variations, it is more appropriate to consider perturbed satellite motion in terms of the average or mean of the orbit elements. This also applies to relative orbit drift whereby any secular growth in mean relative orbital elements represents a drifting apart of the formation. Brouwer (1959) produced a direct mapping between mean and osculating elements for an individual satellite, and a numerical scheme to perform this mapping to first order for relative orbital elements is described by Schaub and Junkins (2003). The mean parameters are convenient from the control design perspective as, for an impulsive control scheme, the mean semi-major axis, eccentricity and inclination remain constant while the argument of perigee, mean anomaly and longitude of ascending node of an orbit vary linearly due to J_2 during the uncontrolled or 'coasting' proportion of the orbit (Vadali and Vaddi, 2000).

Authors at Texas A&M University were the first to report the use of the Lagrange Planetary or 'Gaussian' equations as the orbit elements dynamics model for formation flying control system design (Schaub, Vadali, Junkins and Alfriend (1999) and Vadali, Schaub and Alfriend (1999)). For the single satellite case, equation (3-12) illustrates the orbit elements dynamics architecture subject to control and perturbations. Both matrices are calculated from the Gaussian equations, but have been separated for visibility. The perturbation matrix (elements with subscript p) includes the dynamics of the mean orbit element rates subject to any orbit perturbations. As mentioned above, the Earth oblateness effect (J_2) would cause drifts in Ω_p, ω_p and M_p, but the rates of a_p, e_p, or i_p,

would be zero, and for Keplerian motion, the entire perturbation matrix would be zero. The magnitudes of the rates are always a function of the mean orbit elements ($\underline{e}$).

The control matrix is multiplied by the control force vector $\underline{F}$, and is composed of equations (3-6) to (3-11). This captures the variation in the osculating elements (rates) which would arise due to, for example, corrective control thrust resolved into the LVLH frame. When control is not applied ($\underline{F}=\underline{0}$), the drifts in the perturbation matrix describe the motion of the single satellite. When corrective forces are applied, the mean elements are converted into osculating elements, and allowed to vary according to the Gaussian equations. After an impulse control input, the osculating elements are converted back to mean elements and propagated again according to the perturbation matrix dynamics. For continuous control ($\underline{F}\neq\underline{0}$), a continuous translation between element forms is required as equation (3-12) propagates forward in time. Relative motion in terms of orbit elements can be evaluated by propagating separately the parameters for each satellite, and differencing the results.

$$\begin{bmatrix} \dot{a} \\ \dot{e} \\ \dot{i} \\ \dot{\Omega} \\ \dot{\omega} \\ \dot{M} \end{bmatrix} = \begin{bmatrix} \dot{a}_p(\underline{e}) \\ \dot{e}_p(\underline{e}) \\ \dot{i}_p(\underline{e}) \\ \dot{\Omega}_p(\underline{e}) \\ \dot{\omega}_p(\underline{e}) \\ \dot{M}_p(\underline{e}) \end{bmatrix} + \begin{bmatrix} da/dt(\underline{e}) \\ de/dt(\underline{e}) \\ di/dt(\underline{e}) \\ d\Omega/dt(\underline{e}) \\ d\omega/dt(\underline{e}) \\ dM/dt(\underline{e}) \end{bmatrix} \begin{bmatrix} F_x \\ F_y \\ F_z \end{bmatrix} \qquad (3\text{-}12)$$

Schaub and Alfriend (1999) used the orbit elements approach to establish the existence of J_2 invariant relative orbits for spacecraft formation design. These are reviewed in section 3.1.3 and the J_2 perturbation due to the Earth's oblateness is introduced in section 3.1.4.1. By analysing and imposing a set of conditions on the mean orbit elements of each satellite, orbits were identified which enabled a formation of satellites, subject to the J_2 perturbation, to exhibit bounded motion. The effects of the J_2 perturbation would not be eliminated from each orbit but the removal of relative drift would prevent the formation from diverging over time.

The effects of retaining higher order terms in the derivation of the J_2 invariant orbit constraints were investigated by Alfriend, Yan and Vadali (2002) and Alfriend and Yan (2002). In this case a second order Taylor expansion about the chief satellite orbit elements was performed, and a more accurate expression for the relative semi-major axis to meet a linear orbital period-matching constraint was derived to try to eliminate along-track separation. The inclusion of higher order terms did reduce the relative drift, but it was not possible to derive a new higher order period-matching constraint to prevent this, although some new conditions were proposed.

Schaub, Vadali et al. (1999) designed and compared two Lyapunov controllers to maintain J_2 invariant relative orbits in both the mean orbit elements frame and the inertial Cartesian frame. The orbit element feedback law was found to provide better tracking performance and more flexibility in terms of ΔV reduction by enabling

corrective manoeuvres to be performed over longer periods (using smaller feedback gains). As certain orbit elements are more effectively controlled than others in different parts of the orbit (this can be deduced from equations (3-6) to (3-11)), the control can be more impulsive, although complicated elsewhere by the cross-coupling between orbit elements. Under their inertial Cartesian feedback law, control was continuous, and found costly to engage over many orbits. In both cases transformations had to be made between mean and osculating orbit elements, thus incorporating additional error.

The feasibility of the latter design would also seem limited due to the number of transformations required between the mean element, osculating element and inertial Cartesian systems in order to generate the tracking error. The Cartesian parameters for the chief satellite are converted to osculating and then mean elements, and the chosen relative orbit parameters are added to these to generate the desired mean elements for the deputy. These are then converted back into the Cartesian frame. However, the positions and velocities of the deputy are also converted to mean orbit elements and back to Cartesian before they are differenced with the desired parameters so that the same transformation errors are incorporated into both the sets of desired and actual Cartesian parameters. The conversion between parameters is discussed in numerous references (Battin, 1987), (Prussing and Conway, 1993).

Tan, Bainum and Strong (2000) also designed a Lyapunov controller to maintain desired values of the osculating orbit elements using the same orbit element dynamics of equation (3-12). In this case, J_2 invariant orbits are not considered, but the relative orbits between the chief and deputy satellites are designed to maintain a constant separation around a highly elliptical orbit in the presence of the J_2 disturbance.

Schaub and Alfriend (2000b), (2001) continue to investigate impulsive feedback control techniques using relative mean orbit elements to maintain J_2 invariant orbits. In these studies, the effects of translating between mean and osculating elements are investigated (Brouwer, 1959). In particular, the sensitivity of the mean semi-major axis and eccentricity to corrections in the osculating inclination is found to be significant, and when included in the control model, fuel consumption for the chosen test case is reduced. Schaub and Alfriend conclude by suggesting that the orbit element approach and their impulsive control law lend themselves to autonomous relative orbit station keeping, provided that the satellites are able to perform on-orbit determination. Again, this paper reinforces that the orbit element approach is not appropriate for precision formation flying in LEO. Impulsive control primarily at apogee and perigee means that the relative positions between satellites may vary significantly during the remainder of the orbit. In addition, orbit determination would be in the inertial frame from the ground, or possibly the Hill frame from GPS, both requiring translation into the orbit elements, the mean of which must be evaluated at least once per orbit.

However, while Schaub and Alfriend (2001) are able to counteract some of the problems of formation keeping with the insight that the orbit elements approach provides, there remain modelling limitations, just as for Hill-type equations (the limitations of Hill-type models are investigated in chapter 4). These are summarised by Alfriend and Schaub (2000), again in the context of J_2 invariant orbits where design constraints are found to be impractical for both polar or near-circular chief orbits.

Up to this point, the application of the relative orbit elements approach to satellite formation design and formation flying control has mainly been in the presence of the J_2 perturbation (section 3.1.4.1). In many cases, the Hill equations are described as failing in their inability to capture the primary effects of Earth oblateness on relative motion. However, this is an unfair comparison as the Hill equations can be augmented to incorporate the effects of J_2 (Schweighart and Sedwick, 2001a). Later papers investigate the correction of the orbital rate term (n) in the Hill equations (equations (3-1)) by incorporating drift rates derived through the orbit elements approach. Literature relating to combined studies of the Hill equations and orbit elements approach is reviewed in section 3.1.1.3.

These examples of studies from the literature have illustrated the application of the orbit element approach to satellite formation flying dynamics modelling. The application of this approach for the generation of initial conditions and formation design is reviewed in section 3.1.3. Analytical solutions to describe the variation of relative orbit elements (mean and osculating) have been derived in recent literature, but as they relate to formation separations and relative velocities that have been defined in the Hill frame coordinates (a more practical measurement than relative elements), they are discussed in the following section.

3.1.1.3 The Combination of the Hill and Relative Orbit Elements Approaches

Studies have been performed which compare and contrast the relative orbital elements and Hill equations approaches to satellite formation flying control and formation design, and in some cases, aspects of both approaches have been combined. Alfriend, Schaub and Gim (2000) and Schaub and Alfriend (2000a) have derived an analytical mapping between the relative orbit elements and the Cartesian LVLH Hill frame coordinates (equations (3-13)) by performing a Taylor expansion about the osculating orbit elements of the 'reference' or 'chief' satellite. If the separation between satellites is small and their relative orbit is much smaller than the reference orbit radius, the two forms of relative motion description can be easily translated from one form to the other. The equations apply for elliptic orbits and terms are defined in Table 3-3 and Figure 3-1.

$$\begin{aligned} x &= \delta r \\ y &= r(\delta f + \cos i \delta\Omega) \\ z &= r(\sin f \delta i - \cos f \sin i \delta\Omega) \end{aligned} \qquad (3\text{-}13)$$

An alternative and potentially more useful form of equations (3-13) is derived as a function of true anomaly, θ, in terms of the relative orbit elements ($\delta a, \delta e, \delta i, \delta\Omega, \delta\omega, \delta M$) by Schaub and Junkins (2003). For the near-circular and circular orbit case, terms in e are eliminated and in this special case, the relationship between the Hill parameters and relative orbital elements becomes

$$
\begin{aligned}
x(\theta) &\approx \delta a - a\cos\theta\delta e \\
y(\theta) &\approx a\left(\delta\omega + \delta M + \cos i\delta\Omega\right) + 2a\sin\theta\delta e \\
z(\theta) &\approx a\sqrt{\delta i^2 + \sin^2 i\delta\Omega^2}\cos(f - f_z)
\end{aligned}
\qquad (6\text{-}14)
$$

where the true latitude angle, f_z, is given by

$$
f_z = \tan^{-1}\left(\frac{\delta i}{-\sin i\delta\Omega}\right) \qquad (6\text{-}15)
$$

Relative velocities in the Hill frame can also be expressed in terms of orbit element differences. Schaub and Alfriend (2000a) apply the coordinate transformations in their design of a continuous feedback control law which combines both frames of reference. The desired relative orbit geometry is specified in terms of mean orbit elements, but the actual relative motion is measured in the LVLH Hill coordinate frame. It is claimed that using the linearised relationships between relative motion variables only slightly reduces the system performance compared to the nonlinear transformations. The use of linear transformations for model validation using Hill frame initial conditions and the orbit element user interface of the Satellite Tool Kit (STK) to initialise relative orbits is described in chapter 4.

Alfriend, Schaub and Gim (2000) also derive the state transition matrix (STM) solutions of the perturbed relative dynamics using both reference frames. In later work, Gim and Alfriend (2001) present the analytical STM solutions in closed form for both mean and osculating orbit elements, and these are compared to both the Hill solutions and numerical solutions converted from the Earth Centred Inertial (ECI) frame into the curvilinear Hill frame (Figure 3-1). Transformation matrices are derived between relative positions and velocities in the curvilinear Hill frame, and both the osculating and mean orbit elements, and the linear mapping of equations (3-13) is augmented to include the effects of J_2. The new mean orbit element solution is found to capture relative motion for eccentric orbits in the gravitational perturbation environment well, although short period motion is not captured. Of course, there is no relative mean element motion without the perturbation effects. Very little secular error growth is visible during longer period simulations, and errors are limited to approximately 1 metre for the mean elements solution over 5 orbits. Even when the Hill frame reference orbit is corrected for the effects of drift in the longitude of ascending node, due to J_2, on the mean rate (equation (3-16)), the solution errors are still much greater at around 50 metres in 5 orbits for the test case illustrated.

$$
\bar{n} = \dot{M}_0 + \dot{\omega}_0 + \dot{\Omega}_0\cos i_0 \qquad (3\text{-}16)
$$

Gim and Alfriend (2002) extend these results to remove singularities in the STM which appear when the reference orbit has a zero inclination. Errors at centimetre level were achieved in the radial and cross-track directions, but the along-track drift for all models increased with reference orbit eccentricity. However, the sensitivity of the relative mean-to-oscillating elements transformation to eccentricity is highlighted. For the same

test case, the use of equinoctial variables (alternative combinations of the orbital elements) does not appear to reduce errors in the STM solutions.

Sabol, Burns and McLaughlin (1999) use the Hill equations to design four types of natural formation in the absence of perturbations. The resulting relative motions are visualised in terms of both the LVLH Hill parameters and orbital elements. The motion of the individual satellites within each of the formation designs is then propagated in terms of averaged orbit elements and in the presence of geopotential, atmospheric, third-body and Solar radiation pressure perturbations. The initial conditions are therefore also specified in terms of averaged orbit elements. Corrective velocity impulses for formation maintenance of the different designs are evaluated for the different designs as a function of relative orbit elements (Sabol, Burns, and McLaughlin, 2001).

Vadali and Schaub and Alfriend (1999) describe methods of formation initialisation using the mean orbit elements approach and relative motion visualisation in a Hill-type (in this case, elliptic rotating) reference frame. Vadali, Alfriend and Vaddi (2000) use the Hill equations for orbit design, but consider the perturbative effects of J_2 in terms of mean orbit element drifts. By combining both approaches a new set of relative motion equations are generated which incorporate the effects of J_2. These modified Hill equations are found to improve model fidelity. A set of Hill-type solutions which include the secular J_2 effects expressed in terms of relative orbit elements are presented in Swank et al. (2002).

Vadali (2002) obtains relative motion solutions for satellite formation flying in eccentric, J_2-perturbed orbits using a relative orbit elements approach, again by considering the solution in terms of relative displacements in the LVLH Hill frame. The relative motion is projected onto a unit sphere by normalisation of the Hill coordinates, conversion into relative orbit elements and the series solution to Kepler's equation. The solution is also written as a function of time, and is applicable for mean or osculating orbit elements.

Kormos and Palmer (2002) describe the derivation of a high fidelity relative motion model using epicycle elements which are easily converted to the Hill frame for visualisation of relative motion. A reference (ghost) orbit incorporating just the secular perturbation terms (for J_2 in this case) is specified in epicycle elements, and first and second order element differences are derived including both the effects of J_2 and drag. A number of other studies concerning the effects of the J_2 perturbation are reviewed in section 3.1.4.1.

More recent work, performed since the definition of the thesis aims, has involved the comparison of different modelling methods, and the reconfiguration of satellite formations. Based on work by Junkins et al (2003), Alfriend and Yan (2003) propose a modelling error index and compare linear and nonlinear relative motion models for reference orbits with a range of eccentricities and formations with a variety of separations to determine which is the most accurate. The models considered include the Hill equations, the Gim-Alfriend STM (2002), an STM solution for low eccentricity (a reduced form of the Gim-Alfriend STM), a model similar to the Tschauner-Hempel equations which describe relative motion in an elliptic orbit (Carter, 1998), and a

method for predicting long-term relative motion based on the nonlinear transformation of the mean orbit elements to the LVLH frame. The basic Hill equations are found to model the relative motion the least accurately for all test cases, and predictably the low eccentricity model does not perform well at high eccentricities. The Gim-Alfriend STM approach is consistently the most accurate nonlinear model for smaller satellite separations.

Formation reconfiguration methods based on Hill and orbit element approaches for satellites in LEO are described in section 3.1.5.3, based on more recent work by, for example, McLaughlin, Alfriend and Lovell (2002), Vaddi, Alfriend and Vadali (2003) and Sengupta and Vadali (2004).

3.1.1.4 Discussion

In this section, a summary of the advantages and disadvantages of the Hill equations and relative orbit element approaches for the modelling of satellite formation flying dynamics in LEO is presented (Table 3-4).

If initially the two methods are compared in the absence of orbit perturbations, it is immediately clear that the Hill equations are limited by virtue of their sole application to the circular reference orbit case, whereas the relative orbit elements (where true anomaly is replaced by mean anomaly) remain constant and valid for any orbit eccentricity. The Hill equations only hold for satellites in fairly close proximity, and therefore in the long-term it is necessary for the satellites to maintain bounded relative motion by the appropriate choice of initial conditions. This requirement for the formation not to drift apart significantly limits the number of practical formation configurations. The Hill equations are linearised and will therefore experience associated linearisation errors which are significant. A number of authors investigate the effects of linearisation, and this is discussed in chapter 4. However, due to their simplicity, the linearised differential equations can be solved analytically, enabling the limitations to be observed, and relative orbit shapes to be easily visualised.

For control system design, the Hill equations form the familiar state matrix, but the determination of the relative mean orbit element rates does not require the solution of differential equations. Therefore, the models are suitable for different types of control system design, and can be subject to different types of stability analysis.

The orbit element approach applies the Lagrange equations as the fundamental orbit element model in the literature. While the direct relationship between the variation of orbit elements and control forces provides insight into when a particular element should be adjusted to minimise fuel expenditure (for example, inclination should be adjusted at the equator, but longitude of ascending node should be adjusted at the pole), any feedback control accelerations act on the osculating orbit element dynamics of a single satellite, and not on relative elements.

Although the intention within this literature review is to discuss the effects of orbital perturbations in section 3.1.4, many of the papers describing the application of the orbit

elements approach to formation flying dynamics modelling do so in the presence of the Earth oblateness perturbation, J_2. The orbit elements description of single satellite motion is easily augmented to incorporate the effects of orbit perturbations, and differenced to obtain relative orbit effects. The use of mean orbit elements for formation design and formation flying control has been described from the literature, where it was demonstrated that this approach is effective for efficiently maintaining a formation (preventing relative drift) in the presence of orbit perturbations. However, the primary disadvantage of this approach is that controllers are governed by the mean orbit elements, and the other short (and long) period motions during an orbit are neglected although they may be very significant for practical operations. Relative mean orbit elements enable the orbit geometry to be defined, but do not guarantee that the satellites will remain close together, particularly if impulsive control is applied. However, the Hill equations enable close-proximity relative position and velocity to be continually evaluated and maintained, although it is claimed that the Hill equations in their basic form are not appropriate for control system design for long-term formation flying missions, as they will demand excessive fuel use in eliminating any effects of external perturbations.

LVLH Hill Equations	Relative Orbit Elements
• Limited to circular reference orbit	• Valid for any orbit eccentricity
• Only apply for bounded motion, for satellites in relatively close proximity or contravene model assumptions	• Apply for any satellite separation
• Incorporates linearisation assumptions	• No linearisation assumptions
• Analytical solutions are easily obtained	• No equations to solve
• Initial conditions for bounded motion can be derived, although they are inaccurate for perturbed or eccentric orbits	• Initial conditions for bounded motion can be derived for circular and eccentric orbits in the presence of perturbations
• Easy to visualise relative motion/the relative orbit shape	• Very difficult to visualise relative motion/the relative orbit shape but gives good visibility of individual orbit shape
• Useful for formation design	• Useful for formation design
• Useful form for control system design	• Controllers do not act on relative elements, but on element error dynamics
• No mathematical transformations are required for control system design and implementation	• Transformations between mean and osculating orbit elements is required in the presence of orbit perturbations
• No singularities in the basic form of the equations	• Singularities exist when forces are experienced
• Do not account for orbit perturbations in their basic form – but effects can be incorporated	• Orbit perturbations easily incorporated
• More appropriate for high precision and close proximity formation flying	• Orbit geometry is easily maintained but short period motions are not captured
• Dynamics are described in the frame within which the real relative position and velocity data can be measured by sensors on-orbit	• LVLH frame relative position data must be converted to orbit elements for element feedback control

Table 3-4: A Comparison of Relative Motion Modelling Techniques

The lack of precision formation flying associated with impulsive control of mean elements at different sections in an orbit may hinder certain formation operations and limit applications, although the orbit elements approach appears to be a more practical approach to natural formation design. However, both modelling approaches can be usefully applied to the problem, each providing insight from a different perspective.

The relative mean orbit elements are extremely useful for formation design, and for determining the desired mean elements of the deputy satellite, based on the mean orbital elements of the chief. Using this approach, controllers act on the error between the actual mean orbit elements of a deputy satellite and the desired mean orbit elements, by introducing forces that cause the osculating elements to vary. Any orbit element control law in the presence of perturbations will therefore involve transformations between the mean and osculating elements. This transformation has been found to be significant, and must be included within the control process, and any simplifications of the transformation incorporate error.

Both models also have practical limitations. For example, if forces are applied to the orbit elements model at zero inclination or eccentricity, singularities occur, and if a formation invariant to the J_2 perturbation is to be designed around a polar reference orbit, an impractically large relative eccentricity is required. The Hill equations are limited in the perturbed environment, as they do not incorporate J_2 and other perturbation effects in their basic form. When relative motion is compared to a numerical solution with perturbations included, the most significant error is introduced by the secular drift of the formation away from the circular reference orbit, even when applying the initial conditions for bounded motion. However, authors at MIT have incorporated the averaged J_2 perturbation as a disturbing force in the Hill equations with great success, although in the process introduced other model limitations. These are discussed in more detail in chapter 4. Circular orbit limitations are no longer critical as other Hill-type models are available for elliptic orbits (refer to section 3.1.4.4).

Time explicit relative motion solutions have been obtained for both models. Solutions for the basic Hill equations and higher fidelity versions are used to generate initial conditions for near-bounded relative motion in the perturbed environment. The orbit elements approach does not require solutions in the conventional sense, but the nonlinear algebraic problem has been transformed into a linear one and expressions have been derived for the behaviour of mean and osculating orbit elements over time using a state transition matrix approach in the presence of orbit perturbations. Comparative work showed that the Hill solutions (in their basic form) were the least accurate. This is expected since orbit eccentricity and perturbations are neglected in the Hill equations. However, in section 3.1.2, a number of mission-targeted studies are reviewed, and these illustrate a range of practical uses for natural formations arising from the Hill equations. The evaluation of the orbit elements approach in terms of acceptable modelling error for mission design, and the application of J_2 invariant orbit design for a particular mission application, has not been demonstrated in the literature and further research is required.

It is important to highlight the issues associated with the practical implementation of control systems in terms of the orbit elements. Controller designs inevitably require

consideration of relative position and velocity in terms of the Hill coordinate frame, as in reality, the orbital elements cannot be instantaneously measured and directly applied to onboard control, whereas linear distance between two satellites in the Hill frame could be measured by various metrology systems (refer Table C-1, appendix C). For this reason hybrid models incorporating both modelling approaches are being considered for LEO formation design and control. However, not only must transformations be performed between the osculating relative orbit elements and the relative Hill parameters, but also between the mean and osculating elements for each satellite. For example, when formations are designed using mean orbit elements, these must be converted to osculating elements before control force effects are evaluated. Depending on which relative position measurement strategy is being applied, transformations between the Earth Centred Inertial (ECI) frame, mean and osculating orbit elements and the Hill Cartesian or curvilinear frame parameters (Figure 3-1) may be required. Clearly, although some of them can be carried out in nonlinear form at the expense of time and processing power, these transformations introduce errors.

In conclusion, each model has particular advantages, and the approaches remain complementary. To date, the direct comparisons between model behaviour have found the orbit elements approach to be the most accurate in capturing the relative motion, however the approach is compared only to the basic Hill equations with at most, a modified orbital rate to compensate for some of the along-track drift due to the J_2 perturbation. The inability of the Hill equations to cope with reference orbit eccentricity is also highlighted as a problem. However, it would appear to be an unfair comparison since there exist numerous separate models for relative motion in elliptical orbits, and the Hill equations can be augmented to incorporate J_2 effects. This is addressed further in chapter 4.

The best modelling approach also appears to be task dependent, depending on whether the priority is to retain the overall geometry of the formation, or capture the short-period relative motion for shorter-term high precision formation flying. In the latter case, a set of high fidelity Hill-type equations is likely to be the most practical model. Formation modelling requirements also depend on the application of the mathematical model to control system design. In all cases, a higher fidelity model is desirable, but not at the expense of complexity and significant additional processing power.

For the investigation performed in this thesis, the approach of linearising the gravity gradient at a reference point has been selected. The understanding gained from the development of Hill-type relative motion models and the addition of perturbation terms is applied to the development of a linearised formation flying dynamics model for satellites at the L2 Lagrange point (section 3.2). The primary advantages of this modelling approach have been presented in this section, and while the orbit elements approach has definite benefits for many applications, the emphasis of this study is not formation design, and instead focuses on the requirement for precise control of multiple satellites in close proximity. Complex conversions between the orbital elements and the Hill frame are mostly avoided, and the more practical aspects of relative motion sensor modelling and relative orbit visualisation become straightforward.

3.1.2 Formation Flying Mission Studies and Applications

A summary of the current and planned multi-spacecraft missions was presented in chapter 2. In this section a more detailed review of some of the research performed in direct support of the LEO (and GEO) formation flying missions and other specific scenarios is presented, based on the recent literature. The technical detail is referenced in other sections according to the contributions of each study in each of the categories in Table 3-1. The following subsections group together the studies related by mission type (rather than, for example, author, location, or sponsoring body). These fall into the categories of surveillance systems pointing towards the Earth, astronomical observatories looking away from the Earth, and any additional relevant studies relating to cluster and constellation missions.

3.1.2.1 Interferometric Earth Observation and Imaging

Under the broad funding of the AFRL, both in support of the former TechSat21 mission, and generally in support of research into distributed systems, a number of formation flying studies were performed at MIT for Earth observation and imaging. In these studies, both the ability of the formation to perform the mission task is considered in parallel with orbital mechanics considerations.

Mallory, Jilla and Miller (1998) optimise the orbital elements of a formation of spacecraft in geosynchronous Earth orbit to maximise image quality. Their constellation design method to maximise u-v plane coverage for interferometry almost eliminates the need for propellant (interferometric imaging was introduced in chapter 2). In this case, the system is assumed to operate in the radio regime, where amplitude and phase information can be accumulated in order to reconstruct an image after post-processing. A maximum number of satellites, required for absolute coverage of the u-v plane, is found to exist. However, this number depends on the resolution required, which in turn directly relates to the pixel density at the detector. Path length control, post-processing techniques, coherence lengths, and metrology issues are not considered, but would be important considerations in the design. For a formation at lower altitude, orbital perturbations would have an increasingly significant effect and must also be taken into account.

Kong, Miller and Sedwick (1999) design and optimise a geosynchronous interferometric Earth imager operating in the optical regime, which therefore requires the addition of a combiner spacecraft to interfere the light in real time, rather than by post-processing at radio wavelengths. As a case study, the mass data of the former NASA Deep Space 3 mission satellites are applied to the designs (Sohus, 2001). By considering the basic Hill description of the relative motion dynamics (section 3.1.1.1), an initial estimate is made of the fuel consumed by different satellite formations. Fuel use is evaluated for a range of formation orientations, or in other words, variations in the interferometer line-of-sight (the proposed satellite formations are summarised in section 3.1.3). The use of optical delay lines rather than the fuel-consuming slewing of the formation to ensure the correct wave front interference at the hub is also investigated. Interferometric requirements for the formation were specified at the outset,

and it was found that a for a geosynchronous, visible Earth imager, a six-collector plus combiner system operating as a steered planar circular array was optimum.

A study by Sedwick, Kong and Miller (1998) considers the simplest natural formations of multiple of satellites in LEO, arising from bounded solutions to the Hill equations. Like the figure-of-eight GEO constellation described above, no fuel is required to maintain them (the use of the Hill equations for formation design is described in section 3.1.3.1). The effects of environmental perturbations, including gravitational, atmospheric, Solar radiation and electromagnetic forces, on the fuel used for formation maintenance are estimated. Image formation by interferometry and the effects of baselines are considered, and three types of suitable formation are proposed. Building on this, Sedwick et al. (1999) make improved ΔV estimates for station-keeping of a LEO formation based on the dimensional analysis of environmental perturbations. By counteracting any secular terms (which would drive the formation apart) and smaller periodic motions (which would be likely to affect the ability of the formation to perform interferometric imaging), estimates of fuel use for the TechSat21 mission are made. Although the analysis is simplified by the consideration of polar orbit formations only (although for a formation, the orbit of at least one of the spacecraft needed to be non-polar), they conclude that the fuel requirements for simply preventing the drifting apart of a formation in the perturbed environment are practical. However, actively eliminating small, periodic motions or manoeuvring would be too costly and not viable for a LEO mission. Sabol, Burns and McLaughlin (1999) evaluate the fuel required to maintain natural formations derived from the Hill equations, when subjected to orbit perturbations. Significant fuel is required to counteract the J_2 perturbation for a circular planar TechSat21 formation.

Schaub and Alfriend (2000b) of Texas A&M University, whose formation flying work has primarily involved the analysis of J_2 invariant orbits and control system design using orbit elements, comment that they agree with Sedwick et al. (1999) and Sabol et al. (1999), (2001) about the importance of designing natural LEO formations. Sedwick's results are referenced to justify the use of mean orbit elements which only take into account secular drifts in formation relative orbits, and neglect any smaller, periodic relative motion (the orbital elements description of relative motion dynamics was introduced in section 3.1.1.2). Schaub and Alfriend (2001) claim that to eliminate such periodic motions would create excessive fuel requirements, and that the motions are sufficiently small to lie within the margins of acceptable tracking error. However, no mission-specific study has been performed to demonstrate this, and the magnitudes of these small-scale periodic motions, hidden by mean elements considerations, are not presented.

A later study by Kong and Miller (2001) addresses cluster initialisation and resizing for the three-satellite TechSat21 flight experiment mission. Minimum energy trajectories are proposed using an optimal control approach, for both the manoeuvring of an individual satellite within the formation for deployment or formation initialisation, and for formation resizing. The balance of fuel used against time to perform the manoeuvre is investigated (formation manoeuvring is discussed further in section 3.1.5.3). A low altitude orbit of 600km was specified, and it was therefore necessary to include the

primary perturbation force (J_2) in the Hill relative motion equations (Schweighart and Sedwick, 2001b).

Schweighart and Sedwick (2001b) rectify some of the oversights of earlier analysis by Sedwick et al. (1999) and consider the differential J_2 perturbation effect on a formation at any inclination (rather than just polar). This time, they acknowledge the effect of the perturbation on cross-track relative motion in addition to the along-track and radial directions, and amend the equations to match the orbital rate of the Hill frame origin on an unperturbed circular reference orbit to that of the perturbed cluster to maintain linearisation assumptions. A phenomenon, described as 'tumbling' is identified whereby a circular projection of a formation in LEO reduces to a linear projection due to the difference in period of the in-plane and cross-track terms, caused by the precession of the argument of periapsis. The period of the cross-track motion is found to depend on the moving location of the intersection of orbit planes of different satellites in the formation, and the linearised cross-track equation of motion is found to hold only for equatorial orbits. A more robust cross-track motion model was later developed (since the definition of the thesis aims), based on the geometry of the intersecting orbital planes of J_2 perturbed satellites (Schweighart and Sedwick, 2002). This model development is discussed further in section 3.1.4.1 and chapter 4.

The most recent work on formation flying at MIT is supported by NASA who plan to use electromagnetism (electromagnets and reaction wheels) for formation control (Schweighart and Sedwick, 2004). This eliminates the problem of exhaust plumes affecting other members of the formation, and provides a much longer term propulsive resource for multiple formation manoeuvres in LEO. However, there are spatial limits over which this method of control can be applied as the forces reduce with the fourth power of satellite separation. A testbed is being constructed to examine the feasibility of an electromagnetic system for LEO formation flying control.

A review of progress in a number of research areas that have supported the TechSat21 concept up to 2001 is provided by Garnham et al. (2001). These include a brief overview of formation flying dynamics, relative navigation, cluster management and autonomy, inter-satellite communications, and development of the radar payload. In particular, the three-satellite flight TechSat21 precursor flight experiment is described.

Researchers at CNES have performed a feasibility study and mission analysis of an "interferometric cartwheel" (Amiot et al. (2002)). A formation of three receiver satellites trace an elliptical relative orbit, centred upon and following a single SAR satellite for improved terrain elevation mapping.

3.1.2.2 Interferometric Astronomy

Kong and Miller (1998) at MIT present the first in a series of studies for the NASA Deep Space 3 (DS3) mission to optimise u-v plane coverage without considering any gravitational effects on the formation. The mission aimed to image a distant point source using a two-telescope plus combiner optical interferometer. In a later paper, Kong, Miller and Sedwick (1999b) perform a LEO study into the use of natural

formations derived from the Hill equations (equations (3-1)) to provide the equivalent x-y plane. They apply the geosynchronous Earth imager formation design approach, described in section 3.1.2.1, to a new scenario enabling optical interstellar interferometry from LEO. In their previous Earth imager study (Kong et al, 1999), it was established that interferometry could be performed by placing collector or telescope satellites on a natural relative trajectory in the Hill frame, and a combiner or hub spacecraft at the focus of a paraboloid fitted to the free orbit trajectory. This was contrasted with a steerable planar circular array formation. In this case, the feasibility of these formations in a Sun-synchronous orbit to perform interstellar interferometry was considered. Kong et al. suggest that the advantages of a Sun-synchronous orbit include the provision of a continuous power supply, and the generation of a useful facility for observing objects in the ecliptic. Again, a high altitude was assumed for their study as orbit perturbations are neglected. A significant proportion of the study relates to the use of optical delay lines for steering the interferometer line-of-sight, and the effect of long delay lines on spacecraft dry-mass.

3.1.2.3 Scientific Earth Observation and Communications

In this section, papers relating to non-imaging Earth observation missions are discussed. They include atmospheric and magnetic environmental observation and experimental or communications multisatellite missions that involve some element of formation keeping or collaborative control. Again, the reader is referred to the mission descriptions of the formation flying missions survey in chapter 2 and appendix A.

Mazanek et al. (2000) describe the development of mission analysis software and station-keeping fuel use estimation in the presence of perturbations for GRACE, the Gravity Recovery and Climate Experiment mission. GRACE was launched in March 2002 to perform more accurate geodesy, oceanography, and to support research in other Earth sciences, for example, plate tectonics. The two satellites are loosely formation flying in a leader-follower formation, maintaining a separation of between 170 and 270km using regular station-keeping manoeuvres, and making inter-satellite range measurements to micron level using a K-Band microwave tracking system (Mauldin, Bettadpur, and Fowler, 2004). Stevens, Rodden et al. (2000) describe the development of simulation software verification and validation tools for the attitude and orbit control system for GRACE. This enabled pre-mission investigation of the likely fuel use for mission operations and attitude and formation maintenance.

Bainum proposes a strategy for maintaining a planar satellite formation in elliptical orbits to make simultaneous field measurements. The work is primarily targeted at the Auroral Multiscale Mission (or Auroral Cluster Mission) which aims to measure the curl of the Earth's magnetic field (Tan, Bainum, and Strong, 1999). Formation design, initial deployment and formation maintenance by Lyapunov control are considered (Tan et al, 2000), (Tan and Bainum, 2001).

The first NASA formation flying mission involving the technology demonstrator, Earth Observing-1 (EO-1) and the Landsat7 satellite flying in a ground-track-leader-follower, circular orbit formation is introduced in chapter 2. Folta and Quinn (1998) and Folta and

Hawkins (2002) describe the operation of the control system onboard EO-1 which autonomously maintains the formation. The Landsat7 satellite remains free-flying, and all position data and manoeuvres of this 'leader' satellite are obtained or controlled from the ground. Aspects of the control system are user defined, for example, the manoeuvre timing, but the approach involves onboard software taking the position data of EO-1 (from GPS) and Landsat7 (from the ground), and generating corrective manoeuvres to maintain the formation flying tolerances. Propagating the satellite positions forward in time, a desired target position is specified for EO-1 relative to Landsat7, at a particular time in the future. EO-1 propagates this target position backwards in time to determine a set of desired initial conditions which would allow EO-1 to reach the target without manoeuvring. A reference trajectory involving any desired number of corrective manoeuvres is determined for a given manoeuvre window. During the manoeuvre, at each selected manoeuvre point beyond the actual satellite position, backwards propagation is used to determine the Keplerian trajectory to that next manoeuvre point. This provides new position and velocity error data for the state transition matrix solution to determine the necessary corrective ΔV in three axes which will enable the EO-1 satellite to arrive at the next control point. A subsequent corrective velocity-matching manoeuvre is then performed once the correct position has been attained. This can be repeated many times as a sequence of small manoeuvres or could be implemented via two larger manoeuvres with only the start and end points of the reference being the manoeuvre points. This low frequency manoeuvring, similar to a Hohman transfer was found to be successful during the mission (Folta and Hawkins, 2002). Of course, in this first formation flying mission, relative motion dynamics models are not implemented and on-orbit relative position measurements are not made, however, the autonomous trajectory generation, manoeuvre planning and execution based on relative position tolerances has been successfully demonstrated.

Although, in general, constellations of communications satellites have not been considered as formations, it is appropriate to mention the autonomous station keeping strategy for satellites maintaining equal separations around an orbit proposed by McInnes (1995). By simulating the variation in separations between different satellites in terms of system potential to effectively generate repulsive and attractive forces between satellites, a formation control strategy is derived. The use of potential functions for satellite formation flying guidance and control in the vicinity of the L2 Lagrange point is discussed in section 3.2.5.

3.1.2.4 Discussion

This review has demonstrated that, in general, for the precision formation flying interferometry missions, Hill-type relative motion models have been applied to the formation design, dynamics modelling and control. The orbit element approach advocated by authors at Texas A&M University is not applied in a mission specific context, although very similar work is performed at Howard University in the context of a scientific Earth observation mission (Tan and Bainum, 2001). This mission does not require the same level of formation flying precision as the other applications considered in this section.

3.1.3 Natural Formation Dynamics and Formation Design

A significant proportion of the available literature on LEO (and GEO) formation flying involves some aspect of formation design. To reduce the fuel required to maintain a formation of satellites in LEO to a practical level, it is necessary to design a functional formation using, as far as possible, any naturally available formation dynamics. Approximate natural relative orbits can be derived most easily for Keplerian orbits, in terms of relative orbit elements, or in terms of an axis system based at the reference or 'chief' satellite. The advantages of both approaches in terms of formation design flexibility and visualisation in the perturbed environment were highlighted in section 3.1.1.

In this section a summary of the status of formation design approaches and tools is presented. Formation design using the Hill equations and orbit elements are considered in separate subsections, and the application of both approaches to the design of J_2 invariant relative orbits is included. Mission specific formation designs have already been described in section 3.1.2.

3.1.3.1 The Hill Equations and Formation Design

For the Hill equations, the derivation of natural formations in the unperturbed environment is based completely on the analytical solutions to the equations of relative motion, and the formations are defined through the choice of initial conditions.

Sabol, Burns and Mclaughlin (1999), (2001) present the unperturbed Hill equations, and their solutions as a preliminary formation design tool. The initial condition to avoid along-track secular growth in separation between satellites in near circular orbits is given by

$$\dot{y}_0 = -2nx_0 \tag{3-17}$$

where x_0, $\dot{x}_0$ and y_0, $\dot{y}_0$ are the initial radial and along-track satellite separations and relative velocities respectively (the axis system is illustrated in Figure 3-1). In addition, along-track offset is eliminated by setting

$$y_0 = \frac{2\dot{x}_0}{n} \tag{3-18}$$

Analysis demonstrates that if these conditions are enforced, both satellites have the same orbit energy, and therefore the same semi-major axis, a. Bounded motion of the unperturbed Hill equations is considered further in chapter 4. The closed-form solutions given by equations (3-19) which incorporate the initial conditions of equations (3-17) and (3-18), can then be applied to formation design.

$$x(t) = \frac{\dot{x}_0}{n}\sin nt + x_0 \cos nt$$
$$y(t) = \frac{2\dot{x}_0}{n}\cos nt - 2x_0 \sin nt \qquad (3\text{-}19)$$
$$z(t) = \frac{\dot{z}_0}{n}\sin nt + z_0 \cos nt$$

In linearised form, the oscillatory cross-track (z) motion is decoupled from the in-plane (x-y) motion which traces a 2:1 ellipse in the orbit plane. In combination, a periodic 3-D elliptical relative motion is produced which is the basis for many formation designs.

Sabol et al. (1999) consider four types of formation design. These include the in-plane (or leader-follower) formation where satellites separated by mean anomaly follow each other around the same orbit, an in-track formation which enables the satellites to follow the same ground track, a circular formation which enables the satellites to maintain a circular relative orbit, and a projected circular formation. In the latter case, the relative orbit is elliptical, maintaining a fixed satellite separation distance, and therefore projecting a circle in the y-z plane. Both the circular and projected circular formations occur for specific inclinations.

The stability of these 'natural' formation designs over a year in the presence of orbit perturbations is investigated using a mean orbit element propagator (refer to section 3.1.1.2). The leader-follower formation is found to be stable in the presence of perturbations, although for a planar formation following a frequently repeated ground track, tesseral harmonics were found to cause small but significant long period changes in semi-major axis. The circular and projected circular formations, practical for Earth surveillance and imaging missions, are found to be highly unstable due to the J_2 perturbation. Results demonstrate that the most detrimental effect of Earth oblateness on formation maintenance is the differential drift in longitude of ascending node caused by the difference in inclination of the satellites in the formation. The drift in the line of apsides also introduces error. These and other effects of the J_2 perturbation are considered further in sections 3.1.3.2, 3.1.4.1 and chapter 4.

Relative orbit design software tools have been developed for the AFRL DASL (Distributed Architecture Simulation Laboratory) testbed (Tollefson, 2001) and at ESA (Udrea, 2003), based on the natural formation solutions to the Hill equations. Tollefson implements a form of equations (3-19) for formation design and visualisation, and explores all the possible types of orbit solution in terms of relative orbit amplitudes and phases in the LVLH Hill frame. After the formation has been designed, a two-body orbit propagator determines the actual trajectory of each satellite, highlighting the errors associated with linearisation of the Hill equations. Orbit perturbations are not included. Useful design parameters are obtained from the propagated motions, for example, closest approach distance and time for different combinations of potentially high numbers of satellites in the formation.

For interferometer design, the natural formation dynamics derived from the Hill equations are considered in conjunction with efficient u-v plane coverage and performance metrics based on image quality (Mallory et al. (1998), DeCou (1991)).

Kong, Miller and Sedwick (1999), (1999b) examine formation architectures where only zero-fuel or natural solutions are used as trajectories for the telescope satellites of an optical interferometer. These comprise a 2:1 free ellipse in the vertical plane (x-y in the Hill frame) and oscillatory motion in the cross-track (z) direction, which form natural bounded solutions to the Hill equations (equations (3-19)).

Their formation design proceeds by the fitting of a circular paraboloid to the free elliptical relative motion trajectory, and the combiner spacecraft would then be located at the focus of the selected paraboloid, enforcing the requirement for equal path length from a distant target. Kong et al. (1999) investigate the family of potential paraboloids which can be applied to a given ellipse, and derive an optimum formation based on minimising the fuel required to hold the combiner in a position offset from the Hill origin. Only a limited number of paraboloids can be fitted, thus limiting the number of projected circular formations and therefore operational lines-of-sight. To image any part of the Earth's surface requires the formation to be steerable, and Kong et al. propose that this can be achieved by delay line adjustment to enable the same wave front to be interfered at the combiner spacecraft.

The limitations of this study include the fact that only instantaneous u-v coverage associated with Fizeau interferometry is considered. This requires larger apertures, and for the shortest required baseline these must be located impractically close together (within two aperture diameters) risking collision or plume impingement. The orbital dynamics studied here also does not include perturbations in the equations of motion, although they conclude that the propellant requirement for a GEO Earth imager would be 'rather small to affect the results'. Using similar formation design process, Kong et al. (1999b) proposed an interstellar imager to operate in a low Earth Sun-synchronous orbit (this was reviewed in section 3.1.2.2).

Vaddi, Vadali and Alfriend (2003), (2002) attempt to identify new initial conditions which enable the design of closed relative orbits for satellite formations, and which take into account nonlinearity in the Hill equations and orbit eccentricity. Initially, the Hill equations are extended to include quadratic terms, and solved using a first order perturbation solution, and a bounded solution to the linear Hill equations written in terms of true anomaly is obtained for an eccentric reference orbit. Perturbation solutions are then derived for the combined nonlinear and eccentric problem.

It is also possible to combine the Hill frame initial conditions with relative orbit elements considerations to incorporate the effects of the J_2 perturbation in those conditions and prevent the consequent drift (Vadali, Vaddi, and Alfriend, 2001). Schweighart and Sedwick (2001a) derive new Hill-type linearised relative motion equations, and closed form solutions which include the J_2 perturbation. The effects of J_2 on the formation are considered further below (section 3.1.3.2) and in chapter 4.

3.1.3.2 Orbit Design Using Relative Orbit Elements

The use of relative orbital elements to describe relative motion dynamics was introduced in section 3.1.1 and their particular application to formation design

complements the considerations for the Hill description of relative motion (section 3.1.3.1). The constraint in terms of orbit elements equivalent to that specified in equation (3-17) in the Hill frame is given by equation (3-20).

$$\delta a = 0 \tag{3-20}$$

Of all the orbit elements which describe unperturbed motion of each satellite, the only relative parameter which prevents the formation from drifting apart is semi-major axis, a, as this enforces matching of the orbit period of each individual satellite, and prevents secular growth in along-track separation. The Hill equations conditions hold for circular orbits and small relative orbits, however, the relative orbit elements constraint applies to elliptical orbits and relative orbits of any size. Under this constraint, the formation will expand and contract, but the motion will remain bounded and the maximum amplitude of oscillatory along-track motion y is given by $2a\delta e$. The conversion of equation (3-20) back into the Hill frame using the linear mappings (equations (3-14), section 3.1.1.3) for small eccentricity, e, produces the new Hill frame constraint for bounded motion. When eccentricity is zero, equation (3-21) reduces to equation (3-17) (Schaub and Junkins, 2003).

$$\dot{y}_0 + (2 - 3e)nx_0 = 0 \tag{3-21}$$

In the absence of perturbations, a class of 'rotating formations' which retain their shape when viewed from Earth is defined by Hughes and Hall (2000). The formation size and angular separation between the satellites, which is deemed a measure of formation performance, are designed in terms of orbital elements of the deputy satellites. These are separated by right ascension of the ascending node and true anomaly in order to form an elliptical relative orbit with respect to an equatorial circular reference orbit. Analytical expressions relating design parameters and the orbital elements are derived, and applied to optimal formation design for different numbers of satellites in the formation. No orbit perturbation effects are included in the analysis.

Tan, Bainum and Strong (1999), (2000) propose the design of relative orbits in order to maintain a constant along-track separation between satellites in an elliptic orbit for magnetic field measurements. As the separation would have to be continually controlled at great expense if the satellites followed each other in an identical orbit due, in particular, to their relative motion towards apogee and perigee, an alternative is proposed. Each satellite retains the same semi-major axis, but these are reoriented so that each argument of perigee is slightly different, and the phase angles are correspondingly adjusted so that the satellites retain their separation without control (to around 2.4% in the unperturbed case).

J_2 Invariant Relative Orbits

Significant research at Texas A&M University has been performed into the derivation of constraints that ensure bounded relative motion of satellites in any orbit when subject to the J_2 perturbation, and in this context the bounded relative orbit is defined as a J_2 invariant relative orbit (Schaub and Alfriend, 1999), (Alfriend and Schaub, 2000), (Alfriend, Yan, and Vadali, 2002).

The effect of J_2 on a satellite orbit is discussed further in chapter 4, however in summary the perturbation is known to cause:

- Short and long-period oscillatory effects on relative motion
- Secular drift in the mean longitude of ascending node (Ω)
- Secular drift in the mean argument of perigee (ω)
- Secular drift in the mean anomaly (M)

To overcome the secular drifts, constraints on the mean orbit elements are derived to eliminate their effects on relative motion to first order. (The short period motions due to J_2 are not considered in the derivation of conditions for bounded motion). The following conditions on the relative orbit elements are found to hold (Schaub and Junkins, 2003).

$$\begin{aligned} \delta\eta &= -\frac{\eta}{4}\tan i\delta i \\ \delta L &= \frac{J_2}{4L^4\eta^5}(4+3\eta)(1+5\cos^2 i)L\delta\eta \end{aligned} \tag{3-22}$$

where i is inclination, δ denotes relative parameters, L is a non-dimensional measure of semi-major axis, a, (r_E is Earth radius), and η is a function of eccentricity, e, given by equations (3-23).

$$\begin{aligned} L &= \sqrt{a/r_E} \\ \eta &= \sqrt{1-e^2} \end{aligned} \tag{3-23}$$

The secular drifts in Ω, ω, and M are functions of L(a), η(e) and i, and for these drift rates to be matched ($\delta\dot{\Omega}, \delta\dot{\omega}, \delta\dot{M} = 0$), a, e and i must be equal which does not leave much flexibility in the formation design (Schaub and Junkins, 2003). Instead, the relative argument of latitude rate (the derivative of δf in Table 3-3) is constrained to zero and equations (3-22) result. These conditions are applied to a J_2 invariant relative orbit formation design test case for the verification of a relative dynamics model in chapter 4.

J_2 Invariant Orbits

Koon, Marsden, Murray and Masdemont (2001) use Routh reduction and Poincare section techniques to identify J_2 invariant orbits for a single spacecraft (whose orbit therefore remains periodic in the presence of J_2). A simplified equation of motion for an individual satellite in LEO and subject to the J_2 perturbation is defined. The radial positions and velocities of the spacecraft with respect to the rotation axis of the Earth, are plotted against each other each time the satellite crosses the equator over a number of orbits to create a Poincare map. Concentric lines of constant spacecraft energy are produced on the map for different initial conditions. These lines encircle a single point that represents a periodic orbit, and the initial conditions associated with this periodic J_2 invariant orbit can then be deduced. For formation design, it is possible to select a number of nearly-J_2-invariant orbits from the Poincare map near the periodic orbit point. The authors use this method to identify initial conditions at the equator for each satellite to enable the formation to be maintained for many years without being controlled. This

is because the satellites have the same energy, the same out-of-plane component of angular momentum, and the orbits are near circular (but not quite closed). Ultimately, the effectiveness of this and the mean orbit elements approaches to formation design depends on the additional fuel that would be required to counteract any short-period station keeping requirements of a particular mission.

3.1.3.3 Discussion

The design of practical natural formations of satellites that require no fuel to maintain can be achieved by either a Hill equations or orbit elements approach. While these formations are important to reduce fuel use to practical levels over a mission lifetime, a formation design will be strongly application dependent, and certain manoeuvres may take a satellite outside its natural orbit. It is possible to derive solutions to unperturbed relative motion equations and constraints on orbit elements which will ensure that the formation does not drift apart over time, however in the presence of perturbations, the problem becomes more complex. In this section, examples from the literature have highlighted that both approaches have been applied to mission design. A Hill equations approach has been selected for interferometry mission design where greater continuous relative motion precision is required, and the orbit elements approach has been used for the design of a scientific measurements mission, which did not require precision formation flying to the same degree. Table 3-5 summarises the relative merits of each approach to formation design in LEO.

Hill Equations	Orbit Elements
• In the absence of perturbations the Hill equations are straightforward to solve to provide initial conditions for bounded relative motion.	• No equations need to be solved to derive a suitable bounded motion constraint. In the absence of perturbations, a simple semi-major axis constraint based on orbit period matching satisfies the bounded motion requirement.
• A number of practical formations can be visualised – in-plane, repeat ground-track, circular and projected circular formations.	• More difficult to visualise bounded formations, particularly for specific applications.
• Formation design is limited to circular reference orbits and small relative orbits.	• Formation design is immediately applicable to eccentric reference orbits and any relative orbit.
• In the presence of orbit perturbations, a range of techniques can be used to augment and solve the Hill equations to obtain new bounded initial conditions.	• In the presence of the J_2 perturbation, relationships between relative orbital parameters have been derived to prevent drift.
• Approach applied to precision interferometry mission formation design.	• Approach applied to less precise scientific field measurement formation design.

Table 3-5: Comparison of Hill Equations and Orbit Elements Approaches to Formation Design

3.1.4 Orbit Perturbations and Formation Flying

The orbital perturbations experienced by a satellite in LEO force it to deviate from the ideal Keplerian motion, and significantly complicate formation flying mission analysis. The main LEO perturbations are considered with reference to studies performed in the literature, primarily for comparison with results obtained later in the thesis. The perturbations considered in this section include:

- Earth oblateness
- Atmospheric drag
- Solar radiation pressure (SRP)

Although not an orbit perturbation, reference orbit eccentricity is also considered in this section.

The aim of this section is to summarise qualitatively the studies that have considered the effects of orbit perturbations on formation flying in LEO. The mathematical treatment of relative motion in the presence of perturbations is given in chapter 4 where the effects are independently evaluated. In particular, the focus of chapter 4 is the development and comparison of mathematical models to evaluate the relative effects of the J_2 perturbation.

3.1.4.1 Earth Oblateness

Over the past five years, significant research has been performed into the development of LEO formation flying models which incorporate the perturbing effects of drag, solar radiation pressure and higher order gravitational forces. As stated earlier, the assumption that the Earth is perfect sphere, when it is in fact an oblate spheroid, introduces the most significant error to the relative motion dynamics model for multiple similar spacecraft (Sabol et al, 2001), (Sedwick, Miller, and Kong, 1999). The effects of higher order harmonics in the geopotential on relative satellite motion are relatively small (Wiesel, 2002), however, it would be appropriate to investigate further the long-term effects of these.

The J_2 perturbation has been included in both Hill-type and relative orbit elements dynamics models to improve model fidelity (some of these were introduced in section 3.1.1). In addition, solutions to the equations of motion including J_2 have been obtained for formation design and the derivation of initial conditions for invariant orbits (section 3.1.3). In these contexts, an overview of much of the recent literature has already been provided in earlier sections. In some cases, the models have been used for control system design or the perturbation accelerations imparted to the formation have been evaluated in order to quantify a formation keeping ΔV. A summary of results is presented in Table 3-6 where values of ΔV from each source have been converted to $ms^{-1}yr^{-1}$ for comparison.

In addition, a number of studies incorporate the J_2 acceleration terms into the control system design, but evaluate the ΔV required to eliminate an initial error in relative position, rather than investigating the formation keeping fuel requirements for a greater duration in the perturbed environment (Schaub and Alfriend, 2001), (Tan et al, 2000).

If not included in part of a control system design, the mathematical models of the J_2 perturbation may be applied to numerical simulations of the LEO environment within which the control laws are tested, or used to generate more accurate guidance functions.

Ref.	J_2 Relative Dynamics Model	Control System	ΔV Evaluation Method	Scenario	ΔV $ms^{-1}yr^{-1}$
1	Hill equations describing relative motion of two perturbed satellites with differential J_2 forcing function for a polar orbit only.	No control system considered.	Dimensional Analysis and summation of the perturbing acceleration. Calculates ΔV required to eliminate differential J_2 perturbation between two satellites.	Polar orbit r=800km, 250m separation.	26.1 ($0.005ms^{-1}$ per orbit)
2	Hill equations dynamics model with J_2-related forcing function.	Optimal control of inverse dynamics with optimised formation rotation rate.	Summation of continuous thrust responding to filtered relative motion.	Projected circular formation with elliptic chief orbit.	28.12
3	Hill equations dynamics model with differential J_2 and drag forcing functions.	No control system considered.	Summation of the perturbing acceleration. Calculates ΔV required to eliminate differential J_2 perturbation between two satellites.	In-plane leader-follower in circular orbit, r=600km, i=82°, 100m separation.	30
4	Hill equations without perturbations used to generate desired relative reference trajectory.	LQR control system (Impulsive - In-plane control only with impulses every 1/4 orbit).	Summation of accelerations applied by controller when operations are simulated in the fully perturbed environment.	Projected 1km circular formation, Polar orbit. r=800km.	24.6
5	Hill equations without perturbations, but with a modified orbital rate to account for J_2 used to generate desired relative reference trajectory.	LQR control system (Impulsive - In-plane and cross-track control with impulses every hour).	Summation of accelerations applied by controller when operations are simulated in the J_2 perturbed environment.	Projected 1km circular formation, Polar orbit. r=800km.	49.6
6	Velocity matching condition on the relative orbit is converted to desired orbit elements for each satellite. Semi-major axis of follower satellites is modified to compensate for J_2 perturbation effect on along-track relative drift.	LQR control system (Impulsive - In-plane and cross-track control with burns 3 times per orbit).	Summation of accelerations applied by controller when operations are simulated in the fully perturbed environment.	Circular orbit, r=700km, 1km cluster radius.	10-30

7	Hill equations solutions excluding periodic terms.	LQR discrete control system (In-plane control only).	Summation of accelerations applied by controller when operations are simulated in the fully perturbed environment.	r=500km, i=62.8^o	14.85 at maximum Solar activity.
8	Hill equations with orbit elements consideration of J_2.	Impulsive manoeuvres every 30 hours (from derived relation between J_2 effect on orbit elements and force to counteract this).	Summation of accelerations in the presence of J_2 perturbation.	1km Projected circular formation, r=800km.	50
9	Hill equations without perturbations used to generate desired reference trajectory. The perturbed formation is forced to maintain the same orbital rate as the Hill frame.	Sliding Mode tracking control laws.	Summation of continuous accelerations applied by controller when operations are simulated in the fully perturbed environment.	Circular formation, r=800km, polar chief orbit, 1km separation.	73.9-93.9 depending on control law formulation.
10	Hill equations with J_2 forcing function evaluated at a circular polar orbit only.	No control system considered.	Dimensional Analysis. Calculates ΔV required to maintain a single J_2 perturbed satellite on a circular orbit.	Polar orbit r=800km.	78275 ($15ms^{-1}$per orbit)

Table 3-6: Summary of Formation Keeping ΔV Requirements in the Presence of J_2 Perturbations (Reference Key: [1]Sedwick, Miller and Kong (1999), [2]Vadali, Vaddi and Alfriend (2001), [3]Izzo (2002), [4]Sparks (2000a), [5]Sparks (2000b), [6]Chao, Pollard and Janson (1999), [7]Ulybyshev (1998), [8]Sabol, Burns and McLaughlin (2001) [9]Nelson, Sparks and Kang (2001), [10]Sedwick, Miller and Kong (1999))

A primary source of LEO formation flying modelling literature which incorporates the J_2 perturbation in the relative motion dynamics model has been published through the work of Sedwick at MIT (Sedwick, Miller and Kong (1999), and Schweighart and Sedwick (2001a), (2001b), (2002)), in support of the American military formation flying SAR mission, TechSat21. An overview of the research performed for this target mission was presented in section 3.1.2.1. The first entry in Table 3-6 is a ΔV estimate for formation keeping in LEO by Sedwick et al. (1999), based on dimensional analysis of the environmental perturbations, and the introduction of perturbation forces to the right hand side of the Hill equations. The equations of motion are solved and the accelerations and therefore fuel required to eliminate the secular terms in the solutions are evaluated.

Schweighart and Sedwick (2001a) investigate both the absolute motion of the J_2 perturbed formation relative to a circular reference orbit, and the relative motion of two

J_2 perturbed satellites in LEO through Hill-type dynamics modelling and verification using a numerical orbit propagator.

As described in section 3.1.2.1, in order to capture the differential drift in the longitude of ascending node due to the J_2 perturbation, a new cross-track motion model was developed, based on the geometry of intersecting orbital planes (Schweighart and Sedwick (2001a), (2002)). In addition, a correction to the reference orbit was incorporated into the relative motion equations to compensate for the nodal drift and to reduce linearisation errors. Analytical solutions to the equations were derived, and initial conditions obtained to constrain the satellites to bounded motion. When compared with a numerical orbit propagator, a small amount of drift was observed due to the time averaging of terms in the equations.

While the equations are found to approximate relative motion under the J_2 effect very well, this level of accuracy only holds for the special cases of bounded motion. Schweighart and Sedwick (2002) deduce that it is the averaged linearised differential J_2 perturbation terms in their equations of relative motion which prevented some of the cross-track motion characteristics from being captured. Potential improvements to this modelling approach are investigated in chapter 4.

With an emphasis on orbit determination accuracy and long term formation keeping, rather than precision formation flying, Wiesel (2001), (2002), derives a relative motion solution in a Hill equations form which includes Earth oblateness and higher order geopotential terms. A new near-circular reference orbit is determined in a frame which experiences nodal regression due to oblateness. By linearising about this reference orbit, a set of linear, time periodic relative motion equations result, and are solved using Floquet theory. Sectoral and tesseral harmonics and atmospheric drag effects are evaluated at the reference orbit (they vary with time), and the system is solved numerically to reveal any non-secular relative effects which would not need to be counteracted by a control system. It is found that these do not significantly affect relative motion, but may require further modifications to be made to the periodic reference orbit.

Control system design to counteract the differences between the high fidelity model of Wiesel (2002) and a numerical integration solution highlighted the importance of second order secular terms not captured by linear Floquet theory. However, Wiesel (2003) states that impulsive daily control for the elimination of two forms of linear drift in the Floquet solution (equivalent to the drifts due to J_2 highlighted through the design of J_2 invariant orbits using relative orbit elements by Schaub and Alfriend (1999)) for a 400m formation could be reduced to nearly 0.1mm/s per day (inclination=57^o, altitude=637km). For comparison with the data in Table 3-6, this scales up to a ΔV of $0.0365 ms^{-1}yr^{-1}$ but long period simulations would not necessarily yield this result as Wiesel suggests that the build up in errors of the numerical simulation against which the Floquet guidance trajectory is being compared should be taken into account. This combination of analytical and numerical approaches to formation flying dynamics and control is considered further in chapter 4.

It should be noted that it was not the aim to directly compare the ΔV values listed in Table 3-6 as they have been derived for different scenarios, using different controllers, and for formations of differing sizes. A larger formation will require a greater formation keeping ΔV, and impulsive formation control costs vary depending on the frequency of thruster firing and the acceptable tracking error. In addition, a number of the examples use polar and near-polar orbit test cases where the perturbation effects of J_2 are reduced. In rows 8 and 9, the cost of maintaining a relative circular orbit is estimated by Sabol et al. (2001) and Nelson et al. (2001) respectively. In case 9, the increased fuel cost arises from the forced 'Hill' orbital rate.

Although the focus of the literature survey has been limited to the effects of perturbations on relative dynamics of multiple satellites in LEO, a number of authors have investigated the effects of higher order gravitational perturbations on a single satellite. Hashida and Palmer (2001) incorporate terms up to second order in J_2 into an 'epicyclic' motion model which proved a sufficiently accurate formulation for on-board orbit determination. In row 10 of Table 3-6, the cost of eliminating the perturbing effects of J_2 on a single satellite to enforce a circular orbit is estimated by Sedwick, Miller and Kong (1999). In this case, the Hill frame orbital rate is enforced and a very large ΔV is required to compensate for this drift as expected.

In section 3.1.4.3, the use of solar radiation pressure to counteract the relative nodal drift between satellites in orbits of differing inclination is described. In a study for the TechSat21 mission, Williams and Wang (2000a) evaluate this J_2 perturbation effect, and investigate the use of a Solar wing to counteract the nodal drift.

3.1.4.2 Atmospheric Drag

Carter and Humi (2002) incorporate drag terms that are quadratic in the magnitude of orbital velocity into the equations of relative motion of satellites in LEO, building upon their earlier work and rendezvous studies in which drag terms linear in velocity were included. Firstly, the equations of motion of a single satellite subject to gravitational and drag forces are derived in the inertial frame, and an orbit of low eccentricity is assumed (before degradation due to drag). The geometry of the satellite and atmospheric density are included in the equations as part of the drag term. The equation for a second satellite is then derived in the same frame, and linearised differential forces are calculated and included as forcing terms to the equations of relative motion, now written in a rotating LVLH frame based at the first satellite. The equations are rewritten in terms of true anomaly rather than time, and further simplified by mathematical transformations and substitutions. A general form of the differential gravitational and drag terms is retained in the solution, although a later case study replaces these terms with a simple Newtonian gravity field and an inverse law to represent density variation with altitude. Carter and Humi (2002) present a set of closed form solutions to the relative motion equations including drag. These could only be obtained using the inverse atmospheric density law, as an improved density model would not allow solutions to be obtained. However, other ways of modifying and correcting the model to compensate for this are described.

For an initially circular orbit, the equations reduce to the Hill equations, augmented by a drag term. (Equations (3-24) have been modified to correspond to the LVLH (x,y,z) frame used to describe LEO relative motion throughout the thesis (Figure 3-1)). The derivatives are taken with respect to true anomaly rather than time (denoted by the superscript ‘), and the term, α is a physical constant derived from the satellite geometry and drag coefficient. For the familiar free orbit ellipse relative trajectory derived from the Hill equations, the inclusion of drag serves to increase the size and eccentricity of the relative orbit.

$$\begin{aligned} &x'' - 2y' - 3\left(1 + 4\alpha^2\right)x = 0 \\ &y'' + 2x' = 0 \\ &z'' + z = 0 \end{aligned} \qquad (3\text{-}24)$$

This mathematical study is insightful, but no model validation is performed to establish exactly what the limitations of using a poor atmospheric density model might be, or how easy it would be to perform the modifications suggested. The study has provided an alternative mathematical description of the drag gradient as a perturbation on a LEO formation with which to compare the results of chapter 4, although it has not been evaluated in their reference. The study has illustrated how drag force can be implemented into the orbit equations for a single satellite or for relative satellite motion for both circular and elliptical orbits.

In support of the GRACE mission (introduced in chapter 2 and section 3.1.2.3), Mazanek et al. (2000) highlight atmospheric drag as a critical perturbing effect on the leader-follower formation. The leader spacecraft experiences slightly increased drag compared to the follower satellite at their separation (and the satellites also have very slightly different ballistic coefficients), requiring a station-keeping manoeuvre to regularly raise the semi-major axis of the leader spacecraft. This mean differential drag was estimated from mission analysis software which was developed to capture detailed aerodynamic behaviour of the formation in the free molecular flow regime.

3.1.4.3 Solar Radiation Pressure

The Solar radiation pressure (SRP) has a much smaller influence on the relative motion of satellites in LEO than other perturbations, and therefore it has received relatively little attention. Instead, a number of authors have proposed using SRP as a tool for passive formation control to relieve the demands on propulsive formation keeping.

Williams and Wang (2000a), (2000b), (2001) and Wang and Williams (2002) investigate the use of SRP acting on a Solar wing (a small sail) as a means to control differential J_2 nodal regression for similar Earth-pointing satellites. With the relatively low ΔV requirements over a long duration mission lifetime, this approach is found to be successful in producing the necessary orbit ‘torques’ for controlling average drifts, but does not eliminate short period relative motion.

The motivation for this approach arises through the TechSat21 mission requirements for a formation in near-circular, near-polar orbits. Relative orbit elements analysis revealed the existence, to first order, of J_2 invariant relative orbits which would not diverge significantly over time in the presence of J_2 disturbances (section 3.1.3.2). However for near-polar orbits, the required relative eccentricity for a J_2 invariant relative orbit would compromise formation requirements in the along-track direction. The cost of overcoming the differential J_2 perturbation, as evaluated in a number of simulation studies, is summarised in Table 3-6, section 3.1.4.1.

An optimal scenario occurs when the Sun lies in the orbit plane, with a wing oriented at approximately 45^o to the velocity vector (gravity gradient stabilisation is assumed). However, a net along-track ΔV is also generated when the Sun is outside the orbit plane, but this is much smaller than that required to eliminate differential J_2. Zero corrective torque is generated when the Sun is normal to the orbit plane as the same face of the Solar wing is then illuminated throughout the orbit. Williams and Wang also take into account the fact that the ecliptic does not lie along the equator. This offsets the Solar torque on the orbit and causes both sinusoidal variations in relative orbit inclination and nodal drift.

Techniques to passively overcome the along-track ΔV are investigated and include reorienting the wing, by introducing a periodic yawing motion or aligning it with the velocity vector (without eclipse). A suitable wing size to ensure bounded motion was evaluated by numerical simulation, and it was found that a $3m^2$ wing area was required for a 100kg spacecraft.

In their more recent paper, a full dynamics model for the relative motion is derived using the Gaussian form of the variation of parameters equations describing the change in orbit elements under the SRP perturbation, rather than just considering Solar wing area (Wang and Williams, 2002). A state space equation is derived through linearisation by Taylor expansion of the differential rates of the orbital elements. Their original equations of relative motion allow J_2 to affect both satellites, but only one has a Solar wing and experiences any Solar radiation pressure perturbation. The state matrix expressed in terms of differential orbit elements is unstable without SRP control and therefore a basic regulator feedback control system is implemented using gains determined according to the control authority available from the wing system, and by ensuring system stability.

Burns et al. (2000) examine the effects of SRP on the relative motion of satellites with significantly different area to mass ratio. In this case, simulation results are generated for an orbit altitude of 2000km where forces due to Earth oblateness and atmospheric drag are significantly smaller than in LEO. Earth radiation pressure and albedo are also neglected. The leader satellite is assumed to follow Keplerian motion, and the follower is perturbed by SRP due to its large area to mass ratio. Reflection of the incident light is considered, however the change in projected spacecraft area due to the changing angle between the Sun and vehicle faces during orbit are not considered, and the spacecraft is assumed to be a flat plate. The components of the derived SRP force are expressed in local radial, along-track and cross-track components so that its effects can be evaluated in the Gaussian variation of parameters equations (equations (3-6) to (3-12), section

3.1.1.2) (Chobotov, 2002). Secular growth in the semi-major axis of the perturbed follower satellite orbit is discovered, which would cause the formation to drift apart in both the radial and the along-track direction. Again, a spacecraft reorientation strategy is proposed to counteract the disturbance. The importance of including Earth shadow models in the analysis are demonstrated and this has a significant effect on cross-track relative motion.

The analyses presented here are general and the proposed systems would require considerable redesign for practical implementation on a specific mission. The effects of SRP on relative motion have been established through the calculation of variations in the orbit elements, but the Solar wing strategies for eliminating nodal and along-track drift must be accurately tuned to a particular orbit and scenario.

3.1.4.4 Orbit Eccentricity

Although not strictly an orbit perturbation, the Hill-type relative dynamics models introduced in section 3.1.1 have been augmented to include eccentricity effects as a nonlinear characteristic, and on some occasions, eccentricity is implemented within the equations as a perturbing force. In this section, the intention is to highlight some of the literature where the effects of eccentricity on relative orbits, dynamics models, and initial conditions have been reported, and in particular to introduce literature relevant to the investigations later in the thesis.

Implicit within the Hill equations derivation is the assumption of a circular reference orbit. Of course satellites in LEO do not trace a circle, and the Hill frame description of relative satellite motion is not accurate. A relative orbit elements approach to relative motion modelling in elliptical orbits is straightforward, and often preferred, however, a number of authors have developed and solved analytical models which approximate relative motion about an elliptic reference orbit in a LVLH frame. The result is a selection of relative motion models of varying degrees of accuracy in a Hill equations form.

Useful examples are described below:

- Melton (2000) derives Hill-type equations which incorporate time varying reference orbit radius and angular rate. The equations are converted to cylindrical coordinates and solved by obtaining a state transition matrix where time varying terms are approximated by series expansions in eccentricity.
- Inalhan and How (2000) also investigate closed form solutions to a similar set of linear time varying equations of relative motion based on an elliptic reference orbit. Bounded motion over an orbit period is demonstrated, and initial conditions suitable for formation design (in terms of both time and true anomaly at zero) are derived.
- Tillerson and How (2001) build on the work of Inalhan and How (2000) to find bounded motion initial conditions at any point in the eccentric orbit (true anomaly can take any value). Discrete control using optimal path planning is applied using both the time varying elliptical system and the Hill equations. The initial conditions, determined from the elliptical relative motion model, are

required to achieve a realistic end state in the control problem (using initial conditions derived from the Hill equations is costly), but the basic time-invariant Hill equations dynamics are sufficient for the controller design, and less computationally intensive to implement.

- Broucke (2002) develops linearised elliptical equations of relative motion using an orbit elements approach. A state transition matrix solution is obtained, and the ΔV required to rendezvous with the target in a given period of time is derived.
- Yamanaka and Ankersen (2002) solve the linear relative motion equations for an elliptical orbit and obtain a simpler form of the state transition matrix by performing a number of algebraic transformations. This solution is deemed suitable for practical use, avoiding numerical integration.
- Vaddi, Vadali and Alfriend (2003) investigate the effects of eccentricity on the Hill equations. Corrections to the Hill initial conditions are derived to generate bounded relative motion solutions in terms of time, rather than true anomaly.

Although elliptical orbits have not been investigated in this thesis, the approaches of the authors in their treatment of and solutions for the linear time varying equations of relative motion have provided a useful resource for the research detailed in chapters 4 to 7. Until the more recent work of Yamanaka and Ankersen (2002), the complexity of the elliptical equations and computational effort required to solve them offset the improvements in model fidelity achieved in terms of their practical use. In time varying form, the models appear to be suitable for off-line research into the relative dynamics in the more practical LVLH frame, but unnecessarily complex for the minor fuel use benefits associated with implementing them within formation flying control laws.

3.1.5 LEO Formation Flying Guidance and Control

Feedback control is required to minimise the error between the actual and desired relative satellite motion, and to maintain the formation geometry. A number of different control techniques have already been applied to the problem, and a number of these control strategies, designed using the Hill equations or relative orbit elements, have been performance evaluated in the perturbed environment through numerical simulation.

In this section, a summary of many of the papers on satellite formation flying dynamics and control in LEO is presented. Most are simulation studies involving modelling of the relative dynamics and orbit perturbations, the design of a novel control strategy, implementation of a control system and simulation of the system in the perturbed environment, although most individual papers do not describe all these aspects in a single publication. Instead the focus is usually the control system, the model, or guidance functions. The following subsections focus firstly on those studies which investigate more simple (and perhaps more practical) control systems for satellite formation flying where usually there has been some consideration of operational and subsystems issues. Other studies that focus more on the centralised/decentralised control issues and more advanced control systems are briefly discussed in section 3.1.5.2. It is not the aim of the section to present the mathematical theory of each control technique,

as there are many suitable texts available. An overview of literature with an emphasis on guidance strategies is presented in section 3.1.5.3.

3.1.5.1 Linear Quadratic Regulator Control Systems for Formation Flying

There are many examples of the application of Linear Quadratic Regulator (LQR) control design techniques to spacecraft formation flying, and a number of these are reviewed in this section. The appeal of these techniques is clearly apparent, with the opportunity to reduce fuel consumption, the inherent disturbance rejection properties of the controller, and the relative ease with which this tried and tested technique can be applied, particularly for stabilising the Hill frame dynamics.

In 1985 Vassar and Sherwood (1985) designed a closed loop formation keeping controller for satellites in any circular orbit using digital optimal control theory. In their example they apply the controller to a geosynchronous orbit and maintain an along-track desired separation (700m) within satisfactory error bounds. Sample time and thruster firing intervals are selected by considering the acceptable along-track error (which requires frequent corrections) while minimising onboard processing effort (which requires infrequent corrections). The effects of Solar radiation pressure perturbations are considered, and their work also extends to optical sensor and thruster modelling. A similar discrete LQR control design was performed using the Hill equations by Chao, Pollard and Janson (1999) for a 1km radius cluster in LEO.

Ulybyshev (1998) demonstrates that linear quadratic (LQ) feedback control is a good candidate for formation keeping of a large satellite constellation due to its performance and robustness. A discrete control system is applied to both the along-track secular drift error between satellites and an orbital period error relative to the circular reference orbit (Hill frame). The controller performance is evaluated by simulating relative satellite dynamics in the presence of aerodynamic drag where different satellites decay at different rates.

Irvin and Jacques (2001) implement three forms of LQR controller for performing satellite reconfigurations. Initially, a basic fixed gain LQR control system is designed for the linearised Hill equations. A second approach retains the nonlinear Hill dynamics, and the linear and nonlinear systems are controlled separately by LQR and linearising feedback respectively. A third control approach is proposed using the "State Dependent Riccati Equations (SDRE) technique" with the nonlinear Hill equations. In this final case, the nonlinear dynamics are propagated and a new controller gain matrix is evaluated at each time step.

The test cases for which the control systems are evaluated are based on the relative orbit ellipse, described in the section on formation design (section 3.1.3.1), and relative orbit semi-minor axis reconfiguration manoeuvres are evaluated for small and large relative orbits. For small relative orbits there is no apparent advantage in using the more complex nonlinear techniques, and the linear Hill equations of relative motion are found to be a good approximation. For large relative orbits, the LQR with linearising feedback achieves a much better performance than the linear LQR and SDRE approaches.

However, no perturbations are considered in the simulations. The designs are also compared to an open loop impulsive control system which uses less fuel, but achieves the desired position over a much greater settling time. The findings are summarised below for small reconfiguration manoeuvres:

- Continuous control uses more fuel than discrete control.
- Continuous control methods do not take into account the optimal positions in the orbit to do a burn.
- Truly optimal controllers will need to also take into account the best duration for which to make a burn in the orbit in addition to position.
- Nonlinear control techniques offer little benefit in terms of fuel use and complexity for small relative orbits (the Hill equations are a sufficient approximation to the dynamics in this case).
- For large relative orbits, LQR with linearising feedback demonstrates an improvement in performance over basic LQR as nonlinear effects become more important.

These findings are compared later to those in chapters 4 and 5 where a study is performed into LQR control of a LEO formation in the presence of the J_2 perturbation.

Stansbery and Cloutier (2000) also implement a nonlinear SDRE design for control of two satellites in leader-follower formation in GEO. The same controller acts at each spacecraft forcing the leader to maintain a desired ECI-defined trajectory, and the follower to maintain position relative to the leader by acting upon the targeting error dynamics. The system is evaluated from a range of initial conditions and is found to converge upon the desired trajectories for a large number of test cases, although again, orbit perturbations are not included in the simulations.

A number of sources from the US Air Force Research Laboratory describe the results of research into the design of LQR-type controllers for LEO formation flying control using Pulsed Plasma Thrusters (PPT). Kapila, Sparks, Buffington and Yan (1999), (2000) design full-state feedback discrete controllers to ensure closed loop stability for pulse-type thrusters for formation manoeuvring in GEO (in-plane manoeuvres of 100 metres were performed, perturbed by Solar radiation pressure). Yan, Kapila and Sparks (2000) continue this study using Hill equation dynamics to successfully produce an improved control system with a periodic rather than constant LQR gain. This also has guaranteed closed loop stability for the intermittent pulse-type control action employed throughout the orbit. Yedavalli and Sparks (2000) investigate the stability of discrete control systems derived from continuous models of the relative orbit dynamics. It is proposed but not demonstrated that this hybrid control system, which meets derived stability conditions, will be equivalent to full state feedback (LQR) and will also provide improved efficiency (including smoother responses and smaller control actions). The requirement for the selection of a suitable sample rate for the discrete system is emphasised to ensure the system is controllable.

A switching control system is designed by Yedavalli and Sparks (2001) which switches on and off according to the permitted error in the controlled state variables (relative position and velocity) with the aim of further reducing fuel consumption. The stability of the switched system is investigated, and it is proposed that most of the time, the system does not need to be stable as long as the controlled parameters lie within

acceptable error bounds. The new approach is evaluated using LQR control, and one test case is presented. Additional test cases are required to demonstrate that substantial 'off' times compared to controlled 'on' periods can maintain formation keeping errors within predefined acceptable limits, and again, orbit perturbations are not considered either within the linear model or for controller performance evaluation. Of course the open loop Hill equations dynamics are not stable, and the LEO formation flying problem falls into this framework.

Sparks (2000b) uses a discrete LQ tracker design to minimise the error between actual and desired relative satellite motion in the presence of gravity perturbations. The elliptical formation geometry for a projected 1km circle was maintained within defined error bounds using a controller designed using the Hill equations with a modified orbital rate to account for the J_2 perturbation. In this case, the sampling time for the discrete controller was one hour and tracking error and fuel use performance was evaluated in a gravity-perturbed environment. In a second paper by Sparks (2000a), the formation keeping ΔV using an LQR feedback law is computed as a function of the frequency of the applied control impulses through higher fidelity simulations (including higher degree and order J terms). To maximise their effectiveness, impulses are applied at apogee, perigee and at points mid-way between them. Scenarios using higher frequency impulses are found to use a greater ΔV.

Starin, Yedavalli and Sparks (2001a) design a continuous LQR controller, using non-dimensionalised Hill equations, which allows thrust to be applied coplanar to the local horizon to achieve complete controllability of a two-satellite formation. It is shown that thrust can be avoided completely in the radial direction, and the system is still controllable with controller performance not severely impacted, although it was anticipated that problems would arise in the perturbed environment. Careful selection of the radial control elements in the control weighting matrix for the LQR design enables better fuel efficiency and response time to be achieved, although it is proposed that along-track control has greater authority than radial for a given fuel consumption. The design is assessed using a range of initial separation conditions which are driven to zero (an unrealistic end condition), but the station keeping task in the presence of orbit perturbations is not investigated. In a subsequent paper, manoeuvres between different sized projected circular formations are investigated. The target position of the satellite is transformed into the new virtual origin or leader of the formation, and similar tracking manoeuvres to each 'origin' are performed from different locations on the relative orbit. In this case, LQR control matrix weightings included cross-track control. Again, orbit perturbations were not considered in the evaluation (Starin, Yedavalli, and Sparks, 2001b).

Yamanaka (2000) presents a feedback and feed-forward control law, implementing LQR optimal control theory for relative translation control of satellites. Relative translation and rotation is derived in the ECI frame and converted to a coordinate frame based at the leader satellite. A dynamics model of relative attitude is controlled by simple PID (Proportional-Integral-Derivative) feedback control.

3.1.5.2 Other Formation Flying Control Systems and Strategies

In this section, a brief survey of some of the literature describing the implementation of alternative control systems, or control strategies embedded within guidance, planning and centralised/decentralised control is presented. In addition, LEO controllers derived around orbit elements descriptions of relative motion are reviewed.

Guidance and Control Using a Perceptive Frame

Morton, Weininger and Tierno (1999) and Tierno (2000) design a natural projected circular formation using the Hill equations for a distributed aperture radar concept. Their system has a distributed decentralised control architecture and uses perceptive control theory for formation reconfiguration in the presence of orbit perturbations.

Morton et al. (1999) derive satellite separation functions and characterise the satellite orbits in terms of energy and eccentricity. These orbits provide a framework for a multi-satellite bidding scheme for satellite manoeuvring to ensure fuel use minimisation and optimisation, and satellite separation across the cluster. Tierno (2000) addresses the control of this formation using onboard real-time guidance using an abstract "perceptive action reference" obtained from sensor measurements across the formation. The actual formation centre is derived online from measurements of the other satellite positions and compared to a point on a nominal trajectory closest to the actual centre. The latter is therefore described in a different time frame to the actual motion, and guidance for formation correction is generated in this new perceptive frame. Rather than comparing each individual satellite to its own reference orbit (according to the formation design), formation control in the perceptive frame is possible by combining control of the formation centre (using absolute measurements) with more accurate relative position measurements. A perceptive frame is also intrinsic to the decentralised control system proposed by Kang, Sparks and Banda (2000). Each satellite generates its own control inputs through onboard feedback control (LQR in this case), but coordination of the formation occurs in a perceptive frame based on projected motion of the reference point (an artificial leader) from which relative motion is measured.

Yeh, Nelson and Sparks (2000) design relative motion trajectories to be tracked using a sliding mode control law. The trajectories are derived from Hill equations solutions, with a modified time reference to conserve fuel and increase settling times (a parameterised description of the natural Hill formations is given in Yeh and Sparks (2000)). The control law is adapted for pulse-type formation control, and demonstrated in a fully perturbed simulation environment. They demonstrate that, as expected, most formation keeping fuel is expended in overcoming the J_2 perturbation.

Nelson, Sparks and Kang (2001) combine the above approaches by using a perceptive frame for trajectory planning and sliding mode control for trajectory following. Again, using the Hill equations solutions to prescribe a projected circular formation firstly as standalone reference trajectories, and then modified to include a perceptive frame, the control law is performance evaluated in the perturbed environment. A perceptive frame was found to improve the formation keeping efficiency of a leader-follower hierarchy as the change in orbital rate due to the J_2 perturbation was detected in the leader-based perceptive frame. The follower trajectories generated from this were therefore closer to

reality than those just generated from the solutions to the unperturbed Hill equations. A decentralised approach balanced fuel use more evenly across the formation, but was more costly. The benefits of the new approach are evident for formation reconfiguration of a decentralised formation following the average formation position as a reference. Trajectory planning in the perceptive frame is also presented in greater detail with LQR feedback in Kang, Sparks and Banda (2001), and for attitude control by Kang and Sparks (2002).

Linear Control Systems with Hierarchy Considerations

At Stanford University, Robertson, Inalhan and How (1999a), (1999b) have simulated and tested on a ground-based testbed formation keeping and trajectory planning control systems. They describe their implemented control hierarchy, and evaluate alternative scenarios whereby either each spacecraft operates independently (with relative position knowledge), or optimal control is used to balance fuel use between the two spacecraft. For bang-off-bang feedback control, optimal simultaneous satellite control is found to be more efficient than either classical feedback or by having independent controllers on each satellite. However in contrast, Vadali and Vaddi (2000) show that manoeuvring one satellite to maintain formation with another is more efficient than balancing the manoeuvres between both (for the particular case of formation initialisation requiring the control of relative inclination while holding other relative orbit elements constant).

Robertson et al. (1999a) discuss potential control architectures (forms of centralised, decentralised, and leader-referenced control), and the role of an 'autonomous formation coordinator' in ensuring fuel balancing across the formation is demonstrated. In their study, an outer-loop path planner uses the unperturbed Hill equations as a dynamics model to prescribe optimal relative motion trajectories. These trajectories are provided as inputs for testbed demonstration and fuel use evaluation, and are followed by the onboard controllers of each model.

Although Naasz, Karlgaard and Hall (2002) consider LQ control to be a suitable and adequate technique for satellite formation flying control, they propose that improvements in performance and robustness may be achieved using an H-infinity control system. Again the Hill equations are used for dynamics modelling, and the state equation is written in discrete form as pulsed plasma thrusters will be implemented on their satellite. The problem is expressed as an optimisation problem with a cost function which must be minimised with respect to the control inputs (thruster demands) and maximised with respect to model uncertainty. H-infinity control design is also applied to the European ATV (Automated Transfer Vehicle) rendezvous problem to ensure accurate tracking of a position guidance function (Bourdon, Delpy, Ganet, Quiquis, and Ankersen, 2003).

Nonlinear Controllers for Satellite Formations

Nonlinear Lyapunov control is frequently applied to the LEO formation flying problem. Naasz et al. (2002) also design nonlinear Lyapunov controllers for both the nonlinear Hill equations in a Cartesian frame, and for mean orbit element feedback. The control laws are compared through manoeuvre simulation and convergence to the desired trajectory from an initial offset. Orbit perturbations are not considered, and the Lyapunov control laws are found to achieve the best performance compared to other linear controllers.

A number of researchers at Polytechnic University, New York have derived a series of Lyapunov-based adaptive controllers for formation flying control based on a nonlinear equations of relative motion in an elliptical orbit reference and Hill frames (Yan, Yang, Kapila, and de Queiroz, 2000), (de Queiroz, Kapila, and Yan, 1999), (de Queiroz, Kapila, and Yan, 2000). In the latter case, the ability of this continuous control system to track a desired relative trajectory is demonstrated in the presence of a simplified representation the orbital environment and perturbations.

The relative mean orbital elements approach to relative dynamics modelling and control was introduced in section 3.1.1.2. There, the work of Schaub, Vadali et al. (1999) on the comparison of Lyapunov mean orbit element and inertial Cartesian position and velocity feedback control laws, and the work of Schaub and Alfriend (2000b), (2001) on impulsive control using relative orbit elements for the maintenance of J_2 invariant relative orbits was reviewed (J_2 invariant relative orbits were briefly described in section 3.1.3.2).

In both the continuous and impulsive relative orbit element control laws, the elements of the follower satellite are corrected at optimum points within the orbit, so that the elements being controlled do not affect the remaining osculating elements. The ΔV imparted by the impulsive control system is derived analytically in relation to the mean orbit element being corrected, the size of the correction, and the location on-orbit that the correction would take place. A relationship between the effects of osculating inclination on mean semi-major axis and eccentricity are incorporated into the system model to improve fidelity. Upon implementation, the mean element errors from desired are established at some arbitrary point in the orbit and are then held constant during the orbit. Between impulses, the satellites are allowed to drift uncontrolled. Whether this level of formation keeping accuracy is sufficient is dependent on user requirements. J_2 invariant relative orbits reduce the effects of the gravity-perturbation significantly before the controller is even applied. The suitability of this approach was considered in the context of relative dynamics model development in section 3.1.1.2.

Schaub and Alfriend (2000a) again apply continuous Lyapunov control to a hybrid orbit element-Hill frame system (introduced in section 3.1.1.3). Desired relative motion is specified in terms of relative orbit elements, but these are transformed into a Hill-type Cartesian LVLH frame within which sensor measurements can be compared. Again, asymptotic stability of this type of controller is demonstrated, and despite the number of coordinate transformations between mean and osculating elements and the local LVLH frame, satisfactory performance is achieved in a geopotential-perturbed numerical simulation environment.

A disturbance accommodating control system is proposed for controlling multiple satellites in the presence of the J_2 perturbation, while minimising and balancing fuel consumption across the formation (Vadali, Vaddi and Alfriend (2001), Alfriend, Vadali and Schaub (2001)). The Hill equations, which are solved to generate a relative trajectory for a projected circular formation, are modified to include both along-track rate increases and nodal drifts due to the J_2 perturbation. In particular, the cross-track relative motion equation includes a J_2 related forcing term. The novel control design in this case imparts an additional slow rotation to the circular formation to ensure that all

the satellites in the formation experience a maximum inclination difference, which is the most costly relative position to maintain. The optimum rotation rate is obtained by minimising a cost function based on control inputs that have been defined to impose a rotation rate and to counteract the J_2 forcing term in the cross-track equation of motion. For the test case evaluated, an optimal formation rotation rate was identified and fuel consumption was reduced using this disturbance cancellation technique.

3.1.5.3 Low Earth Orbit Formation Flying Guidance Strategies

A number of guidance strategies have already been introduced in sections 3.1.5.1 and 3.1.5.2. In their simplest forms, the natural solutions to the unperturbed Hill equations can form reference trajectories that satellites within a formation can be forced to follow. In section 3.1.5.2, the concept of the perceptive frame for leader-follower and decentralised formation path planning and control has already been used by a number of authors (Nelson et al, 2001), (Tierno, 2000). A survey of satellite formation flying literature where guidance strategies form the primary focus of the GNC system is presented below. In particular, strategies for fuel balancing or load levelling while manoeuvring a satellite formation in LEO are highlighted.

Satellite formation flying guidance systems generate the desired trajectories for satellites to follow as a control system reference. Their complexity can range from simply producing a 'constant' reference, for example a fixed relative position that a satellite must maintain with respect to a second, or a time varying trajectory that is predetermined offline. More complicated guidance systems integrate onboard parameter measurements with planning algorithms which may intelligently update in real time. Guidance can be provided to both leader and follower satellites in a formation or to a formation adopting decentralised control. The functions will vary depending on application and operational mode, and may involve switching logic. The primary modes of operation considered here are formation maintenance and reconfiguration in LEO.

The simplest form of guidance trajectory has a profile of straight lines, defining constant values of acceleration, deceleration and velocity in order to perform a manoeuvre. The desired profile may be augmented with limiters to prevent excess velocities and accelerations being demanded.

For satellite formation flying in LEO the effect of the gravity well environment must be taken into account for a practical guidance system and suitable reference trajectories can be generated through dynamics models of relative motion. Since relative motion measurements are likely to be made in a Hill LVLH frame (refer to section 3.1.1) based at the leader satellite or designated reference position, rather than in terms of orbit elements, the natural solutions to these equations can be used to produce bounded reference trajectories for practical formations. For the basic linear, unperturbed Hill equations, these are prescribed by Sabol et al. (2001). However, a higher fidelity model will generate trajectories closer to the real orbits, and the fuel used to follow these trajectories will therefore be reduced. A set of natural trajectories including the J_2 perturbation are derived in chapter 4.

Two of the primary benefits of analytical relative dynamics models (in terms of both the Hill frame and relative orbit elements) for formation guidance include:

- The insight provided by the bounded solutions which can be used to:
  - Control particular orbit elements at optimum positions in the orbit (Schaub and Alfriend, 2001),
  - Control multiple elements simultaneously with a carefully selected single burn (Lovell, Tragesser, and Tollefson, 2004),
  - Derive the sequence of a combination of burns to achieve a desired reconfiguration manoeuvre (McLaughlin, Alfriend, and Lovell, 2002), (Vaddi, Alfriend, and Vadali, 2003).
- The facility to express natural orbits as terminal constraints for optimal trajectory generation (Kong and Miller, 2001).

In the first instance, some authors use the relative dynamics models to plan individual burns to optimally or strategically reconfigure a formation. Where a continuous manoeuvre is required, for example to reorient or resize a LEO formation, the problem becomes one of optimisation.

Kong and Miller (2001) derive minimum energy trajectories to manoeuvre a formation in LEO for initialisation and resizing, using a numerical optimal control approach. After selecting a quadratic cost function to minimise fuel use, and establishing the initial and end states of the system on natural orbits, calculus of variations is used to generate suitable trajectories. A significant proportion of the work is concerned with establishing suitable terminal states for the formation, using computationally expensive shooting and iterative methods. An early form of the time invariant relative dynamics model incorporating the J_2 perturbation, derived by Schweighart and Sedwick (2001a), is applied to the optimal control problem, and a number of test cases are evaluated. The ΔV required is found to reduce significantly for increasing manoeuvre time, and beyond a one orbit period manoeuvre duration, the peak thrust used is reduced, although the total ΔV requirement does not reduce. Neither limiting power constraints nor plume avoidance are considered in this study, but the latter is incorporated into the linear programming optimisation strategy described by Richards, Schouwenaars, How, and Feron (2002) and the minimum time and fuel manoeuvres derived by Campbell (2002).

Massari et al. (2004) also generate real time optimal reconfiguration manoeuvre trajectories in LEO by integrating a discretised linearised time varying elliptical relative motion dynamics model in the Hill frame (section 3.1.4.4). The solution is augmented to account for control inputs and disturbances. Collision avoidance constraints are applied, and the optimisation problem is simply reduced to a fuel minimisation requirement. An error threshold is defined, and if exceeded, the trajectory is updated in real time. The same terminal condition is reached in the desired time, and the technique is found to significantly reduce fuel consumption.

Milam, Petit and Murray (2001) use optimal control to actively control a satellite formation in real time. Their Nonlinear Trajectory Generation software is designed for onboard computation of formation keeping and reconfiguration manoeuvres in LEO, using an inertial dynamics model which incorporates the J_2 perturbation.

A Hamiltonian mechanics approach to finding optimal control laws and guidance functions by solving two point boundary value problems associated with satellite formation manoeuvring within a fixed period of time is adopted by Scheeres, Park and Guibout (2003) and Guibout and Scheeres (2004a).

Fuel Balancing Considerations for LEO Formation Flying

In general, the most fuel consuming phase of satellite formation flying operations in low Earth orbit is formation reconfiguration where spacecraft are forced to manoeuvre from one natural relative orbit to another. Depending upon the type of actuation system on board the different spacecraft, and the spacecraft masses, it may be important to balance the fuel use across the formation to ensure all spacecraft have an equal lifetime. Of the references already considered earlier in this section, the following consider fuel balancing control:

- Robertson Inalhan and How (1999a) assess the effects of relative fuel usage through simulations of manoeuvres with different fuel use weightings on different spacecraft in the formation, however, the weighting selections are not autonomous.
- Vadali et al. (2001) design a disturbance accommodating control system to counteract the effects of the J_2 perturbation while minimising and balancing fuel consumption across a circular formation in LEO through enforced formation rotation.

3.1.5.4 Formation Flying Control Systems Summary

This review of recent literature has revealed a significant number of alternative approaches taken to simulate and control a satellite formation in LEO. The most popular control techniques identified through the review are summarised below. In some cases, combinations of the control techniques have been applied or different techniques have been directly contrasted:

- Linear Quadratic Regulator (LQR)
- Sliding Mode
- H-infinity
- Lyapunov
- Classical

A popular technique is the LQR method, primarily in discretised form and applied to the control of both the linear and nonlinear Hill equations (examples of its application were described in section 3.1.5.1). Some research relates to the control of satellites in GEO, subject to Solar radiation pressure, but the majority investigate the performance and stability of discretised LQR controllers for LEO formations. These formations are derived from the linear Hill equations solutions, and actuated with pulsed plasma thrusters (PPT). The flexibility of the technique to assign different weightings to different thrust directions is demonstrated, and a number of useful conclusions are drawn regarding the fuel consumption of continuous and discrete controllers, and the use of nonlinear models for improved control system design. Only two studies have been identified whereby the LQR control laws are evaluated in a gravity-perturbed environment, using a controller designed with the Hill equation dynamics with a

modified orbital rate to allow for the effects of the J_2 perturbation. (The modified orbital rate is, however, not analytically derived). This is not directly contrasted with any other controller designs using any other models to demonstrate whether any benefits have been gained, although useful estimates of ΔV to counteract the J_2 perturbation are evaluated (Table 3-6).

Some evaluations of trajectory generation and control using a 'perceptive frame' for centralised and decentralised formation control architecture have been performed. Interestingly, when the perceptive frame modified its orbital rate due to the J_2 perturbation, fuel use for the maintenance of the follower trajectories was reduced. However, although a decentralised control architecture was more fuel costly overall, it was easier to balance fuel use more evenly across the formation.

The majority of other control designs applied to the formation flying problem in LEO are based on nonlinear Lyapunov control. These have been successfully applied to both relative orbit elements and nonlinear Hill equations dynamics.

A brief survey of some of the more recent literature addressing guidance functions for LEO formation flying has highlighted only a couple of sources where fuel balancing across the formation has been directly addressed. This is clearly an area for future work. Further discussion of the literature is presented in the chapter summary (section 3.3) and the introductory sections of chapters 4 to 7 to support the justification for the research presented in the thesis.

3.2 Formation Flying in the Vicinity of L2

In this section, an overview of basic Lagrange or 'libration' point celestial mechanics for the Sun-Earth (or Earth-Moon) three body problem is presented to provide the necessary background context for the dynamics and control literature review (a more detailed mathematical treatment of the problem is reserved for chapter 6). The majority of the early literature describes the orbital mechanics and control of single satellites in the vicinity of the collinear Lagrange points. While this is not the focus of the research, insight is gained into the dynamics of the environment (stability, orbit type and perturbations), and the mathematical models which describe satellite motion and which can be used to investigate orbit maintenance. Aspects of formation design in the Lagrange point environment are addressed, and relative dynamics models for formation flying modelling are described according to the literature. In the final section, an overview of formation flying control and guidance strategies applied to formation flying in deep space is presented.

3.2.1 The Three Body Problem

The problem of describing the motion of a satellite in the presence of two massive celestial bodies, for example, the Earth and Sun, or Moon and Earth, is termed the 'three body problem'. The satellite is assumed to have infinitesimally small mass compared to the two massive bodies or 'primary bodies'. The problem can only be solved

numerically unless certain assumptions are made to simplify the problem. The simplest case is the circular restricted three body problem (CR3BP) which requires the primary bodies to have circular orbits about the centre of mass of the whole three body system (the 'barycentre'). Following linearising assumptions it is also possible to derive analytical solutions to the slightly more complicated elliptical restricted three body problem (ER3BP) which assumes that the primary bodies trace elliptical orbits about the barycentre. In both cases, the spacecraft does not affect the motion of the primary bodies. The CR3BP is illustrated in Figure 3-2.

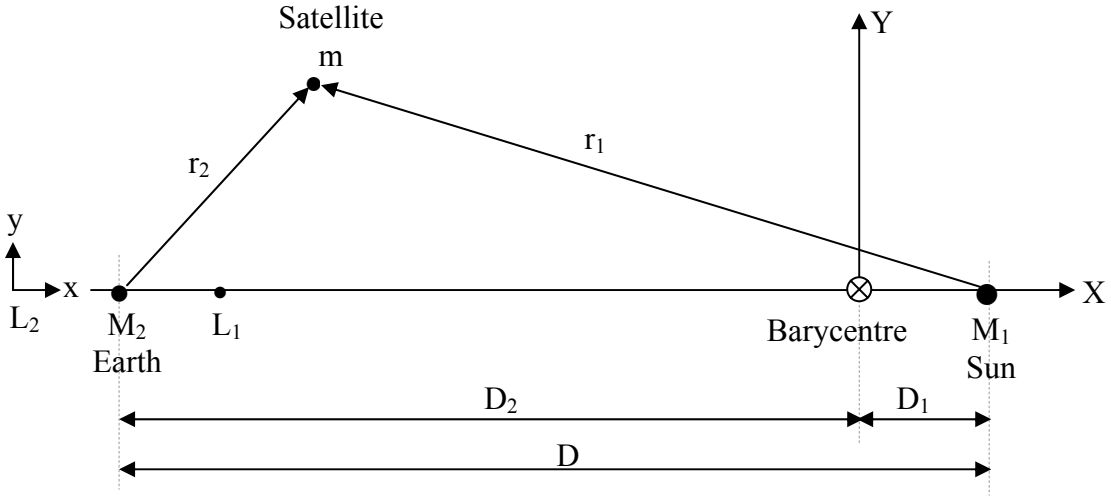

Figure 3-2: The Circular Restricted Three Body Problem (Wie, 1998)

Equations of motion for the satellite moving in the presence of the three bodies are derived in many texts, for example, Wie (1998), Szebehely (1967). The following equations are taken from Wie (1998), and the terms correspond to those in Figure 3-2.

$$\ddot{X} - 2n\dot{Y} - n^2X = -\frac{\mu_1(X - D_1)}{r_1^3} - \frac{\mu_2(X + D_2)}{r_2^3}$$

$$\ddot{Y} + 2n\dot{X} - n^2Y = -\frac{\mu_1 Y}{r_1^3} - \frac{\mu_2 Y}{r_2^3} \qquad (3\text{-}25)$$

$$\ddot{Z} = -\frac{\mu_1 Z}{r_1^3} - \frac{\mu_2 Z}{r_2^3}$$

The X-Y-Z axis system, based at the barycentre, rotates with orbital rate, n where

$$n = \sqrt{G(M_1 + M_2)/D^3} \qquad (3\text{-}26)$$

and equations (3-25) therefore contain Coriolis and centrifugal terms. Multiplying each equation in (3-25) by $\dot{X}$, $\dot{Y}$, and $\dot{Z}$ respectively, and summing them produces an expression which can be numerically integrated to give equation (3-27) (Wie, 1998).

$$\frac{1}{2}(\dot{X}^2 + \dot{Y}^2 + \dot{Z}^2) - \frac{1}{2}n^2(X^2 + Y^2) - \left(\frac{\mu_1}{r_1}\right) - \left(\frac{\mu_2}{r_2}\right) = C \qquad (3\text{-}27)$$

C is a (negative) measure of energy called the Jacobi Integral, and remains constant during simulation of the motion of a satellite in the CR3BP. Given specific initial conditions (satellite

position and velocity), the value of C will have a particular value, and uncontrolled, the satellite will follow a trajectory along which C remains constant. For the purposes of formation design, regions of constant C define where the satellites may orbit without additional energy consumption. The outer boundaries of these regions can be defined by setting the velocity terms in equation (3-27) to zero to create "zero-relative-velocity surfaces" (Schaub and Junkins, 2003), and these surfaces can be used to identify minimum energies required for a satellite to translate between or orbit within particular zones in the region of the CR3BP. Dynamical systems theory provides additional mathematical descriptions of the regions within the surfaces (Koon, Lo, Masdemont, and Ross, 2000).

Five stationary points exist in the CR3BP, as discovered by Lagrange in 1772. Their location can be established by setting the acceleration and velocity terms to zero in the equations of motion (3-25) as they occur where the gravitational and centrifugal forces balance. For the Sun-Earth system, where the barycentre lies within the volume of the Sun, the equilibrium points can be visualised as locations where the centrifugal force due to the rotation of the Earth about the Sun is equal to the gravitational attraction of the Sun and Earth, and the resultant force acting on a third infinitesimally small body at that location is zero.

Finding the exact location of each equilibrium point involves the solution of a series of quintic equations (these are solved for the Sun-Earth system in chapter 6). All the equilibrium points lie on the X-Y plane, and rotate with the primary bodies around the barycentre. Three points lie along the axis joining the primary bodies (L1, L2 and L3 are the collinear points), and two form an equilateral triangle with the primary bodies, as illustrated in Figure 3-3 (L4 and L5 can be called the triangular libration points).

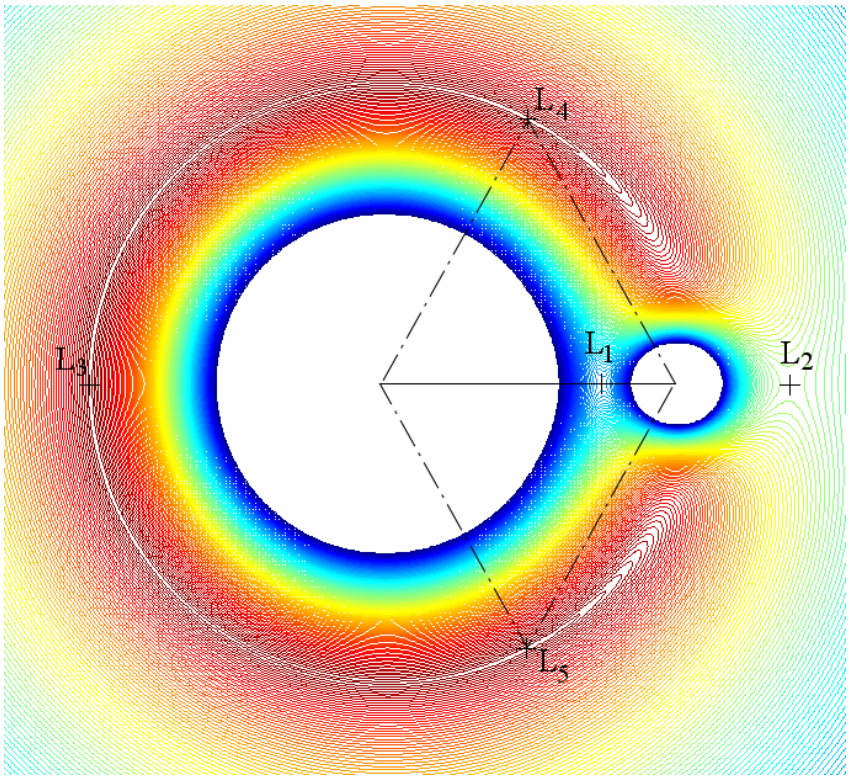

Figure 3-3: Contour Plot of the Gravitational Force Field Associated with the Circular Restricted Three Body Problem

Analysis of Lagrange point stability is also presented in many texts (Szebehely, 1967), (Marchal, 1990), (Schaub and Junkins, 2003). Their stability can be determined by linearising the equations of motion at each Lagrange point, and extracting the eigenvalues of the system. The collinear points are all unstable, and the equilateral (triangular) points are stable. This can be partially visualised through simple representation of the interactions of the rotating gravitational field for the two primary bodies. Figure 3-3 illustrates the saddle points associated with the collinear libration points and the gravity well of the triangular points. However, it should be noted that the potential is also velocity dependent, and a full stability analysis is therefore required.

3.2.2 Lagrange Point Orbits and Their Control

A summary of the approaches taken for determining the motion of spacecraft in the vicinity of the Lagrange points is presented in this section. The first subsection introduces the analytical descriptions of satellite motion, and the types of orbits that this approach can represent. Numerical tools and strategies for Lagrange point orbit analysis published in the literature are then reviewed. Examples of orbit maintenance control are discussed. In this section, the emphasis is placed on the Sun-Earth L2 Lagrange point as this is the target location for the ESA Darwin mission.

3.2.2.1 Analytical Description of Lagrange Point Orbits

By translating the equations of motion for a spacecraft travelling in the three body problem (equations (3-25)) to a reference frame based at one of the collinear Lagrange points, and linearising, the following equations of motion for a spacecraft in the vicinity of a Lagrange point can be derived

$$\begin{aligned} &\ddot{x} - 2\dot{y} - (2\sigma + 1)x = 0 \\ &\ddot{y} + 2\dot{x} + (\sigma - 1)y = 0 \\ &\ddot{z} + \sigma z = 0 \end{aligned} \qquad (3\text{-}28)$$

where σ is a function of the masses of the primary bodies, and also of the location of the equilibrium point in the coordinate frame based at the barycentre (Wie, 1998). x, y, and z describe the position of the satellite in a Cartesian frame aligned with the barycentre frame, and centred on the Lagrange point (Figure 3-2). The in-plane (ecliptic) x-y motion is coupled, and the out-of-the-ecliptic z motion is simple harmonic. The in-plane solutions contain both divergent and oscillatory modes, however, careful selection of the initial conditions can eliminate these secular terms. These initial conditions are given by equations (3-29) and (3-30), where ω_{xy} is in-plane frequency

$$\dot{x}_0 = \frac{\omega_{xy}}{k} y_0 \quad \text{and} \quad \dot{y}_0 = -k\omega_{xy} x_0 \qquad (3\text{-}29)$$

and k is given (for a collinear point) by

$$k = \frac{\omega_{xy}^2 + 2\sigma + 1}{2\omega_{xy}} \qquad (3\text{-}30)$$

With these conditions applied, the solutions to equations (3-28) are given by equations (3-31)

$$\begin{aligned} x(t) &= x_0 \cos\omega_{xy} t + \frac{y_0}{k} \sin\omega_{xy} t \\ y(t) &= y_0 \cos\omega_{xy} t - kx_0 \sin\omega_{xy} t \\ z(t) &= z_0 \cos\omega_z t + \frac{\dot{z}_0}{\omega_z} \sin\omega_z t \end{aligned} \qquad (3\text{-}31)$$

If the initial positions, x_0 and z_0, are zero and $\dot{z}_0 = -y_0\omega_z$, the solutions simplify to the following (equations (3-32)). These equations are considered in the formation flying model development described in chapter 6.

$$\begin{aligned} x(t) &= -A_x \sin\omega_{xy} t \\ y(t) &= -kA_x \cos\omega_{xy} t \\ z(t) &= kA_x \sin\omega_z t \end{aligned} \qquad (3\text{-}32)$$

When the ratio of in-plane and out-of-the-ecliptic frequencies (ω) is a rational number, the solutions will be bounded in three dimensions. The resulting trajectory is therefore closed and a halo orbit around the Lagrange point is produced. When the ratio of frequencies is not a rational number, the orbit does not close and a Lissajous is formed.

Large halo orbits may be hundreds of thousands of kilometres in amplitude, and the linearisation assumptions associated with the equations of motion based at the Lagrange point will no longer hold, and therefore the linear equations (3-32) are not sufficiently accurate to form a reference trajectory (numerical solutions are discussed in section 3.2.2.2). The solutions to the linearised equations of motion about the L2 Earth-Moon Lagrange point (in the form of equations (3-28)) are applied to LQR feedback control by Wie (1998), who demonstrates that the spacecraft is able to follow the first order reference halo orbit trajectory, but at great ΔV expense.

An iterative method for determining a more accurate halo reference trajectory is obtained through disturbance modelling and filtering (disturbance accommodating control), and the ΔV is reduced as the spacecraft does not respond to all the disturbance frequencies, and instead only responds to eliminate secular motion. Cielaszyk and Wie (1994) improve the halo orbit maintenance cost further by repeating the analysis in the context of the elliptical restricted three body problem. The nonlinear equations of motion for the motion of a satellite in the ER3BP are presented by Wie (1998), (1994).

Farquhar (1970) focussed on the control of libration point satellites at the collinear points in the three body problem. In his report the linear equations of motion are derived for a selection of the libration points and solved in the presence of nonlinearity, eccentricity and perturbations to improve the quality of the nominal trajectory beyond that described by equations (3-32). Stability analyses are performed and a method of feedback control is proposed using classical techniques for the linearised constant coefficient equations in the vicinity of the Lagrange points. The effect of the time varying coefficients in either the linearised equations of motion due to the inclusion of

eccentric orbit effects, or the equations of motion of a satellite relative to the nominal trajectory, on stability are investigated by Floquet analysis. Station keeping strategies using a variety of control systems, including basic linear feedback control and a Solar sail are proposed and evaluated.

In a later work, Farquhar and Kamel (1973) develop analytical solutions for quasi-periodic orbits around the Earth-Moon L2 point while, as before, taking into account nonlinearity, eccentricity and Solar gravitational effects. Linstedt-Poincare techniques are applied whereby orbit amplitudes are related to in and out-of-plane frequencies to eliminate secular terms to find a solution. The aim is to develop accurate analytical descriptions of a nominal trajectory for small amplitude orbits which would reduce station keeping costs. They find that above a certain in-plane orbit amplitude, a halo orbit will result where the in and out-of-the ecliptic frequencies of motion are equal (a finding also reported via numerical studies of halo orbits reviewed in section 3.2.2.2). Third order solutions for small-amplitude Lissajous orbits about the Earth-Moon L2 point are obtained, but it is proposed that a fourth order solution is required for sufficient accuracy. The amplitude relationship between in-plane (Y) and out-of-plane (Z) motion to produce a larger halo orbit is established. Richardson and Cary (1975) perform a similar analysis for a satellite near a collinear libration point in the Sun-Earth ER3BP in the presence of Lunar perturbations.

Three further publications by Richardson (1980b), (1980a), and (1980c) describe the subsequent development of a third order analytical solution for a periodic halo orbit around the Sun-Earth collinear Lagrange points in the CR3BP, in support of the first Lagrange point mission, ISEE-3 (International Sun-Earth Explorer – 3, introduced in section 3.2.4). A new formulation of the nonlinear equations of motion at the collinear libration points is proposed using Lagrangian mechanics and Legendre polynomials. This approach produces a more concise and robust analytical solution due to its improved ability to describe higher order terms in the equations of motion. The solution is obtained using the same approach as that of Farquhar and Kamel (1973), described above. The Richardson solutions are considered further for the formation flying dynamics model development in chapter 6.

Kim and Hall (2001) refine the initial conditions derived by the Richardson third order analytical solution using an iterative procedure to numerically produce a halo orbit. The tool then applies the same procedure to numerically generate the family of halo (or planar) orbits through gradual variation in orbit amplitude. Although a numerical study (section 3.2.2.2), Junge, Levenhagen, Seifried and Dellnitz (2002) also simulate a halo family using a similar approach for the design of the Darwin formation flying mission. The halo solution is designated the centre of the four-spacecraft formation investigated, and the trajectories of each spacecraft in the CR3BP are propagated. The deformation of the formation and the cost of halo orbit maintenance are measured for each scenario investigated. The formation is found to be more stable in halo orbits further away from the Earth, and halo orbits requiring a maximum control acceleration of $10^{-9}ms^{-2}$ to maintain are identified. The latter are deemed suitable for continuous thrust control for Darwin.

More recently, Gomez, Masdemont and Simo (1998) report the semi-analytical computation of 'quasihalo' orbits also using a Lindstedt-Poincare method. Quasihalo Lissajous orbits form a torus around the halo orbit (forming another class of Lagrange point orbit), but these are not considered further here.

The simplest description of controlled satellite motion in deep space is of course the double integrator, representing Newton's third law, and neglecting the influence of any of the primary bodies in the system dynamics. This dynamics model is often adopted for detailed work on formation control, formation architecture design, and formation manoeuvring where the scale of the relative motion is much smaller than the scale of a halo orbit (for example, Smith and Hadaegh (2002b)).

3.2.2.2 Numerical Solutions in the Three Body Problem

An extensive range of literature is available regarding the numerical solutions in the three body problem and the nature of Lagrange point orbits. However, researchers continue to identify more accurate descriptions of satellite motion in an effort to improve orbit design, control system design, and develop sufficient knowledge of particularly the gravitational environment for autonomous operations which would greatly facilitate complex missions. It is argued that, particularly for the family of large halo orbits around a Lagrange point, that the linearisation assumptions associated with the derivation of linear equations and solutions at the Lagrange point (introduced in section 3.2.2.1) are no longer valid, and that even the higher order analytical solutions derived above for all practical purposes should be evaluated numerically. This is considered further in chapter 6 where a description of the Lagrange point orbit (analytical or numerical) is incorporated into the description of the relative dynamics for the formation flying model.

Early literature relates to the search for analytical solutions for the identification of periodic orbits in the vicinity of the Lagrange points (for example, Lanzano (1967)), however a significant proportion of recent published literature on the identification and classification of periodic orbits in the restricted three body problem has been produced using numerical techniques by Howell at Purdue university. The research can be categorised into two main areas:

- The identification, classification and recording of families of libration point orbits (Howell, 1984), (Howell, 1998), (Howell, 2001).
- Orbit transfers from Earth to the Lagrange points using Dynamical Systems Theory (DST) (Howell, Barden B.T. and Lo, 1997).

Related work with JPL involves research into the link between the DST techniques and low thrust trajectory design around other bodies within the Solar System, for example, Europa (Lo, Anderson, Whiffen, and Romans, 2004).

Howell and Campbell (1999) and Howell, Barden and Lo (1997) describe the motivation for the development of solutions to the three body problem in the two areas listed above:

- The identification and classification of a potentially infinite number of periodic orbit solutions is useful in anticipation of a range of potential mission

applications. The discovery of a strategy to numerically produce a desired orbit given a number of specific mission requirements would be a valuable tool for mission analysis and design. In particular, the insight afforded by the understanding of the relationship between sets of initial conditions and the subsequent orbit trajectory would be extremely valuable.

- The conic sections approach to the design of transfer trajectories to a Lagrange point orbit is not appropriate due to the sensitivity of the problem to initial conditions and nonlinearities. Numerical targeting of the desired orbit is possible by manually selecting initial conditions until the desired orbit is achieved. However, this approach is inefficient and does not provide insight into the dynamics of the L2 environment.

Instead Dynamical Systems Theory (DST, originating from the work of Poincare) and the development of manifold theory is proposed as a suitable tool for trajectory design between the collinear L1 and L2 Sun-Earth Lagrange points and the Earth (Howell et al, 1997). The establishment, initialisation and control of Lagrange point orbits is so sensitive to the nature of the arrival and potential departure dynamics of spacecraft at the Lagrange point, that in much of the subsequent literature, the emphasis of DST is stronger on its application to low thrust trajectory design for orbit transfers. However, insight into the unstable behaviour of satellites in Lagrange point orbits is gained.

Folta and Richon (1998) describe the use of DST in the design of libration point trajectories. They describe how this numerical procedure uses knowledge of the equilibrium points, periodic and quasi-periodic solutions in the three body problem, and then generates invariant manifolds, which are essentially a set of orbits that form a surface. In a study to investigate low energy transfer trajectories to the Moon, Koon, Lo, Marsden and Ross (2000) present a useful overview of the dynamic environment in the vicinity of the collinear Lagrange points. Their figure (Figure 3-4) illustrates four types of orbit in the vicinity of the L2 Lagrange point, as identified using Poincare sections and DST:

- *Planar (Lyapunov) Orbit*: A single periodic orbit which exists for a specific energy level.
- *Asymptotic Orbit*: Winds on and off the periodic orbit. The orbit is on the stable manifold of the periodic orbit when it is winding on, and on the unstable manifold when winding off (the manifolds form tubes).
- *Transit Orbit*: Passes the Lagrange point through the Lyapunov orbit but is not captured.
- *Non-Transit Orbit*: This orbit never reaches the Lagrange point or enters a manifold tube.

Howell (2001) provides a summary of the families of orbits in the vicinity of the collinear Lagrange points. These can be categorised into:

- Periodic Orbits: Halo (Northern and Southern), Lyapunov (planar), Vertical
- Quasi-periodic: Lissajous, Quasihalo

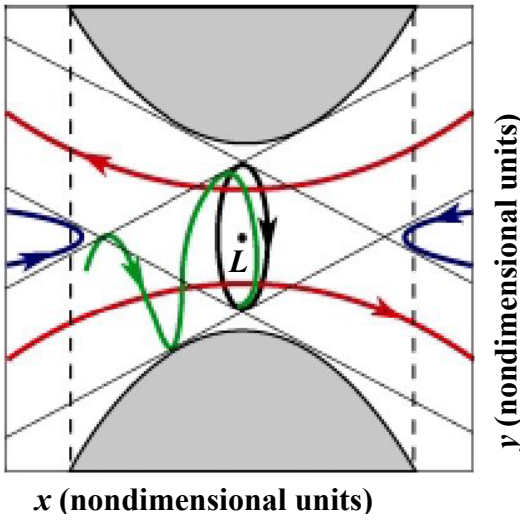

Figure 3-4: The L2 Region and 4 Major Classes of Orbits (Koon et al, 2000)

Two types of periodic motion are possible in the centre manifold, including Lyapunov orbits (planar in the ecliptic) and vertical orbits (almost vertical and dominated by out-of-plane motion). However, when a critical amplitude of planar orbit is reached, eigenstructure analysis of the planar orbit reveals the existence of bounded orbits with an out-of-plane component. These are halo orbits which are classified into two families, northern and southern (reflected in the ecliptic). The halo orbits lie in the centre manifold and the stable and unstable manifolds are used to generate transfer trajectories. The family of halo orbits around L1 and L2 collapse back to the planar orbit near the Lagrange points, and as they extend towards the smaller primary body the orbits become perpendicular to the plane of motion of the primaries. Lissajous orbits are unbounded, and are not constrained to be a certain size. Both analytical and numerical studies have demonstrated a class of Lissajous orbits ('quasihalo') with trajectories which form a surface around the vertical orbit or halo trajectories, forming a torus (Howell (1998), Gomez et al. (1998)).

Alternative approaches to orbit design in the vicinity of the Lagrange points are presented by Roithmayr and Kay-Burnell (2004) who evaluate the cost of maintaining a spacecraft at the Lagrange point (both analytically and numerically), and Shen, Kumar and Seywald (2004), who design alternative periodic orbits in the presence of Solar radiation pressure and subject to a size constraint which does not permit a halo around the Sun-Earth L2 point.

Lagrange point orbit design and control is influenced by mission objectives (science and communications requirements), and fuel cost in the mission analysis. While the former largely determines the size and location of the operational orbit, most papers describe the orbit transfer analysis and its optimisation according to energy criteria and orbit insertion ΔV. Also related to the orbit design are the permitted directions of thrusting, for example, to prevent plume impingement on sensitive optics for the observatory missions. Many related references describe low energy or zero cost transfers between, to or from libration point orbits, rather than the control of the orbits themselves (Howell,

Guzman, and Anderson, 2001), (Gomez and Masdemont, 2000). Improvements to standard numerical determination of transfer trajectories are also presented in the literature, for example, Kechichian (2001) describes the development of an iterative optimisation procedure (involving integration and interpolation) that can determine the trajectory of a satellite between LEO and the Sun-Earth L1 point to meet boundary conditions with 1m accuracy.

Two types of control of the numerically determined orbits are discussed by Howell and Keeter (1995), and other examples in the literature fall into these categories:

- Trajectory following by periodic control with optimal targeting of a future position in the orbit.
- Analysis of the stability characteristics of the dynamics continuously along the reference trajectory, and elimination of the unstable mode (using Floquet analysis which is discussed further in chapter 4).

3.2.3 Perturbations and the Sun-Earth L2 Environment

A number of sources in the literature describe the perturbations experienced by satellites travelling in the vicinity of the Lagrange points. They are incorporated into dynamics models, and applied to orbit control. Gravitational and radiation forces influence the natural spacecraft motion, but are considered as perturbations in the context of the circular restricted three body problem where the Lagrange equilibrium points are considered fixed in the rotating frame.

Analysis of the Sun-Earth L2 Lagrange point environment is presented by Evans (2001) in support of the Next Generation Space Telescope (now the James Webb Space Telescope, JWST) mission design. The main perturbing forces, which uncorrected will prevent a satellite maintaining its location at the L2 point, include:

- Elliptical motion of the Sun and Earth about the Barycentre
- Lunar Perturbations
- Planetary Perturbations
- Solar Radiation Pressure (SRP)

From a systems design point of view it is also important to take into account the characteristics of the radiation environment, including the:

- Dynamic Plasma Environment
- High Energy Radiation
- Thermal Radiation

Meteoroid impact would also be a feature of the L2 environment, but this has not been considered here. Earth-based measurements have provided initial estimates of the quantity, location and velocity of meteoroids in the vicinity of L2. However, for future astronomy missions, the effects of impacts on the telescope mirrors and optical path stability should be investigated as part of the system design.

Elliptical Motion about the Barycentre

The greatest improvement that can be made to the accuracy of analytical descriptions of a Lagrange point orbit is to include the effects of eccentricity in the motion of the primary

bodies of the circular R3BP to formulate the elliptical R3BP. In determining analytical descriptions of Lagrange point orbits, Farquhar (1970) demonstrates that for the Earth-Moon restricted three body problem, perturbations due to the eccentricity of the Moon's orbit are greater than the nonlinearity in the equations of motion (at the Lagrange point), and also the effect of the Sun's gravitational field and Solar radiation pressure. The effect of eccentricity in the Sun-Earth three body problem is also significant.

Lunar and Planetary Perturbations

Table 3-7 summarises the maximum perturbing accelerations due to Lunar and planetary perturbations in the in-plane X-Y and out-of-the-ecliptic Z directions (as described by Figure 3-2). The Lunar perturbations arise from the effect of the Moon rotating about the Earth, and are more significant than the perturbations due to other planets in the Solar system (Uranus and Neptune also have an effect but this is smaller than Mercury). Jupiter and Venus have the most significant effect on accelerations experienced by a body at the L2 Sun-Earth Lagrange point. In each case the accelerations are cyclic with different periods.

	X $x10^{-10}kms^{-2}$	Y $x10^{-10}kms^{-2}$	Z $x10^{-10}kms^{-2}$
Lunar Perturbation	±5.5346	±5.8480	±0.7017
Mercury	-0.0360	±0.0085	±0.0044
Venus	-2.0789	±0.5972	±0.1231
Mars	+0.1529	±0.0623	±0.0049
Jupiter	+3.6769	±2.6124	±0.0838
Saturn	+0.2662	±0.2169	±0.0116

Table 3-7: Maximum Perturbations at the L2 Sun-Earth Lagrange Point (Evans, 2001)

Solar Radiation Pressure

The effect of Solar Radiation Pressure (SRP) on satellite formations in LEO was considered in section 3.1.4.3, and is evaluated in chapter 4 (section 4.2.2.4). At the L2 Lagrange point in the Sun-Earth system, the effect of SRP as a perturbing force will depend on the spacecraft area to mass ratio, the orientation of the spacecraft, and particularly for the infrared observatories (JWST and Darwin), the size of the thermal shields. Tene, Richon, Folta and Tene (1998) state that for the Microwave Anisotropy Probe (MAP) and the NGST (JWST) missions, the SRP is the largest perturbing force and has the effect of shifting the orbit centre (an overview of mission applications of Lagrange point orbits is presented in section 3.2.4).

Folta and Richon (1998) investigate the use of SRP to control the unstable mode of a Sun-Earth L2 orbit as part of the analysis for MAP and NGST (JWST) missions. The magnitudes of the perturbing accelerations due to the Moon and Solar System planets are very small, yet over a few months they are able to cause the orbit to diverge. SRP offers the opportunity to continuously control the L2 orbit, and as described above, its effectiveness and control authority will depend on the size, shape and orientation of the Solar sail or shield. The average SRP acceleration calculated for MAP is $0.2\mu ms^{-2}$. They propose that the satellite can be moved a few hundred kilometres closer to the Sun to counteract the Lunar perturbations, and reorientation of the Sun-shields can control the spacecraft and force it to remain in the vicinity of L2.

3.2.4 Mission Applications

The nature of the low perturbation, thermally stable environment with the opportunity to have permanent visibility or coverage of particular celestial bodies makes missions to the Lagrange points of any three body system attractive. In particular, for the Sun-Earth and Earth-Moon systems, the Lagrange points offer the potential for uninterrupted science observations and measurements, and access to the entire surface of the different bodies through appropriate orbit design. The applications proposed or flown to date include science (Solar or Lunar observation, deep space astronomy, scientific field measurements in the vicinity of the Lagrange points) and inter-planetary communications. In this section, the orbital characteristics of some of the proposed and ongoing Lagrange point missions are summarised.

An overview of practical control of satellites in Lagrange point orbits is presented by Dunham and Roberts (2001) who review the control strategies applied to recent Lagrange point missions. Of note for consideration in chapters 6 and 7 are the following points:

- The location of a Lagrange point satellite must be monitored for 3-4 weeks for orbit determination prior to a corrective manoeuvre.
- Launch injection and halo orbit insertion manoeuvres are much more costly (two orders of magnitude) than the ΔV required for station keeping.
- Maintaining a prescribed reference trajectory through regular orbit corrections (ISEE-3 mission) is more costly than balancing orbit energy using periodic thrust to eliminate the unstable components (SOHO mission).
- Better orbit determination is likely to contribute to a reduction in mission ΔV.

The first spacecraft to be flown in a libration point orbit was the International Sun-Earth Explorer-3 (ISEE-3) in 1978, thus demonstrating the feasibility of using the Lagrange points for a range of potential missions. Farquhar, Muhonen, Newman and Heuberger (1980) and Richardson (1980c) describe the trajectories and orbital manoeuvres performed by ISEE-3. In this case the spacecraft adopted a 700,000km y-amplitude (in the ecliptic plane and perpendicular to the Sun-Earth line) and 110,000km z-amplitude (out-of-the-ecliptic) halo orbit around the Sun-Earth L1 point to monitor Solar flares and the Solar wind prior to its arrival at Earth. The data acquisition was designed to complement two other ISEE missions within the Earth's magnetosphere. The design halo orbit was tightly controlled with manoeuvres performed on average every 82 days. Annual average station keeping ΔV was approximately $10ms^{-1}$.

Farquhar (1970) suggested that the Earth-Moon L2 point would be suitable for communications and operations on the far side of the moon. A halo orbit would be sufficiently large to enable the spacecraft to be permanently visible from Earth, and yet behind the moon. Another spacecraft at L1 would give full lunar coverage, and permit communications to be relayed to Earth. Farquhar (1991) introduces a number of other missions that were to be operated at the Sun-Earth L1 and L2 points during the 1990s.

The Solar Heliospheric Observatory (SOHO), launched 1995 adopted a halo orbit about the Sun-Earth L1 libration point with amplitude similar to ISEE-3. This is controlled in the x-axis (along the Sun-Earth line) only which has reduced station keeping fuel use to

approximately 2.3ms^{-1}yr^{-1}. Unlike the ISEE-3, SOHO does not maintain its orbit by tracking an analytically derived trajectory. Instead station keeping manoeuvres are performed to guarantee that the spacecraft will maintain the halo for the next orbit. Orbit determination using the DSN established accuracies of 10km in position, 5mm/sec in velocity and 1mm/sec velocity along the Sun-Earth line.

Tene et al. (1998) describe the mission design criteria and transfer trajectories considered for MAP (the Microwave Anisotropy Probe mission, launched 2001). The small Lissajous orbit around the Sun-Earth L2 point was selected according to the upper design limit of the orbit amplitude (260,000km), based on considerations of Earth shadow, communications, and science requirements associated with avoiding thermal radiation from the Earth and Moon (Folta and Richon, 1998). The station keeping strategy for Lissajous maintenance is described in Rohrbaugh and Schiff (2002).

The Advanced Composition Explorer (ACE), launched 1997, was the third NASA libration point mission, and performed measurements of the Solar wind and Galactic cosmic rays at the Sun-Earth L1 point (Roberts, 2001). The operational orbit was a Lissajous, maintained to prevent escape from the L1 region, and selected to enable a smaller orbit to be achieved. The orbit was maintained by out-of-the-ecliptic control once per orbit and applied where the z-velocity is zero to avoid the 'Solar exclusion zone' where communications are overcome by background radio noise. Attitude and orbit control and determination is planned and performed from the ground, with command functions relayed through the Deep Space Network (DSN).

DST has also been applied to mission design. The Genesis mission was launched in 2001 to retrieve samples of the Solar wind from a region of space in the vicinity of the Sun-Earth L1 point. The transfer trajectory design technique was able to reduce the ΔV for orbit insertion to just 6ms^{-1}.

The Sun-Earth L2 libration point is particularly suitable for infrared observatory missions. Using a combination of DST and Astrogator targeting software, mission analysis has been performed for the NGST (JWST) by Folta, Cooley and Howell (2001). A combination of numerical techniques enabled an orbit, which takes into account SRP, to be derived so that orbit maintenance could be performed in the anti-Sun direction only (the orbit y-amplitudes of 800000km and 400000km were investigated). Direct transfer to the orbit under constant acceleration was also incorporated into the design. Once in the target halo orbit, one of the proposed orbit maintenance strategies involves four corrective manoeuvres per orbit. The controller imparts a ΔV to reduce position errors with respect to the design trajectory to zero at a target time. This is based on the linear propagation of errors using the state transition matrix associated with the design solution (and the target time is that of the next manoeuvre). The proposed control interval is not claimed to be ideal, but sufficient to demonstrate that the mission can be performed and meets ΔV design requirements of 4ms^{-1}yr^{-1}.

Strizzi, Kutrieb, Damphouse and Carrico (2001) propose the use of the Sun-Mars L1 and L2 points for communications relays for future Martian expeditions. In their study using the Satellite Tool Kit (Astrogator) numerical orbit propagator, the costs of transferring and station keeping two spacecraft in Lissajous orbits, one at each Lagrange

point, are evaluated. The attraction of this arrangement is that almost half of Mars would be visible to each spacecraft throughout the mission, and the Sun is always visible for power.

A number of future Lagrange point missions will involve formation flying. These are summarised in appendix A.

3.2.5 Dynamics and Control of Relative Motion for Satellites Formation Flying in the Three Body Problem

Compared to single satellite operations, satellite formation flying in the three body problem has received relatively little attention. While the subject of formation dynamics and control are interrelated, and most of the references address both of these aspects of formation flying, the role and methods of dynamics modelling for Lagrange point formations is emphasised in this section. The section comprises a review of the research involving both analytical and numerical approaches to relative dynamics modelling and formation control. It is appropriate to note at this point that the dynamics model development research presented in chapter 6 was proposed in 2002, and prior to some of the more recent publications on the subject described below.

As recently as 2000, Lo, Koon, Marsden and Murray (2000) presented an overview of the technology gaps which must be filled in order to implement a spacecraft formation flying mission in the vicinity of the Lagrange points. A number of points were emphasised:

- The need to exploit the natural trajectories of members of the formation and to generate the individual trajectories of each satellite in the three body problem.
- The complexity of formation deployment.
- The need for control system design for both loose and precision control.
- For interferometry applications, it must be possible to measure and control the shape and orientation of the formation.
- The need to estimate control effort and performance metrics that enable formation and system designs to be compared.
- The need for autonomous operations.

As an extension to the work on single satellite trajectories using the numerical approaches of DST and manifold theory, Barden and Howell (1998) investigate the families of Lagrange point orbits that would be appropriate for formation flying at the Earth-Moon L1 point. The role of quasihalo orbits (which form a torus around a halo) is proposed for formation design. With the appropriate initial conditions, the formation could remain planar and rotate as all the satellites move along the torus. However, a test case nonlinear solution revealed that the out of plane motion was 1% of the satellite separation. In this study the feasibility of performing formation and trajectory design using DST is demonstrated, although this was applied to a formation of diameter 130000km. The use of the approach for satellite separations of a few metres using halo orbit tori is not discussed, and the presence of small diameter tori around halo orbits is unknown without further investigation.

In section 3.2.2.2, Howell and Keeter (1995) are referenced in the description of the two main approaches to the control of unstable orbits. Scheeres and Vinh (2000) adopt the second of these approaches to stabilise the relative motion of two satellites in Sun-Earth L2 Lagrange point orbits. Initially, a halo design is identified numerically for one of the spacecraft, and it is assumed that this is maintained separately from the formation. Instead of controlling the second satellite to another (numerically sensitive) trajectory which has the same period, and therefore cannot also be a halo, the dynamics of relative motion are controlled. At each point along the halo trajectory a Taylor expansion is performed to describe the variation in position and velocity of a second spacecraft relative to the first. This is satisfactory for satellites in close proximity, and can be reduced to a time invariant form over short time intervals. At each point, the eigenstructure of the relative motion state matrix is evaluated and feedback gains are designed which control and eliminate the divergent modes. An example of formation control whereby the second satellite follows a quasihalo around the first (as described above) is presented, and the controller is found to successfully control nonlinear motion. This does not achieve precision formation flying, but will maintain the satellites in the vicinity of L2. Hsaio and Scheeres (2002) continue this work and attempt to parameterise the toroidal relative motion. The proposed application is interferometric imaging using natural spacecraft formations around L2, complementing innovative image reconstruction work which does not require precision formation flying (Hyland, 2001).

Gomez, Lo, Masdemont and Museth (2001) performed an investigation of formation flying in the vicinity of the Sun-Earth L2 point for the NASA Terrestrial Planet Finder (TPF) mission. As one of the first investigations into precision formation control, the objective of their research was to assess the feasibility and ΔV costs associated with the following mission phases:

- Launch and Transfer to L2
- Deployment into Initial Formation
- Pattern Maintenance
- Formation Reconfiguration

Initially a baseline halo orbit and a quasi-periodic orbit in the vicinity of the halo were selected to construct the planar formation travelling along the halo (both unstable orbits). The baseline halo was the target reference for formation deployment, but for the science phase, no satellite was rigidly maintained on the halo. In addition to halo maintenance, the spacecraft formation is made to slowly rotate through the use of impulsive burns to control satellites on the circumference of the formation. This causes them to move linearly between points on the circumference approximated by a many sided polygon. Impulsive manoeuvres to maintain desired formation rotation rates were estimated using numerical targeting techniques. The mission was found to be feasible, and other findings relating to rotating pattern maintenance phase included the following:

- Formation manoeuvres were practically independent of baseline orbit.
- Halo orbit maintenance manoeuvres can be absorbed into formation flying manoeuvres since the latter are relatively frequent.
- The mission can be achieved using linear control in the nonlinear environment.

An analytical approach to formation control in the CR3BP is presented in a series of papers by Gurfil and Kasdin (2001), and Gurfil, Idan and Kasdin (2002), (2003). In

earlier work (2001), the equations of motion of a satellite in the Sun-Earth CR3BP are derived in terms of distance from the Earth in a rotating frame. The solution to the equations provides a reference trajectory, and the equations of motion of a follower satellite relative to the reference are obtained by linearisation about the reference. The stability and controllability of the time varying system are investigated and a time varying LQR control law is designed. Weighting matrices in the LQR design are selected by tuning the formation response to a baseline expansion scenario (on a scale required for TPF of 50-500m). In this case, the reference trajectory is initialised in LEO, and then projected into an out-of-the-ecliptic trajectory using the nonlinear equations. The resizing manoeuvre thrust levels required are evaluated, and continuous micro-Newton thrusters (for example, FEEP) are deemed suitable for the task.

Gurfil Idan and Kasdin (2002) develop a nonlinear control law for formation control in the ER3BP, thus avoiding the linearisation assumptions of the previous study. A relative position controller is designed using approximate feedback linearisation via dynamic model inversion, LQR controller design and a neural network design to compensate for the inversion error. For a similar approach applied in the CR3BP, sub-millimetre tracking is achieved (Gurfil et al, 2003). In all cases, the out-of-the ecliptic trajectory initialised in LEO is presented as a test case, and the approach is not demonstrated for Lagrange point orbits.

Hamilton, Carpenter and Folta (2002) apply LQR control with Kalman filtering (Linear Quadratic Gaussian, LQG, control) to formation station keeping and manoeuvring control around L2 in the CR3BP. The dynamics models used are obtained from software, developed at Purdue university (Howell, Barden and Lo (1997)), which calculates the Lissajous reference orbits including Lunar and planetary perturbations, Solar radiation pressure, and Earth orbit eccentricity. A linearised dynamics matrix is calculated by the software at each epoch along the numerical trajectory for LQR design. The hub is found to track the reference orbit satisfactorily but the telescopes only achieve a tracking accuracy of a few metres when process and measurement noise are included in the simulation. Station keeping and formation slewing are simulated and the ΔV is evaluated. Instead of linearising and redesigning the controller at each time step, Howell and Marchand (2003a) perform a related study using the same trajectory generation software, and simultaneously integrate the differential Riccati equation with the equations of motion to achieve a guarantee of optimal control. This is contrasted with input and output feedback linearisation controllers for different formation scenarios. These include the now familiar quasi-halo planar rotating relative trajectory, station keeping and orientation keeping. The nonlinear techniques are found to be more efficient for formation control.

During the model development research presented in chapter 6, a publication by Segerman and Zedd (2003) was released. They derived high order solutions to the equations of relative motion for two satellites orbiting L2. The nonlinear equations of motion for the hub (leader) satellite and the telescope satellite are derived separately in the CR3BP, assuming that both are ‘in the vicinity’ of L2. The hub equation is subtracted from the telescope equation to produce an equation of motion for the telescope relative to the hub. A series expansion is performed and the terms are evaluated and ordered by magnitude. Also, the frequency of out of plane motion is adjusted to have the same fundamental period as the in-plane motion to create a planar

formation. The analytical solutions to the equations of motion are derived using a Lindstedt-Poincare-type method (Richardson, 1980a) and compared to numerically integrated solutions. Due to the divergent nature of the relative motion, comparisons were only made over 20 day periods using initial conditions derived from the analytical solutions at time t=0. It was found for one test case that their solutions approximated well the numerical integration of the two separate CR3BP equations of motion (one for each satellite) for approximately 5 days in all directions. This high order analytical model of the relative motion dynamics was implemented for comparison with the dynamics model developed in chapter 6 and the Satellite Tool Kit (STK).

In more recent research, Marchand and Howell (2003b), (2004) continue to apply numerical techniques to the natural formation design and control problem, finding that the inclusion of planetary bodies and Solar radiation pressure has an insignificant impact on formation keeping near the Sun-Earth L1 and L2. In fact the control requirements for formation keeping are so small that they may not be achievable with current thruster technology, and the role of impulsive control should be investigated further (Carlson, Pernicka, and Balakrishnan, 2004).

3.2.6 Formation Flying Guidance and Control in Deep Space

In this section an overview of formation flying control and guidance strategies applied to formation flying in deep space is presented, with an emphasis on the guidance. The nature of the problem means that guidance and control systems are often designed together, using simple double integrator dynamics to represent satellite motion in the deep space environment. Also, in the absence of natural orbits and large perturbations, the guidance and control system is designed specifically to enable efficient task-specific manoeuvring of the formation.

A number of different formation flying guidance systems for LEO were introduced in section 3.1.5.3, and these also apply to satellite formations in the vicinity of the L2 Lagrange point. To reiterate, satellite formation flying guidance systems generate the desired trajectories for satellites to follow as a control system reference. In general they vary in complexity depending upon the nature of the manoeuvre, the conditions enforced during the manoeuvre, whether the desired trajectory has been predetermined offline, or whether the planning algorithms are continually being updated online with measured information. A significant factor influencing system complexity is the level of autonomy of the system and the number of satellites within the formation that must be simultaneously manoeuvred. The conditions of manoeuvre can include, for example:

- Plume avoidance from nearby satellite propulsion systems.
- Collision avoidance (permits certain manoeuvres only, and maintains exclusion zones).
- Operational constraints (maximum accelerations and velocities permitted, maximum thrust available).
- Initial and terminal conditions on the manoeuvre.
- Global fuel minimisation.
- Fuel balancing.

At the Lagrange points, the modes of operation of the formation considered in the literature include:

- Autonomous formation deployment and initialisation upon arrival at L2.
- Interferometry mission specific manoeuvres – slewing, resizing, rotation.
- Formation keeping in the presence of disturbances.

A number of references by Hadaegh investigate advanced control strategies outside of Earth's gravity well (often a heliocentric Earth-trailing orbit rather than L2). These more theoretical approaches to satellite formation flying guidance and control would be applicable in both LEO and deep space, and include:

- Model Predictive Control with linearising feedback for formation keeping and attitude control (Manikonda, Arambel, Gopinathan, Mehra, and Hadaegh, 1999),
- Graph Theory, Matrix Inequalities and Switching Schemes (Mesbahi and Hadaegh (2001b), (1999)),
- Linear Matrix Inequalities (LMI) based on relative position measurement only, and incorporating control architecture redundancy and fuel optimisation (Smith and Hadaegh, 2002b).

Mesbahi and Hadaegh (2001a), (2000) define the modes of operation of the three-satellite ST-3 optical interferometer which was intended to perform imaging of distant astrophysical objects from a heliocentric orbit (this mission has now been cancelled). Fringe acquisition modes similar to those identified for Darwin are defined qualitatively, and the level of permitted thruster use is described. Control laws are designed for two of the modes:

- Translation between u-v points on the Fourier plane.
- Stabilisation of the formation to engage imaging mode.

In the first case, optimal bang-coast-bang laws are derived for a minimum fuel/time balance, although precision manoeuvre requirements are not specified. The fuel use requirements and the mission duration for the control of a single satellite are evaluated as a function of the number of sources being observed. The results are extended to the simultaneous control of two spacecraft and the fuel/time cost is found to be higher (agreeing with the findings of Vadali and Vaddi (2000) for the LEO case in section 3.1.5.2).

Through simulation, Mesbahi and Hadaegh (2000) demonstrate that the optimal control laws are not suitable for the formation stabilisation and imaging phase. Following the translation manoeuvre, the final position error, although small and acceptable for this phase, is too great for the precision control system to capture and correct. Instead a classical proportional-integral-derivative (PID) controller is applied (and contrasted with an alternative controller based on Linear Matrix Inequalities (LMIs)). The definition of acceptable regions of the u-v plane within which control law switching can occur is investigated. The controllers are not evaluated in the presence of perturbations.

Lawton, Beard and Hadaegh (1999) design a strategy to rigidly rotate an interferometer formation with two collectors in the u-v plane, and a hub satellite on the pointing axis while equalising optical path lengths. A decentralised approach is applied to trajectory generation for each individual satellite. The trajectories are derived by imparting a virtual torque to the formation, considering it as a rigid body formation. Trajectory following is enforced using adaptive control which updates according to spacecraft mass, and incorporates actuator saturation constraints. Also, formation rotation while

maintaining attitude for the same free flying interferometer problem is demonstrated using centralised and decentralised control approaches (Lawton, Beard, and Hadaegh, 2000). Control of a rotation manoeuvre while maintaining precise relative position between formation members is also investigated by Beard and Hadaegh (1999a). In this case a position error box for trajectory following during the manoeuvre is derived. When a satellite approaches the edge of the error box, or 'tube' for a satellite performing a planar rotation, the thrusters are fired in a predictive manner to prevent any overshoot (maximum thrust limitations are incorporated into the control). Specifying an acceptable position error in this manner reduces the frequency of thruster firings, and minimises fuel use.

Kong and Miller (1998) define a series of imaging locations in deep space to enable interferometric image reconstruction of a point spread function. Trajectory optimisation is then performed using Travelling Salesman algorithms to enforce the motion of the spacecraft through the u-v imaging points according to a minimum time or minimum fuel law.

The imaging phase of an optical interferometry mission is also considered by Bailey, McLain and Beard (2000). Fuel optimisation strategies to minimise global fuel use are investigated by solving the Travelling Salesman problem in order to cover the necessary u-v points on the Fourier plane and move to different targets. They identify the core interferometry manoeuvres to be rotation, resizing and slewing, and find that combining these manoeuvres can be more fuel efficient than performing them separately. However, the manoeuvres prescribed are suitable for imaging and not nulling interferometry, which is the ultimate objective of this research. Their approach to fuel balancing during the manoeuvres is described below.

Also for the astrophysical interferometric imaging task, PID control is employed by van der Avoort, D'Arcio and den Herder (2003) to enable telescopes to follow prescribed trajectories for the Darwin mission. The guidance trajectory combines translation and rotation of the planar circular Darwin formation to cover the u-v plane and enable imaging while manoeuvring. In this case, noise on the relative metrology and actuation systems is included in the simulation to ensure that any relative position errors can be compensated by the onboard optical path length control system in terms of path difference and bandwidth of response. They conclude a fringe tracker is necessary during imaging, and that the FEEP thrusters (Table C-2, appendix C) are saturated when responding to measurement noise. Incorporation of a suitable estimator (Kalman-filter) into the control system is recommended.

For the Darwin mission, Lagadec, Lebas and Ankersen (2003) combine optical path difference control and formation position control in the presence of noise and disturbances using LQG. A trade-off study is performed to justify whether more than one optical delay line is required, and whether a centralised or decentralised control scheme should be implemented. A centralised multi-delay line approach is selected for the baseline study. LQG is demonstrated to be a suitable control technique, meeting performance requirements for the formation.

A number of authors report the use of potential function methods, which are widely used in robotics, for formation flying formation keeping and manoeuvring (McQuade, Ward, and McInnes, 2002). McQuade et al. (2002) apply this method to the deployment of a formation of satellites near L2 using a description of the linearised dynamics of each satellite relative to the L2 point. Wang and Hadaegh (1999) investigate fuel minimisation for larger scale formations using optimal control laws and a strategy for breaking down the formation and manoeuvring a few spacecraft at a time. In later works, they apply potential function methods to formation reconfiguration with collision avoidance for decentralised formations (Wang and Hadaegh, 2000), and reduce the computational requirement by designing control laws whereby each satellite only needs to know about its nearest neighbours, and not the entire formation (Wang and Hadaegh, 2001). Singh and Hadaegh (2001) also design an autonomous onboard guidance system incorporating collision avoidance.

Guibout and Scheeres (2004b) again demonstrate the use of Hamiltonian mechanics to find optimal guidance functions, and solve two point boundary value problems with specified beginning and end times and positions for spacecraft reconfiguration in the vicinity of the Sun-Earth L2 point.

Fuel Balancing Considerations for Deep Space Formation Flying

The role of fuel balancing or load levelling for satellite formation manoeuvring was introduced in section 3.1.5.3. Unlike in LEO, formation manoeuvring and reconfiguration in deep space does not necessarily require the consideration of natural relative orbits, and for example, the optimum orbit positions to control particular orbit elements. Fuel balancing manoeuvres in deep space can therefore be considered more conceptually as an offline optimisation problem. A summary of the fuel balancing strategies considered in the literature is presented below:

- Beard, McLain and Hadaegh (1998) investigate trajectory design for an interferometer "retargeting" task, and force the satellites to follow the trajectories using proportional-derivative PD control and bang-off-bang thrust profiles to minimise time/fuel. One approach finds an optimal fixed point of rotation for the formation, based on completion of the entire manoeuvre, whereas a second approach allows this point to continually move according to the mass of remaining fuel on each spacecraft during the manoeuvre. The latter method is found to be more computationally and fuel-costly overall, and more fuel is required to achieve fuel equalisation rather than fuel minimisation across the formation. In this case, the research relates to a control architecture where the planar formation was treated as a rigid body, thus oversimplifying the problem, and manoeuvres were limited to two dimensions. Similar results were obtained in a further study where the formation was not treated as a rigid body and the satellites did not need to maintain formation during the manoeuvre (Beard and Hadaegh, 1999b). In both cases, the manoeuvres were not simulated in the perturbed environment.
- Bailey, McLain and Beard (2000), (2001) incorporate the fuel balancing strategies derived by Beard and Hadaegh (1999b) described above into a global optimisation problem. The fuel balancing laws are applied to a series of rotation, resizing and slewing manoeuvres for the imaging task of the NASA ST-3 two-telescope interferometer.

- Vadali, Bae and Alfriend (2004) use the analytical halo orbit solution derived by Richardson (1980a) for formation design. Formation keeping, slewing and fuel-balanced reconfiguration are addressed for a rotating formation, using a similar approach to their LEO work (Vadali, Vaddi, and Alfriend, 2001).

3.2.7 Discussion

Following the introduction to the three body problem, and a review of the design and control of trajectories for single satellite Lagrange point missions in the Sun-Earth (and Earth-Moon) system, an overview of the recent research into formation flying dynamics and control has been presented. In this section the findings are summarised and discussed.

Earlier investigations provided insight into the problem of designing natural formation trajectories around Lagrange points using numerical techniques. However, the resulting planar formations travelling around a halo did not seem to be appropriate for precision formation flying applications. Also inappropriate was the strategy to control the divergent modes in the relative motion, rather than relative position and velocity directly for precision formation flying.

LQR control techniques in different forms (time varying, time invariant, and redesign at different points around the trajectory in deep space) have successfully been applied to the formation control problem. To design these control systems, a range of numerical and semi-analytical approaches have been taken for modelling the relative motion of satellites in the three body problem, and in particular in the vicinity of the Lagrange points. In each case, linearised dynamics have been evaluated along a reference orbit, which in all the formation flying control examples identified so far, has been numerically generated with varying degrees of accuracy in the three body problem. The reference trajectories reported, which do not necessarily have a satellite located or maintained along them, have been generated in different ways, using:

- Nonlinear equations of motion in the three body problem which are based at different points (the Earth, the Sun-Earth barycentre or a Lagrange point).
- Nonlinear equations in a simplified form.
- Full nonlinear equations in the presence of planetary, Lunar and Solar radiation pressure perturbations.

No fully analytical approaches to deriving a linearised dynamics model were identified prior to the work performed in chapter 6. A higher order analytical solution of relative motion around the Sun-Earth Lagrange point has, however, recently been developed. This solution is therefore compared to those obtained from the new dynamics model.

Although formation keeping control for L2 formations may require an extremely small continuous thrust, the station keeping cost for real missions is small but significant, and the thrust levels required for science manoeuvres may also be significant. The guidance literature review demonstrated a number of control techniques could be applied to rotate and expand/contract a formation, governed by simple integrator dynamics. However, different controllers may be required for different mission tasks, depending on precision requirements, and it is proposed that formation manoeuvring be investigated in the

presence of a gravity gradient. Of current interest is the ability to perform Lagrange point formation control and manoeuvring in the presence of sensor/actuator noise and dynamics, and to perform manoeuvres in an optimal manner, ideally while balancing fuel use across the formation.

3.3 Summary and Rationale for Research

A significant proportion of the literature on satellite formation flying dynamics and control in both LEO and in deep space (near L2) has been reviewed in this chapter. The material presented in this review has been used to establish a more detailed definition of the research objectives, however it should be noted that a proportion of the literature was not available at the start of the programme (2001). Where appropriate, additional literature from 2003 and 2004 has been incorporated into the review, although the majority of the work undertaken was motivated through an appreciation of papers published prior to mid-2002.

This summary comprises a brief review of the main findings of the LEO and deep space formation flying literature presented in sections 3.1 and 3.2, and concludes with a general outline of how the literature review influenced the direction of research. More detailed analysis of the motivation and justification for different aspects of the research is presented in the introductory sections of chapters 4 to 7.

3.3.1 Chapter Summary

In section 3.1, a thorough survey of literature relating to LEO formation flying dynamics and control was presented. This highlighted the scope and depth of research, primarily during the last five years, in the areas of dynamics model development, missions, applications, formation design, relative orbit perturbations, and formation flying control systems and their evaluation.

Two main approaches to the modelling of relative dynamics in LEO were identified:

- Linear Hill equations in a Cartesian frame based at a satellite on a circular reference orbit.
- Relative orbit elements.

The advantages and disadvantages of each approach for formation design and formation flying control were established by considering the following:

- Mathematical assumptions incorporated into the model derivation and the resulting model limitations (linearisation, singularities).
- Solutions to the formation flying equations and their applicability to formation design and orbit visualisation.
- The ease with which perturbations can be included in the model.
- The practical implementation of the dynamics model in the wider control system (sensors, actuators, use of the dynamics matrix for controller design).

Upon consideration of the literature, the Hill equations were found to be limited in a number of ways, but sufficiently flexible in terms of the methods by which

perturbations, eccentricity and nonlinear terms could be incorporated to more accurately describe relative motion. They describe relative motion in the frame of on-orbit relative position and velocity measurement, thus eliminating the need for complex transformations from orbit elements to the Hill frame coordinates. The orbit elements approach appears to be better for formation design and maintenance when long term bounded motion is required, however the dynamics model does not capture short period motions which may be important for interferometry applications. The Hill equations approach has therefore been selected for the LEO formation flying dynamics and control research performed in later chapters.

A number of applications of LEO formations were established through a review of formation flying mission studies for the following mission types:

- Interferometric Earth observation and imaging.
- Interferometric Astronomy.
- Scientific Earth observation and communications.

It was found that a Hill equations dynamics model approach was used almost exclusively in all this research where precision formation flying was required.
Much of the available literature on LEO formation flying involves some aspect of formation design. To reduce the fuel required to maintain a formation to a practical level, it is necessary to design the formation using any naturally available formation dynamics. Both relative orbit elements and the Hill equations provide solutions or constraints which will enforce the bounded motion of satellites over time, thus meeting this requirement. In particular the existence of J_2 invariant relative orbits was investigated for later consideration as a test case in chapter 4.

The effects of orbit perturbations and orbit eccentricity on satellite relative motion in LEO, according to research published in recent literature, were also investigated. In particular, the effects of the following were considered:

- Earth oblateness
- Atmospheric Drag
- Solar Radiation Pressure
- Reference orbit eccentricity

The Earth oblateness (J_2) perturbation has the most significant effect on satellite formation keeping in LEO, and the findings of this part of the review are discussed further in chapter 4 where alternative formation flying models incorporating the effects of J_2 are developed. In support of the research presented in chapters 4 and 5, any fuel use ΔV evaluations performed for formation keeping in the presence of the J_2 perturbation were collated for later comparisons, and techniques for augmenting relative dynamics models to incorporate these effects were surveyed.

A number of linear and nonlinear control techniques have been successfully applied to the satellite formation flying formation keeping and manoeuvring problem. The most commonly applied techniques include LQR and Lyapunov control using both Hill-frame and orbit elements relative dynamics models, and both continuous and discrete control systems. Less emphasis has been placed on the detailed review of guidance for LEO satellite formations, as much of the literature has only become available more recently, and after the LEO formation flying research performed for chapters 4 and 5.

In section 3.2 an overview of basic Lagrange or 'libration' point celestial mechanics for the circular restricted three body problem (CR3BP) is presented. A basic linear description of a Lagrange point orbit is derived and forms the background necessary for the model development research presented in chapter 6. An overview of the literature associated with the derivation of higher order solutions for halo orbit motion in the vicinity of the collinear libration points is also presented for later application.

An appreciation of the unstable dynamic environment in the vicinity of, in particular, the Sun-Earth L2 libration point is important as it is the planned destination of a number of future formation flying missions which require different orbital characteristics. Numerical methods are able to provide increased insight into both transfer trajectories and the stability and types of orbits that can be used for formations at the Lagrange points. In parallel is the need for an appreciation of the perturbation environment, and its effect on orbit control and formation control. This is found to be much more significant in the former case.

A brief overview of the single satellite missions, both past and present, to the Lagrange points is provided. Of particular interest is the ISEE-3 mission which adopted a trajectory following orbit maintenance approach using both analytically and numerically derived trajectories (the latter was found to reduce fuel use as this enable the satellite to adopt a more natural motion). An awareness of the cost of satellite formation keeping has therefore been gained.

In the final sections of 3.2, the relative motion dynamics models applied to control system design have been identified, and guidance strategies for formation manoeuvring, including some load-levelling, have been reviewed.

A Dynamical Systems Theory approach to formation design and control appears to be inappropriate for precision formation flying. Instead, either neglecting the orbital dynamics altogether, in favour of investigating formation manoeuvres for the science tasks of TPF or Darwin, or linearising the dynamics about a reference trajectory in the three body problem is preferred. No fully analytical approaches to deriving a linearised dynamics model were identified at the outset, and the analytical approach was therefore considered for relative motion model development prior to the formation control analysis performed in chapter 7.

3.3.2 Rationale For Research

This literature review has supported the rationale for and definition of the objectives for the dynamics and control simulation studies in the following chapters (refer to Figure 1-3, chapter 1, for the Thesis Road Map). The following sections summarise the original research plan, and particular conclusions of the literature survey that have contributed to motivating the research performed.

3.3.2.1 Original Research Plan

The original objectives for performing research into both LEO and L2 formation flying were reinforced by the literature review, and can be summarised as follows:

- A LEO study would demonstrate the methods of relative motion modelling (in the presence of significant orbit perturbations) that could be applied at L2.
- A greater insight into different approaches to tackling the formation flying problem would be gained by focussing on LEO due to the wealth of available literature.
- Familiarity would be gained with the necessary mathematical techniques for solving equations of motion and control system design.
- Performing a precursor study would enable the development of software tools for simulation and visualisation of the formation flying results that could also be applied to L2.
- Continuation of work initially carried out in support of the MUSTANG project at the Cranfield University Space Research Centre would be an appropriate starting point (Roberts, Bowling, and Hobbs, 2002).

3.3.2.2 Application of the Literature Review to the Research Plan

The more detailed conclusions from the literature review, which were directly applied to the research presented in chapters 4 to 7 are summarised below:

- The review confirmed that for the LEO case, the selection of a Hill-type dynamics model was appropriate and justified (section 3.1.1.4).

- A number of authors have attempted to incorporate the J_2 perturbation into relative dynamics models of varying complexity. The perturbing force is either included as a forcing function within the equations of motion, or the effects on orbit element drifts and secular terms in the relative motion have been identified and incorporated into the model. The effects of the J_2 perturbation have been evaluated using both numerical and analytical approaches. However, although some comparisons between different models have been made, regarding their ability to capture perturbed relative satellite motion, the comparisons have not been performed in the context of their application to control system design.

- Equations with nonlinear terms and other effects (quadratic drag and eccentricity) have been used for linear and nonlinear control system design. For the LQR technique, nonlinear control was found to be of no benefit for satellites in relatively close proximity, and controllers designed using the basic Hill equations were sufficient. However, many systems were not evaluated in the perturbed environment in order to appreciate fully their limitations. The contrasts in control law design technique did not include J_2.

- It is claimed that compensating for the smaller scale periodic motions associated with the J_2 perturbation would require excessive and impractical levels of fuel use.

- In terms of control system design, continuous thrust is anticipated for the science manoeuvres of Darwin. As the LEO study is a precursor, a more costly continuous LQR control method was selected. This approach is easily discretised for formation control using Pulsed Plasma Thrusters (PPT), and there are many examples of discrete, but not continuous, LQR control in the literature.

Further details of the control law selection are presented in the introductory sections of chapter 5.

- Relatively few studies performance evaluate control systems in the presence of a full set of LEO perturbations. No descriptions of the use of the Satellite Tool Kit (STK) for model validation and controller evaluation have been identified.

- An analytical description of the relative dynamics of satellite formation flying around a halo orbit at the Sun-Earth was not available at the time of proposing the research.

- The load-levelling strategies designed for deep space applications have not been evaluated in the perturbed environment, and while maintaining a halo trajectory.

These conclusions generated a number of questions which, in combination with the overall thesis aims, and recent work at Cranfield University on MUSTANG, were assembled into the following more detailed objectives for the LEO research in chapters 4 and 5.

- Evaluate the magnitude of the different relative orbit perturbations in LEO.
- Identify and compare suitable methods for incorporating the differential J_2 perturbation force into the equations of relative motion in the Hill frame (based on existing models).
- Establish any limitations of the models, and improve these accordingly.
- Solve equations of motion and establish initial conditions for bounded relative motion.
- Verify the analytical models against STK numerical orbit propagators.
- Apply the models to continuous LQR control system design for formation flying scenarios in the perturbed environment.
- Evaluate the ΔV required for a range of formation keeping tasks.
- Compare the higher fidelity J_2 models against the basic Hill equations to see if benefits can be achieved.
- Develop a software interface tool for formation flying scenarios using Matlab/Simulink and STK.

The research associated with these objectives has been split between chapters 4 and 5. Model development, solution and verification is described in chapter 4, and control law design and evaluation is performed in chapter 5. For the study of a Darwin-type formation performing science manoeuvres, the following objectives have been defined:

- Derive an analytical description of absolute and relative motion for a formation in a halo orbit around the Sun-Earth L2 point.
- Implement control and guidance strategies to perform a sequence of tasks while load-levelling across the formation, and maintaining a halo orbit around L2.
- Evaluate the formation flying fuel requirements (using continuous control).
- Visualise the controlled formation flying scenario in STK.

Again, the research associated with these objectives has been split between two chapters. The model development and preliminary verification is presented in chapter 6, and the formation flying control law design and visualisation is addressed in chapter 7.

4 THE DEVELOPMENT OF LOW EARTH ORBIT FORMATION FLYING MODELS

In order to perform any aspect of design and control of a satellite formation, it is necessary to model the motion of the spacecraft in the space environment. An interferometric astronomy mission research focus was selected in chapter 2. This and the literature review, presented in chapter 3 have supported the general research aim, which ultimately involves the development of a relative motion dynamics model at the Sun-Earth L2 Lagrange point and its application to control system design for a Darwin-type mission.

Following the literature review, the LEO formation flying research enabled familiarity to be gained with the software tools and mathematical techniques that could be applied to the problem. In addition, the significant proportion of formation flying literature identified in chapter 3 related to LEO rather than deep space, and the results of many LEO studies were therefore available for comparison with those generated here.

An extensive study of the types of models which could be used for formation flying control (refer to section 3.1.1, chapter 3) was performed, and a Hill-type dynamic system was selected for a LEO interferometry application; a context adopted in preparation for the later research into the L2 formation flying problem. A significant area of interest within the literature is the effect of orbit perturbations, and in particular the effects of J_2 (Earth oblateness) on the formation. Schweighart and Sedwick (2001a) derived a relative motion model by extending the Hill equations to include linearised perturbations due to the Earth's oblateness (J_2) and Izzo (2002b), referencing this work, tried to capture relative motion better by retaining time varying perturbation terms, but did not perform any model validation. In this case, the limitations of both models are explored, and a new one is developed by incorporating corrective terms from the analytical model into the time varying model. The resulting dynamics are verified against the Satellite Tool Kit (STK) Astrogator high precision numerical orbit propagator. Through model verification the new formation flying model limitations are also assessed, and STK is evaluated as a suitable environment in which to fly the controlled formation.

A complete discussion of the research context, drawing on the rationale outlined in section 3.3.2.2 (chapter 3), and providing justification for the approach taken is presented in section 4.1. The research into the development of LEO relative dynamics models is presented in the following sections, and the application of the models to control system design for formation keeping is presented in chapter 5.

In section 4.2, the Hill equations and their solutions are discussed, and orbit perturbation expressions are presented. A preliminary evaluation of the magnitudes of the aerodynamic drag, gravitational, third body, and Solar radiation pressure perturbation accelerations on satellites in LEO is made, and more importantly for this research, their effects on relative motion are assessed. The perturbation due to J_2 is

found to be the most significant disturbance acceleration affecting the relative motion of two satellites in LEO.

In the first stage of model development (section 4.3), the work performed at MIT, now published in more complete form by Schweighart and Sedwick (2002), is derived and implemented independently. A review of their analytical model development theory is therefore presented. Solutions and initial conditions associated with the equations of motion are derived for the analytical, time varying, and Hill equations LEO formation flying models. Their limitations are established by model verification against STK and the verification method and key test case results are presented. Supporting material in the form of theory and derivations from the literature are included in appendix D.

The time invariant and time varying J_2 models are both found to approximate fairly well the motion of a perturbed cluster of satellites relative to a circular reference orbit. This is fundamental to the modelling of the relative motion between multiple J_2 perturbed satellites. However, for bounded formations, the time invariant model captures the relative motion of two J_2 perturbed satellites more accurately than the time varying J_2 model or the Hill equations. Reasons for the lack of accuracy of the time varying model are sought. However, the retention of time varying parameters was found to capture the shape of the small-scale motion dynamics for a wider range of conditions (including non-bounded formations) than the time invariant model and Hill equations.

4.1 The Context of LEO Model Development

A preliminary evaluation of the relative accelerations experienced by satellites in LEO revealed that the Earth's oblateness was the primary perturbation. Over the past five years, significant research has been performed into the development of LEO formation flying models that incorporate the effects of the J_2 perturbation, and many of these were reviewed in chapter 3. In this section, the J_2 modelling research performed in this chapter is described in the context of the reviewed literature. The ultimate aim of the LEO research is to find a way to maintain a formation of satellites in the perturbed environment in a more fuel efficient and spatially accurate manner.

The research detail was motivated by the following considerations:

- Why mathematical models of relative satellite motion are required.
- Whether the J_2 perturbation is the most disturbing factor on the formation and to understand how this can be included in the equations of motion.
- Whether there was a simple way to incorporate the J_2 perturbation into the equations, to improve model fidelity without introducing significant complexity.
- The way in which modelling approaches in LEO could be adapted to model development in the vicinity of L2.
- The fact that the selected models already developed had limitations (and the importance of establishing what these are).
- The model verification processes and results of other researchers in terms of ΔV estimates for formation keeping in LEO.

- Whether it was possible to further develop recent models and use them for controller design.
- The fact that in the literature, model nonlinearity has been incorporated into control law design and compared to linear model control, and has been found not to demonstrate improved performance for very close formations. However, this was in the absence of J_2, and the nonlinear system did demonstrate improvements for the formation keeping control of larger formations.

4.1.1 Relative Dynamics Models and Model Fidelity

The advantages of a Hill-type relative dynamics model for satellite formation flying over orbit elements approaches were presented in chapter 3 (sections 3.1.1.4 and 3.3), and the literature review revealed a number of techniques for including perturbations in relative motion models. The curvilinear or Cartesian Hill frame based on a circular or elliptical reference orbit respectively would appear to be the most practical coordinate system for formation flying dynamics modelling and controller design. In the Hill frame, it is more straightforward to visualise the relative motion between satellites, and there are fewer variables to control. Linearised disturbance accelerations can also be more easily implemented. It is easier to model and describe sensor and thruster behaviour, and their measurement of relative motion parameters (relative positions, velocities and accelerations) to higher accuracy in the context of a satellite-based Cartesian coordinate frame rather than through conversions to orbital elements.

A relative dynamics model is less complex for establishing relative motion, compared to obtaining the individual positions and velocities of satellites and differencing them. The relative dynamics models can be more easily applied to formation flying controller design, where the relative motion parameters become the controlled state variables, rather than the orbital elements of separately controlled satellites within the formation.

The unperturbed Hill equations (introduced in section 3.1.1.1 and considered further in section 4.2.1) were described as sufficient for modelling and control design for the rendezvous of satellites in LEO over short periods of time, but not sufficient to predict the relative motion of spacecraft flying in formation over longer periods. However, these equations can be developed to allow relative motion to be predicted more accurately for the duration of the mission lifetime (section 4.3).

A case for the development of high fidelity analytical models describing satellite relative motion was made in chapter 2. Relative dynamics models have a role to play in primarily:

- On-board orbit determination (autonomous).
- Control system design (and simulation studies).
- Providing physical insight into formation dynamics for formation design and control.

Improvements in model fidelity will improve the accuracy with which simulations of the relative behaviour of two or more satellites in the perturbed environment can be performed, either as a stand-alone model, or as a more representative environment for

controller evaluation. A high fidelity analytical model will also provide increased insight into the relative motion dynamics caused by the additional perturbations (rather than by observation of individual trajectories in the ECI frame). An improved dynamics model may enable controller designs to be tuned to provide a more optimal response to state errors, and higher fidelity solutions can be used to optimise guidance for a particular application by enabling as much of the natural relative orbit dynamics to be taken into account as possible. Also, given a measured set of conditions, the higher fidelity models can more accurately predict future relative spacecraft motion as part of onboard guidance systems.

In this case, the J_2 perturbation is included in the Hill equations, as this is the most significant relative perturbation on a LEO formation, with short period dynamic effects which will disrupt precision formation keeping. Through the following model developments, the effects of J_2 on the relative dynamics are identified, and although the dynamics of the secular drift are slow, and the state matrices for the Hill and time invariant J_2 models are similar, these are applied to control system design in chapter 5. Here, the solutions of the Hill and J_2 models are also used as guidance functions prescribing relative trajectories for satellites separated by up to 1km. Feedback control is used for trajectory following by the follower satellite in a leader-follower architecture, and the implementation of alternative control strategies using the time averaged and time varying models is explored, and any performance benefits noted. In order to assess the benefits of including the J_2 perturbation in trajectory planning, continuous linear quadratic regulator (LQR) control is applied. The motivation for exploring this particular control technique is discussed further in chapter 5 (section 5.1).

4.1.2 The Context of J_2 Model Development

The assumption that the Earth is a perfect sphere, rather than an oblate spheroid, introduces the most significant error to LEO formation flying models. Therefore, it is necessary to investigate the modelling and potential controller design improvements that could be achieved if the acceleration specifically due to J_2 was included in the linearised equations of relative motion. Likely improvements include reduced fuel use for formation keeping and the provision of greater facility for choosing the optimum operational orbits for the formation. The effects of relative aerodynamic drag and relative spacecraft attitude also need to be included in any dynamics model when the spacecraft are dissimilar and have different ballistic coefficients, however here we assume this is not the case. The perturbing effects of aerodynamic drag, higher order zonal harmonics (J_3), and higher order Hill equations terms are briefly considered at the end of this chapter.

Schweighart and Sedwick (2002), (2001a) developed a high fidelity linearised set of differential equations for describing the relative motion of satellites in the presence of the Earth oblateness (J_2) gravity perturbation. In their model, the accelerations due to the J_2 effect are linearised and included in the equations of relative motion, and the Hill equations are also modified further to take into account the change in orbit period and drift of the longitude of ascending node caused by the J_2 perturbation (discussed in section 4.2.2.2). The cross-track motion is not captured in the first instance by the

linearised equations because the gradient of J_2 disturbance is modelled by taking its time average. In their study, their equations of relative motion are compared to their own in-house numerical orbit propagator. However, when first investigated, they had only published model verification data for one test case. Since then they have published maximum error measurements over 10 orbits for different combinations of reference orbit altitude and inclination, but did not define the model limitations or apply the model to control law design.

In the formation flying work performed for MUSTANG at Cranfield (Izzo, 2002b), (Roberts, Bowling, and Hobbs, 2002) the gradient of J_2 term in the equations of relative motion was allowed to remain time varying, thus removing the problems associated with time averaging of the perturbation term. However, no corrective terms (due to the effects of J_2 on the orbital period and longitude of ascending node) were included in the model, rendering the linearisation assumption invalid. Initial conditions analyses that are required for an accurate, useable set of equations of motion were not included in the study, and no model validation was performed.

Because of the limitations of the analytical model developed by Schweighart and Sedwick, and the omissions in the time varying study by Izzo, the derivation of a new orbit period and nodal drift-corrected version of the time varying model is proposed. The three (Hill, time averaged J_2, and time varying J_2) models are then verified against STK to establish their fidelity and comparative limitations. A significant proportion of the model development work in this chapter is based on the work of Schweighart and Sedwick (2001a), although the publication of their new geometric cross-track model and additional model validation results occurred after this study had already begun. A detailed overview of their model is presented in section 4.3, and referenced as appropriate, as it is integral to the development of the time varying model, and in this way the differences between the models can be highlighted.

4.1.3 Incorporating the J_2 Perturbation into Relative Dynamics Models

In section 4.2.1, the linearised Hill equations describing relative motion of one satellite relative to a reference satellite are introduced. To derive analytical solutions and initial conditions the J_2 perturbation is included in the equations as a periodic forcing function, and then in linearised form. The Hill equations are firstly extended to examine the effects of the perturbation due to J_2 on a circular reference orbit, and secondly to examine the effects of J_2 on the relative motion behaviour of two perturbed satellites, neither being constrained to the circular reference orbit. In this case, the contributions of different terms are presented in more detail to highlight aspects of the relative motion dynamics due to J_2.

In addition to exploring the model limitations, the purpose of model verification against STK is to also to gain familiarity with the implementation of initial conditions in non-Hill frame coordinates, and to assess the use of STK as a ‘real environment’ within which a controller (effectively onboard a satellite) could be evaluated. Neither the time averaged or time varying models have been applied and evaluated in the control law design process before, and this model development and verification is therefore an

essential step in preparing for future model application, and the contrast in performance of the unperturbed and perturbed Hill equations.

4.1.4 Conclusion on Model Development

In conclusion, relative dynamics models are more practical for control system design, and require much less processing power to solve for relative motion compared to the propagation of the absolute motion parameters of individual satellites and differencing them. In the former case, only approximately half of the calculations would be required.

The Hill frame (illustrated in Figure 3-1, section 3.1.1.1) is suitable for the implementation of perturbing accelerations within the equations of relative motion, and the inclusion of additional perturbations is relatively simple. Before investigating the use of higher fidelity models on improved controller design to minimise fuel use in the formation keeping task in LEO, it is necessary to compare model performance and their suitability for the task, and to verify them to establish their limitations. In the absence of available, prior modelling and simulation work in the field of satellite formation flying at Cranfield, the motivation for the model derivation and verification has been presented, and the modelling approach proposed as a suitable way forward.

4.2 Background and Theory

The derivation of the Hill equations and their basic solutions are described in this section as a precursor to the development of perturbed relative motion equations. The important LEO disturbance forces and their effects on the orbit of a single satellite are introduced and a preliminary assessment of their relative effects on a satellite formation is also presented.

4.2.1 The Hill Equations

Although only the linearised form of the Hill equations are applied to the formation flying modelling and control problem in this work, the nature of the higher order and nonlinear behaviour of Hill's equations is briefly considered. In the first section, the basic equations of motion are introduced, and in the second section the higher order terms and their effects are discussed.

4.2.1.1 Basic Equations of Motion

The basic relative motion equations were originally developed by Hill (1878), and later applied to satellite rendezvous by Clohessy and Wiltshire (1960) (refer to the review of the original papers in section 3.1.1.1). These linearised equations describe the relative motion of two satellites under the point-mass gravitational influence of a central body, each governed by the inverse square gravity law in the form of equation (4-1).

$$\underline{g}(\underline{r}) = \frac{-\mu}{r^3}\underline{r} \qquad (4\text{-}1)$$

For the Hill equations, the Earth is assumed to be a perfect sphere and approximates point mass behaviour. In equation (4-1) μ is the Earth gravitational parameter (GM_E) and r is the orbit radius of the satellite from the centre of the Earth.

In this case, the equations of relative motion are based in a Cartesian coordinate frame, made to travel around a circular orbit with an angular velocity, ω. The circular orbit traced by this 'Hill' frame will be referred to as the 'reference orbit' from which relative motion is described, and the radius of the reference orbit is r_{ref}. In this case one of the satellites in the formation may be considered to be located on the reference orbit as perturbations are not considered. The role of the reference orbit in the presence of perturbations is discussed further in section 4.3.6. The equations can be derived using either an ECI coordinate frame (I, J, K), or the moving Hill frame (i, j, k) (Kaplan, 1976), (Wie, 1998). Both coordinate frames are illustrated in Figure 4-1. The relative acceleration of P_1 with respect to P_0 can be simply transformed between the ECI and Hill frames.

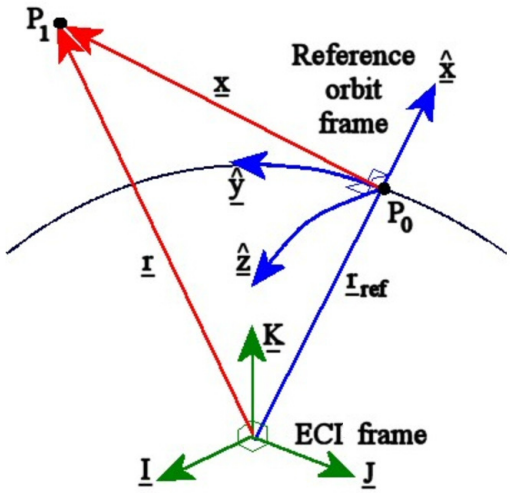

Figure 4-1: Earth-Centred-Inertial and Rotating Hill Frames

Because the main source of reference for the development of the analytical models (Schweighart and Sedwick, 2002) uses '$\underline{x}$' as the relative position vector, this is maintained for ease of comparisons with later model derivations. In the local vertical local horizontal (LVLH) x-y-z Cartesian coordinate system (Figure 4-1), relative position, velocity and acceleration are given by equations (4-2).

$$\begin{aligned}
\underline{x} &= \underline{r} - \underline{r}_{ref} \\
\underline{x} &= x\underline{i} + y\underline{j} + z\underline{k} \\
\dot{\underline{x}} &= \dot{x}\underline{i} + \dot{y}\underline{j} + \dot{z}\underline{k} \\
\ddot{\underline{x}} &= \ddot{x}\underline{i} + \ddot{y}\underline{j} + \ddot{z}\underline{k}
\end{aligned} \qquad (4\text{-}2)$$

The local coordinate frame is in fact an approximation to a curvilinear coordinate system. In this curvilinear system (Figure 4-1), the $\hat{x}$ axis lies along the radius vector (radial direction), the $\hat{y}$ axis is on the orbital plane, normal to the radius vector and curving around the orbit, and the $\hat{z}$ axis curves around the Earth in the out-of-plane direction. The LVLH x-y-z Cartesian coordinate system is related to the curvilinear $\hat{x}$-$\hat{y}$-$\hat{z}$ system by equations (4-3) to (4-5). For small distances between satellites, the Cartesian x-y-z frame approximates the true curvilinear frame.

$$\hat{x} = \frac{\left(r_{ref} + x\right)}{\cos\left(\tan^{-1}\left(\frac{y}{r_{ref} + x}\right)\right)\cos\left(\tan^{-1}\left(\frac{z}{r_{ref} + x}\right)\right)} - r_{ref} \tag{4-3}$$

$$\hat{y} = r_{ref}\tan^{-1}\left(\frac{y}{r_{ref} + x}\right) \tag{4-4}$$

$$\hat{z} = r_{ref}\tan^{-1}\left(\frac{z}{r_{ref} + x}\right) \tag{4-5}$$

For the second satellite, P_1, in the vicinity of the reference, P_0, the velocity relative to the centre of the Earth is given by equation (4-6). This velocity ($\underline{\dot{r}}$) can be expressed in terms of the velocity at P_0 plus relative motion terms in the Hill frame that takes into account both its translation and rotation.

$$\underline{\dot{r}} = \underline{\dot{r}}_{ref} + \underline{\dot{x}} + \underline{\omega} \times \underline{x} \tag{4-6}$$

The rotation vector is expressed as

$$\underline{\omega} = n\underline{k} \tag{4-7}$$

For a constant orbital velocity, ω (for a satellite tracing a circular reference orbit), the acceleration of P_1 is given by equation (4-8)

$$\underline{\ddot{r}} = \underline{\ddot{r}}_{ref} + \underline{\ddot{x}} + 2\left(\underline{\omega} \times \underline{\dot{x}}\right) + \left(\underline{\omega} \times \left(\underline{\omega} \times \underline{x}\right)\right) \tag{4-8}$$

$\underline{\ddot{x}}$ is the relative acceleration of P_1 to P_0 in the Hill frame, $2\left(\underline{\omega} \times \underline{\dot{x}}\right)$ is the Coriolis acceleration due to the rotation of the axis system, and the centrifugal acceleration due to the angle between ω and $\underline{x}$ is $\underline{\omega} \times \left(\underline{\omega} \times \underline{x}\right)$. The terms in r in equation (4-8) are point-mass gravitational accelerations of the satellite at the reference orbit, P_0 (r_{ref}) and at P_1 (r). In linearised form the relative acceleration at P_1 relative to P_0 is given by equation (4-9) (Kaplan, 1976).

$$\underline{\ddot{r}} - \underline{\ddot{r}}_{ref} \approx \frac{\mu}{r_{ref}^3}\left(-\underline{x} + 3\left(\frac{\underline{r}_{ref} \cdot \underline{x}}{r_{ref}^2}\right)\underline{r}_{ref}\right) + O\left(\underline{x}^2\right) \tag{4-9}$$

In the Hill frame, equation (4-9) can be rewritten in component form to give equation (4-10)

$$\ddot{\underline{r}} - \ddot{\underline{r}}_{ref} \approx \begin{bmatrix} \frac{2\mu}{r_{ref}^3} & 0 & 0 \\ 0 & -\frac{\mu}{r_{ref}^3} & 0 \\ 0 & 0 & -\frac{\mu}{r_{ref}^3} \end{bmatrix} \begin{bmatrix} x \\ y \\ z \end{bmatrix} = \begin{bmatrix} 2n^2 x \\ -n^2 y \\ -n^2 z \end{bmatrix} = \nabla \underline{g}(\underline{r}_{ref}) \cdot \underline{x} \qquad (4\text{-}10)$$

where the orbital rate, or mean motion of a satellite on the reference orbit is given by equation (4-11)

$$n = \sqrt{\frac{\mu}{r_{ref}^3}} \qquad (4\text{-}11)$$

By substituting expression (4-10) into equation (4-8), the linear differential equations of relative motion between a satellite at P_1 and a satellite on a circular reference orbit, P_0, in the Hill frame result. The x-y-z components in the expressions are measured in the curvilinear frame.

$$\ddot{x} - 2n\dot{y} - 3n^2 x = 0 \qquad (4\text{-}12)$$

$$\ddot{y} + 2n\dot{x} = 0 \qquad (4\text{-}13)$$

$$\ddot{z} + n^2 z = 0 \qquad (4\text{-}14)$$

The Hill equations can be easily solved analytically, and form the basis for the development of expressions for relative satellite motions in a perturbed environment, and a baseline with which to compare analytical solutions and control law behaviour.

4.2.1.2 Higher Order Terms

In section 4.2.1.1, all the nonlinear, higher order terms in the Hill equations were neglected, however, it is appropriate to perform at least some preliminary analysis to quantify these terms, and the errors associated with linearization. The full nonlinear relative equations are given by equations (4-15).

$$\begin{aligned} \ddot{x} - 2n\dot{y} - n^2(r_0 + x) &= -\frac{\mu(r_0 + x)}{\left[(r_0 + x)^2 + y^2 + z^2\right]^{3/2}} \\ \ddot{y} + 2n\dot{x} - n^2 y &= -\frac{\mu y}{\left[(r_0 + x)^2 + y^2 + z^2\right]^{3/2}} \\ \ddot{z} &= -\frac{\mu z}{\left[(r_0 + x)^2 + y^2 + z^2\right]^{3/2}} \end{aligned} \qquad (4\text{-}15)$$

Richardson and Mitchell (2002) derive the third order Hill equations in non-dimensional form, and find an accurate periodic solution by the method of successive approximations. The nonlinear contributions are on the right hand side of their

equations (4-16) and include both unidirectional and cross-coupled terms. Clearly, without these terms, the equations reduce to the linear Hill equations (4-12) to (4-14).

$$\ddot{x} - 2\dot{y} - 3x = -\frac{3}{2}\left(2\dot{x}^2 - y^2 - z^2\right) + 2x\left(2x^2 - 3y^2 - 3z^2\right)$$
$$\ddot{y} + 2\dot{x} = 3xy - \frac{3}{2}y\left(4x^2 - y^2 - z^2\right) \qquad (4\text{-}16)$$
$$\ddot{z} + z = 3xz - \frac{3}{2}z\left(4x^2 - y^2 - z^2\right)$$

Their evaluation of the numerical solution to these equations and their analytical solutions was found to be consistent with the truncation errors arising from the solution method. Physically, the relative position errors encountered by the analytical solution were of the order of centimetres radially, millimetres along-track, and tenths of a millimetre in the cross-track direction over one day when the initial separations were 20km and 4km in the radial direction and cross-track directions respectively. The contribution of nonlinear terms are compared to the effects of orbit perturbation accelerations on relative motion in section 4.2.2.5.

4.2.1.3 Solutions and Initial Conditions

In all cases, the model development work has been separated into in-plane and cross-track analysis. The in-plane (x-y) equations are coupled and therefore solved together. The cross-track (z) motion analysis is summarised separately.

The in-plane equations of motion are combined by integrating equation (4-13) and substituting the resulting y velocity (equation (4-17)) into equation (4-12) to give equation (4-18).

$$\dot{y} = -2nx + 2nx_0 + \dot{y}_0 \qquad (4\text{-}17)$$

$$\ddot{x} + n^2 x = 4n^2 x_0 + 2n\dot{y}_0 \qquad (4\text{-}18)$$

Using the standard complementary function and particular integral solution method to solve equation (4-18), a general solution for the x-motion is obtained. This can be substituted back into equation (4-17) to derive a solution for the y-motion. The terms containing the subscript '$_0$' represent the initial position and velocity conditions at time t = 0. The in-plane and cross-track relative position solutions to the Hill equations are given by equations (4-19) to (4-21) and the velocity expressions are included in the Hill equations summary in appendix D.

$$x(t) = x_0(4 - 3\cos nt) + \frac{\dot{x}_0}{n}\sin nt + \frac{2\dot{y}_0}{n}(1 - \cos nt) \qquad (4\text{-}19)$$

$$y(t) = x_0(6\sin nt - 6nt) + y_0 + \frac{2\dot{x}_0}{n}(\cos nt - 1) + \dot{y}_0\left(\frac{4}{n}\sin nt - 3t\right) \qquad (4\text{-}20)$$

$$z(t) = z_0 \cos nt + \frac{\dot{z}_0}{n}\sin nt \qquad (4\text{-}21)$$

4.2.1.4 Relative Motion

An overview of model implementation in Matlab/Simulink for both the Hill equations and the other analytical models investigated in this chapter is given in section 4.5. Also, the equations are compared to individually propagated satellites as part of the model verification process in section 4.7. At this stage, the purpose of this section is to illustrate the relative motion behaviour of two satellites according to the Hill equations derived above for some example sets of initial conditions.

The undisturbed relative motion behaviour exhibited here is important for later comparisons with perturbed results. The satellites separated in the along-track y-direction with zero relative velocity simply follow the same track at the same rate around the circular reference orbit. Therefore, only a constant along-track (y) offset is observed in Figure 4-2a.

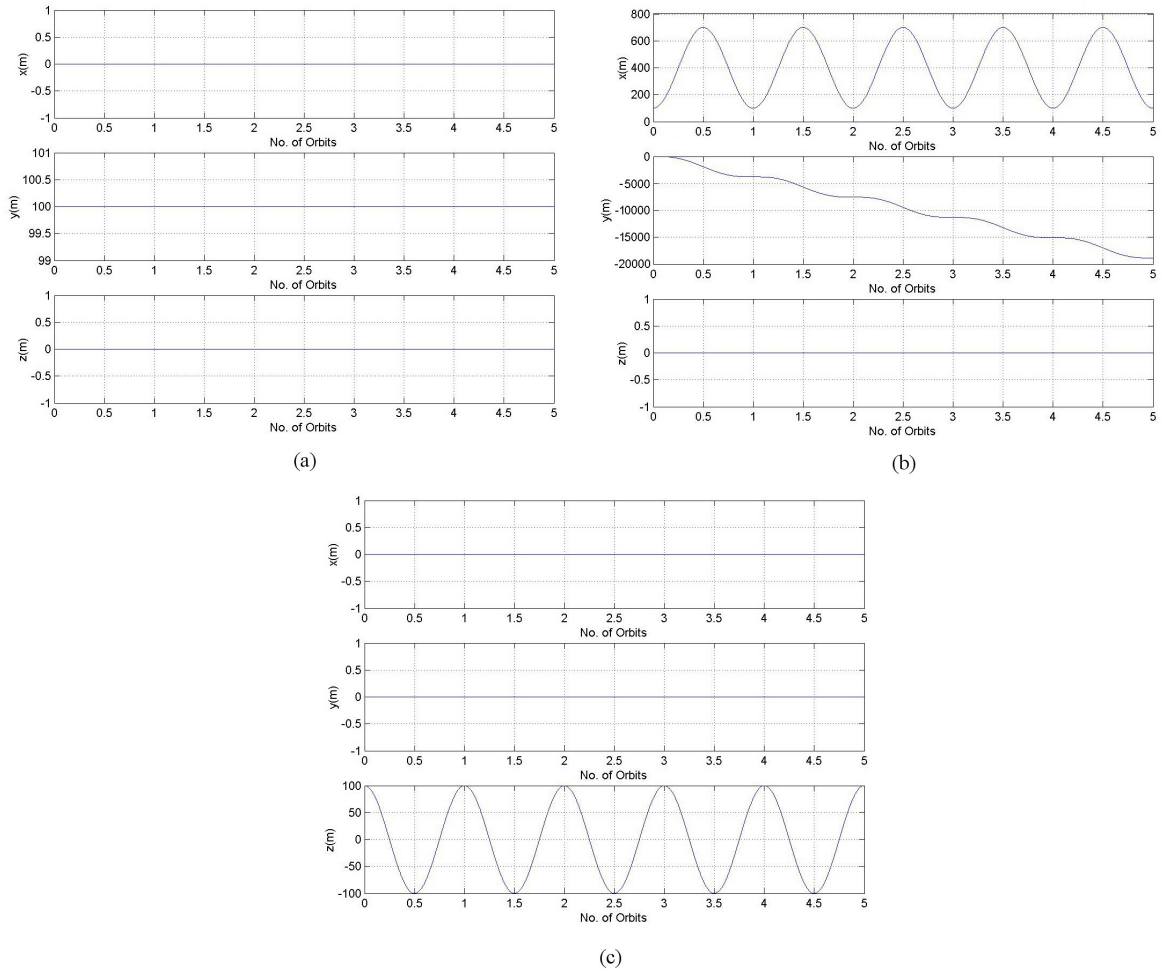

Figure 4-2: Effects of Initial Separation (x,y,z in metres) on Relative Motion in the Hill Frame for: (a) y-Separation (0,100,0) (b) x-Separation (100,0,0) (c) z-Separation (0,0,100)

When the satellites are separated radially by 100m (x), and again have zero relative velocity, the slower satellite at the higher altitude begins to lag behind the satellite in the reference orbit, and the radial relative motion is oscillatory (Figure 4-2b). The relative motion due to a cross-track z-separation is oscillatory and uncoupled to the in-plane motion (Figure 4-2c).

4.2.2 Orbital Perturbations

In the following subsections, the orbit perturbations experienced by a satellite formation in Low Earth Orbit (LEO) are described. Figure 4-3 illustrates the relative magnitude of the accelerations from different sources that affect individual satellites in LEO. Note that the accelerations on the chart are normalised with respect to the point mass acceleration on the Earth's surface at the equator. The dominant force of 'primary gravity' is of course the point mass gravity effect of the central body, spherical Earth, which maintains the satellite on a basic circular or elliptical orbit. The former was considered in the derivation of the Hill equations in section 4.2.1.1. The other perturbations each prevent the satellite from maintaining and exactly repeating its orbit, and cause small deviations from the two-body motion. The different perturbation contributions are described in order of descending importance in the following subsections and analytical expressions to describe these accelerations are presented.

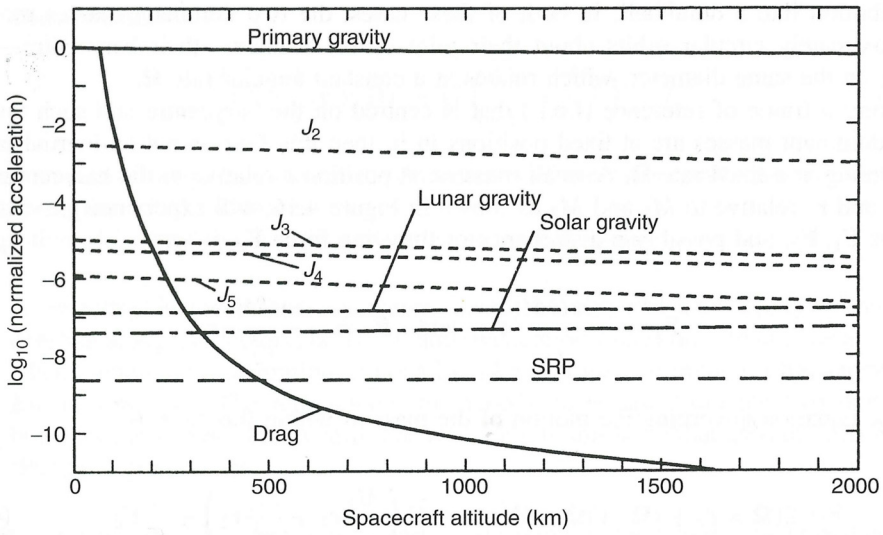

Figure 4-3: Orbit Perturbations (Fortescue, Stark, and Swinerd, 2003)

4.2.2.1 Atmospheric Drag

Atmospheric drag is the most significant perturbing force for satellites in very low altitude orbits, and reduces quickly with decreasing atmospheric density and therefore increasing altitude. According to Figure 4-3, beyond approximately 130km altitude other gravitational perturbations become more important.

Newtonian free molecular flow aerodynamics can be used to describe the forces experienced by a satellite in LEO. Drag forces will act in opposition to the direction of travel relative to the atmosphere, and are greater at lower altitude, and therefore at perigee for an elliptic orbit. Drag removes energy from the system, causing an elliptic orbit to circularise and the semi-major axis to reduce. For a circular orbit, the orbital period and radius will continuously reduce, eventually causing re-entry. The atmosphere rotates at almost the same speed as the Earth, and generates small sideways forces that will reorient the orbit plane. King-Hele (1987) describes expressions for the drag force experienced by a single satellite in a rotating atmosphere in terms of the orbital elements: Drag causes changes in i which slowly increase, small periodic changes in Ω, a reduction in e and a, and it also affects ω, particularly for near-circular orbits when drag levels vary around the orbit at the same altitude due to atmospheric oblateness and diurnal density variations. Relative motion will also be affected as these variations will cause density gradients whose effects will be accentuated for satellites in a formation with different ballistic coefficients. Perpendicular to the direction of motion, the body will experience lift, but this is usually much less significant than drag (although may be included in the perturbation calculations). Fortescue et al. (2003) describe the drag force in standard form as

$$\underline{D} = \frac{1}{2}\rho V^2 S C_D \left(\frac{-\underline{V}_r}{|V_r|} \right) \tag{4-22}$$

where V_r is the satellite velocity (relative to the atmosphere), S is the vehicle area exposed to the flow, C_D is the satellite's drag coefficient, and ρ is atmospheric density. The value of C_D depends on the flow regime within which the satellite is flying. This is usually free molecular flow where the molecules that impact on the satellite do not interact further with the flow field, and typically C_D~2.2.

4.2.2.2 Gravitational Perturbations

The effects of the Earth's oblateness on an orbiting satellite are significant. The Earth bulges at the equator and the path of an orbiting satellite is distorted. The expression for the most significant LEO perturbation force above approximately 130km altitude, the J_2 geopotential force, can be derived from the expression for the gravitational potential for the oblate Earth.

$$U(r,\varphi) = -\frac{GM_E}{r}\left\{1 - \sum_{n=2}^{\infty}\left(\frac{R_E}{r}\right)^n J_n P_n(\sin\varphi)\right\} \tag{4-23}$$

This is described in terms of Legendre Polynomials (P_n), and in spherical coordinates where r is geocentric distance, R_E is equatorial radius, and φ is geocentric latitude. The J parameters are dimensionless coefficients (zonal harmonic constants) for the Earth (Sidi, 1997). At three orders of magnitude greater than the other J terms, J_2 is the largest constant, and for initial modelling purposes the higher order terms will be neglected. Further detail of the effects of tesseral and sectoral harmonic coefficients associated

with equation (4-23) can be obtained from orbital mechanics texts, for example Fortescue et al. (2003) and Chobotov (2002). The corresponding gravitational force in geocentric spherical coordinates (r, φ, θ) is given by

$$F_{J2} = -\nabla U \tag{4-24}$$

In order to be able to introduce the J_2 force into the equations of relative motion (equations (4-12) to (4-14)), the forces in equation (4-24) must be transformed so that they are expressed in terms of the rotating curvilinear reference orbit frame (Figure 4-1). The transformation uses the relationship between the geocentric latitude and the orbital elements, and is obtained by spherical trigonometry. The resulting force acting on a single satellite due to J_2 in the curvilinear reference orbit frame is given by equation (4-25), where i and θ are inclination and true latitude respectively (Wie, 1998).

$$\underline{J}_2(r) = -\frac{3J_2\mu R_e^{\,2}}{2r^4}\left[\left(1-3\sin^2\theta\sin^2 i\right)\underline{\hat{x}} + \left(2\sin^2 i\sin\theta\cos\theta\right)\underline{\hat{y}} + \left(2\sin i\cos i\sin\theta\right)\underline{\hat{z}}\right] \tag{4-25}$$

In terms of orbital elements, the primary effects of J_2 on a single satellite orbit are the regression of the line of nodes and the precession of the line of apsides (variation in Ω and ω). For a prograde orbit, the secular rate of nodal regression can be shown to be

$$\Delta\Omega = -\frac{3\pi J_2 R_E^2}{a^2\left(1-e^2\right)^2}\cos i \ \text{ rad/rev} \tag{4-26}$$

and the precession of the line of apsides can be shown to be given by equation (4-27).

$$\Delta\omega = 3\pi\frac{J_2 R_E^2}{a^2\left(1-e^2\right)^2}\left(2-\frac{5}{2}\sin^2 i\right) \ \text{ rad/rev} \tag{4-27}$$

4.2.2.3 Third Body Perturbations

Solar and Lunar (and Jovian to a lesser extent) gravity cause periodic variations in all of the orbit elements, and secular variation in the longitude of ascending node, Ω, argument of perigee, ω, and mean anomaly, M (Larson and Wertz, 1996). The Sun causes a regression of the orbit around an axis normal to the ecliptic, and the Moon will have a similar effect normal to its orbit plane. The effects are more significant for high altitude orbits, for example, for orbits with a period of 12 hours or more (Chobotov, 2002).

To include these effects, the equations of motion for the two-body problem can be extended for an n-body problem. This is discussed further in chapter 6 when orbits in the vicinity of Lagrange points are considered in the context of the three-body problem. In the general case, the acceleration due to a j^{th} perturbing body in an Earth centred coordinate frame is given by equation (4-28)

$$\underline{a}_j = \mu_j \left[\frac{\underline{\rho}_j}{\rho_j^3} - \frac{\underline{r}_j}{r_j^3} \right] \tag{4-28}$$

where μ_j is the gravitational parameter for the j^{th} body, ρ_j is the separation between the satellite in Earth orbit and the perturbing body, and r_j is the distance from the centre of the Earth to the perturbing body. The maximum acceleration experienced by a satellite in LEO will occur when the satellite is nearest the perturbing body and the Earth, satellite and j^{th} body are aligned. Equation (4-28) is simply the direct gravitational effect of the j^{th} body on the satellite minus the perturbing effect of the j^{th} body on the Earth itself. For multiple-perturbing bodies, the total acceleration would be the sum of all the components forces. The multi-body problem cannot be solved analytically without simplifying assumptions.

4.2.2.4 Solar Radiation Pressure

A satellite experiences Solar radiation pressure (SRP) perturbations when its surfaces are illuminated by Solar radiation, and photon momentum is exchanged. In Earth orbit, SRP produces periodic variations in all the orbital elements, although this effect is less significant compared to other perturbations in LEO, and the variations produced depend on the nature of the desired orbit. SRP becomes a primary perturbing force at high altitudes and in deep space.

In LEO, the mean Solar energy flux incident on a satellite is $W_E = 1400 W/m^2$ and this energy flux is proportional to the inverse square of the distance from the Sun (Sidi, 1997). The perturbing acceleration along the Sun-spacecraft (a_{SRP} in equation (4-29)) line due to SRP depends on this, the area to mass ratio of the satellite (A is the cross-sectional area perpendicular to the Sun-line), the mean Earth-Sun and satellite-Sun distances (a_Θ, r_Θ respectively), and the SRP coefficient, C_p, which varies between 0 and 2, depending on the transmission/absorption/reflection properties of the illuminated material (C_p=1 for a black body, and C_p=2 for perfect reflection) (McInnes, 2004).

$$a_{SRP} = C_p \frac{A}{m} \left(\frac{W_E}{c} \right) \left(\frac{a_\Theta}{r_\Theta} \right)^2 \tag{4-29}$$

4.2.2.5 The Effect of Orbit Perturbations and Nonlinearity on Relative Motion

The primary orbit perturbation accelerations have been introduced, and clearly the aerodynamic drag and J_2 perturbation forces have the greatest influence on the motion of a single satellite in LEO (Figure 4-3). However, in formation flying, it is the relative magnitude and direction of the perturbations experienced by the satellites that are the most important, and not the absolute accelerations individually experienced. In this section a preliminary assessment of the maximum magnitude of the relative acceleration between two satellites in LEO, using the equations presented in sections 4.2.2.1 to 4.2.2.4 for each type of disturbance is made. This involves the evaluation of the

acceleration at selected points, and differencing the results, depending on the satellite separation. In this case, the two satellites are separated by 100m in altitude (radial x-direction in the Hill frame), and in the absence of perturbations they will experience the relative motion illustrated in Figure 4-2b, section 4.2.1.4. Sample calculations of relative accelerations are repeated for altitudes of 200km, 600km and 1000km and the results are presented in Table 4-1.

The drag force at each altitude was calculated using equation (4-22). The different values of atmospheric density (ρ) were obtained by performing a logarithmic fit to density-altitude data (obtained from tables in Larson and Wertz (1996)). The velocity of the first satellite was taken to be the circular orbit velocity at that altitude, and the second satellite was assumed to be at apogee when separated radially by 100m from the first. The results obtained are given in a generalised form as an acceleration parameter multiplied by area over mass (S/m), and also as a pure acceleration, by multiplying the acceleration parameter by a typical value for S/m. A typical satellite ballistic coefficient, B_o, is 100kg/m^2 where $B_o=m/C_DS$, giving a typical S/m ratio of $4.5\text{x}10^{-3}$m^2/kg (Larson and Wertz, 1996). The relative drag accelerations correspond only to a radial satellite separation, as there would be zero relative drag experienced by satellites separated in the along-track or cross-track directions.

The acceleration at each satellite due to J_2 was evaluated at different altitudes for zero inclination and true anomaly using equation (4-25). The resulting relative radial accelerations are given in Table 4-1. Also, the magnitudes of the maximum perturbing accelerations of a third body in the satellite reference frame at different altitudes were evaluated using equation (4-28). By differencing these results, relative accelerations were obtained for both Solar and Lunar perturbations.

Equation (4-29) was applied to calculate the SRP on satellites in the different orbit altitudes. Table 4-1 includes relative accelerations, acting along the Sun-satellite line, between two satellites separated in altitude by 100m. The first row of terms is given as a function of the satellite area to mass ratio, A/m. (The area, A, is perpendicular to the incident radiation). For the second row of terms, A/m takes the typical ballistic coefficient value used for determining the relative drag acceleration ($4.5\text{x}10^{-3}$m^2/kg).

Relative Acceleration (m/s^2)	200km	600km	1000km
Aerodynamic Drag	$6\text{x}10^{-5}$S/m	$6\text{x}10^{-9}$S/m	$8\text{x}10^{-11}$S/m
	($3\text{x}10^{-7}$)	($3\text{x}10^{-11}$)	($4\text{x}10^{-13}$)
Oblateness (J_2)	$7\text{x}10^{-7}$	$5\text{x}10^{-7}$	$4\text{x}10^{-7}$
Solar Gravity	$7.92800\text{x}10^{-12}$	$7.92805\text{x}10^{-12}$	$7.92812\text{x}10^{-12}$
Lunar Gravity	$1.817\text{x}10^{-11}$	$1.822\text{x}10^{-11}$	$1.828\text{x}10^{-11}$
Solar Radiation Pressure	$4.67956\text{x}10^{-15}$A/m	$4.67958\text{x}10^{-15}$A/m	$4.67960\text{x}10^{-15}$A/m
	($2.12707\text{x}10^{-17}$)	($2.12708\text{x}10^{-17}$)	($2.12709\text{x}10^{-17}$)
Nonlinear Hill Terms	$-6.3863\text{x}10^{-9}$	$-5.0432\text{x}10^{-9}$	$-4.0353\text{x}10^{-9}$

Table 4-1: Magnitude of Relative Perturbation Accelerations for Two Satellites in LEO, Separated Radially by 100m, and for Different Reference Orbit Altitudes (terms in brackets include values for S/m=A/m=$4.5\text{x}10^{-3}$m^2/kg and additional significant figures are included to distinguish between results)

These relative accelerations are either cyclic, secular or both. Non-cyclic terms will produce secular drifts in relative position that will grow over time. In this case, the order

of magnitude of the relative accelerations at the instant where the satellites are separated by 100m radially are of primary interest. These results show a significant decrease in relative aerodynamic drag with altitude, paralleling the behaviour of drag experienced by a single satellite with altitude. The drag experienced by a single satellite at 200km altitude is approximately $2x10^{-2}$S/m which is much greater than the relative motion value of $6x10^{-5}$S/m.

The relative acceleration due to J_2 will vary around the orbit, however, the values shown here, acting along the radial reveal that it has the most significant effect on relative satellite motion throughout LEO. The effect of the J_2 perturbation on relative satellite motion is therefore the focus of this chapter. The implementation of linearised J_2 effects within formation flying models and the justification for this approach were discussed in section 4.1.

The third-body and SRP accelerations experienced by the satellites individually are smaller than those due to J_2 and drag, at approximately 10^{-6}m/s^2. The Lunar perturbations are greater than the Solar perturbations, both on individual satellites and in terms of relative motion. However, in all cases, the relative accelerations are much smaller (Table 4-1), and in LEO these perturbations have little effect on the formation.

For this test case, the effects of nonlinearity in the Hill equations can be evaluated by differencing the forcing term in the radial (x) equation (of equations (4-15)) in its nonlinear and linearised form. (This is equivalent to differencing equations (D-6) and (D-7) in section D.1, appendix D). The nonlinear acceleration omitted by linearising the Hill equations in this 100m radial separation example is just 10^{-9}m/s^2 at all three altitudes investigated, and is therefore more significant than the SRP and third body effects in LEO, but less significant than drag or the relative J_2 perturbation.

4.3 Development of the J_2-Perturbed Equations of Relative Motion

A summary of the mathematical model development is presented in this section in order to highlight the differences between the time averaged and the proposed alternative periodic time varying linearised relative motion models, both including the perturbation due to J_2. The reader is also referred to Schweighart and Sedwick (2002) for further details relating to the time averaged model, particularly in relation to the cross-track motion. The use of their model as a starting point for the research was proposed following earlier studies performed at Cranfield, and justified through the literature review (refer to section 3.3.2 and the introductory discussions of this chapter (section 4.1)).

The model development work of Schweighart and Sedwick (2001a) was reviewed and implemented as one of the three relative dynamics models considered in this study. In this section both of the J_2 models are derived (the Hill equations were introduced in section 4.2.1). They are developed by initially considering the relative motion between one satellite tracing a circular reference orbit under the gravitational influence of a spherical Earth (at orbit altitude r_{ref}) and another satellite subject to the additional J_2 perturbation. Throughout much of the model development, the effects of J_2 on only one

of the two satellites are considered. The 'gradient of J_2' terms, derived using a Taylor series expansion about the reference orbit, are then implemented as time averaged and time varying coefficients in the state matrix. Eventually, the more realistic formation scenario concerned with the relative motion of two perturbed satellites (neither being constrained to the circular reference orbit) is considered. Corrective terms are applied to maintain the assumptions associated with linearisation, and at each stage of development, the performance of the models is evaluated (section 4.7). The analytical solutions to and associated initial conditions of the equations of motion are derived in section 4.4.

4.3.1 The Basic Equations

The model is developed by considering the relative motion between one satellite tracing a circular orbit, not subjected to any disturbance forces, and another satellite subject to the J_2 perturbation. The equation of motion for an unperturbed satellite in a circular orbit, under the gravitational influence of a spherical Earth, can be expressed as equation (4-30).

$$\ddot{\underline{r}}_{ref} = \underline{g}(\underline{r}_{ref}) \tag{4-30}$$

This satellite orbits at a chosen reference orbit altitude, r_{ref}, at P_0 (Figure 4-1). The second satellite (P_1) experiences the same gravitational force as the reference, but in addition is acted upon by J_2 (equation (4-31))

$$\ddot{\underline{r}} = \underline{g}(\underline{r}) + \underline{J}_2(\underline{r}) \tag{4-31}$$

where g and J_2 were given by equations (4-1) and (4-25) respectively.

The motion of the perturbed satellite, P_1 at $\underline{r}$, can be linearised by applying a Taylor series expansion at the reference orbit (r_{ref}) to give

$$\ddot{\underline{r}} = \underline{g}(\underline{r}_{ref}) + \nabla \underline{g}(\underline{r}_{ref}) \cdot \underline{x} + \underline{J}_2(\underline{r}_{ref}) + \nabla \underline{J}_2(\underline{r}_{ref}) \cdot \underline{x} \tag{4-32}$$

where $\underline{x}$ is the relative position vector between the reference and perturbed satellites in the curvilinear $\hat{\underline{x}} - \hat{\underline{y}} - \hat{\underline{z}}$ frame based at P_0. $\underline{x}$, initially introduced in section 4.2.1.1 (equations (4-2)) must remain relatively small for the linearisation to hold. In this equation, the values of $\underline{g}(\underline{r}_{ref})$ and $\underline{J}_2(\underline{r}_{ref})$ are evaluated at the reference orbit and the gradient of each term is also calculated at this point.. The relative acceleration of the perturbed satellite to the reference in the rotating Hill frame was also derived in section 4.2.1.1 and is repeated here as equation (4-33).

$$\ddot{\underline{x}} = \ddot{\underline{r}} - \ddot{\underline{r}}_{ref} - 2\underline{\omega} \times \dot{\underline{x}} - \dot{\underline{\omega}} \times \underline{x} - \underline{\omega} \times (\underline{\omega} \times \underline{x}) \tag{4-33}$$

For two satellites tracing circular orbits of similar altitude, undisturbed by additional external forces, equation (4-33) reduces to the basic Hill equations given by expressions (4-12) to (4-14).

4.3.2 Basic Equations of Relative Motion Including the J_2 Perturbation

In this section the effects of J_2 are incorporated into the equations of relative motion between a single perturbed satellite and the reference, but before any linearisation of J_2 has been performed. In other words, there is no gradient of J_2 term (∇J_2) being considered. The reason for looking at the relative motion equations in their basic form is so that the effects of including ∇J_2 can be assessed as the model is developed further. The gravity gradient term ($\nabla \underline{g}$) is given by equation (4-10) (section 4.2.1.1). The equations are derived by substituting for the acceleration terms, $\ddot{\underline{r}}_{ref}$ and $\ddot{\underline{r}}$ in equation (4-33) before the J_2 linearisation has been performed. In this case equation (4-34) is obtained.

$$\ddot{\underline{x}} + 2\underline{\omega} \times \dot{\underline{x}} + \dot{\underline{\omega}} \times \underline{x} + \underline{\omega} \times (\underline{\omega} \times \underline{x}) = \nabla \underline{g}(\underline{r}_{ref}) \cdot \underline{x} + \underline{J}_2(\underline{r}_{ref}) \qquad (4\text{-}34)$$

Expanded from the vectorial form, the radial, in-track, and cross-track relative motion equations subjected to J_2 in their simplest form are given by equations (4-35) where t is time since perigee passage (with ω=0). For a circular reference orbit, the orbital rate is constant, and therefore $\dot{\underline{\omega}} = 0$.

$$\begin{aligned}
\ddot{x} - 2n\dot{y} - 3n^2 x &= -\frac{3J_2 R_e^2 n^2}{2r_{ref}}\left(1 - 3\sin^2 i \sin^2 nt\right) \\
\ddot{y} + 2n\dot{x} &= -\frac{3J_2 R_e^2 n^2}{r_{ref}}\left(\sin^2 i \sin nt \cos nt\right) \qquad (4\text{-}35) \\
\ddot{z} + n^2 z &= -\frac{3J_2 R_e^2 n^2}{r_{ref}}\left(\sin i \cos i \sin nt\right)
\end{aligned}$$

4.3.3 Basic Equations of Relative Motion Including the Gradient of J_2

In this section, the equations to describe the motion of the perturbed satellite with respect to the reference on a circular orbit are derived using the linearised expressions for the perturbed satellite acceleration (given by equation (4-32) in vectorial form). By substituting for the acceleration terms, $\ddot{\underline{r}}_{ref}$ and $\ddot{\underline{r}}$, this time from equations (4-30) and (4-32), equation (4-36) is obtained.

$$\ddot{\underline{x}} + 2\underline{\omega} \times \dot{\underline{x}} + \dot{\underline{\omega}} \times \underline{x} + \underline{\omega} \times (\underline{\omega} \times \underline{x}) = \nabla \underline{g}(\underline{r}_{ref}) \cdot \underline{x} + \underline{J}_2(\underline{r}_{ref}) + \nabla \underline{J}_2(\underline{r}_{ref}) \cdot \underline{x} \qquad (4\text{-}36)$$

In this study the gradient of J_2 term (∇J_2) is expressed in both time averaged and time varying form. Written in this form, the coefficients in the equations of motion become

time varying and in the state space form, the state matrix will therefore vary with each time step. ∇J_2 is only constant for an equatorial orbit.

Using tensor calculus in the spherical coordinate frame (Figure 4-4), an expression for the J_2 gradient tensor can be derived (equation (4-37)). Partial derivatives of the components of the J_2 perturbation force given by equation (4-25) are taken with respect to the spherical coordinate directions illustrated below. Note that the curvilinear and spherical coordinate systems can be aligned. The $\hat{\underline{r}} - \hat{\underline{\theta}} - \hat{\underline{i}}$ vectors coincide with the curvilinear $\hat{x}$ - $\hat{y}$ - $\hat{z}$ vectors respectively (Figure 4-1), and θ is the true latitude.

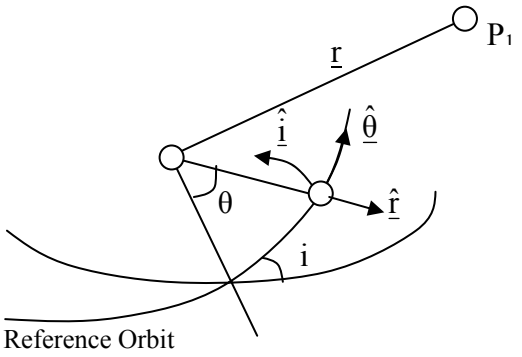

Figure 4-4: Spherical Coordinate System, $\hat{\underline{r}} - \hat{\underline{\theta}} - \hat{\underline{i}}$, on the Reference Orbit

$$\nabla \underline{J}_2(\underline{r}) = \begin{pmatrix} \dfrac{\partial J_{2\hat{r}}}{\partial \hat{r}} & \dfrac{\partial J_{2\hat{\theta}}}{\partial \hat{r}} & \dfrac{\partial J_{2\hat{i}}}{\partial \hat{r}} \\ \dfrac{1}{r}\left(\dfrac{\partial J_{2\hat{r}}}{\partial \hat{\theta}}\right) - \dfrac{J_{2\hat{\theta}}}{r} & \dfrac{1}{r}\left(\dfrac{\partial J_{2\hat{\theta}}}{\partial \hat{\theta}}\right) + \dfrac{J_{2\hat{r}}}{r} & \dfrac{1}{r}\left(\dfrac{\partial J_{2\hat{i}}}{\partial \hat{\theta}}\right) \\ \dfrac{1}{r\sin\theta}\left[\left(\dfrac{\partial J_{2\hat{r}}}{\partial \hat{i}}\right) - J_{2\hat{i}}\sin\theta\right] & \dfrac{1}{r\sin\theta}\left[\left(\dfrac{\partial J_{2\hat{\theta}}}{\partial \hat{i}}\right) - J_{2\hat{i}}\cos\theta\right] & \dfrac{1}{r\sin\theta}\left[\left(\dfrac{\partial J_{2\hat{i}}}{\partial \hat{i}}\right) + J_{2\hat{\theta}}\cos\theta + J_{2\hat{r}}\sin\theta\right] \end{pmatrix} \tag{4-37}$$

By substituting for $\underline{J}_2$ from equation (4-25), ∇J_2 can be derived (equation (4-38)).

$$\nabla \underline{J}_2(r,\theta,i) = \frac{6J_2\mu R_e^2}{r^5}\begin{bmatrix} (1-3\sin^2 i\sin^2\theta) & \sin^2 i\sin 2\theta & \sin 2i\sin\theta \\ \sin^2 i\sin 2\theta & -\frac{1}{4} - \sin^2 i(\frac{1}{2} - \frac{7}{4}\sin^2\theta) & -\frac{\sin 2i\cos\theta}{4} \\ \sin 2i\sin\theta & -\frac{\sin 2i\cos\theta}{4} & -\frac{3}{4} + \sin^2 i(\frac{1}{2} + \frac{5}{4}\sin^2\theta) \end{bmatrix} \tag{4-38}$$

In order to derive analytical solutions to the equations of relative motion, the ∇J_2 expression (equation (4-38)) must be time averaged over one orbit. Schweighart and Sedwick (2002) calculate the time average, but do not derive these equations. The vectorial equation of relative motion including the time averaged gradient of J_2 is given by equation (4-39).

$$\ddot{\underline{x}} + 2\underline{\omega} \times \dot{\underline{x}} + \dot{\underline{\omega}} \times \underline{x} + \underline{\omega} \times (\underline{\omega} \times \underline{x}) = \underline{\nabla g}(\underline{r}_{ref}) \cdot \underline{x} + \underline{J}_2(\underline{r}_{ref}) + \frac{1}{2\pi} \int_0^{2\pi} \underline{\nabla J}_2(\underline{r}_{ref}) d\theta \cdot \underline{x} \qquad (4\text{-}39)$$

where

$$\frac{1}{2\pi} \int_0^{2\pi} \nabla J_2(\underline{r}) d\theta = \frac{\mu}{r^3} \begin{bmatrix} 4s & 0 & 0 \\ 0 & -s & 0 \\ 0 & 0 & -3s \end{bmatrix} \quad \text{and} \quad s = \left(\frac{3J_2 R_e^2}{8r^2} \right) (1 + 3\cos 2i) \qquad (4\text{-}40)$$

In full, the equations of relative motion (with $\dot{\underline{\omega}} = 0$) in the radial (x), in-track (y), and cross-track (z) directions become

$$\begin{aligned} \ddot{x} - 2n\dot{y} - 3n^2 x - 4n^2 sx &= -\frac{3J_2 R_e^2 n^2}{2r_{ref}} (1 - 3\sin^2 i \sin^2 nt) \\ \ddot{y} + 2n\dot{x} + n^2 sy &= -\frac{3J_2 R_e^2 n^2}{r_{ref}} (\sin^2 i \sin nt \cos nt) \\ \ddot{z} + n^2 z + 3n^2 sz &= -\frac{3J_2 R_e^2 n^2}{r_{ref}} (\sin i \cos i \sin nt) \end{aligned} \qquad (4\text{-}41)$$

Equations (4-41) and (4-35) were implemented in Matlab/Simulink to investigate the effects of time averaging the gradient of J_2 term in the equations of relative motion.

4.3.4 Equations of Relative Motion with the Orbital Rate and Nodal Drift Correction Terms

In equation (4-36), the values of $\underline{g}(\underline{r}_{ref})$ and $\underline{J}_2(\underline{r}_{ref})$ and the gradients of these terms are evaluated at the reference orbit. $\underline{x}$ must remain relatively small for the first order Taylor expansion to apply and therefore, the mean radii and orbital rates of the perturbed and reference satellites must be similar. An effect of the J_2 perturbation is to cause a change in the orbital rate as well as a drift in the longitude of ascending node. The J_2 perturbed satellite will experience this drift, but the reference orbit will not, thus the two orbits will gradually separate unless some correction to the orbital rate and nodal drift of the reference satellite is included in the model.

Schweighart and Sedwick (2002) determined that the change in the orbital rate experienced by the perturbed satellite is, on average, related to the time averaged J_2 acceleration. Averaged over the orbit, this additional acceleration is related to the orbital rate as it effectively modifies the gravitational constant. They also determined that the drift in the longitude of ascending nodes is due to the cross-track component of J_2 (this can be shown by analysis of the variation of orbital parameters due to J_2). The time averaged J_2 acceleration is given by equation (4-42).

$$\frac{1}{2\pi}\int_0^{2\pi} J_2(\underline{r})d\theta = \begin{bmatrix} -n^2 rs \\ 0 \\ 0 \end{bmatrix} \text{ where } s = \left(\frac{3J_2R_e^2}{8r^2}\right)(1+3\cos 2i) \tag{4-42}$$

This results in a non-zero value for acceleration in the radial $\hat{\underline{x}}$ direction only. This can be visualised as equivalent to a force acting to increase or decrease the Keplerian gravity term (depending on the sign of 's'). Therefore, if a perturbed satellite is to remain in close proximity to the circular reference orbit, the reference orbital rate must be increased or decreased.

Originally, the reference orbit had a basic equation of motion including only the gravitational influence of a spherical Earth ($\underline{g}(\underline{r})$). The reference orbit with the modified time orbital rate has a new equation of motion (equation (4-43)) incorporating the time averaged J_2 acceleration and cross-track component of J_2. ($\hat{\underline{z}}$ is the unit vector in the cross-track direction).

$$\ddot{\underline{r}}_{ref} = \underline{g}(\underline{r}_{ref}) + \frac{1}{2\pi}\int_0^{2\pi} \underline{J}_2(\underline{r}_{ref})d\theta + [\underline{J}_2(\underline{r}_{ref})\cdot\hat{\underline{z}}]\hat{\underline{z}} \tag{4-43}$$

As the rate of the reference orbit has changed, so has the average angular velocity of the reference satellite, and the coordinate system which is based there. The new angular velocity can be found by equating the accelerations to give

$$\underline{\omega}\times(\underline{\omega}\times\underline{r}_{ref}) = \underline{g}(\underline{r}_{ref}) + \frac{1}{2\pi}\int_0^{2\pi} \underline{J}_2(\underline{r}_{ref})d\theta \tag{4-44}$$

The new angular velocity becomes

$$\underline{\omega} = nc\hat{\underline{z}} \quad \text{where } c = \sqrt{1+s} \tag{4-45}$$

The resulting linear vectorial equation of relative motion of one J_2-perturbed satellite relative to the reference, including the reference orbital rate and nodal drift correction terms is given by equation (4-46) for the time averaged case.

$$\ddot{\underline{x}} + 2\underline{\omega}\times\dot{\underline{x}} + \dot{\underline{\omega}}\times\underline{x} + \underline{\omega}\times(\underline{\omega}\times\underline{x}) = \underline{\nabla g}(\underline{r}_{ref})\cdot\underline{x} + \underline{J}_2(\underline{r}_{ref}) + \frac{1}{2\pi}\int_0^{2\pi}\underline{\nabla J}_2(\underline{r}_{ref})d\theta\cdot\underline{x} - \frac{1}{2\pi}\int_0^{2\pi}\underline{J}_2(\underline{r}_{ref})d\theta - [\underline{J}_2(\underline{r}_{ref})\cdot\hat{\underline{z}}]\hat{\underline{z}} \tag{4-46}$$

In full, the equations of relative motion in the radial (x), in-track (y), and cross-track (z) directions become

$$\begin{aligned}
&\ddot{x} - 2nc\dot{y} - (5c^2-2)n^2x = -\frac{3J_2R_e^2n^2}{r_{ref}}\left(\frac{1}{2} - \frac{3}{2}\sin^2 i\sin^2 kt\right) + \frac{3J_2R_e^2n^2}{r_{ref}}\left(\frac{1}{8}+\frac{3}{8}\cos 2i\right) \\
&\ddot{y} + 2nc\dot{x} = -\frac{3J_2R_e^2n^2}{r_{ref}}(\sin^2 i\,\sin kt\cos kt) \\
&\ddot{z} + (3c^2-2)n^2z = 0
\end{aligned} \tag{4-47}$$

The orbital period correction factor, c, remains within the dynamics on the left hand side of equations (4-47). The forcing terms on the right hand side of the in-plane equations now occur at a modified frequency, k. The cross-track (z) motion now has a zero forcing function due to the nodal drift correction term. Physically, k can be considered as the frequency of equator crossing of the satellites which is modified by the shift in the line of nodes after each orbit.

$$k = nc + \frac{3nJ_2R_e^2}{2r_{ref}^2}\cos^2 i \tag{4-48}$$

By integrating the perturbation equations which describe the variation with time of the orbital elements due to the normal component of the J_2 acceleration, the true latitude can be expressed as

$$\theta = kt \tag{4-49}$$

The model described by equation (4-46) was implemented both with and without the nodal drift correction term, and also in time varying form (equation (4-50)) to investigate the effects of time averaging the gradient of J_2, and including nodal drift.

$$\ddot{\underline{x}} + 2\underline{\omega}\times\dot{\underline{x}} + \dot{\underline{\omega}}\times\underline{x} + \underline{\omega}\times(\underline{\omega}\times\underline{x}) = \underline{\underline{\nabla g}}(\underline{r}_{ref})\cdot\underline{x} + \underline{J}_2(\underline{r}_{ref}) + \underline{\underline{\nabla J}}_2(r_{ref})\cdot\underline{x} - \frac{1}{2\pi}\int_0^{2\pi}\underline{J}_2(\underline{r}_{ref})d\theta - [\underline{J}_2(\underline{r}_{ref})\cdot\underline{z}]\underline{z} \tag{4-50}$$

4.3.5 Cross-Track Modelling

Schweighart and Sedwick (2002) derived a new model specifically to capture the cross-track motion due to J_2. This was developed in order to rectify a problem introduced by taking the time average of the gradient of J_2 (equation (4-47)). Instead of rotating about the Earth's polar axis, the orbit plane was caused to rotate about a vector normal to the reference orbit. Their new equation describing cross-track motion was derived using a geometric approach based on the movement of the intersection of the orbit planes of the perturbed satellite and the reference orbit and is given as equation (4-51).

$$\ddot{z} + q^2 z = 2lq\cos(qt + \varphi) \tag{4-51}$$

The argument of the cross-track periodic motion in the absence of J_2 is equal to the orbital rate, n. When the reference orbit is modified to take into account the time averaged J_2 acceleration over the orbit, this rate becomes 'nc' (equation (4-45)), and the point of intersection of the orbit planes of the reference orbit and J_2 perturbed satellites remains the same over time. However, Schweighart and Sedwick (2002) identified that this should not be the case, and time averaging of the J_2 acceleration introduced an error by preventing the perturbed orbit from rotating about the polar axis. The model was therefore modified to capture the new orbital rate, 'q' which is defined in appendix D.2 (equation (D-23)) as 'nc minus the rate of change in location of the intersection of the orbit planes due to J_2'. The maximum separation between the planes therefore also

varies with time at a rate given by 'l' (defined through spherical trigonometry and given by equation (D-26)). φ in equation (4-51) is the phase angle of the satellite in the cluster, as determined by the formation initialisation. (A brief summary of the model is included for reference in section D.2 of appendix D and further detail can be found in Schweighart and Sedwick (2002)). Equation (4-51) was also implemented within the Matlab models and compared to STK.

4.3.6 Equations of Relative Motion for Two Perturbed Satellites

The relative motion between two perturbed satellites is the application towards which the model development has been directed in sections 4.3.1 to 4.3.5. The notation used by Schweighart and Sedwick (2002) to describe the relative position of the two perturbed satellites is adopted in Figure 4-5 which illustrates the relative positions ($\underline{x}_1$ and $\underline{x}_2$) of two J_2 perturbed satellites (P_1 and P_2) with respect to the reference orbit (P_0).

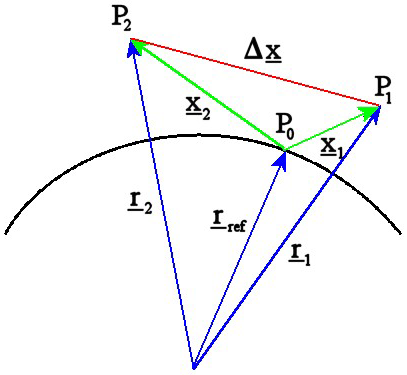

Figure 4-5: Relative Motion of Two Perturbed Satellites

By subtracting the relative motion equations which describe the motion of any two J_2 perturbed satellites, P_1 and P_2, with respect to the reference satellite, P_0, the equation describing the relative motion between the two perturbed satellites is given in linear time invariant form by equation (4-52). The time averaged ∇J_2 was derived in equation (4-40). It is important to note that the only terms affecting the relative motion are the gradients.

$$\underline{\Delta\ddot{x}} + 2\underline{\omega}\times\underline{\Delta\dot{x}} + \underline{\dot{\omega}}\times\underline{\Delta x} + \underline{\omega}\times(\underline{\omega}\times\underline{\Delta x}) = \underline{\nabla g}(\underline{r}_{ref})\cdot\underline{\Delta x} + \frac{1}{2\pi}\int_0^{2\pi}\underline{\nabla J}_2(\underline{r}_{ref})d\theta\cdot\underline{\Delta x} \qquad (4\text{-}52)$$

where

$$\underline{\Delta x} = \underline{x}_1 - \underline{x}_2 \qquad (4\text{-}53)$$

In full, the equations of relative motion for two perturbed satellites, from equation (4-52) in the radial (x) and along-track (y) directions are given by equations (4-54) and (4-55). The cross-track (z) equation (4-56) is derived by the same process from equation (4-51). Clearly these equations are much simplified and comparable in form to the Hill equations.

$$\Delta\ddot{x} - 2nc\Delta\dot{y} - \left(5c^2 - 2\right)n^2\Delta x = 0 \tag{4-54}$$

$$\Delta\ddot{y} + 2nc\Delta\dot{x} = 0 \tag{4-55}$$

$$\Delta\ddot{z} + q^2\Delta z = 2lq\cos\left(qt + \varphi\right) \tag{4-56}$$

The corresponding equation with time varying coefficients describing the relative motion of two J_2 perturbed satellites is given by equation (4-57).

$$\underline{\Delta\ddot{x}} + 2\underline{\omega}\times\underline{\Delta\dot{x}} + \underline{\dot{\omega}}\times\underline{\Delta x} + \underline{\omega}\times\left(\underline{\omega}\times\underline{\Delta x}\right) = \underline{\nabla g}\left(\underline{r}_{ref}\right)\cdot\underline{\Delta x} + \underline{\nabla J}_2\left(\underline{r}_{ref}\right)\cdot\underline{\Delta x} \tag{4-57}$$

The substitution of expressions into equation (4-57) results in the following equations of motion in the radial, along-track and cross-track directions. Note that the expression for cross-track motion contains terms from equation (4-38), and is not related to the geometric model described by equation (4-56). In this model, θ is given by equation (4-49).

$$\Delta\ddot{x} - 2nc\Delta\dot{y} - n^2\left[c^2 + 2 + \left(\frac{6J_2R_e^2}{r_{ref}^2}\right)\left(1 - 3\sin^2 i\sin^2\theta\right)\right]\Delta x - \left(\frac{6J_2n^2R_e^2}{r_{ref}^2}\right)\sin^2 i\sin 2\theta\Delta y - \left(\frac{6J_2n^2R_e^2}{r_{ref}^2}\right)\sin 2i\sin\theta\Delta z = 0 \tag{4-58}$$

$$\Delta\ddot{y} + 2nc\Delta\dot{x} - \left(\frac{6J_2n^2R_e^2}{r_{ref}^2}\right)\sin^2 i\sin 2\theta\Delta x - n^2\left[c^2 - 1 - \left(\frac{6J_2R_e^2}{r_{ref}^2}\right)\left(\frac{1}{4} + \sin^2 i\left(\frac{1}{2} - \frac{7}{4}\sin^2\theta\right)\right)\right]\Delta y + \left(\frac{6J_2n^2R_e^2}{r_{ref}^2}\right)\left(\frac{\sin 2i\cos\theta}{4}\right)\Delta z = 0 \tag{4-59}$$

$$\Delta\ddot{z} - \left(\frac{6J_2n^2R_e^2}{r_{ref}^2}\right)\sin 2i\sin\theta\Delta x + \left(\frac{6J_2n^2R_e^2}{r_{ref}^2}\right)\left(\frac{\sin 2i\cos\theta}{4}\right)\Delta y + n^2\left(1 + \left(\frac{6J_2R_e^2}{r_{ref}^2}\right)\left(\frac{3}{4} - \sin^2 i\left(\frac{1}{2} + \frac{5}{4}\sin^2\theta\right)\right)\right)\Delta z = 0 \tag{4-60}$$

If equations (4-58) to (4-60) are written together in state space form, the gradient of J_2 (∇J_2) terms create a periodic time varying state matrix as the true anomaly varies with time.

For the development of an analytical relative dynamics model (particularly when perturbations are included), it is necessary to define a reference orbit as a virtual orbit with a known trajectory which remains as close as possible to the satellite formation. This enables force gradients in the vicinity of the formation to be quantified and ensures that any modelling linearisation assumptions hold. The existence of a known reference point travelling with the formation enables the coordinate frame for relative motion measurement to be transferred to a real satellite in the formation without significant loss of accuracy. A numerically generated satellite trajectory, based on the orbit of a member of the formation, could be used as a reference orbit, but this requires orbit determination from the ground and adds complexity to the model, as the positions of the individual spacecraft must be measured in addition to the relative positions between spacecraft. This formulation does not provide the necessary insight for formation design in the perturbed environment, and the force gradients would have to be reevaluated at every time step as the reference satellite position was determined.

4.3.7 Summary

The main aim of this description of model development has been to introduce the new equations of relative motion, (4-58) to (4-60). These and other previously undocumented interim equations of motion (for example, equations (4-41)), derived during the model development process, are compared to STK in section 4.7. A detailed overview of the analytical model derived by Schweighart and Sedwick (2001a) (equations (4-54) to (4-56)) has also been presented, although the majority of their expressions were separately derived in support of the development of the time varying equations of motion.

4.4 Solutions and Initial Conditions

The following sections summarise the solutions and initial conditions associated with the time averaged model and their application to formation design and trajectory generation for bounded relative satellite motion. The techniques used to analyse the solutions and initial conditions for the time varying model are also explored. In the former case, the solutions to the equations of relative motion at a selection of stages of model development have been derived. In most cases, these analytical solutions have been implemented in Matlab in order to compare the results with numerical solutions.

4.4.1 Solutions and Initial Conditions for Bounded Motion from the Time Averaged J_2 Model

The linear time averaged equations describing the relative motion of one J_2 perturbed satellite relative to a reference or another J_2 perturbed satellite can be solved using standard techniques. The in-plane model equations are coupled and are therefore solved together. The cross-track motion analysis is performed separately. If the equations of motion are initialised so that the satellites cross the equator at $t = 0$, and bounded motion is enforced for formation flying (refer to section 3.1.3, chapter 3), the relationships between the initial relative position and velocity in Table 4-2 are required. The initial conditions are based on the fact that any secular drift and offset terms in the analytical solutions are equated to zero when $t = 0$. Effectively, bounded motion causes the reference or 'chief' satellite to be the point about which all the perturbed 'deputy' satellites describe a relative orbit.

All the parameters within the equations in Table 4-2 were introduced through the model development overview in section 4.3, except for the leader-follower conditions. These and the time varying model are both discussed further below.

The first entry comprises the initial conditions for bounded motion as described by the unperturbed Hill equations. These conditions and their implications for formation design were introduced in section 3.1.3.1, and the periodic solutions obtained were given as equations (3-19). The elliptical relative motion in the orbit plane ensures that the satellites do not drift apart during the orbit, but appear to circle around each other.

The next three entries in the left column of Table 4-2 refer to the early stages of the time averaged model development where the relative motion of a reference satellite and a second satellite perturbed by J_2 is considered. There are similarities between the initial condition formulae. The addition of the J_2 perturbation force (not including the gradient term) affects the initial y-velocity. When orbital rate and nodal drift correction terms are applied to the reference orbit, terms in s and c (from equations (4-40) and (4-45) respectively) are introduced, reflecting the inclusion of the time averaged gradient of J_2 perturbation term in the equations of motion. The only difference between the orbital rate and nodal drift conditions lies in the initial y-velocity where k becomes the new rate parameter on the denominator (k is given by equation (4-48)).

Model (including satellite conditions)	**Initial x-Condition**	**Initial y-Condition**
Hill Equations (no perturbations)	$\dot{x}_0 = \frac{y_0 n}{2}$	$\dot{y}_0 = -2nx_0$
Basic Equations including J_2 only (1 reference, 1 J_2-perturbed)	$\dot{x}_0 = \frac{y_0 n}{2}$	$\dot{y}_0 = -2nx_0 + \frac{3J_2 R_e^2 n}{8r_{ref}}(1-\cos 2i)$
Orbital Rate Corrected Model* (1 reference, 1 J_2-perturbed)	$\dot{x}_0 = \frac{y_0 n(1-s)}{2c}$	$\dot{y}_0 = -2ncx_0 + \frac{3J_2 R_e^2 n}{8cr_{ref}}(1-\cos 2i)$
Nodal Drift Corrected Model* (1 reference, 1 J_2-perturbed)	$\dot{x}_0 = \frac{y_0 n(1-s)}{2c}$	$\dot{y}_0 = -2ncx_0 + \frac{3J_2 R_e^2 n^2}{8kr_{ref}}(1-\cos 2i)$
Two Perturbed Satellites* (2 J_2-perturbed)	$\Delta\dot{x}_0 = \frac{n\Delta y_0(1-s)}{2\sqrt{1+s}}$	$\Delta\dot{y}_0 = -2n\Delta x_0\sqrt{1+s}$
Two Perturbed Satellites in Leader-Follower Formation (2 J_2-perturbed)	$\Delta\dot{x}_0 = \frac{n(\Delta y_0 - \Delta y_d)(1-s)}{2\sqrt{1+s}}$	$\Delta\dot{y}_0 = 0$

Table 4-2: Initial Conditions for Bounded In-Plane Motion (*entries from Schweighart and Sedwick (2002), Note: Δy_d is desired satellite separation)

The initial conditions simplify considerably when the equations are describing the relative motion of two J_2 perturbed satellites. By the same solution methods, the analytical model described by equations (4-54) to (4-56), can be solved to give the following closed-form expressions for relative radial, along-track and cross-track motion respectively (Schweighart and Sedwick, 2002), and the corresponding initial conditions for bounded motion are given in Table 4-2.

$$\Delta x = \Delta x_0 \cos\left(nt\sqrt{1-s}\right) + \frac{\Delta\dot{x}_0}{n\sqrt{1-s}}\sin\left(nt\sqrt{1-s}\right) \tag{4-61}$$

$$\Delta y = \frac{2\Delta\dot{x}_0\sqrt{1+s}}{n(1-s)}\cos\left(nt\sqrt{1-s}\right) - \frac{2\Delta x_0\sqrt{1+s}}{\sqrt{1-s}}\sin\left(nt\sqrt{1-s}\right) \tag{4-62}$$

$$\Delta z = (lt + m)\sin(qt + \phi) \tag{4-63}$$

The initial conditions associated with the cross-track motion for the time averaged analytical model were user defined. Equations (4-64) and (4-65) then provided values for the parameters l, m, q and φ in equation (4-63) (refer to section D.2 of appendix D or

Schweighart and Sedwick (2002)). For the analytical model, the inclinations of both satellites, and the initial separation and velocity are specified, and the motion is deemed uncoupled to the in-plane x-y motion, therefore no bounded motion initial conditions have been derived in this case.

$$\Delta z_0 = m \sin \phi = \Delta\Omega_0 r_{ref} \sin i_{ref} \tag{4-64}$$

$$\Delta \dot{z}_0 = l \sin \phi + qm \cos \phi = (i_{sat1} - i_{sat2}) k r_{ref} \tag{4-65}$$

For the leader-follower formation, with a desired separation in y (along-track) of Δy_d at an inclination of i, the initial conditions for generating the relative motion of two perturbed satellites, according to the analytical model, would need to be $\Delta x_0 = 0, \Delta y_0 = \Delta y_d, \Delta z_0 = 0, \Delta \dot{z}_0 = 0$ with i_{sat1}, i_{sat2} = i. In this case it is necessary to consider the full solution to the equations of motion including the drift and offset terms. When t = 0, the secular term disappears, leaving a desired offset. The initial conditions that result are given in the final row of Table 4-2.

All the forms of bounded initial conditions summarised in Table 4-2 relate in-plane radial and along-track positions and velocities. Different types of bounded formations, as natural solutions to the Hill equations, were introduced in section 3.1.3.1 in chapter 3. The initial conditions presented in Table 4-2 are shown later (section 4.7) to be the circumstances under which the analytical models are most accurate due to the assumptions inherent within the derivation of the linearised Hill equations. Any deviation from these initial conditions and the model describes the real relative motion less accurately.

4.4.2 The Application of Analytical Solutions to Formation Design

The derivation of natural formations in the unperturbed environment from the Hill equations was described in section 3.1.3.1. Sabol et al. (1999), (2001) considered the following formations:

- Along-track (leader-follower)
- In-track (ground-track repeating)
- Circular
- Projected Circular (relative elliptical orbit)

The relative motion solutions provide useful reference trajectories for formation keeping control (trajectory following), and formation design and visualisation. However, the development of the analytical linearised J_2 model offers the opportunity to modify the reference trajectories to include the effects of the J_2 perturbation, and improve formation stability in the perturbed environment.

The along-track separation can be implemented as described above with an initial y-offset. The circular formation initial conditions can be derived by considering the geometry of the relative orbit.

For an unperturbed orbit, equations (3-19) in chapter 3, section 3.1.3.1, give the closed form solutions to the Hill equations. If these are compared to equations (4-61), (4-62), and (4-63) above, in the in-plane direction, bounded motion is now given by a new ratio in x-y amplitude. For the Hill equations this ratio produces a 1 by 2 ellipse, however for the J_2 perturbed orbit, this is now a 1 by $[2\sqrt{(1+s)/(1-s)}]$ ellipse. For a bounded circular orbit, the following condition must hold.

$$x^2 + y^2 + z^2 = r^2 \tag{4-66}$$

This requires the following initial conditions for the Hill bounded solutions (equations (4-67) (Sabol et al, 2001))

$$\dot{y}_0 = -2nx_0 \qquad y_0 = \frac{2\dot{x}_0}{n} \qquad z_0 = \pm\sqrt{3}x_0 \qquad \dot{z}_0 = \sqrt{3}\dot{x}_0 \tag{4-67}$$

and the equivalent for J_2 near-bounded motion (equations (4-68))

$$\Delta\dot{y} = -\frac{2n}{\sqrt{1+s}}\Delta x_0 \qquad \Delta y_0 = \frac{2\sqrt{1+s}}{n(1-s)}\Delta\dot{x}_0$$

$$\Delta z_0 = \sqrt{\frac{3+5s}{1-s}}\Delta x_0 \qquad \Delta\dot{z}_0 = \sqrt{\frac{3+5s}{1-s}}\Delta\dot{x}_0 \quad \text{and} \quad q = n\sqrt{1-s} \tag{4-68}$$

where from equation (4-42), s is given by

$$s = \left(\frac{3J_2R_e^2}{8r^2}\right)(1+3\cos 2i) \tag{4-69}$$

Of course, the assumption in this case is that the cross-track frequency, q, is equal to the rates in equations (4-61) and (4-62), otherwise a closed formation is not possible. This slight change in rate worsens the cross-track model, but controlling the formation to this modified circular formation should be less costly than forcing the satellites to trace a Hill solution in the perturbed environment. The modelling errors associated with this approach are presented in section 4.7, and any benefits in terms of station keeping cost are investigated in chapter 5.

Although part of formation design considerations (refer to section 3.1.3), the phasing of multiple satellites around a relative orbit has not been considered in this chapter. The relative motion models and control system design (chapter 5) have been restricted to description of just two satellites. A cluster of three or more spacecraft could be modelled by simultaneous computation of a number of relative motion models, for example calculating motion of each satellite relative to a communal hub.

4.4.3 Solutions and Initial Conditions for the Time Varying Model

The in-plane and cross-track time varying equations are clearly coupled, and it is appropriate to investigate the relationship between relative positions and velocities for formation flying in all three axes. Both state transition matrix (STM) and numerical approaches were pursued to investigate the solutions and initial conditions of the time varying equations of relative motion.

For a linear time varying system described by equation (4-70),

$$\dot{\underline{x}} = \underline{A}(t)\underline{x} \tag{4-70}$$

a state transition matrix (STM), $\underline{\Phi}$, maps the initial state vector to a final state vector at time t. according to equation (4-71)

$$\underline{x}(t) = \underline{\Phi}(t, t_0)\underline{x}(t_0) \tag{4-71}$$

if and only if the state matrix and integral matrix multiplication is commutative (and equation (4-72) holds) (Schaub and Junkins, 2003).

$$A(t)\int A(t)dt = \int A(t)dtA(t) \tag{4-72}$$

Note that the STM has the following properties.

$$\dot{\underline{\Phi}}(t, t_0) = A(t)\underline{\Phi}(t, t_0) \text{ and } \underline{\Phi}(t_0, t_0) = \underline{I} \tag{4-73}$$

In this case, the state matrix describing equations (4-58), (4-59) and (4-60) does not obey (4-72) Instead, the terms in A(t) were split between constant, A_0, and time varying, A_{TV}, components (equation (4-74)).

$$A(t) = A_0 + A_{TV}(t) \tag{4-74}$$

However, the new state matrix, A_{TV}, could also not yield useful analytical initial conditions using the approach proposed in equations (4-75) to (4-77)

$$\underline{x}(t) = \phi(t, t_0)\underline{x}_0 = e^{\int A(t)dt}\underline{x}_0 \tag{4-75}$$

where the exponential can be obtained by expansion

$$e^{At} \approx I + At \tag{4-76}$$

and therefore for the time varying and constant terms the form of solution is given by

$$\underline{x}(t) = \left[I + A_0 t + \int_0^t A_{TV}(t)dt \right]\underline{x}_0 \tag{4-77}$$

Instead, the time varying model behaviour was investigated using the initial conditions derived from the analytical model, and by numerical analysis. The latter are derived using a 'targeting' function within STK (section 4.7).

In its original form, the state matrix of equations (4-58) to (4-60), A(t), is time varying, and in particular, time periodic. It is therefore possible to derive solutions and perform a stability analysis using Floquet theory (Calico and Wiesel, 1984). According to Floquet theory, the STM can be factored into the following form.

$$\underline{\Phi}(t, t_0) = F(t)e^{Jt}F^{-1}(t_0) \tag{4-78}$$

The diagonal matrix, J, comprises constant Poincare exponents which can be interpreted as eigenvalues of the state matrix, and demonstrate system stability. F(t) is equivalent to the eigenvector matrix, but remains time varying and periodic. It is relatively straight forward to obtain values for J, and $F(t_0)$ through numerical simulation of equation (4-73) but the transformation of the time periodic equations into equations with constant coefficients is less so. A new set of variables, $\eta(t)$, are introduced by Calico and Wiesel (1984) (equation (4-79)),

$$x(t) = F(t)\eta(t) \tag{4-79}$$

leading to the constant coefficient equations of relative motion below.

$$\dot{\eta} = J\eta \tag{4-80}$$

F(t) can be calculated over one orbit by solving equation (4-81) numerically. Wiesel (2001) states that periodic F(t) can eventually be expressed as a Fourier series expansion.

$$\dot{F}(t) = A(t)F(t) - F(t)J \tag{4-81}$$

This enables a numerically determined STM solution (equation (4-82)) to be obtained which gives greater insight into the relative dynamics than a purely numerical integration of the time varying state matrix, A(t). Equation (4-82) is derived by substituting equation (4-78) into equation (4-71).

$$\underline{x}(t) = F(t)e^{Jt}F^{-1}(t_0)\underline{x}(t_0) \tag{4-82}$$

Techniques for solving time varying equations and examples of their application were sought in the literature. A number of sources describe the solution of time varying relative dynamics for elliptical orbits (Izzo, 2002), (Melton, 2000), (Yamanaka and Ankersen, 2002), (Inalhan and How, 2000), and others relate to other fields of research (dynamic buckling of structures (Natarajan, Kapania, and Inman, 2001) and RF communications (Demir, 2000)). These involved either Floquet analysis, or the less generally applicable approximation and transformation of terms in the time varying state matrix to generate a set of time invariant equations. Wiesel (2003) is tackling the general solution of any periodic time varying system, using an extension of Floquet theory in the decomposition of the time varying state matrix.

For the time varying J_2 dynamics model described by equations (4-58) to (4-60), the numerical solutions were obtained using a 4th order Runge-Kutta solver, and elements of Floquet analysis were performed. Initial conditions were either obtained numerically, or derived from the same scenarios implemented in the time invariant J_2 model. The results are discussed in section 4.7.

4.5 Model Implementation in Matlab/Simulink

The equations of relative motion in their various levels of complexity have been implemented in Matlab/Simulink. The vectorial equations, derived in section 4.3, are implemented as separate models in Simulink. An m-file associated with each model requests orbital parameters (inclination, radius and initial satellite separations) which the user can input through the workspace. The m-file runs the model for the specified duration using discrete (usually 1 or 10 second) interval time steps and a fourth order Runge Kutta solver, and then plots the relative motion results.

For all the models where either there was no gradient of J_2 term (∇J_2) (including the Hill equations), or the term was time averaged, the equations of motion had constant coefficients and it was possible to implement them using an inbuilt Simulink block as the state space model.

Figure 4-6 illustrates a model of this type. The remainder of the diagram implements any forcing functions on the right hand side of the equations of motion. In this example, the Basic Time Averaged model, derived as equation (4-39) in section 4.3.3, and repeated below as equation (4-83) is implemented.

$$\ddot{\underline{x}} + 2\underline{\omega}\times\dot{\underline{x}} + \dot{\underline{\omega}}\times\underline{x} + \underline{\omega}\times(\underline{\omega}\times\underline{x}) = \underline{\nabla g}(\underline{r}_{ref})\cdot\underline{x} + \underline{J}_2(\underline{r}_{ref}) + \frac{1}{2\pi}\int_0^{2\pi}\underline{\nabla J}_2(\underline{r}_{ref})d\theta\cdot\underline{x} \quad (4\text{-}83)$$

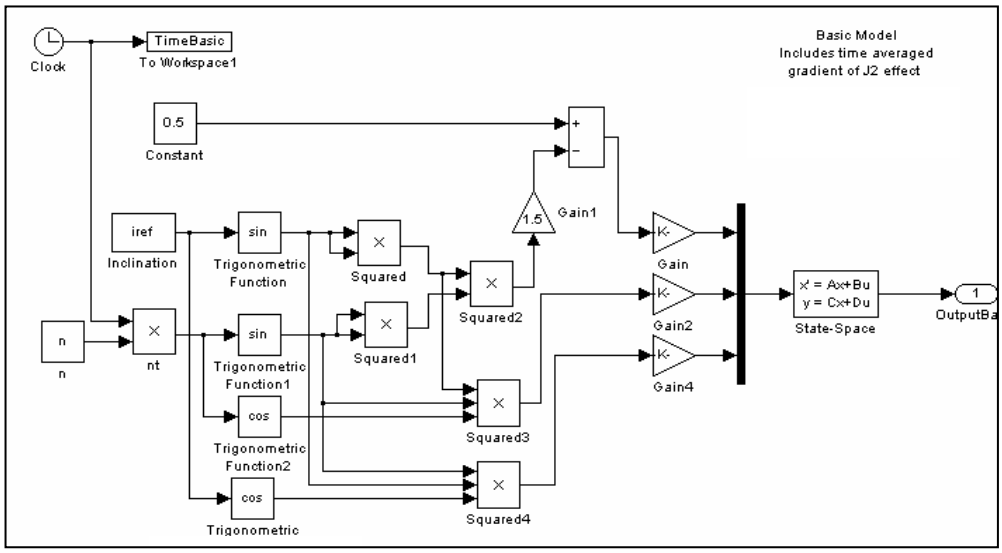

Figure 4-6: Matlab/Simulink Implementation of the Basic Time Averaged Model

For the equations where ∇J_2 is time varying, the coefficients of the state matrix vary at each time step. In these cases, the Simulink state space block cannot be applied. Instead, the new state matrix is computed at each time step and integrations are performed on each state separately. Despite their additional complexity, the time varying models run quickly.

Figure 4-7 illustrates the top level diagram of one of the time varying Simulink models. This example illustrates the Orbital Period Corrected Time Varying Model, described by equation (4-84).

$$\ddot{\underline{x}} + 2\underline{\omega} \times \dot{\underline{x}} + \dot{\underline{\omega}} \times \underline{x} + \underline{\omega} \times (\underline{\omega} \times \underline{x}) = \underline{\nabla g}(\underline{r}_{ref}) \cdot \underline{x} + \underline{J}_2(\underline{r}_{ref}) + \underline{\nabla J}_2 \cdot \underline{x} - \frac{1}{2\pi} \int_0^{2\pi} \underline{J}_2(\underline{r}_{ref}) d\theta \quad (4\text{-}84)$$

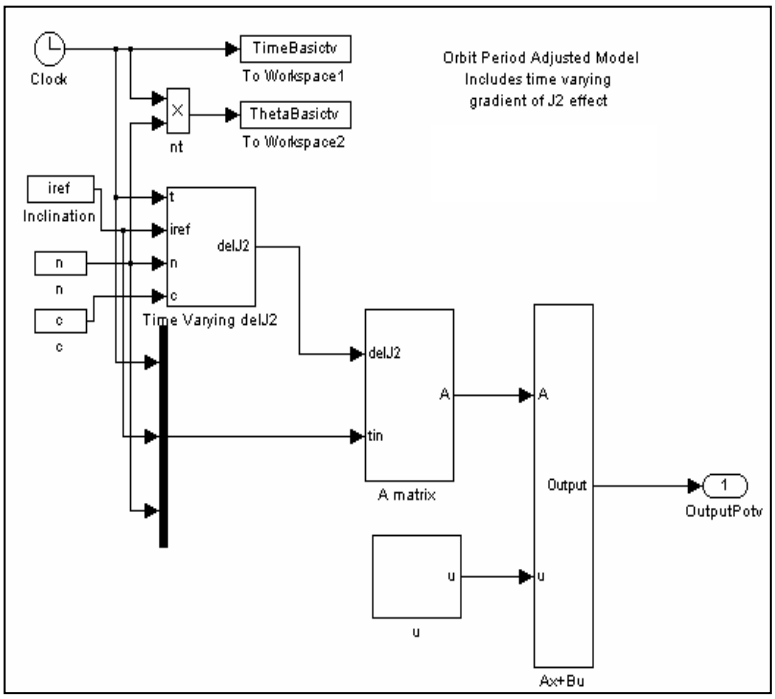

Figure 4-7: Matlab/Simulink Implementation of the Orbital Period Corrected Time Varying Model (Top Level)

The model outputs are the relative position and velocity of the perturbed satellite compared to either another satellite on the circular reference orbit, or another perturbed satellite. All measurements are in a curvilinear coordinate system based at the reference satellite. These data were either written to an Excel spreadsheet or used in other Matlab programs where the final comparisons between the theoretical and numerical scenarios from STK could be made.

The solutions obtained for different sets of analytical equations have also been implemented in Matlab. This has served as a check for the model implementation, and the derivation of the analytical solutions. For each set of relative motion equations, the corresponding set of expressions (the analytical solutions) were implemented term by term in a Matlab m-file, and evaluated for a range of values of time. The results were plotted in Matlab and could be compared with the state space model output from Simulink.

4.6 Model Verification

Before the models are applied to control law design and evaluation, it is necessary to verify their response in a range of conditions. A suitable tool for model verification is the Satellite Tool Kit Astrogator software (Satellite Tool Kit, 2005). Astrogator is essentially a highly accurate numerical orbit propagator application with the facility to incorporate a full range of external disturbances to the simulation. The purpose of verifying the Matlab model against STK is twofold. Firstly it is appropriate to verify the solutions and initial conditions for the analytical Hill and J_2 models, and also the time varying model for a number of test cases using this commercially available software. It is important to ensure that the models function correctly and are sufficiently accurate in a range of conditions, and also to define their limitations. Secondly, the suitability of STK to be used as a 'real environment' within which a controller (effectively on board a satellite) can be evaluated is being assessed. By embedding the Matlab controller in the STK software, the facility of this technique will be tested in chapter 5, in particular with a view to simulating formation flying scenarios of greater complexity in the future.

4.6.1 General Application of the Satellite Tool Kit to Model Verification

In initial simulations, one satellite was created to orbit in a perfect circle at the reference orbit altitude, subject to point mass gravity, and a second satellite with the same basic properties was made to experience the J_2 perturbation. Comparisons were later made with the relative motion predicted by the Matlab model where two satellites experienced J_2. The scenario used to validate each stage of model development is described in turn later in this section. A number of settings associated with the propagator and satellite properties within STK remained constant throughout all the scenarios:

- The axis system in STK was selected to be the Earth Centred Inertial (ECI) J2000 which is defined by the following description. 'X points toward the mean vernal equinox and Z points along the mean rotation axis of the Earth on 1 Jan 2000 at 12:00:00.00 TDB'. To minimise errors, all satellite orbit propagation runs were performed during an epoch beginning 1 Jan 2000 at 12:00:00.00.
- The satellite properties were selected so that there was no aerodynamic drag or Solar radiation pressure affecting either satellite at this stage.

It is also necessary to include any initial conditions that are applied to the analytical model to the STK simulation. For example, if the satellites have an initial separation in the radial (x), in-track (y) or cross-track (z) directions in the Matlab model, the same separations can be implemented in STK. For the radial separation, the orbit eccentricity and the semi-major axis can be adjusted. For the in-track separation (curvilinear), a non-zero value for the initial true anomaly (true latitude with $\omega=0$) can be entered, and for the cross-track separation (also curvilinear), the initial inclination, longitude of ascending node, and true anomaly can be altered. The conversion between relative orbit elements and the Hill frame coordinates described by equations (3-13) (section 3.1.1.3) were applied where appropriate.

If initial relative velocities in the x-y-z directions are non-zero in the Matlab model, it is also possible to simulate these within the STK Astrogator software by applying an impulse equivalent to the value of the relative velocity in any direction to one or both of the satellites. (The impulse magnitude is also related to the initial orbit element settings already applied). An illustration of the STK Astrogator window is included as Figure 4-8. The orbital parameters were entered on the right hand side of the window, and the initial relative velocities were entered through the 'Impulsive Manoeuvre' segment using the 'Thrust Vector' option with LVLH axes.

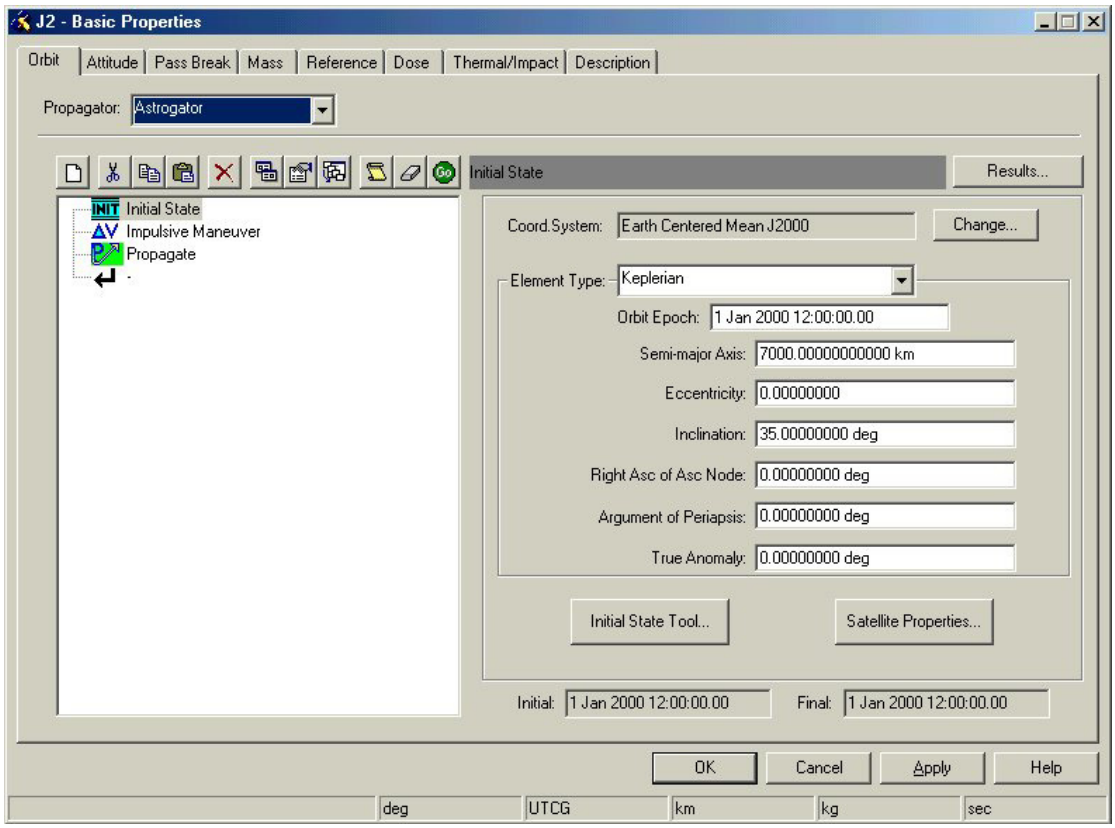

Figure 4-8: An example of the STK Astrogator window (Satellite Tool Kit, 2005)

For each scenario, the two satellites were propagated simultaneously and their motion reported using a selected time step size (1 or 10 seconds) within STK for the chosen number of orbits (usually 5). A routine within the STK software enables the relative position between any number of satellites to be computed as a Cartesian LVLH set, based at one of the satellites (the reference). Absolute and relative motion data can be produced in graphical or report format. The STK reports containing the relative position data were either copied into an Excel spreadsheet, or extracted from STK through its Matlab Engine. The STK report data was converted to curvilinear coordinates using expressions (4-3) (4-4) and (4-5) (section 4.2.1.1) before being compared to the Matlab model solutions.

4.6.2 Verification of the Basic Equations

The same 'Basic' STK scenario was compared to all three of the Matlab models where the relative motion between one J_2 perturbed satellite and one reference satellite was calculated. The three basic models, derived in sections 4.3.2 and 4.3.3, all incorporated the J_2 perturbation force with the following different characteristics.

- The J_2 perturbation force before it was linearised.
- The J_2 perturbation force plus the time average of the gradient of J_2 (∇J_2).
- The J_2 perturbation force plus the time varying gradient of J_2 (∇J_2).

The Basic scenario in STK was established by creating one satellite, P_0, which would orbit in a perfect circle (eccentricity set to zero), subject to point mass gravity. A second satellite (P_1) with the same basic properties was created, but the J2 Propagator within Astrogator was selected to propagate this satellite. P_0 and P_1 are illustrated in Figure 4-1 (section 4.2.1.1).

The radius of the circular reference orbit for the reference satellite was made equal to the initial orbit radius of the perturbed satellite. The initial conditions for zero drift and offset, summarised in section 4.4, Table 4-2, were applied to the perturbed satellite. These initial relative positions and velocities effectively make the mean radius of the perturbed satellite equal to the reference orbit radius, and create a formation with a bounded relative orbit. Despite experiencing different disturbances, the satellites remain together throughout the scenario without any orbit correction. Without this initial relative velocity, the satellites would rapidly drift apart, and this is easily visualised in both Matlab and STK at the output of the relative dynamics model (Matlab) or for two separate satellites whose relative motion is computed following individual spacecraft propagation in STK. It is important to use the relative dynamics model under conditions where the satellites (or reference points if the reference is not located at one of the spacecraft) remain in close proximity as the model is linearised. (The gravity gradients will not be representative when the spacecraft are separated over long distances). The effects of zero drift and offset initial conditions are demonstrated in the results section (4.7). For the verification of the particular set of equations list above, the same initial conditions were applied to the Matlab model, and the STK and Matlab data compared. The differences between the results (denoted as 'error') were evaluated and are also presented in section 4.7.

4.6.3 Verification of the Orbital Rate and Nodal Drift Corrected Model

For the reference orbit corrected for both the change in mean angular velocity and for nodal drift, the implementation of an equivalent scenario in STK was possible using either of the following approaches. In both cases it was first necessary to generate an orbital rate and nodal drift corrected reference orbit in Matlab (rather than STK). This was achieved by implementing the expressions for the variation in orbital elements due to the cross-track component of the J_2 perturbation according to the Lagrange Planetary Equations (equations (3-6) to (3-11)). Schweighart and Sedwick (2002) proposed an

alternate expression for inclination which improves reference orbit accuracy, and this was therefore also implemented.

Method 1 - ECI Conversion

- Convert the osculating orbit elements of the reference orbit at each time step to positions and velocities in ECI coordinates (Prussing and Conway, 1993).
- Write the ephemeris file to STK and import it to produce the artificial reference orbit in the STK environment.
- Propagate the J_2 perturbed satellite with the initial conditions for the nodal drift corrected case given in Table 4-2, section 4.4.
- Generate STK reports of relative position and velocity with respect to the new reference orbit in the local LVLH frame.
- Convert the relative data into the curvilinear frame in Excel and compare to the Matlab dynamics model (equations (4-47)).

Method 2 - Relative Orbit Elements

- Propagate the J_2 perturbed satellite with the initial conditions for the nodal drift corrected case given in Table 4-2, section 4.4.
- Generate STK report for the perturbed satellite of the osculating orbit elements during the orbit.
- Copy the orbit element data into Excel, and subtract the reference orbit elements derived for the Matlab reference orbit to obtain relative orbit elements.
- Convert the relative orbit elements to the Hill curvilinear Hill frame using equations (3-13).
- Compare results to the Matlab dynamics model (equations (4-47)) output, also copied into Excel.

Both approaches were successful in extracting the relative motion data, and the model verification results are presented in section 4.7.

4.6.4 Verification of the Cross-Track Model

A separate test scenario was implemented in STK for comparison with the cross-track relative motion model implemented in Matlab (refer to section 4.3.5). For a simple initial cross-track offset, measured from the equator, the equivalent changes in the orbital elements (longitude of ascending node and true latitude) had to be calculated as inputs to the satellite properties in STK. By using approximations and spherical trigonometry (equations (4-85)), the same initial satellite separation was generated in STK.

$$\Omega = -\frac{z_0}{r_{ref}\sin i}$$
$$\theta = \frac{z_0}{r_{ref}\tan i} \qquad (4\text{-}85)$$

In addition to the cross-track relative motion data, the radial and along-track data from STK also had to be obtained to enable the conversion of z-axis results to curvilinear coordinates so that the model verification could be performed.

4.6.5 Verification of the Time Averaged Model for Relative Motion of Two Perturbed Satellites in STK

For the purposes of dynamics model verification using an STK scenario where the relative motion of two perturbed satellites is to be evaluated, there is no need to include a reference orbit satellite on a circular orbit (only the relative positions and velocities of two perturbed satellites need to be measured to examine the effect of J_2 on relative motion). In this case one of the perturbed satellites becomes the 'reference' and the relative position data is generated within STK in terms of a Cartesian LVLH set based at the J_2 perturbed reference satellite.

The inclination and reference orbit radius data for a particular case are set for the perturbed reference satellite, and the position of the second satellite is established by varying the semi-major axis (for x separation), true anomaly (for y separation), and longitude of ascending node and true anomaly (for z separation). Impulsive manoeuvres (initial relative velocities) must be applied to both perturbed satellites in order to eliminate drift and offset with respect to the 'invisible' circular reference orbit. This is to ensure that like scenarios are being compared. The proximity of both J_2 perturbed satellites to the reference orbit (with modified orbital rate and nodal drift) is implicit within the Matlab model. This must therefore still be accounted for through the STK initial conditions in order to allow fair comparisons between the model and STK to be made.

The initial relative positions of the first perturbed (reference) satellite with respect to the circular reference orbit are zero, and the initial relative velocities are given by equations (4-86) (introduced in Table 4-2, section 4.4)

$$\begin{aligned} \dot{x}_{01} &= \frac{y_{01} n}{2c}(1-s) \\ \dot{y}_{01} &= -2ncx_{01} + \frac{3J_2 R_e^2 n^2}{8kr_{ref}}(1-\cos 2i) \end{aligned} \tag{4-86}$$

where the x_{01} and y_{01} terms are separations and velocities with respect to the circular reference orbit (and not the second satellite). The $\dot{y}_{01}$ expression was derived for the nodal drift and orbital period corrected model, and represents the most accurate initial condition achieved through the model development stages.

Even though the reference satellite is collocated with the circular reference initially, a y-velocity must still be applied in STK. The additional J_2 effect (described in the second part of the y-equation above) is applied to both perturbed satellites. Equations (4-86) represent an in-track relative velocity change over and above the relative velocity

change due to the orbital rate, n, becoming nc. Therefore, equation (4-87) gives the velocity which must be applied to the perturbed reference satellite in STK.

$$\dot{y}_{1STK} = \dot{y}_{01STK} + ncr_{ref} - nr_{ref} \tag{4-87}$$

The second perturbed satellite will have an offset applied through changes in the initial orbital parameters in STK. Equations (4-88) describe the initial relative velocities of the second satellite relative to the circular reference, based on these initial separations.

$$\begin{aligned} \dot{x}_{02} &= \frac{y_{02}n}{2c}(1-s) \\ \dot{y}_{02} &= -2ncx_{02} + \frac{3J_2R_e^2n^2}{8kr_{ref}}(1-\cos 2i) \end{aligned} \tag{4-88}$$

These equations are the same as equations (4-86), but the y-velocity will be different due to the initial separations between the satellites. Equation (4-89) is used to calculate the initial velocity to be implemented in STK.

$$\dot{y}_{2STK} = \dot{y}_{02STK} + ncr_{ref} - \left(\frac{\mu}{(r_{ref}+x_{02})^3}\right)^{\frac{1}{2}}(r_{ref}+x_{02}) - \text{factor} \tag{4-89}$$

The first two terms are the derived initial velocity, and the reference orbit velocity with the modified period. The term containing x_{02} is equivalent to 'nr_{ref}', but allows for an initial separation in the radial (x) direction. 'Factor' is the remaining term that must be included to ensure that the STK and Matlab initial conditions are matched. The initial relative velocities in Matlab are given by equations (4-90) and (4-91) (also in Table 4-2).

$$\Delta\dot{x}_0 = \frac{n\Delta y_0(1-s)}{2\sqrt{1+s}} \tag{4-90}$$

$$\Delta\dot{y}_0 = -2n\Delta x_0\sqrt{1+s} \tag{4-91}$$

It is important that the initial relative along-track (y) velocity computed by STK is equal to $\Delta\dot{y}_0$ of equation (4-91). Whether the factor is required depends on how the initial x separation was implemented using the orbital elements. For example, a different factor is required if the eccentricity was used to define the offset. The reasons for these small but necessary adjustments are unknown, but probably due to the methods used by STK to read and apply initial orbit element conditions within its own software. One of the limitations of STK is the lack of visibility of the initialisation process and propagation algorithms.

With the correct initial conditions implemented in STK, the relative motion data can be extracted in LVLH coordinates. These are converted to curvilinear coordinates before

being compared to the time averaged equations of relative motion implemented in Matlab.

4.6.6 Verification of the Time Varying Model for Relative Motion of Two Perturbed Satellites in STK

The generation of initial conditions for the time varying J_2 relative dynamics model was important in order to identify the conditions in which reliable model verification could be performed. The time varying model is linear, and as soon as the formation begins to drift away from the reference orbit, the same assumptions regarding the validity of the equations as the time averaged case no longer hold. In section 4.4, two approaches for obtaining initial conditions for the time varying model were introduced.

As demonstrated in section 4.6.5, the initial conditions specified for the Matlab model for the case of two perturbed satellites cannot be applied directly to the STK orbit propagator, and instead some measure of the absolute motion of both satellites is required in relation to the reference orbit, correcting for the effects of the J_2 perturbation on orbital rate and nodal drift. This is also the case for the time varying model, and therefore both absolute and relative initial conditions must be defined.

Earlier analysis demonstrated that it was not possible to derive a set of analytical conditions with sufficient accuracy using the time varying A matrix and state transition matrix approach to the solutions. However, instead they could be derived numerically within STK. The time varying model is very similar in basis to the time averaged model but requires a numerical solution and therefore at this stage it is not clear whether the analytically derived initial conditions (described in section 4.6.5) will produce more closely bounded motion than a purely numerical approach using STK. It is possible that neither set of initial conditions will create bounded motion for the time varying model, preventing the best performance of the model to be achieved in the verification. The effects of both sets of initial conditions were investigated and the results are presented in section 4.7.

In this section (4.6), the use of STK for model verification is presented. Applying the STK 'targeter' routine to derive numerically initial conditions is therefore part of this process for the time varying model, and the method is described below.

- In STK, specify the orbit elements of two satellites, separated according to formation requirements (select one satellite to be the reference).
- Set the desired terminal conditions of each satellite to be equal to the initial conditions after one orbit.
- Compute the $\Delta V(x,y,z)$ required to enforce the final conditions using the STK targeter algorithm.
- Apply the corrective $\Delta V(x,y,z)$ to the non-reference satellite, and specify the terminal conditions to be the new initial conditions (positions and velocities).
- Repeat the cycle until the initial and terminal conditions are the same, and no additional ΔV is required. In this case bounded motion has been achieved.

This function was found to be a reasonably efficient method of determining bound initial conditions for the numerical propagator as few iterations were required. Over a large number of orbits, the motion ceases to remain bounded, but the drift is extremely gradual. However, early simulations revealed the sensitivity of the model behaviour to the initial conditions, and therefore, the results obtained for the time varying model could be deemed an unfair comparison to the other linear time invariant models.

4.7 Results of Model Verification

In this section, the results of the comparisons between the Matlab models and STK scenarios are presented for a number of test cases. In some cases, the model output and scenario data are included separately, but most graphical results display the difference in relative position predicted by the Matlab model and STK, or 'modelling error', although it should be noted that this error may arise from the minor uncertainties associated with the implementation of initial conditions through the graphical user interface in STK. The areas addressed through these comparisons include the effects of the initial conditions, the limits of linearisation, the effects of leaving the gradient of J_2 term in the equations of relative motion time varying and establishing model limitations in the test cases described below.

The test cases considered in this results section are listed below, where i_{ref} is the reference orbit inclination.

- General Test Case ($i_{ref} = 35^o$)
- Polar Orbit
- Equatorial Orbit
- Sun Synchronous Orbit
- Circular Formation
- J_2 Invariant Relative Orbit and Critical Inclination Orbit
- MUSTANG Orbit
- Zero Orbital Rate Change Orbit ($i_{ref} = 54.74^o$)

All test cases apart from the MUSTANG orbit have a reference orbit radius (r_{ref}) of 7000km, whereas the MUSTANG mission design radius is 6978.1km (600km altitude). Additional model comparisons were made at orbits of different inclinations and altitudes, but the above cases were better able to highlight different features of the models and aspects of model behaviour.

Some of the results illustrate model behaviour at a general test case with a reference orbit inclination (i_{ref}) of 35^o and orbit radius (r_{ref}) of 7000km. This was originally the only test case published by Schweighart and Sedwick (2001a), and therefore the results of this general case, produced early in the verification process, were used to ensure correct implementation of their analytical model and to confirm their results. The general test case has been more extensively applied here.

The remaining test case not already introduced is the 'Zero Orbital Rate Change' orbit. In this case, the J_2 perturbation on average does not speed up or slow down the

perturbed satellite relative to the 'uncorrected' circular reference orbit, thus simplifying the rate matching problem. (The orbit rate correction factor, c defined in the model derivation by equation (4-45) is equal to one, and the corresponding inclination is calculated by setting 's' equal to zero in equation (4-40)).

In the following subsections, the Hill equations model is first compared to STK, and the effects of bounding the initial conditions are demonstrated. The mathematical descriptions of the motion of one J_2 perturbed satellite relative to the reference orbit are then verified. In the next subsection, the more realistic scenarios where both satellites are perturbed by J_2 are investigated. The findings are summarised in section 4.7.4

4.7.1 The Hill equations

The relative motion predicted by the Hill equations for initial separations in the radial (x), along-track (y) and cross-track (z) directions was illustrated in Figure 4-2, although the conditions for bounded motion described in section 3.1.3.1 (chapter 6) and section 4.4 were not applied.
Figure 4-9 illustrates the effect of the bounded initial conditions which remove the along-track drift in the absence of J_2 perturbations.

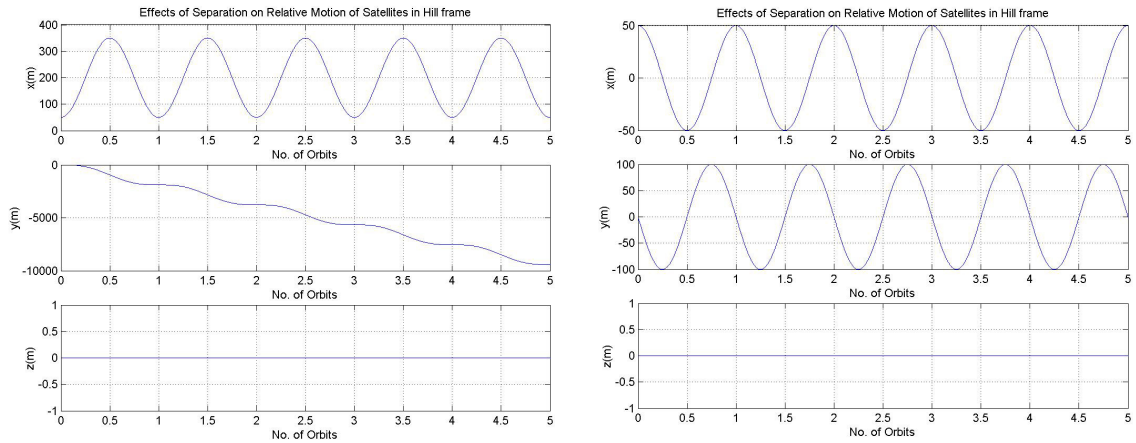

(a) **(b)**

Figure 4-9: The Effects of Bounded Initial Conditions on Hill Relative Motion for the General Test Case (r_{ref}=7000km, i_{ref}=35°) (a) Radial Offset x_0 = 50m, y_0 = 0, z_0 = 0, $\dot{x}_0 = 0$, $\dot{y}_0 = 0$, $\dot{z}_0 = 0$ (b) Bounded Initial Conditions x_0 = 50m, y_0 = 0, z_0 = 0, $\dot{x}_0 = 0$, $\dot{y}_0 = -0.1078$m/s, $\dot{z}_0 = 0$

Figure 4-10 demonstrates that despite the bounded motion initial conditions, the Hill equations do not capture relative motion in the presence of the J_2 perturbation. The radial error (x) increases to approximately 1m over 5 orbits, the along-track error (y) increases to approximately 2m over 5 orbits, and the small cross-track (z) motion in the third graph is not captured at all. The errors encountered are later compared to those arising from the analytical and time varying J_2 models for the equivalent test case.

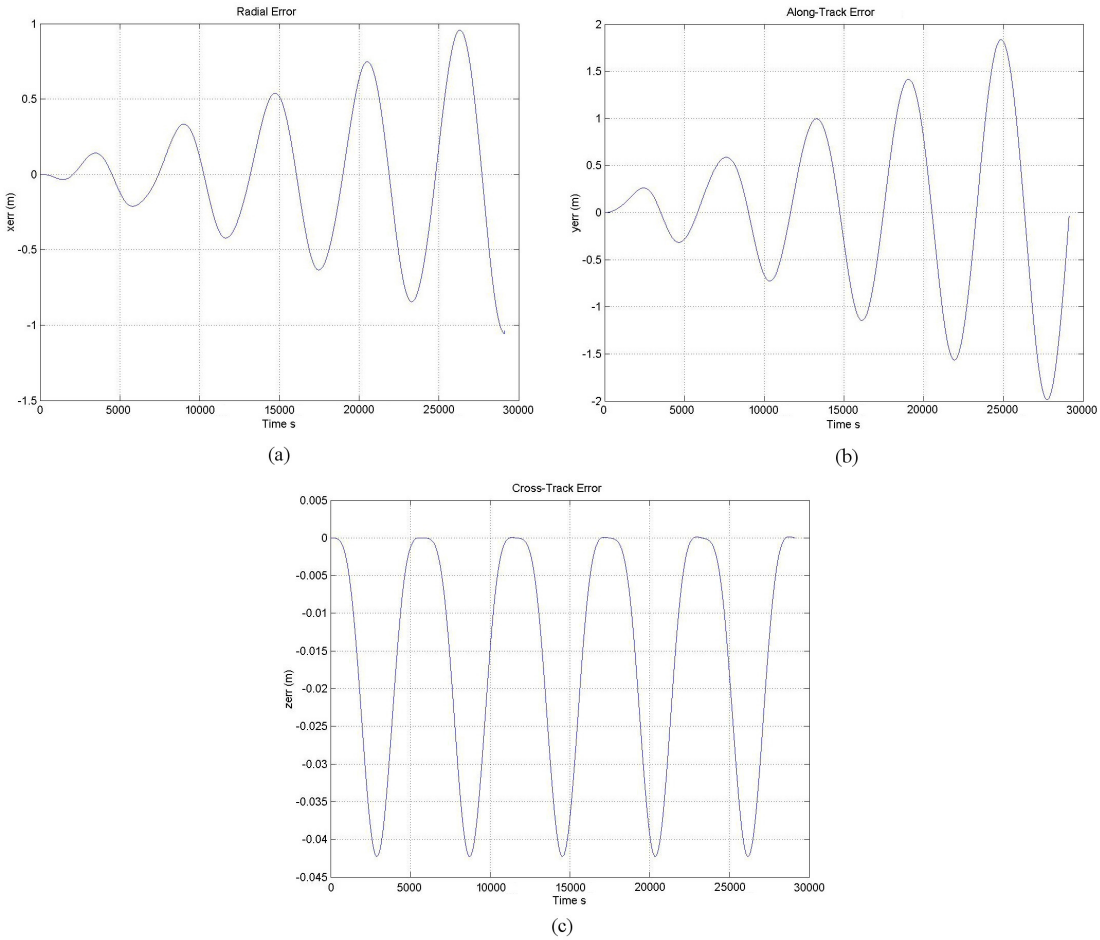

Figure 4-10: Modelling Error Between the Unperturbed Relative Motion Predicted by the Hill Equations and the J_2 Perturbed STK Scenario for Two Perturbed Satellites for the General Test Case (r_{ref}=7000km, i_{ref}=35°) and Initial Conditions Δx_0=0, Δy_0=50m, Δz_0=0, $\Delta\dot{x}_0 = 0.02695$m/s, $\Delta\dot{y}_0 = 0$, $\Delta\dot{z}_0 = 0$

4.7.2 Equations of Relative Motion for One Perturbed Satellite

In this section, the motion of one J_2 perturbed satellite relative to a circular reference orbit is considered. The relative motion is equivalent to that which a cluster of satellites would experience relative to a Keplerian circular orbit at the same altitude. This motion is significant if the relative motion between perturbed satellites is to be controlled in an efficient manner. It is also an extremely important aspect of the relative model development as the whole formation must remain in close proximity to the circular reference orbit along which linearised forcing terms are evaluated. However, as described in section 4.3, rather than forcing the perturbed satellites to essentially follow Keplerian orbits at great and impractical fuel expense, it is necessary to modify the reference orbit which does not have a satellite physically located on it, and can remain 'virtual'. This modification was applied to both time averaged and time varying equations of motion. The equations considered in this section are included below with

the descriptions of figures for ease of reference, although the reader is referred to section 4.3 for their development.
In this section the following models are compared and verified (equations (4-92) to (4-96)) in order to establish:

- The effects of J_2 on a single satellite compared to the Keplerian orbit without reference orbit correction.

$$\ddot{\underline{x}} + 2\underline{\omega} \times \dot{\underline{x}} + \dot{\underline{\omega}} \times \underline{x} + \underline{\omega} \times (\underline{\omega} \times \underline{x}) = \underline{\nabla g}(\underline{r}_{ref}) \cdot \underline{x} + \underline{J}_2(\underline{r}_{ref}) \tag{4-92}$$

- The effects of including the time averaged gradient of J_2 (∇J_2) without reference orbit correction.

$$\ddot{\underline{x}} + 2\underline{\omega} \times \dot{\underline{x}} + \dot{\underline{\omega}} \times \underline{x} + \underline{\omega} \times (\underline{\omega} \times \underline{x}) = \underline{\nabla g}(\underline{r}_{ref}) \cdot \underline{x} + \underline{J}_2(\underline{r}_{ref}) + \frac{1}{2\pi}\int_0^{2\pi} \underline{\nabla J}_2(\underline{r}_{ref}) d\theta \cdot \underline{x} \tag{4-93}$$

- The effects of including the time varying ∇J_2 without reference orbit correction.

$$\ddot{\underline{x}} + 2\underline{\omega} \times \dot{\underline{x}} + \dot{\underline{\omega}} \times \underline{x} + \underline{\omega} \times (\underline{\omega} \times \underline{x}) = \underline{\nabla g}(\underline{r}_{ref}) \cdot \underline{x} + \underline{J}_2(\underline{r}_{ref}) + \underline{\nabla J}_2(\underline{r}_{ref}) \cdot \underline{x} \tag{4-94}$$

- The effects of J_2 on a single satellite compared to a circular reference orbit with orbit rate correction.

$$\ddot{\underline{x}} + 2\underline{\omega} \times \dot{\underline{x}} + \dot{\underline{\omega}} \times \underline{x} + \underline{\omega} \times (\underline{\omega} \times \underline{x}) = \underline{\nabla g}(\underline{r}_{ref}) \cdot \underline{x} + \underline{J}_2(\underline{r}_{ref}) - \frac{1}{2\pi}\int_0^{2\pi} \underline{J}_2(\underline{r}_{ref}) d\theta \tag{4-95}$$

- The effects of including time averaged ∇J_2 with orbit rate correction.

$$\ddot{\underline{x}} + 2\underline{\omega} \times \dot{\underline{x}} + \dot{\underline{\omega}} \times \underline{x} + \underline{\omega} \times (\underline{\omega} \times \underline{x}) = \underline{\nabla g}(\underline{r}_{ref}) \cdot \underline{x} + \underline{J}_2(\underline{r}_{ref}) + \frac{1}{2\pi}\int_0^{2\pi} \underline{\nabla J}_2(\underline{r}_{ref}) d\theta \cdot \underline{x} - \frac{1}{2\pi}\int_0^{2\pi} \underline{J}_2(\underline{r}_{ref}) d\theta \tag{4-96}$$

- The effects of including time varying ∇J_2 with orbit rate correction.

$$\ddot{\underline{x}} + 2\underline{\omega} \times \dot{\underline{x}} + \dot{\underline{\omega}} \times \underline{x} + \underline{\omega} \times (\underline{\omega} \times \underline{x}) = \underline{\nabla g}(\underline{r}_{ref}) \cdot \underline{x} + \underline{J}_2(\underline{r}_{ref}) + \underline{\nabla J}_2(\underline{r}_{ref}) \cdot \underline{x} - \frac{1}{2\pi}\int_0^{2\pi} \underline{J}_2(\underline{r}_{ref}) d\theta \tag{4-97}$$

- The effects of including time varying ∇J_2 with orbit rate and nodal drift correction.

$$\ddot{\underline{x}} + 2\underline{\omega} \times \dot{\underline{x}} + \dot{\underline{\omega}} \times \underline{x} + \underline{\omega} \times (\underline{\omega} \times \underline{x}) = \underline{\nabla g}(\underline{r}_{ref}) \cdot \underline{x} + \underline{J}_2(\underline{r}_{ref}) + \underline{\nabla J}_2(\underline{r}_{ref}) \cdot \underline{x} - \frac{1}{2\pi}\int_0^{2\pi} \underline{J}_2(\underline{r}_{ref}) d\theta - [\underline{J}_2(\underline{r}_{ref}) \cdot \underline{z}]\underline{z} \tag{4-98}$$

It should be noted that most of the graphs presented in section 0 have a horizontal axis quantifying the 'number of orbits' according to the period of the reference orbit in the Matlab model (usually this has been selected to be 5). The data comparison between the Matlab models and STK simulations are made at the same points in time to obtain a measure of modelling error. For each test case evaluated, the reference (virtual) and perturbed satellites were initialised at the same position on orbit, but an additional velocity was imparted to the perturbed satellite to enforce the zero drift and offset conditions where appropriate.

Figure 4-11 illustrates relative motion predicted by equations (4-92)-dashed line, (4-93)-solid line and (4-96)-dotted line. In order to perform a direct comparison between these models, the satellites start at the same point with zero relative velocity, resulting in an unbounded solution.

The dashed lines in Figure 4-11 illustrate the effect of including the J_2 term as a disturbing function to the Hill equations of motion. The radial (x) response does not drift (due to the implementation of a curvilinear coordinate system) or vary in amplitude. However, the along-track drift between the J_2 perturbed satellite and the reference is significant due to the effect of J_2 in speeding up the perturbed satellite relative to the reference. The cross-track relative motion gradually increases in amplitude. For a reference orbit with an inclination greater than 54.74^o (for Zero Orbital Rate Change where the orbit rate correction factor, c is one) J_2 actually slows the perturbed satellite relative to the reference. This effect is also captured by the analytical and time varying models.

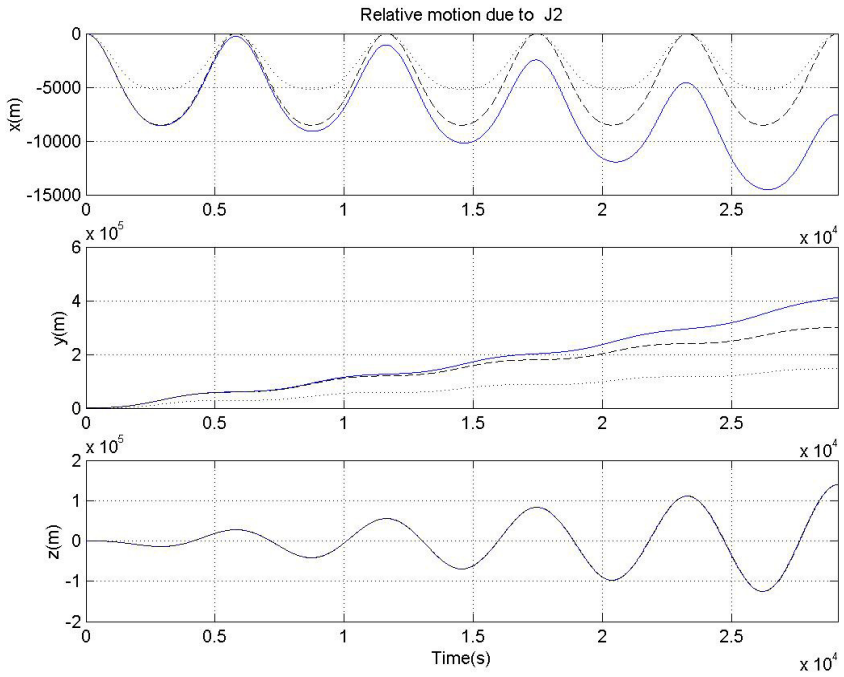

Figure 4-11: Motion of a J_2 Perturbed Satellite Relative to a Satellite on the Circular Reference Orbit for the General Test Case (r_{ref}=7000km, i_{ref}=35^o), with all Initial Conditions=0. Note: This demonstrates the need for the reference orbit to take J_2 effect into account.

In contrast, the solid line in Figure 4-11 illustrates the effect of including the time averaged ∇J_2, also with zero initial conditions. The ∇J_2 term multiplied by separation distance causes significant drift in the radial (x) and along-track (y) directions and in this case, the inclusion of ∇J_2 increased the modelling error in all axes. This would be expected in the absence of orbit rate correction due to linearisation errors introduced by the along-track drift. The physical magnitude of the J_2 perturbation acceleration, according to equation (4-25), is of the order 10^{-2}m/s^2 whereas the ∇J_2 has a magnitude

of the order of $10^{-9}/s^2$. The ∇J_2 in the equations of motion is multiplied by the separation of the perturbed and reference satellites to give an acceleration in m/s^2. When this separation reaches 100km, the gradient of J_2 acceleration is of order $10^{-4}m/s^2$, and for the General test case this occurred after just one orbit. When this term becomes large, the linearisation of the J_2 force in the equations of motion no longer holds. This example illustrates and reinforces the need to adjust the circular reference orbit so that the reference satellite can maintain the orbital rate of the perturbed satellite, and linearisation error can be reduced.

A similar result was obtained for the time varying ∇J_2 (equation (4-94)). Any differences in the effects of including either the time averaged ∇J_2 or time varying ∇J_2 in the equations were far outweighed by the linearisation error associated with the large separation between the reference and perturbed satellites.

The dotted line in Figure 4-11 illustrates the relative motion achieved when the orbital rate correction was applied to the reference orbit (equation (4-96)). Clearly the radial drift has been eliminated, but the along-track drift remains because of the zero initial conditions. The cross-track motion is only slightly affected (by approximately 1km in 5 orbits) compared to the scale of the motion when ∇J_2 and the orbital rate correction are included in the equations.

Figure 4-11 illustrates the effects of the component terms in the time averaged ∇J_2 equation (4-96). However, the ability of equations (4-95) and (4-96) to capture satellite behaviour is established by comparing the analytical Matlab models to bounded motion scenarios in STK and measuring the modelling error. In the following case, bounded initial conditions for the in-plane motion were provided to the perturbed satellite.

Figure 4-12 illustrates modelling error between the analytical model and STK, with and without time averaged ∇J_2 for a Sun synchronous orbit (with one J_2 perturbed satellite and one orbit rate corrected reference orbit). The lighter line represents the error associated with equation (4-95) and the darker line represents the modelling error associated with equation (4-96). The in-plane (x,y) results show a significant modelling error reduction when the time averaged ∇J_2 term is included in the model. However, in time averaged form, ∇J_2 does not correctly capture cross-track motion and actually increases modelling error. This supports the motivation for investigating the effects of retaining ∇J_2 in time varying form within the equations of relative motion. The relative dynamics model being compared to STK in Figure 4-12 is simplified by linearisation, time averaging of the J_2 acceleration, and decoupling of in-plane and cross-track motion. Clearly for matched initial conditions (initial errors are zero in all three axes), the cross-track error is significant and the dynamics are not captured, and associated with this, a growing along-track error is expected, despite the inclusion of an orbit rate correction term in the reference orbit equation.

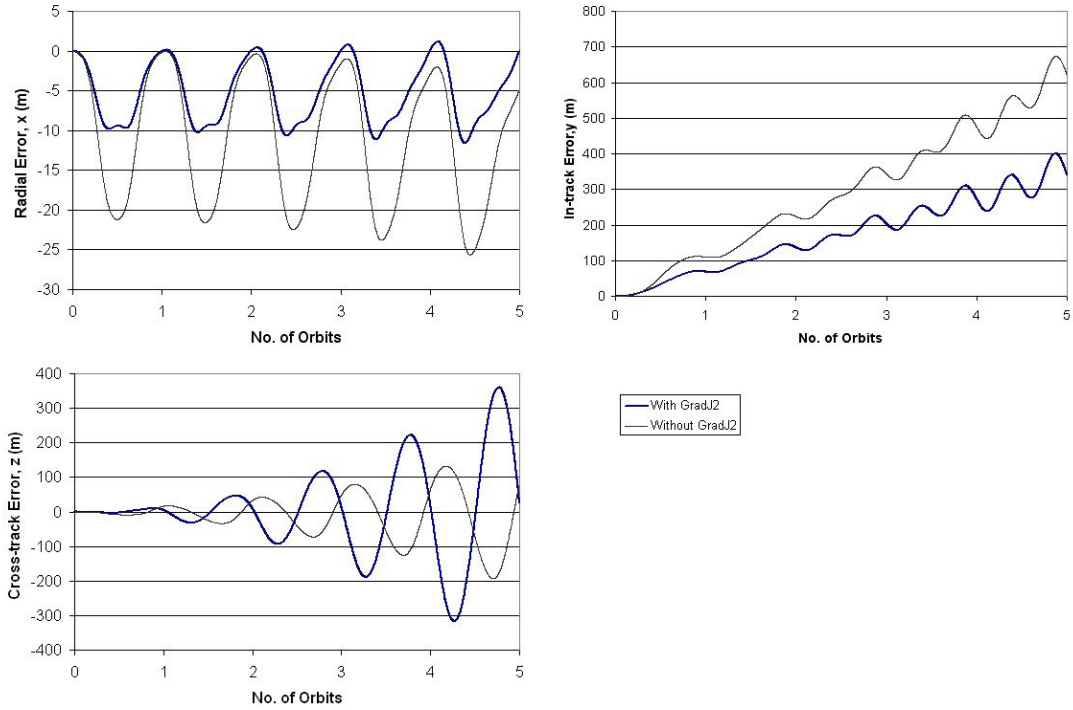

Figure 4-12: The Effect of the Time Averaged Gradient of J_2 Term on Modelling Error for a Sun Synchronous Orbit (i_{ref}=97.87^o at r_{ref}=7000km, Note: Orbit Rate Corrected Reference Orbit)

A Sun synchronous orbit maintains its initial orientation relative to the Sun, and in order to achieve this, the orbit must have nodal regression rate equal to the Earth's mean rate of revolution about the Sun. The Sun synchronous orbit inclination is dependent on the orbit radius and can be calculated by equating nodal regression rates described by equations (4-99) and (4-100).

$$\Delta\Omega_{\text{required}} = \frac{2\pi T}{T_{ES}} \quad \text{rad/rev} \tag{4-99}$$

where T is the orbit period of the satellite and T_{ES} is the orbit period of the Earth around the Sun (3.155815x10^7 seconds).

$$\Delta\Omega = -\frac{3\pi J_2 R_e^2}{r_{ref}^2}\cos(i) \quad \text{rad/rev} \tag{4-100}$$

For a circular orbit of radius 7000km (621.9km altitude), the Sun synchronous reference inclination, i_{ref}, is 97.87^o.

The Sun synchronous orbit test case was implemented both during model development to examine the relative motion of one perturbed satellite with respect to the reference and also for the two perturbed satellites case. By applying the Sun synchronous conditions, the errors introduced by the nodal drift of the perturbed orbit away from the reference are reduced, allowing the performance of models with just orbit rate correction to be evaluated (equations (4-95), (4-96) and (4-97)). A polar inclination would be required to completely remove the nodal drift, and enable improved model

verification, but this could not be implemented in the cross-track model as singularities in the spherical trigonometry arise. This and other model limitations associated with the polar orbit test case are considered later for two perturbed satellites.

The actual relative motion predicted by the model including time averaged ∇J_2 and the orbit rate correction (equation (4-96)), and therefore associated with the darker line in Figure 4-12, is illustrated in Figure 4-13.

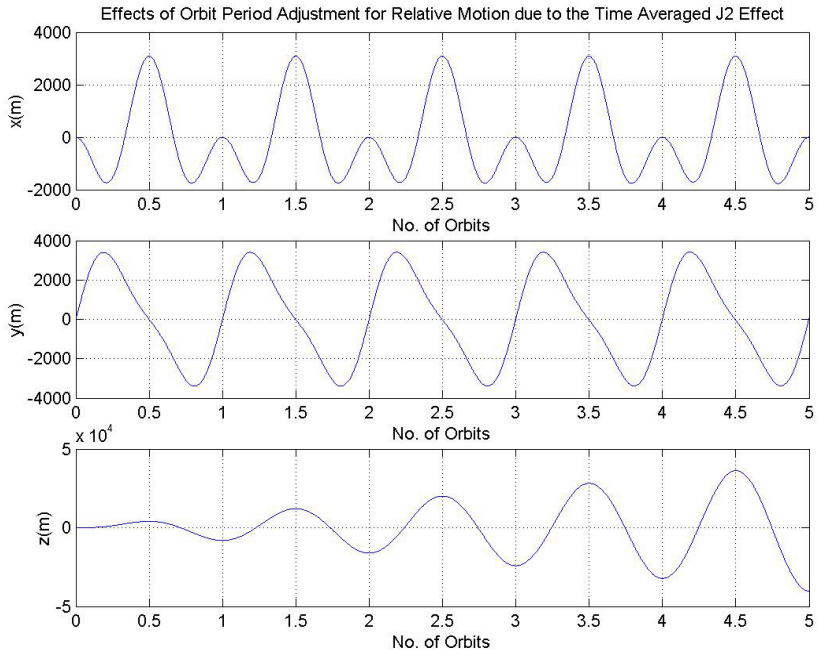

Figure 4-13: Bounded Relative Motion of a J_2 Perturbed Satellite Relative to a Satellite on the Circular Reference Orbit with Corrected Rate and Time Averaged Gradient of J_2 for a Sun Synchronous Orbit (Relative Dynamics Model Output) (r_{ref}=7000km, i=97.87° and Initial Conditions x_0=0,y_0=0,z_0= 0, $\dot{x}_0 = 0$, $\dot{y}_0 = 4.9931$m/s, $\dot{z}_0 = 0$)

More generally, all test cases demonstrated that the orbit rate correction term was required to eliminate along-track drift, and that modelling error increased the further away from the ideal bounded motion conditions that the satellite formation operated. Where changes were made to the in-plane initial conditions, for example changing them from zero to bounded motion conditions, the cross-track initial conditions remained unchanged (zero in this case). The cross-track equations are decoupled from the in-plane equations for the time averaged models, and therefore the motion predicted by the Matlab models remains the same. However, the modelling errors differed because of the changing initial conditions applied to STK. The fact that changing the in-plane initial conditions in STK causes a change in cross-track relative motion predicted by the propagator highlights the level of cross-coupling between the in-plane and cross-track motion. Again, a further justification for retaining the time varying gradient of J_2 terms in the linear equations is provided. The only other way of incorporating the coupling effects between the cross-track and in-plane dynamics is by including nonlinear terms in the equations (refer to equations (4-15) and (4-16) in section 4.2.1.2).

The scenario implemented in Figure 4-13 was repeated for the time varying model including orbit rate correction (equation (4-97)). The model response is illustrated in Figure 4-14.

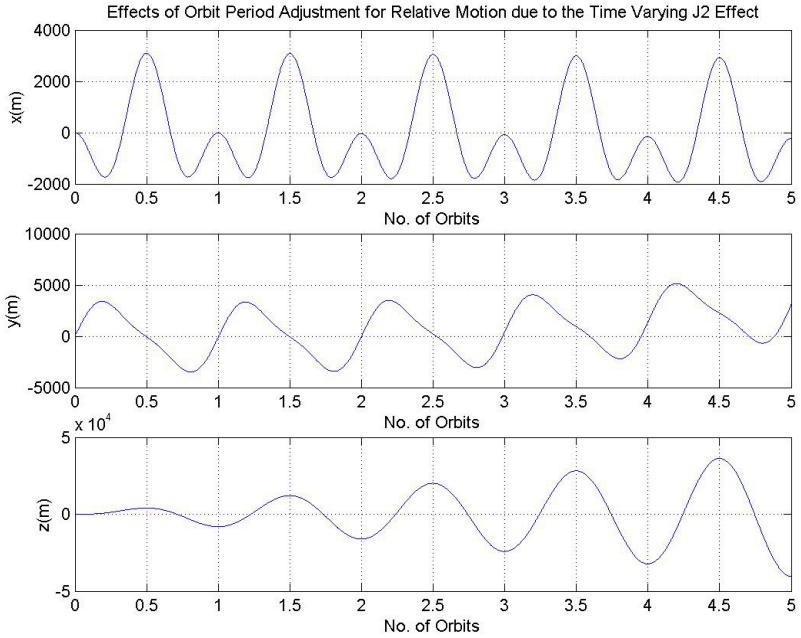

Figure 4-14: Relative Motion of a J_2 Perturbed Satellite Relative to a Satellite on the Circular Reference Orbit with Corrected Rate and Time Varying Gradient of J_2 for a Sun Synchronous Orbit (Relative Dynamics Model Output) (r_{ref}=7000km, i=97.87° and Initial Conditions x_0=0, y_0=0, z_0=0, $\dot{x}_0 = 0$, $\dot{y}_0 = 4.9931$m/s, $\dot{z}_0 = 0$)

Upon comparing Figure 4-13 and Figure 4-14, an additional drift can be observed in the along-track response for the time varying case. The same bounded motion initial conditions, derived from the analytical solutions to the time averaged equations, were applied to both models. When compared to STK, the in-plane modelling error was found to be greater for the time varying model with analytical initial conditions, however, the cross-track modelling errors were reduced.

For the scenario illustrated in Figure 4-12, the new cross-track modelling error resulting from the inclusion of time varying ∇J_2 is shown in Figure 4-15a, superimposed on the results of Figure 4-12. For a relative cross-track motion of ±40km over 5 orbits (Figure 4-15b), the maximum modelling error is +60m to –110m over the same period. In contrast, the time averaged ∇J_2 model produced errors of approximately +350m to –310m. Of concern for the time varying model verification is the magnitude of the oscillatory cross-track relative motion displayed in Figure 4-14. Due to the cross coupling between all axes, the magnitude of this motion is likely to be detrimental to the linearisation approximations inherent in the equations. However, the results displayed in Figure 4-15 are as expected. The nodal drift effect of J_2 has not been included in the reference orbit and therefore cross-track relative motion will grow with time. The associated modelling error therefore also grows for all three relative dynamics models considered. However, the time varying model captures relative motion the most accurately as expected.

The targeting procedure in STK, introduced in section 4.6.6, was applied to identify the initial along-track velocity required to produce bounded in-plane motion. Further investigations were performed which involved varying the initial conditions of the Matlab model to visually reduce the along-track drift. However, the resulting numerically determined initial conditions from STK were found to be almost exactly the same as those predicted by the analytical equations for the Sun Synchronous case (with orbit rate correction). The trial and error approach suggested that improved performance would be obtained with a slightly higher initial relative along-track velocity. In conclusion, a more likely cause of the error for the time varying model was due to the omission of another significant effect of the J_2 perturbation in the model – the drift in longitude of ascending node. The verification of the orbital rate corrected time varying model was deemed too unphysical to warrant sensible results without taking into account the nodal drift.

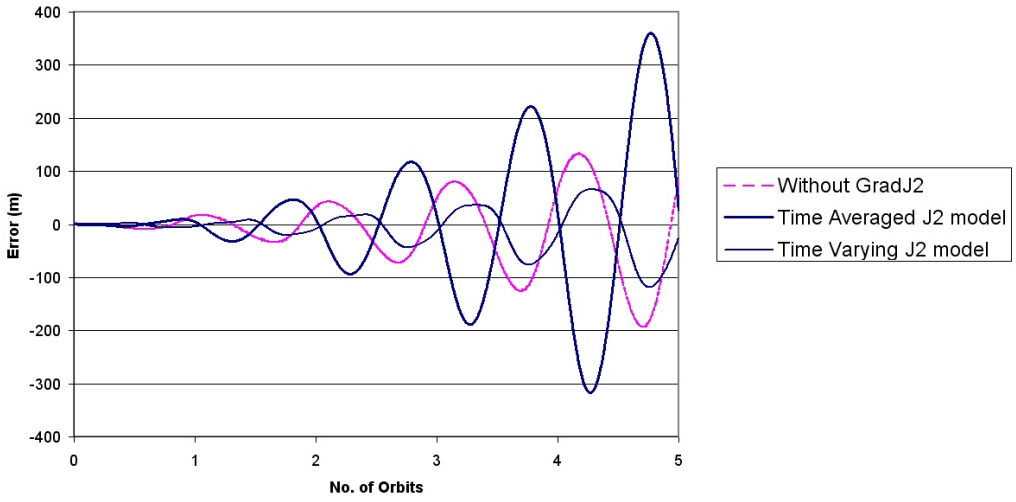

(a)

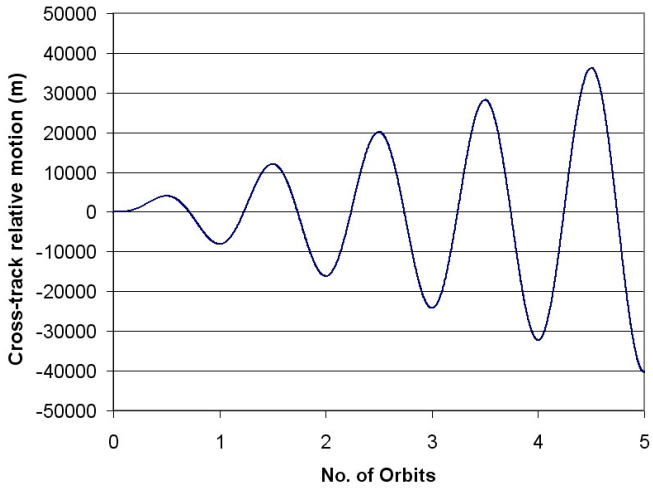

(b)

Figure 4-15: (a) Modelling Error Associated with Cross-track Relative Motion of a J_2 Perturbed Satellite Relative to a Satellite on the Circular Reference Orbit with Corrected Rate and Time Varying Gradient of J_2 for a Sun Synchronous Orbit (r_{ref}=7000km, i=97.87^o and Initial Conditions x_0=0, y_0=0, $z_0 = 0$, $\dot{x}_0 = 0$, $\dot{y}_0 = 4.9931$m/s, $\dot{z}_0 = 0$) (b) Cross-track Relative Motion

The nodal drift term 'k' was included in the time averaged and time varying equations of motion (equations (4-46), (4-47) and (4-50) in section 4.3.4)). Figure 4-16 illustrates the same motion for a Sun synchronous orbit with all correction terms included. Compared to Figure 4-14, the along-track drift has been reduced and its direction changed, but the motion is not completely bounded even though the analytically derived bounded initial conditions were applied (listed in Table 4-2 - Nodal drift corrected model). Of particular note is the reduced cross-track motion of the perturbed satellite relative to the nodal drift and orbit rate corrected circular reference orbit.

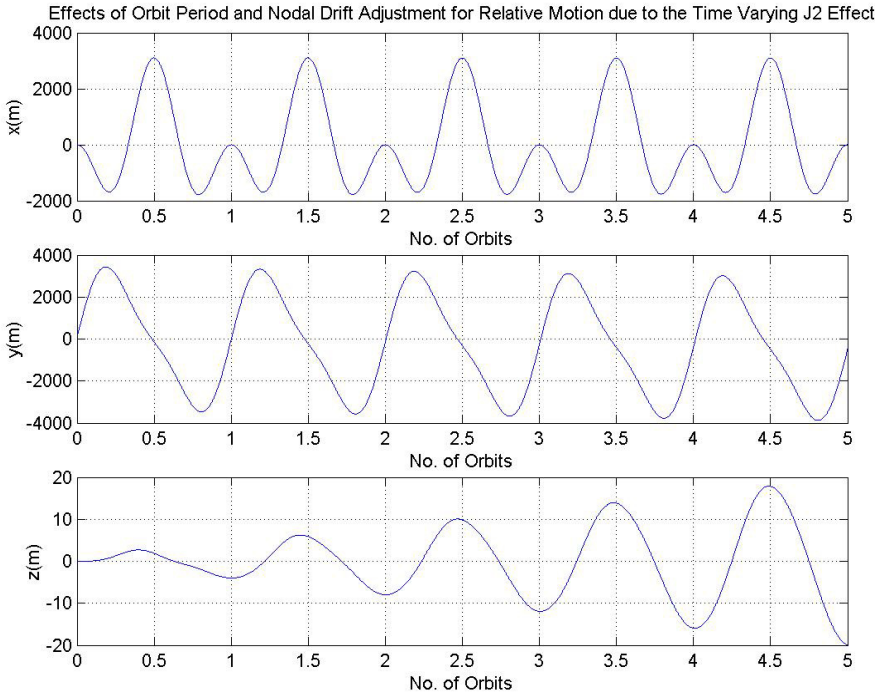

Figure 4-16: Relative Motion of a J_2 Perturbed Satellite Relative to a Satellite on the Circular Reference Orbit with Corrected Rate, Corrected Nodal Drift and Time Varying Gradient of J_2 for a Sun Synchronous Orbit (Relative Dynamics Model Output) (r_{ref}=7000km, i=97.87° and Initial Conditions x_0=0, y_0=0, z_0=0, $\dot{x}_0 = 0$, $\dot{y}_0 = 4.9929$m/s, $\dot{z}_0 = 0$)

Figure 4-17 superimposes the results of Figure 4-16 and the equivalent scenarios generated by both STK and the time averaged J_2 model. Both models capture relative motion fairly well, apart from the cross-track time averaged model. However, examination of the modelling error this time demonstrated that the initial conditions derived from the analytical model including both orbit rate and nodal drift correction are not suitable for creating near bounded motion in STK for model verification.

For the STK scenario, the new nodal drift corrected reference orbit was firstly generated in Matlab by integrating the Lagrange Planetary Equations subject to J_2 forces (equations (3-6) to (3-11), section 3.1.1.2, chapter 3). The resulting orbit elements were evaluated around the reference orbit, and in this case, converted to positions and velocities in the ECI frame. The data was written to an ephemeris file in STK and a reference orbit with nodal drift was visualised. This is illustrated for a Sun synchronous orbit in Figure 4-18.

A J_2 perturbed satellite was created in STK with the initial conditions derived from the analytical model, and relative positions in the Cartesian Hill frame were extracted using the reporting tool before being converted to curvilinear coordinates in Excel. The differences between the responses of both the time averaged and time varying Matlab models and the STK data were evaluated and these are displayed in Figure 4-19. This and an alternate verification procedure are summarised in section 4.6.3 (the alternative verification procedure involves conversion between the relative orbit elements and the Hill frame, and was found to produce similar results).

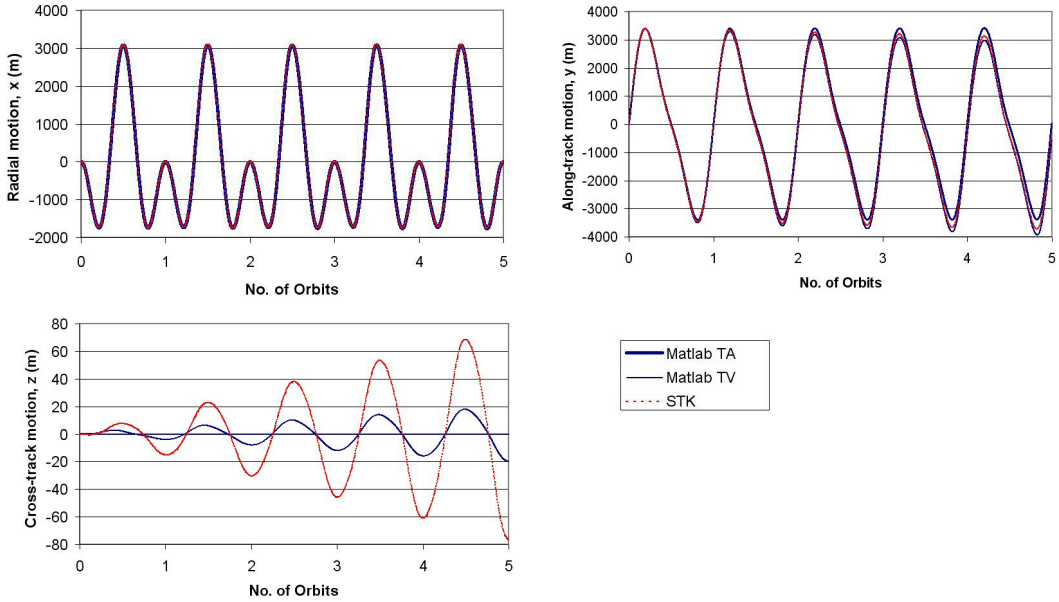

Figure 4-17: Relative Motion Predicted by STK, the Time Averaged J_2 Model, and the Time Varying J_2 Model for a Sun Synchronous Orbit (r_{ref}=7000km, i_{ref}=97.87^o and Initial Conditions x_0=0, y_0=0, z_0=0, $\dot{x}_0 = 0$, $\dot{y}_0 = 4.9929$m/s, $\dot{z}_0 = 0$)

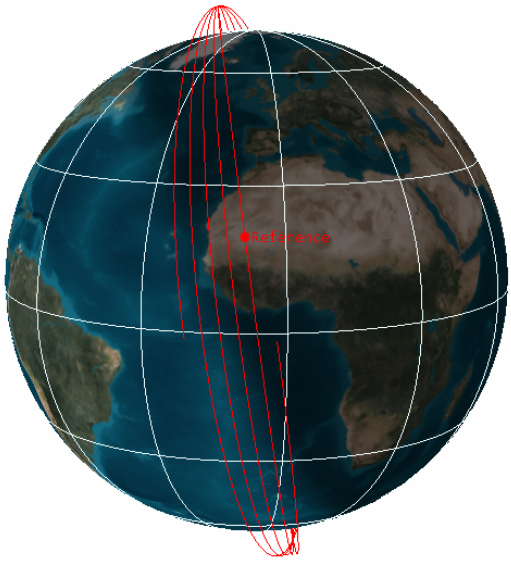

Figure 4-18: STK Scenario with Orbital Rate Corrected Circular Reference Orbit with Nodal Drift (r_{ref}=7000km, i_{ref}=97.87^o) Note: Nodal Drift is Exaggerated for Illustration

Figure 4-19 illustrates the modelling error corresponding to the scenario in Figure 4-17. In the radial direction a much greater error was obtained for the time varying model after 5 orbits and this is likely to be due to a mismatch in radial frequency, and may be overcome by a slight change in the initial conditions. However, for a third of the first orbit, the time varying modelling error is significantly smaller. The modelling error is not zero after every orbit for both the time averaged and time varying models, and therefore both models do not exactly capture the correct period in radial motion. The relative motion is a maximum of 3km, and the error over one orbit is approximately 10m for both models.

In the along-track direction neither model matched the STK results perfectly and the error is greater for the time averaged model over 5 orbits. The time averaged model experiences a large secular error (approximately 70m per orbit), and the time varying model error is more oscillatory although it returns close to zero every half orbit. Over the first third of an orbit, the time varying model is again more accurate, and the oscillatory motion is likely to be coupled to the more extreme radial error. Figure 4-17 clearly shows the closely matched along-track relative motion over the first orbit, and then the drift separates the plots slightly. The relative motion is also on a 3km scale with errors of 50-70m over one orbit.

For the initial condition where the perturbed satellite starts on the reference frame, the time averaged cross-track model has a zero response according to the cross-track analytical model given by equation (4-47). However, the time varying model captures the shape but not the magnitude of the cross-track motion. The modelling error arises due to a cross-track magnitude and frequency mismatch. The horizontal axis (orbit number) in each case corresponds to the reference orbit equator crossing, including the effects of nodal drift.

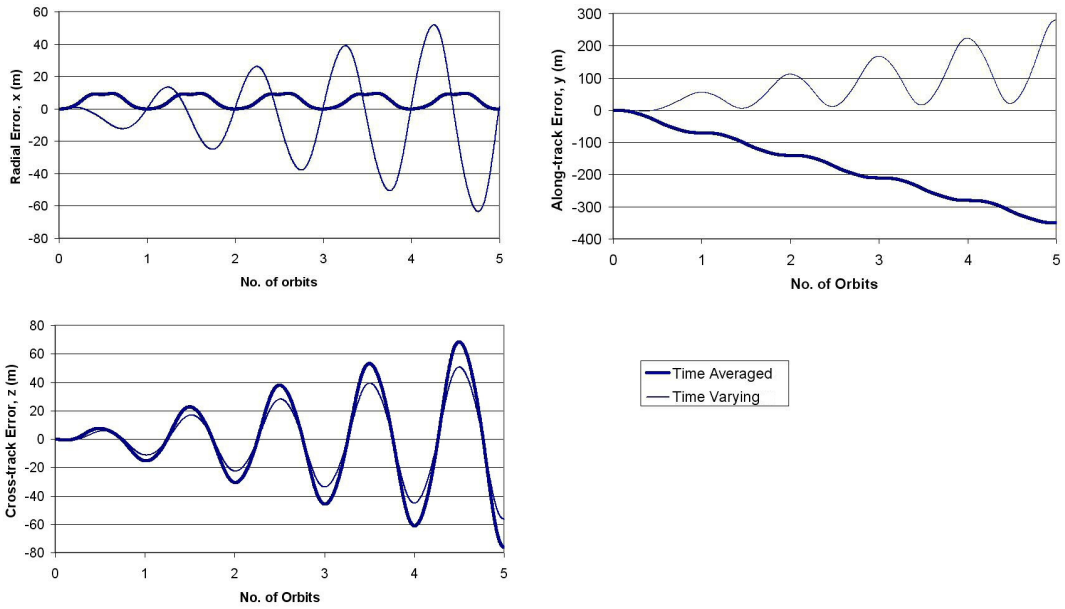

Figure 4-19: Modelling Error Associated with the Relative Motion of a J_2 Perturbed Satellite Relative to a Satellite on the Circular Reference Orbit with Corrected Rate, Corrected Nodal Drift and Time Averaged and Time Varying Gradient of J_2 for a Sun Synchronous Orbit (r_{ref}=7000km, i_{ref}=97.87^o and Initial Conditions x_0=0, y_0=0, z_0=0, $\dot{x}_0 = 0$, $\dot{y}_0 = 4.9929$m/s, $\dot{z}_0 = 0$)

A new cross-track model derived by Schweighart and Sedwick (2002) (equation (4-51)) was also implemented in Matlab. The model was evaluated for small initial offsets in cross-track position, and for a perturbed satellite initialised 50m from the reference orbit, the error increased to approximately 2.5m over 5 orbits. All in-plane parameters were initialised to zero as the motion was decoupled from the in-plane motion in the analytical model. However, this does not provide a meaningful comparison of relative behaviour when in-plane bounded conditions caused a 40km cross-track motion (Figure 4-15b). Generally, the modelling error increases with increased relative motion, and extrapolating these results would give errors of the same order of magnitude as the error associated with the time varying model (Figure 4-15a). Again, the significant coupling between the in-plane and cross-track motion is demonstrated in the STK scenario, but is still not captured by the time averaged model with new cross-track component.

Tuning the STK initial conditions to prevent drift was proposed as a better basis from which to compare the time averaged and time varying models. As the analytical initial conditions do not create bounded motion in STK, the targeter (introduced in section 4.6.6) was applied to derive fully coupled initial velocity impulses which would give close to bounded motion of a J_2 perturbed satellite relative to the new orbit rate and nodal drift corrected reference orbit (Figure 4-18). Clearly these would not produce bounded motion in the analytical model, and therefore would be expected to reduce its performance, although they may improve the time varying results.

Figure 4-20 illustrates the errors associated with modelling this STK-bounded scenario. In the radial direction, the time varying model captures the relative motion for longer during the first orbit. Subsequently the errors increase, again due to a mismatch in the period of relative motion. Secular drift is lower for the time varying model than the analytical model, however, surprisingly, the cross-track modelling error is greater. This may be due to coupling between in-plane and cross-track motion associated with the change in initial conditions. The cross-track modelling is more accurate for the time varying model during the first third of the first orbit. The errors are slightly greater for both models using the STK bounded initial conditions than those derived from the analytical model.

It is therefore not clear which model captures the numerical scenario more accurately for bounded relative motion in STK, and cumulatively there is little difference in performance between the J_2 models. It is here that model application should be considered. It is likely that a satellite formation would be controlled at certain intervals during an orbit, and therefore, although it is important to look at the longer term dynamics, it is also useful to just consider the model behaviour during the first quarter or third of an orbit. In this case, the time varying model captures the motion of a J_2 perturbed satellite relative to an orbital rate and nodal drift corrected reference orbit more accurately than the time averaged model.

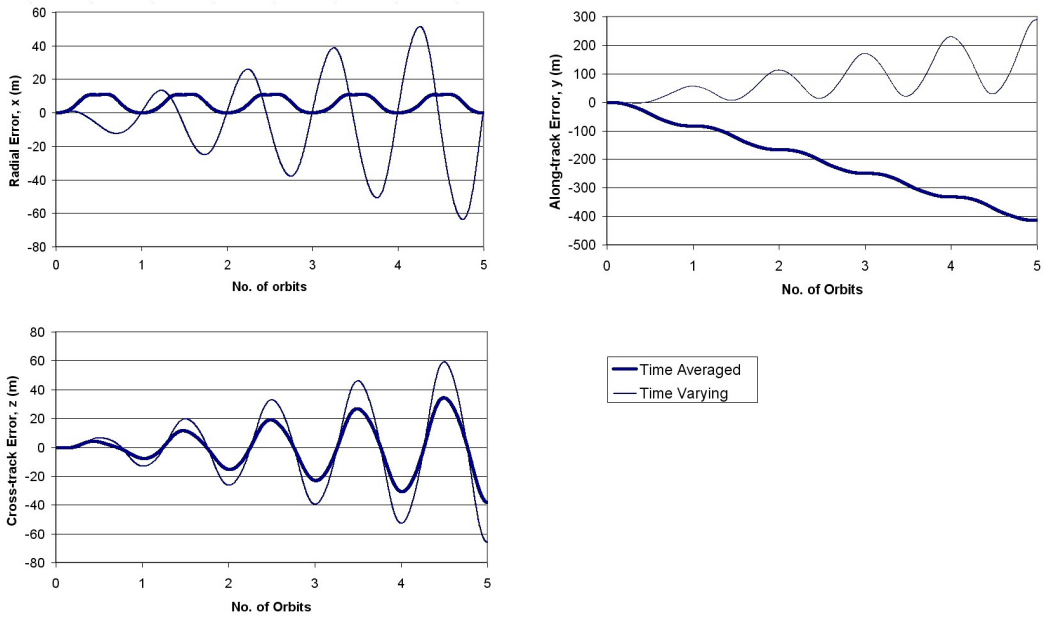

Figure 4-20: Modelling Error Associated with the Relative Motion of a J_2 Perturbed Satellite Relative to a Satellite on the Circular Reference Orbit with Corrected Rate, Corrected Nodal Drift and Time Averaged and Time Varying Gradient of J_2 for a Sun Synchronous Orbit (r_{ref}=7000km, i_{ref} =97.87° and Numerically Determined Initial Conditions x_0=0, y_0=0, z_0=0, $\dot{x}_0 = 0, \dot{y}_0 = 4.9889\text{m/s}, \dot{z}_0 = -1.9723\text{m/s}$)

Summary

For the case of one J_2 perturbed satellite moving with respect to a circular reference orbit, some modelling improvement is visible from the time varying model compared to the time averaged model for bounded motion in STK, and particularly for periods of one third of an orbit when analytical initial conditions are applied to both models and STK. These initial conditions ensure that the performance of the time averaged model is at its best, but clearly the relative motion predicted by STK is not captured. For very short periods of time, the time averaged model predicts relative motion sufficiently accurately, but the time varying model predicts relative motion for slightly longer. In practice, this might enable the frequency of impulsive formation control to be lowered while station keeping. However, the analytical initial conditions do not create sufficiently bounded motion in STK, and these were therefore tuned numerically while incorporating the important cross coupling between both in-plane and cross-track behaviour. However, with the new STK-bounded conditions, increased error resulted for both models.

Initial tests incorporating the orbital rate correction to the reference orbit but no nodal drift correction demonstrated the importance of the latter. Without this, the separation of the perturbed satellite from the reference orbit in the cross-track direction became very large, and cross coupling between axes caused an increasing along-track error. When nodal drift was included in the reference orbit, the cross-track relative motion between the reference orbit and perturbed satellite was significantly reduced, and consequently, along-track drift was also reduced. However, with nodal drift included in the reference orbit, the along-track drift error for the time averaged model changed direction.

One factor not taken into consideration is the precession in the argument of perigee due to the assumption of a circular orbit. It is proposed that this effect is investigated further. It should also be noted that although initial conditions for STK and the dynamics models were matched to high order (sixteen decimal places) any small differences would affect long term propagation results and modelling errors. A summary of the results and conclusions from this part of the model verification process is presented in section 4.7.4.

4.7.3 Equations of Relative Motion for Two Perturbed Satellites

In this section, the relative motion of two J_2 perturbed satellites is considered. The motion of each satellite relative to the circular reference orbit is implicit within the relative motion equations in either time averaged (invariant) or time varying form and remains important for the verification process in STK. The test cases considered in this section were introduced at the start of section 4.7. Graphical results for every test case have not been included due to the large amount of data available, and instead the main findings have been summarised. The analytical model based on the time averaged gradient of J_2 is verified in section 4.7.3.1, and the time varying dynamics model is verified in section 4.7.3.2.

4.7.3.1 Time Averaged J_2 Model

For the first four test cases listed in the introduction to section 4.7, bounded initial conditions are applied according to equations (4-95) and (4-96) for the time averaged model given by equations (4-101). The terms are defined in section 4.3.

$$\begin{aligned} &\Delta\ddot{x} - 2nc\Delta\dot{y} - \left(5c^2 - 2\right)n^2\Delta x = 0 \\ &\Delta\ddot{y} + 2nc\Delta\dot{x} = 0 \\ &\Delta\ddot{z} + q^2\Delta z = 2lq\cos\left(qt + \varphi\right) \end{aligned} \qquad (4\text{-}101)$$

General Test Case ($i_{ref}=35^o$)

The following graphs (Figure 4-21, Figure 4-22 and Figure 4-23) illustrate the predicted relative motion and the modelling error associated with offsets in the radial (x), along-track (y) and cross-track (z) respectively in the General test case described earlier in the section.

The zero drift and offset in-plane initial conditions in the Matlab model for two perturbed satellites cause them to orbit around each other (Figure 4-21a). The model compares well to the relative motion predicted by STK, and captures the period of the motion. In Figure 4-21 the small radial error is due to the time averaging of the gradient of J_2, which does not capture these 13cm periodic variations. The error in the along-track direction increases by approximately 65cm per orbit, and this is due to the initial along-track velocity conditions, calculated from the derived formulae in the analytical model. The cross-track motion was only 3cm, but the model predicted zero motion due to the decoupling of the in-plane and cross-track equations.

For an initial along-track offset, the radial error is periodic with a maximum magnitude of just over 1cm, and the along-track error is just over 5cm (Figure 4-22). The cross-track motion is not captured, but the maximum magnitude of the motion is approximately 4.2cm. A slight drift is still visible from the along-track error graph of 1mm per orbit.

In both cases, the nature of the radial and along-track errors could be investigated further by matching exactly the periods of the circular reference orbit and perturbed satellite orbits using numerical methods in STK. It has already been shown that the conditions that create bounded motion for the analytical model are not the same as those which will create motion even closer to bounded in STK (section 4.7.2). However, any deviation from the analytically derived initial conditions will prevent bounded motion in the analytical model, although this may improve results for the time varying model (this was investigated in section 4.7.3.2).

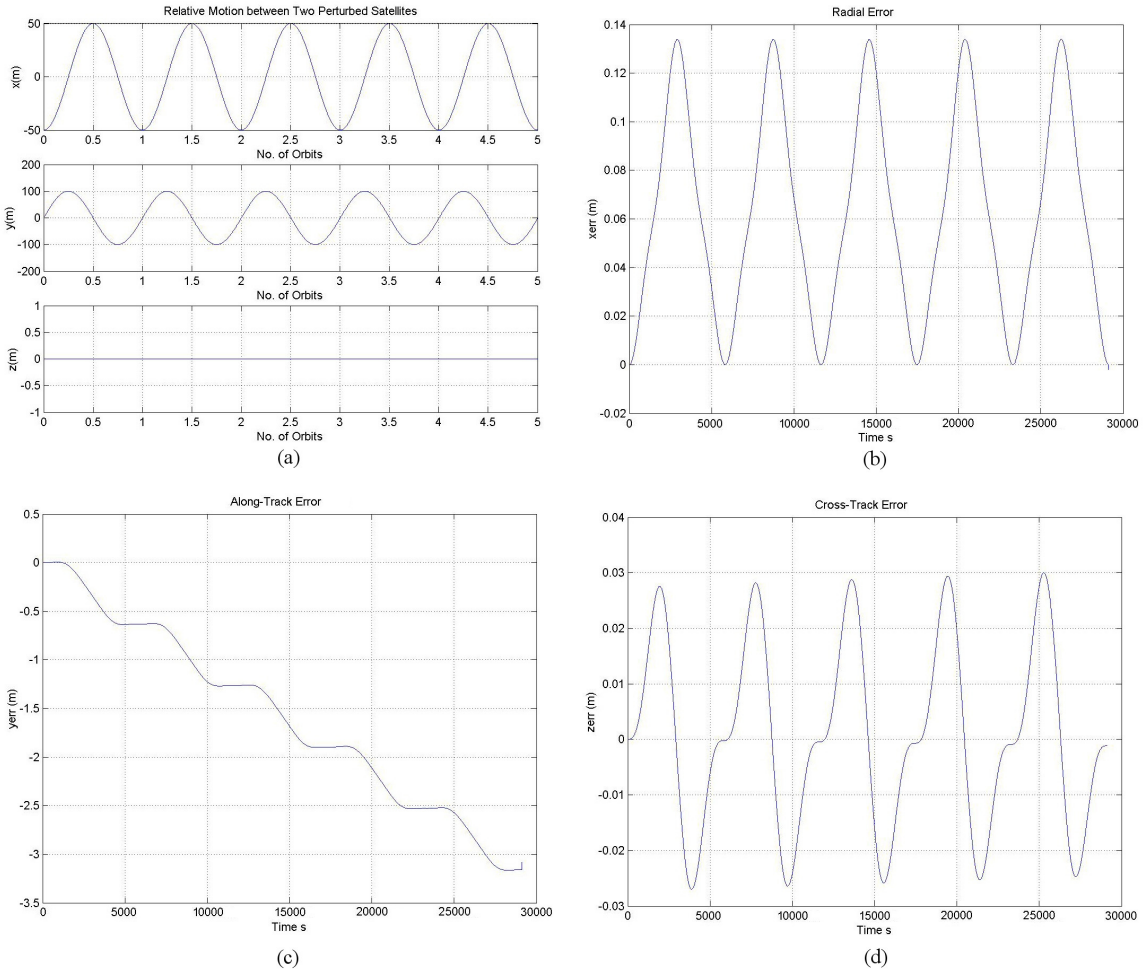

Figure 4-21: Time Averaged Relative Motion and Modelling Error for Initial Radial Offset – General Test Case with Initial Conditions $\Delta x_0 = -50\text{m}$, $\Delta y_0 = 0$, $\Delta z_0 = 0, \Delta \dot{x}_0 = 0$, $\Delta \dot{y}_0 = 0.10784\text{m/s}$, $\Delta \dot{z}_0 = 0$ (a) Relative Motion (b) Radial Error (c) Along-Track Error (d) Cross-Track Error

The modelling error in Figure 4-22 can be directly compared to Figure 4-10, which describes the modelling error between the Hill equations and equivalent STK scenario for an initial along-track offset. In the presence of the J_2 perturbation, the analytical J_2 model captures the radial and along-track motion much more accurately.

For the cross-track model (derived from the geometric model, appendix D.2), the initial conditions must be non-zero in order to generate a non-zero response. The values of Δz_0 and $\Delta \dot{z}_0$ enable the relative inclination of the orbit planes to be calculated without the knowledge of the reference orbit inclination, i_{ref}. However, i_{ref} must still be selected and input into the model so that other terms can be calculated. It is therefore still necessary to retain a physical insight into the initial position of the satellites relative to the reference orbit, rather than just their relative cross-track position. In this implementation of the model, one of the perturbed satellites is initialised at the reference orbit inclination, although this does not have to be the case, and instead the reference can be considered the 'virtual' centre of a constellation.

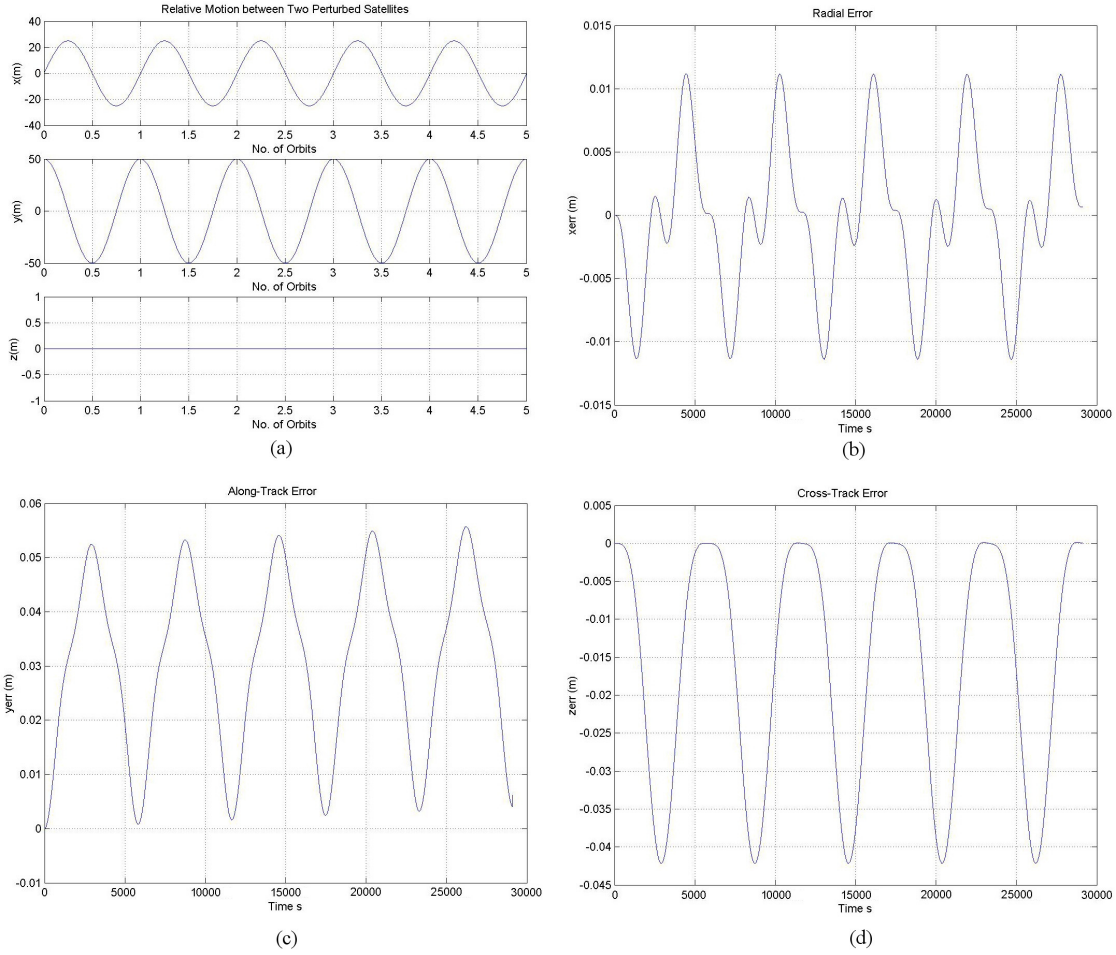

Figure 4-22: Time Averaged Relative Motion and Modelling Error for Initial Along-Track Offset – General Test Case with Initial Conditions Δx_0=0, Δy_0=50m, Δz_0=0, $\Delta \dot{x}_0 = 0.02692$m/s , $\Delta \dot{y}_0 = 0$, $\Delta \dot{z}_0 = 0$ (a) Relative Motion (b) Radial Error (c) Along-Track Error (d) Cross-Track Error

Figure 4-23a illustrates the model response for two perturbed satellites with an initial cross-track offset and velocity. The in-plane responses remain constant at zero as all the in-plane initial conditions are zero and the in-plane and cross-track equations are uncoupled. An equivalent scenario was implemented in STK using the true anomaly and longitude of ascending node to effect the initial 50m offset (equations (4-90)). Both of the satellites required an additional y-velocity to be applied as an initial impulse so that their resultant angular velocities were equal to that of the time period corrected circular reference orbit in the presence of J_2. An initial z-velocity of 0.1m/s was applied as a cross-track impulse.

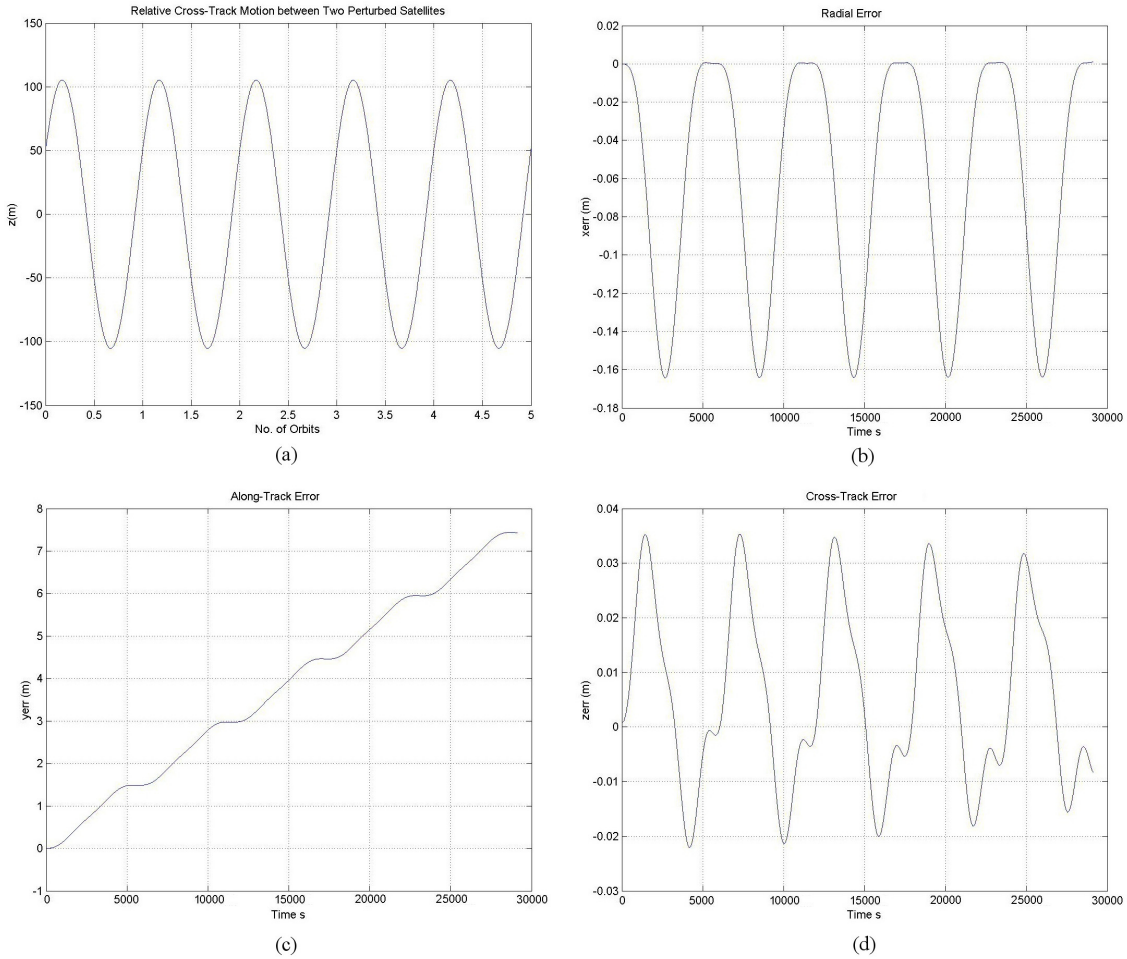

Figure 4-23: Cross-Track Geometry Model Relative Motion and Error for Initial Cross-Track Offset – General Test Case with Initial Conditions $i_{ref} = i_{sat2} = 35^o$, $\Delta z_0 = 50\text{m}$, $\Delta \dot{z}_0 = 0.1\text{m/s}$, $\Omega = -0.0007135^o, \theta = 0.0005845^o$, (a) Relative Cross Track Motion (b) Radial Error (c) Along-Track Error (d) Cross-Track Error

Figure 4-23 (b and c) illustrates the radial and along-track motion predicted by STK (since the Matlab model predicts zero relative motion). The final graph (d) shows that the cross-track model captures the ±100m out of plane relative motion with a maximum error of approximately 3.5cm. In this case the error actually decreases during the 5 orbits.

The initial z-velocity will change the velocity vector just as much as an initial velocity in x or y. The cross-track motion is coupled to the radial and along-track motion although the analytical model of Schweighart and Sedwick (2002) does not capture this. In fact, the same observations made regarding the coupling of in-plane and cross-track motion for the case of the single perturbed satellite moving with respect to the reference also apply here. Effectively, by adding an initial cross-track velocity to the model, the 'zero drift and offset' conditions cannot be applied as before and the STK results show that the satellites will drift apart in the along-track direction. This drift can be compensated for by applying additional y-velocity impulses as initial conditions to the satellites in STK. It was found that for cross-track velocities of the order of 0.1m/s, as in this test case, there was a negligible effect on the perturbed orbit period, and no y-velocity adjustments were actually necessary. The correction parameter is calculated in the Matlab model and the software user can choose whether to include this value as an initial condition in STK, depending on the size of the initial z-velocity.

Polar Orbit

This test case ($i_{ref}=90^o$) revealed that singularities arise in the cross-track model and it is unable to compute the relative motion in its current form. The cross-track initial conditions were therefore set to zero just to enable the in-plane part of the model to function.

The bounded motion Polar orbit scenarios in STK for in-plane offsets demonstrated that the relative cross-track motion was negligibly small (μm), as predicted by the J_2 equations. These indicate that there should be zero cross-track motion for a polar orbit cluster relative to a 90^o reference orbit, and for satellites with small separation about a polar orbit, the cross-track motion would be extremely small. Setting the model response to zero in this case is therefore within the limits of model accuracy. However, the modelling errors both along-track and radially were both (three times) greater than for the General test case ($i_{ref}=35_o$) for the same along-track separation. Very similar results were obtained for the near-polar Sun synchronous orbit.

Equatorial Orbit

As for the polar orbit, the cross-track model is unable to compute relative motion for an equatorial reference orbit ($i_{ref}=0^o$). This is because the separation in longitude of ascending node between the satellites cannot be defined (refer to appendix D.2 for the cross-track model derivation).

The decoupled in-plane model was given bounded initial conditions for the same range of offsets as the other models and the resulting relative motion was found to be the most accurately captured when compared to STK (Figure 4-24). For example, for an along-track separation of 50m, the radial error (on a motion of ±25m) was 0.3mm, the along-track error was secular at 1mm per orbit, and the cross-track error was a few μm (the actual motion predicted by STK for this scenario). In this scenario, the satellites had to be given the greatest initial along-track ΔV in addition to the prescribed bounded motion initial conditions.

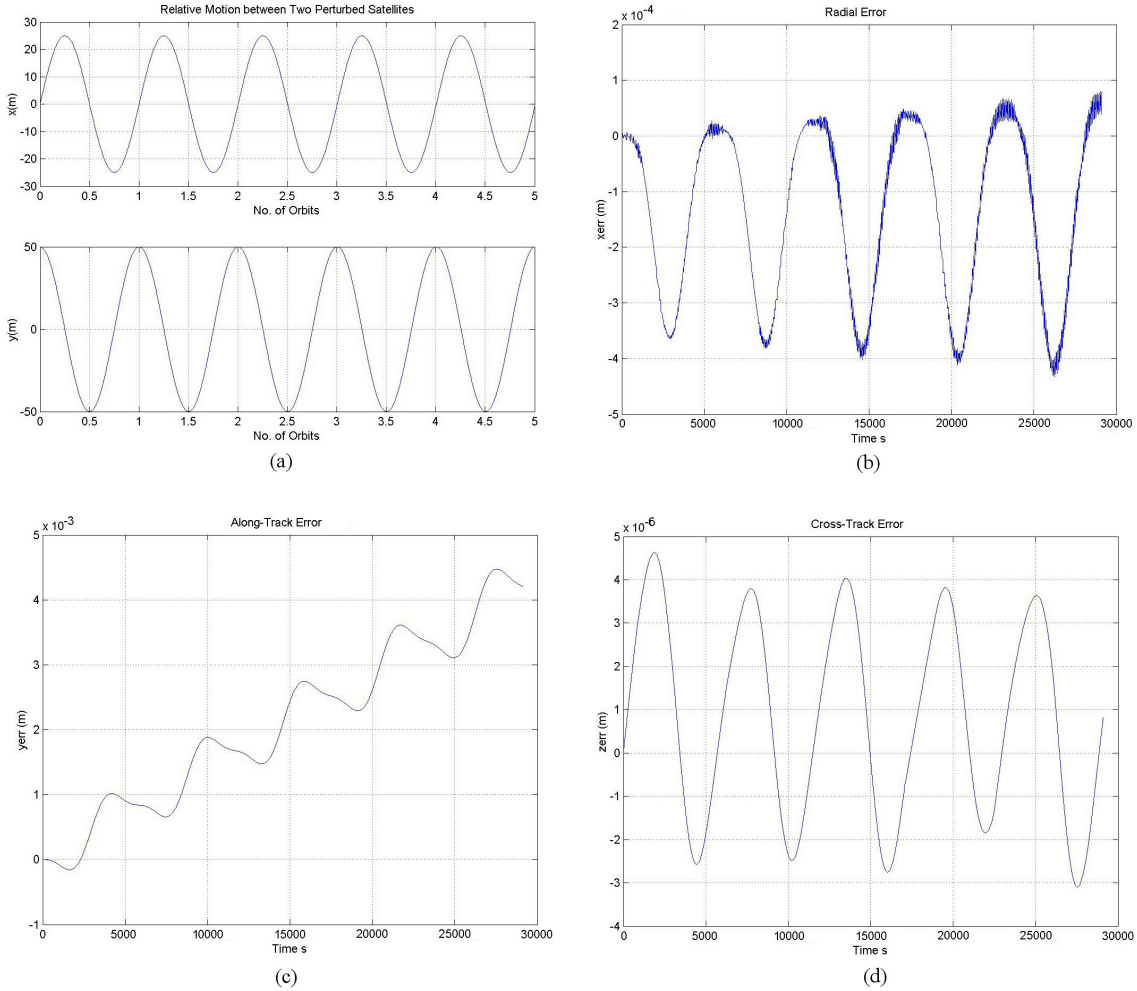

Figure 4-24: Time Averaged Relative Motion and Modelling Error for Initial Along-Track Offset – Equatorial Orbit Test Case with Initial Conditions Δx_0=0, Δy_0=50m, Δz_0=0, $\Delta \dot{x}_0 = 0.02689$m/s, $\Delta \dot{y}_0 = 0$, $\Delta \dot{z}_0 = 0$ (a) Relative Motion (b) Radial Error (c) Along-Track Error (d) Cross-Track Error

Circular Formation

This formation was generated using the new formulae derived in section 4.4 (equations (4-68)). Figure 4-25a and Figure 4-25b illustrate the relative orbits of the time averaged J_2 model and those generated by STK for the same analytically derived initial conditions. Of course, the STK relative orbits will drift over time as a circular formation cannot naturally occur in the presence of the J_2 perturbation. To create the bounded circular orbit in the analytical model, a cross-track rate error must be introduced. It is proposed, however, that this circular orbit will be less costly to maintain than that derived from the solutions to the Hill equations in the J_2 perturbed environment. Figure 4-26 illustrates the relative motion and modelling error associated with the circular relative orbit. For a 100m radial motion, the periodic error is 40cm in amplitude. The cross-track error is steadily increasing due to the forced mismatch in the frequency of the model and STK. The introduction of the cross-track motion to create this formation in STK contributes to increasing the along-track drift. For the same scenario, without cross-track motion (Figure 4-21c), the along-track drift was approximately 65cm per orbit. This has increased to 1.88m per orbit for the circular formation.

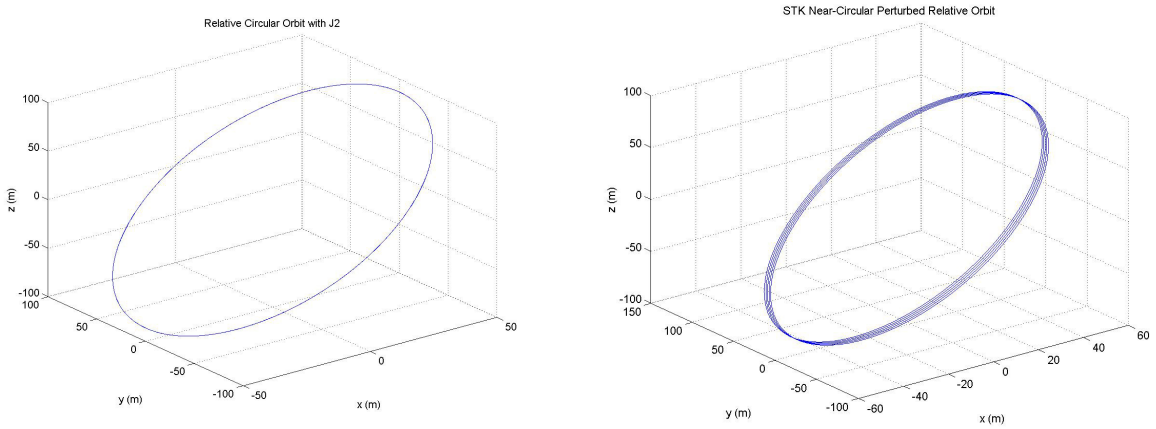

(a) (b)

Figure 4-25: Circular Formation for Two J_2 Perturbed Satellites over 5 Sun Synchronous Orbits with Initial Conditions Δx_0=-50m, Δy_0=0, Δz_0=-86.53m, $\Delta\dot{x}_0 = 0$, $\Delta\dot{y}_0 = 0.1078$m/s $\Delta\dot{z}_0 = 0$ (r_{ref}=7000km,i_{ref}=97.87^o) (a) Time Averaged J_2 Model with Modified Cross-Track Frequency (b) STK

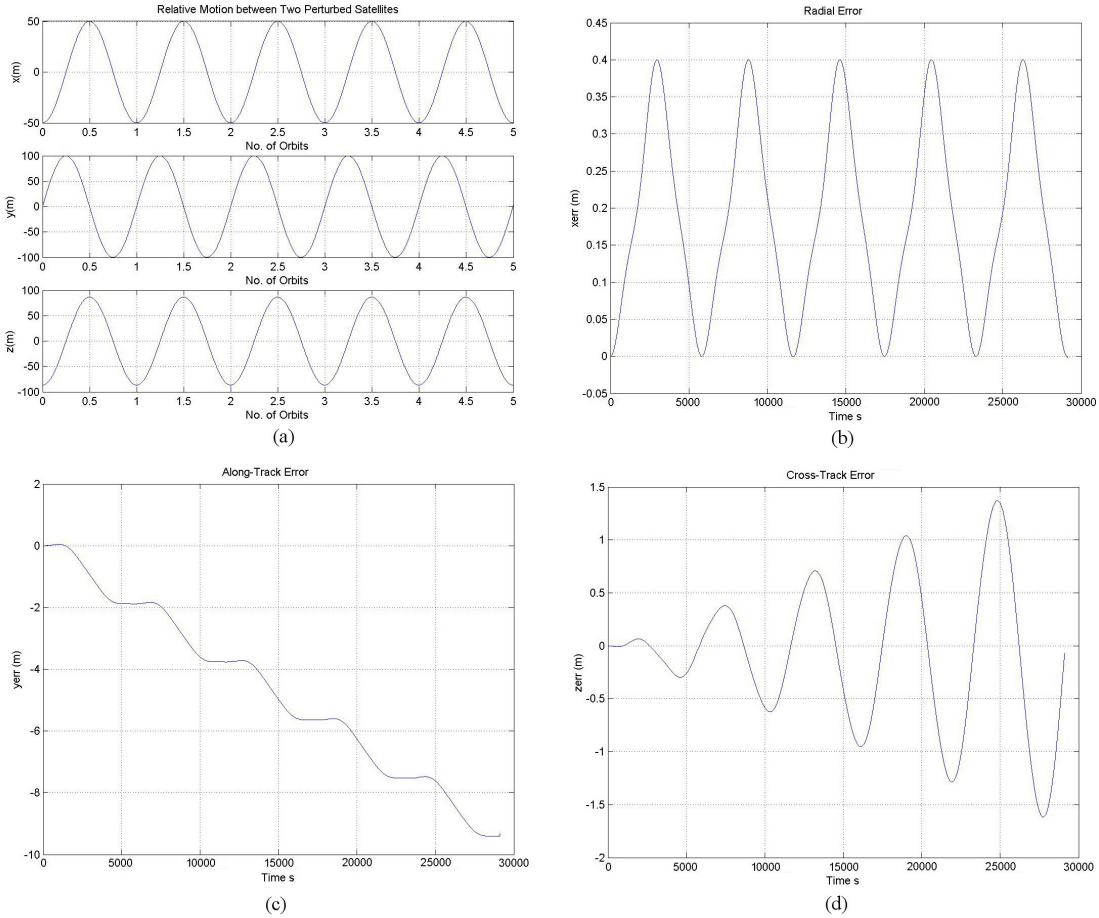

Figure 4-26: Time Averaged Relative Motion and Modelling Error for the Sun Synchronous Circular Formation over 5 Orbits with Initial Conditions Δx_0=-50m, Δy_0=0, Δz_0=-86.53m, $\Delta\dot{x}_0 = 0$, $\Delta\dot{y}_0 = 0.1078$m/s $\Delta\dot{z}_0 = 0$ (r_{ref}=7000km, i_{ref}=97.87^o) (a) Relative Motion (b) Radial Error (c) Along-Track Error (d) Cross-Track Error

If the analytical model retains the more accurate cross-track model and therefore replicates the natural motion to create an elliptical formation (and not a circular formation), for this test case the radial and along-track errors remain almost exactly the same, but the much reduced cross-track error fluctuates between 0 and 5cm for the 86m amplitude motion.

J_2 Invariant Relative Orbit

The J_2 invariant relative orbit was introduced in section 3.1.3.2 and a test case was selected from recent literature for comparison with the time averaged J_2 relative motion model. Since the concept has arisen from the relative orbit elements approach to LEO dynamics modelling, the initial conditions were defined in this form, and converted to the Hill frame either by using the relations described by equations (3-13), or through parameter conversions implemented within STK. The mean anomaly was converted to true anomaly using Kepler's equation. Table 4-3 summarises the initial conditions supplied to STK and the relative motion model.

Reference Orbit Elements	**Relative Orbit Elements**	**Hill Parameters**
$a = 7555\text{km}$	$\delta a = -0.00192995\text{km}$	$\Delta x_0 = 2008.481\text{m}$
$e = 0.05$	$\delta e = 0.000576727$	$\Delta y_0 = 0.021149\text{m}$
$i = 48^o$	$\delta i = 0.006^o$	$\Delta z_0 = 598.8061\text{m}$
$\omega = 10^o$	$\delta\omega = 0$	$\Delta \dot{x}_0 = 3.549801\text{ms}^{-1}$
$\Omega = 0^o$	$\delta\Omega = 0$	$\Delta \dot{y}_0 = -3.87772\text{ms}^{-1}$
$M = 120^o$	$\delta M = 0$	$\Delta \dot{z}_0 = -0.47580\text{ms}^{-}$
$\theta = 122.4183^o$	$\delta\theta = 0$	

Table 4-3: Initial Conditions for the J_2 Invariant Orbit Test Case (Reference Orbit Elements and Relative Orbit Elements taken from Schaub, Vadali, Junkins and Alfriend (1999))

Figure 4-27 illustrates the J_2 invariant relative orbit defined by the parameters in Table 4-3. The near-bounded conditions achieved in STK (Figure 4-27a) were applied to the model, but since these were not the same as the analytically derived 'bounded' initial conditions, drift is visible in the time averaged model response over 5 orbits (Figure 4-27b). The errors illustrated in figures (c), (d), and (e) demonstrate that the model is unsuitable for mildly eccentric orbits with large satellite separations.

An alternative set of initial relative velocities, derived from the analytical model for bounded motion, rather than from the orbit elements were also compared to the STK scenario and the errors were found to increase further.

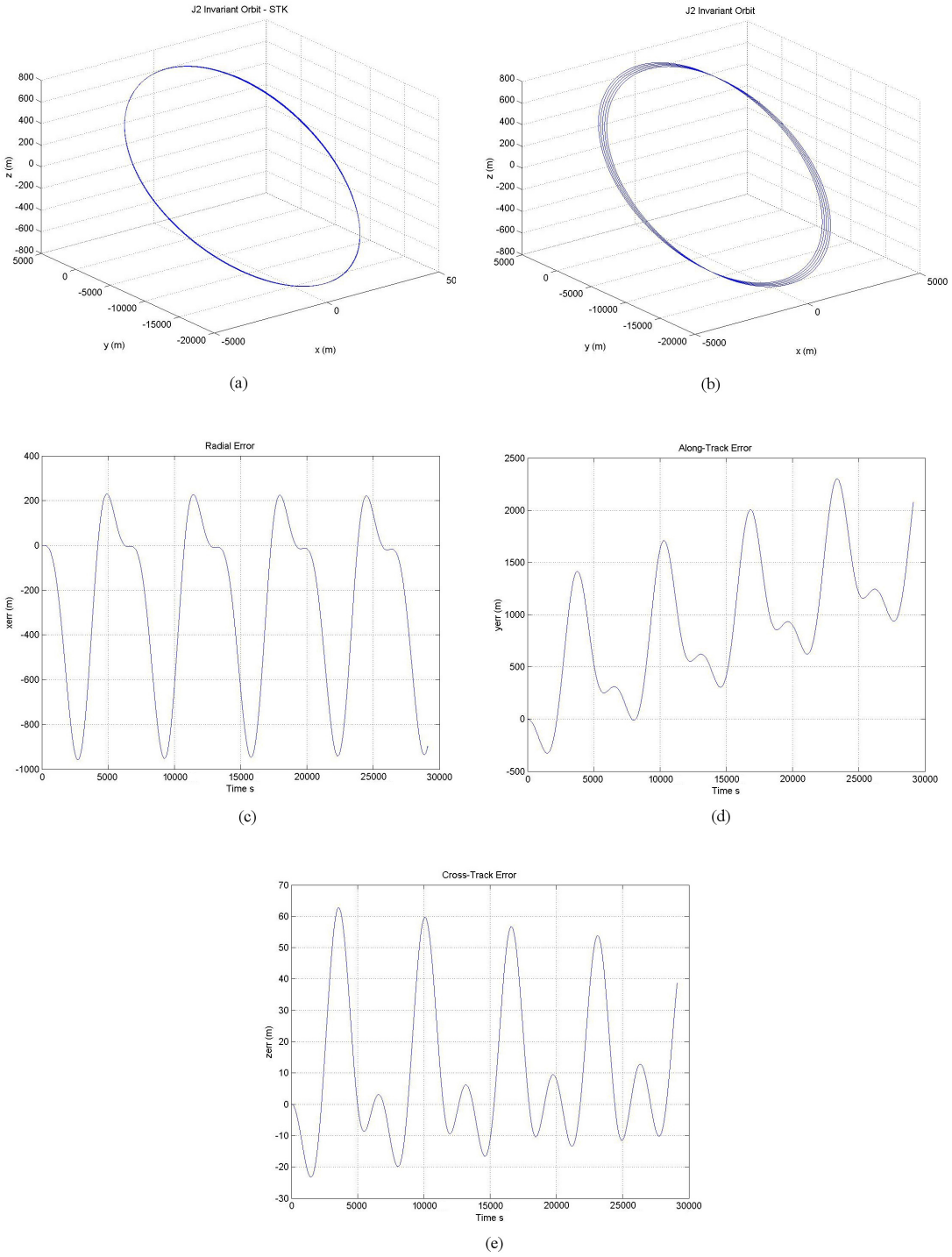

Figure 4-27: STK Relative Motion, Time Averaged Model Relative Motion and Modelling Error for the J_2 Invariant Orbit defined in Table 7-3 (a) STK Relative Motion (b) Time Averaged Model Relative Motion (c) Radial Error (d) Along-Track Error (e) Cross-Track Error

MUSTANG Leader-Follower

For this leader-follower example, the time averaged model reduces to the Hill equations (Figure 4-28a). The satellites are separated in the along-track direction, and this time, they are not provided with additional impulses to create a 'zero drift and offset' formation. This leads the STK orbit propagator to predict the relative motion illustrated in Figure 4-28b. Clearly, the time averaged model does not capture the relative motion at all, highlighting the specific nature of the formations which the analytical model can represent.

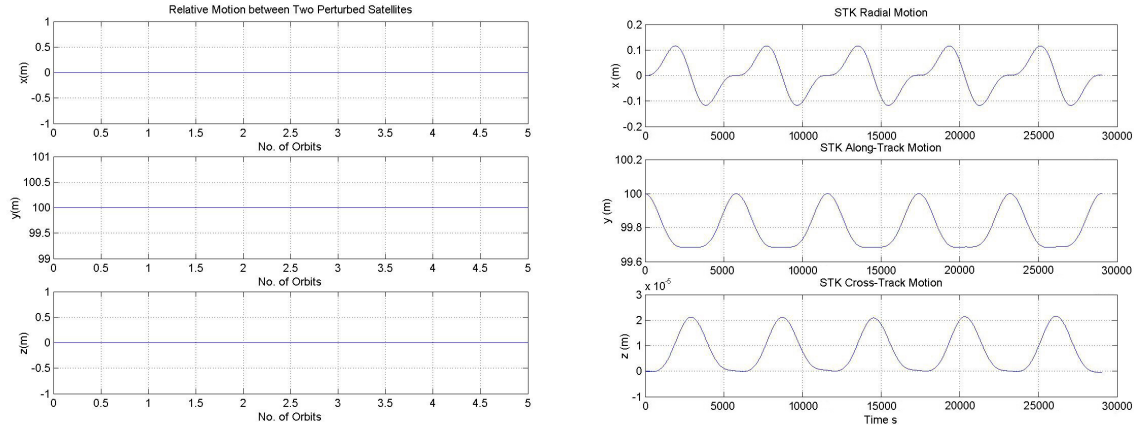

(a) (b)

Figure 4-28: Relative Motion of Two J2 Perturbed Satellites in Leader-Follower Formation with 100m Initial Along-Track Separation for i=85o, radius=6978.1km over 5 Orbits (a) Time Averaged Model (b) STK

4.7.3.2 Time Varying J_2 Model

In this section, almost all the model verification was performed using the initial conditions derived from the time averaged model since these achieved better performance in the test cases for one J_2 perturbed satellite considered in section 4.7.2. The equations derived in section 4.3.6 (equations (4-58) to (4-60)) were implemented in Matlab and solved numerically for comparison with the STK fully numerical solution.

General Test Case ($i_{ref}=35^o$)

The same STK scenarios for the General test case were simulated for two J_2 perturbed satellites with an initial x, y and z offset. In each case the relative motion appeared bounded in both STK and the time varying model output. However, evaluation of the modelling errors revealed a poorer performance than that achieved by the time averaged model in section 4.7.3.1. The following examples include the relative motion predicted by the time varying model, and the error between this and STK for initial x and y offsets.

For an initial radial offset, Figure 4-29a appears to show that bounded relative in-plane motion is captured by the time varying model. For the scale of the motion (50 to 100m), the errors only increase to 70cm in x over 5 orbits due to a frequency mismatch in the radial motion, and along-track a secular error grows at the rate of 75cm per orbit.

Although these results are worse than those achieved by the time averaged model in Figure 4-21 (the equivalent test case), relative motion is still well approximated by the model. That the time varying model is less accurate is unexpected and reasons for this are investigated in the following subsections.

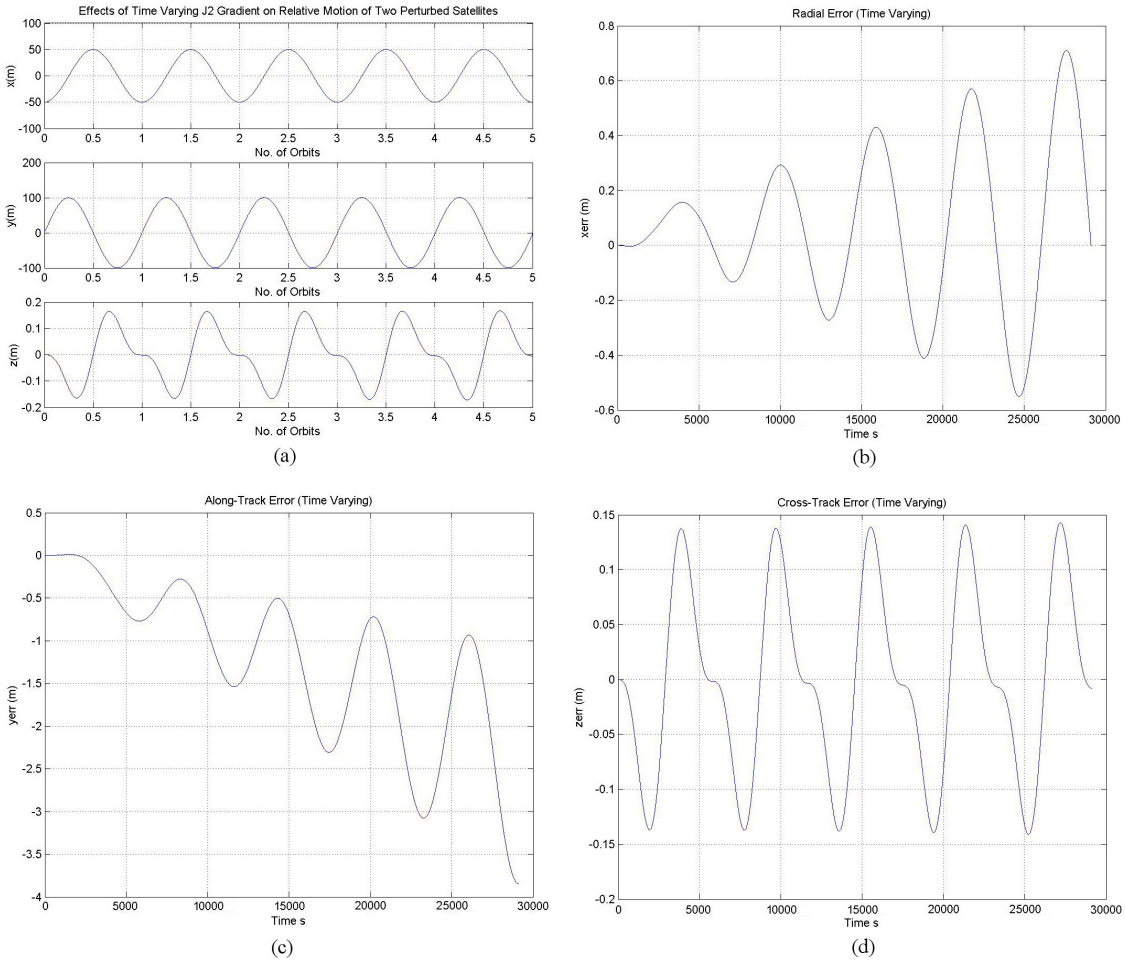

Figure 4-29: Time Varying Modelling Error for Initial Radial Offset – General Test Case with Initial Conditions Δx_0=-50m, Δy_0=0m, Δz_0=0, $\Delta \dot{x}_0 = 0$, $\Delta \dot{y}_0 = 0.10784$m/s, $\Delta \dot{z}_0 = 0$ (a) Relative Motion Predicted by Time Varying Model (b) Radial Error (c) Along-Track Error (d) Cross-Track Error over 5 Orbits

Figure 4-30a illustrates the bounded relative motion predicted by the time varying model due to an initial along-track offset of 50m. Again, the model output appears to capture the motion, but the errors between this and STK remain larger than those for the time averaged model (Figure 4-22). However, if the time varying results are compared to those of the equivalent scenario for the Hill equations (Figure 4-10) (section 4.7.1), the in-plane errors from the time varying model over five orbits are still significantly smaller. The cross track motion is not captured at all by the Hill equations, but the shape of the motion is captured by the time varying model. However, because the motion is so small, the zero response approximation to the motion is actually closer to the STK results than the time varying model response.

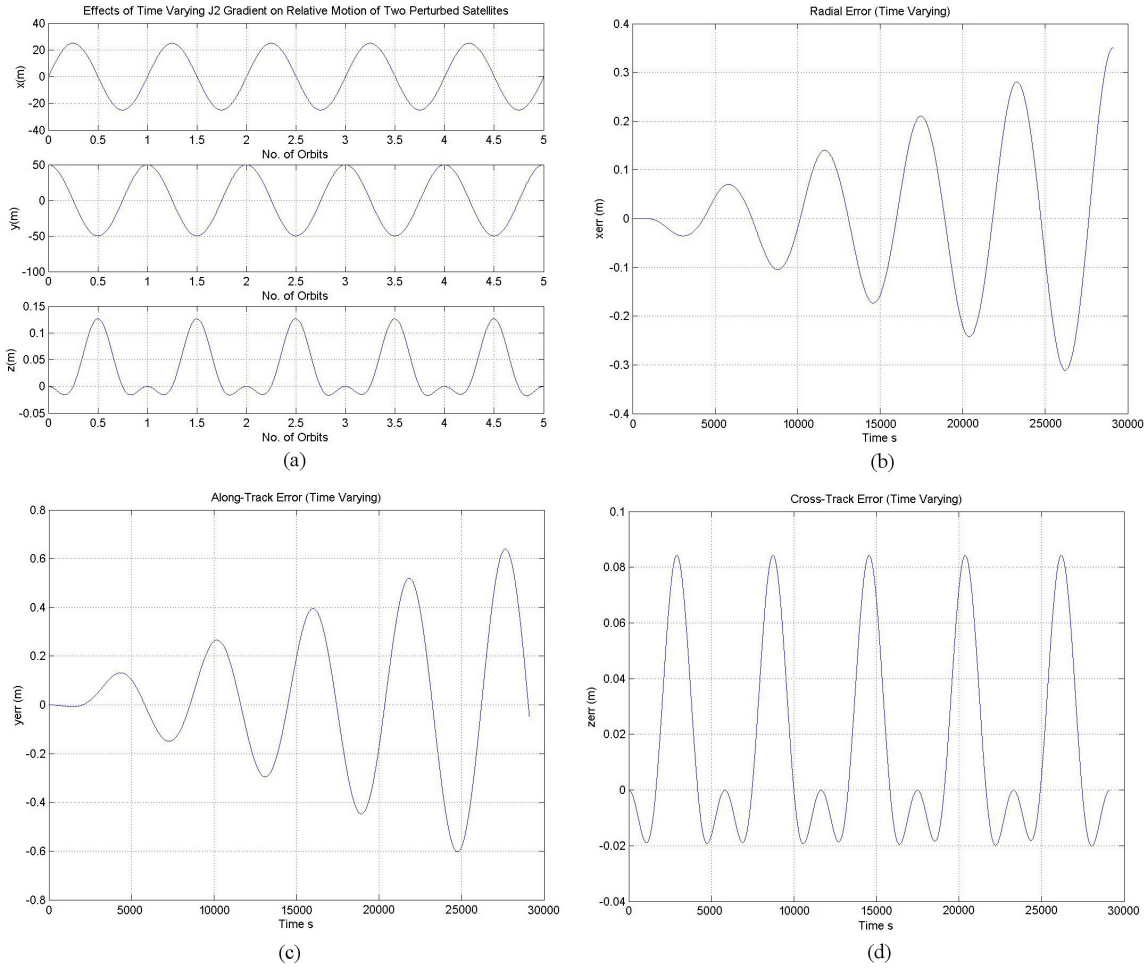

Figure 4-30: Time Varying Modelling Error for Initial Along-Track Offset – General Test Case with Initial Conditions Δx_0=0, Δy_0=50m, Δz_0=0, $\Delta \dot{x}_0 = 0.02692$m/s, $\Delta \dot{y}_0 = 0$, $\Delta \dot{z}_0 = 0$ (a) Relative Motion Predicted by Time Varying Model (b) Radial Error (c) Along-Track Error (d) Cross-Track Error over 5 Orbits

Polar Orbit

Unlike the time averaged model, the time varying model does not experience implementation problems in polar orbits. This is due to the change in cross-track modelling approach. The time varying model appears to produce a good approximation to bounded motion for this test case (i_{ref}=90^o). However, even with the negligible cross-track motion, the in-plane modelling errors exhibited growth to 1 or 2 metres over 5 orbits radially and along-track respectively for relative motion over 100m. Errors at the cm level were achieved for the time averaged model. Again, similar results were obtained for the near-polar Sun synchronous orbit.

Equatorial Orbit

In this case, the time varying cross-track model also does not experience implementation problems. The time varying gradient of J_2 simplifies to the time averaged case, and the same results are achieved (Figure 4-24).

Circular Formation

Although errors of a similar magnitude to those observed for the General test case were expected, this example has been included here for the time varying model as it is implemented as one of the test cases for formation control in chapter 5.

The circular formation initial conditions (equations (4-68)) were again applied to the time varying model to investigate its behaviour, although only a near-circular formation could be achieved (as for STK). The time varying model cross-track equation cannot be decoupled from the in-plane equations, and therefore the frequency cannot be modified. The circular relative orbits obtained from the time varying model are illustrated below (Figure 4-31a). The errors between STK and the time varying model motion are also illustrated, and again are greater in the radial and along-track directions than those for the time averaged model with cross-track frequency modification (Figure 4-25 and Figure 4-26). Of course, the cross-track errors are reduced for the time varying model as the cross-track frequency modification is not applied.

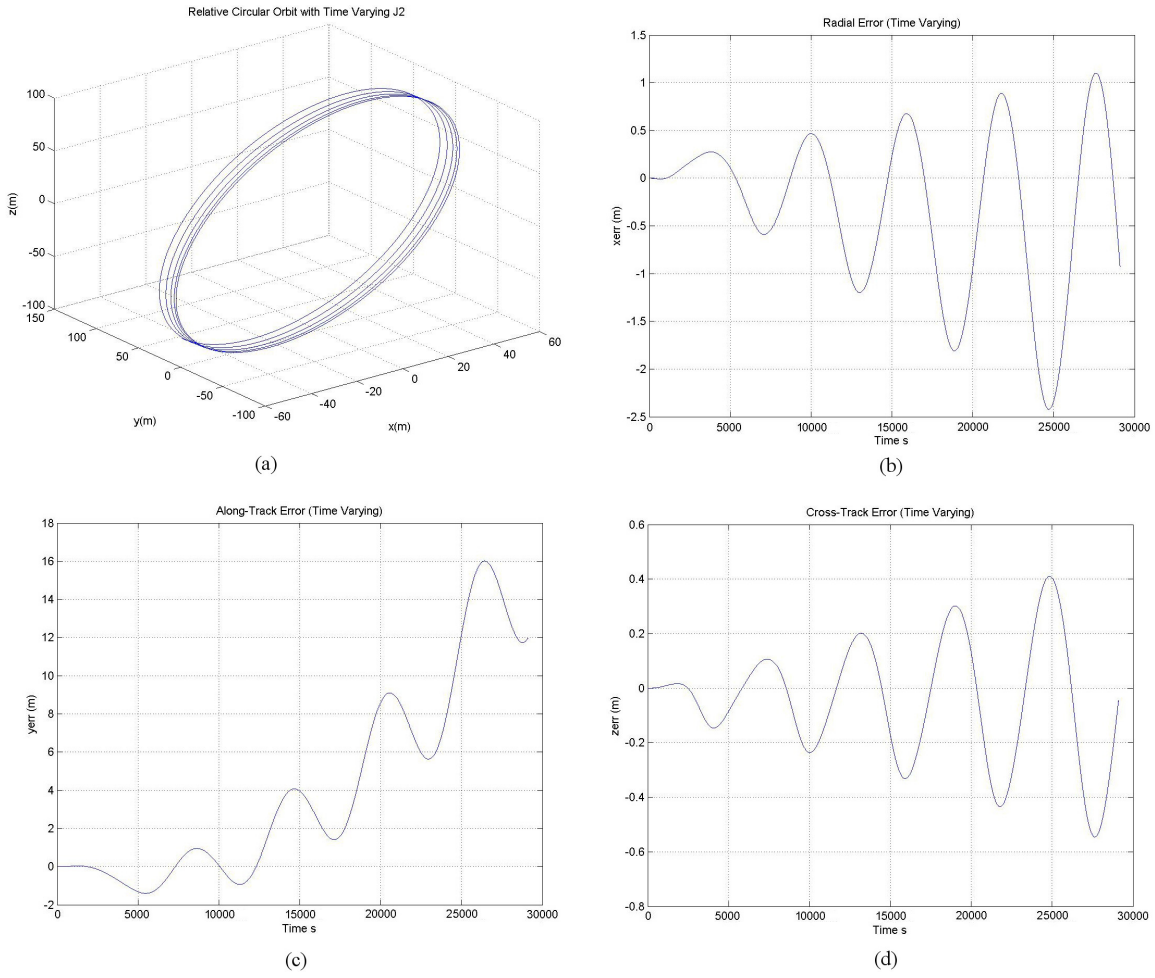

Figure 4-31: Near-Circular Formation Relative Motion and Modelling Error for the Time Varying J_2 Model over 5 Sun Synchronous Orbits with Initial Conditions Δx_0=-50m, Δy_0=0, Δz_0=-86.53m, $\Delta \dot{x}_0 = 0$, $\Delta \dot{y}_0 = 0.1078$m/s $\Delta \dot{z}_0 = 0$ (r_{ref}=7000km, i_{ref}=97.87°) (a) Time Varying J_2 Model (b) Radial Error (c) Along-Track Error (d) Cross-Track Error

Due to the unexpected lower performance of the time varying model compared to the time averaged model observed in the test case results so far, further test cases were implemented to reduce the number of variables in the model. It was anticipated that allowing the gradient of J_2 terms to remain time varying in the model would improve the fidelity, and enable the model to be applied to additional scenarios beyond those for zero drift and offset. Further analysis of the role of different terms in the equations of motion was performed (this is discussed further below and in section 4.7.4).

Critical Inclination Orbit

The time varying model takes into account the effect of the J_2 perturbation on the orbital rate and the drift in longitude of ascending node of the reference orbit, but because a circular reference orbit is assumed, the rotation of the line of apsides has not been considered. As a potential source of error, a critical inclination test case was evaluated to set this rotation rate to zero. Even though this does not affect the time varying model, the secular terms intrinsic to the STK scenario should be reduced. The precession of the line of apsides is described by equation (4-27) (section 4.2.2.2). By setting this to zero, the critical inclination to prescribe a frozen orbit is either 63.43^o or 116.57^o. The prograde orbit was selected for this test case.

Errors of a similar magnitude to those shown in Figure 4-29 and Figure 4-30 were achieved, and no further modelling improvement was visible by using a critical inclination.

MUSTANG Leader-Follower

This scenario was implemented in the time averaged model in section 4.7.3.1. The satellites are separated in the along-track direction, but are not provided with additional velocity impulses to generate relative motion around each other in a 'zero drift and offset' formation. Again the STK relative motion is presented for comparison in Figure 4-32a. The relative motion predicted by the time varying model is presented in Figure 4-32b. The time varying model captures the shape of the in-plane orbit propagator relative motion, but is subject to an along-track drift. The cross-track model does not capture the STK motion in this case, but this approaches zero for both the time varying model and STK as the inclination increases towards 90^o.

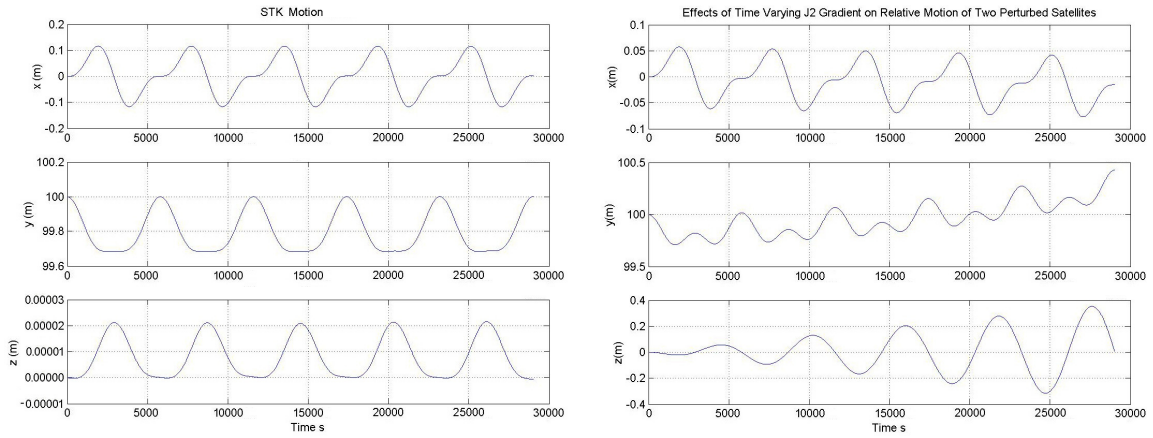

(a) (b)

Figure 4-32: Relative Motion of Two J_2 Perturbed Satellites in a Leader-Follower Formation with 100m Initial Along-Track Separation for i=85°, radius=6978.1km over 5 Orbits (a) STK (b) Time Varying Model

Zero Orbital Rate Change Orbit (i=54.75 ^{o} c=1, s=0)

This test case was briefly introduced in the introduction to section 4.7. One of the reasons for the mismatch between the STK, time averaged and time varying models was potentially the orbit rate correction term. Clearly a drift can be observed in the time varying model response for the MUSTANG test case (above). It was proposed that the orbital rate may need to vary around the orbit for the time varying model to hold, or that perhaps it needed tuning to the new model to improve performance. By allowing the orbit correction term to equal one such that the average effect of J_2 is to neither speed up nor slow down a perturbed satellite relative to a satellite on a circular Keplerian orbit at the same orbit radius, the ability of the other terms in the equations of motion to capture the perturbed relative motion were explored.

However, with the orbit rate correction eliminated from the problem, along-track drift was still experienced by the time varying model for an initial along-track offset, and results similar to those obtained for MUSTANG were obtained.

Additional Investigation

Beyond the basic test cases reported in this section, and a review of the model implementation, a number of further investigations into the behaviour of the time varying model were performed. These included:

- The removal of different cross coupling terms in the time varying state matrix to identify their effects.
    - The removal of potentially erroneous terms, or terms deemed to be causing adverse effects, in different combinations did not reduce the modelling errors.
- Taking the numerical time average of the time varying state matrix and comparing this to the time averaged model.
    - The average values summed over an orbit in small time steps were found to be the same as those predicted analytically, thus confirming model implementation.
- Implementing a Floquet solution to confirm model implementation.
- Tuning of the orbital rate parameters ‘c’ and ‘k’ in the equations of relative motion.
    - This did not prevent the growing errors.
- Incorporating an expression for time varying orbital rate in the time varying equations of relative motion.
    - The following expression was derived for the orbital rate correction factor, and replaced the constant correction factor, ‘c’ in the time varying equations of motion.
    - $$c(t) = \left(1 + \frac{3J_2 R_E^2}{2r_{ref}^2}\left(1 - 3\sin^2 i \sin^2 kt\right)\right) \qquad (4\text{-}102)$$
    - Modelling error was found to marginally reduce, but the errors were still greater than those observed for the time averaged model.
- Comparing the forces arising from the gradient of J_2 terms to those evaluated analytically using the J_2 force equation (4-25).

This final investigation was revealing, as the gradient term multiplied by a separation in a particular direction was not equivalent to the difference in force for the same satellite separation, also derived analytically from equation (4-25). An example is included below:

Radial Force due to an Offset in y

Consider a formation of two satellites separated along-track by angle δ.

According to equation (4-25) the force due to J_2 acting radially at satellite 1 (designated the reference) is given by equation (4-103), where θ is true latitude and all other terms were defined in section 4.3.

$$F_{radial1} = -\frac{3\mu J_2 R_E^2}{2r_{ref}^4}\left(1 - 3\sin^2 i \sin^2 \theta\right) \tag{4-103}$$

The force acting on satellite 2 is therefore be given by equation (4-104).

$$F_{radial2} = -\frac{3\mu J_2 R_E^2}{2r_{ref}^4}\left(1 - 3\sin^2 i \sin^2 (\theta + \delta)\right) \tag{4-104}$$

The relative force is given below.

$$F_{radial2} - F_{radial1} = \frac{9\delta\mu J_2 R_E^2 \sin^2 i \sin 2\theta}{2r_{ref}^4} \tag{4-105}$$

The gradient of J_2 (∇J_2) for the equivalent offset is given by equation (4-106).

$$F_{\nabla J2} = \frac{6\mu J_2 R_E^2 \sin^2 i \sin 2\theta}{r_{ref}^5}\Delta y \quad \text{where } \Delta y \approx r_{ref}\delta \tag{4-106}$$

Equations (4-105) and (4-106) should be equal, and yet the results suggest a factor of 0.75 difference between them. The equivalent analysis was performed for all terms and offset directions, and all the gradients relating to radial (x) offsets were found to be equivalent for both models. However, factors of between 0.571 and 2 arose from the algebra for along-track (y) and cross-track (z) offsets. Implementing these as correction factors to the state matrix of the time varying model revealed much improved radial modelling, however further investigation of these model characteristics and additional model verification is required to justify the approach. This is proposed as further work and is beyond the scope of the current research. While the time varying model performance did not demonstrate the improvements in model fidelity proposed or expected, the test cases presented here have demonstrated its ability to capture relative motion well, and show modelling improvements over the Hill equations in the presence of J_2.

The time varying model should demonstrate an improved ability to predict the relative motion of satellites subject to the J_2 perturbation, and it is proposed that both the

modelling assumptions associated with the force comparisons outlined above are investigated in more detail, and the STK scenarios also be reconsidered, possibly by comparison of results with an alternative propagator due to the lack of visibility associated with implementation of the initial conditions and integrator routine in STK. However, it is believed by the author that the STK implementation is unlikely to be a source of significant error.

4.7.4 Summary of Results

The results of the analysis presented in section 4.7 are summarised below for both the model development phase and relative dynamics models for two J_2 perturbed satellites.

Models Excluding the Gradient of J_2

- The Hill equations did not capture the J_2 perturbation. The basic force caused the perturbed satellite to orbit at a different rate and separate from the circular reference orbit thus violating linearisation assumptions.
- The zero drift and offset initial conditions for the in-plane J_2 motion did not eliminate along-track drift of the perturbed satellite away from the reference as they are unphysical conditions unless they also take into account the change in orbital rate.
- However, the zero drift and offset initial conditions did reduce the drift, and demonstrated that the closer the satellites are to bounded motion, the smaller the modelling error will be.
- Although the cross-track initial conditions remain decoupled from those derived for the in-plane motion, modelling errors are different for the different models because of the change in initial conditions supplied to STK. Cross-track motion is clearly coupled to the in-plane motion in the numerical simulation environment.

Models Including the Gradient of J_2

A Sun synchronous orbit was selected for much of the model development phase due to the implicit reduction of drift in the longitude of ascending node due to J_2 in a near polar orbit. For the Sun synchronous orbit test case:

- The modelling error is increased if the time averaged or time varying ∇J_2 term is included in the model unless an orbit rate correction is also applied.
- The time averaged ∇J_2 term reduced the in-plane modelling error but increased the cross-track error in a number of test cases.
- The time varying ∇J_2 term causes a drift, particularly in the along-track relative motion unless the effects of nodal drift are also taken into account at the reference orbit (in addition to orbit rate correction).
- The time varying ∇J_2 term reduces the cross-track modelling error below that of the time averaged model or the basic J_2 model (without ∇J_2).
- For the initial conditions for bounded motion derived from the time averaged model, the time varying model and time averaged model achieve a similar performance when compared to the same scenario in STK.

- For the numerically derived initial conditions that enforce bounded motion in STK, a slight degradation in performance of both models is observed.
- The analytically derived initial conditions which create bounded motion in the time averaged model do not create sufficiently bounded motion in the STK 'real' environment (although exactly bounded motion cannot be achieved in STK).
- During the first third of the first orbit, the time varying model captures relative motion in all directions more accurately than the time averaged model.
- Over five orbits, both models exhibit increased error growth to a similar extent and it is not clear which model captures relative motion of one J_2 perturbed satellite relative to an orbit rate and nodal drift corrected reference orbit.

Relative Motion of Two J_2 Perturbed Satellites

- The time averaged model captures relative motion very accurately in all axes for 'zero drift and offset' initial conditions.
- Without further modifications to the implementation of the model, the cross-track model cannot compute at inclinations of 0 and 90 degrees, and at certain other inclinations for zero initial cross-track position and velocity.
- The time averaged model can be used to generate a circular formation in the presence of J_2 which should be less costly to maintain than the equivalent, derived using the Hill equations.
- The time averaged model does not capture relative motion accurately for formations with large inter-satellite separations (error increases roughly in proportion to satellite separation).
- The time averaged model is also not able to model relative motion in eccentric orbits, and therefore will not capture a J_2 invariant orbit.
- The time averaged model reduces to the Hill equations for a leader-follower along-track formation, and is fundamentally flawed for other non-bounded motion formations by virtue of the decoupled nature of the in-plane and cross-track dynamics (these are clearly coupled in reality).
- The time varying model captures relative motion more accurately than the Hill equations, but less accurately than the time averaged model (the latter was unexpected).
- The time varying model will run for any orbit inclination, and reduces to the time averaged model for equatorial orbits.
- For a leader-follower formation, the time varying model captures the shape of the relative motion, but the amplitude is regularly about half that observed in STK numerical environment.
- Investigations into the performance degradation of the time varying model have been performed and should continue as further work as the model shows a promising ability to capture more features of the relative motion in a wider range of scenarios than those which apply to the time averaged model (bounded motion only in the time averaged case).
- Despite the minor differences between them, overall, both the time varying and time averaged models capture relative motion well in the presence of the J_2 perturbation.

General Conclusions Regarding Model Verification and Future Application

- The process of model verification has highlighted how many conditions must hold before an analytical description of satellite relative motion in the perturbed LEO environment will be representative with a degree of accuracy. In particular the satellites must not only have specific bounded initial conditions to keep them relatively close together, but the whole cluster must also have a defined orbital rate to retain the concept of a nearby virtual reference orbit about which the equations of motion are derived. This would be difficult to implement in practice.
- When performing model verification it was necessary to match the initial relative positions in the Matlab models and STK simulations to 10^{-6}m in position and 10^{-9}ms^{-1} in velocity to make a fair model comparison.
- The inclusion of time varying terms was not found to add significant complexity and computational effort to the running of the model.
- When the time averaged J_2 model was compared to the same bounded scenario in STK including higher order geopotential terms, only very small increases in modelling error were observed (errors at the cm level in all axes for 100m amplitude relative motion).
- Clearly there are a number of useful LEO formations where the zero drift and offset conditions do not apply. These include some of the test cases highlighted in this section (circular and projected circular formations, along-track leader-follower and J_2 invariant orbits). All these test cases have highlighted the limitations of the time averaged J_2 model in terms of practical application.

4.8 Summary

Following the literature review in chapter 6, a Hill-type dynamics modelling approach was selected for a precursor phase of research into satellite formation flying dynamics and control in LEO. Building on earlier work performed at MIT and at Cranfield University, in this chapter a new dynamics model is developed to capture the relative motion of satellites in LEO, subject to the J_2 perturbation. The context of this phase of research is established prior to a preliminary evaluation of a variety of perturbation accelerations acting on satellites in LEO, where the J_2 perturbation is shown to be the primary differential disturbance force on a formation of similar satellites.

A summary of the mathematical model development of three relative dynamics models is presented:

- The Hill equations (no J_2 perturbation effects)
- A time invariant or 'time averaged' J_2 model originally proposed by researchers at MIT (Schweighart and Sedwick, 2002)
- A time varying J_2 model

The well known Hill equations provide the baseline for relative motion modelling in the presence of point mass gravity, and these are compared to the J_2 models to highlight any modelling improvements achieved by augmenting the equations of motion.

For the J_2 models, the extensive model development phase highlights the need for both cluster motion (the motion of perturbed satellites relative to a circular reference orbit upon which the frame of reference is based, and the force gradients are evaluated), and relative motion between the perturbed satellites to be simultaneously considered in order to truly capture the relative dynamics. At each stage of model development, verification has been performed against the STK Astrogator high precision numerical orbit propagator using reference orbits modified for the effects of J_2 on orbital rate and drift in the longitude of ascending node. A variety of strategies have been successfully devised to compare the J_2 perturbed satellite motion with an unphysical reference orbit.

Solutions and initial conditions have been obtained where possible for all the relative motion models. New initial conditions have been derived for leader-follower and circular formations in the presence of J_2. For the time varying model, a number of solution approaches are investigated and ultimately numerical solutions are obtained, although further insight into the dynamics is obtained using a Floquet approach. For model verification, both analytically derived and numerically determined initial conditions which produce bounded relative motion between the satellites in the LEO formation are applied to establish both the optimal and limiting conditions of model accuracy.

The methods of dynamics model implementation and STK scenario execution are described in some detail (related techniques are employed for the L2 model verification reported in chapter 9). These highlight the role of the parameters and initial conditions derived during the model development, and also the complexity of the verification task.

The detailed findings of the model verification are presented for a number of test cases. In particular, the areas addressed through the model verification include the effects of initial conditions, the limits of linearisation within the models, the effects of retaining time varying terms within the equations of motion, and the determination of model limitations (mathematical and operational).

The time averaged and time varying J_2 models were found to achieve a similar performance for cluster motion relative to a circular reference orbit. However, for two J_2 perturbed satellites, the time averaged model captured bounded relative motion the most accurately. The time varying model captured the relative motion well, but not as accurately, and for both J_2 models, performance was improved above that of the Hill equations. However, the time varying model captures the shape of the relative motion for a wider range of formation flying scenarios. Investigations into the reasons for the difference in performance between the time averaged and time varying J_2 models, and particularly the lack of superiority of the time varying J_2 model, have been performed and are being continued. Of particular interest for further research is the nature of the cross-coupling initial conditions for the time varying model and bounded STK scenarios. The analytically derived initial conditions provide the optimal conditions for operation of the time averaged model, but conditions for motion closer to bounded in the STK environment can be established numerically. In addition, the role of cluster motion as well as bounded relative orbit motion in formation design should be formalised. A number of additional suggestions for further model development work are proposed in chapter 11.

In addition to being a useful formation flying simulation tool, the models are all appropriate for control system design. STK has been evaluated as a suitable perturbation environment in which to fly a controlled formation, and the verification process has demonstrated that the Matlab and STK software can be successfully interfaced. The inclusion of the J_2 effect in the Hill equations model allows greater insight into the formation dynamics, the opportunity to investigate alternative feedback control strategies for station keeping of a formation of satellites, thus enabling the potential reduction of lifetime ΔV requirements, and provides greater facility for choosing the optimum operational orbit. The models are applied to control system design and evaluation for LEO formation flying in chapter 8. This will determine whether the high fidelity J_2 models will enable more efficient formation flying control compared to controller design using the Hill equations.

5 FORMATION FLYING CONTROL IN LOW EARTH ORBIT

In this chapter, the LEO dynamics models derived and verified in chapter 4 are applied to control system design and performance assessment in the Satellite Tool Kit (STK) numerical simulation environment.

The aim of this research is to compare the ease with which the Hill equations, and the time averaged and time varying relative J_2 dynamics models can be utilised for control law design, and to demonstrate any benefits of using the more accurate formation flying models. The dynamic properties of the models are compared further and applied to linear quadratic regulator (LQR) design. The station keeping performance and ΔV requirements of the LQR designs when the models are subjected to a range of initial conditions and disturbances in the STK environment are evaluated.

The method of selection and justification for the control approach taken for this analysis, the overall research plan, and a review of the literature in chapter 3 is described in section 5.1. An overview of LQR theory and design for different types of control system is presented in section 5.2, providing the theoretical background for the controller designs described in chapter 7 for formation flying control of a Darwin-type formation.

Continuous control laws are designed to optimise station keeping accuracy against fuel use for the formation keeping task, while limiting peak thrust and maintaining a suitable manoeuvre time during any corrective manoeuvres. The controllers derived from the Hill equations and time averaged or time 'invariant' J_2 model are designed offline and remain constant for all scenarios. The controllers for the time varying system equations are redesigned at sampling intervals during the orbit. All these are compared for formation keeping scenarios in the perturbed environment. Constant offset and circular formation test cases are investigated, and a range of disturbance forces are applied to the satellites (in addition to the J_2 perturbation). The role of the initial conditions for the Hill equations and time invariant J_2 models are investigated and the results of the control system evaluations are presented in section 5.5.

The controller gains obtained from both the Hill equations and high-fidelity J_2 models were very similar, and this led to similar controller performance being observed in the STK environment. However, the designs did demonstrate that acceptable response characteristics could be achieved using both models, and that the controllers could perform the formation keeping task. The Matlab/STK interface was successfully developed to implement controller gains effectively onboard the non-reference satellite for the leader-follower architecture employed. A slightly smaller ΔV was required for comparable formation keeping tasks using the high-fidelity J_2 model formation design, initial conditions, and control concepts. The measures of ΔV used for formation keeping were compared to those in the literature, and found to be realistic. The chapter concludes with a discussion and summary of the main results.

5.1 Introduction

The Hill equations and time invariant J_2 models discussed at length in chapter 4 are intrinsically unstable. Unless they are given specific initial conditions for bounded motion to a great degree of accuracy, an initial disturbance to the system dynamics will cause relative spacecraft positions to diverge in the absence of corrective control. Even by using numerically derived initial conditions, bounded motion is never truly achieved in STK for J_2 perturbed orbits, and although lesser in effect on a formation of similar spacecraft, other LEO perturbations will also cause the satellites to drift away from their desired relative and absolute positions in orbit. Feedback control is therefore required to minimise the error between the actual and desired relative satellite motion, and to maintain the formation geometry.

A review of the recent literature, presented in chapter 3, revealed that a number of different linear and nonlinear control techniques have already been applied to the satellite formation flying problem in LEO. The most commonly applied techniques were Linear Quadratic Regulator (LQR) and Lyapunov control using both Hill frame and orbit elements dynamics models, and both continuous and discrete control systems. However, while nonlinear terms and eccentricity have been considered in contrasting designs, the effects of the J_2 perturbation have not been contrasted, and most of the systems reviewed were not evaluated in the perturbed environment. This finding has motivated the research presented in chapters 4 and 5.

The accuracy and limitations of three different dynamics models were identified in chapter 4. These models were the:

- Hill equations (no J_2 perturbation)
- Time invariant J_2 model (Schweighart and Sedwick, 2001a)
- Time varying J_2 model

Significant improvements in modelling accuracy were observed for the J_2 models for specific satellite formations. Of particular interest are the initial conditions resulting from the model solutions. These conditions appear to limit the conditions under which the models can capture relative motion, but also they provide insight into the design of fuel-minimising natural formations. The effects of initial conditions on controlled formations are therefore investigated here.

In preparation for the later dynamics and control simulation work for Lagrange point orbits, the LEO case was deemed an essential precursor to develop the necessary Matlab/STK interface for formation control. In particular, it was important to investigate the feasibility of interfacing the STK simulations with the time varying J_2 dynamics model in Matlab. The Hill equations and the time invariant J_2 model control designs are simplified due to the decoupling of the in-plane and cross-track dynamics, but for the time varying J_2 model, the in-plane and cross-track control gains must be evaluated together.

The aspects considered when choosing the multivariable control methodology for this application were identified as follows:

- Application – Suitability of the technique for the task. This is a trade-off between complexity, functionality, performance and prior implementation. The

latter points facilitate the comparison of results with other research and indicate that the approach will be successful.

- Complexity – Related to performance improvements and retention of insight into the dynamics problem.
- Stability – Full-envelope stability and stability margins.
- Robustness – Guaranteed stability and performance across a wide range of operating conditions and in the presence of significant noise and external disturbance.

Feedback is important to compensate for external disturbances, model uncertainty, and instability. In this case Linear Quadratic optimal control has been selected for this LEO study. The design process can be applied for continuous and discrete control, and also to time varying systems in a continuous or discretised manner. The basic LQR design can be augmented to include compensation for measurement and disturbance noise (Linear Quadratic Gaussian (LQG) control). However, in this case only basic LQR designs have been investigated for the different models due to the perturbing effects of J_2 on the dynamics being of primary interest. While important, the effects of sensor and actuator noise on formation control has not been considered and full state knowledge is assumed. For a mission specific scenario, much more detailed analysis would be required.

There are many examples of the application of LQR control design techniques to spacecraft formation flying. The appeal of these techniques is clearly apparent, with the opportunity to optimise fuel consumption and speed of response to disturbances or for manoeuvring demands from a guidance system, the inherent disturbance rejection properties of the controller, and the relative ease with which this tried and tested technique can be applied. However, it is also possible to use a number of alternative techniques, and in future work it may be appropriate to compare their performance. In the absence of a specific mission with defined spacecraft systems, software capability, and operational requirements, it is difficult to categorically state which control technique will be the best approach.

Mission specification will determine the type of formation and reference orbit which will determine different levels of orbit perturbations to which the formation will be exposed and the inter-satellite separations. Other operational requirements, for example, the acceptable maximum relative position error bounds, fuel use limits, thruster saturation levels, frequency of control inputs, type of thrusters and sensors, and the level of autonomy and guidance strategy (which will also dictate how trajectory tracking would need to be implemented onboard the spacecraft) would need to also be considered to tune the design. In this case, three different leader-follower scenarios have been investigated. These include a 10m manoeuvre to an along-track formation (used to tune the controller design), an along-track station keeping scenario, and trajectory following for a circular formation.

The literature review in chapter 3 revealed significant interest in pulsed plasma thruster (PPT) propulsion systems, and a number of authors, particularly at the US Air Force Research Laboratory (AFRL) considered discrete and pulse-based LEO formation control using LQR. In this case continuous LQR control has been selected for the J_2

relative dynamics and Hill equations comparisons for simplicity, and in preparation for the continuous propulsion system considered in the Darwin-type simulation (chapter 7). Irvin and Jacques (2001) propose that continuous control is more fuel costly than discrete control. However, this will depend on the acceptable position error and the precision with which the satellites can be controlled to their desired position during the impulsive manoeuvre for a discretised system. For a slightly increased cost, more highly precise formation flying may be achieved using continuous control. An evaluation of fuel cost for formation maintenance over a mission lifetime will enable the feasibility of a continuous control system to be established. Also, De Quieroz, Kapila and Yan (2000) suggest that continuous control laws can provide an idealised response for comparison with the actual responses obtained from impulsive control controllers. The results obtained in this chapter will be compared and contrasted with other relevant studies reported in the literature, and in particular the ΔV required to maintain precisely a formation in the presence of the J_2 perturbation.

The stability and robustness characteristics of the LQR control technique are described in a number of texts (Bryson and Ho, 1975), (Skogestad and Postlethwaite, 2001). A system with continuous LQR stabilising feedback will have an infinite gain margin and substantial phase margin, however, this is not necessarily the case for LQG. In the LEO formation flying literature, the application of discretised LQR control could also not be proven stable in all circumstances (discussed in Yan, Kapila and Sparks (2000)). A summary of the LQR theory applied in this chapter is presented in section 5.2.

The application of the more accurate relative dynamics models to the control law design process is presented in this chapter. The station keeping performance, formation keeping performance and ΔV requirements of the LQR designs, when the models are subjected to a range of initial conditions and disturbances in the STK environment, are evaluated.

5.2 Linear Quadratic Regulator Theory

A brief overview of the basic LQR theory that is applied to the time invariant and time varying dynamics models is presented in this section. Control system designs using the theory in its different forms are described in section 5.3.

5.2.1 Linear Time Invariant LQR Theory

The first step in the application of the LQR theory to the problem of formation flying control of two satellites in the J_2 perturbed environment is to establish the controllability and observability of the states in the system. One definition of state controllability requires that the input (u) is able to move the system from one state to any other state in the state space in a finite time. If the states are not controllable then state feedback cannot be applied. A system is observable if for any initial state, knowledge of the zero input response (y) is sufficient to determine the initial state.

There are a number of conditions, of which only one must be satisfied, which will ascertain whether a system, described by the state and output equations below, is controllable (Wie, 1998).

$$\dot{x} = Ax + Bu \tag{5-1}$$

$$y = Cx + Du \tag{5-2}$$

The state response to initial condition, x_0, and system input, u, over time can be expressed as (Whidborne, 2005)

$$x(t) = e^{At}x_0 + \int_0^t e^{A(t-\tau)}Bu(\tau)d\tau \tag{5-3}$$

For a controllable system, it must be possible to achieve x(t) = 0 in a finite time with an appropriate input, such that

$$x_0 = -\int_0^t e^{-A\tau}Bu(\tau)d\tau \tag{5-4}$$

Equation (5-4) can only be solved for $u(\tau)$ if the rows of $e^{-A\tau}B$ are linearly independent. A controllability criterion can therefore be derived through a Taylor series expansion of the exponential (Kwakernaak and Sivan, 1972). In n-dimensional space, there will be a maximum of n linearly independent vectors given by the exponential matrix sequence arising from the Taylor expansion. Written in the form of a criterion, the controllability matrix is given by equation (5-5). For system controllability (all modes can be controlled by input, u), this matrix must have rank 'p', where p represents the number of inputs to the system.

$$\begin{bmatrix} B & AB & A^2B & A^3B & \dots & A^{p-1}B \end{bmatrix} \tag{5-5}$$

A system is unobservable if $Ce^{At}x_0$ is zero for all 't' greater than or equal to zero (Whidborne, 2005). For an observable system, the columns of Ce^{At} must be linearly independent, and using the same approach (Taylor series expansion of the exponential), an observability criterion can be derived. A system is observable if the observability matrix in equation (5-6) has rank 'w', where w represents the number of outputs, y.

$$\begin{bmatrix} C & CA & CA^2 & CA^3 & \dots & CA^{w-1} \end{bmatrix}^T \tag{5-6}$$

Having established the controllability and observability of each system, the linear time invariant (LTI) models (Hill equations and time averaged J_2 model) were used directly in the LQR design process. With the LQR technique, it is possible to perform either a tracker or regulator design.

A 'tracker' design will cause the output to follow or 'track' the input, and this is appropriate for constellation designs incorporating 'zero drift and offset' conditions. When zero drift and offset conditions are applied to a model, the in-plane (and cross-

track for circular and projected circular formations) relative motion is periodic and bounded. There is no secular drift or fixed offset maintained between the satellites.

A 'regulator' has constant or zero input and feedback is used to keep the output constant (usually zero) or to 'regulate' the output. A state regulator will derive the control signal required as a function of the state of the system so that any non-zero initial condition will be driven to zero at the output. An optimal state regulator will achieve this while minimizing a performance index or cost function.

In state feedback control, the state vector is multiplied by a gain matrix, K, and fed back into the control input, u where

$$u = -Kx \tag{5-7}$$

giving a closed loop system described by equation (5-8).

$$\dot{x} = (A - BK)x \tag{5-8}$$

A simple illustration of the closed loop state regulator system is given in Figure 5-1.

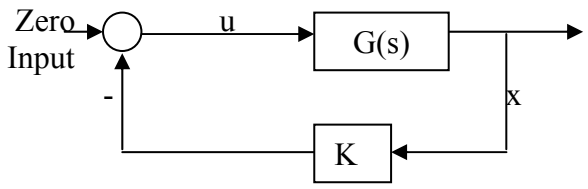

Figure 5-1: Basic State Regulator

In this LQR design the gain matrix can be determined by minimising the linear quadratic performance index or 'cost' given by J in equation (5-9) (Skogestad and Postlethwaite, 2001).

$$J = \int_0^\infty x(t)^T Qx(t) + u(t)^T Ru(t)dt \tag{5-9}$$

The designer must choose values for the matrices Q and R to design a controller which will achieve an optimal response from the system, depending upon the design requirements. Q is the state weighting matrix, and by increasing Q, the error between desired and actual system output is reduced more quickly. R is the control input weighting matrix, and by increasing R, the fuel used and maximum accelerations permitted during the elimination of the error are reduced. The relative magnitude of Q and R are also selected according to the relative importance of minimising the states or control effort. Increasing Q and R together in proportion will not affect the feedback. The Q and R matrices must be positive and semi-definite to ensure that the cost function, J, is greater than or equal to zero.

For the general application of optimal control theory, the cost function does not have to be quadratic and the system does not have to be linear or time invariant. However, for the LTI models and continuous control system required here, relatively simple techniques are available for obtaining a feedback gain matrix. In order to minimise the

cost function (equation (5-9)), it is necessary define a symmetric positive definite matrix, P, such that (Whidborne, 2005)

$$-\frac{d\left(x^T P x\right)}{dt} = x^T Q x + u^T R u \tag{5-10}$$

and therefore, for a stable closed loop system

$$J = x_0^T P x_0 \tag{5-11}$$

The cost function can also be written in terms of feedback gain, K (equation (5-7)) by substituting for u in equation (5-9). Algebraic manipulation of equations (5-1), (5-7), (5-8) and (5-10) produces equation (5-12) (Whidborne, 2005).

$$A^T P + PA - (K^T B^T P + PBK) + K^T R K + Q = 0 \tag{5-12}$$

If the feedback gain, K is K_0 when P is P_0 and the cost function, J, is minimised to J_0, then in a different situation $K=K_0+\Delta K$ when $P=P_0+\Delta P$. Selecting K_0 for ΔP to be zero produces a relationship between K and P such that control is optimal. In this case, the feedback gain matrix is given by equation (5-13).

$$K = R^{-1} B^T P \tag{5-13}$$

By substitution into equation (5-12) the algebraic Riccati equation (5-14) is obtained.

$$A^T P + PA + Q - PBR^{-1} B^T P = 0 \tag{5-14}$$

For this research, the optimal feedback gains were evaluated off line using Matlab before being implemented within the STK simulation environment onboard the satellites. Further details of the derivation of the Riccati equation can be found in suitable control texts, for example, Kwakernaak and Sivan (1972).

5.2.2 Application of LQR Theory to the Time Varying Model

There are two approaches that could be taken to implement continuous LQR controllers for the time varying model. The more complicated approach involves the offline solution of the differential algebraic Riccati equation to obtain time varying gains prior to simulating the scenario (Bryson and Ho, 1975). The Riccati equation and gain matrix are given by equations (5-15) and (5-16) respectively (where in this case B, Q and R are not time varying).

$$\dot{P}(t) = -A^T(t)P(t) - P(t)A(t) - Q + P(t)BR^{-1}B^T P(t) \tag{5-15}$$

$$K(t) = R^{-1} B^T P(t) \tag{5-16}$$

However, for a periodic state matrix, the solution matrix, P(t), of the Riccati equation will also be periodic, and there is likely to be relatively little benefit gained from solving this complex problem. Instead it is proposed that similar results would be achieved by redesigning the controller using the standard algebraic Riccati equation at regular intervals during the orbit to produce a continually optimised control system which should provide long term fuel consumption reduction. The variable gains could

be evaluated offline and stored for a particular formation design. These would have to be called across the Matlab/STK interface to be implemented on the follower satellite in the formation flying scenario.

In this case, a generalised tool is developed whereby the controller is redesigned at selected intervals onboard the spacecraft. Specifically in the test cases presented here, the redesign is performed at every timestep in the simulation as continuous control conditions are being compared and contrasted for the different dynamic models. Conceptually this is a more practical approach as the dynamic model could regularly be updated with on-orbit position measurements (used to update, for example, orbital rate correction terms within the model itself in the same way that an orbit rate correction due to J_2 was applied to the reference orbit in the J_2 models in chapter 4), before the next series of periodic gains are derived.

5.3 Control Law Design

This section summarises the controller design process applied in the Matlab environment. For this investigation one satellite is designated the leader, and the relative motion is always measured in a curvilinear axis system based at this satellite (Figure 5-2). The leader satellite does not regulate its own position, and follows the cluster or 'absolute' motion due to the J_2 perturbation relative to a circular reference orbit, as discussed in chapter 4. The scenario always begins with the leader satellite located on the circular reference orbit as illustrated. P_0 represents the leader satellite, and P_1 represents the follower.

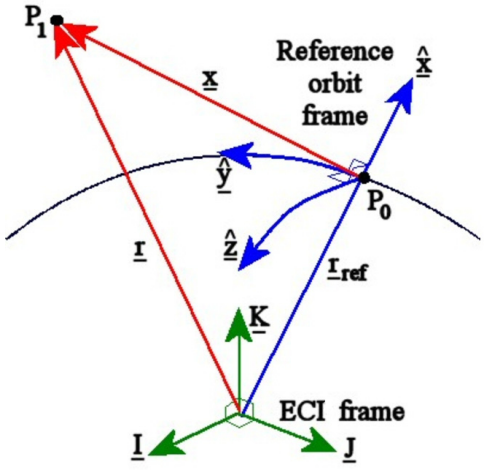

Figure 5-2: Axis System for Relative Motion Measurement

The second satellite also experiences the J_2 perturbation, and maintains its position relative to the leader satellite using its own on-board sensors and thrusters. Recent literature has suggested that controlling one satellite rather than distributing the corrective control between spacecraft is less costly (Vadali and Vaddi, 2000). However, the selected control strategy would also depend on whether the divergence of the

formation from their ideal operational orbit was tolerable. For this assessment of formation keeping ΔV it is assumed that all the states are accurately known and there is no sensor noise.

The model has not been discretised at this stage although the frequency and magnitude of thruster firings is normally an important variable in the design process. The frequency of thruster input must be optimised in terms of desired station keeping accuracy and fuel use, and the design would need to be mission specific. Minimising position error implies frequent corrections whereas minimising disturbances to the spacecraft and fuel use implies that a long time between formation keeping corrections is required.

The control law designs for the linear time invariant (LTI) and linear time varying (LTV) systems are summarised in the following subsections.

5.3.1 Linear Time Invariant Models

In the following sections, the LQR design procedure, its implementation in Matlab/Simulink, and any assumptions made are summarised for the time invariant Hill and J_2 models. Examples of the results obtained are then presented and compared for both models prior to the control system evaluation in the STK environment.

5.3.1.1 Design Procedure

The Hill equations and time invariant J_2 models, derived in chapter 4, are both composed of two highly coupled sets of equations (in-plane, x-y), and one decoupled equation (cross-track, z). Expressed in state space form (equations (5-1) and (5-2)), they are given by equations (5-17) and (5-18). A_{xy} represents the in-plane motion, and A_z represents cross-track motion for both models. The output equation matrices are C (identity matrix) and D (zero matrix) for this system.

Hill Equations Model

$$A_{xy} = \begin{bmatrix} 0 & 2n & 3n^2 & 0 \\ -2n & 0 & 0 & 0 \\ 1 & 0 & 0 & 0 \\ 0 & 1 & 0 & 0 \end{bmatrix} \qquad A_z = \begin{bmatrix} 0 & -n^2 \\ 1 & 0 \end{bmatrix} \qquad (5\text{-}17)$$

Time Invariant J_2 Model

$$A_{xy} = \begin{bmatrix} 0 & 2nc & (5c^2-2)n^2 & 0 \\ -2nc & 0 & 0 & 0 \\ 1 & 0 & 0 & 0 \\ 0 & 1 & 0 & 0 \end{bmatrix} \qquad A_z = \begin{bmatrix} 0 & -q^2 \\ 1 & 0 \end{bmatrix} \qquad (5\text{-}18)$$

The terms in these state matrices are defined in chapter 4. In both the Hill equations and high-fidelity J_2 models, n is the mean angular rate for a satellite on the Keplerian circular reference orbit. This is the fundamental parameter describing relative motion in the Hill equations. The parameter c represents a correction factor applied to the mean orbital rate of a satellite on a 'virtual' circular reference orbit to match the orbital rate to that experienced by a J_2 perturbed satellite. In the time invariant J_2 cross-track model, q is the argument in the equation describing relative cross-track position. This was derived by considering the effects of the J_2 perturbation on the location of the intersection of the different orbital planes of two satellites (Schweighart and Sedwick, 2002). The state vector (x) in equations (5-1) and (5-2) is given for the in-plane models by

$$x_{xy} = \begin{bmatrix} \dot{x} & \dot{y} & x & y \end{bmatrix} \tag{5-19}$$

and for the cross-track models by

$$x_{z} = \begin{bmatrix} \dot{z} & z \end{bmatrix} \tag{5-20}$$

A separate design was performed in Matlab for each of the four models:

- Hill Equations – In-plane
- Hill Equations – Cross-track
- Time Invariant J_2 Model – In-plane
- Time Invariant J_2 Model – Cross-track

In order to perform the design, it was necessary to choose a suitable design point to give the system a realistic behaviour in the deterministic initial value problem. The details are summarised in Table 5-1.

Design Parameters	**Target Values**
Manoeuvre	10m in x,y,z simultaneously
Satellite Mass	100kg
Maximum Thrust	10mN
Maximum Acceleration	$10^{-4}ms^{-2}$
Manoeuvre Duration	½ Orbit

Table 5-1: Controller Design Point

The initial error from desired position in the radial, along-track and cross-track directions was set to 10 metres. The mass of the satellite being controlled (the follower in this case) was assumed to be 100kg, and the maximum thrust in any direction 10mN. The acceptable acceleration was therefore $10^{-4}m/s^2$. The controller was tuned to allow the 10m manoeuvre (in all directions) to occur over an acceptable period of time, for example, half of an orbit.

For rapid tuning of the controllers, the design process was automated for each model. The resulting program architecture, applied separately to each model, performs the following tasks:

- Obtains desired reference orbit parameters.
- Calculates additional orbital parameters for inclusion in the state space model of the formation flying dynamics (Hill and time invariant J_2 models).
- Confirms the Controllability and Observability of the coupled system.
- Computes the Q and R matrices, given the matrix elements provided by the user.
- Performs the LQR design by solving the algebraic Riccati equation.
- Returns values for the feedback gain matrix, K.
- Returns the eigenvalues of the closed loop system.
- Takes the initial error values that will be driven to zero.
- Runs the closed loop simulation (Simulink model) using the feedback gain matrix in the loop around the formation flying dynamics.
- Extracts and plots relative positions and velocities from the model.
- Calculates the maximum thrust applied in each direction.
- Calculates the total ΔV over a user-specified period of time.

Only at the final stage of evaluating total ΔV are the in-plane and cross-track design processes combined.

The control accelerations acting on the spacecraft are given by a_x, a_y, and a_z in the radial, along-track and cross-track directions respectively (as expressed in the Hill equations example below).

$$\begin{aligned} \ddot{x} - 2n\dot{y} - 3n^2 x &= a_x \\ \ddot{y} + 2n\dot{x} &= a_y \\ \ddot{z} + n^2 z &= a_z \end{aligned} \qquad (5\text{-}21)$$

An initial estimate of the total station keeping ΔV can be determined by the summation of instantaneous values of the continuous accelerations provided to the follower spacecraft (equation (5-22)).

$$\mathbf{\Delta V} = \int_0^{\mathbf{Lifetime}} \sqrt{\mathbf{a_x^2 + a_y^2 + a_z^2}}\,\mathbf{dt} \qquad (5\text{-}22)$$

In this case, the total ΔV is calculated by taking the absolute value of controller acceleration demand in each direction, finding the resultant, and multiplying by the time step of the simulation. In order to combine the in-plane and cross-track accelerations, both models have to operate at the same fixed simulation time step.

$$\Delta V = \left[\sum \left(a_x^2 + a_y^2 + a_z^2 \right)^{1/2} \right] * \text{TimeStep} \qquad (5\text{-}23)$$

The initial controller design was performed using the basic state regulator illustrated in Figure 5-1 to drive all the states to zero in an optimal manner. The implementation of the state regulator in Matlab-Simulink is illustrated in Figure 5-3.

In Figure 5-3, Aip is the in-plane state matrix, Bip is the in-plane input matrix. The initial offsets are applied through the constant block in the top left hand side of the

diagram, and integrations are performed separately on each state. The behaviour of the output is monitored through the Matlab workspace, and the accelerations applied to the follower satellite are extracted through the 'Acceleration' output port. This acceleration data is used to calculate the ΔV.

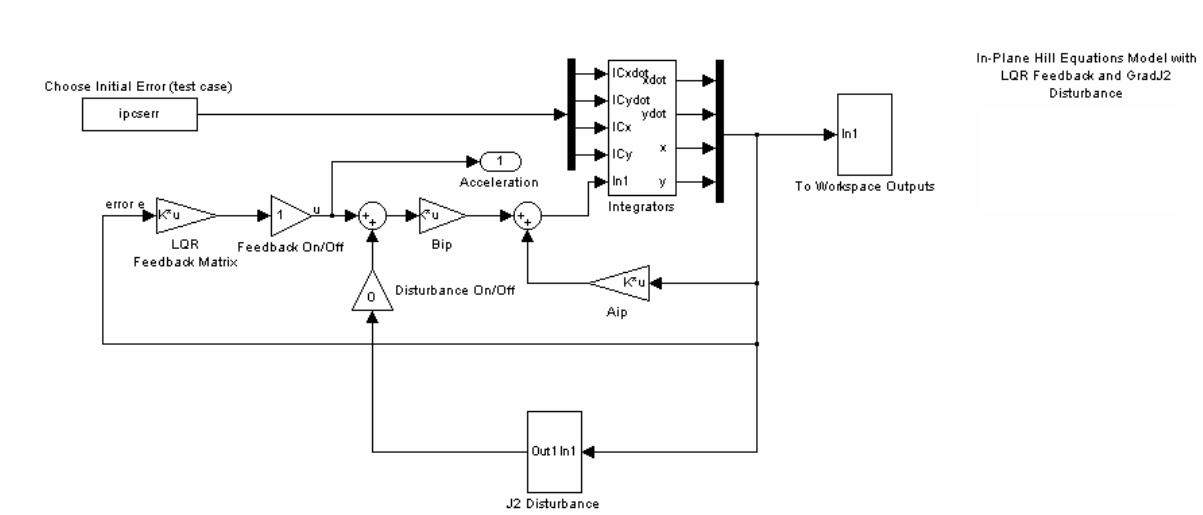

Figure 5-3: In-plane Hill Equations Implemented as State Space Model with LQR feedback and J_2 Disturbance (Simulink Diagram)

The Q and R matrices were varied, and the responses of the model were observed. The design and response parameters evaluated for each design included:

- Closed loop eigenvalues for stability
- Maximum acceleration
- % Overshoot in response
- Time to reach within 1mm of desired offset
- ΔV over 1 orbit (including the initial manoeuvre)

The Simulink model was then executed with the gradient of J_2 perturbation as a disturbance (this was introduced in chapter 4 and is given by equation (4-38)). The ability of the controller to reject these disturbances in the Matlab environment was observed.

5.3.1.2 LTI Controller Designs

The General test case, used for model verification in section 4.7, chapter 4, is presented as an example for the design evaluation. The reference orbit parameters for this test case are as follows:

- Orbit radius $r_{ref} = 7000$km
- Orbit inclination $i_{ref} = 35^o$

This was deemed a suitable design case (although others were also investigated) as greater differences between the Hill equations and both of the J_2 models were

anticipated away from polar and equatorial orbits, and the case has already been used for verification of all three models.

Hill Equations Model

The weighting matrices, Q and R were selected as diagonal matrices with zero or positive elements, and defined according to the relative importance and direction of the output states and control inputs. The values in Q were made equal to achieve equal speed and precision of manoeuvre for positions and velocities in all directions (x, y, and z). The R matrix was initially selected to have the same magnitude elements to equalise fuel use in each direction. However, tuning the response to limit the maximum thrust to 10mN for a 10m manoeuvre required the R matrix values to differ on the diagonal. A larger weighting was therefore given to the along-track control which, according to the literature, can achieve a greater authority than radial control for the same thrust (Starin, Yedavalli, and Sparks, 2001a). The critical measure of Q and R is their ratio. For the LQR designs performed here, the ratio of diagonal elements varied between $R/Q = 10^9$ radially to 10^{10} along-track and cross-track.

The following feedback gain matrices were obtained.

$$K_{xy} = \begin{bmatrix} 0.006683919 & -0.001547667 & 0.000019195 & -0.000009208 \\ -0.000251324 & 0.003309947 & 0.000003780 & 0.000006214 \end{bmatrix}$$

$$K_z = \begin{bmatrix} 0.004471255 & 0.000009996 \end{bmatrix} \qquad (5\text{-}24)$$

The terms in the gain matrix are small as the state matrix was not non-dimensionalised. However, in this form, the gains can be directly implemented into STK and the relative position and velocity data passed between the Matlab/STK interface does not have to be repeatedly converted. (The operation of the Matlab/STK interface is discussed in section 5.4). This closed loop system had the following stable complex eigenvalues.

$$E_H = \begin{matrix} -0.002766047 + 0.003470272i \\ -0.002766047 - 0.003470272i \\ -0.002230886 + 0.001321740i \\ -0.002230886 - 0.001321740i \\ -0.002235627 + 0.002481949i \\ -0.002235627 - 0.002481949i \end{matrix} \qquad (5\text{-}25)$$

When the controller was applied to the Hill formation flying model, and used to eliminate a 10m error in the radial and along-track directions, the accelerations, velocities and relative positions, illustrated in Figure 5-4, Figure 5-5 and Figure 5-6 respectively, were observed.

The maximum acceleration experienced by the follower satellite is tuned to be less than 10mN ($10^{-4}ms^{-2}$ acceleration) in either direction in accordance with the design point requirements in Table 5-1. The maximum relative velocity between the satellites is 13.9mm/s, around 407 seconds into the manoeuvre, and the position error is reduced from 10 metres to zero. The overshoot and time to reach within 1mm of desired

separation were measured by observation of more detailed graphical data, and the maximum thrust and ΔV were calculated as described above.

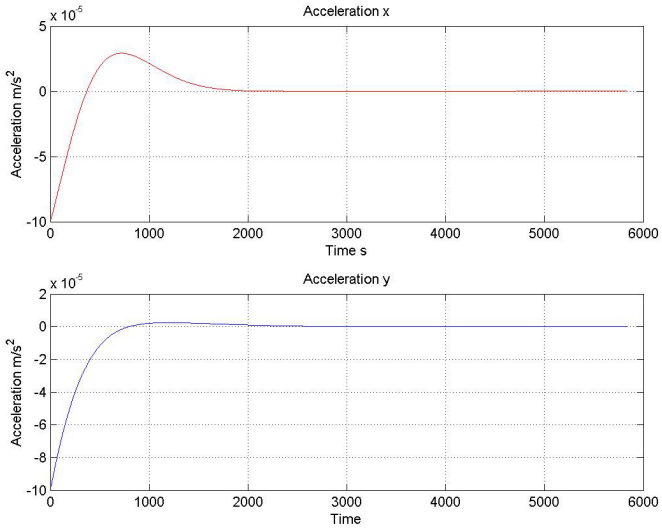

Figure 5-4: Acceleration Applied by the Hill controller to a Follower Satellite to Eliminate a 10m Initial Position Error in the Radial (x) and Along-Track (y) Directions

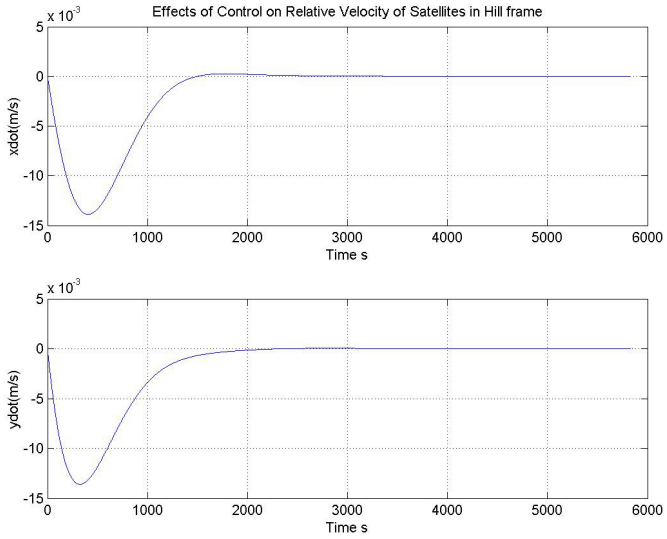

Figure 5-5: Relative Radial and Along-Track Velocity During the Elimination of a 10m Initial Position Error in the Radial (x) and Along-Track (y) Directions Using the Hill controller

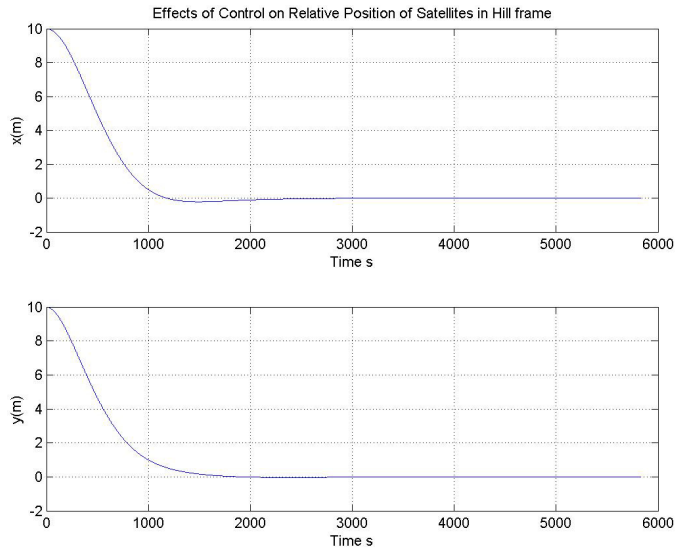

Figure 5-6: Relative Radial and Along-Track Position During the Elimination of a 10m Initial Position Error in the Radial (x) and Along-Track (y) Directions Using the Hill Controller

The cross-track feedback, K_z, was applied to the cross-track Hill equations model and the acceleration, velocity and position responses for the design are illustrated in Figure 5-7 and Figure 5-8.

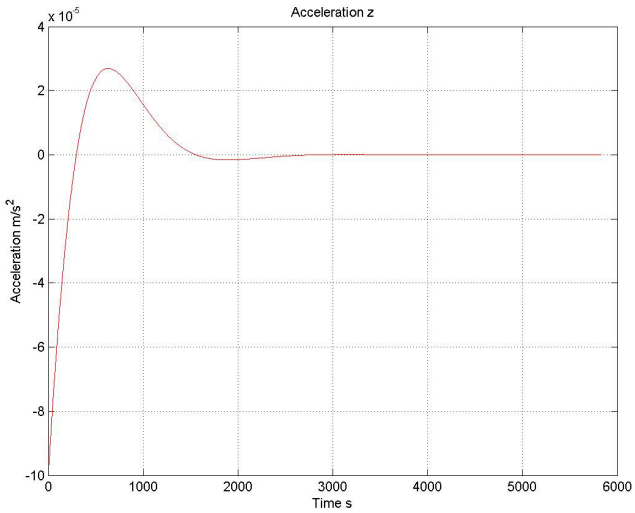

Figure 5-7: Acceleration Applied by the Hill Controller to the Follower Satellite to Eliminate a 10m Initial Position Error in the Cross-Track (z) Direction

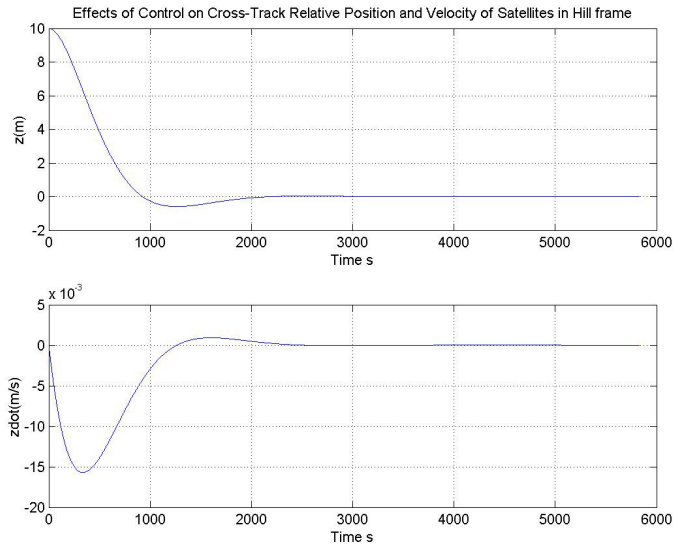

Figure 5-8: Relative Cross-Track Velocity and Position During the Elimination of a 10m Initial Position Error in the Cross-Track (z) Direction Using the Hill Controller

The response parameters for the in-plane and cross-track controlled relative motion are given in Table 5-2.

Hill Model	Initial Offset (m)	Max. Thrust (mN)	% Overshoot	Settling Time (s) to 1mm
X (Radial)	10	9.98731	2.150	3534
Y (Along-track)	10	9.99388	0.363	3853
Z (Cross-track)	10	9.99600	5.902	4227

Table 5-2: Response Parameters (Hill Equations Design)

The total ΔV for the manoeuvre within one orbit (evaluated for 1-second time steps) was found to be

$\Delta V = 0.06113\ ms^{-1}$

High-Fidelity Time Invariant J_2 Model

The controller design and evaluation procedure described in section 5.3.1.1 to meet the design requirements in Table 5-1 was also applied to the time invariant J_2 model (maximum accelerations were limited to $10^{-4} ms^{-2}$). The state (Q) and control (R) weighting matrices were selected using the procedure described above (for the Hill controller design). The following in-plane and cross-track feedback matrices were obtained.

$$K_{xy} = \begin{bmatrix} 0.006684559 & -0.001547683 & 0.000019198 & -0.000009210 \\ -0.000251326 & 0.003309708 & 0.000003781 & 0.000006214 \end{bmatrix}$$

$$K_z = \begin{bmatrix} 0.004472147 & 0.000010000 \end{bmatrix} \qquad (5\text{-}26)$$

The closed loop system had the following stable complex eigenvalues.

$$E_{J2} = \begin{matrix} -0.002766057 + 0.003470425i \\ -0.002766057 - 0.003470425i \\ -0.002231077 + 0.001321379i \\ -0.002231077 - 0.001321379i \\ -0.002236074 + 0.002236062i \\ -0.002236074 - 0.002236062i \end{matrix} \quad (5\text{-}27)$$

Figure 5-9, Figure 5-10, and Figure 5-11 illustrate the controlled response using the high-fidelity J_2 formation flying model.

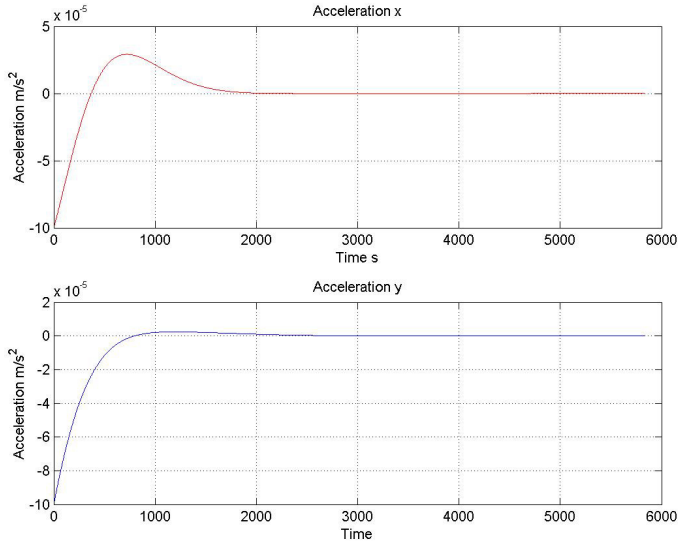

Figure 5-9: Acceleration Applied by the Time Invariant J_2 Model Controller to the Follower Satellite to Eliminate a 10m Initial Position Error in the Radial (x) and Along-Track (y) Directions

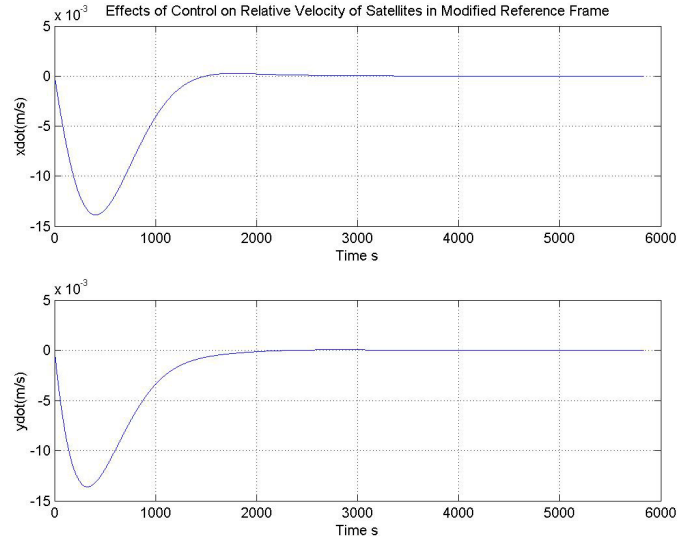

Figure 5-10: Relative Radial and Along-Track Velocity During the Elimination of a 10m Initial Position Error in the Radial (x) and Along-Track (y) Directions Using the Time Invariant J_2 Controller

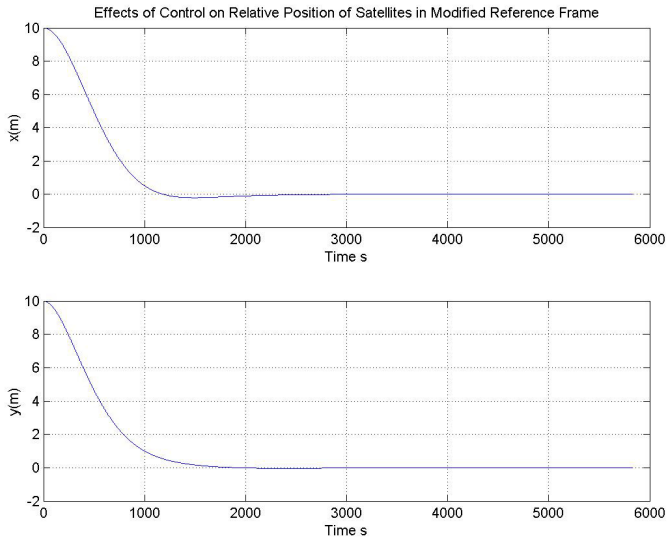

Figure 5-11: Relative Radial and Along-Track Position During the Elimination of a 10m Initial Position Error in the Radial (x) and Along-Track (y) Directions Using the Time Invariant J_2 Controller

The cross-track feedback, K_z, was applied to the cross-track time invariant J_2 model, and the acceleration, velocity and relative position responses are illustrated in Figure 5-12 and Figure 5-13.

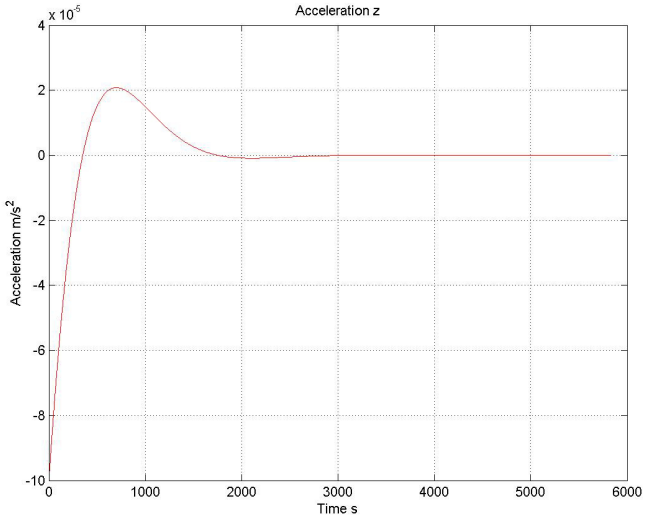

Figure 5-12: Acceleration Applied by the Time Invariant J_2 Controller to the Follower Satellite to Eliminate a 10m Initial Position Error in the Cross-Track (z) Direction

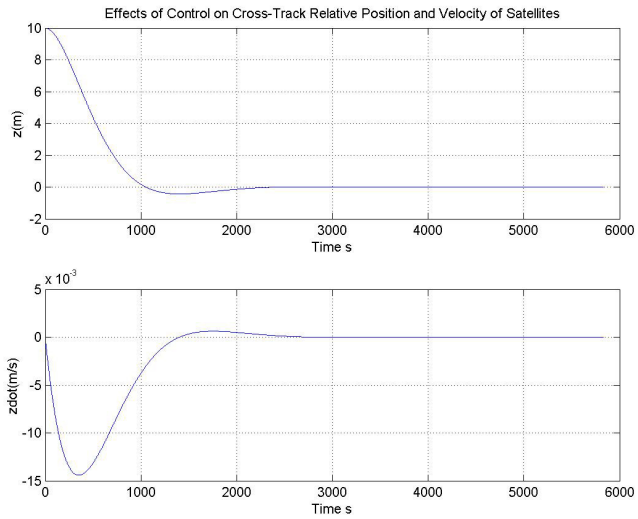

Figure 5-13: Relative Cross-Track Velocity and Position During the Elimination of a 10m Initial Position Error in the Cross-Track (z) Direction Using the Time Invariant J_2 Controller

For the in-plane responses using the time invariant J_2 model, similar features can be observed when compared to the Hill model responses. This is expected due to the similarity of the dynamics captured in the Hill and time invariant J_2 models. The only significant observable difference is in the cross-track motion where the accelerations applied are smaller for the J_2 model. The response parameters for the high-fidelity J_2 model design are given in Table 5-3.

Time Invariant J_2 Model	Initial Offset (m)	Max. Thrust (mN)	% Overshoot	Settling Time (s) to 1mm
X (Radial)	10	9.98794	2.148	3534.5
Y (Along-track)	10	9.99445	0.362	3853
Z (Cross-track)	10	10.00000	4.322	3729

Table 5-3: Response Parameters (Time Invariant J_2 Model Design)

The total ΔV for the manoeuvre within one orbit (evaluated for 1-second time steps) was found to be

$$\mathbf{\Delta V = 0.05968\ ms^{-1}}$$

5.3.1.3 LTI Controller Design Comparison

The design study reported in this section is tailored to a specific scenario. However, it has demonstrated that acceptable response characteristics can be achieved using both the Hill and high-fidelity time invariant J_2 models. Only very small differences between the designs could be observed from the response graphs and gains (the latter were slightly higher for the J_2 model). Comparisons are more easily made using the response data in Table 5-2 and Table 5-3.

The design for the time invariant J_2 controller enabled marginally greater maximum thrust to be applied within the design requirements. The most visible effect of this and the improved dynamics modelling was through the cross-track model behaviour. Clear reductions in both % overshoot and settling time were visible, and the total ΔV over one orbit (including the 10m offset manoeuvres).

One potential issue with the control designs so far is the size of the elements of the constant gain matrices as these are very small. In addition, the state matrices are not well conditioned, and a more robust design procedure would involve the normalisation of the equations of relative motion to eliminate the orbital rate term, n. However, for this investigation, the addition of further complexity by converting between non-dimensional and dimensional parameters was avoided as STK requires the dimensional physical values of relative position, velocity and acceleration, and the effect of introducing additional complexity on the processing time and general implementation of the Matlab/STK interface was unknown.

In the Matlab environment, and for this particular manoeuvring task, the reduction in ΔV due to the J_2 model was found to be 2.37%. However, this is not an important parameter as the design evaluations performed using the Hill controller used the Hill equations as the formation flying model in the loop, and the time invariant J_2 controller was used with the time invariant J_2 model in the loop. Also, only simple observations could be made of the ability of the controllers to perform station keeping tasks. In order to make a physical comparison between the controllers, they need to be implemented in the same J_2 perturbed (and realistic) space environment, for example, that created by the STK Astrogator numerical orbit propagator.

The scenario proposed for implementation in STK can be more easily visualised with the block diagram in Figure 5-14. A desired separation is specified to the follower satellite through the 'Reference' input. The satellite 'onboard processor' uses the measured relative position and velocity information to calculate the error from desired position and velocity, and multiply the error by the feedback gains designed using the Hill and time invariant J_2 models. A corrective acceleration is calculated by the controller and output to the satellite thrusters within STK. STK then propagates the satellite in the perturbed environment (the range of disturbances applied can be user selected) while controller inputs are applied. From this model, formation keeping measurements are extracted from STK and the accelerations applied can be used to calculate fuel use as ΔV.

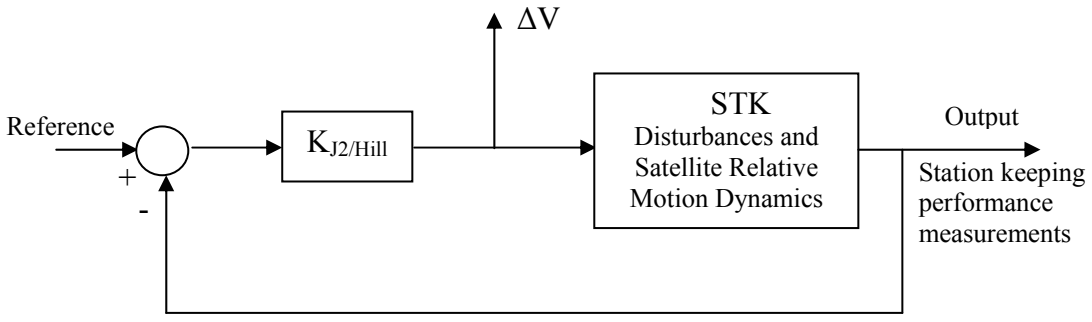

Figure 5-14: Block Diagram to Illustrate the Control Law Implementation with STK in the Loop

5.3.2 Linear Time Varying J_2 Model

An offline study was not performed for the time varying J_2 dynamics model. One of the advantages of the approach described in section 5.2.2 is that the off-line analysis is not required provided that certain parameters are monitored during the controlled formation flight in STK. In particular, the effects of the weighting matrices, Q and R, (which remain constant although the state matrix updated at each time step) should be investigated through the simulation of a range of scenarios. The elements of Q and R selected for the time averaged (invariant) J_2 model provide a suitable starting point. In addition to examining the controller performance and evaluating the ΔV, the variation in the gains throughout the orbit can be identified. The details of the time varying J_2 controller design are therefore considered during the controller evaluation and comparison in section 5.5.

5.4 Control Law Implementation

In this section, the implementation of the Hill, time invariant and time varying J_2 controllers within the STK environment is discussed. The feasibility of this approach to control system evaluation is explored for a number of test cases, and the strategy for scenario initialisation is presented. Control system performance is evaluated in section 5.5.

5.4.1 Plug-In Scripts for the Onboard Controller

The Matlab controller must be implemented in the STK environment through the Matlab/STK interface. This level of interaction is achieved through the STK Plug-In Scripts tool which allows the user to create scripts (written, for example, in Matlab) that integrate with STK's in-built software.

Scripts can be used to perform tasks such as modelling additional forces and time varying parameters which act on or affect an object which is being propagated within the STK Astrogator propagator application. Effectively, the script becomes the 'onboard controller' for the satellite selected, and each script will contain one input argument and one output argument. The script has two main functions

- To register inputs and outputs for the compute function
- To compute outputs based on the inputs

For the registration of inputs and outputs, a descriptor for each of the requested arguments is specified with an identifier for STK to interpret. Settings were also selected to ensure that the additional control accelerations computed by the script were added to the STK orbit accelerations experienced by the satellites in a Cartesian manner. After the declaration of inputs and outputs, the remainder of the Matlab script computes the accelerations to be applied to the controlled satellite (effectively through its own thrusters) and outputs the values back to STK under the variable name specified during

the registration of variables. The resulting script must be then embedded at the correct point within the Astrogator propagator in STK.

All propagators have five Entry Points which define where the script will be calculated in the overall propagation of a scenario. These are Pre-propagation, Post-propagation, Segment start, Update, and Eval. Eval means that the script is called at every force model evaluation to return an additional acceleration or to change parameter values, which is the operation that is performed in this series of simulations.

The propagation routine takes considerably longer when a script file is included. For the scenario operating without a Matlab script, the propagation of one satellite for one orbit take approximately 2 seconds. When the Matlab script was included to calculate motion using the simple feedback gains designed using the Hill or time invariant J_2 model, the propagation time for the satellite was substantially increased. On the same processor, the propagation time for the satellite with the time varying gain recalculation increased by a further 60%.

After propagation, the relative motion of the satellites can be viewed through the STK visualisation windows, and relative positions and velocities and other parameters can be obtained through the STK graph and reporting functions. Any parameters declared in the script and the Matlab workspace as global can also be extracted through Matlab. The calculation of ΔV was performed after the propagation using separate data extraction programs to obtain thruster accelerations from STK.

5.4.2 Data Extraction

Following the successful integration of the controller with the numerical orbit propagator, the simulation results can be accessed through the Matlab/STK interface. The variables accessed from the Plug-In script in Matlab are:

- Computation number
- Time
- Radial acceleration (Fx)
- Along-Track Acceleration (Fy)
- Cross-Track Acceleration (Fz)

Figure 5-15 and Figure 5-16 illustrate the variation in time and radial acceleration with iteration step respectively.

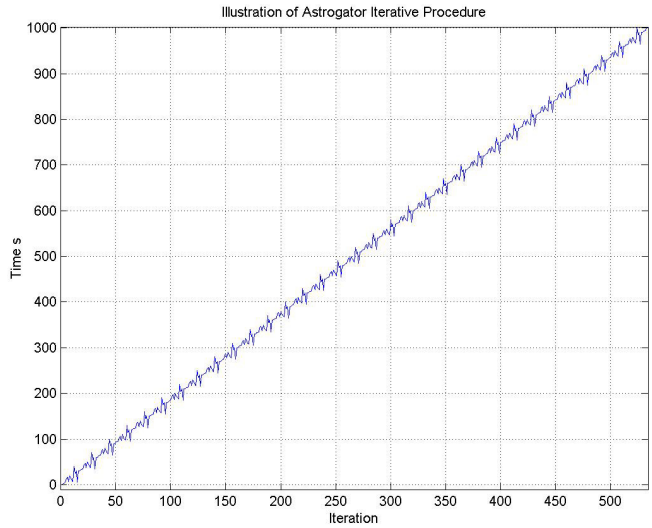

Figure 5-15: Variation of Time with Iteration in the Astrogator Propagator

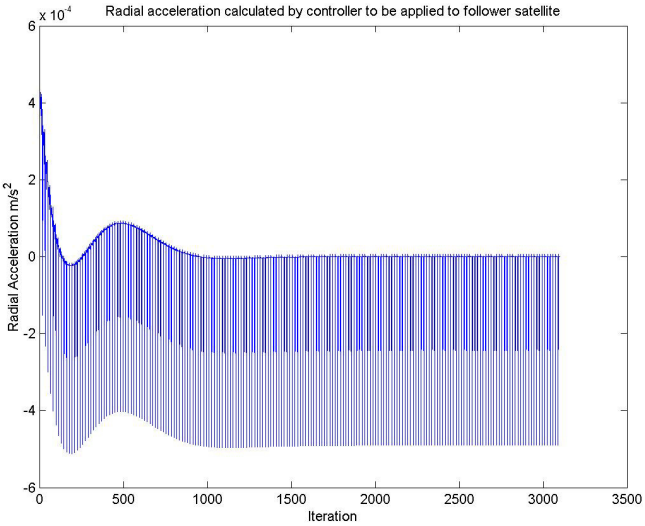

Figure 5-16: Radial Acceleration Computed by the Controller at Each Iteration for an Along-Track Manoeuvre from 97.7m Separation to a Desired 50m Separation

For the purposes of control law evaluation, it is necessary to ascertain the fuel requirements for the station keeping task. This is measured in velocity (acceleration over time) and therefore it is necessary to establish suitable points for the extraction of acceleration and time data from the script file. In its current form, the output accelerations cannot be summed directly over a prescribed period of time. Figure 5-15 illustrates how the time data points jump backwards and forwards as Astrogator iterates until it reaches the set tolerances and progresses to the next calculation. Both of the figures show that the Matlab script is also computed at each of these iterations as well and the result is the static around a sensible acceleration profile.

In order to evaluate the acceleration data at suitable intervals, and avoid the problem with static, it is necessary to select Astrogator Numerical Integrator properties so that

the Astrogator ephemeris time steps are the same for both the leader and follower satellites. The STK reporting function can then be applied to calculate highly accurate relative position data and also the accelerations at the ephemeris time step. In this study, the ephemeris time step was set to 30 seconds, below the minimum naturally selected by the propagator at the defined tolerance (10^{-13}). Of course in general for the same number of orbits, the smaller the time step, the longer the propagation will take. The effects of using a smaller time step in the simulations are considered in section 5.5.

The data extraction routine uses the STK relative position and velocity to calculate the error from the desired state, and applies the LQR gains to these errors. The resulting accelerations that would have been applied during the scenario are summed over the duration of the simulation (this can be restricted to the duration of a particular manoeuvre if necessary) and divided by the measured time to compute the ΔV. Graphs illustrating the cumulative ΔV during the simulation are produced, although any other variables of interest can be easily accessed.

Figure 5-17 illustrates the radial acceleration output for the same example illustrated in Figure 5-16. This method of data extraction was found to be successful in eliminating the static on the earlier results.

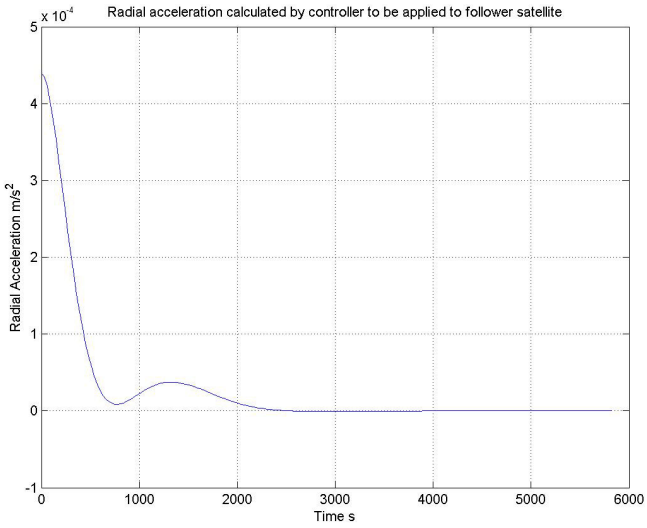

Figure 5-17: Radial Acceleration Computed by the Controller Using Astrogator Propagating at 30 second Time Steps for an Along-Track Manoeuvre from 97.7m Separation to a Desired 50m Separation.

5.5 Control System Evaluation

The results of the control system evaluations are presented in this section. Two types of practical satellite formation are investigated to demonstrate the performance of each controller for station keeping (fixed offset) or formation keeping (trajectory following) of two satellites in LEO. These include:

- ***Along-Track Formation*** (General Test Case r_{ref}=7000km, i_{ref}=35^o)
- ***Circular Formation*** (Sun Synchronous orbit r_{ref}=7000km, i_{ref}=97.87^o)

The along-track formation investigation comprises two scenarios. The follower satellite is constrained to follow the leader (or 'reference') while maintaining a constant along-track offset. In addition, the basic operation of the controllers is investigated by giving the formation an error offset from desired, equivalent to the design manoeuvre described in section 5.3.1.1.

The circular formation also comprises two related scenarios. Both scenarios involve the maintenance of a 1km circular formation; one derived from the solutions to the Hill equations, and the second derived from the solutions to the time invariant J_2 model (refer to section 4.4 chapter 4). Comparisons of the cost of maintaining the circular formations in the presence of J_2 perturbations using the different control systems are performed. A 1km radius was selected to enable the formation to experience greater disturbance and inter-satellite separation than the along-track case, and thus offer the potential to provide greater contrast in formation design and control system performance. In addition, the ΔV evaluated for this scenario can be compared to the results of other related studies in the literature (Table 3-6, chapter 3).

The final subsection presents the results of further investigations into the effects of initial conditions (derived from the relative dynamics models) and additional external environmental disturbances imposed upon the formation in the STK environment.

5.5.1 Along-Track Station Keeping

The General test case is the scenario considered for the controller design in section 5.3, and also applied in the model verification process in chapter 4. For the control system evaluation, the following scenario details were specified:

- *Formation-type:* Along-track, leader-follower architecture.
- *Task 1:* Station keeping, with the follower satellite given a y-offset of 50m from the leader or reference. This must be maintained in the presence of the J_2 perturbation.
- *Task 2:* Performing a manoeuvre from a radial offset of 10m, cross-track offset of 10m, and along-track offset of 60m back to the desired y-offset of 50m (simultaneously controlling all three axes).
- *Reference Orbit:* Orbit radius r_{ref}=7000km, inclination i_{ref}=35^o.

As the design test case (Table 5-1) optimises the controller for the second (manoeuvring) task, the required accuracy for the station keeping task was not specified, other than that a significant reduction in the relative motion should be observed. In this section the STK response of the uncontrolled formation is presented (note that only an along-track offset was provided in the initial conditions, and zero relative velocity). The following subsections evaluate the performance of the Hill equations, time invariant J_2 model and time varying J_2 model controllers for these along-track formation flying scenarios. (Note that the manoeuvre scenario (Task 2) was also used for controller design for the time varying J_2 model).

Initially, the J_2 perturbation force was selected to be the only disturbing force applied to the satellites within the STK Astrogator propagator. Figure 5-18 a, b and c illustrate the

effects of this force on the relative motion over one orbit of two uncontrolled satellites in the leader-follower formation described above.

The relative radial motion over one orbit is small, and varies between ±1.9cm. The along-track relative position is displaced by a maximum of just over 16cm before returning to desired separation after one orbit, and the peak cross-track motion is very small at almost 0.115mm half way around the orbit. For illustration, the corresponding in-plane and cross-track relative velocities are included as Figure 5-19.

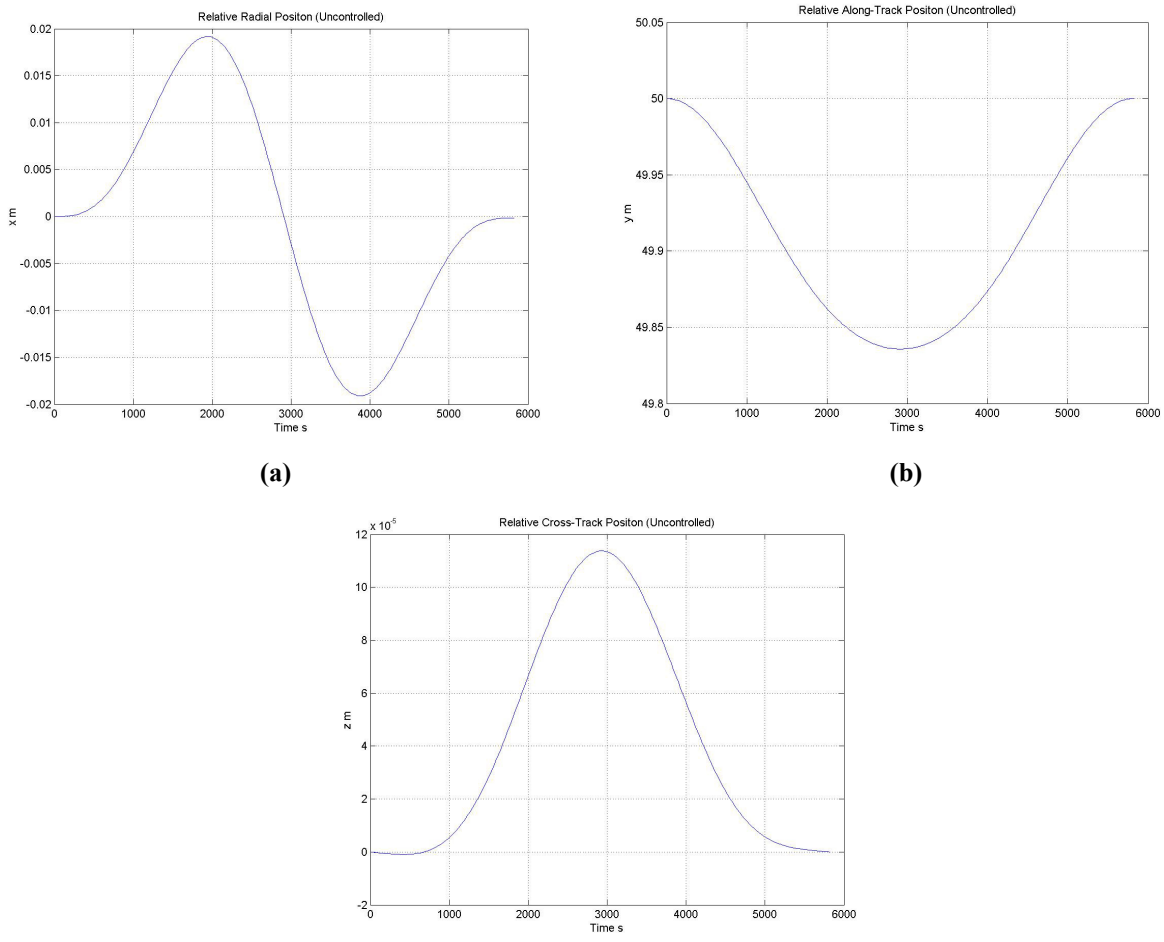

Figure 5-18: Relative Position of Two J_2 Perturbed Satellites (STK results for i=35°, r_{ref}=7000km, Initial Along-Track Separation 50m) (a) Radial (b) Along-Track (c) Cross-Track

If the initial relative position or velocity is offset from desired, then the controller is expected to eliminate this velocity error and drive the satellites back to their correct position efficiently. For the purposes of comparing the controllers and evaluating the ΔV for the station keeping task, it is however important that in all cases the initial conditions be the same.

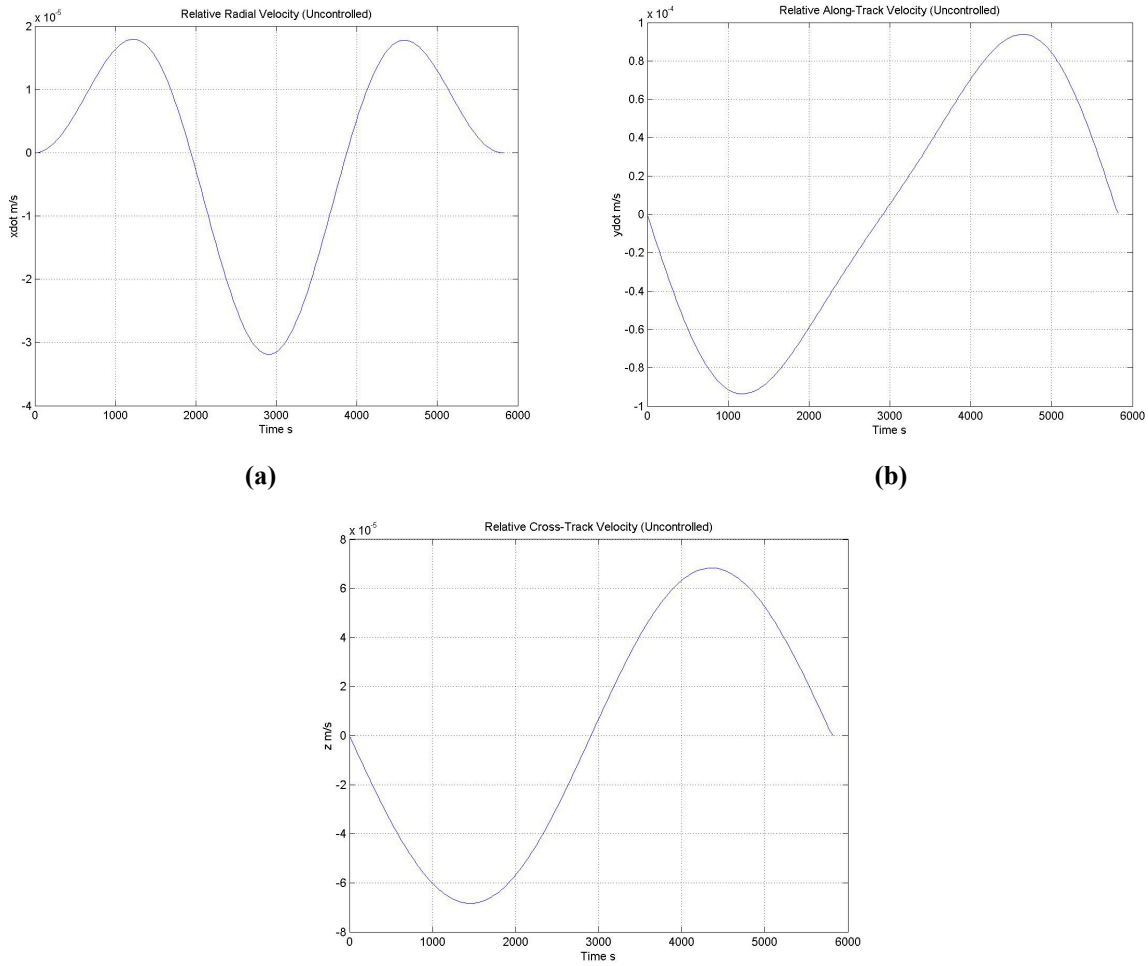

Figure 5-19: Relative Velocity of Two J_2 Perturbed Satellites (STK results for i=35°, r_{ref}=7000km, Initial Along-Track Separation 50m) (a) Radial (b) Along-Track (c) Cross-Track

5.5.1.1 Hill Controller

The feedback gains designed using the Hill equations were applied to the follower satellite in all three axes (equations (5-24)). The satellites were given an initial along-track separation and the initial relative velocity of the spacecraft was zero. Additional initial impulsive manoeuvres to minimise formation separation from the virtual circular reference orbit were not applied in the first instance (the role of these initial conditions was established in chapter 4, and is investigated further in section 5.5.3.1).

The relative motion observed for the station keeping task over one orbit when the Hill controller was applied to the follower satellite is illustrated below.

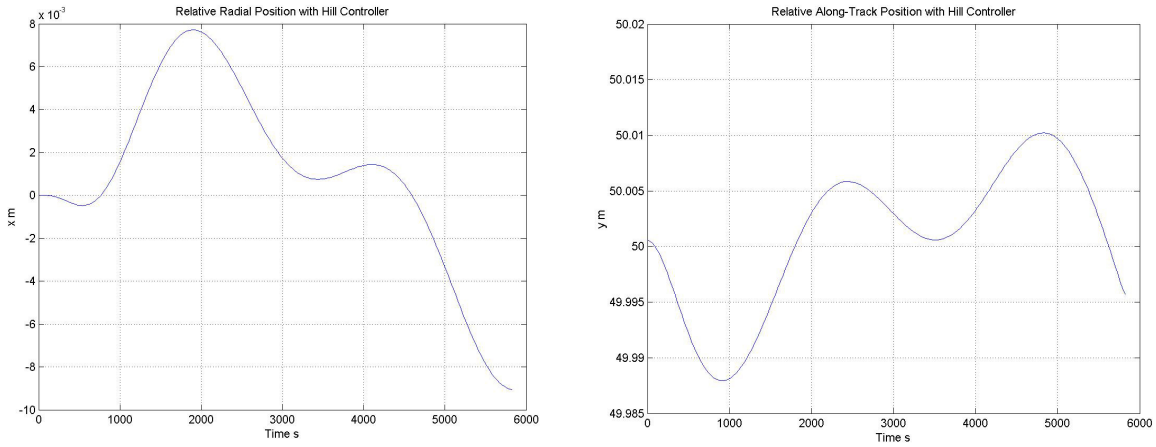

(a) **(b)**

Figure 5-20: Effect of the Hill Controller on the Relative In-Plane Motion Between Satellites in the J_2 Perturbed Environment (STK Results for i=35°, r_{ref}=7000km, Initial Along-Track Separation 50m) (a) Radial (b) Along-Track

When compared to Figure 5-18a, Figure 5-20a shows that the relative radial motion has been reduced with the application of the controller. Figure 5-20b illustrates a reduction in along-track motion compared to Figure 5-18b from over 16cm to less than 1.5cm. The shape of the response results from the cross-coupled proportional and derivative feedback from the along-track and radial directions. The scenario was propagated for five orbits, and the relative in-plane motion illustrated above repeated with very small, almost negligible drift. These results are included as Figure 5-21. Cross-track relative motion remains negligible in all cases.

Clearly the controller has proved beneficial in reducing the relative motion for the station keeping task. For a continuous controller with acceleration evaluations made at 30-second time steps, the total ΔV to achieve station keeping at this level was found to be (based on the extrapolation of a 5-orbit simulation):

$$\mathbf{\Delta V_{year} = 4.04735\ ms^{-1}yr^{-1}}$$

Controller performance can be observed more clearly in terms of response to an initial 10m error simultaneously in the radial, along-track and cross-track directions. Figure 5-22a and Figure 5-22b illustrate the successful operation of the controller in response to an initial position error. The manoeuvre takes place over approximately half an orbit, and applies a maximum initial acceleration of approximately $0.29 mms^{-2}$. (Identical results to those of the design case are not expected, and this slightly higher initial acceleration is perfectly acceptable). For particular design requirements, the weighting matrices in the LQR design could be adjusted again.

The cumulative acceleration applied over one orbit, including the 10m manoeuvre, was converted to ΔV. The resulting 'fuel use' for the Hill controller was found to be:

$$\mathbf{\Delta V = 0.0818806\ ms^{-1}}$$

This is comparable to the design point ΔV, evaluated in idealised conditions, which was found to be $\Delta V = 0.06113 ms^{-1}$ (refer to section 5.3.1.2).

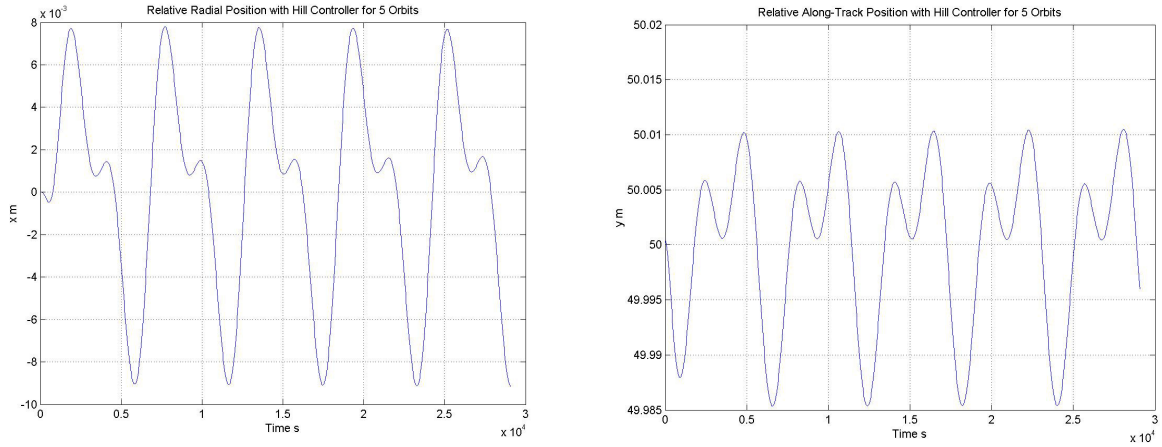

(a) **(b)**

Figure 5-21: Effect of the Hill controller on the Relative Position Between Satellites in the J_2 Perturbed Environment over 5 Orbits (STK Results for i=35°, r_{ref}=7000km, Initial Along-Track Separation 50m) (a) Radial (b) Along-Track

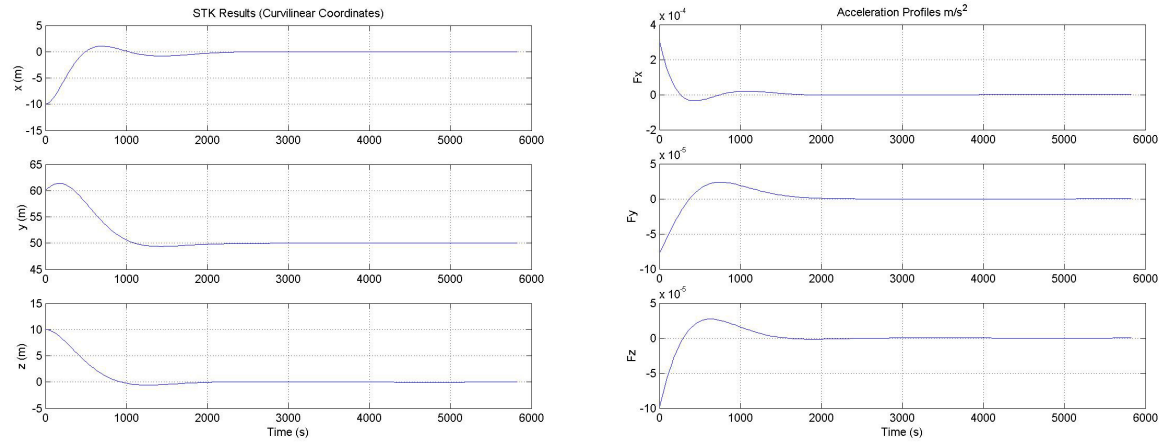

(a) **(b)**

Figure 5-22: Response of the Hill Controller to a 10m Relative Position Error Between Satellites in the J_2 Perturbed Environment Over 1 Orbit (STK Results for i=35°, r_{ref}=7000km, Desired Initial Along-Track Separation 50m) (a) Relative Position (b) Corrective Accelerations Applied

5.5.1.2 Time Averaged J_2 Controller

The same test case was applied using the time averaged (invariant) J_2 model controller gains to replace the Hill model gains. The new controller was applied within STK to the follower satellite of the leader-follower two-satellite formation. Again, the satellites were required to maintain a 50 metre along-track (y) separation in an orbit inclined at 35° and with an orbital radius of 7000km. No 'zero drift and offset' conditions were applied, and for the evaluation of the station keeping task, the scenario was initialised with the satellites already at their desired location, with zero relative velocity.

The relative motion observed for the station keeping task over one orbit when the time invariant J_2 controller was applied to the follower satellite is illustrated in Figure 5-23.

Compared to Figure 5-18, Figure 5-23 also shows that the relative motion has been reduced with the application of the time invariant J_2 controller. However, the responses are almost identical to those obtained with the Hill controller (Figure 5-20).

The same conclusions can therefore be drawn for the time invariant J_2 controller as for the Hill controller. The controller has proved beneficial in all axes in reducing the relative motion for the station keeping task. For a continuous controller with acceleration evaluations made at 30-second time steps, the total ΔV required to perform the station keeping task was found to be (based on the extrapolation of a 5-orbit simulation):

$$\mathbf{\Delta V_{year} = 4.04695\ ms^{-1}yr^{-1}}$$

This is a small reduction in ΔV compared to that achieved by the Hill controller. However, unlike the design case, the time invariant J_2 controller was marginally less efficient when subject to the 10m manoeuvre. The relative position and acceleration responses were almost identical to those illustrated in Figure 5-22. Over one orbit the ΔV required was found to be:

$$\mathbf{\Delta V = 0.0818941\ ms^{-1}}$$

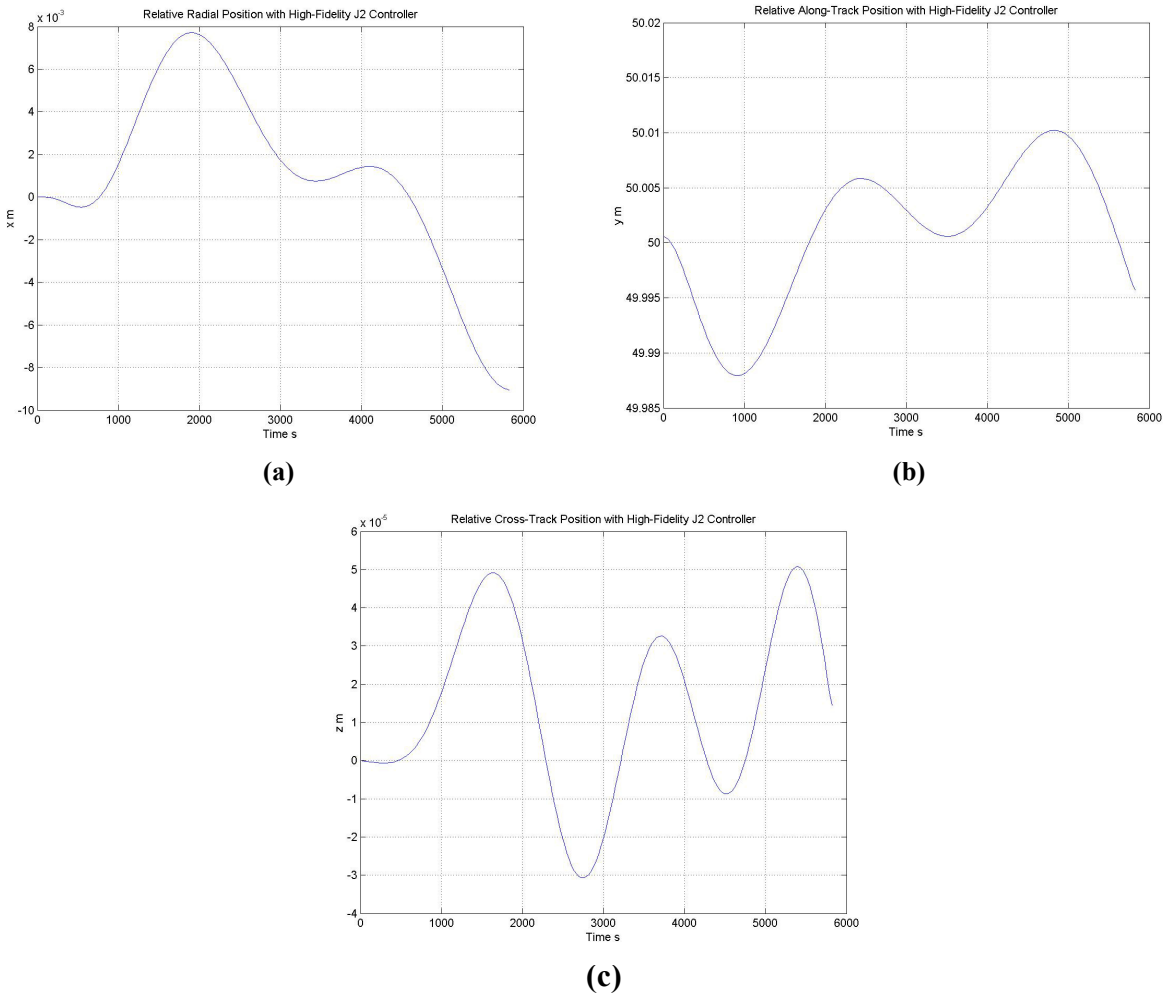

Figure 5-23: Effect of the Time Invariant J_2 Controller on the Relative Motion Between Satellites in the J_2 Perturbed Environment (STK Results for i=35°, r_{ref}=7000km, Initial Along-Track Separation 50m) (a) Radial (b) Along-Track (c) Cross-Track

5.5.1.3 Time Varying J_2 Model

An offline study was not performed for the time varying J_2 dynamics model and instead, the effect of the weighting matrices was investigated through observation of controlled relative motion in STK. The design test case was the three-axis 10m manoeuvre scenario, already performed using the Hill and time averaged J_2 model controllers.

The design process involved the initial selection of Q and R (which remained constant during the scenario), and the propagation of two J_2 perturbed satellites with 10m offsets in x, y and z from the desired along-track relative position. At each propagation time step (30 seconds), the state matrix was evaluated and applied to LQR design to obtain a time varying gain matrix. The gain values were recorded during the simulations for monitoring, and relative positions, velocities, and controller accelerations were observed as a measure of design performance. The design parameters identified for the LTI models could not be directly applied here, as the numerically perturbed environment did not represent an equivalent situation. For example, the 'settling time to within 1mm' criterion did not occur as controlled relative position continually varied at the 10mm level. Instead, the gains were tuned to produce similar results to those observed in Figure 5-22. The resulting Q and R matrices were similar to those obtained using the LTI models (the in-plane weightings in R were slightly increased), and the mean gain matrix for this example is given by equation (5-28). The equivalent terms in the coupled matrix (5-28) are of similar order of magnitude to the time invariant J_2 model gains, decoupled in x-y and z, in equation (5-26). Terms representing feedback between in-plane and cross-track motion, highlighted by underlining in the matrix, are very small.

$$K_{xyz} = \begin{bmatrix} 5.7399e-3 & 1.3602e-4 & \underline{1.243e-9} & 1.6776e-5 & -5.7983e-6 & \underline{2.38e-12} \\ 1.3602e-4 & 5.1348e-3 & \underline{-4.016e-9} & 5.9723e-6 & 1.290e-5 & \underline{-1.430e-11} \\ \underline{6.2130e-10} & \underline{2.0082e-9} & 4.2195e-3 & \underline{6.2e-13} & \underline{-1.284e-11} & 8.9020e-6 \end{bmatrix} \quad (5\text{-}28)$$

However, the gains vary around the orbit, some at twice the frequency of the others, according to the frequency of terms in the time varying state matrix (given by equations (4-58) to (4-60) in chapter 4). Table 5-4 illustrates the maxima and minima of the gains throughout their cycle, and demonstrates that the cross-coupling gains not present in the LTI models do contribute to the controlled response even though they average to almost zero around the orbit.

	x velocity	**y velocity**	**z velocity**	**x position**	**y position**	**z position**
Radial	5.741e-3 5.739e-3	1.366e-4 1.354e-4	1.695e-6 -1.695e-6	1.678e-5 1.677e-5	-5.794e-6 -5.803e-6	6.550e-9 -6.548e-9
Along-Track	1.366e-4 1.354e-4	5.135e-3 5.134e-3	5.643e-7 -5.642e-7	5.975e-6 5.970e-6	1.290e-5 1.290e-5	1.601e-9 -1.601e-9
Cross-Track	8.476e-7 -8.475e-7	2.822e-7 -2.821e-7	4.220e-3 4.219e-3	5.598e-9 -5.597e-9	1.305e-9 -1.305e-9	8.904e-6 8.900e-6

Table 5-4: Maximum and Minimum Gains for the Along-Track Formation Flying Scenario

For the 10m manoeuvring scenario, a slightly reduced fuel consumption was observed over 1 orbit compared to the ΔV calculated for the Hill and time invariant J_2 controllers,

however the manoeuvre response observed was marginally slower. In this case, fuel consumption was given by:

$\Delta V = 0.0806151\ ms^{-1}$

Evaluating the controller in this 'real' perturbed environment revealed that varying the Q and R matrices significantly affects control system performance. For example, by increasing Q by a factor of 10 (to reduce the error more quickly in the optimal response), the time varying controller produced a more rapid manoeuvre response using a greater initial thrust, and ultimately consumed more fuel over 1 orbit while keeping tighter control of the formation. Of course, further refinement of the design requires mission specific criteria to be provided as a baseline. Figure 5-24 illustrates the relative position response and accelerations applied by the time varying J_2 controller for an along-track satellite formation requiring the elimination of a 10m initial offset error in all three axes. Figure 5-24a and Figure 5-24b illustrate the relative position response and controller accelerations for the design point gains (equation (5-28)), and Figure 5-24c and Figure 5-24d illustrate the same manoeuvre response for the high-Q design. A higher Q weighting caused an increase in mean gain for most elements of the gain matrix, but not in all. On-axis gains increased, and the feedback of radial position and velocity to along-track motion also increased. The feedback of along-track velocity and radial position to radial motion decreased. The associated response, illustrated in Figure 5-24 (c and d), is more rapid with less overshoot, and demonstrates the ability of the controller to hold the desired relative position more accurately in the presence of J_2 perturbations. The acceleration demands are clearly increased, particularly for the initial corrective manoeuvre.

Table 5-5 summarises the main response parameters and their change due to the ten-fold increase in the state weighting matrix (Q) in the controller design for the time varying J_2 model (for a 30-second simulation time step). This increase in Q caused a 40% increase in ΔV, but the response amplitude data demonstrates that a better precision is achieved.

	ΔV (1 orbit) (ms^{-1})	**Maximum Acceleration (ms^{-2})**	**x Response Amplitude (mm)**	**y Response Amplitude (mm)**	**z Response Amplitude (mm)**
Low Q	0.0806	2.3×10^{-4}	11	8	29
High Q	0.1317	5.1×10^{-4}	4	2	17

Table 5-5: Response Parameters for Two Different LQR Designs for the 10m Manoeuvre in the General test case Along-Track Formation Flying Scenario

Having established suitable weighting matrices (Q and R), the variation in reference orbit characteristics (inclination and radius) are automatically taken into account in the onboard controller design. These changes produce small variations in the gain matrix for all the designs (time invariant and time varying).

Another important variable to confirm the validity of the ΔV measurements established in the test cases performed so far is the effect of simulation time step. This was initially selected to be 30 seconds for the following reasons:

- To provide an interval sensitive enough for ΔV measurement and controller comparisons.
- To limit computational effort and propagation time during the analysis.

This time scale lies well within the ability of most sensors to measure the relative position and velocity of satellites in orbit (approximately 1 second for systems with dedicated processing support).

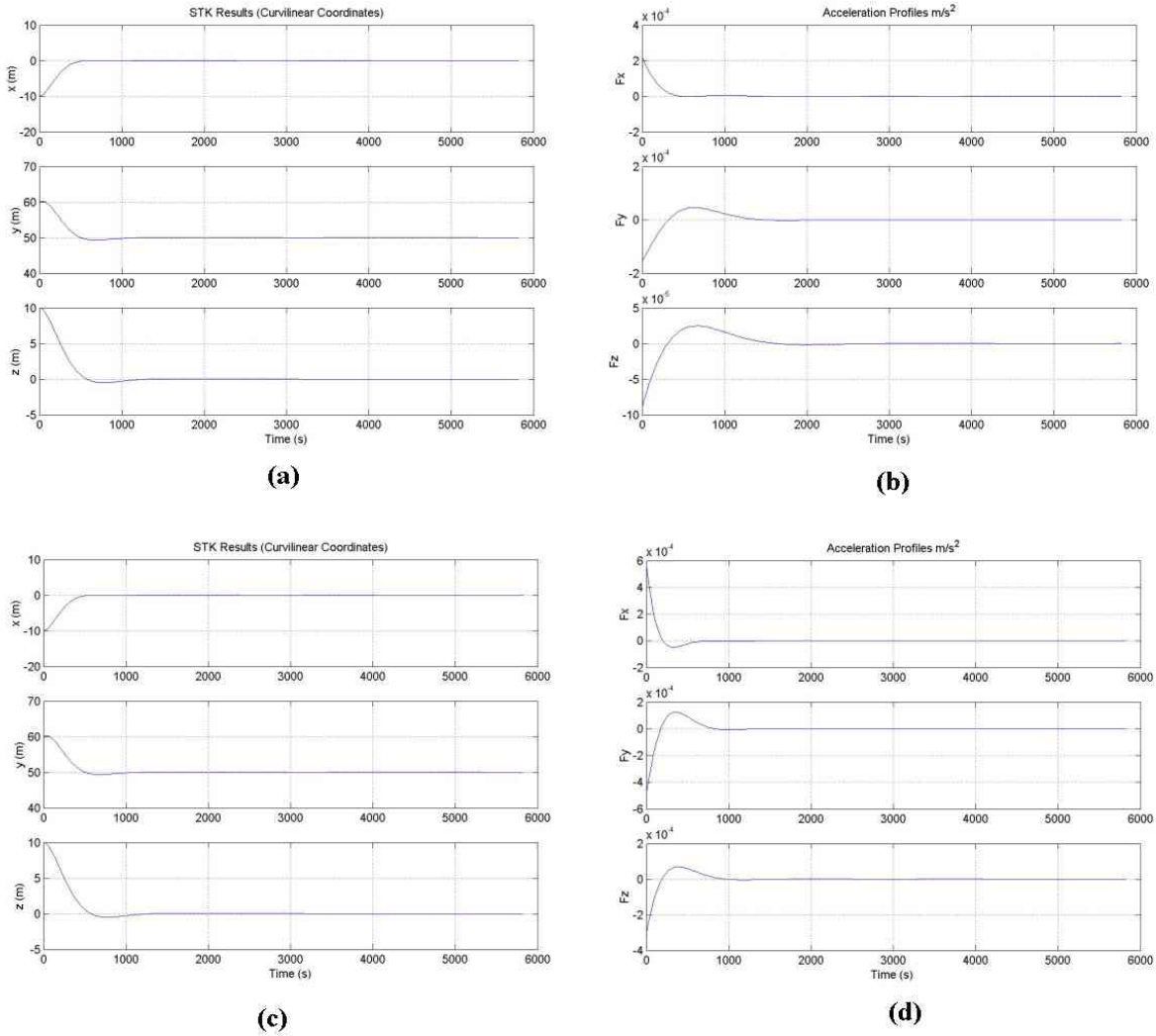

Figure 5-24: Response of the Time Varying J_2 Controller to a 10m Relative Position Error Between Satellites in the J_2 Perturbed Environment Over 1 Orbit (STK Results for i=35°, r_{ref}=7000km, Desired Initial Along-Track Separation 50m) (a) Relative Position (low gain) (b) Corrective Accelerations Applied (low gain) (c) Relative Position (high gain) (d) Corrective Accelerations Applied (high gain)

The time step was reduced to 10 seconds in STK and the data extraction programmes for the time varying model controller, and a 10m manoeuvre was performed (for the General test case). The fuel use over 1 orbit was found to be:

$$\Delta V_{10sec} = 0.0776764 \text{ ms}^{-1}$$

This represents a 3.6% reduction in ΔV compared to the 30-second time step results. However, in this part of the along-track formation flying study, many other design factors have not been taken into account, for example, sensor error and measurement

noise, and other orbit perturbations. Running the models at a 30-second time step will still produce representative results for fuel consumption and provide insight into relative model behaviour.

A summary and analysis of these and other LEO along-track formation flying simulation study results are presented in section 5.6.

5.5.2 Circular Formation Keeping

The results presented in this section demonstrate the ability of the time invariant control systems to maintain a circular formation of 1km radius in the presence of the J_2 perturbation. Two trajectory following scenarios are proposed, the first associated with the solutions to the Hill equations, and the second derived from the time invariant J_2 equations of motion. In each case, the solutions are used to define the relative motion trajectories (positions and velocities), which assume the leader is at the centre of the circle. The leader satellite is free flying, and the deputy is controlled by the LQR gains (designed for the reference orbit radius and inclination) to follow each trajectory. The circular formation is unstable in the presence of J_2, primarily due to the effective inclination difference of satellites in the formation. The drift in longitude of ascending node is therefore different for each satellite, and the orbital precession must be controlled.

Due to the increase in spacecraft separation, these scenarios expose the formation to increased levels of relative orbit perturbations, and in particular, enable the investigation of cross-track performance. In addition, the use of the Hill equations solutions as trajectories can be compared to those derived from the J_2 model analysis in section 4.4.

- *Formation-type:* Circular Formation, leader-follower architecture.
- *Task:* Formation keeping, by maintaining the follower satellite in a 1km radius circular relative orbit around the leader or reference satellite in the presence of the J_2 perturbation, based on trajectories derived from the:
    - Hill equations
    - Time averaged J_2 equations
- *Reference Orbit:* Sun Synchronous, radius r_{ref}=7000km, inclination i_{ref}=97.87^o.

5.5.2.1 Trajectory Development and Test Case Description

The Sun synchronous orbit test case was selected as in addition to being a practical orbit for many applications, the relative dynamics models were verified at this condition in chapter 4 (although for a formation of much smaller radius).

The bounded solutions to the Hill equations were introduced in section 3.1.3.1, and the circular formation initial conditions were derived in section 4.4.2. The bounded solutions to the time averaged J_2 equations of motion are given for the in-plane dynamics by equations (4-61) and (4-62), and the cross-track solution was modified in rate to enable a circular formation trajectory to be generated (also described in section

4.4.2). Table 5-6 summarises the relative motion trajectories for both the Hill and time averaged J_2 models. In both cases, the relative position solutions have been differentiated to provide velocity trajectories which must also be followed to create a stable circular formation. All terms in Table 5-6 are defined in chapter 4. For the J_2 solutions, the x-y-z parameters represent relative motion between two J_2 perturbed satellites, rather than the relative motion of a single perturbed satellite relative to the reference orbit (the Δ has been omitted). n is orbital rate and s is given as a function of J_2, Earth radius, orbit radius and inclination by equation (4-69).

Three test cases are presented in this section. These include:

- Hill Trajectory Following
- J_2 Trajectory Following
- J_2 Trajectory Following with Bounded Cluster Motion

	Hill Solutions	**Time Averaged J_2 Model Solutions (Modified)**
x	$x(t)=\frac{\dot{x}_0}{n}\sin nt + x_0\cos nt$	$x(t)=\frac{\dot{x}_0}{n\sqrt{1-s}}\sin\left(n\sqrt{1-s}t\right)+x_0\cos\left(n\sqrt{1-s}t\right)$
y	$y(t)=\frac{2\dot{x}_0}{n}\cos nt - 2x_0\sin nt$	$y(t)=\frac{2\dot{x}_0\sqrt{1+s}}{n(1-s)}\cos\left(n\sqrt{1-s}t\right)-\frac{2x_0\sqrt{1+s}}{\sqrt{1-s}}\sin\left(n\sqrt{1-s}t\right)$
z	$z(t)=\frac{\sqrt{3}\dot{x}_0}{n}\sin nt + \sqrt{3}x_0\cos nt$	$z(t)=\sqrt{\frac{3+5s}{1-s}}\frac{\dot{x}_0}{n}\sin\left(n\sqrt{1-s}t\right)+\sqrt{\frac{3+5s}{1-s}}x_0\cos\left(n\sqrt{1-s}t\right)$
$\dot{x}$	$\dot{x}(t)=\dot{x}_0\cos nt - nx_0\sin nt$	$\dot{x}(t)=\dot{x}_0\cos\left(n\sqrt{1-s}t\right)-x_0n\sqrt{1-s}\sin\left(n\sqrt{1-s}t\right)$
$\dot{y}$	$\dot{y}(t)=-2\dot{x}_0\sin nt - 2x_0n\cos nt$	$\dot{y}(t)=-\frac{2\dot{x}_0\sqrt{1+s}}{\sqrt{1-s}}\sin\left(n\sqrt{1-s}t\right)-2x_0n\sqrt{1+s}\cos\left(n\sqrt{1-s}t\right)$
$\dot{z}$	$\dot{z}(t)=\sqrt{3}\dot{x}_0\cos nt - \sqrt{3}x_0n\sin nt$	$\dot{z}(t)=\sqrt{3+5s}\dot{x}_0\cos\left(n\sqrt{1-s}t\right)-\sqrt{3+5s}x_0n\sin\left(n\sqrt{1-s}t\right)$

Table 5-6: Circular Formation Reference Trajectories

For a circle of radius 1km, the initial along-track relative position of the satellites can be set to zero, and the initial radial and cross-track relative positions derived from the initial conditions specified by equations (4-67) or (4-68) for the Hill and J_2 models respectively. For the Hill scenario, the follower satellite must also be given an additional along-track velocity to create bounded in-plane motion relative to the leader.

For the J_2 trajectory analysis, two sets of initial velocity conditions were applied in turn to the formation. In both cases the follower satellite was given an additional along-track velocity to create bounded in-plane motion relative to the leader. The effects of including the initial velocity conditions to enable both satellites to maintain the orbital rate of the reference orbit were then investigated in the final test case as this is an important part of the trajectory derivation. The initial conditions applied to the three circular formation test cases are summarised in Table 5-7.

The Hill controller applied for the along-track formation flying scenario remained the same for the circular formation as the same optimal response to position and velocity error from the desired trajectory was required. The Hill equations state matrix is independent of the reference orbit inclination, therefore no further controller design was required for this Sun synchronous orbit.

Initial Conditions (m or ms^{-1})	Relative Radial Position x_0	Relative Along-Track Position y_0	Relative Cross-Track Position z_0	Relative Radial Velocity $\dot{x}_0$	Relative Along-Track Velocity $\dot{y}_0$	Relative Cross-Track Velocity $\dot{z}_0$	Additional Cluster Velocity
1. Hill	500.00	0	866.00	0	-1.078	0	0
2. J_2	500.32	0	865.84	0	-1.079	0	0
3. J_2 Bounded	500.32	0	865.84	0	-1.079	0	2.592

Table 5-7: Circular Formation Initial Conditions for 1Hill Scenario 2 J_2 Scenario 3 Bounded J_2 Scenario

However, the time averaged (invariant) J_2 controller was redesigned for the new reference orbit. The gains for i=97.87° reference orbit were slightly reduced in-plane, and the same as the i=35° design for the cross-track dynamics for the same weighting matrices. The gains were implemented in the follower satellite, and the ΔV for formation maintenance evaluated.

5.5.2.2 Simulation Results

The uncontrolled relative motion of two spacecraft subject to the J_2 perturbation in STK over 5 orbits is illustrated in Figure 5-25 for both the Hill initial conditions (blue) and the J_2 model initial conditions with bounded cluster motion (red), defined in Table 5-7. Clearly the differences are subtle, and some drift is visible for both formations. The drift associated with the Hill initial conditions is greater.

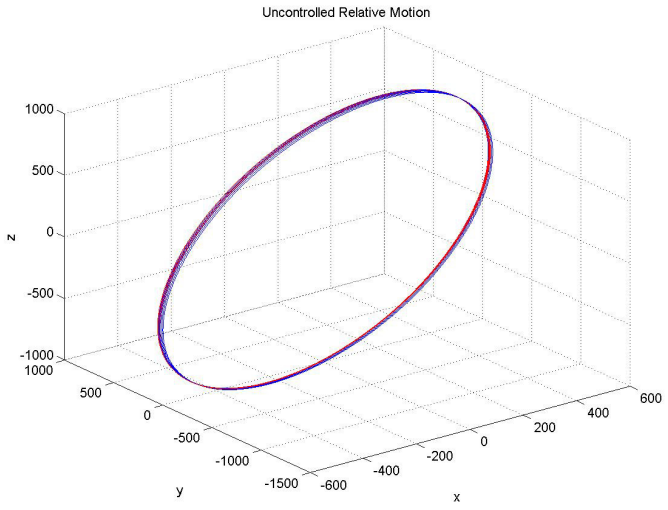

Figure 5-25: Uncontrolled Sun Synchronous Circular Formations (key blue line – Hill ICs red line J2 bounded ICs)

Figure 5-26a illustrates the Hill guidance trajectory and superimposed controlled formation response for the Hill controller, demonstrating that the drift has been

eliminated, although 20-40cm of varying position error remains (Figure 5-26b). The control accelerations imparted to the follower spacecraft during 5 orbits for formation maintenance are shown in Figure 5-26c. Similar performance can be observed for the J_2 controller maintaining the circular formation along the J_2 trajectory with bounded cluster motion (Figure 5-27). However, the cost of formation maintenance per year is reduced. The ΔV evaluated for each scenario is included in Table 5-8.

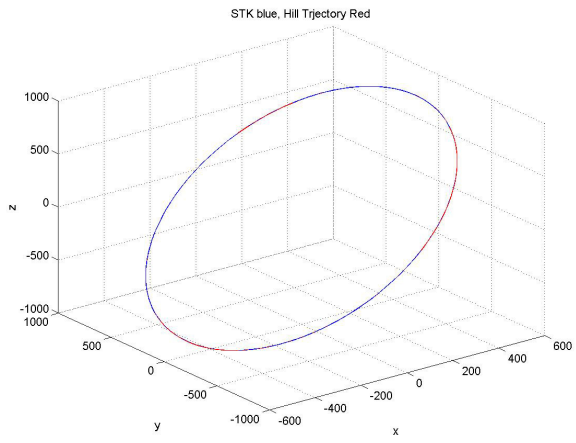

(a)

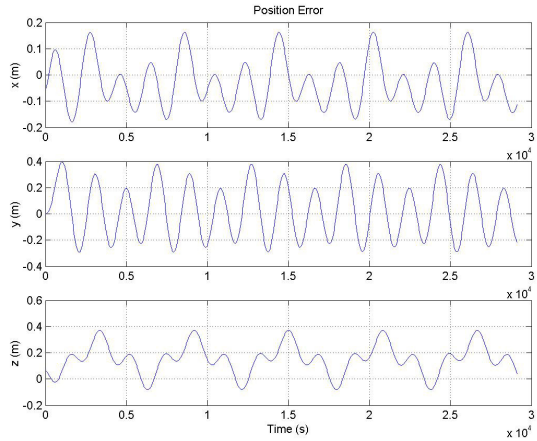

(b)

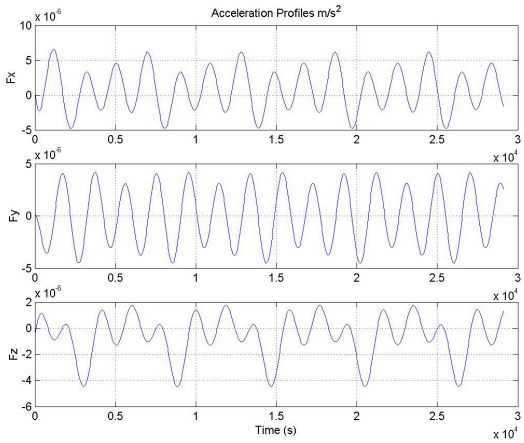

(c)

Figure 5-26: Controlled Sun Synchronous Circular Formation over 5 Orbits (Hill Trajectory and Controller) (a) Controlled STK Response (b) Position Error (c) Acceleration Profile

Trajectory/Controller	Hill	J_2	J_2 Bounded
ΔV $ms^{-1}yr^{-1}$	136.248	132.344	131.443

Table 5-8: Annual ΔV for Maintenance of a Circular Formation in the Presence of the J_2 Perturbation (based on a 5 orbit extrapolation)

Following the trajectory that takes into account the effects of the J_2 perturbation, even when a lower fidelity cross-track solution is imposed to describe a circular formation,

reduces the cost of formation maintenance compared to the cost of the Hill scenario. Giving each spacecraft in the cluster an additional along-track velocity to force the formation to maintain the orbital rate described by the reference orbit, about which the trajectory solutions are derived, reduces the ΔV further. For the circular formation, the difference between the Hill and J_2 trajectories for a 1km radius circular formation design and maintenance therefore offers a small but significant 3.32% fuel saving for a Sun synchronous orbit.

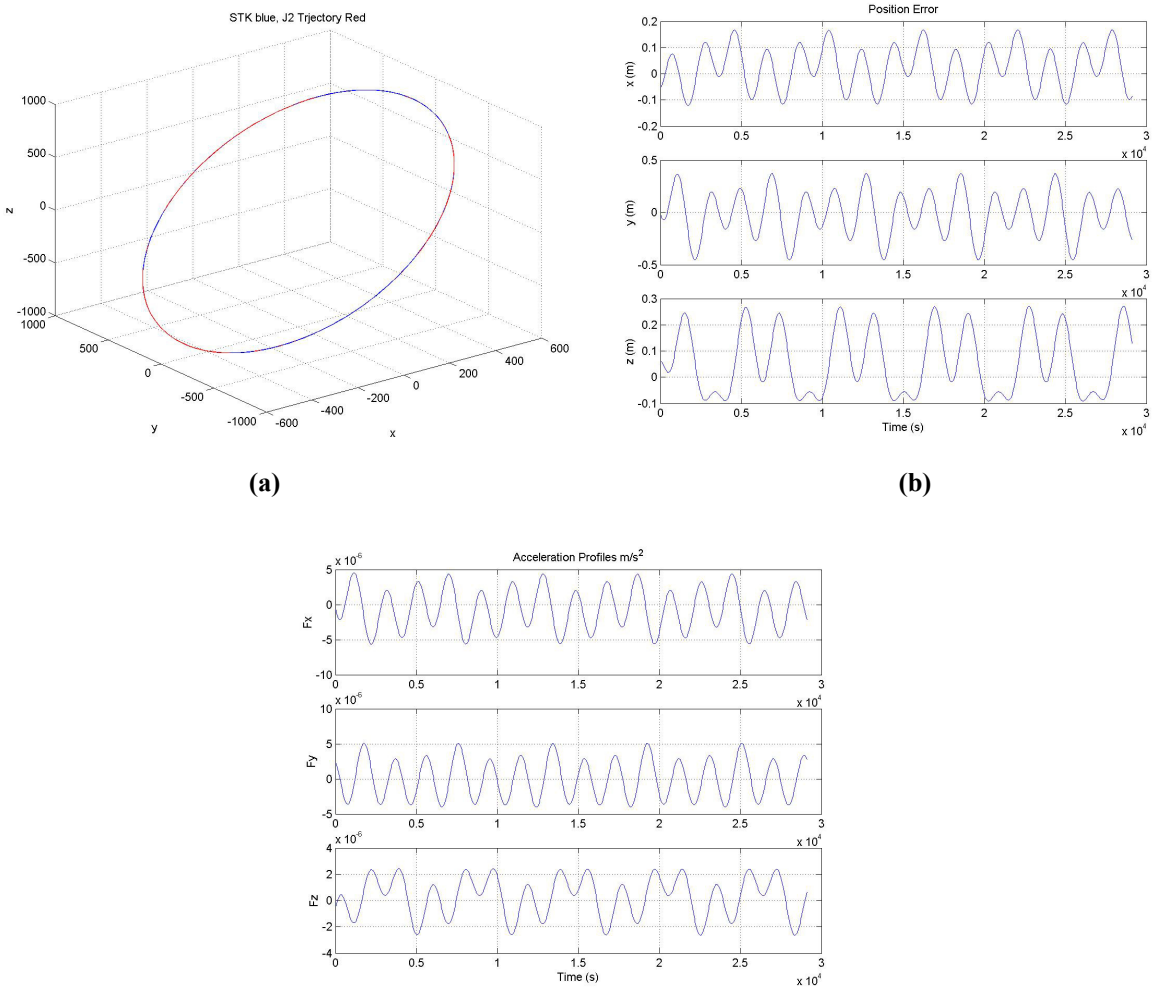

Figure 5-27: Controlled Sun Synchronous Circular Formation over 5 Orbits (J_2 Trajectory with Bounded Cluster Motion and Constant J_2 Controller) (a) Controlled STK Response (b) Position Error (c) Acceleration Profile

The effect of bounding the cluster with respect to the virtual reference orbit offers a minor ΔV reduction for the J_2 trajectory design. Analysis summarised in section 5.5.3.1 reveals that these initial conditions can have a much more significant effect at lower orbit inclinations.

Finally, it is appropriate to compare the ΔV estimates obtained for the 1km circular formation with the results published by other authors (refer to Table 3-6, section 3.1.4.1,

chapter 3). The most relevant comparisons are those for the circular and projected circular formations of 1km radius, controlled in the fully perturbed or J_2 perturbed environment. In particular, entry number 9 in the table measures the ΔV for continuous control of a circular formation using the Hill equations and sliding mode control for a 1km circular formation in the fully perturbed environment (Nelson, Sparks, and Kang, 2001). The ΔV estimated per year was $73.9 ms^{-1}$ to $93.9 ms^{-1}$ depending on the control law formulation, but the level of precision at which the relative position is maintained is not revealed. However, for the levels of precision achieved in the STK analysis presented in this section, a ΔV per year of between 136 and $131 ms^{-1}$ would seem realistic for continuous control.

5.5.3 The Effects of Initial Conditions and Additional Disturbances

This final subsection presents the results of further investigations for the along-track formation into the effects of initial conditions and additional external disturbances imposed upon the formation in the STK environment.

5.5.3.1 Initial Conditions

The effects of both zero and non-zero initial velocity conditions were investigated using both the Hill and time invariant J_2 controllers respectively. Following the results obtained in sections 5.5.1.1 and 5.5.1.2, the along-track investigations were repeated with additional initial velocity conditions which would force the formation to maintain proximity to the orbit rate and nodal drift corrected virtual reference orbit (this was referred to as bounded cluster motion in section 5.5.2.2). Additional along-track velocity was therefore applied to both the leader and follower satellites in the STK environment.

The equations describing the initial conditions to be applied were derived through the model development phase (initial conditions and their application in STK are described in sections 4.4 and 4.6 of chapter 4 respectively). Equation (5-29) describes the velocity which was applied to both the leader and follower satellites with the time invariant J_2 controller onboard the follower. The relative velocity between the satellites, which are separated by 50 metres in the along-track direction, remained zero.

$$\dot{y}_{01} = \dot{y}_{02} = \frac{3J_2 R_e^2 n^2}{8kr_{ref}}(1 - \cos 2i) \qquad (5\text{-}29)$$

Figure 5-28 illustrates the relative motion in the radial, along-track and cross-track directions, obtained when the time invariant J_2 controller was applied to an along-track formation flying scenario with modified initial conditions for the General test case ($i_{ref} = 35^o$). The initial along-track velocity applied to each satellite was 4.2475 ms^{-1} (from equation (5-29)).

One of the effects of imposing an additional along-track velocity to the spacecraft is a reduction in relative motion, leading to improved station keeping accuracy in the controlled scenario (compare Figure 5-28 to Figure 5-23). The total ΔV using the time invariant J_2 controller to achieve the improved station keeping accuracy illustrated in Figure 5-28 was found to be:

$$\Delta V_{year} = 2.970 \text{ ms}^{-1}\text{yr}^{-1}$$

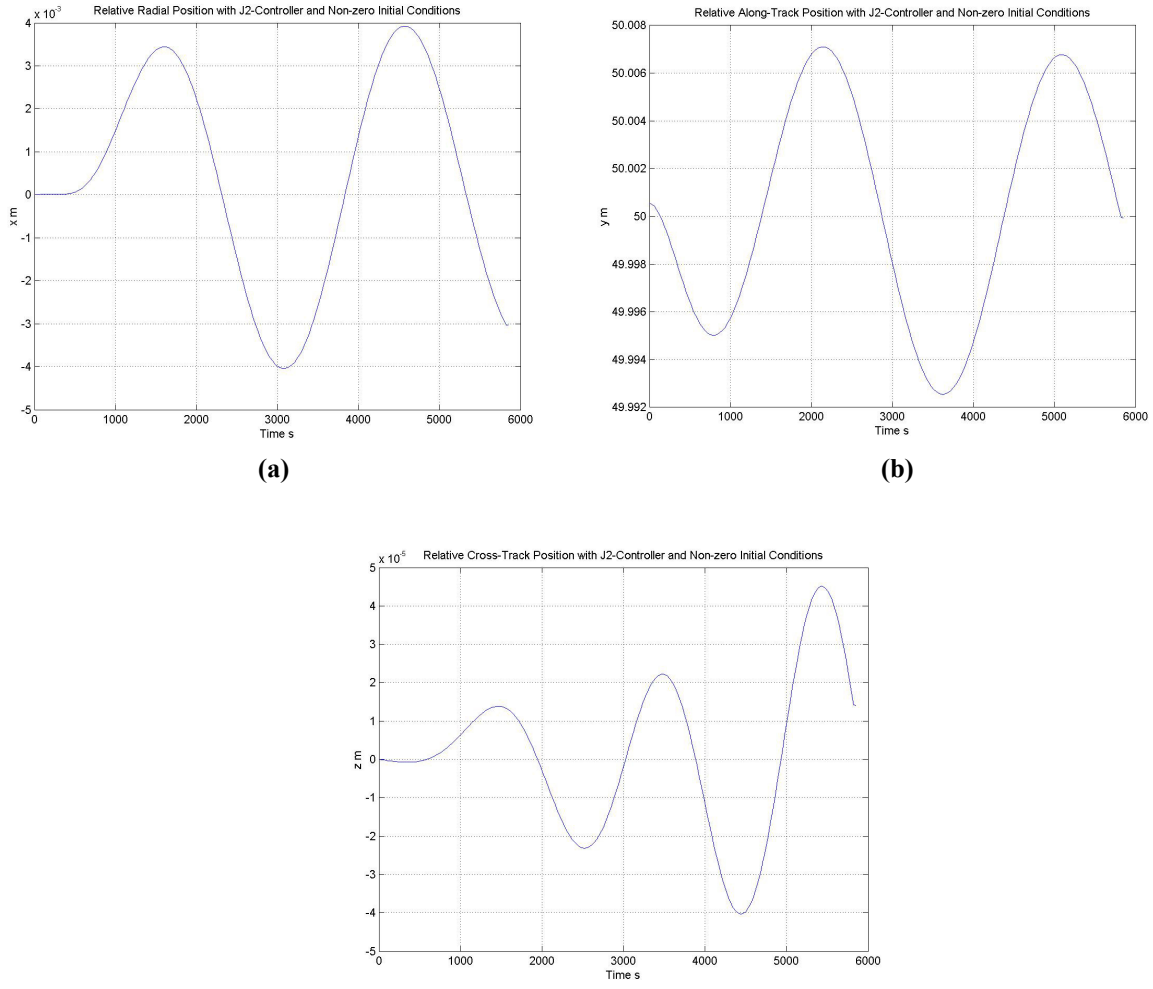

Figure 5-28: Relative Motion with the Time Invariant J_2 Controller and Non-Zero Intial Conditions (STK Results for i=35°, r_{ref}=7000km, Initial Along-Track Separation 50m) (a) Radial (b) Along-Track (c) Cross-Track

This is a reduction of 26.6% compared to the ΔV required for the zero cluster initial conditions.

The model derivation and validation work completed in chapter 4, and applied to the station keeping task described here, allows the design of along-track orbits that reduce the influence of the J_2 perturbation force and therefore reduce the control effort for the station keeping task. The addition of these initial velocities effectively circularises the

orbit and reduces the eccentricity that the J_2 perturbation force would immediately apply. The same ΔV reduction was observed for the Hill controller applied to the same scenario. The variation in effects of these initial conditions with reference orbit inclination is discussed in section 5.6.

5.5.3.2 Additional Disturbances

The in-plane relative motion of the two perturbed satellites with the follower controlled by the time invariant J_2 controller was found to be almost identical when other environmental disturbances were introduced to the scenario. The additional disturbances applied to both satellites included Solar radiation pressure, aerodynamic drag and additional geopotential terms. The magnitude of these disturbance forces depended on the satellite properties which were set in the propagator. These included drag area ($0.082m^2$), Solar radiation pressure area ($1m^2$), coefficient of drag (2) and coefficient of reflectivity (2). The controlled in-plane motion was indistinguishable from the relative motion observed in Figure 5-23 when all disturbances were applied.

The total ΔV per year required for the station keeping task was found to be:

$$\mathbf{\Delta V_{year} = 3.925\ ms^{-1}yr^{-1}}$$

In this case, the additional environmental perturbations applied to both satellites actually reduced the ΔV requirement for the along-track station keeping task. It should be noted however, that the two satellites in this formation are identical in terms of their Solar and aerodynamic ballistic coefficients, reducing further the relative effects of the additional disturbances applied.

5.6 Discussion of Results

A summary of the main conclusions from the controller evaluation is presented in this section, and the ΔV measurements for the formation flying scenarios are collated for comparison.

Along-Track Leader-Follower Formation Flying

A number of observations were made during the design and evaluation of the controlled along-track formation flying scenario. The main findings are summarised below:

- The station keeping ΔV is approximately $4ms^{-1}yr^{-1}$ for an along-track formation maintaining a 50m separation in a 35^o inclined orbit of radius 7000km, with centimetre-level precision.
- An alternative design point could easily be selected to maintain the formation to greater precision.
- The station keeping cost is increased if greater precision is required, but this can be significantly reduced by formation and initial condition design.
- The offline design of LQR controllers using the Hill and time invariant J_2 dynamics models can produce a practical system for counteracting the effects of J_2 on the formation when flown in the numerical environment.

- The controllers are able to counteract an initial offset from desired relative position (10m) in approximately half an orbit or less (deemed an appropriate period of time), while demanding suitable levels of thrust (accelerations of $10^{-4}ms^{-2}$) and velocity (cms^{-1}) in any axis, as approximated in the design case.
- Controller design can be performed online or offline using the Matlab/STK interface. In this case the time invariant controllers were designed offline, and the time varying controllers were designed online.
- Gains of a similar order of magnitude to those for the LTI models are obtained for the time varying model and similar controller performance is achieved. However, the technique provides reduced insight into the detailed effects of the varying gains on the time responses in the perturbed environment.
- The Hill equation gains, derived for a given Q and R, are the same for any inclination, but vary with reference orbit radius.
- The time invariant J_2 controller gains vary with both inclination and orbit radius for a given Q and R, but not significantly.

The context of the numerical ΔV values obtained should be noted. It has been assumed throughout this study that there is no measurement error or sensor noise, and that the system has full state knowledge. In reality, the $4ms^{-1}$ is likely to be larger to maintain a 50m offset along-track leader-follower formation and this also depends on the level of precision station keeping required, yet this is a practical value which could be implemented in a real mission.

It has been demonstrated that a greater relative position precision requirement will be more expensive for a given formation design. However, improvements in formation design can significantly reduce fuel consumption. In particular for the along-track formation, modifying the along-track velocity of the cluster at a given orbit radius to 'circularise' the orbit can achieve a significantly reduced fuel consumption in the presence of the J_2 perturbation for a given inclination.

There is minimal difference between the control gains obtained for the Hill and time averaged J_2 models when optimised for the same design point. It was clear from the design phase that the two models were very similar, and this can be observed from the in-plane state matrices of both models given below (equation (5-30)) for the General test case ($i_{ref} = 35^o$, $r_{ref} = 7000km$).

$$A_{Hill} = \begin{bmatrix} 0 & 0.002156015 & 0.000003486 & 0 \\ -0.002156015 & 0 & 0 & 0 \\ 1 & 0 & 0 & 0 \\ 0 & 1 & 0 & 0 \end{bmatrix}$$

$$A_{J2} = \begin{bmatrix} 0 & 0.002156751 & 0.000003490 & 0 \\ -0.002156751 & 0 & 0 & 0 \\ 1 & 0 & 0 & 0 \\ 0 & 1 & 0 & 0 \end{bmatrix} \qquad (5\text{-}30)$$

The dynamics are slightly different, but their effects are completely masked by the rest of the design process (the choice of Q and R). The benefits of improving model fidelity are therefore not apparent in simple LQR control for along-track relative motion. Also, only small differences in the gains were observed for the time varying J_2 model design for the same test case. However, the effects of the LQR design parameters have been established. Varying Q and R affects the controlled formation response according to the predictions of LQR theory. Most notably, increasing Q holds the formation more precisely, but demands greater acceleration and ΔV from the control system.

The role of improved dynamics models is therefore likely to be more apparent for larger formations and discretised control systems. Greater distinction between the results are anticipated if the dynamics models are used for model predictive control, and techniques which correct the relative motion errors to an advanced point in time as predicted by the controller dynamics. In this case the controllers act on the immediate error at every time step.

The effect of the simulation time step was also investigated. More accurate (and usually smaller) ΔV measurements were made using a smaller time step, but the differences were relatively small (within the margins of error associated with the simulation of a practical system), and the increase in processing time was significant. Instead, the ΔV measurements taken from this study should be considered primarily in a comparative or relative sense, rather than absolute, although they represent a good first estimate of practical formation keeping (and basic manoeuvring) ΔV.

The use of the formation design parameters associated with the derivation of the high fidelity models provides the opportunity for more efficient formation control in the presence of orbit perturbations. The effects of bounded initial conditions (with respect to the reference orbit, rather than the leader satellite) on an along-track and large (1km) circular formation were investigated and found to reduce the ΔV.

A summary of the ΔV measurements associated with the along-track scenarios described in this section and others for the MUSTANG mission are presented in Table 5-9.

The following observations were made from the results presented in Table 5-9:

- For all the 10m design manoeuvres performed, the time varying J_2 controller consumed less fuel, but produced a slightly slower and more damped response than the time invariant controllers.
- Similar fuel consumption was observed for the station keeping task for both time invariant models (Hill and J_2).
- Although not presented here, the station keeping accuracy achieved by a controller was proportional to the desired satellite separation.
- A much greater ΔV is required for station keeping at a higher inclination.
- ΔV reduction can be achieved by applying additional along-track velocity to the cluster, but the reduction is much greater at lower inclination orbits.

Scenario	Initial Conditions	Controller	Reference Orbit	ΔV (and duration)
Design 10m Initial Error Manoeuvre (3-axis) +1orbit	Δx_0=10m => 0 Δy_0=60m =>50m Δz_0=50m =>0	Hill	General (i=35^o r_{ref}=7000km)	0.0818806 ms^{-1}
Design 10m Initial Error Manoeuvre (3-axis) +1 orbit	Δx_0=10m => 0 Δy_0=60m =>50m Δz_0=50m =>0	LTI J_2	General (i=35^o r_{ref}=7000km)	0.0818941 ms^{-1}
Design 10m Initial Error Manoeuvre (3-axis) +1 orbit	Δx_0=10m => 0 Δy_0=60m =>50m Δz_0=50m =>0	LTV J_2	General (i=35^o r_{ref}=7000km)	0.0806151 ms^{-1}
Along-track Station keeping	No initial error Δy_0=50m	Hill	General (i=35^o r_{ref}=7000km)	4.04735 $ms^{-1}yr^{-1}$
Along-track Station keeping	No initial error Δy_0=50m	LTI J_2	General (i=35^o r_{ref}=7000km)	4.04695 $ms^{-1}yr^{-1}$
Along-track Station keeping	No initial error Δy_0=50m Cluster velocity 4.248ms^{-1}	LTI J_2	General (i=35^o r_{ref}=7000km)	2.970 $ms^{-1}yr^{-1}$
Along-track Station keeping	No initial error Δy_0=100m	Hill	MUSTANG (i=85^o r_{ref}=6978.1km)	17.10189 $ms^{-1}yr^{-1}$
Along-track Station keeping	No initial error Δy_0=100m	LTI J_2	MUSTANG (i=85^o r_{ref}=6978.1km)	17.10131 $ms^{-1}yr^{-1}$
Along-track Station keeping	No initial error Δy_0=100m	LTV J_2	MUSTANG (i=85^o r_{ref}=6978.1km)	14.46830 $ms^{-1}yr^{-1}$
Along-track Station keeping	No initial error Δy_0=100m Cluster 2.584ms^{-1}	LTI J_2	MUSTANG (i=85^o r_{ref}=6978.1km)	17.07668 $ms^{-1}yr^{-1}$

Table 5-9: Summary of ΔV Calculations (Along-Track Formation Flying Scenarios)

At near polar orbits, J_2 (Earth oblateness) will have a much more significant effect on an along-track spacecraft formation. The satellites will try to separate near the equator and move closer together nearer the poles, and therefore the formation is more costly to control.

Table 5-9 shows that for the 35^o inclination orbit, the additional circularising velocity reduces the station keeping ΔV by 26.6% whereas for the near polar MUSTANG 85^o orbit, the ΔV is reduced by just 0.14% (and a similar reduction is observed for the Sun synchronous circular formation scenario discussed below). This additional velocity must be higher for equatorial orbits where the net gravitational acceleration including J_2 is strongest, and it will therefore have a greater effect on the ΔV when applied. Investigating further the effects of inclination on formation keeping ΔV and formalising how this relates to the circularisation initial conditions is proposed as further work.

Formation Flying in a Circular Relative Orbit

The main results from the circular formation analysis presented in section 5.5.2 are summarised below:

- Trajectory following for circular formation keeping in the J_2 perturbed environment is possible using the Hill, time averaged J_2, and time varying J_2 controllers.
- Following the trajectory that takes into account the effects of the J_2 perturbation, even when a lower fidelity cross-track solution is imposed to describe a circular formation, reduces the cost of formation maintenance compared to the cost of maintaining trajectories defined by solutions to the Hill equations.
- The difference between the Hill and J_2 trajectories for circular formation design and maintenance therefore offers a small but significant 3.32% fuel saving for a Sun synchronous orbit and 1km formation. The potential for further ΔV reductions at other mid-inclinations (away from polar and equatorial) where cross-track relative motion is more significant should be investigated.
- Providing the circular cluster with a 'circularisation' ΔV to force the formation to maintain the orbital rate described by the virtual reference orbit, reduces the ΔV further. This additional along-track cluster velocity is likely to have a more significant effect at lower inclinations for the circular formation, as observed for the along-track scenario.
- The ΔV estimated per year for circular formation keeping ($136ms^{-1}$) is greater than that published by other researchers for a similar scenario. However, levels of station keeping accuracy were not compared, and other refinements to the control law and simulation design (for example, evaluating the ΔV using smaller simulation time steps) may reduce the ΔV.

5.7 Summary

In this chapter, the Hill equations and higher fidelity J_2 models derived in chapter 4 have been applied to control system design and performance assessment in the perturbed environment using the Satellite Tool Kit (STK). In addition, the insight into formation design and the effects of initial conditions provided through the process of model development in chapter 4 has enabled alternative methods of reducing fuel consumption for the formation keeping task in LEO to be proposed and evaluated.

The selection of the LQR technique for formation control has been justified and basic theory presented. Following the selection of a suitable design point test case (section 5.3.1.1), LQR feedback controllers were designed using three relative dynamics models:

- Hill equations (no J_2 perturbation)
- Time invariant J_2 model (Schweighart and Sedwick, 2001a)
- Time varying J_2 model

The controllers performed well when integrated into the numerical, perturbed simulation environment through the Matlab/STK interface. The opportunity to improve the design to meet different requirements was also investigated through controller tuning to achieve tighter control of relative position in the presence of different

perturbations. Control system evaluations were presented for two practical formation flying scenarios:

- Along-Track (50m separation, General test case, $r_{ref} = 7000$km, $i_{ref} = 35^o$)
- Circular Formation (1km radius, Sun synchronous orbit r_{ref}=7000km, i_{ref}=97.87^o)

Constant and time varying LQR controllers were found to reject the J_2 disturbance (although this depended on the controller design and spacecraft separation). By including the effects of J_2 in the circular formation design, and 'circularising' the absolute orbits of each satellite in the cluster by imparting an additional along-track velocity to each, formation keeping ΔV was reduced. The degree to which trajectory design or initial conditions contributed to the reduction in ΔV was found to be dependent primarily on orbit inclination.

It is proposed that additional benefits of improved model fidelity could be better demonstrated through the use of alternative control techniques, for example discretised, dynamic inversion, or predictive control, which would make more extensive use of the model to predict spacecraft relative motion. However, the important effects of orbit selection and formation initialisation and their relationship to the station keeping ΔV should be investigated further as this could prove consistently more important than the refinement of controllers in reducing fuel requirements over a mission lifetime. A number of suggestions for future work associated with this chapter are proposed in chapter 8. The results presented in this chapter have demonstrated the suitability of the LQR technique for simple, functional multivariable control design for LEO formation keeping, and the feasibility of the Matlab/STK interfacing approach for simulating the control of a satellite formation in the perturbed environment. The approach will therefore be applied for formation flying scenarios near L2 in chapters 6 and 7.

6 THE DEVELOPMENT OF AN L2 FORMATION FLYING DYNAMICS MODEL

The role of analytical models in formation flying control system design, implementation and mission analysis has already been presented in earlier chapters. Following the literature review in chapter 3, it was proposed that a purely analytical relative dynamics model be developed for formation flying simulation and control at the Sun-Earth L2 Lagrange or 'libration' point.

In section 6.1 the context of the model development is briefly outlined. A review of the techniques being applied to identify the structure of the gravity field in the vicinity of the equilibrium points was presented in chapter 3, and in this case the dynamics modelling described in section 6.2 is based on the circular restricted three body problem. The technique for satellite formation flying modelling in LEO (chapter 4) is applied at L2 whereby analytical solutions to the equations of motion of a satellite relative to L2 are used to define a halo reference orbit, and an expression for the gravity gradient is obtained along the reference. The linearised equations of relative motion in a frame based at the reference trajectory are then derived. The relative motion model is implemented in Matlab/Simulink and evaluated for different initial conditions. In section 6.3 comparisons are made between the relative motion solutions obtained from the new model, the higher order solutions recently developed by Segerman and Zedd (2003), and the Satellite Tool Kit numerical orbit propagator.

6.1 The Context of L2 Model Development

The motivation for this element of the research was provided initially by the requirement to gain insight into the formation flying dynamics at the Sun-Earth L2 libration point in order to investigate formation manoeuvring for a Darwin-type mission. In addition, any onboard autonomous operations would require an analytical description of orbit and formation dynamics. At the outset, the model development was deemed an important part of gaining an appreciation for:

- The time scales and stability characteristics of the relative motion.
- The potential role of the relative dynamics in guidance, navigation and control system design.
- The effects of perturbations in the L2 environment on both halo orbit maintenance and formation keeping.

The development of a dynamics model derived from the circular restricted three body problem (CR3BP) was proposed as a suitable initial approach, and later, this could be developed for the elliptical case (ER3BP). In the proposed form, the effects of relative perturbations on the formation could also be easily added.

In a flurry of recent research, many of the open questions formulated at the beginning of the research have been addressed. For example it has been established that the cost of formation control in the L2 environment is negligible even in the presence of

perturbations (refer to the literature review in chapter 6, section 6.2), and numerical and analytical solutions have been derived which provide insight into the scales of relative motion in the vicinity of the Sun-Earth L2 point. Many control techniques (particularly LQR) have been successfully applied to the problem. Amongst the conclusions of the literature survey, it was found that sensor and actuator noise and thrust limitations were of greater concern for formation flying than the orbit perturbations, and TPF studies suggested that orbit maintenance could be performed at the same time as science manoeuvres (slewing, rotating, translating)

However, although some load levelling strategies had been published in the literature, the combination of orbit and formation and manoeuvring control while fuel balancing had not been demonstrated in the perturbed environment, and this application of the formation flying model was therefore proposed. This model would provide insight into both the relative satellite motion and the halo orbit motion.

In the literature survey, the following approaches to relative dynamics modelling were identified:

- *Full Nonlinear Model*: The solutions to separate equations of motion for two satellites in the CR3BP or the ER3BP are subtracted. Equations are based at:
    - One of the primaries
    - Barycentre
    - A Lagrange point
- *Dynamic System Theory (DST) Trajectories*: Comparison of separate DST spacecraft trajectories for planar rotating formation design (suitable for non-precision formation flying applications) (DST was introduced in section 3.2.2.2).
- *Nonlinear Model and Dynamics Matrix*: DST trajectory generation software is also able to output a linearised dynamics matrix at each time step (this has been used for formation control by Hamilton et al. (2002)).
- *Nonlinear Hill Model*: The gradient of the nonlinear equations which are a simplified form of the CR3BP in a rotating frame, is derived by Scheeres and Vinh (2000).
- *Analytical Model*: Bounded relative motion solutions to third order have been derived from truncated forms of the nonlinear relative motion equations (but not applied to formation control).
- *Double Integrator*: This has been used for guidance system and formation manoeuvring analysis, but does not capture relative dynamics.

In this study, the linearised system dynamics are evaluated at each point on a reference orbit described by the Richardson (1980a) third order analytical solution for a periodic halo orbit around L2. This continues previous LEO formation flying work where the relative motion was governed by force gradients. The analytical approach also enables expressions for initial formation conditions, to which relative motion is so sensitive, to be derived.

The recent research by Segerman and Zedd (2003) was reviewed in chapter 3. They define a truncated set of relative motion equations in the CR3BP which are linear in satellite separation and quadratic in the distance of the formation from L2. Analytical solutions to the equations for satellites in a planar formation describing a halo orbit

around L2 are derived. The equations of motion require the substitution of a halo orbit description, and in the test case presented, a lower fidelity linear halo description (first order) is defined as the reference. However, the analytical solutions integrate the solutions to the halo orbit around L2 with a periodic relative motion, and therefore require the specification of the amplitudes of both forms of periodic motion. In this case, for third order analytical solutions, a second order description of halo reference motion is required. However, in this chapter it is proposed that the full third order halo reference solution be incorporated into the new model.

The motivation for the proposed approach involving linearisation about a higher order reference trajectory is the application of the model to control system design, away from the purely numerical environment. The analytical approach enables initial conditions to be determined which create halo orbit motion for at least part of an orbit in the numerical environment (this would be bounded motion in terms of the analytical solution), although a Poincare map could also be used. The solutions determined by Segerman and Zedd (2003) are particularly appropriate for formation trajectory design. Their solutions also provide estimates of initial conditions that can be compared with those derived using the linear gravity gradient model.

In chapter 7, the controlled spacecraft formation will be flown in the Satellite Tool Kit (STK) Astrogator software, and this was therefore used for model comparison. The gravity gradient model solution in terms of linear (third order) distance from L2 is compared to similar scenarios in STK, and also the solution of the truncated equations of Segerman and Zedd (augmented with a third order halo reference orbit description rather than the first order solution implemented in their paper).

It was also possible to derive equations of motion that were quadratic in the distance from L2 (the distance described by the third order halo solution), however, the model is significantly simplified by expressing the third order halo reference in terms of linear distance. The modelling accuracy is therefore investigated to establish the duration for which the model accurately captures relative and halo motion. This may be much less than an orbit (approximately 6 months), but most manoeuvres will be of much shorter duration.

6.2 Model Development

In this section, an introduction to the model development is presented, and any assumptions made are discussed. The formation flying dynamics model is then derived, and solutions and initial conditions are investigated.

6.2.1 Modelling Assumptions in the Circular Restricted Three Body Problem

A basic introduction to the circular restricted three body problem (CR3BP) was given in chapter 3, section 3.2. The nonlinear equations of motion of a satellite subject to the gravitational effects of the primary bodies in the rotating system were also introduced in

chapter 3 as equations (3-25). The equations were used to define the locations of the 5 equilibrium points (Lagrange points), and these were visualised on a generalised contour plot of the gravitation field associated with the CR3BP (Figure 3-3). The L2 point possesses the widest gravity force saddle point of the collinear libration points (note that the contours represent zero velocity conditions). Figure 6-1 illustrates the gravitational field around the Earth, and specifically, the regions of L1 and L2 in the Sun-Earth CR3BP. The stationary points lie approximately 1.5 million kilometres from the Earth along the Sun-Earth line.

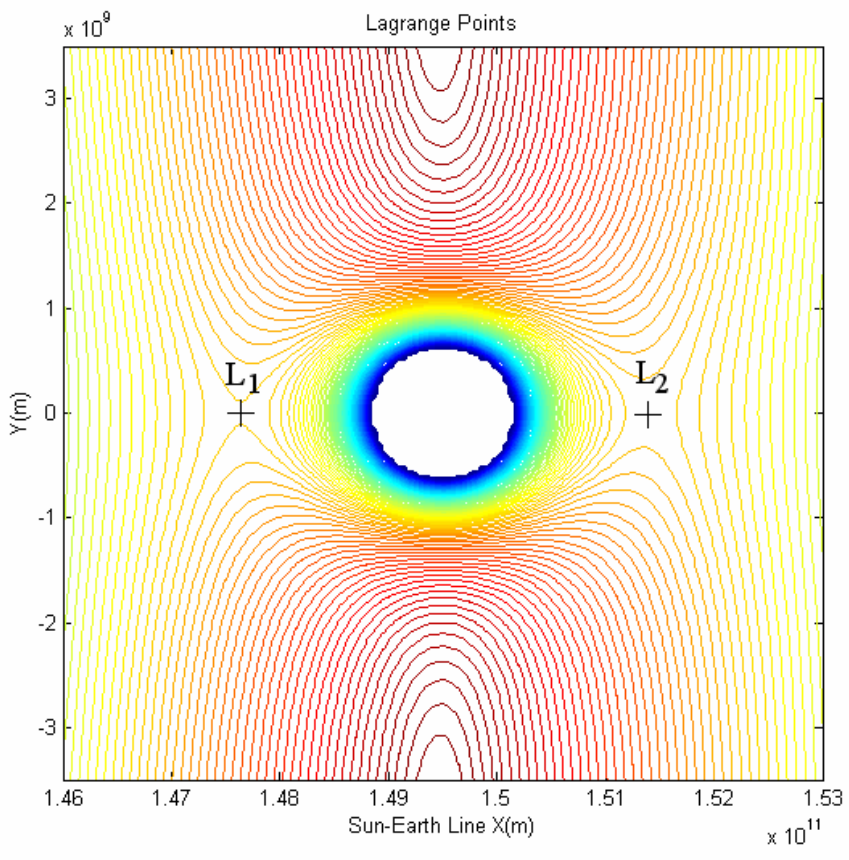

Figure 6-1: L1 and L2 in the Sun-Earth System

In the CR3BP, the following assumptions are made:

- The presence of only three bodies is considered.
- The two more massive (primary) bodies move in circular orbits about their combined centre of mass (the barycentre).
- The satellite (third body) has infinitesimally small mass.

In this case, the model derivation is carried out specifically for the L2 Lagrange point in the Sun-Earth system, although a similar approach could be adopted for any of the collinear libration points. In the Sun-Earth system, the mass of the Earth and Moon are combined, and an equivalent second primary body is placed at the Earth-Moon barycentre. The ecliptic is defined to lie along the Sun-Earth/Moon barycentre line, rather than the Sun-Earth line in this analysis. It should be noted that for the Sun-Earth system, the mass ratio between the two primary bodies is such that the barycentre actually lies within the spherical volume of the Sun.

For ease of analysis, the nonlinear equations of motion based at the barycentre (equations (3-25)) can be non-dimensionalised. This improves the conditioning of the linearised equations developed later, and allows the dynamics analysis to be easily scaled to any test case. Distance is normalised with respect to the Sun-Earth/Moon separation, D, and time is expressed in terms of the rotation rate of the three body system about the barycentre, n. The masses of the Sun (M_s) and Earth (M_e) are normalised by the total mass, and the mass ratio ρ_m (equations (6-1)) replaces mass terms in the equations.

$$\rho_m = \frac{M_e}{M_e + M_s} \quad \text{and} \quad (1-\rho_m) = \frac{M_s}{M_e + M_s} \tag{6-1}$$

This mass ratio term is equivalent to the distance ratio about the barycentre of the primaries (by definition of the barycentre). Consequently, ρ_m is equivalent to $-x_s$ and $(1-\rho_m)$ is equivalent to x_e, where x_s and x_e are the non-dimensional distances illustrated in Figure 6-2. The non-dimensional nonlinear equations of motion for a satellite in the CR3BP are therefore given by equations (6-2). In these equations, x, y and z are the non-dimensional forms of X, Y, and Z at the barycentre in Figure 6-2. x and y lie in the plane of the ecliptic, and z describes the out of plane motion.

$$\begin{aligned}
\ddot{x} - 2\dot{y} - x &= -\frac{(1-\rho_m)}{\rho_s^3}(x - x_s) - \frac{\rho_m}{\rho_e^3}(x - x_e) \\
\ddot{y} + 2\dot{x} - y &= -\frac{(1-\rho_m)}{\rho_s^3} y - \frac{\rho_m}{\rho_e^3} y \\
\ddot{z} &= -\frac{(1-\rho_m)}{\rho_s^3} z - \frac{\rho_m}{\rho_e^3} z
\end{aligned} \tag{6-2}$$

Figure 6-2 illustrates the three body problem and coordinate frames used in for the formation flying model development. Two 'third' bodies have been defined for this analysis as relative motion between them will be described. The 'Hub' and 'Telescope' can be considered a reference (leader) and non-reference (follower) satellite respectively for an interferometry mission, although the follower may not trace the path of the leader exactly, hence the preferred term of 'reference'. In equations (6-2) only the motion of the reference satellite is being considered, and its positions relative to the primaries (ρ_s and ρ_e) are labelled on Figure 6-2.

In preliminary analysis, the effects of the following assumptions on the location of the Sun-Earth/Moon system barycentre, and the location of the collinear Lagrange points were assessed:

- The Earth and Moon can be combined and treated as a single body in the Sun-Earth CR3BP.
- The Sun-Earth barycentre is located at the centre of the Sun.

The results are summarised in Table 6-1, based on Solar System constants provided by Dunham and Muhonen (2001). In the first case, the distance of the barycentre from the centre of the Sun for just the Sun-Earth system is 449km. This is 6.68km closer to the Sun than the barycentre of the Sun-Earth/Moon system, thus demonstrating that this

approximation shifts the barycentre by less than 1.5% of that distance, and 0.0000045% of the Sun-Earth separation.

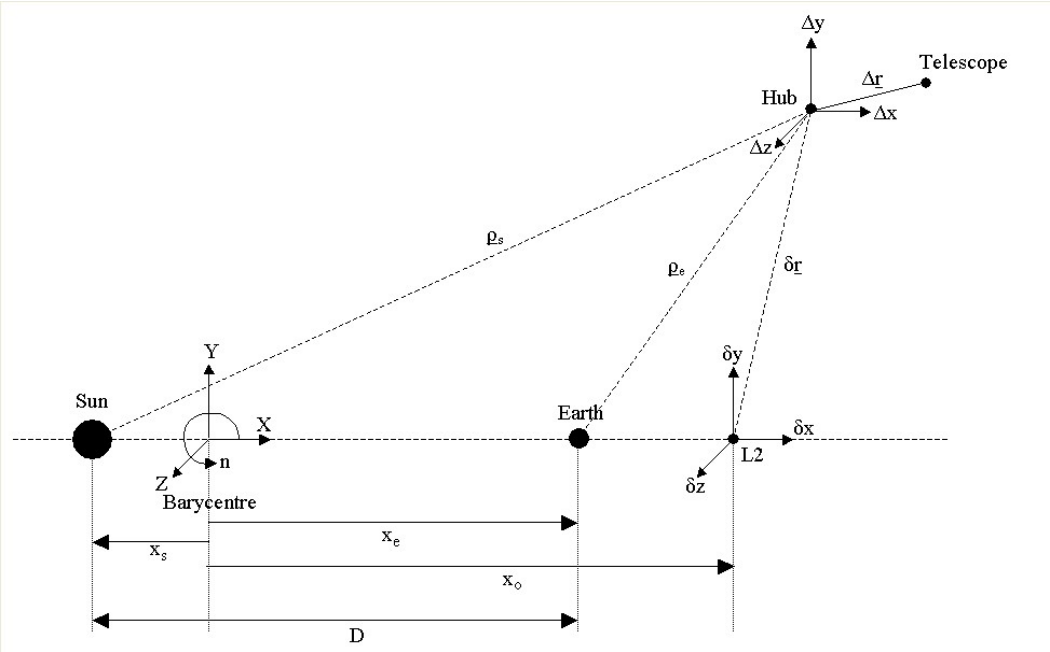

Figure 6-2: Formation Flying Parameters in the Three Body System

In the second case, the barycentre location is just a few hundred kilometres from the centre of the Sun. Scaled to the Sun-Earth separation of 1AU (1.4996×10^8km), the assumption that the barycentre lies at the centre of the Sun therefore has a negligible effect.

% Change in Distance	**Single Earth/Moon Body**	**Barycentre at Sun**
Between Sun-Earth/Moon Barycentre and Sun	0.0000045	0.0003
Between L2 and Earth/Moon Barycentre	0.660	0.0034

Table 6-1: The Effects of CR3BP Modelling Assumptions on Barycentre and L2 Position

Having established the scale of the changes in barycentre position due the inclusion of the Moon in the model and the placing of the barycentre at the Sun, the effect of these assumptions on the location of the collinear Lagrange points were also considered. The locations of the collinear libration points can be derived by eliminating velocity and acceleration terms from equations (6-2). These locations form one set of solutions to the equations of motion, which in this case reduce to a series of quintic equations for the collinear points, and these can be solved numerically (or algebraically using series expansions (Szebehely, 1967)). The non-dimensional quintics are given by equations (6-3), (6-4) and (6-5), where ξ is the distance of the Lagrange point from the nearest primary (the Earth for L1 and L2, and the Sun for L3).

L1: $$\xi^5 - (3-\rho_m)\xi^4 + (3-2\rho_m)\xi^3 - \rho_m\xi^2 + 2\rho_m\xi - \rho_m = 0 \quad (6\text{-}3)$$

L2: $$\xi^5 + (3-2\rho_m)\xi^4 + (3-2\rho_m)\xi^3 - \rho_m\xi^2 - 2\rho_m\xi - \rho_m = 0 \quad (6\text{-}4)$$

L3: $$\xi^5 + (2+\rho_m)\xi^4 + (1+2\rho_m)\xi^3 - (1-\rho_m)\xi^2 - 2(1-\rho_m)\xi - (1-\rho_m) = 0 \quad (6\text{-}5)$$

When the barycentre is placed at the Sun (x_s is zero in Figure 6-2), the quintics simplify to equations (6-6) to (6-8).

L1: $$\xi^5 - 3\xi^4 + 3\xi^3 - 2\rho_m\xi^2 + 2\rho_m\xi - \rho_m = 0 \quad (6\text{-}6)$$

L2: $$\xi^5 + 3\xi^4 + 3\xi^3 - 2\rho_m\xi - \rho_m = 0 \quad (6\text{-}7)$$

L3: $$\xi^5 - 2\xi^4 + \xi^3 + \xi^2 - 2(1-\rho_m)\xi + (1-\rho_m) = 0 \quad (6\text{-}8)$$

For L2, the error in Lagrange point location due to the assumption that the barycentre lies at the Sun was found to be 0.0034% of the Earth/Moon-L2 separation, and the error associated with not including the Moon was 0.66% (Table 6-1). For the remaining quantitative analysis, these assumptions were therefore allowed to hold, and L2 was found to be located 1.5114 million kilometres away from the Earth-Moon barycentre along the Sun-Earth/Moon line. The model derivation is however performed for a more general case where the barycentre is assumed to lie between the primaries. Note that further references to 'Earth' now actually refer to the Earth/Moon combined mass and barycentre.

6.2.2 Derivation of the Relative Motion Model

The nonlinear equations of motion with respect to the L2 point for a single satellite flying in the vicinity of L2, in the inertial (non-rotating) Cartesian coordinate frame in the CR3BP are given by equations (6-9) to (6-11) in dimensional form (as indicated by subscript 'dim'). The subscripted μ terms represent the gravitational constants of the Sun and Earth, n is the orbital rate of the system about the barycentre, and the remaining terms are dimensional forms of the distances in Figure 6-2.

$$\delta\ddot{x}_{dim} = -\left(\frac{\mu_s\delta x}{\rho_s^3} + \frac{\mu_e\delta x}{\rho_e^3}\right) - \left(\frac{\mu_s(x_o - x_s)}{\rho_s^3} + \frac{\mu_e(x_o - x_e)}{\rho_e^3}\right) + n^2 x_o \quad (6\text{-}9)$$

$$\delta\ddot{y}_{dim} = -\left(\frac{\mu_s\delta y}{\rho_s^3} + \frac{\mu_e\delta y}{\rho_e^3}\right) \quad (6\text{-}10)$$

$$\delta\ddot{z}_{dim} = -\left(\frac{\mu_s\delta z}{\rho_s^3} + \frac{\mu_e\delta z}{\rho_e^3}\right) \quad (6\text{-}11)$$

In non-dimensional form, these become

$$\delta\ddot{x} = -\left(\frac{(1-\rho_m)}{\rho_s^3} + \frac{\rho_m}{\rho_e^3}\right)\delta x - \left(\frac{(1-\rho_m)(x_o+\rho_m)}{\rho_s^3} + \frac{\rho_m(x_o-1+\rho_m)}{\rho_e^3}\right) + x_o \tag{6-12}$$

$$\delta\ddot{y} = -\left(\frac{(1-\rho_m)}{\rho_s^3} + \frac{\rho_m}{\rho_e^3}\right)\delta y \tag{6-13}$$

$$\delta\ddot{z} = -\left(\frac{(1-\rho_m)}{\rho_s^3} + \frac{\rho_m}{\rho_e^3}\right)\delta z \tag{6-14}$$

Equations (6-12) to (6-14) can be summarised in vector form by equation (6-15) which describes the motion of satellite number N. Initially just two satellites are considered, the hub or beam combining spacecraft (N=1) and a single telescope (N=2).

$$\delta\ddot{\underline{r}}_N = \underline{f}_N \tag{6-15}$$

To calculate the relative motion, the nonlinear equations of motion for each satellite must be subtracted and solved, however, the relative motion can be written in linearised form by evaluating the gravity gradient at the hub and multiplying by the distance between the hub and telescope (equation (6-16)). The same concept applies when only a virtual satellite is considered as the reference, and the relative positions and velocities between two offset satellites in close proximity to the reference are modelled.

$$\Delta\ddot{\underline{r}} = \delta\ddot{\underline{r}}_2 - \delta\ddot{\underline{r}}_1 = \underline{f}_2 - \underline{f}_1 = \nabla\underline{f}_1 \cdot \Delta\underline{r} \tag{6-16}$$

The gradient of the components of each gravity force in the δx, δy, and δz directions were derived for the general case (anywhere in the CR3BP). For the L2 case, the components of equations (6-12) to (6-14) were linearised. In the linearisation, the distance measures illustrated on Figure 6-2 are described by equations (6-17).

$$\begin{aligned}\rho_s^{-3} &= R_s^{-3}\left(1 - 3R_s^{-2}\left(\delta x(x_0+\rho_m) + y_0\delta y + z_0\delta z\right)\right)\\ \rho_e^{-3} &= R_e^{-3}\left(1 - 3R_e^{-2}\left(\delta x(x_0-1+\rho_m) + y_0\delta y + z_0\delta z\right)\right)\end{aligned} \tag{6-17}$$

where

$$\begin{aligned}R_s &= x_0 - x_s\\ R_e &= x_0 - x_e\end{aligned} \tag{6-18}$$

For the L2 formation flying model, referenced to a collinear point, y_0 and z_0 are zero. In the full derivation, these terms were retained in the gravity gradient terms, and the relative motion equations specifically for the L2 scenario were extracted afterwards.

Equations (6-19), (6-20), and (6-21) describe the relative motion for two satellites orbiting in the vicinity of the Sun-Earth L2 point, in non-dimensional form, and

linearised with respect to distance from L2. The rotation of the Sun-Earth system about the barycentre is taken into account (the acceleration and velocity terms in the equations have a similar form to those in the rotating frame in equations (3-25) and (3-28) in chapter 3 which describe the motion of a single satellite in the CR3BP). The relative motion is described by the variation of Δx, Δy, and Δz, which are the components of the vector $\Delta \underline{r}$ in equation (6-16). Again, all other terms are defined in Figure 6-2 and in the preceding equations.

$$\Delta\ddot{x} - 2\Delta\dot{y} - \Delta x = \left[-(1-\rho_m)\left(\frac{1}{R_s^3} - \frac{3}{R_s^5}(x_o + \rho_m)\{2\delta x + x_o + \rho_m\} \right) \ldots \right.$$
$$\left. \ldots - \rho_m \left(\frac{1}{R_e^3} - \frac{3}{R_e^5}(x_o - 1 + \rho_m)\{2\delta x + x_o - 1 + \rho_m\} \right) \right] \Delta x \qquad (6\text{-}19)$$

$$\Delta\ddot{y} + 2\Delta\dot{x} - \Delta y = \left[3\delta y \left(\frac{(1-\rho_m)(x_o + \rho_m)}{R_s^5} + \frac{\rho_m (x_o - 1 + \rho_m)}{R_e^5} \right) \right] \Delta x \ldots$$
$$\ldots + \left[-(1-\rho_m)\left(\frac{1}{R_s^3} - \frac{3(x_o + \rho_m)\delta x}{R_s^5} \right) - \rho_m \left(\frac{1}{R_e^3} - \frac{3(x_o - 1 + \rho_m)\delta x}{R_e^5} \right) \right] \Delta y \qquad (6\text{-}20)$$

$$\Delta\ddot{z} = \left[3\delta z \left(\frac{(1-\rho_m)(x_o + \rho_m)}{R_s^5} + \frac{\rho_m (x_o - 1 + \rho_m)}{R_e^5} \right) \right] \Delta x \ldots$$
$$\ldots + \left[-(1-\rho_m)\left(\frac{1}{R_s^3} - \frac{3(x_o + \rho_m)\delta x}{R_s^5} \right) - \rho_m \left(\frac{1}{R_e^3} - \frac{3(x_o - 1 + \rho_m)\delta x}{R_e^5} \right) \right] \Delta z \qquad (6\text{-}21)$$

In the case considered for the model development, the gravity gradient must be evaluated at the hub, and therefore its location must be known. In these equations, this is achieved by providing values or expressions for the δx, δy, δz terms, which are the separation of the hub or reference satellite from the L2 point. This also provides the user with the opportunity to prescribe the orbit of the hub or reference telescope (eliminating the divergent modes of halo motion) in order to focus on the control of relative satellite motion.

The hub orbit was selected to be a periodic halo orbit, although a Lissajous could also be prescribed. The third order analytical solution to the full three-dimensional equations of motion for periodic motion about L2 in the CR3BP developed by Richardson (1980a) was applied (this was introduced in section 3.2.2.1 in chapter 3). The hub motion is given by equations (6-22), (6-23), and (6-24) where A_x, A_y, and A_z are the amplitudes of the linearised halo solution (non-dimensionalised with respect to the distance between the Earth-Moon barycentre and L2) in the δx, δy, δz directions respectively, τ_1 is the independent variable relating frequency correction and orbital rate to time and the remaining terms are constants associated with the Linsdstedt-Poincare type method of solution used. An amplitude constraint relationship was derived and the satellites can be initialised at any point on the halo. The terms are defined in appendix E (section E.1), and the reader is referred to Richardson (1980a) for further details.

$$\delta x = a_{21}A_x^2 + a_{22}A_z^2 - A_x\cos\tau_1 + \left(a_{23}A_x^2 - a_{24}A_z^2\right)\cos 2\tau_1 + \left(a_{31}A_x^3 - a_{32}A_xA_z^2\right)\cos 3\tau_1 \quad (6\text{-}22)$$

$$\delta y = kA_x\sin\tau_1 + \left(b_{21}A_x^2 - b_{22}A_z^2\right)\sin 2\tau_1 + \left(b_{31}A_x^3 - b_{32}A_xA_z^2\right)\sin 3\tau_1 \quad (6\text{-}23)$$

$$\delta z = \delta_n A_z\cos\tau_1 + \delta_n d_{21}A_xA_z(\cos 2\tau_1 - 3) + \delta_n\left(d_{32}A_zA_x^2 - d_{31}A_z^3\right)\cos 3\tau_1 \quad (6\text{-}24)$$

These equations are higher order, and significantly more accurate than the first order solutions included as equations (3-32) in chapter 3. This analytical description of an L2 halo orbit (and its numerical equivalent) was used for station keeping of the ISEE-3 spacecraft (section 3.2.4). Specific constants for halo orbits about either L1, L2 or L3 in the Sun-Earth system are listed in Richardson (1980a), and were implemented to simulate a Darwin-type halo orbit around L2. It should be noted that while on the halo orbit, the hub axes do not rotate, and instead remain aligned with those fixed at L2. The solutions do however take into account the rotation of the Sun-Earth system about the barycentre.

Unlike the linearised equations of motion of a single satellite relative to the L2 libration point, the equations of relative motion are coupled in the in-plane and out-of-plane directions (equations (6-19) to (6-21)). However this is not the case in the simplest form when the reference orbit trajectory is the Lagrange point ($\delta x,\delta y,\delta z=0$). In this case, the equations simplify to

$$\begin{aligned} &\Delta\ddot{x} - 2\Delta\dot{y} - (2\sigma+1)\Delta x = 0 \\ &\Delta\ddot{y} + 2\Delta\dot{x} + (\sigma-1)\Delta y = 0 \\ &\Delta\ddot{z} + \sigma\Delta z = 0 \end{aligned} \quad (6\text{-}25)$$

where

$$\sigma = \frac{(1-\rho_m)}{R_s^3} + \frac{\rho_m}{R_e^3} \quad (6\text{-}26)$$

which are similar in form to the linear equations for single satellite motion (equations (3-28)). Due to the non-dimensional nature of equations (6-19), (6-20), and (6-21), it is straightforward to factor the linear expressions (6-25) into them to facilitate the generation of a solution. The resulting equations of motion are given below.

$$\begin{aligned} &\Delta\ddot{x} - 2\Delta\dot{y} - (2\sigma+1)\Delta x = 6\alpha\delta x\Delta x \\ &\Delta\ddot{y} + 2\Delta\dot{x} + (\sigma-1)\Delta y = 3\alpha(\delta y\Delta x + \delta x\Delta y) \\ &\Delta\ddot{z} + \sigma\Delta z = 3\alpha(\delta z\Delta x + \delta x\Delta z) \end{aligned} \quad (6\text{-}27)$$

where

$$\alpha = \left(\frac{(1-\rho_m)(x_o+\rho_m)}{R_s^5} + \frac{\rho_m(x_o-1+\rho_m)}{R_e^5}\right) \quad (6\text{-}28)$$

6.2.3 Solutions and Initial Conditions

Analytical solutions to the linearised relative motion equations (6-27) were sought. Initially, the reference orbit terms were held constant, and the halo orbit expressions were not substituted into δx, δy, or δz. Without these terms (δx, δy, δz = 0), the solutions to equations (6-25) can be expressed simply as equations (6-29) (from equations (3-32)).

$$\begin{aligned}\Delta x(t) &= -A_{xrel}\sin\omega_{xy}t \\ \Delta y(t) &= -k_{rel}A_{xrel}\cos\omega_{xy}t \\ \Delta z(t) &= k_{rel}A_{xrel}\sin\omega_{z}t\end{aligned} \qquad (6\text{-}29)$$

However, these bounded solutions only result if the initial conditions listed in Table 6-2 hold (k_{rel} is of the form given in equation (6-30), and arises from the elimination of exponential terms in the linearised solutions for relative motion).

Initial Conditions	
Δx_0	0
Δy_0	free
Δz_0	0
$\Delta\dot{x}_0$	$\frac{\omega_{xy}}{k_{rel}}\Delta y_0$
$\Delta\dot{y}_0$	$-k_{rel}\omega_{xy}\Delta x_0$
$\Delta\dot{z}_0$	$-\Delta y_0\omega_z$

Table 6-2: Initial Conditions for Bounded Relative Motion (Linear Case with Reference at L2)

By differentiating the in-plane equations of motion (equations (6-27)), substitutions can be made to decouple the Δx and Δy motion. The in-plane characteristic equation is given by equation (6-30) (terms are defined in section 6.2.2).

$$\lambda^4 + (2 - \sigma - 9\alpha\delta x)\lambda^2 - 6\alpha\delta y\lambda - (2\sigma^2 - \sigma - 9\alpha\delta x - 1) = 0 \qquad (6\text{-}30)$$

This can be solved algebraically, but the resulting expressions do not factorise simply due to the presence of the -6αδyλ term, and instead the quartic must be reduced to a cubic form and solved (Howatson, Lund, and Todd, 1991). However the halo orbit reference terms (δx, δy) also remain variable, as described by equations (6-22) and (6-23). In this case an approximate set of solutions and initial conditions, which would give non-secular motion near time zero, were derived using a state transition matrix approach. The approach was introduced in section 4.4.3 of chapter 4. Initially, the δx, δy and δz terms were held constant, and the solution expressed in approximate form (for constant A) by

$$x(t) = e^{At}x(0) \approx [I + At]x(0) \qquad (6\text{-}31)$$

to give lowest order approximate solutions

$$\begin{aligned}\Delta\dot{x}(t) &= \Delta\dot{x}_0 + 2t\Delta\dot{y}_0 + (2\sigma + 1 + 6\alpha\delta x)t\Delta x_0 \\ \Delta\dot{y}(t) &= -2t\Delta\dot{x}_0 + \Delta\dot{y}_0 + 3\alpha\delta y t\Delta x_0 + (1 - \sigma + 3\alpha\delta x)t\Delta y_0 \\ \Delta\dot{z}(t) &= \Delta\dot{z}_0 + 3\alpha\delta z t\Delta x_0 + 3\alpha\delta x t\Delta z_0\end{aligned} \tag{6-32}$$

To eliminate any secular drift, but retain the periodic terms in δx, δy and δz, the constant elements only of the Richardson solutions (equations (6-22), (6-23) and (6-24)) were substituted into the equations. Approximate initial conditions were derived by equating coefficients of secular terms at time t equal to zero.

$$\Delta\dot{y}_o = -\left[\frac{1}{2} - \frac{(1-\rho_m)}{2}\left[\frac{1}{R_s^3} - \frac{3(x_o+\rho_m)^2}{R_s^5}\right] - \frac{\rho_m}{2}\left[\frac{1}{R_e^3} - \frac{3(x_o-1+\rho_m)^2}{R_e^5}\right] + \left(\frac{3(1-\rho_m)(x_o+\rho_m)}{R_s^5} + \frac{3\rho_m(x_o-1+\rho_m)}{R_e^5}\right)\left(a_{21}A_x^2 + a_{22}A_z^2\right)\right]\Delta x_o \tag{6-33}$$

$$\Delta\dot{x}_o = \frac{1}{2}\left[1 - \frac{(1-\rho_m)}{R_s^3} - \frac{\rho_m}{R_e^3} + \left(\frac{3(1-\rho_m)(x_o+\rho_m)}{R_s^5} + \frac{3\rho_m(x_o-1+\rho_m)}{R_e^5}\right)\left(a_{21}A_x^2 + a_{22}A_z^2\right)\right]\Delta y_o \tag{6-34}$$

$$\Delta x_0 = \frac{a_{21}A_x^2 + a_{22}A_z^2}{3d_{21}A_xA_z}\Delta z_0 \tag{6-35}$$

The relative dynamics model described by equations (6-19) to (6-24) was implemented in Matlab/Simulink and also solved numerically. The reference halo motion is described by the Richardson solutions, and initial conditions were derived directly from the equations by setting τ_1 to zero. The initial relative positions and velocities were obtained from the relationships in equations (6-33) to (6-35).

6.3 Model Comparisons

The relative dynamics model based at the third order halo orbit around the Sun-Earth L2 Lagrange point was compared to STK for a selection of scenarios. In the following subsections, the implementation and initialisation of the linear gravity gradient model in Matlab/Simulink, and the initialisation of an equivalent scenario in STK are described. A higher order linear model, recently developed by Segerman and Zedd (2003), is introduced and also implemented for comparison.

6.3.1 Linear Model and Halo Reference Trajectory Implementation

The formation flying model described by equations (6-19) to (6-24) was implemented in Matlab/Simulink. Firstly, a halo reference orbit generator was constructed according equations (6-22) to (6-24). These solutions were derived by the method of successive approximations as described by Richardson (1980a), and are constructed in terms of non-dimensional distances, mass ratios and system rotation rate. A listing of the coded formulae is included as appendix E.1.

In the Simulink model, the simulation duration was defined by τ_{halo} where for orbital mean motion, n_1, the real time, t, is given by

$$t = \frac{\tau_{halo}}{n_1} \tag{6-36}$$

The halo generator operates in terms of τ_1, where

$$\tau_1 = n_1 \omega \lambda t \tag{6-37}$$

According to the Richardson (1980a) nomenclature, λ is the in-plane frequency, and ω is a frequency correction term associated with the solution method applied. In addition, the halo amplitudes, A_x, A_y, and A_z were non-dimensionalised with respect to the distance between the Earth and L2. However, the output halo positions were inputs to a non-dimensional relative motion model which was derived by scaling to different measures of time and length. Further correction factors were therefore applied to the generator outputs before the parameters were passed to the relative dynamics model (Figure 6-3).

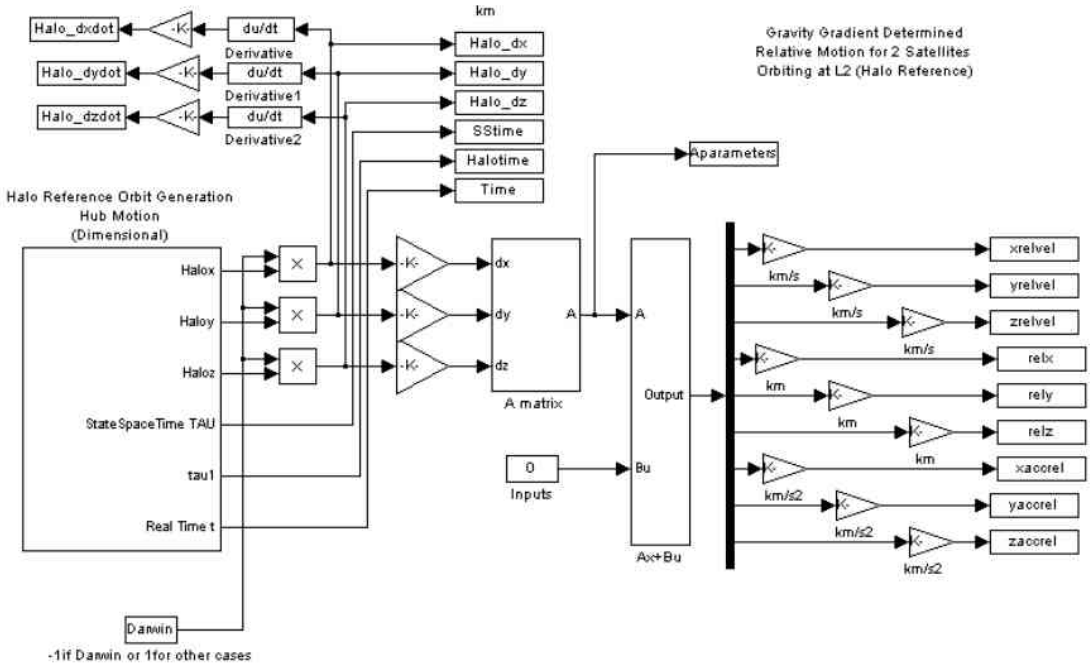

Figure 6-3: Matlab/Simulink Implementation of the Relative Dynamics Model

For ease of simulation, in this case the hub is located on the reference halo and is also designated the formation leader. The initial position of the reference relative to L2 is found by setting time t=0 (equivalent to τ_1=0) in equations (6-22), (6-23) and (6-24). δy_0 becomes zero, but δx_0 and δz_0 are non-zero functions of the constants and linear solution halo amplitudes A_x and A_z. The initial velocity conditions, $\delta \dot{x}_o, \delta \dot{y}_o, \delta \dot{z}_o$ can be found by differentiating equations (6-22), (6-23) and (6-24) and setting time τ_1=0. These were verified by differentiating the halo position outputs during the first time steps of the numerical simulation (using small time steps). These values were also compared to

the initial conditions approximated by the linear solution conditions for removal of divergent modes (equations (3-29) and (3-30) in chapter 3, section 3.2.2).

Given a set of user-defined halo orbit amplitudes, and desired formation relative positions, the simulation model applied the initial relative conditions given by equations (6-33) to (6-35).

6.3.2 L2 Lagrange Point Formation Flying Scenario in STK

For the model comparisons, the two satellites in the formation were propagated separately in STK. The 'real' satellite behaviour was propagated using STK Astrogator, a high precision orbit propagator, able to incorporate Solar, terrestrial and Lunar effects. For the model comparisons Lunar and planetary perturbations are included and the L2 coordinate system is centred on the Sun-'Earth/Moon barycentre' line. However, Solar radiation pressure was not included in the simulations. The eccentricity of the Earth's orbit around the Sun was, however, also implicit in the numerical solution, and the L2 point therefore moves during the simulation in addition to rotating with the Earth around the Sun. The use of STK for model verification was established for the LEO environment in chapters 4 and 5. In this case, a Cartesian axis system was created at the L2 point, and initial conditions were provided to each satellite as Cartesian position and velocity relative to L2 (Figure 6-2).

The hub was given the prescribed halo initial conditions (as described in section 6.3.1), and the telescope was provided with initial conditions given in form by equation (6-38), where X_0 is the vector of initial positions and velocities.

$$\delta X_0^{\text{Telescope}} = \delta X_0^{\text{Hub}} + \Delta X_0^{\text{Relative}} \tag{6-38}$$

Absolute motion of each satellite was extracted through the STK reporting tool and differenced to obtain relative motion of the telescope with respect to the hub.

Unlike the equations of motion in the CR3BP, the eccentricity of the Earth's orbit affects the location of the L2 point. STK propagations were therefore run at two different epochs, six months apart, but this did not appear to affect the relative motion dynamics significantly. The propagation time step was fixed at 1 hour for both the Matlab models and STK during the scenarios (for the test cases investigated, the duration of the analytically derived halo orbit period was approximately 180 days). Subsequent analyses focussed on the first 20 days of orbit, as without control, the numerical solution would diverge from the 'ideal' halo orbit.

6.3.3 Higher Order Analytical Models

During the model development research, Segerman and Zedd (2003) produced a higher order set of relative motion equations for satellites in the vicinity of the Sun-Earth L2 point, and proceeded to obtain analytical solutions for an uncontrolled periodic orbit using techniques similar to those applied by Richardson (1980a) for a halo orbit around

the collinear Lagrange points. As for the halo, relative motion solutions were obtained to third order and were also restricted to ensure periodic motion. An overview of their model development strategy was presented in section 3.2.5, and the differences between this model and the gravity gradient model in section 6.2.2 were highlighted in section 6.1. A brief summary of the main equations in their model is presented in appendix E.2, however, for a full explanation it is necessary to refer to their publications.

The equations of motion implemented in Matlab/Simulink are given by equations (6-39). The subscript h refers to the location of the hub (reference) satellite with respect to L2. The (x,y,z) terms represent relative motion in the hub reference frame, also aligned with the axis system at L2, and A, B, and C are given in appendix E.2. It should be noted that the term Δ in the out-of-plane dynamics arises from the selection of a periodic motion of the telescopes about the hub. This term counteracts the effects of defining the frequency, λ, in the z-dynamics model to match the fundamental frequencies of in-plane and out-of-plane motion for periodic planar relative motion.

$$\begin{aligned}
&\ddot{x} - 2n\dot{y} - n^2 x = 2Ax + B(-6xx_h + 3yy_h + 3zz_h) + C(12xx_h^2 - 12yx_h y_h - 12zx_h z_h - 6xy_h^2 - 6xz_h^2)\\
&\ddot{y} - 2n\dot{x} - n^2 y = -Ay + B(3xy_h + 3yx_h) + C(-12xx_h y_h + \tfrac{9}{2} yy_h^2 + 3zy_h z_h - 6yx_h^2 + \tfrac{3}{2} 6yz_h^2)\\
&\ddot{z} + \lambda^2 z = \Delta z + B(3xz_h + 3zx_h) + C(-12xx_h z_h + 3yy_h z_h - 6zx_h^2 + \tfrac{3}{2} zy_h^2 + \tfrac{9}{2} zz_h^2)
\end{aligned} \qquad \text{(6-39)}$$

All terms in equations (6-39) are in dimensional form, and therefore for implementation in Matlab/Simulink and integration with the third order halo reference orbit model (x_h, y_h, z_h in this notation), the expressions were non-dimensionalised.

Observation of equations (6-39) reveals the similarities in form of the equations at low order to those in equations (6-27). The differences lie in the x and z expressions. In this case it has been assumed that the x equation contains a positive '2Ax' term, unlike the equations in the paper, as this matches the vectorial form of the equations (equation (E-37) in appendix E.2) and produces better results. In the x equation, the equivalent expressions in B differ because Segerman and Zedd expand their equations of motion in terms of both powers of the distance between the hub and L2 as well as between the hub and telescope, and additional terms therefore arise. Terms in y and z disappear from the gravity gradient model derivation since L2 is a collinear point. In the z equation, the frequency correction term, Δ, is not part of the linear model development. (The higher order terms, multiplied by C, are also not included in the linear model).

In their solution, the hub motion is included at progressively higher order as the order of the relative motion solution increases. For their second order relative motion solutions, the linear motion of the hub is implicit. For their third order relative motion solutions, the second order components of the halo reference orbit (traced by the hub) are incorporated. However, for the truncated equations of motion, the hub initial conditions are defined by the first order linear solutions (equations (3-29), chapter 3). In the model derived in section 6.2.2, the third order hub solution is included in the equations instead.

For the model comparisons to STK, the relative motion equations defined by equations (6-39) were implemented in Matlab/Simulink. The hub position terms (x_h, y_h, z_h, which when non-dimensionalised appropriately are equivalent to δx, δy, δz) were supplied with the same third order reference halo as the new linear model. It was not the purpose of the investigation to consider the accuracy of the analytical solutions, but the equations were implemented to generate higher fidelity initial relative motion conditions (at time $\tau=0$). The solutions are included in appendix E.2 (equations (E-40) to (E-42)). Differentiating these expressions for time equal to zero ($\tau=0$) provides a set of initial velocity conditions.

6.3.4 Results of Model Comparisons

In this section, two test cases are presented for the model comparisons. These include:

- *The SZ scenario*: The single example presented by Segerman and Zedd (2003).
- *The Darwin scenario*: A Darwin-type mission scenario (ESA Report, 2000).

A full model verification requires many additional test cases and is beyond the scope of the thesis due to time constraints. Without a full implementation of the analysis leading to the development of the higher order analytical solutions derived by Segerman and Zedd (2003), it was not possible to implement any additional test cases (unless the model was supplied with initial conditions from the gravity gradient model or from for example, a Poincare map). The process was also limited due to the inability of the initial conditions for any of the analytical models to produce bounded relative motion, or even a bounded reference halo orbit without controller input in the unstable environment.

However, the examples illustrated here demonstrate the effects of the initial conditions derived from the three different models on both halo and relative motion, and some measure of the ability of the model to capture the numerical behaviour of the satellites in STK. The Darwin test case is also investigated as this scenario is applied for the load-levelling simulations in chapter 7.

6.3.4.1 The SZ Scenario

For the SZ test case (Segerman and Zedd, 2003), it was not possible to replicate the initial conditions presented in the paper. There the dimensional hub initial conditions were set equal to the initial halo amplitudes (equations (6-40)). The A_z amplitude was initially selected, and A_y and A_x were derived from the amplitude constraint relationships for a halo orbit.

$$\begin{aligned} x_h(0) &= A_x \\ y_h(0) &= 0 \\ z_h(0) &= A_z \end{aligned} \qquad (6\text{-}40)$$

The initial hub velocities were calculated using the linear halo conditions introduced in chapter 3, (and now given by equations (6-41)).

$$\dot{x}_h(0) = \left(\frac{\lambda}{k}\right) y_h(0)$$
$$\dot{y}_h(0) = -k\lambda x_h(0) \qquad (6\text{-}41)$$
$$\dot{z}_h(0) = 0$$

In the test case presented here, the halo amplitude values were instead retained for implementation in the Richardson halo equations (at τ_1=0), and the initial velocities from equations (6-22) to (6-24) and equations (6-41) were evaluated. The results for the hub or reference initial conditions are tabulated below (Table 6-3). The initial y-velocity from the linear solution is an approximation to the equivalent value from the Richardson halo solutions, but the values are similar.

The relative initial conditions were derived from the SZ test case where a formation relative motion amplitude was selected to be A_{xrel}=50m. By implementing this amplitude into the SZ solutions (in appendix E) along with the linear hub amplitudes, the initial relative satellite positions were found to be approximately -65m in x, zero in y, and 27m in z. Differentiating their expressions provided an initial relative y-velocity of approximately 4.4m/day. The relative initial condition from the linear gravity gradient model described by equation (6-33) produced a slightly higher initial y-velocity of approximately 4.9m/day. The results are summarised in the right hand columns of Table 6-3.

HUB Initial Conditions		**TELESCOPE-HUB Relative Initial Conditions**	
Linear Amplitude Ax (km)	227219.42	Position Δx_o (m)	-64.7796
Linear Amplitude Ay (km)	724200.94	Position Δy_o (m)	0
Linear Amplitude Az (km)	250000.00	Position Δz_o (m)	26.7391
Velocity $\dot{x}_{01}$ (km/s)	0	Velocity (SZ model) $\Delta\dot{x}_o$ (m/day)	0
Velocity (Richardson) $\dot{y}_{01}$ (km/s)	0.3134925	Velocity (SZ model) $\Delta\dot{y}_o$ (m/day)	4.4205
Velocity $\dot{z}_{01}$ (km/s)	0	Velocity (SZ model) $\Delta\dot{z}_o$ (m/day)	0
Velocity (Linear Approx.) $\dot{y}_{01}$ (km/s)	0.3631100	Velocity (Gravity gradient model) $\Delta\dot{x}_o$ (m/day)	0
		Velocity (Gravity gradient model) $\Delta\dot{y}_o$ (m/day)	4.9011

Table 6-3: Hub and Telescope Initial Conditions (SZ Test Case)

The following results were obtained for the SZ and gravity gradient model responses to initial conditions derived from the SZ model.

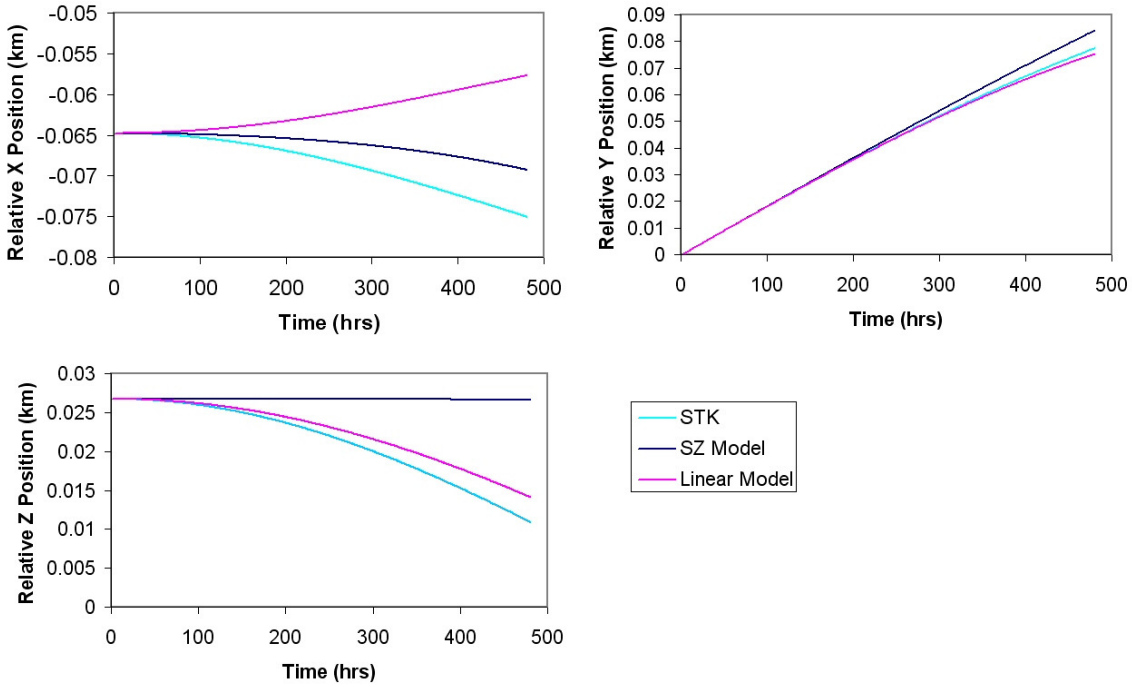

Figure 6-4: Comparison of Relative Position Over 20 Days As Predicted by the Modified SZ Model, Gravity Gradient Linear Model and STK for the SZ Scenario (Initial Conditions are in Table 6-3: Using Richardson Hub Initial Conditions and the SZ Relative Initial Conditions)

The SZ model was expected to capture relative motion more accurately than the linear model, and without reproducing their analysis in full, the reasons for the differences in model performance are not clear. With the initial relative velocity conditions derived from the SZ model:

- In the x direction, the SZ model response follows the path of the STK trajectory but with increasing error. The gravity gradient model response drifts away from the STK trajectory, although this is very gradual (5m in 20 days).
- In the y direction, the linear y response is closer to the STK response than the higher order SZ model.
- In the z direction, the STK response is also better approximated by the linear model.

The implementation of the z-equation in the SZ model was investigated further, but similar results showing very little change in the relative position over 20 days were also achieved by Segerman and Zedd (2003). This was expected as their initial conditions were defined to produce a 'planar' formation by design. However, it would appear that the form of their integration of the full nonlinear equations is not matched by the numerical solution in STK. This could be due to the use of the higher order hub or reference orbit initial conditions in the STK scenario (equations (6-22) to (6-24)). In addition, Lunar and planetary perturbations in STK are likely to slightly affect the STK relative motion. However, the effects of the circularisation assumption in the CR3BP apply to both models and this assumption is therefore not the source of error in this case. STK includes Earth orbit eccentricity effects, but evaluation of the scenarios at different epochs demonstrated that this had a negligible effect on satellites in close proximity. It should be noted that relative motion between the spacecraft occurs on a completely different scale (a few metres) compared to other dimensions in the three

body problem (1.5 million kilometres), and numerical noise and other issues that are masked by the STK user interface may also affect the results.

The analysis was repeated using the gravity gradient model initial conditions, also included in Table 6-3, and the results of the model comparison are illustrated below (Figure 6-5). Very similar results are obtained, and the choice of initial y-velocities as determined by each model is not critical in the simulations in terms of model performance.

With the gravity gradient initial conditions, the relative y-velocity is slightly greater and therefore all models produce a slightly greater relative y-position after 20 days. In the x-direction, the SZ model and STK exhibit slightly reduced relative position divergence, but the linear model response very slightly increases. The change in initial conditions has little effect on the out-of-the-ecliptic relative motion.

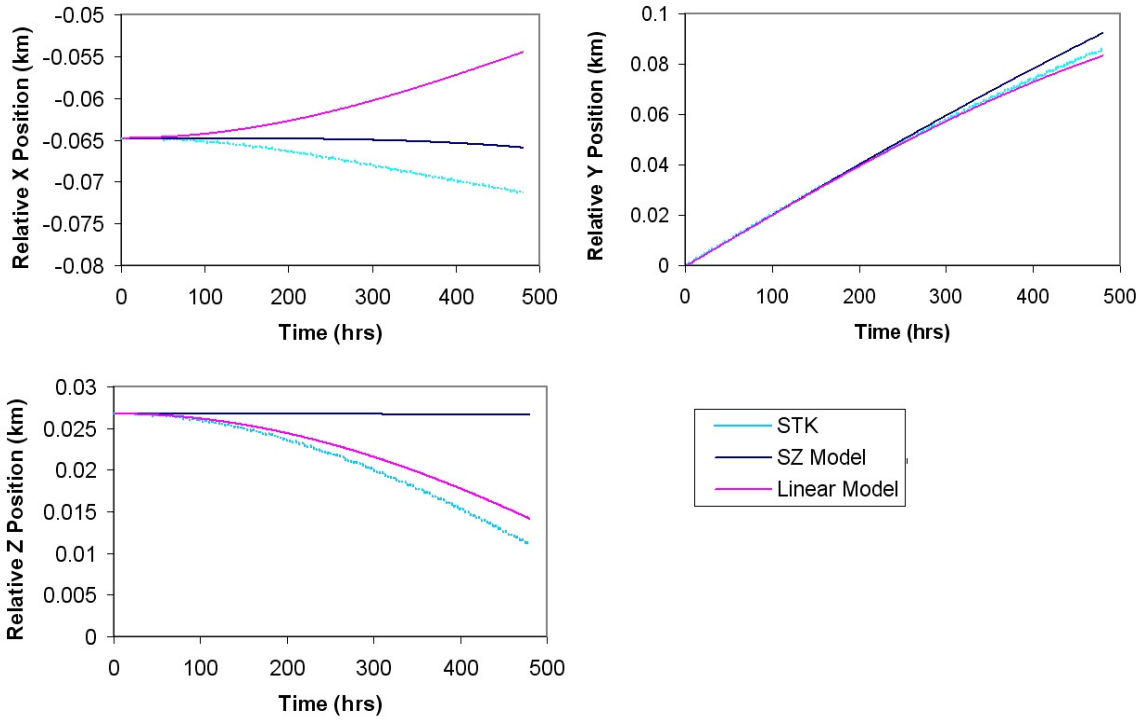

Figure 6-5: Comparison of Relative Position Over 20 Days As Predicted by the Modified SZ Model, Gravity Gradient Linear Model and STK for the SZ Scenario (Initial Conditions in Table 6-3: Using Richardson Hub Initial Conditions and Gradient Model Relative Initial Conditions)

However, to investigate the difference between the initial conditions from the two models, another test case was evaluated. For comparison, the initial conditions are included in Table 6-4. This time, the hub halo orbit around L2 was given a z-amplitude (A_z) of twice the size of the SZ test case (A_z=500000km). The formation amplitude, A_{xrel}, was 200m (four times larger than the SZ test case).

For a halo orbit with twice the amplitude of the SZ test case, the difference between the linear model and third order model initial velocity conditions for the hub is

approximately doubled. The relative velocity initial conditions for a formation with an amplitude four times greater than the SZ test case were found to be also approximately four times larger. The values obtained from both the SZ analytical solutions and the gravity gradient model remained similar.

HUB Initial Conditions		**TELESCOPE-HUB Relative Initial Conditions**	
Linear Amplitude Ax (km)	269798.65	Position Δx_o (m)	-234.74
Linear Amplitude Ay (km)	859910.64	Position Δy_o (m)	0
Linear Amplitude Az (km)	500000.00	Position Δz_o (m)	246.49
Velocity $\dot{x}_{01}$ (km/s)	0	Velocity (SZ model) $\Delta\dot{x}_o$ (m/day)	0
Velocity (Richardson) $\dot{y}_{01}$ (km/s)	0.3845289	Velocity (SZ model) $\Delta\dot{y}_o$ (m/day)	16.306
Velocity $\dot{z}_{01}$ (km/s)	0	Velocity (SZ model) $\Delta\dot{z}_o$ (m/day)	0
Velocity (Linear Approx.) $\dot{y}_{01}$ (km/s)	0.4970369	Velocity (Gravity gradient model) $\Delta\dot{x}_o$ (m/day)	0
		Velocity (Gravity gradient model) $\Delta\dot{y}_o$ (m/day)	17.751

Table 6-4: Hub and Telescope Initial Conditions (Large Halo – Large Formation Example)

As a final test case associated with the SZ scenario, the initial relative y-velocity was set to zero for both models and STK, while all other parameters in Table 6-3 were retained. The relative positions over 20 days are illustrated in Figure 6-6.

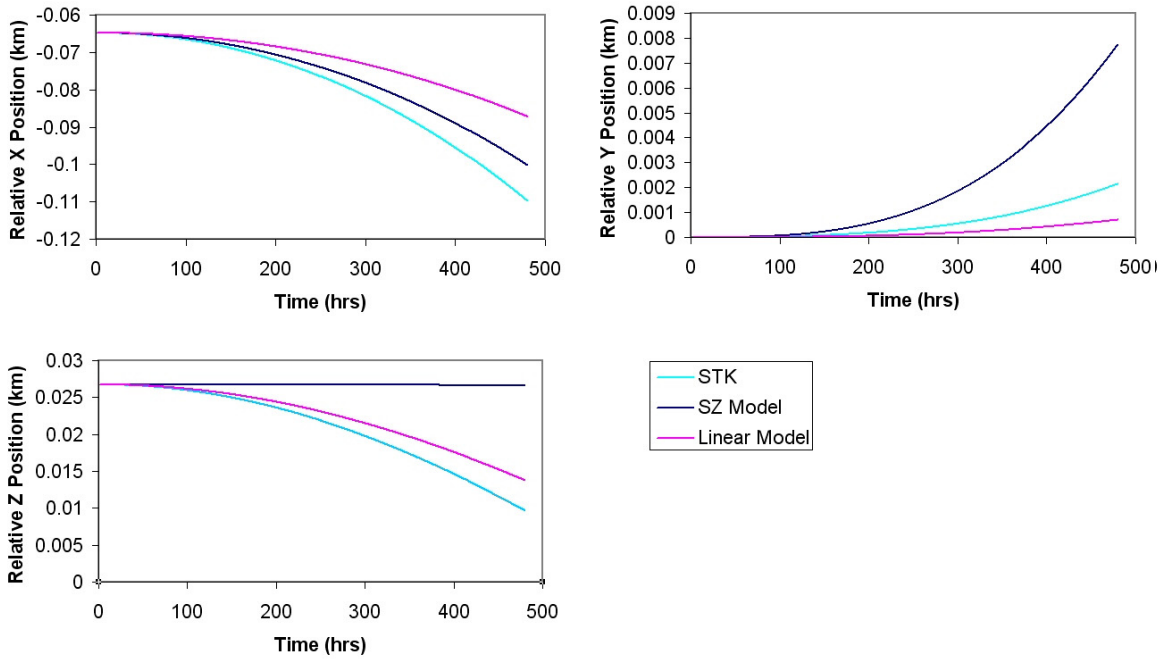

Figure 6-6: Comparison of Relative Position Over 20 Days As Predicted by the Modified SZ Model, Gravity Gradient Linear Model and STK for the SZ Scenario (Initial Conditions in Table 6-3 with Richardson Hub Initial Conditions and an Initial Relative y-Velocity Set to Zero)

Again the gravity gradient linear model captures relative motion in y and z more accurately than the SZ model. Without an initial relative y-velocity, with which motion in the x direction is strongly coupled, the natural dynamics is still captured more accurately by the higher order SZ model, but this time the gradient model results are significantly improved. A slow drift is produced in the same direction as the STK results, thus demonstrating the importance of the y-velocity on model performance.

6.3.4.2 The Darwin Scenario

A Darwin-type scenario was derived from the ESA Darwin Concept and Feasibility Study (ESA Report, 2000) and the relationship between insertion ΔV and amplitude of a halo orbit derived by Farquhar (1998). The initial conditions applied to the Darwin formation are summarised in Table 6-5. For zero insertion ΔV into a halo orbit, Ay was selected to be 780000km (and therefore Ax was 244726.7km, and Az was 368380.8km). For these linear amplitudes of motion, the hub satellite initial position was out-of-the-ecliptic by z_{01}km, and on the Earth side of L2 on the Sun-Earth line.

The telescope was initially separated from the hub by 100 metres (Δx_0), parallel to the Sun-Earth line, and in the hub plane. According to the initial conditions prescribed by the models, an initial out-of-the-ecliptic position is associated with an initial displacement along the Sun-Earth line. Equation (6-35) defines an initial relative z-position of approximately 61m. However in Darwin the scenario considered here, the formation was assumed to be initially planar in the ecliptic to improve insight into the in-plane motion (since an initial offset in z did not significantly affect model performance).

The gravity gradient model for the reduction of secular motion suggests an initial relative y-velocity of 7.5659m/day, which is equivalent to the very small value of 87.6μm/sec.

HUB Initial Conditions		**TELESCOPE-HUB Relative Initial Conditions**	
Initial Position x_{01} (km)	-319112	Position Δx_o (m)	-100
Initial Position y_{01} (km)	0	Position Δy_o (m)	0
Initial Position z_{01} (km)	329681	Position Δz_o (m)	(60.616)
Velocity $\dot{x}_{01}$ (km/s)	0	Velocity (Gravity gradient model) $\Delta\dot{x}_o$ (m/day)	0
Velocity (Richardson) $\dot{y}_{01}$ (km/s)	0.3422590	Velocity (Gravity gradient model) $\Delta\dot{y}_o$ (m/day)	7.5659
Velocity $\dot{z}_{01}$ (km/s)	0	Velocity $\Delta\dot{z}_{01}$ (km/s)	0

Table 6-5: Hub and Telescope Initial Conditions (Darwin Mission Scenario)

Halo Motion

The third order analytical solution for the prescribed halo orbit was compared to the motion of the hub satellite in STK. Figure 6-7 illustrates the analytical halo motion and

the difference between this and the hub motion propagated in STK over a period of 20 days. The hub motion in STK does appear to perform a partial halo before diverging onto an alternative trajectory.

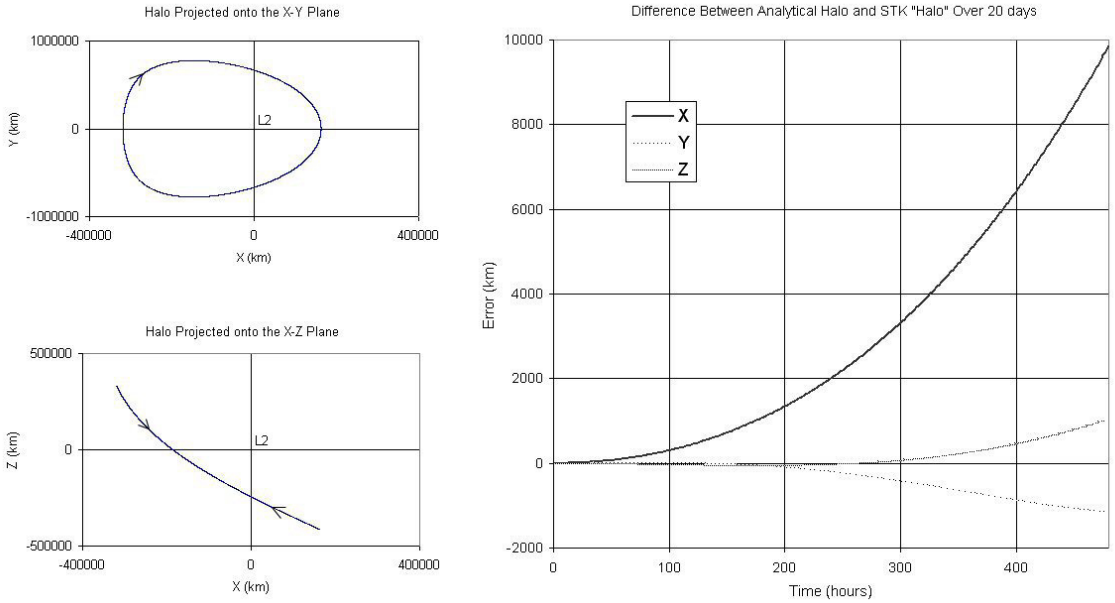

Figure 6-7: Darwin-type Halo Orbit, and Halo Modelling Error

After 20 days, the uncontrolled STK 'halo' has diverged from the analytical halo motion by 9854km in X, 1044km in Y, and 1150km in Z for a halo orbit of approximately 780000km in Y-dimension. The divergence is significantly less over shorter periods of time, and if we assume frequent control of the hub satellite (for example, every quarter of a halo orbit), the analytical halo is sufficiently accurate to represent the hub motion on the scale of the halo amplitude. This was confirmed by evaluating the gravity gradient model along both the analytical and STK numerical reference orbits and examining their effects on relative motion over a few days. A few kilometres in hub halo error did not significantly affect the relative motion predicted by the gravity gradient model.

Relative Motion

The relative motion in the x, y and z directions, predicted by both STK and the gravity gradient model are illustrated in Figure 6-8. In the x direction, STK predicts that the satellites will separate by a further 14.2m in 20 days. However, the gravity gradient model indicates that the satellites will in fact be moving closer together (by 18.5m). The error in predicted motion is very small at 1.6m/day and upon examination of the x-equation of motion (equation (6-19)), it was found that as for the SZ scenario (section 6.3.4.1), the cause of the change in the x direction was due to the y-velocity contribution. The equation was extremely sensitive to the relative y-velocity, which at 87.6μm/s is very small and difficult to control. This initial condition was evaluated using an approximate model, and a very small error in the approximation would make a very large difference to the relative motion obtained (and therefore the ability of the dynamics model to capture this).

In the CR3BP, the physical location of the satellites can be visualised. The telescope is nearer to the Earth than the hub, while the hub is closer to L2. The hub is given an initial y-velocity ($\dot{y}_{01}$ in Table 6-5) and increases in altitude, pulling away from the Earth. The hub then experiences a growing centrifugal force, which in combination with the Earth's attraction will cause it to rotate in a halo. The telescope requires a larger initial y-velocity to stay near the hub as it is 'lower' in altitude with respect to the Earth. If the hub starts to rotate in a halo and the additional y-velocity given to the telescope is not quite sufficient, they will appear to separate. The fact that the gravity gradient model appears to move the satellites closer together suggests that relative y-velocity ($\Delta\dot{y}_o$) is overestimated. In Figure 6-8, the y and z relative positions predicted by the gravity gradient model approximate the STK relative motion fairly well.

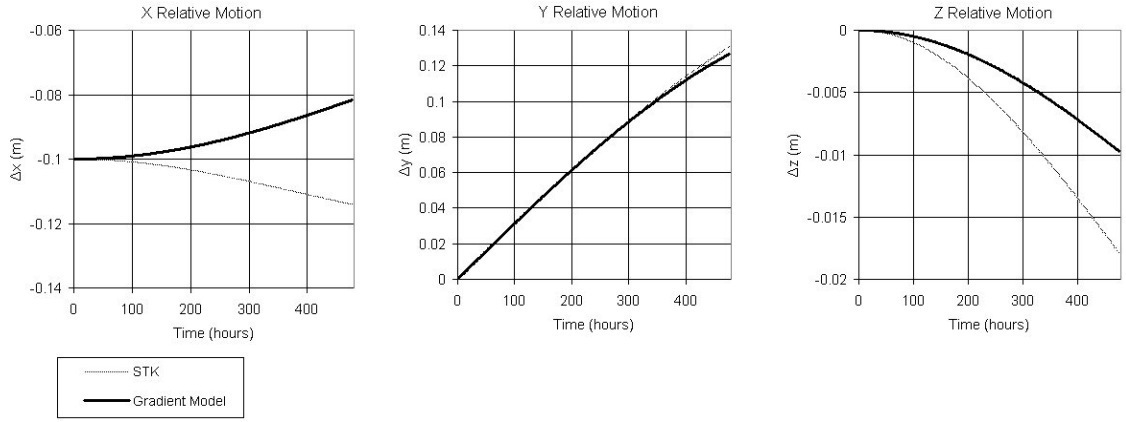

Figure 6-8: Model Comparison of Relative Hub-Telescope Motion Over 20 Days

6.3.5 Discussion

A preliminary conclusion from the analysis presented in section 6.3.4 is that the higher order relative motion model will not necessarily offer significant improvement in formation modelling for controller design and that a linear gravity gradient model may be sufficient. Both models provided similar values for initial conditions to eliminate drift or produce bounded relative motion in the numerical STK environment. However, the STK scenarios solve the nonlinear problem and include additional perturbations not considered in the CR3BP, and a bounded formation tracing a bounded halo reference orbit was therefore not physically viable. A summary of the main findings resulting from the modelling approach investigated in this chapter is given below:

- Use of the Richardson third order solution as a reference halo orbit enables the improved definition of hub initial conditions and reference trajectory about which both of the relative motion models can operate.
- The difference between the linear halo initial conditions and the third order solution initial conditions grows proportionately with halo orbit amplitude. The initial hub velocities also increase slightly with orbit amplitude.

- The Richardson halo is currently the best analytical description for halo motion available and has been successfully applied for spacecraft station keeping (ISEE-3).
- A multi-satellite mission scenario involving spacecraft orbiting in the vicinity of L2 was implemented in STK, and relative position and velocity data was successfully extracted.
- For any set of initial relative positions, the initial velocity conditions derived using the gravity gradient or higher order relative dynamics models were similar, and scaled for both models with formation inter-satellite separation.
- Comparisons between the gravity gradient and higher order models and the STK scenario did not reveal the steady improvements in dynamics capture anticipated. The sensitivity of the system behaviour to the initial conditions was apparent, and the difficulty in using STK to establish a 'truth' model was demonstrated.

The differences between the direction of the gravity gradient model and STK responses were found to be due to the selection of initial y-velocity. Neither dynamics model therefore predicted appropriate initial relative conditions. However this cannot be concluded for certain without further analysis and investigation since STK includes additional perturbation effects beyond the CR3BP. It is proposed that additional test cases be implemented with alternative tolerances in the numerical integrator.

Without the initial relative velocity conditions, the gravity gradient model was able to capture the shape of the gravity environment in the vicinity of the hub, and also produce relative motion responses closer to those of STK than the SZ model in the y and z directions. Both models were found to predict similar initial conditions, and the model comparison has therefore proved useful in demonstrating that the gravity gradient model produces a sensible result. The model can therefore be applied to controller design, pending the outcome of further model verification work.

6.4 Summary

Following the literature review in chapter 3, the need for an analytical description of relative satellite motion in the vicinity of L2 was established. As part of the process of model development, initially the physical parameters associated with the Sun-Earth three body problem were identified, and the effects of the Moon on the location of the collinear Lagrange points and system barycentre were quantified.

Equations of motion in a relative frame based at a reference point near L2 in the CR3BP were derived using an approach similar to that applied to the LEO formation flying model development in chapter 4.

The reference satellite could either be placed at the L2 libration point in the simplest case (although for large amplitude halo orbits the linearisation assumptions break down), or at a moving reference tracing a halo orbit near L2. Third order analytical solutions to the CR3BP for bounded halo motion around the Sun-Earth L2 Lagrange point were therefore proposed as the formation reference trajectory. However, the

linearised expressions for the gravity gradient in the CR3BP are applicable to either an analytically or numerically generated reference trajectory.

Solutions are considered, and used to derive some approximate initial conditions to eliminate secular motion for a limited period of time. However it was important to establish whether the model provided sensible results. Recently a new higher order relative motion model was developed by Segerman and Zedd (2003) (the SZ model), and this was deemed appropriate for some limited model comparisons. Both analytical models produced similar relative motion initial conditions, and when integrated with the third order reference halo (this had not been demonstrated previously for either model), overall model performance was similar in all three axes. The model performance was investigated further by investigating a wider range of initial conditions, and formation responses were found to be extremely sensitive to these. However, a feature of the CR3BP environment is the lack of stability of both the halo reference orbit and the formation without control. Comparisons with STK were therefore limited as although Solar radiation pressure was not considered, Lunar and planetary perturbations were incorporated in the simulations. As part of the model comparisons, a Darwin mission scenario was also investigated. When smaller initial relative velocities than those predicted by the analytical models were applied to the simulations, the gravity gradient model was found to perform sufficiently well.

Significant additional work is required involving the comparison of further test cases, and the investigation of the sensitivity of the relative motion to initial conditions and orbit perturbations. Additions to the complexity of the linear model should be avoided until the magnitude of errors over a wider range of conditions has been established. Potential modelling improvements include extension of the model to the ER3BP, the inclusion of higher order terms and relative perturbations in the initial equations of motion.

7 CONTROLLED FORMATION FLIGHT IN THE VICINITY OF L2

Within the stated aim of the research, chapter 7 describes the procedure and results of simulations of controlled mission manoeuvres for a Darwin-type mission. The mission needs to hold formation position or manoeuvre the formation sufficiently accurately to enable multiple telescopes and a beam combining hub to perform optical interferometry. The mission tasks involve extrasolar planet detection and astrophysical imaging from the vicinity of the Sun-Earth L2 Lagrange point.

In this chapter, an overview of the dynamics and control approach is presented. Initially, the cost of controlling a single satellite in a halo orbit is investigated using time invariant LQR control, and simulation in the perturbed environment using the Matlab/STK interface. The stability of a formation following a halo reference orbit in the vicinity of L2 is then established by eigenstructure analysis of the relative motion.

Formation control system design and preliminary analysis is performed using the dynamics models derived in chapter 6 which describe the relative motion of two spacecraft near L2. The concepts are extended to a general case with multiple telescopes and a hub for formation keeping and manoeuvring simulations in both Matlab and STK. Guidance functions are designed according to the manoeuvres derived in chapter 2 for integration with the control system, and a load-levelling strategy is derived to balance fuel use across the formation for a baseline expansion manoeuvre. As STK is unable to simulate interdependent controlled satellites, the simulation of a manoeuvre sequence requires a combination of off-line and on-line construction. However, total fuel consumption may be evaluated across the formation by summing the requirements for each manoeuvre, and once the solutions are compiled, the manoeuvres can be observed using STK visualisation tools. A global optimal solution is not considered for minimisation of overall fuel use, and instead the focus is fuel balancing.

7.1 Conceptual Control System and Simulation Design

The aim of the control system and simulation design is to produce preliminary fuel consumption and relative motion precision estimates for formation keeping and load-levelling manoeuvring of a formation of satellites performing infrared interferometry for extrasolar planet identification and observation. At this stage, a functional feedback controller rather than fully optimal controller was sought with the ability to integrate load-levelling guidance strategies. The emphasis of the work presented in this and subsequent sections has therefore been:

- The simple application of the relative dynamics model derived in chapter 6 to controller design.
- The investigation of load-levelling strategies for extrasolar planet observation and astrophysical imaging tasks.

- The implementation of the controlled formation in the perturbed numerical environment in STK to obtain greater insight into the effects of the local dynamics on formation keeping and load-levelling.

In chapter 3 (section 3.2.6), a number of different approaches to formation guidance and control in the vicinity of L2 were identified from the literature where fuel balancing manoeuvres for the interferometric imaging task for the ST-3 mission (comprising just three spacecraft, not in a planar formation) have been performed. However, these were not evaluated in the perturbed environment, or considered in the context of halo orbit maintenance which requires a sequence of different manoeuvres to be investigated. Guidance functions are produced for each satellite, and the individual spacecraft dynamics are simply represented by a double integrator (Bailey, McLain, and Beard, 2001). Trajectory following is performed using classical SISO control (van der Avoort, D'Arcio, and den Herder, 2003), (Beard, McLain, and Hadaegh, 1998), whereas here, a controller derived by considering the coupling between in-plane and out-of-plane dynamics is proposed instead. Bailey, McLain and Beard (2001) investigated global optimisation of a sequence of load-levelling manoeuvres for sampling the u-v plane (for interferometric imaging) and observing different targets, however, the formation is not maintained during the manoeuvres. Guidance for a Darwin-type mission that takes into account the local natural environmental dynamics, and performs accurate science manoeuvres (maintaining the formation during the manoeuvres) is therefore proposed. Also, all relative motion is governed by practical telescope-hub inter-satellite measurements of relative position and velocity.

The following aspects of guidance and control system design in this context are acknowledged, but are proposed as considerations for future work:

- The potential need for switching between different modes of interferometer operation and manoeuvre guidance and control.
- Optimisation of the manoeuvres and global fuel minimisation.
- Incorporation of additional manoeuvre limitations and additional modes of operation (for example, deployment, reconfiguration in the event of failure).
- Development of alternative control techniques and a thorough system evaluation (stability, robustness, disturbance rejection response across a full range of operating conditions).
- Autonomous operations.
- Inclusion of sensor noise and actuator dynamics.

Due to the strong coupling between particularly the in-plane (parallel to the ecliptic) relative dynamics, multivariable LQR is proposed as a suitable technique for simple feedback control system design. Continuous control will adequately represent a pulsed control system if the frequency of pulses is much greater than the local system dynamics, and for cold gas thrusters used for load-levelling manoeuvres, continuous operation is assumed. In addition, since measurement noise and sensor and actuator dynamics may also be critical to precision formation flying, the technique can be extended to Linear Quadratic Gaussian (LQG) control. In chapter 5, basic LQR controllers were implemented in LEO formation flying scenarios for formation keeping and trajectory following tasks, and ΔV was evaluated. In this case, the dynamic environment is completely different, and the scenario more complex, comprising

additional numbers of satellites, different levels of precision control, and simultaneous formation flying and halo orbit maintenance. The controller design concepts are also linked to the simulation approach taken due to the complications associated with interfacing the control system to the STK Astrogator numerical orbit propagator, particularly for the load-levelling tasks.

In the subsequent implementation of formation flying scenarios for a Darwin-type mission, full state knowledge is assumed. For the single satellite maintenance of a halo orbit, LQR gains are derived from the linearised time invariant three body problem equations of motion based at L2 and briefly compared to those derived from the time varying dynamics model in chapter 6. The latter are evaluated by integrating the differential Riccati equation and gravity gradient dynamics around the analytically derived reference halo orbit, also introduced in chapter 6 (Richardson, 1980a). A halo orbit trajectory following scenario can be easily implemented in STK using the Matlab/STK interface, and the simulation is described by the schematic of the formation control system inside the dashed line for the hub satellite in Figure 7-1.

A second scenario is then investigated whereby, in addition to the halo orbit maintenance (which is not necessarily continuously controlled), a formation keeping task is performed using new LQR gains for precision control. The telescopes are controlled relative to the hub as the formation moves around a near-halo orbit.

An alternative control system design, to be investigated as future work could involve the conversion of guidance commands to spacecraft actuator commands through the inverse of the model dynamics developed in chapter 6. Inversion errors and disturbances experienced by the satellites in STK could then be eliminated by LQR feedback control. In chapter 5 the trajectory following was really a form of model following since the trajectories were bounded solutions to the equations describing the natural dynamics to high fidelity. However, the dynamics are so slow in the vicinity of L2, that often they have not been considered at all (Beard et al, 1998). It is also therefore anticipated that a simple feedback gain will be sufficient to maintain the load-levelling trajectories prescribed to each satellite without dynamic inversion. The control and simulation system implemented within Matlab/STK for the two-spacecraft formation is illustrated in Figure 7-1.

The system design and operation is influenced by the fact that STK is unable to simultaneously propagate multiple controlled satellites which need to interact in order to determine their relative trajectories or control requirements. The control systems onboard each spacecraft cannot interact, or react to the accelerations provided to different members of the formation, or respond to relative measurements between different numbers of spacecraft collectively. However, a leader-follower architecture can be implemented where the leader spacecraft (hub) is free flying or controlled to follow a particular trajectory, and the followers (the telescopes) are controlled relative to the hub, but this arrangement is not practical for load-levelling manoeuvring. In addition, STK limitations prevent the development of complex controllers which, given a desired relative acceleration between members of the formation, are able to optimally distribute the load in real time. In this case (prior to load-levelling considerations), the

hub is propagated separately on the halo orbit, and each telescope is then also propagated separately relative to the hub.

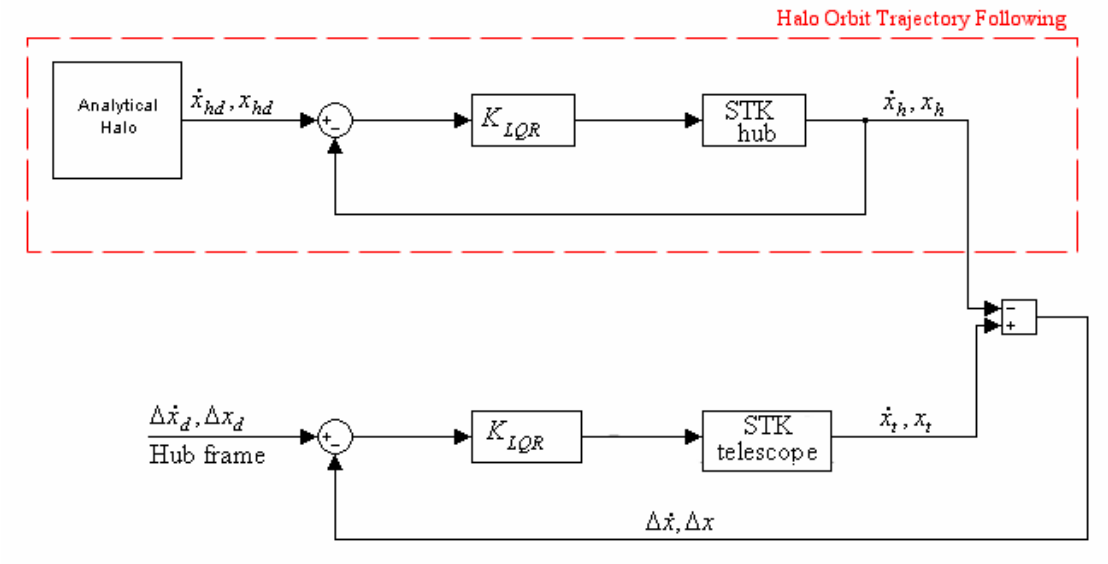

Figure 7-1: Control and Simulation System for Formation Flying around L2

In the low disturbance environment, potential propulsion systems include FEEP thrusters, mini ion engines and miniature cold gas thrusters. Load-levelling or fuel balancing across the formation is particularly relevant to cold gas thrusters to prevent the fuel supply from being exhausted on one spacecraft before another, and to ensure that the spacecraft fuel masses are equalised. According to d'Arcio and Karlsson (2004), a combination of thruster systems is being considered for the Darwin interferometry mission:

- mN-level thrust in the manoeuvring and reconfiguration modes.
- μN-level thrust for fine baseline and attitude control in the nulling mode.

Finally, a guidance strategy for a load-levelling system for a greater number of telescopes formation flying with a central hub is proposed, although some assumptions have to be made regarding the system implementation in STK. This time no satellite is forced to follow the halo reference trajectory, drift is permitted during the manoeuvres, and a virtual point is maintained with respect to the analytical halo trajectory at intervals around the orbit. In this case the LQR controller initially acting on the hub can now be applied to the virtual formation reference point, and the formation (including the hub) can be controlled relative to this. The control and simulation system architecture is illustrated in Figure 7-2.

Again, the implementation and complexity of the load-levelling guidance and control system is restricted due to the formation interaction and simultaneous propagation limitations of STK. In future analysis, a Matlab/Simulink simulation of the nonlinear equations of motion of the three body problem with perturbations would be more appropriate for analysing controller designs.

The framework illustrated in Figure 7-2 enables load-levelling guidance to be generated effectively on board each satellite. However, this is based on a virtual reference point whose location cannot update as fuel is consumed by each spacecraft. Due to the duration of the selected manoeuvres, the formation is not controlled rigidly to the halo, as the natural dynamics will maintain the formation in the vicinity of the halo for a significant period before it is able to diverge away. Instead the performance of the system in making halo orbit corrections simultaneously with station keeping (spectroscopy) tasks is investigated. In this case the relative satellite positions are maintained between periods of load-levelling manoeuvres.

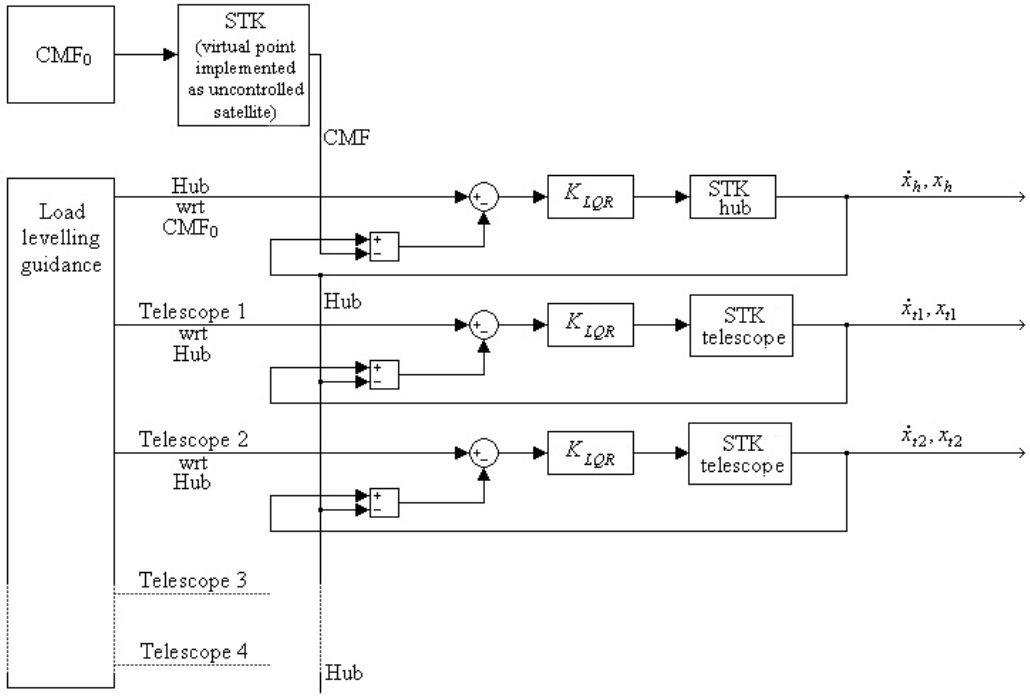

Figure 7-2: Control and Simulation System for a Load-Levelling Manoeuvre around L2

A manoeuvre sequence may be compiled as an Astrogator sequence in STK, but the benefits of making this fully autonomous from a simulation implementation perspective are not sufficient compared to the complexity of the Matlab/STK interface required. Instead, it is proposed that the selected sequence manoeuvres be evaluated one at a time, and the next be given the initial conditions derived from the last so that load-levelling performance can be measured and total ΔV evaluated for the whole sequence. The manoeuvres can still be arranged sequentially for visualisation using STK tools, and this facility is also investigated.

7.2 Single Satellite Control in a Halo Orbit

In this section, LQR controllers are designed using three techniques:

- Solution of the algebraic Ricatti equation using the linear time invariant equations of relative motion given by equations (7-1), based at the L2 point.
- Solution of the algebraic Ricatti equation to derive gains at intervals around the periodic halo reference orbit using the periodic time varying dynamics given by equations (7-2) to (7-4) (introduced in chapter 6).
- Integration of the differential Riccati equation simultaneously with the relative dynamics model around the halo reference orbit.

The following models were derived in section 6.2.2.

Linear Time Invariant L2 Model

$$\begin{aligned} &\Delta\ddot{x} - 2\Delta\dot{y} - (2\sigma + 1)\Delta x = 0 \\ &\Delta\ddot{y} + 2\Delta\dot{x} + (\sigma - 1)\Delta y = 0 \\ &\Delta\ddot{z} + \sigma\Delta z = 0 \end{aligned} \tag{7-1}$$

Linear Time Varying Gravity Gradient Model Based at a Halo Reference

$$\begin{aligned} &\Delta\ddot{x} - 2\Delta\dot{y} - (2\sigma + 1)\Delta x = 6\alpha\delta x\Delta x \\ &\Delta\ddot{y} + 2\Delta\dot{x} + (\sigma - 1)\Delta y = 3\alpha(\delta y\Delta x + \delta x\Delta y) \\ &\Delta\ddot{z} + \sigma\Delta z = 3\alpha(\delta z\Delta x + \delta x\Delta z) \end{aligned} \tag{7-2}$$

where

$$\sigma = \frac{(1-\rho_m)}{R_s^3} + \frac{\rho_m}{R_e^3} \qquad \alpha = \left(\frac{(1-\rho_m)(x_o + \rho_m)}{R_s^5} + \frac{\rho_m(x_o - 1 + \rho_m)}{R_e^5} \right) \tag{7-3}$$

and where the halo reference orbit is defined by Richardson (1980a).

$$\begin{aligned} \delta x &= a_{21}A_x^2 + a_{22}A_z^2 - A_x\cos\tau_1 + (a_{23}A_x^2 - a_{24}A_z^2)\cos 2\tau_1 + (a_{31}A_x^3 - a_{32}A_xA_z^2)\cos 3\tau_1 \\ \delta y &= kA_x\sin\tau_1 + (b_{21}A_x^2 - b_{22}A_z^2)\sin 2\tau_1 + (b_{31}A_x^3 - b_{32}A_xA_z^2)\sin 3\tau_1 \\ \delta z &= \delta_n A_z\cos\tau_1 + \delta_n d_{21}A_xA_z(\cos 2\tau_1 - 3) + \delta_n(d_{32}A_zA_x^2 - d_{31}A_z^3)\cos 3\tau_1 \end{aligned} \tag{7-4}$$

Linear Quadratic Regulator theory was described in section 5.2, chapter 5, and is therefore not repeated in detail here. The control weighting matrices, Q and R, in the quadratic cost function, J relate to the dynamic states and control inputs respectively.

$$J = \int_0^\infty x(t)^T Qx(t) + u(t)^T Ru(t)dt \tag{7-5}$$

The weighting matrices were tuned according to the maximum thrust limits for different scale manoeuvres, and in the following subsections, two scenarios are considered. In the

first case, the LQR gains are tuned to achieve basic halo orbit maintenance with a representative fuel consumption. In the second case, the ability of the formation to manoeuvre back to the halo reference within the capacity of micro-Newton thrusters used in the science manoeuvres is investigated. (This may be required between load-levelling manoeuvres and during the spectroscopy task).

ΔV evaluations are made using equation (7-6) for comparative purposes only. For the simulations performed in this chapter, there are too many variables associated with the STK simulation to make accurate ΔV estimates without in-depth analysis. However, the investigation performed here provides insight into the capacity of such low thrust levels to control the halo orbit formation, for station keeping, manoeuvring and halo orbit maintenance.

$$\Delta V = \left[\sum \left(a_x^2 + a_y^2 + a_z^2 \right)^{1/2} \right] * \text{TimeStep} \qquad (7\text{-}6)$$

In the following sections, feedback gains are evaluated offline using both models (equations (7-1) and (7-2)) before being implemented within the STK simulation environment for evaluation of the control of a single satellite in a halo orbit around the Sun-Earth L2 point.

7.2.1 Halo Orbit Maintenance

In this scenario, the ΔVs are likely to be higher than those reported in the literature, and experienced in practice with the Lagrange point missions, as in this simulation, the reference for trajectory following is an approximate analytical solution and continuous control is applied. In reality, halo orbit maintenance would be performed at intervals around the halo orbit to retain a natural near-halo. This has proven less costly in practice for the ISEE-3 mission. In addition, the flexibility associated with the choice of weighting matrices in the LQR design can increase or decrease the ΔV depending on how closely the analytically described halo should be maintained.

For the simplified dynamics given by equation (7-1), the effects of the weighting matrices were investigated through both Matlab simulation and STK formation control. In this case, a design point was not defined at the outset as the objective was to design a controller which would satisfactorily maintain the analytical halo orbit around L2 using milli-Newton level thrust and a reasonably low ΔV. Using weightings of 10^{-3} in position (Q), 10^{-6} in velocity (Q), and 1 in control (R), a set of feedback gains, decoupled in the x-y (ecliptic) and z (out-of-the-ecliptic) directions were derived. These are given by equation (7-7).

$$K_{LQR} = \begin{bmatrix} 3.8111 & 2.0784 & 0 & 13.5645 & -2.4449 & 0 \\ 2.0748 & 1.1497 & 0 & 7.4149 & -1.3363 & 0 \\ 0 & 0 & 0.0160 & 0 & 0 & 0.0001 \end{bmatrix} \qquad (7\text{-}7)$$

The offline response which regulates an initial 10km error to zero in all three axes during a single halo is illustrated in Figure 7-3. This figure demonstrates the difficulty with offline controller design in this context as the response to an initial 10km error (in x, y and z) is clearly very poorly damped. However, accelerations at the $10^{-9}ms^{-2}$ level are being applied to the spacecraft, and yet in the formation flying scenario in STK, this level of continuous control is adequate for maintaining the halo over a number of orbits. The gains associated with a fully damped offline response produced large thrusts, increased fuel consumption significantly, and over-controlled the satellite in the perturbed STK environment.

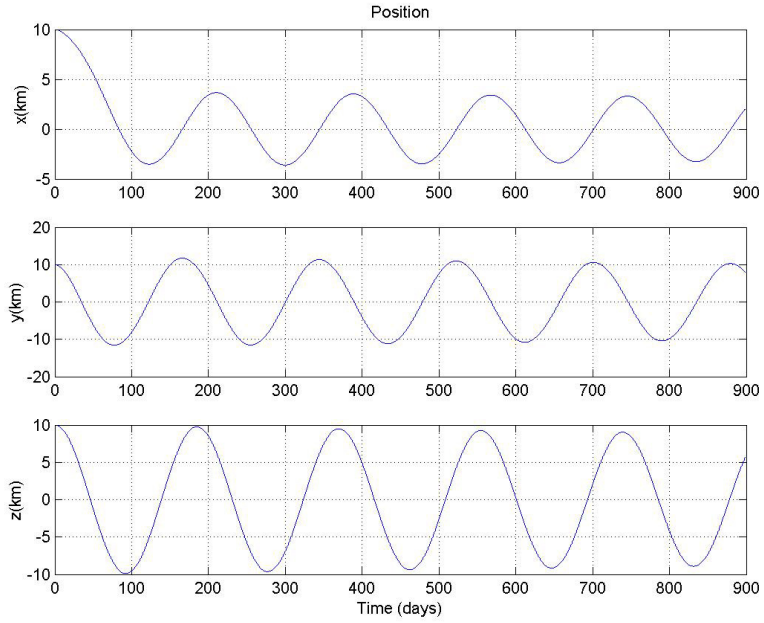

Figure 7-3: Offline (Matlab Dynamics Model) Response over 5 Orbits to an Initial 10km Error in x-y-z Position (Darwin Halo Scenario)

A halo maintenance scenario was implemented in STK for a Darwin-type mission. The orbit characteristics for Darwin are given in Table 6-5, and the third order halo reference trajectory is illustrated in Figure 6-7. The halo orbit defined by equations (7-4) was used to define the desired trajectory for a satellite flying in STK. A single satellite was provided with an onboard controller using the Matlab/STK interface, which was originally developed in chapter 5 for LEO formation flying control. The controller successfully maintained the halo orbit, using a ΔV of 58.94m/s over 1 orbit in the presence of Lunar and planetary perturbations. The uncontrolled and controlled trajectories are illustrated in Figure 7-4. When Solar Radiation Pressure (SRP) is included in the simulation (for a Darwin-type hub with a Sun shield of 5m diameter – refer to Table B-3, appendix B.2) the ΔV was found to decrease to 56.12m/s though this maybe due to a fortuitous set of initial conditions rather than a general trend. In the literature, a number of authors have proposed the use of SRP for halo orbit maintenance, however, for the remainder of the analysis presented here, the SRP is not included in the simulations.

Figure 7-5 illustrates the thrust profile generated by a 500kg satellite during the halo orbit maintenance manoeuvres illustrated in Figure 7-4. (The mass of the hub spacecraft was defined as a combination of the Darwin hub and the Master satellite masses (Table B-3, appendix B.2). The results indicate that the required thrust level can be achieved by cold gas milli-Newton thrusters.

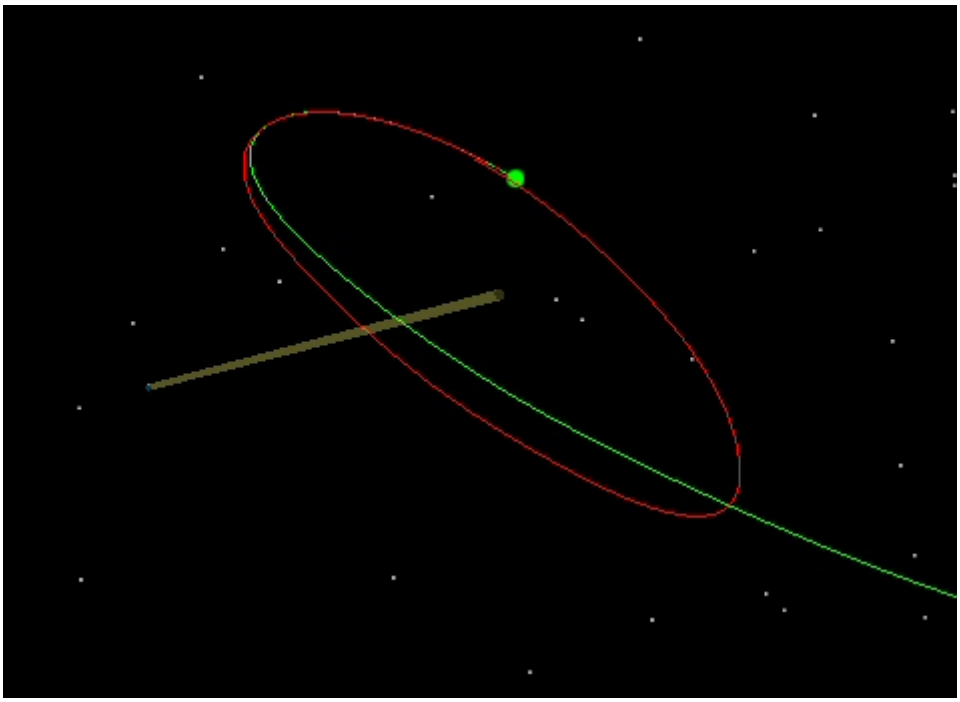

Figure 7-4: Uncontrolled and Controlled Trajectories for the Darwin Halo Orbit in STK

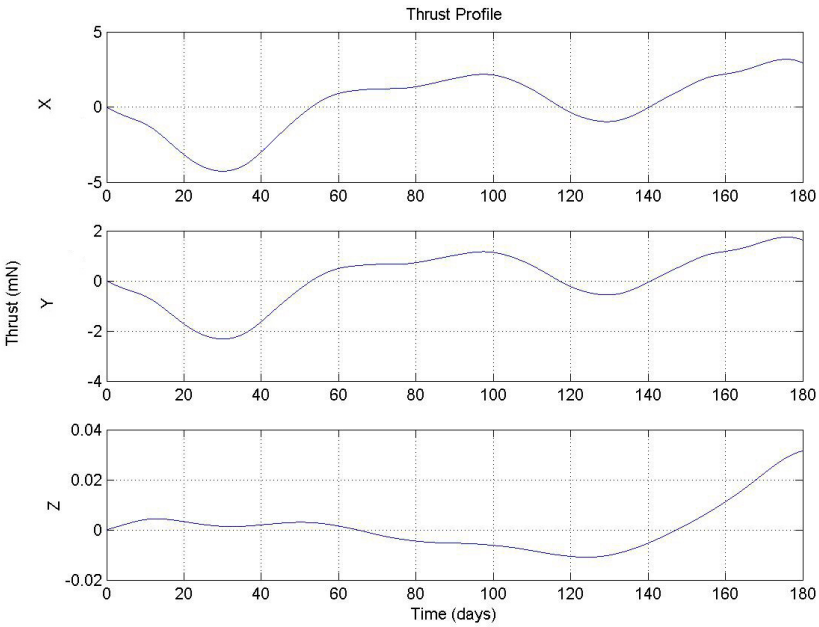

Figure 7-5: Thrust Profile for Halo Orbit Maintenance

For comparison, controller gains were evaluated around the halo reference orbit for a similar scenario. Numerical solutions to equations (5-15) and (5-16) were evaluated by implementing them in Simulink, within the linear gravity gradient dynamics model (Figure 6-3), and propagating the system for one orbit. However, a full implementation of the results to investigate the cost of halo orbit maintenance using this technique is reserved for future work. The elements of the gain matrix for the same Q and R values defined above were found to be similar in proportion, with increase coupling in the z axis, as expected due to the coupling in the equations. For example, the initial gain matrix was given by equation (7-8).

$$K_{LQR_{TV}} = \begin{bmatrix} 2.6201 & 2.0784 & -0.0055 & 7.5819 & -2.5271 & -0.0176 \\ 1.5070 & 1.1497 & -0.0013 & 4.4042 & -1.4703 & 0.0122 \\ -0.0055 & -0.0013 & 0.0079 & -0.0017 & -0.0107 & 0.00005 \end{bmatrix} \quad (7\text{-}8)$$

For the following investigations, different gains were derived from the time invariant model since the benefits of applying the time varying gains were not clear, and fuel economy achieved may be masked by other aspects of the simulation.

7.2.2 Station Keeping for Spectroscopy

In the absence of corrective control, it was established in chapter 6 (Figure 6-7) that the degree of drift for a halo orbit (with a maximum amplitude of approximately 780000km in Y) from the analytical reference, over 20 days, was:

- 9854km in X (along the Sun-Earth line)
- 1044km in Y (in the ecliptic)
- 1150km in Z (out of the ecliptic)

The initial velocity of the spacecraft on the halo was approximately $342ms^{-1}$ (Table 6-5). For this test case, a design point was selected which would control a spacecraft offset from the halo orbit and gradually manoeuvre it back towards the reference halo trajectory in an optimal manner. Of particular interest was whether this could be achieved during precision station keeping spectroscopy modes using micro-Newton level thrust.

Formation flying requirements for an example spectroscopy task were defined in section 2.3.1.2 of chapter 2, but in this case, the gradual manoeuvre of the whole formation back to the halo reference orbit is considered (where halo orbit maintenance cannot be performed during a load-levelling manoeuvre). Equivalently, this can be considered in terms of the control of a single satellite in a halo orbit using very low thrust levels, appropriate for the station keeping spectroscopy task.

Implementation of this scenario in STK revealed that to achieve such low levels of thrust, the spacecraft (formation) would not be able to trace the prescribed halo trajectory. However, although a consistent halo trajectory was not obtained during the simulation, the spacecraft did not diverge from a near halo-type orbit with the control system provided (Figure 7-6).

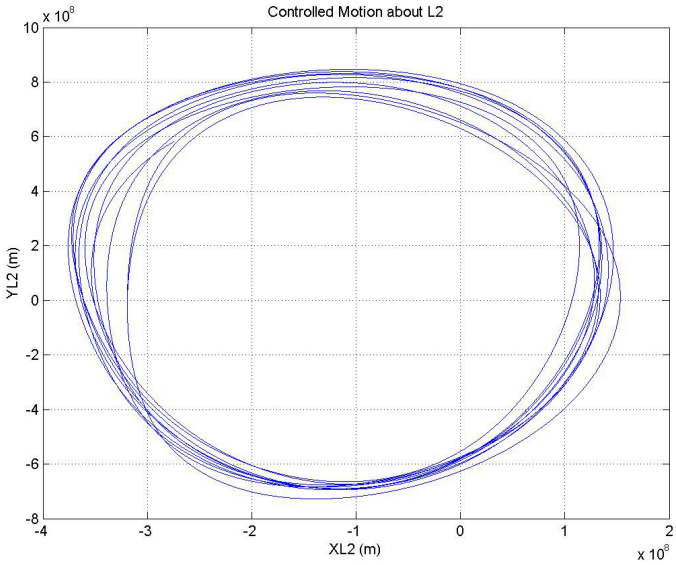

Figure 7-6: Controlled Halo Orbits over a 5 Year Period

7.3 Formation Flying in a Halo Orbit with Basic Guidance

Building upon the preliminary single satellite halo orbit control implementation in section 7.2, the stability of the region around the reference trajectory was investigated by evaluating the eigenvalues of the relative dynamics matrix around the Darwin halo (based on equations (7-2)). The loci representing eigenvalue variations around the halo orbit are illustrated in Figure 7-7. In all cases the open loop eigenvalues have real parts which transition between the positive and negative around the orbit, and therefore stability augmentation is required for formation control around L2.

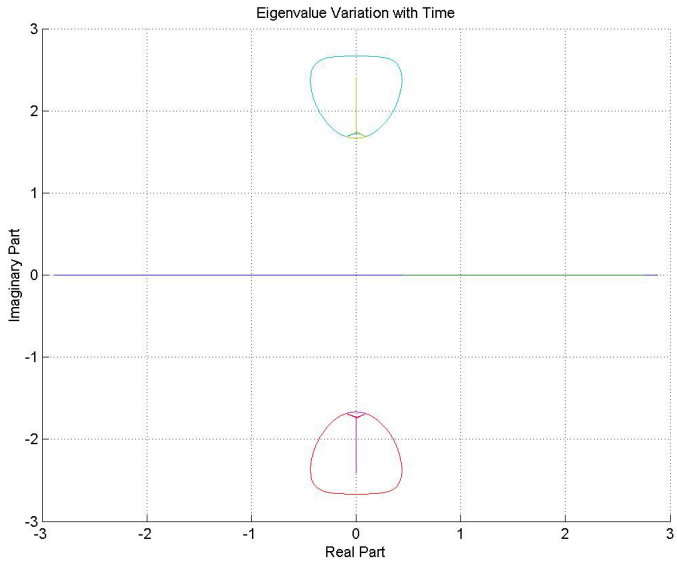

Figure 7-7: Eigenvalues Around the Halo Orbit

In this section, the LQR design process summarised in section 7.2 using the relative dynamics models was repeated for a new design criterion which required higher gain control for relative trajectory following. In this case, the formation must remain tightly controlled to the relative motion trajectories prescribed by a guidance function, implemented in STK using the control and simulation system architecture introduced in section 7.1.

In this case a station keeping task and a formation rotation around the reference or hub satellite were investigated. In both cases the hub is allowed to remain free flying, and a guidance trajectory relative to the hub is implemented onboard a follower satellite (note that load-levelling is not considered).

Station Keeping

A station keeping manoeuvre (derived in chapter 2) was simulated in STK using one free flying satellite in a near-halo orbit, and a second satellite controlled relative to the first (to maintain a constant relative position offset), according to the following specifications:

- No permitted formation rotation
- Relative position maintenance to 1cm accuracy
- Formation baseline = 74.25m (x-axis separation)
- Manoeuvre duration = 6days

The basic LQR controller, tuned for precision trajectory following over short distances (compared to halo orbit maintenance), demanded a total ΔV of 10^{-5}m/s, and a thrust profile at the 0.01μN level for station keeping in the perturbed STK environment. Relative position was maintained to well within the 1cm requirements, experiencing only sub-millimetre position error.

Rotation Manoeuvre

The rotation manoeuvre specified in Table 2-12 was also implemented by providing a circular relative position trajectory and circumferential velocity to the follower satellite to force it to rotate about the free-flying reference. The following manoeuvre characteristics were specified:

- A rotation rate of 0.00333^{o}/sec (to be precisely maintained)
- Hub-telescope separation = 63.3m (half the maximum baseline)
- A 30hr manoeuvre duration for a 360^{o} formation rotation
- Relative position maintenance to 1cm accuracy

The resulting relative motion in the perturbed STK environment is illustrated in Figure 7-8. However, Figure 7-9 clearly shows that with the controller gains selected, the relative position accuracy is not achieved. In Figure 7-10, the thrust profile demonstrates that milli-Newton level thrust is required for this type of formation manoeuvre, and a total ΔV requirement of 0.125m/s was determined from the analysis. Further tuning of the controller is therefore required.

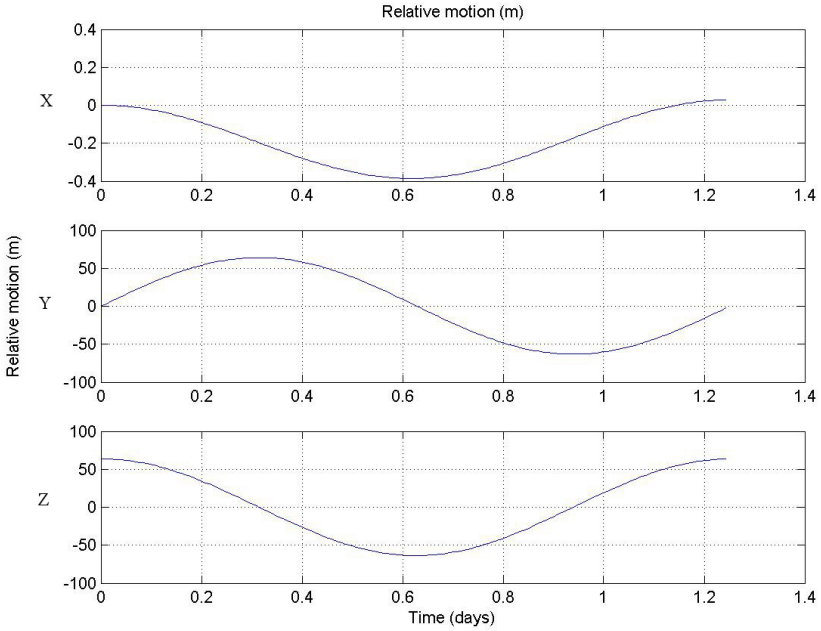

Figure 7-8: Relative Rotation of the Hub and Telescope for a Extrasolar Planet Detection Maneouvre

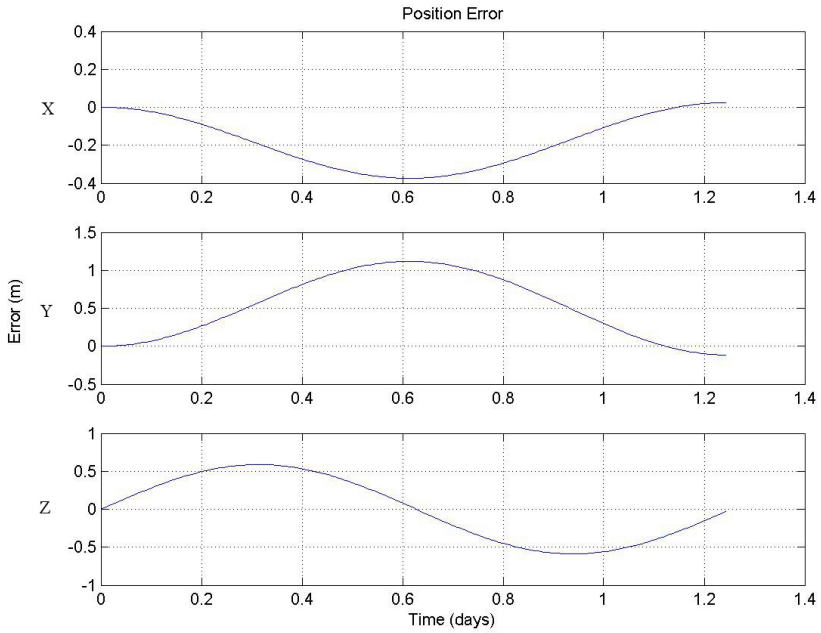

Figure 7-9: Position Error Associated with the Formation Rotation Manoeuvre

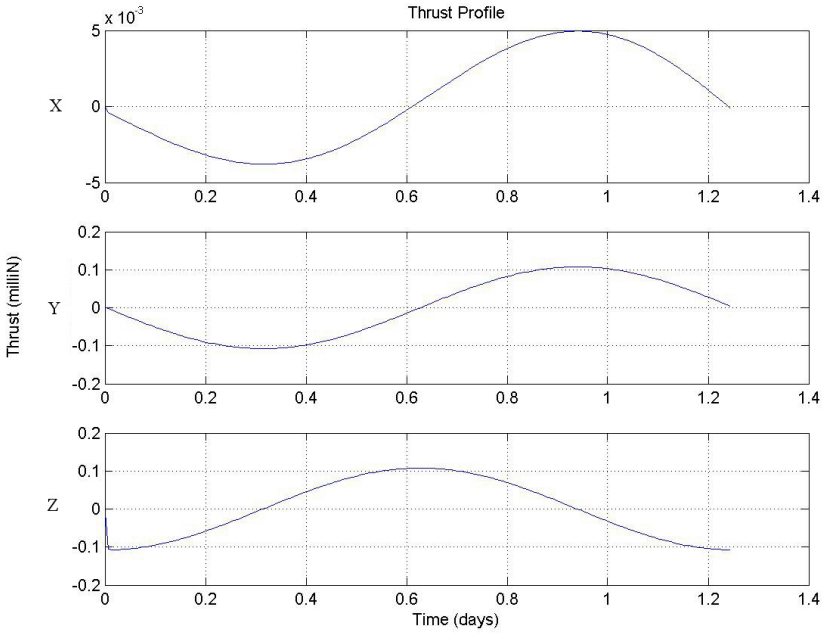

Figure 7-10: Thrust Profile for the Rotation Manoeuvre

7.4 Guidance Strategy for Load Levelling Manoeuvres

To manoeuvre a formation while balancing fuel or 'load-levelling' across the formation, it is necessary to define the concept of load-levelling as applied to this study more precisely. In this case the following definitions were considered:

- From an initially un-balanced configuration, the manoeuvre would drive the formation to be fuel-balanced by the end of the desired manoeuvre.
- Load-levelling is a mission-duration objective.

Sometimes it will not possible to achieve a completely balanced load-levelling manoeuvre due to the magnitude of the differences in fuel mass on each spacecraft, the relative masses of the spacecraft themselves, or other manoeuvring restrictions (for example, duration of manoeuvre, maximum individual spacecraft acceleration, maximum relative velocity).

The problem is therefore not as straightforward as it initially might appear. In this section, the guidance for a load-levelling formation expansion is derived. The manoeuvre specification was identified in chapter 2 and would be appropriate for the Darwin mission. The formation is assumed to comprise a number of telescopes in a planar formation with a central hub. The objective is, from an initial un-balanced state, to achieve a fuel-balanced formation following manoeuvres described in the following sections. Deriving the trajectories for collision avoidance and using optimisation routines, while important, is saved for future work.

7.4.1 Guidance Architecture

In order to formulate the load-levelling guidance strategy, the axes systems and reference points in which and about which the manoeuvres are derived must be defined. The combination of formation and halo-orbit maintenance is also considered in a load-levelling context.

Figure 7-11 illustrates the axis systems and reference points considered when deriving the formation load-levelling manoeuvres.

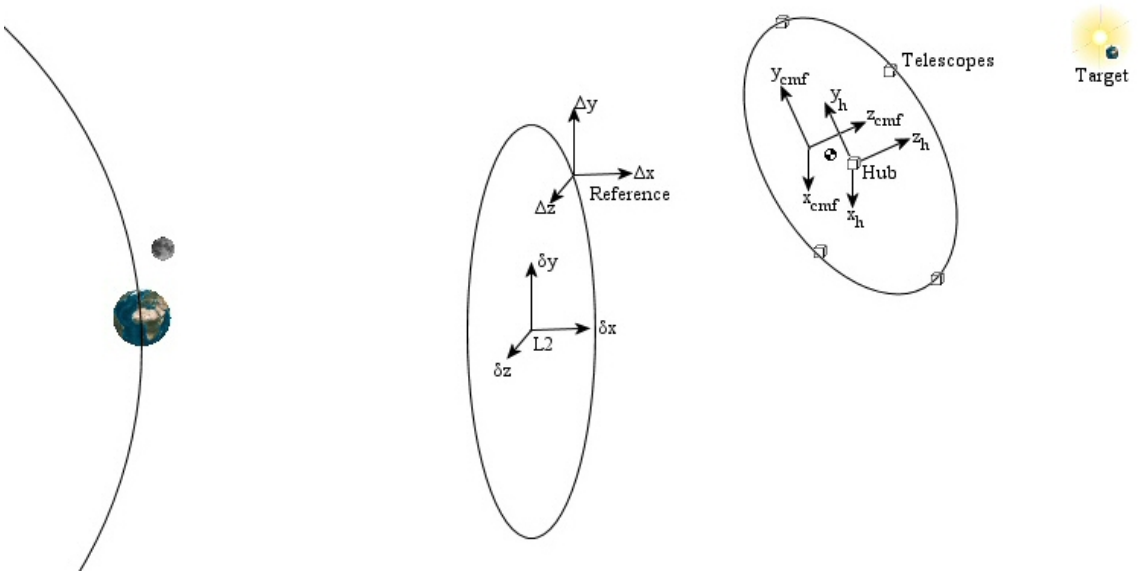

Figure 7-11: Axis Systems and Reference Points for Load-Levelling Guidance (h = hub, cmf = centre of minimum fuel mass)

The familiar halo reference orbit forms the reference point and axis system from which the centre of mass of the formation and an alternative virtual reference point termed the 'centre of minimum fuel' are measured. The location and definition of these virtual reference points are described below.

By mission definition (chapter 2), the Darwin formation is planar, and when prescribing relative motion between the telescopes and the hub, it is useful to reorient the axis system into this plane. The halo reference frame is aligned with the axes on the Sun-Earth barycentre line at L2 and can be easily converted into the formation plane at any pointing direction. During the science manoeuvres, the inertial pointing direction and therefore the plane of the formation must remain constant (gently slewing over time with respect to the halo/L2 axes to remain pointing at a target).

Control of the whole formation for halo orbit maintenance is performed by continually updating throughout the mission, the centre of mass of the formation. The key to achieving load-levelling during a manoeuvre is the identification of the centre of minimum fuel mass. This is calculated in the same manner as a centre of mass of the system, but instead only considers the mass of fuel onboard each spacecraft, or in the case of large differences in spacecraft mass across the formation, the ratio of the mass of

each spacecraft to the fuel it contains. In the latter case, this means that as a guidance manoeuvre is generated, the masses of the spacecraft themselves are also considered, rather than just the distances by which they have to travel as both factors contribute to the ΔV consumed. The centre of minimum fuel mass is given by equation (7-9) with respect to the halo reference orbit in the halo orbit axis system where L is the distance between members of the formation and the halo reference orbit, β is the spacecraft fuel mass fraction, and m is the sum of the 'lack of fuel' (the total mass of fuel minus the fuel fraction, summed across the formation).

$$CMF = \frac{\sum_{i=1}^{5}(1-\beta_i)L_i}{\sum_{i=1}^{5} m_i} \tag{7-9}$$

In the (non-STK) load-levelling simulations, this is continually updated as fuel is used on the satellites, so that the degree of significance of the effect can be investigated. For the manoeuvres implemented in STK, the initial centre of minimum fuel (CMF) is assumed constant for the duration of that manoeuvre, and it is re-evaluated at the start of the next manoeuvre. For a more optimal solution, the variation in CMF during a manoeuvre must be taken into account. The size of the variation of centre of minimum fuel mass during the manoeuvre may be critical for a formation that is initially significantly unbalanced.

An additional important factor to consider in the selection of reference points is whether the virtual reference points are an appropriate place from which to generate guidance functions. It is unknown whether these virtual points could be instantaneously determined during a manoeuvre in practice, as all the spacecraft may be moving. For some manoeuvres it may only be possible to locate a reference point at one of the spacecraft, and define manoeuvres from there, although as sequences of manoeuvres build up, the reference spacecraft could switch as part of the load-levelling strategy.

During a manoeuvre, the relative motion guidance may be able to load-level across the formation, but the formation may drift in the vicinity of the halo reference orbit. This is a desired effect as to maintain a precise halo, for example by controlling the hub, and forcing all the telescopes to maintain position or manoeuvre relative to the hub, would be too costly. Instead, it is conceptually more appropriate for the centre of mass of the system to be considered the formation frame or 'centre' which must be maintained in the vicinity of the halo.

Integrating the halo maintenance into the forms of load-levelling guidance system proposed is not possible. It has been suggested for TPF (Gomez, Lo, Masdemont, and Museth, 2001) that that halo orbit maintenance could be integrated into the formation science manoeuvres for the TPF mission, but this did not require fuel balancing, and simply evaluated the thrust levels required to ascertain whether the appropriate levels of thrust for both types of manoeuvres could be simultaneously obtained. Also, it is known (Farquhar, Muhonen, Newman and Heuberger, 1980) that only periodic corrections are required to maintain a halo around the Sun-Earth L2 point. In this analysis, it is

therefore proposed that halo orbit maintenance is performed during station keeping science operations. In this case, the whole formation would be translated until the formation centre of mass is relocated to the halo reference (in this case the analytical solution is the reference halo, although in practice, and for a more detailed study, a numerical solution would be used).

7.4.2 Formation Expansion

In this subsection, the approach to load-levelling guidance for initial investigation of the problem is presented. Two formation expansion manoeuvres were described in chapter 2 (Table 2-12), and the proposed trajectory generation tool would be applicable to either. The trajectory expansion is performed from the centre of minimum fuel (CMF), evaluated at manoeuvre initialisation, and allowed to vary as fuel is used during the manoeuvre. By Newton's laws of motion, the maximum acceleration required by each satellite is given by equation (7-10)

$$a_{max} = -\frac{v_{max}^2}{d - v_{max} t_{man}} \qquad (7\text{-}10)$$

where d is the absolute distance a satellite must move, t_{man} is the duration of the manoeuvre, and v_{max} is the maximum relative velocity between the spacecraft. The manoeuvre limitations and requirements are given in relative terms, and therefore it is necessary to consider the following:

- Maximum absolute acceleration (according to maximum allowable thrust for each satellite)
- Maximum relative velocity between members
- Manoeuvre duration
- For what proportion of the manoeuvre a constant relative velocity between the satellites and the hub is required in order to perform science tasks.

The most efficient trajectory for this manoeuvre type has a bang-coast-bang profile with a constant mid-manoeuvre velocity. A relative position and velocity profile relative to the hub is provided to each telescope, and a manoeuvre profile is also provided to the hub to enable load-levelling across all the formation (and not just the telescopes). The hub profile is expressed relative to the centre of minimum fuel, but in the halo reference coordinates. Figure 7-12 illustrates the baseline expansion manoeuvre. These profiles can be followed using tight feedback control based on measured relative position data between the hub and telescopes. An alternative simulation model is currently under construction, which will not require STK to behave as the perturbing 'real' environment (although this research extends beyond the scope of this thesis). Instead increased visibility of the dynamics and control problem is preferred for early analysis. In addition, the ability to simulate multiple controlled and interacting spacecraft is required to investigate formation load-levelling and obtain meaningful results.

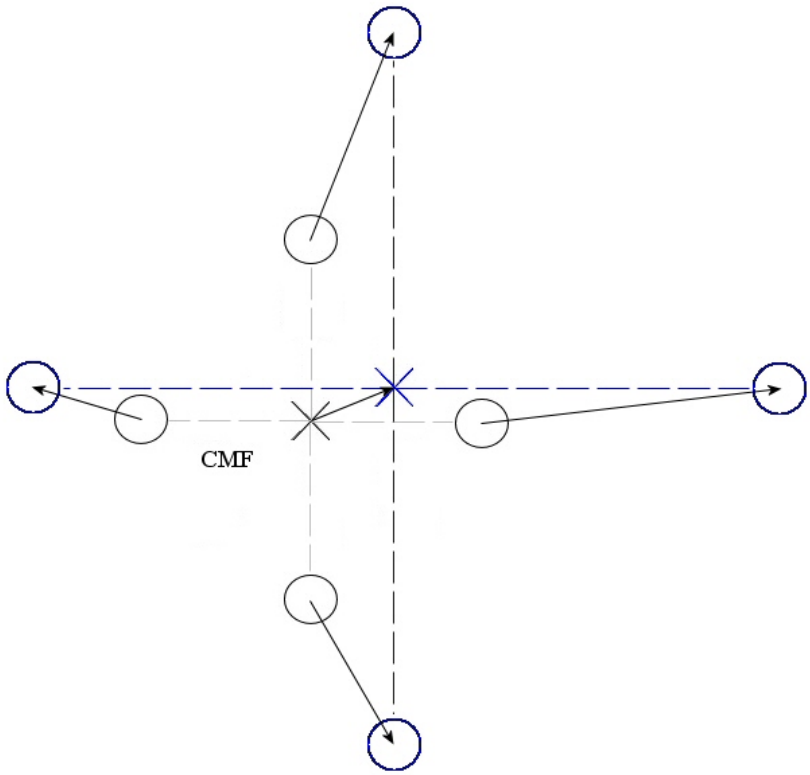

Figure 7-12: Load-Levelling Formation Expansion Manoeuvre, With Each Spacecraft Moving Away from the Centre of Minimum Fuel Mass to Achieve the New Baseline.

7.5 Discussion and Proposed Further Work

The results presented in this chapter represent the start of another fascinating phase of research which must be investigated in much greater detail in order to draw reliable conclusions. Part of the issue is the lack of visibility of the dynamics and effects of controller gains in the STK simulation environment. To date, the dynamics models derived in chapter 6 have not yet been exploited to their full potential, and it is proposed that these be used for more detailed offline formation manoeuvring studies prior to any further control system evaluations in STK. Initial findings have demonstrated that a simple LQR controller is not necessarily appropriate for all types of manoeuvre, and gain scheduling or mode switching within a more complicated control system is required to transfer between the nulling interferometry and extrasolar planet detection operational modes.

Early results have demonstrated that, using different controllers for different operational modes, halo orbit maintenance and formation rotation manoeuvres require thrust at the milli-Newton level, and high-gain precision station keeping manoeuvres can be performed at the micro-Newton thrust level for satellites with a relatively small separation. It is possible to maintain a near-halo orbit around L2 using low levels of thrust, but whether this can be achieved for a full mission lifetime, when only periodic

corrective manoeuvres can be applied between load-levelling modes, should be investigated.

The application of the relative dynamics model to a very basic LQR controller design has been successfully demonstrated, and a design and visualisation tool which will be useful for further research, has been developed using Matlab and STK. It is suggested that future load-levelling simulations be implemented in a Matlab environment to maximise visibility of the dynamics, and to enable time varying fuel mass to be fed back into the load-levelling control system.

The load-levelling strategy presented here for the baseline expansion manoeuvre can apply to any other type of formation manoeuvre. The critical concept is the role of load-levelling, which does not apply to every manoeuvre, and the use of a variable centre of minimum fuel mass as a reference point from which the balancing manoeuvres can be defined.

Some of the remaining tasks relating to this particular investigation have been identified as follows:

- Complete the load-levelling simulation tool in Matlab
- Adapt the tool for the more up-to-date Darwin configurations.
- Analyse a wider range of formation manoeuvres (include slewing).
- Investigate further the differences in simulation results (precision of formation maintenance, fuel consumption estimates) between an offline control system, designed using the derived dynamics models and STK.
- Augment the relative dynamics models to include relative attitude.
- Analyse further the benefits of applying feedback gains derived from the gravity gradient model (chapter 6), rather than the time invariant relative motion equations defined at L2.
- Investigate further the claim that relative position can be simultaneously controlled while performing halo orbit maintenance.
- Incorporate sensor noise and actuator limits into the controller design.
- Investigate the application of the gravity gradient relative motion model to navigation or relative trajectory generation.
- Combine load-levelling manoeuvre generation with the new gravity gradient dynamics model to take into account the local dynamic environment, and minimise fuel use further (possibly by dynamic model inversion).
- Combine fuel balancing strategies with overall fuel minimisation strategies to solve the global optimal control problem.

8 CONCLUSIONS AND FURTHER WORK

In this final chapter, the main findings of the research are summarised and conclusions are drawn. Proposed areas of future work relating to all the areas investigated in the thesis are also presented, although more detailed suggestions have often been presented during the discussion of results, conclusions or summary of the relevant chapter. Here, proposed further work is presented at a more general level.

8.1 Summary and Conclusions

The investigation process and results of three years of research have been presented in this thesis. Detailed investigations into satellite formation flying applications, systems, dynamics and control have been performed. Following the definition and role of satellite formation flying and a survey of current and future missions, a target mission with the purpose of detecting and characterising extrasolar planets was selected as a focus for the research. In the absence of an astronomy background, it was necessary to gain insight and understanding of the purposes of such a mission, and the techniques that could be applied to achieve the mission objectives. This is due to be published in a separate report (Roberts, 2006).

The spacecraft system and science application requirements were found to be critical to the formation flying dynamics and control analysis which has formed the ultimate focus of the research. Chapters 1 and 2 therefore present the background and motivation for the research, leading to the preliminary design of a Planet Imager mission and definition of formation manoeuvring requirements for science operations, and chapters 3 to 7 have focused on formation flying dynamics and control. In this section, a summary of the thesis is presented, and supplemented with a concise statement of the conclusions.

8.1.1 Thesis Summary

Defining satellite formation flying was not as straightforward as might be anticipated. Three types of spacecraft formation were identified, but a formation was only deemed to be formation flying when on-orbit position maintenance of the spacecraft was controlled through measured relative separation, combined with a minimal level of collective autonomy. The applications of the different types of formations were identified, and these could be broadly categorised into military, communications and scientific missions. In particular the science applications included:

- Simultaneous scientific field measurements
- Earth surveillance from LEO (by interferometry or aperture synthesis)
- Interferometry for astronomical observations

Following a survey of current and future formation flying missions, the third application was selected for further study, and in particular, the ESA Darwin mission. Darwin has the primary objective “to detect and study Earth-type planets and characterize them as

possible abodes of life" (Fridlund, 2002). The mission aims to detect Earth-like planets in the Habitable Zone, determine planetary characteristics, and analyse the planetary spectrum. A second mission objective also exists to perform astrophysical imaging.

The complexity of the optical systems and the formation control problem associated with the operation of multiple telescopes as a single observatory was highlighted in chapter 2. Through the consideration of optical theory, the processes by which different types of single and multi-aperture optical systems capture astrophysical images, and perform extrasolar planet detection and spectral analysis was established and the findings are discussed in Roberts (2006). The ability of interferometry to increase the resolution of the optical system was established, although the dual application of extrasolar planet observation and astrophysical imaging using the same optical system remains a challenge at the high level system design. The former is more effectively achieved by pupil-plane interferometry, and the latter by image-plane interferometry, capturing image signals in the time and spatial domains respectively. The theory of nulling interferometry was ultimately applied to an interferometry mission design (discussed below), which aimed to remove the stellar light from the image to reveal the presence of a planet, by placing a zone of destructive interference in the transmission map over the bright star, thus enabling light from the dimmer planet to be detected.

Supported by a summary of the technical requirements and performance specifications for the Darwin mission, and significant background research into the optical, astronomical and astrobiological design drivers associated with interferometry mission design, the following tasks were performed:

- Derivation of suitable manoeuvres for a Darwin-type mission performing extrasolar planet detection, observation and characterisation.
- A preliminary Planet Imager mission design

The operational modes of the interferometer were established in order to appreciate the precision formation flying requirements, and to identify the necessary formation manoeuvres. However, the defined modes for Darwin were found to be limited to deployment, coarse baseline control, a fringe acquisition sequence requiring fine control, and a 'staring' high precision science mode. This provided the opportunity to derive additional formation flying manoeuvres appropriate for completion of the mission tasks, not already reported in the available literature. Additional modes based on the mission science objectives and on an appreciation of the optical systems were therefore identified. With a research objective to investigate load-levelling, formation manoeuvres including formation rotation, translation (expansion and contraction), slewing and station keeping, were defined for the astrophysical imaging and extrasolar planet detection and observation phases of a Darwin-type mission. In this case, emphasis was placed on the planet detection and spectroscopy phases.

Each manoeuvre type was identified as having a number of applications, and therefore constraints, depending on the science measurements being taken. For example, baseline expansion may take three forms:

- Large scale interferometer resolution adjustment during retargeting (probably combined with a slew).

- Relatively rapid formation expansion/contraction for u-v plane coverage during imaging.
- Precision relative manoeuvres during fringe acquisition.

The manoeuvre constraints are complicated further by load-levelling requirements (these were considered later in the research). The manoeuvres were quantified by defining suitable manoeuvre rates, relative positions, accelerations, thruster sizes and manoeuvre durations for each application.

Spacecraft data was drawn from the Darwin mission specifications and the manoeuvres were originally derived in the context of the six-telescope planar Darwin formation, however since performing the majority of the work, a new scaled-down Darwin mission has been proposed to achieve the same mission objectives with fewer telescopes. Although some of the system parameters (for example, spacecraft mass and maximum baseline), and manoeuvre rates and constraints may change slightly, similar manoeuvres are anticipated for both mission specifications.

A planet imager mission would be a natural successor to Darwin/TPF, and would also provide an unparalleled astrophysical imaging facility. The requirement for images of extrasolar planets, following their detection and atmospheric analysis by Darwin/TPF, is the next step in the process of identifying an extrasolar life-supporting environment. Spectroscopy primarily indicates the constituents of the planetary atmosphere, although some surface composition information from the ground may be deduced. Imaging, however, remains necessary to examine thoroughly the planet surface (in the absence of cloud) and it is anticipated that in the future, images will become increasingly important in the search for life as experience in the identification of surface features is gained.

In chapter 2, the results of a preliminary design of a nulling interferometry planet imaging mission capable of higher resolution than Darwin were also presented. The motivation for the study was to identify and evaluate some of the key optical and astrobiological design parameters for this large scale mission to highlight the challenges of both the nearer-term Darwin mission and a more futuristic interferometry mission.

Only a preliminary design was performed due to the refocus of the dynamics and control research to the nearer-term Darwin mission. However, the analysis and design revealed the significant increase in scale of the mission, and some of the challenges associated with this. Particularly salient were the issues of thermal control, the complexity of the formation flying problem due to the large number of apertures (or control of fewer extremely large apertures), and the development of image post-processing techniques to reduce imaging integration times. During the design, the following were considered:

- Star/Planet emission and contrast
- Photon capture at the aperture
- Resolution and baseline
- Starlight cancellation
- Observation wavelength and range
- Number and sizing of apertures
- CCD operation
- Fringe patterns / image reconstruction

The main findings of the design study are summarised in the list of conclusions. Analysis revealed that a formation of ‘sub-aperture’ nulling interferometer formations would be required to image an Earth-like planet orbiting a Solar-type star, separated by

1AU and at an observation distance of 25pc, and that the formation flying challenges are as great as the optical challenges. This is due to the increased number of satellites which must operate collectively and autonomously in a coordinated and efficient manner.

Having established the motivation, application, and justification for the research, a thorough survey of satellite formation flying dynamics and control literature was performed following a refocusing of the research towards the investigation of formation manoeuvres for a Darwin-type mission.

Initially, some of the wider aspects of guidance, navigation and control (GNC) systems, and in particular, relative navigation and thruster technologies, suitable for application in different gravitational environments were explored in conjunction with the formation flying missions survey in chapter 2. This highlighted the types of technology required for different formation flying missions and the abilities of sensor and actuation technologies to achieve different levels of precision. In addition, research presented in chapter 2 also highlights the nature of other closely related GNC research areas which although not investigated here, could easily be integrated with the modelling and control developments of chapters 4 to 7 (including for example, formation autonomy, sensor data fusion, control hierarchy). The role of simulation in the design of a formation flying mission GNC system was also identified as a precursor to hardware implementation and technology demonstration.

The context of the dynamics and control research performed in chapters 4 to 7 was set by a thorough survey of formation flying literature to identify potential areas for dynamics modelling and control development. The review covered both the basic theory of and advanced research work in satellite formation flying for both LEO and deep space, and the following topics were considered:

- Relative dynamics models
- Formation flying missions and further potential applications
- Formation design
- Orbit perturbations
- Formation flying guidance and control systems

For a LEO formation flying mission, the advantages and disadvantages of different techniques and reference frames for relative dynamics modelling were established, and for an interferometry application, a reference frame based at a circular reference orbit was found to be the most appropriate for precision formation flying metrology and control. Orbit perturbations and the magnitude of their effects on formation stability were investigated both in the literature, and through independent evaluation, and perturbations due to Earth oblateness (J_2) were found to be the most significant.

The potential to develop relative dynamics models incorporating the Earth oblateness effect was identified, initially as a development to early work on the MUSTANG mission at Cranfield University, and then for application to trajectory design and formation control analysis. Although the ultimate aim of the research was to investigate formation manoeuvring for the Darwin mission, the original objectives for performing research in LEO as a precursor to the dynamics and control investigation near the Sun-

Earth L2 Lagrange point were reinforced by the literature review. Many recent publications on the LEO formation flying problem, mainly stemming from rendezvous analyses, were available during early phases of the research, however, little material was available regarding formation flight around L2. At the outset it was therefore deemed necessary to investigate both fields of research. Detailed research objectives for the dynamics and control part of the thesis were formulated accordingly.

Dynamics and control analysis for a J_2 perturbed LEO formation was performed, and three mathematical models describing relative satellite motion were investigated:

- The Hill equations (no J_2 perturbation)
- A time invariant J_2 model originally proposed by researchers at MIT (Schweighart and Sedwick, 2002)
- A time varying J_2 model

All the models were verified against the Satellite Tool Kit (STK) Astrogator high precision numerical orbit propagator, and the effects of the perturbation due to J_2 on the absolute cluster motion and on relative motion were established. Analytical and numerical solutions of the models were investigated and initial conditions derived for bounded relative satellite motion in the presence of J_2. Following the evaluation of a number of verification test cases involving satellite separations in radial, along-track and cross-track directions, in J_2 invariant relative orbits, and circular and along-track formations, the ability of each model to capture relative satellite motion in the presence of J_2 was assessed. Test cases were also performed at a series of different inclinations, including equatorial, polar, critical, Sun synchronous, and others.

The time averaged and time varying J_2 models were found to achieve a similar performance for cluster motion relative to a circular reference orbit. However, unexpectedly, the time averaged model performed better than both the Hill equations and time varying J_2 model, but only for bounded motion conditions. The time varying J_2 model consistently performed better than the Hill equations, and unlike the time invariant models, for an along-track leader-follower formation, it captured the shape of the relative dynamics. Model limitations were established, and the time varying model was more robust to variations in operating conditions.

All three models were applied to continuous LQR controller design and performance assessment in the Satellite Tool Kit (STK) numerical orbit propagator environment which could incorporate a range of external disturbances in the simulation. A controlled follower satellite was forced to maintain a prescribed formation with respect to an uncontrolled reference or leader spacecraft. Fuel use and formation keeping precision were evaluated for the formation designs highlighted in the model verification process, and the effects of modifying well known natural relative motion trajectories to include the effects of the J_2 perturbation were evaluated. Formation keeping ΔV was found to be particularly sensitive to orbit inclination and the initial along-track cluster velocity. The LQR control systems maintained the formations in the presence of a range of orbit disturbances, in addition to the effects of J_2. The application of STK as an environment within which controlled formations could propagate was also established.

In chapter 6, a linearised gravity gradient model has been derived and evaluated for formation flying around the Sun-Earth L2 point. Initial model comparisons with STK

scenarios have been performed and satisfactory model behaviour achieved. The results of the gravity gradient model comparisons against a higher order model and numerical solutions in STK demonstrated that the linearised model is sufficiently accurate for controller design and relative motion analyses. In the final technical chapter of the thesis, and in support of one of the final research aims, the role of the L2 dynamics models (of chapter 6) in the design of simple LQR feedback control for formation flying around L2 is investigated. A preliminary evaluation of the controllers for the extrasolar planet detection and observation manoeuvres defined in chapter 2 was performed in STK, and the thrust levels required for different manoeuvres were established. Halo orbit maintenance was investigated, and considered in the context of both load-levelling and general science task manoeuvring. The concept of formation load-levelling is defined, and a guidance strategy for a load-levelling baseline expansion manoeuvre is derived. Due to the preliminary nature of this final study, a number of further work suggestions are proposed.

8.1.2 Conclusions

The following points provide a concise summary of the main findings and conclusions of the research at all stages. From the initial mission surveys and general familiarisation with the role and potential applications of satellite formation flying it was found that:

- To achieve a continual increase in mission performance, many applications will require a formation of satellites to replace a single satellite.
- However, although there are many benefits to using a distributed satellite system, this is not necessarily a less costly option.
- The use of multiple satellites for astronomy applications is essential if improved resolution is to be achieved, although this introduces many technical challenges.

Following the selection of an optical interferometry astronomy mission as a focus for the research it was found that:

- There is a general trend towards increased aperture size for single satellite observatories, and to achieve adequate resolution in the future, these will become impractical to launch and deploy with current or near-term launcher technology.
- A multi-satellite interferometer can achieve a significantly higher resolution that a single aperture telescope with a mirror diameter equal to the separation between the interferometer apertures, and is an ideal system for astrophysical imaging and extrasolar planet detection and observation.
- Interferometer resolution can be altered by adjusting the separation between elements of the formation, and this provides an opportunity to improve the resolution even further.
- By careful formation and manoeuvre design, apertures can be efficiently manoeuvred across the image plane to collect sufficient information to enable image reconstruction.
- Potential tools for extrasolar planet detection and observation include the nulling interferometer, and single and multi-aperture coronagraphs.

- In the Darwin time-frame, for a mission focussed on planet detection and spectral analysis, infrared nulling interferometry is the most appropriate multi-aperture technique.
- Observing planets in the infrared and visible wavelength regimes is complementary, and will highlight different features of the planet and its orbit, however, operations in the infrared require less precise optical instruments, and at this waveband, the star/planet contrast is reduced.
- Astrobiology research has enabled the identification of the life indicators, the characteristics of potentially habitable planets, the likelihood of the existence of other Earths, and other scientific drivers for planet detection and observation missions.
- The role of manoeuvres for interferometry applications has been established for the imaging and extrasolar planet detection and observation tasks.
- For planet detection and observation, formation rotation (for planet signal modulation), baseline variation (to alter the resolution of the interferometer), formation slewing (to retain an object in the field-of-view for the duration of an observation) and station keeping (to maintain the formation orbit) were identified.
- The feasibility of a planet imager mission has been investigated by the successful application of basic optical theory to the conceptual design of a large nulling interferometer with the objective of imaging any Earth-like planet identified by Darwin out to 25pc at a minimum resolution of 12x12 pixels.

The findings of the planet imager study demonstrated that:

- Implementing and operating a planet imager on this scale would be prohibitively costly in terms of technology readiness and scale. Given current estimates of noise contributions and the weak planet signal, an extremely large telescope collecting area is required in order to meet the short integration time.
- The justification for applying infrared nulling interferometry to a planet imager design did not take into account SNR issues which were found to be fundamental in driving the design requirements.
- A larger wavelength range than that selected for Darwin is required for a larger scale mission looking at more distant targets, as even fewer photons are gathered at the aperture per unit of observation wavelength.
- More specific technical challenges associated with the development of a planet imager mission include thermal control, particularly at the detector, the scale and complexity of the formation flying problem due to the large number of satellites (or the large mirror diameters required if fewer apertures are used), and the development of suitable optical systems and image production capability.

In the area of satellite formation flying dynamics and control:

- The role of relative dynamics models for formation flying GNC system analysis was established, and the need for simple (analytical where possible) and yet high-fidelity dynamics models was identified, including:
    - Linearised models for controller design.
    - High-fidelity models for advanced control laws designs, for example, predictive, model-following, or dynamic inversion control laws.
    - A tool for relative motion analysis, and controller evaluation.

    - Kalman filter design.
    - Relative trajectory generation (onboard).
    - To provide insight into the orbital dynamics.
    - Formation design and mission analysis to identify natural orbits which require as little correction as possible to maintain.
- The role of simulation in GNC system development, mission analysis and feasibility studies prior to ground or microgravity testbed, on-orbit technology demonstration or implementation on a full mission has been identified, and is an essential part of the design process, facilitating the investigation of more complex operations to achieve higher performance.

For the LEO dynamics model and control analysis:

- The time averaged J_2 model performed better than both the Hill equations and time varying J_2 models, but only for bounded motion conditions and specific inclination. However, it fails to capture coupling between in and out-of-plane relative motion dynamics.
- Modelling limitations were established for all three models.
- The poorer performance of the time varying J_2 model was unexpected. Investigative analysis of the limitations of the time varying J_2 model provided significant insight into the importance of initial conditions, relative drifts in the orbit elements due to J_2, and the effects of J_2 on relative motion at particular orbital conditions.
- The benefits of the new time varying model in capturing relative motion more accurately than the Hill equations were established.
- All the models were applied to LQR control system design through the development of the Matlab/STK interface. This was then applied to formation flying in the vicinity of the Sun-Earth L2 point.
- Formation keeping fuel use requirements were established for along-track and circular relative formations.

For the L2 dynamics model and control analysis:

- A survey of potential navigation and thruster systems revealed that FEEP or miniature cold gas thrusters, and a variety of relative navigation systems would be suitable for the precision formation flying task around L2.
- A suitable relative dynamics model for control system design was independently derived, and upon comparison to STK and a higher order model, was found to capture relative motion and the gravity gradient conditions around a halo orbit. However, the model was more susceptible to initial relative velocity conditions.
- Similar performance was achieved for the new linear model as the higher order analytical model for the test cases considered.
- The application of the L2 relative dynamics model to controller design has been successfully demonstrated, and a design and visualisation tool which will be useful for further research, has been developed.
- It is possible to simulate a controlled satellite formation in STK as long as continuous interaction between the systems is not required. This seriously limits the application of the propagator tool for load-levelling and other manoeuvre research.

- Using the architectures derived, it is not possible to simultaneously perform halo orbit maintenance control and precision formation manoeuvring for a science application using a basic LQR control system as the thruster requirements differ too widely. However, simultaneous station keeping and 'loose' halo orbit maintenance can be performed.
- Different manoeuvres in the vicinity of L2 have different propulsion system requirements.
- A strategy for developing load-levelling guidance trajectories has been identified and applied to the design of a baseline expansion manoeuvre.

8.2 Further Work

The aim of this research was established and refined during the earlier phase of the study, and therefore ultimately focuses on the final stages of research. The aim was defined as follows (chapter 1):

To assess the feasibility of achieving high precision formation flying of a fleet of satellites in both the Low Earth Orbit and Lagrange point (L2) environments using a variety of dynamics models which can be compared and contrasted. Ultimately, the satellites need to operate autonomously and hold position sufficiently accurately to enable them to perform the appropriate formation manoeuvring and optical interferometry tasks associated with imaging a distant extrasolar planet from L2, in support of an ESA Darwin-type mission.

Within the stated aim, a number of objectives were defined and these are summarised below:

- To develop, evaluate and validate analytical and time varying formation flying dynamics models for multiple spacecraft operating in different orbits (in LEO and within the three body problem, in particular near L2) so that their relative motion can be calculated when they are subject to a range external disturbances.
- To develop robust, stable and practical control laws which will enable precise relative position maintenance of the satellite formation in the presence of disturbances.
- To calculate the fuel required to maintain these orbits.
- To extend the guidance and control laws to meet more detailed mission requirements, including manoeuvring to perform specific imaging and spectroscopy tasks.
- To apply the L2 formation flying model to the problem of 'load-levelling'.
- To develop the necessary software to visualise multiple satellites interacting and formation flying in a 'real space' perturbed numerical orbit propagator environment.

The objectives have been met within the limits of the available simulation tools and time, and at each stage, the justification for the research and analysis has been presented. However, the analysis has revealed many areas for further investigation and research. These are summarised below, firstly in relation to the general research area

associated with an optical interferometry mission, and secondly, in relation to dynamics, control and simulation for satellite formation flying.

Interferometry Mission Analysis

Following the preliminary mission design, it is clear that there are many opportunities to develop further the relationship between imaging processes, optical system design and formation flying dynamics and control.

- During the planet imager design, image processing and reconstruction techniques, and simulations of the optical systems were not performed. In order to demonstrate fully the feasibility of a nulling interferometer and integrate image quality metrics with formation flying manoeuvre design and formation control, further analysis of image processing, (for example, time scales and attainable quality) would be required. Image quality could also be measured as a feedback control parameter for the generation of guidance functions for autonomous formation manoeuvres.
- Review and investigate further proposals by Hyland (2001) to avoid the need for actively transmitting light to the hub and interfering it. It is suggested that image reconstruction techniques can be used to replace stringent precision formation flying requirements.

The following are also proposed for further work:

- Repeat a preliminary planet imager design based on the hypertelescope concept (Roberts, 2006) to contrast the optical system requirements directly with the nulling interferometer presented in chapter 2.
- Design a visible light coronagraph and interferometer to establish whether planet imaging could be achieved using fewer telescopes compared to the infrared interferometer. Imaging a planet in the visible will provide greater contrast between continents and oceans, although circulation, indicated by temperature variation across the planetary surface can be determined more easily in the infrared.
- Perform a preliminary thermal analysis of a planet imager to see if the low temperatures can be achieved for the optical systems using sun shields and thermal insulation.
- Define further and quantify more accurately noise contributions to the SNR calculations as the SNR directly influences to so many aspects of the conceptual design.

Formation Flying Dynamics and Control

Following the detailed analysis of relative dynamics models, and their application to GNC system design and evaluation, proposed future work is summarised below.

In Low Earth Orbit:

- Investigate further the differences between the time averaged and time varying J_2 models to build upon the findings detailed at the end of chapter 4. Here it was found that the gradient terms in the model (evaluated by deriving a tensor in spherical coordinates) multiplied between the separation between the satellites were not equal to the absolute differences between the forces acting at each satellite. This may clarify why the time varying model did not demonstrate the level of modelling improvement expected.

- For all models, further improvements in model fidelity could be investigated, although this would not significantly affect LQR controller design and performance.
- It is important to be able to measure both absolute and relative positions and velocities in both LEO and at L2. Although the orbit determination challenges of these two regions differ, the sensitivity of the formation behaviour to the initial conditions, particularly in LEO, means that to provide, for example, the additional 'circularising' ΔV to a formation to minimise formation keeping fuel use, accurate orbit determination is required. The practical implementation of this should be considered.
- Investigate LEO formation manoeuvres and applications.
- Integrate the relative dynamics models with relative navigation systems, and implement these in the formation flying scenarios to gain a truer estimate of formation flying fuel consumption for different control systems and architectures in both LEO and at L2.

For the L2 dynamics and control research:

- Investigate orbit determination strategies for formation flying near L2 for application to interferometry missions of both Darwin and Planet Imager size.
- The relative dynamics model fidelity could be improved by incorporating relative disturbances and considering the elliptical restricted three body problem or higher order terms.
- The relative dynamics model should be augmented to include relative attitude.
- It is proposed that the development of a new tool be continued (to replace STK) specifically for load-levelling manoeuvre analysis.
- Extend formation manoeuvring analysis to solve optimal trajectory generation problems for the manoeuvres with fewer constraints (to tackle the global fuel use optimisation problem).

REFERENCES

Abbas, O. and Schulze-Makuch, D. (2002), 'Acetylene-Based Pathways for Prebiotic Evolution on Titan', *Proceedings of the Second European Workshop on Exo/Astrobiology,* Vol. SP-518, Graz, Austria, ESA, pp. 345-348.

Adams, J., Robertson, A., Zimmerman, K., and How, J. (1996), 'Technologies for Spacecraft Formation Flying', *ION GPS-96 Conference,* Kansas City, MO,

Agee, F.J., Janni, J.F., King, Y.J., Witt, G., and Fender, J.S. (2001), 'Research for an Innovative Approach to Satellite Technology', *AIAA Space 2001,* Albuquerque, NM, AIAA 2001-4555.

Aldiss, B.W. (2001), ' Desperately Seeking Aliens', *Nature,* Vol. 409, pp. 1080-1082.

Alfriend, K.T. and Schaub, H. (2000), 'Dynamics and Control of Spacecraft Formations: Challenges and Some Solutions', *Richard H. Battin Astrodynamics Symposium,* College Station, Texas, pp. 205-223, AAS 00-259.

Alfriend, K.T. and Yan, H. (2002), 'An Orbital Elements Approach to the Nonlinear Formation Flying Problem', *Proceedings of the Ineternational Symposium: Formation Flying Missions and Technologies,* Toulouse, France, CNES.

Alfriend, K.T. and Yan, H. (2003), 'An Evaluation and Comparison of Relative Motion Theories', *Proceedings of the AAS/AIAA Astrodynamics Conference,* Vol. 116 pt.2, Big Sky, Montana, AAS, San Diego, CA, pp. 1049-1065.

Alfriend, K.T., Schaub, H., and Gim, D. (2000), 'Gravitational Perturbations, Nonlinearity and Circular Orbit Assumption Effects on Formation Flying Control Strategies', *AAS Guidance and Control Conference,* Breckenridge, Colorado, AAS 00-012.

Alfriend, K.T., Vadali, S.R. and Schaub, H. (2001), 'Formation Flying Satellites: Control by An Astrodynamicist', *Celestial Mechanics and Dynamical Astronomy,* Vol. 81, No. 1-2, pp. 57-62(6).

Alfriend, K.T., Yan, H., and Vadali, S.R. (2002), 'Nonlinear Considerations in Satellite Formation Flying', *AIAA/AAS Astrodynamics Specialist Conference and Exhibit,* Monterey, California, AIAA 2002-4741.

Allard, F., Baraffe, I., Chabrier, G., and Barman, T. (2003), 'Atmospheres of Extrasolar Giant Planets and Brown Dwarfs', *Proceedings 'Towards Other Earths: DARWIN/TPF and the Search for Extrasolar Terrestrial Planets',* Vol. SP-539, Heidelberg, Germany, ESA, pp. 247-252.

ALMA Website (2003), *The ALMA Project,* available at: http://www.eso.org/projects/alma/info/ (accessed 2004).

Alonso, R., Crassidis, J.L., and Junkins, J.L. (2000), 'Vision-Based Relative Navigation for Formation Flying of Spacecraft', *AIAA Guidance, Navigation and Control Conference and Exhibit,* Denver, Colorado, pp. 1384-1394, AIAA 2000-4439.

Amiot, T., Massonnet, D., Douchin, F., Thouvenot, E., Souyris, J.C., and Cugny, B. (2002), 'The Interferometric Cartwheel: Feasibility Studies, Performances and Stability of Topographic Accuracy', *International Symposium: Formation Flying Missions and Technologies,* Toulouse, France, CNES.

Amos, J. (2005), *Plenty of Earths Await Discovery,* available at: http://news.bbc.co.uk/1/hi/sci/tech/4411865..stm (accessed 2005).

Angel, J.R.P. and Woolf, N.J. (1997), 'An Imaging Nulling Interferometer to Study Extrasolar Planets', *Astrophysical Journal,* Vol. 475, pp. 373-379.

Angel, R. (2003), 'Direct Detection of Terrestrial Exoplanets: Comparing the Potential for Space and Ground Telescopes', *Proceedings 'Towards Other Earths': DARWIN/TPF and the Search for Extrasolar Terrestrial Planets,* Vol. SP-539, Heidelberg, Germany, ESA, pp. 221-230.

Arida, M. (2001), *The ROSAT X-Ray Mirror Assembly,* available at: http://heasarc.gsfc.nasa.gov/docs/rosat/rosgof.html (accessed 2002). Notes: original website no longer available

Arnett, W.A. (2004), *The Nine Planets,* available at: http://www.nineplanets.org (accessed 2004).

Bailey, C.A., McLain, T.W. and Beard, R.W. (2000), 'Fuel Saving Strategies for Separated Spacecraft Interferometry', *AIAA Guidance, Navigation, and Control Conference and Exhibit,* Denver, Colorado, pp.1405-1413, AIAA 2000-4441.

Bailey, C.A., McLain, T.W. and Beard, R.W. (2001), 'Fuel-Saving Strategies for Dual Spacecraft Interferometry Missions', *The Journal of the Astronautical Sciences,* Vol. 49, No. 3, pp. 469-488.

Barbieri, M., Piotto, G., Claudi, R.U., Crescenzio, G., Desidera, S., Baruffolo, A., Bedin, L.R., Bertelli, G., Gratton, R., Marzari, F., Montalto, M., and Ortolani, S. (2004), 'Search For An Optimal Eddington Planet Finding Field', *Proceedings of the 2nd Eddington Workshop 'Stellar Structure and Habitable Planet Finding',* Vol. SP-538, Palermo, Italy, ESA , pp. 163-175.

Barden, B.T. and Howell, K.C. (1998), 'Formation Flying in the Vicinity of Libration Point Orbits', *Advances in the Astronautical Sciences,* Vol.99 Pt.2 , pp. 969-988.

Barnes, D., Summers, P., and Shaw, A. (2000), 'An Investigation Into Aerobot Technologies for Planetary Exploration', *6th ESA Workshop on Advanced Space Technologies for Robotics and Automation. ASTRA 2000,* ESA.

Bartolini, C., Benelli, M., Campana, G., Guarnieri, A., and Beskin, G. (2002), 'Search for Exoplanets at Bologna University', *Proceedings of the Second European Workshop on Exo-Astrobiology,* Vol. SP-518, Graz, Austria, ESA, pp. 499-500.

Battin, R.H. (1987), *An Introduction to the Mathematics and Methods of Astrodynamics*, AIAA, New York, USA.

Bauer, F., Bristow, J., Folta, D., Hartman, K., Quinn, D., and How, J.P. (1997), 'Satellite Formation Flying Using an Innovative Autonomous Control System (AUTOCON) Environment', pp. AIAA 97-3821.

BBC News Website (2005a), *Mars Pictures Reveal Frozen Sea,* available at: http://news.bbc.co.uk/1/hi/sci/tech/4285119.stm (accessed 2005).

BBC News Website (2005b), *Spitzer Sees Far-Off Planet Light,* available at: http://news.bbc.co.uk/1/hi/sci/tech/4379007.stm (accessed 2005).

Beard, R.W. and Hadaegh, F.Y. (1999a), 'Finite Thrust Control for Satellite Formation Flying with State Constraints', *Proceedings of the American Control Conference,* San Diego, California, pp. 4383-

4387.

Beard, R.W. and Hadaegh, F.Y. (1999b), 'Fuel Optimized Rotation for Satellite Formations in Free Space', *Proceedings of the American Control Conference,* San Diego, California, pp. 2975-2979.

Beard, R.W., McLain, T.W., and Hadaegh, F.Y. (1998), 'Fuel Equalized Retargeting for Separated Spacecraft Interferometry', *Proceedings of the American Control Conference,* Philadelphia, Pennsylvania, pp. 1580-1584.

Beichman, C.A. (2000), 'NASA's Terrestrial Planet Finder (TPF)', *Proceedings of the Conference 'Darwin and Astronomy - The Infrared Space Interferometer',* Vol. SP-451, Stockholm, Sweden, ESA, pp. 239-244.

Beichman, C.A. (2004a), *Memo to the TPF Science Working Group,* available at: http://planetquest.jpl.nasa.gov/TPF/SWG_AnnoucementV2.pdf (accessed 2005).

Beichman, C.A. (2004b), *New Directions for TPF,* available at: http://planetquest.jpl.nasa.gov/TPF/TPFDownselectUpdate.pdf (accessed 2005).

Bennet, C. (2004), *WMAP Mission Overview,* available at: http://map.gsfc.nasa.gov/m_mm/ob_tech1.html (accessed 2004).

Bennet, D. and Hong Rhie, S. (1999), *Astronomers Observe Distant Solar System with Possible Neptune-Like Planet,* available at: http://bustard.phys.nd.edu/MPS/98-BLG-35/press.html (accessed 2004).

Bennet, D.P. and Hong Rhie, S. (1996), 'Detecting Earth-Mass Planets with Gravitational Microlensing', *The Astrophysical Journal,* Vol. 472, pp. 660-664.

Bhasin, K. and Hayden, J.L. (2001), 'Inter-Spacecraft Communication Architectures and Technologies for Coordinated Spacecraft Missions', *AIAA Space 2001,* Albuquerque, New Mexico, AIAA 2001-4709.

Blair, B. (2004), *FUSE Mission Overview,* available at: http://fuse.pha.jhu.edu/overview/mission_ov.html#FHOW (accessed 2004).
Notes: Mirror details at: http://fuse.pha.jhu.edu/photos/mirror.html

Boboltz, D. and Wittkowski, M. (2004), *The Very Long Baseline Array,* available at: http://www.aoc.nrao.edu/vlba/html/VLBA.html (accessed 2004).

Boccaletti, A., Riand, P., Moutou, C. and Labeyrie, A. (2000), 'Snapshot Coronagraphy with an Interferometer in Space', *Icarus,* Vol. 145, pp. 628-636.

Boccaletti, A., Riaud, P., Baudrand, P., Reess, J.M., and Rouan, D. (2003), 'Exoplanet Imaging at Mid-IR Wavelengths with JWST', *Proceedings 'Towards Other Earths': DARWIN/TPF and the Search for Extrasolar Terrestrial Planets,* Vol. SP-539, Heidelberg, Germany, ESA, pp. 355-360.

Boggess, N.W., Mather, J.C., Weiss, R., Bennett, C.L. and Cheng, E.S.e.al. (1992), 'The COBE Mission: Its Design and Performance Two Years After Launch', *The Astrophysical Journal,* Vol. 397, pp. 420-429.

Borucki, W., Koch, D., Boss, A., Dunham, E., Dupree, A., Geary, J., Gilliland, R., Howell, S., Jenkins, J., Kondo, Y., Latham, D., Lissauer, J., and Reitsema, H. (2004), 'The Kepler Mission: A Technical Overview', *Proceedings of the 2nd Eddington Workshop 'Stellar Structure and Habitable Planet Finding',* Vol. SP-538, Palermo, Italy, ESA, pp. 177-182.

Borucki, W.J., Koch, D., Basri, G., Brown, T., Caldwel, D., DeVore, E., Dunham, E., Gautier, T., Geary, J., Gilliland, R., Gould, A., Howell, S., and Jenkins, J. (2003), 'Kepler Mission: A Mission to Find Earth-Size Planets in the Habitable Zone', *Proceedings 'Towards Other Earths': DARWIN/TPF and the Search for Extrasolar Terrestrial Planets,* Vol. SP-539, Heidelberg, Germany, ESA, pp. 69-81.

Bourdon, J., Delpy, P., Ganet, M., Quiquis, I., and Ankersen, F. (2003), 'Application of H-infinity Design on ATV Control Loop During the Rendezvous Phase', *Proceedings of the 5th International ESA Conference on Spacecraft Guidance, Navigation and Control Systems,* Vol. SP-516, Frascati, Italy, ESA, pp. 289-296.

Bowey, J.E. and Yates, J.A. (2000), 'Spectroscopy with Darwin: The Case for R>100', *Proceedings of the Conference 'Darwin and Astronomy - The Infrared Space Interferometer',* Vol. SP-451, Stockholm, Sweden, ESA, pp. 173-177.

Bracewell, R.N. and MacPhie, R.H. (1979), 'Searching for Nonsolar Planets', *Icarus,* Vol. 38, pp. 136 .

Brack, A. (2000a), 'The Exobiology Exploration of Mars: A Survey of the European Approaches', *Planetary and Space Science,* Vol. 48, pp. 1023-1026.

Brack, A. (2000b), 'Life in the Universe', *Proceedings of the Conference 'Darwin and Astronomy - The Infrared Space Interferometer',* Vol. SP-451, Stockholm, Sweden, ESA, pp. 151-158.

Briot, D., Schneider, J., Francois, P., and Arnold, L. (2002), 'A Test for the Detectability of Vegetation on Extrasolar Planets: Observing the Terrestrial Vegetation in the Earthshine Spectrum', *Proceedings of the Second European Workshop on Exo/Astrobiology,* Vol. SP-518, Graz, Austria, ESA, pp. 505-506.

Broucke, R.A. (2002), 'A Solution of the Elliptic Rendezvous Problem With The Time As Independent Variable', *AAS/AIAA Space Flight Mechanics Conference,* Vol. 112 pt.2, San Antonio TX, pp. 585-604, AAS 02-144.

Brouwer, D. (1959), 'Solution of the Problem of Artificial Satellite Theory', *The Astronautical Journal,* Vol. 64, No. 1274, pp. 378-397.

Bryson, A.E. and Ho, Y. (1975), *Applied Optimal Control*, Hemisphere Publishing Corporation, Washington, D.C.

Burns, R., Gabor, M., McLaughlin, A., Luu, K., and Sabol, C. (2000), 'Solar Radiation Pressure Effects on Formation Flying of Satellites with Different Area to Mass Ratios ', *AIAA/AAS Astrodynamics Specialist Conference,* Denver Colorado, Virginia, USA, AIAA 2000-4132.

Busse, F.D., Inalhan, G., and How, J.P. (2000), 'Project Orion: Carrier Phase Differential GPS Navigation for Formation Flying', *AAS Guidance and Control Conference,* Breckenridge, Colorado, pp. 197-212, AAS 00-016.

Calico, R.A. and Wiesel, W.E. (1984), 'Control of Time-Periodic Systems', *Journal of Guidance, Control, and Dynamics,* Vol. 7, No. 6, pp. 671-676.

Campbell, M.E. (2002), ' Planning Algorithm for Large Satellite Clusters', *AIAA Guidance, Navigation, and Control Conference and Exhibit,* Monterey, California, AIAA 2002-4958.

Caramagno, A., Araujo, J., Bastante, J.C., and Penin, L.F. (2005), Unpublished Presentation at ESA-ESTEC.

Carlson, B.A., Pernicka, H.J., and Balakrishnan, S.N. (2004), 'Spacecraft Formation Flight about Libration Points', *AAS/AIAA Astrodynamics Specialist Conference,* Providence, RI, pp. 48-64, AIAA 2004-4737.

Carme, J. (2003), *Gaia - Taking the Galactic Census,* available at: http://astro.estec.esa.nl/GAIA/Assets/Papers/IN_astro_telescope.pdf (accessed 2004).

Carrel, A. (2003), *Alternative Attitude Determination Technologies for Formation Flying Satellites, MSc Thesis*, Cranfield University, Cranfield, UK .

Carroll, S.B. (2001), 'Chance and Necessity: The Evolution of Morphological Complexity and Diversity', *Nature,* Vol. 409, pp. 1102-1109.

Carter, T. and Humi, M. (2002), 'Clohessy-Wilthsire Equations Modified to Include Quadratic Drag', *Journal of Guidance, Control and Dynamics,* Vol. 25, No. 6, pp. 1058-1063.

Carter, T.E. (1998), ' State Transition Matrices for Terminal Rendezvous Studies: Brief Survey and New Example', *Journal of Guidance, Control, and Dynamics,* Vol. 21, No. 1, pp. 148-155.

Chan, K.W. (2003), *X-ray Mirror at Lhea,* available at: http://lheawww.gsfc.nasa.gov/docs/xray/astroe/MirrorLab/mir_make.html (accessed 2004).

Chandler, D.L. (2003) SETI is About to Get Serious. *New Scientist* http://www.newscientist.com/hottopics/astrobiology/setiabout.jsp (accessed 2005)

Chandra Website (2004), *The Chandra Mission,* available at: http://chandra.harvard.edu/about/axaf_mission.html (accessed 2004).
Notes: For telescope image: http://chandra.harvard.edu/about/telescope_system.html

Chao, C.C., Pollard, J.E., and Janson, S.W. (1999), 'Dynamics and Control of Cluster Orbits for Distributed Space Missions', AAS 99-126.

Chela-Flores, J. (2001), 'Search for Microorganisms on Europa and Mars in relation with the Evolution of Intelligent Behaviour on Other Worlds', *Proceedings of the First European Workshop on Exo/Astro-Biology,* Vol. SP-496, Frascati, Italy, pp. 219-222.

Chela-Flores, J. (2002), 'Can Evolutionary Convergence be Tested on Europa?', *Proceedings of the Second European Workshop on Exo/Astrobiology,* Vol. SP-518, Graz, Austria, ESA, pp. 337-340.

Chobotov, V.A. (2002), *Orbital Mechanics* (Third edition), AIAA, Virginia, USA.

Chow, N., Gralla, E., Chase, J., and Kasdin, N.J. (2004), 'Low Earth Orbit Constellation Design Using The Earth-Moon L1 Point', *14th AAS/AIAA Space Flight Mechanics Conference,* Maui, Hawaii, AAS 04-248.

Chown, M. (2004) The Planet that Stalked the Earth. *New Scientist* **183** (2460):27-30. England: Reed Business Information Ltd.

Cielaszky, D. and Wie, B. (1994), 'Halo Orbit Determination and Control for the Elliptic Restricted Three-Body Problem', *AIAA/AAS Astrodynamics Conference,* Scottsdale, Arizona, USA, Washington D.C., AIAA 94-3729.

Clohessy, W.H. and Wiltshire, R.S. (1960), 'Terminal Guidance System for Satellite Rendezvous', *Journal of the Aerospace Sciences,* pp. 653-658,674.

Cobb, R., Das, A., and Denoyer, K. (1999), 'TechSat21: Developing Low-Cost Highly Functional Micro-Satellite Clusters for 21st Century Air Force Missions', *International Astronautical Federation Specialists Symposium: Novel Concepts for Smaller, Faster and Better Space Missions,* Redondo Beach, California.

Cohen, J. and Stewart, I. (2001), 'Where Are The Dolphins?', *Nature,* Vol. 409, pp. 1119-1122.

Cordoba-Jabonero, C., Patel, M.R., Zorzano, M.P. , and Cockell, C.S. (2004), 'Assessments for Possible Habitability in Martian Polar Environments: Fundaments Based in Ice Screening of UV Radiation', *Proceedings of the Third European Workshop on Exo-Astrobiology. Mars: The Search for Life,* Vol. SP-545, Madrid, Spain, ESA, pp. 187-188.

Cornwell, T.J. (1994), 'A Novel Principle for Optimization of the Instantaneous Fourier Plane Coverage of Correlation Arrays', *IEEE Transactions on Antennas and Propagation,* Vol. 2, No. 31 Jul - 4 Aug, pp. 1165-1167.

Costes, V., Bodin, P., Levacher, P., and Auvergne, M. (2004), 'COROT Mission: Accurate Stellar Photometry', *Proceedings of the 5th International Conference on Space Optics,* Vol. SP-554, Toulouse, France, ESA, pp. 281-284.

Coulter, D.R. (2003), 'NASA's Terrestrial Planet Finder Mission: The Search for habitable Planets', *Proceedings 'Towards Other Earths': DARWIN/TPF and the Search for Extrasolar Terrestrial Planets,* Vol. SP-539, Heidelberg, Germany, ESA, pp. 47-54.

Curtis, H.D. (2005), *Orbital Mechanics for Engineering Students*, Elsevier, Boston.

D'Arcio, L. and Karlsson, A. (2004), 'Search for Extraterrestrial Planets: The Darwin Mission', *Proceedings of the 5th International Conference on Space Optics 2004,* Vol. SP-554, Toulouse, France, ESA.

D'Arcio, L. and Le Poole, R. (2003), 'Beam Combiner Concept for the Darwin Imaging Mode', *Proceedings 'Towards Other Earths': DARWIN/TPF and the Search for Extrasolar Terrestrial Planets,* Vol. SP-539, Heidelberg, Germany, ESA, pp. 393-398.

Darling, D. (2004), *Microlensing,* available at: http://www.daviddarling.info/encyclopedia/M/microlensing.html (accessed 2004).

Davidson Web Page (2004), *The Fabry-Perot Interferometer,* available at: http://www.phy.davidson.edu/StuHome/cabell_f/diffractionfinal/pages/Fabry.htm (accessed 2004).

de Queiroz, M.S., Kapila, V. and Yan, Q. (1999), 'Adaptive Nonlinear Control of Satellite Formation Flying', *Proceedings of the AIAA Guidance, Navigation and Control Conference,* Potland, Oregon, AIAA 99-4270.

de Queiroz, M.S., Kapila, V. and Yan, Q. (2000), 'Adaptive Nonlinear Control of Mulitple Spacecraft Formation Flying', *Journal of Guidance, Control, and Dynamics,* Vol. 23, No. 3, pp. 385-390.

Decou (1991), 'Orbital Station-Keeping for Multiple Spacecraft Interferometry', *Journal of the Astronautical Sciences,* Vol.39, No. 3, pp. 283-297.

Deeg, H.J. (2004), 'Should Eddington Concentrate on M Stars?', *Proceedings of the 2nd Eddington Workshop 'Stellar Structure and Habitable Planet Finding',* Vol. SP-538, Palermo, Italy, ESA, pp. 231-237.

Deeg, H.J. and Horne, K. (2002), 'Eddington's Planet Finding Capabilities', *Proceedings of the First Eddington Workshop 'Stellar Structure and Habitable Planet Finding',* Vol. SP-485, Cordoba, Spain, pp. 123-128.

Demir, A. (2000), 'Floquet Theory and Non-Linear Perturbation Analysis for Oscillators with Differential-Algebraic Equations', *International Journal of Circuit Theory and Applications,* Vol. 28, pp. 163-185.

Donges, A. (1998), 'The Coherence Length of Black-Body Radiation', *European Journal of Physics,* Vol. 19, pp. 245-249.

Drossart, P., Semery, A., Reess, J., and Combes, M. (2004), 'Miniaturisation of Imaging Spectrometer for Planetary Exploration', *Proceedings of the 5th International Conference on Space Optics (ICSO 2004),* Vol. SP-554, Toulouse, France, ESA, pp. 63-65.

Dunham, D.W. and Muhonen, D.P. (2001), 'Tables of Libration-Point Parameteers for Selected Solar System Objects', *Journal of the Astronautical Sciences,* Vol.49 No.1, pp. 197-217.

Dunham, D.W. and Roberts, C.E. (2001), 'Stationkeeping Techniques for Libration-Point Satellites', *Journal of the Astronautical Sciences ,* Vol.49 No.1.

Eiroa, C., Fridlund, M., and Kaltenegger, L. (2003), 'The Darwin Target List: Observational Properties of the G-Type Stars', *Proceedings 'Towards Other Earths: Darwin/TPF and the Search for Extrasolar Terrestrial Planets',* Vol. SP-539, Heidelberg, Germany, ESA, pp. 403-407.

Encrenaz, Th. (2002), 'From Solar-System Planets to Exoplanets', *Proceedings of the First Eddington Workshop 'Stellar Structure and Habitable Planet Finding',* Vol. SP-485, Cordoba, Spain, pp. 129-135.

ESA Cosmic Vision 2020 Programme (2002), *'Cosmic Vision 2020': The New ESA Science Programme*: http://www.esa.int/export/esaCP/ESA2KPG18ZC_index_2.html (accessed 2004).

ESA Report (2000), *DARWIN The Infrared Space Interferometer*, Report no. ESA-SCI(2000)12, European Space Agency, The Netherlands.

ESA Website (2001), *Gaia - To Chart the Billion Brightest Objects,* available at: http://sci.esa.int/content/doc/3c/6204.htm (accessed 2002).
Notes: no longer available

ESA Website (2003), *Darwin: Fact Sheet,* available at: http://sci.esa.int/science-e/www/object/index.cfm?fobjectid=31167 (accessed 2005).

ESA Website (2003a), *ISO's Facts,* available at: http://www.iso.vilspa.esa.es/outreach/bck_grnd/iso_fact.htm#1 (accessed 2004).

ESA Website (2003b), *IUE Factsheet,* available at: http://sci.esa.int/science-e/www/object/index.cfm?fobjectid=31285 (accessed 2004).

ESA Website (2003c), *Hubble Fact Sheet,* available at: http://hubble.esa.int/science-e/www/object/index.cfm?fobjectid=33008 (accessed 2004).

ESA Website (2004), *XEUS Overview,* available at: http://www.esa.int/export/esaSC/120369_index_0_m.html (accessed 2004).

ESA Website (2004a), *INTEGRAL,* available at: http://integral.esa.int/science-

e/www/area/index.cfm?fareaid=21 (accessed 2004).

ESA Website (2004b), *Herschel,* available at: http://sci.esa.int/science-e/www/object/index.cfm?fobjectid=34682 (accessed 2004).

ESA Website (2004c), *Integral Instruments - IBIS,* available at: http://integral.esa.int/science-e/www/object/index.cfm?fobjectid=31175&fbodylongid=720 (accessed 2004).

ESA Website (2004e), *XMM-Newton Factsheet,* available at: http://sci.esa.int/science-e/www/object/index.cfm?fobjectid=31250 (accessed 2004).

ESA Website (2004f), *The Scientific Performance of Planck,* available at: http://www.rssd.esa.int/index.php?project=PLANCK&page=perf_top (accessed 2004).

ESA Website (2005), *Gaia Overview,* available at: http://www.esa.int/science/gaia (accessed 2005).

ESA-ESO Working Group (2005), *Report by the ESA-ESO Working Group on Extrasolar Planets,* available at: http://www.eso.org/gen-fac/pubs/esaesowg/espwg_report.pdf (accessed 2005).

ESO Publication (2004), *Is this Speck of Light an Exoplanet?,* available at: http://www.eso.org/outreach/press-rel/pr-2004/pr-23-04.html (accessed 2004).

ESO Website (2004), *OWL Design,* available at: http://www.eso.org/projects/owl/OWL_design.html (accessed 2004).

Essenburg, B., Sarokhan, J., and Kasdin, J. (2004), 'Hovercraft Satellite Simulation Test-Bed', *14th AAS/AIAA Space Flight Mechanics Conference,* Maui, Hawaii, AAS.

Evans, S.W. (2001), *Natural Environment Near the Sun/Earth-Moon L2 Libration Point ,* available at: http://snap.lbl.gov/pub/bscw.cgi/d84104/SNAP-TECH-03009.pdf (accessed 2005).

Farquhar, R.W. (1970), *The Control and Use of Libration-Point Satellites*, Report no. NASA TR R-346, National Aeronautics and Space Administration, Washington D.C.

Farquhar, R.W. (1991), 'Halo-Orbit and Lunar-Swingby Missions of the 1990's', *Acta Astronautica,* Vol. Vol. 24, pp. 227-234.

Farquhar, R.W. (1998), 'The Flight of the ISEE-/ICE Origins, Mission History, and a Legacy', AIAA 98-4464.

Farquhar, R.W. and Kamel, A.A. (1973), 'Quasi-Periodic Orbits about the Translunar Libration Point', *Celestial Mechanics,* Vol.7, pp. 458-473.

Farquhar, R.W., Muhonen, D.P., Newman, C.R. and Heuberger, H.S. (1980), 'Trajectories and Orbital Maneuvers for the First Libration-Point Satellite', *Journal of Guidance and Control,* Vol.3 No.6, pp. 549-554.

Favata, F. (2002), 'The Eddington Baseline Mission', *Proceedings of the First Eddington Workshop 'Stellar Structure and Habitable Planet Finding',* Vol. SP-485, Cordoba, Spain, pp. 3-10.

Fehse, W. (2003), *Automated Rendezvous and Docking of Spacecraft*, Cambridge University Press, Cambridge, UK.

Ferguson, P., Busse, F., Engberg, B., How, J.P., and Tillerson, M.e.al. (2001), 'Formation Flying Experiment on the Orion-Emerald Mission', *AIAA Space 2001,* Albuquerque, New Mexico, AIAA 2001-4688.

Folta, D. and Hawkins, A. (2002), 'Results of NASA's First Autonomous Formation Flying Experiment: Earth Observing-1 (EO-1)', *AIAA?AAS Astrodynamics Specialist Conference ,* Monterey, California, AIAA 2002-4743.

Folta, D. and Quinn, D. (1998), 'A Universal 3-D Method for Controlling the Relative Motion of Multiple Spacecraft in Any Orbit', AIAA 98-4193.

Folta, D. and Richon, K. (1998), 'Libration Orbit Mission Design at L2: A MAP and NGST Perspective', AIAA 98-4469.

Folta, D., Cooley, S., and Howell, K. (2001), 'Trajectory Design Strategies for the NGST L2 Libration Point Mission', AAS 01-205.

Fortescue, P., Stark, J., and Swinerd, G. (2003), *Spacecraft Systems Engineering* (Third edition), Wiley, Chichester, UK.

Fosbury, R. and Hook, R. (1998), *Future Large Telescopes in Space (Prepared for the 46th ESO-STC Meeting),* available at: http://www.stecf.org/~rfosbury/ngst/ngst_documents/ESO_STC_Oct98.pdf (accessed 2002).

Franck, S., Block, A., von Bloh, W., Bounama, C., Schellnhuber, H.J. and Svirezhev, Y. (2000), 'Habitable Zone for Earth-Like Planets in the Solar System', *Planetary and Space Science,* Vol. 48, pp. 1099-1105.

Franck, S., Bounama, C., and von Bloh, W. (2004), 'On the Habitability of Earth and Mars', *Proceedings of the Third European Workshop on Exo-Astrobiology. Mars: The Search for Life,* Vol. SP-545, Madrid, Spain, ESA, pp. 205-206.

Freudenrich, C.C. (2004), *How Planet Hunting Works,* available at: http://www.howstuffworks.com/planet-hunting2.htm (accessed 2004).

Fridlund, C.V.M. (2004), 'Darwin: The Scientific Constraints', *Proceedings of the Second Eddington Workshop: "Stellar Structure and Habitable Planet Finding",* Vol. SP-538, Palermo, Italy, ESA, pp. 225-229.

Fridlund, M. (2001), 'The Darwin Mission and Exo/Astrobiology', *Proceedings of the First European Workshop on Exo-/Astro-Biology,* Vol. SP-496, Frascati, Italy, ESA, pp. 267-271.

Fridlund, M. (2002), 'The Darwin Mission and Exo-Planets', *Proceedings of the First Eddington Workshop 'Stellar Structure and Habitable Planet Finding',* Vol. SP-485, Cordoba, Spain, pp. 235-242.

Fridlund, M. and Kaltenegger, L. (2002), 'ESA's Search for Extra-Solar terrestrial Planets: Mission Update of the Darwin Project ', *Proceedings of the Second European Workshop on Exo/Astrobiology,* Vol. SP-518, Graz, Austria, ESA, pp. 359-364.

GALEX Website (2004), *GALEX The Galaxy Evolution Explorer - Quick Facts,* available at: http://www.galex.caltech.edu/QUICKFACTS/quickfacts.html (accessed 2004).

Garnham, J., Wainwright, R., and Burns, R. (2001), 'Enabling Research and Development for Flight Demonstration of Sparse Aperture Sensing', *AIAA Space 2001 - Conference and Exposition,* Albuquerque, New Mexico, AIAA 2001-4552.

GBT Website (2003), *Robert C. Byrd Green Bank Telescope,* available at: http://www.gb.nrao.edu/GBT/GBT.shtml (accessed 2004).

Gim, D.W. and Alfriend, K.T. (2001), 'The State Transition Matrix of Relative Motion for the Perturbed Non-Circular Reference Orbit', *Proceedings of the AAS/AIAA Space Flight Mechanics Meeting,* Santa Barbara. California, pp. 913-934, AAS 01-222.

Gim, D.W. and Alfriend, K.T. (2002), 'The State Transition Matrix for Relative Motion of Formation Flying Satellites', *Proceedings of the AAS/AIAA Space Flight Mechanics Meeting,* San Antonio, Texas, pp. 1021-1041, AAS 02-186.

Gomez, G. and Masdemont, J. (2000), 'Some Zero Cost Transfers Between Libration Point Orbits', AAS 00-177.

Gomez, G., Lo, M., Masdemont, J., and Museth, K. (2001), 'Simulation of Formation Flight Near Lagrange Points for the TPF Mission', *AAS/AIAA Astrodynamics Conference,* Quebec, Canada, American Astronautical Society, AAS 01-305.

Gomez, G., Masdemont, J. and Simo, C. (1998), 'Quasihalo Orbits Associated with Libration Points', *Journal of the Astronautical Sciences,* Vol. Vol.46, pp. 135-176.

Gondoin, P., Absil, O., den Hartog, R., Kaltenegger, L., Eiroa, C., and Erd, C.e.al. (2003), 'The Ground-Based European Nulling Interferometry Experiment (DARWIN-GENIE)', *Proceedings 'Towards Other Earths': DARWIN/TPF and the Search for Extrasolar Terrestrial Planets,* Vol. SP-539, Heidelberg, Germany, ESA, pp. 121-131.

Grady, J.F. and Gadwal, G.R. (2001), 'The Constellation X-ray Mission: Exploring the Mysteries of Matter in the Universe', *IEEE Aerospace Conference 2001,* Vol. 7, IEEE, pp. 7-3629 to 7-3635.

GSFC Cos-B Website (2003), *Cos-B,* available at: http://heasarc.gsfc.nasa.gov/docs/cosb/cosb_about.html#overview (accessed 2004).

GSFC EXOSAT Website (2003), *The EXOSAT Observatory,* available at: http://heasarc.gsfc.nasa.gov/docs/exosat/exosat.html (accessed 2004).

Guibout, V.M. and Scheeres, D.J. (2004a), 'Spacecraft Formation Dynamics and Design', *AAS/AIAA Astrodynamics Conference,* Providence, RI, pp. 27-47, AIAA 2004-4736.

Guibout, V.M. and Scheeres, D.J. (2004b), 'Solving Relative Two-Point Boundary Value Problems: Spacecraft Formation Flight Transfers Application', *Journal of Guidance, Control, and Dynamics,* Vol. 27, No. 4, pp. 693-704.

Gurfil, P. and Kasdin, J. (2001), 'Dynamics and Control of Spacecraft Formation Flying in Three-Body Trajectories', AIAA 2001-4026.

Gurfil, P., Idan, M. and Kasdin, N.J. (2003), 'Adaptive Neural Control of Deep-Space Formation Flying', *Journal of Guidance, Control, and Dynamics,* Vol. 26, No. 3, pp. 491-501.

Gurfil, P., Idan, M., and Kasdin, J. (2002), 'Neurocontrol of Spacecraft Formation Flying in the Elliptic Restricted Three-Body Problem', *AIAA Guidance, Navigation and Control Conference and Exhibit,* AIAA 2002-4962, Monterey, California, USA.

Gutierrez, J.L. (2002), 'Terrene Meteorites in the Moon: Its Relevance for the Study of the Origin of Life in the Earth', *Proceedings of the Second European Workshop on Exo/Astrobiology,* Vol. SP-518, Graz, Austria, ESA, pp. 187-191.

Guyon, O., Ridgway, S., and Otsubo, M. (2003), 'Phase-Induced Pupil Apodization: A New Concept for A Simpler Darwin/TPF', *Proceedings 'Towards Other Earths': DARWIN/TPF and the Search for*

Extrasolar Terrestrial Planets, Vol. SP-539, Heidelberg, Germany, ESA, pp. 435-440.

Hablani, H.B., Tapper, M., and Dana-Bashian, D. (2001), 'Guidance Algorithms for Autonomous Rendezvous of Spacecraft with a Target Vehicle in Circular Orbit', *AIAA Guidance, Navigation, and Control,* Montreal, Canada, AIAA 2001-4393.

Hamilton, N. (2002), 'Formation Flying Satellite Control around the L2 Sun-Earth Libration Point', *AIAA Guidance, Navigation and Control Conference and Exhibit,* AIAA 2002-4528, Monterey, California, USA.

Haniff, C. (2003), *Optical Interferometry - A Gentle Introduction to the Theory,* available at: http://msc.caltech.edu/school/2003/2003_mss/07_Monday/haniff_finalv2.pdf (accessed 2005).

Hardacre, S. (1996), *Control of Collocated Geostationary Satellites, PhD Thesis*, Cranfield, Cranfield University.

Hariharan, P. (1985), *Optical Interferometry*, Academic Press Australia, Australia.

Harrison, R. (2004), *Welcome to the Very Large Array,* available at: http://www.vla.nrao.edu/ (accessed 2004).
Notes: Further information at: http://www.vla.nrao.edu/genpub/overview/

Hashida, Y. and Palmer, P.L. (2001), 'Epicyclic Motion of Satellites About an Oblate Planet', *Journal of Guidance, Control, and Dynamics,* Vol. 24, No. 3, pp. 586-596.

Hecht, E. (1998), *Optics* (Third edition), Addison Wesley Longman, Inc., Massachusetts.

Helvajian, H. ed. (1999), Microengineering Aerospace Systems. El Segundo, California, The Aerospace Press.

Hill, G.W. (1878), 'Researches in the Lunar Theory', *American Journal of Mathematics,* Vol. 1, pp. 5-26.

Hill, T. (2005), *Rice University Electromagnetic Field Model,* available at: http://image.gsfc.nasa.gov/poetry/art/mviews.html (website for NASA IMAGE mission – Imager for Magnetopause-to-Aurora Global Exploration) (accessed 2005).

Horneck, G. (2000), 'The Microbial World and the Case for Mars', *Planetary and Space Science,* Vol. 48, pp. 1053-1063.

Hough, J.H.L.P.W. (2003), 'Polarimetry as an Aid to the Detection of Extra-Solar Planets', *Proceedings 'Towards Other Earths': DARWIN/TPF and the Search for Extrasolar Terrestrial Planets,* Vol. SP-539, Heidelberg, Germany, ESA, pp. 11-17.

Howatson, A.M., Lund, P.G., and Todd, J.D. (1991), *Engineering Tables and Data* (2nd edition), Chapman & Hall, London.

Howell, K.C. (1984), 'Three-Dimensional Periodic Halo Orbits', *Celestial Mechanics,* Vol. Vol.32, pp. 53-71.

Howell, K.C. (1998), 'Families of Orbits in the Vicinity of the Collinear Libration Points', *AAS/AIAA Astrodynamics Specialists Conference,* Boston, MA, USA, AAS 98-4465.

Howell, K.C. (2001), 'Families of Orbits in the Vicinity of the Collinear Libration Points', *Journal of the Astronautical Sciences,* Vol.49 No.1, pp. 107-125.

Howell, K.C. and Campbell, E.T. (1999), 'Three-Dimensional Periodic Solutions that Bifurcate from Halo

Families in the Circular Restricted Three-Body Problem', AAS 99-161.

Howell, K.C. and Keeter, T. (1995), 'Station-Keeping Stategies for Libration Point Orbits - Target Point and Floquet Mode Approaches', *Advances in the Astronautical Sciences,* Vol. Vol.89 Pt.2, pp. 1377-1396.

Howell, K.C. and Marchand, B.G. (2003a), 'Control Strategies for Formation Flight in the Vicinity of the Libration Points', *AAS/AIAA Space Flight Mechanics Meeting,* Ponce, Puerto Rico, American Astronautical Society, AAS 03-133.

Howell, K.C. and Marchand, B.G. (2003b), 'Design and Control of Formations Near the Libration Points of the Sun-Earth/Moon Ephemeris System', *2003 Space Flight Mechanics Symposium,* Goddard Space Flight Centre, Greenbelt, MD, USA,

Howell, K.C., Barden B.T. and Lo, M.W. (1997), 'Application of Dynamical Systems Theory to Trajectory Design for a Libration Point Mission', *Journal of the Astronautical Sciences,* Vol.45 No.2, pp. 161-178.

Howell, K.C., Guzman, J.J., and Anderson, J.P. (2001), 'Trajectory Arcs with Lunar Encounters for Transfers to Small Amplitude Lissajous Orbits', AAS 01-207.

Hsaio, F.Y. and Scheeres, D.J. (2002), 'The Dynamics of Formation Flight about a Stable Trajectory ', *AAS/AIAA Space Flight Mechanics Meeting,* Vol. Vol. 112 Pt.2, San Antonio, TX, USA, Advances in the Astronautical Sciences, AAS 02-189.

Hughes, S.P. and Hall, C.D. (2000), 'Optimal Configurations for Rotating Spacecraft Formations', *Richard H. Battin Astrodynamics Symposium,* College Station, Texas, pp. 163-185, AAS 00-257.

Hyland, D. and Vesecky, J. (2002), 'Basic Advances in System Architecture for Interferometric Imaging', *International Symposium: Formation Flying Missions and Technologies,* Toulouse, France, CNES,

Hyland, D.C. (2001), 'Interferometric Imaging Concepts with Reduced Formation-Keeping Constraints', *AIAA Space 2001 - Conference and Exposition,* Albuquerque, New Mexico, AIAA 2001-4610.

Inalhan, G. and How, J.P. (2000), 'Relative Dynamics and Control of Spacecraft Formations in Eccentric Orbits', *Proceedings of the AIAA Guidance, Navigation, and Control Conference,* Denver. Colorado, AIAA 2000-4443.

Irvin, D.J. and Jacques, D.R. (2001), 'Linear vs. Nonlinear Control Techniques for the Reconfiguration of Satellite Formations', *Proceedings of the 2001 AIAA Guidance, Navigation, and Control Conference,* Montreal, Canada, AIAA 2001-4089.

Irwin, L.N. and Schulze-Makuch, D. (2002), 'Origin and Evolution of Life on Other Worlds: Lessons from the History of Life on Earth', *Proceedings of the Second European Workshop on Exo/Astrobiology,* Vol. SP-518, Graz, Austria, ESA, pp. 463-464.

Izzo, D. (2002), *MSc Group Design Project Report*, Cranfield University, Cranfield .

Izzo, D. (2002b), 'Formation Flying Linear Modelling', *5th Cranfield Conference on the Dynamics and Control of Systems and Structures in Space,* Cambridge, UK, Cranfield University Press, Cranfield, UK, pp. 283-289.

Jackson, R. (2004), *Origins: Missions: Planet Imager,* available at: http://planetquest.jpl.nasa.gov/science/finding_life.html (accessed 2005).

Jackson, R. (2004a), *Two Architectures Chosen for Terrestrial Planet Finder,* available at:

http://planetquest.jpl.nasa.gov/TPF/tpf_architectures.cfm (accessed 2005).

Jackson, R. (2004b), *Origins: Missions: Life Finder,* available at: http://planetquest.jpl.nasa.gov/science/finding_life.html (accessed 2005). Notes: Same material as on webpage viewed in February 2002

Jackson, R. (2004c), *Keck Interferometer,* available at: http://planetquest.jpl.nasa.gov/Keck/astro_tech.cfm (accessed 2004).

Jackson, R. (2005a), *PlanetQuest: the Search for Another Earth: Missions> Spitzer,* available at: http://planetquest.jpl.nasa.gov/Spitzer/spitzer_index.html (accessed 2005).

Jackson, R. (2005b), *SIM PlanetQuest,* available at: http://planetquest.jpl.nasa.gov/SIM/sim_index.html (accessed 2005).

Jacquinot, P. (1960), 'New Developments in Interference Spectroscopy', *Reports on Progress in Physics,* Vol. 23, pp. 267-312.

Jones, B., Underwood, D.R., and Sleep, P.N. (2003), 'The Stability of the Orbits of Earth-Mass Planets In and Near the Habitable Zones of Known Exoplanetary Systems ', *Proceedings 'Towards Other Earths: DARWIN/TPF and the Search for Extrasolar Terrestrial Planets',* Vol. SP-539, Heidelberg, Germany, ESA, pp. 625-630.

Jones, B.W. (1999), *Discovering the Solar System*, John Wiley & Sons, Chichester, UK.

JPL Presentation (1997), *Origins Technology Roadmap,* available at: http://origins.jpl.nasa.gov/library/techroadmap/techroadmap.pdf (accessed 2002).

JPL Publication (1999a), *SIM: Taking the Measure of the Universe,* available at: http://origins.jpl.nasa.gov/library/techreports/SIM_response.pdf (accessed 2002a).

JPL Publication (1999b), *The Terrestrial Planet Finder,* available at: http://planetquest.jpl.nasa.gov/TPF/tpf_book/index.cfm (accessed 2002b).

JPL Web Site (2004), *Precision Formation Flying: Distributed Spacecraft Technology: Formation Control Testbed,* available at: http://dst.jpl.nasa.gov/test_beds/, also http://dst.jpl.nasa.gov/test_beds/testbeds.htm (accessed 2005).

JPL, P.I.O. (1997), *Mars Pathfinder Winds Down After Phenomenal Mission,* available at: http://mars.sgi.com/MPF/mpf-pressrel.html (accessed 2004).

Junge, O., Levenhagen, J., Seifried, A., and Dellnitz, M. (2002), 'Identification of Halo orbits for energy efficient Formation Flying', *International Symposium: Formation Flying Missions and Technologies,* Toulouse, France, CNES.

Junkins, J.L. and Singla, P. (2003), 'How Nonlinear Is It?', *Proceedings of the John L. Junkins Astrodynamics Symposium,* College Station, Texas, AAS 03-286.

Kaltenegger, L., Karlsson, A., and Hanslmeier, A. (2002), 'Darwin: A Nulling Space Interferometer', *Proceedings of the Second European Workshop on Exo/Astrobiology,* Vol. SP-518, Graz, Austria, ESA, pp. 519-520.

Kaltenegger, L., Karlsson, A., Fridlund, M., and Absil, O. (2003), 'Overview of the Darwin Mission', *Proceedings 'Towards Other Earths': DARWIN/TPF and the Search for Extrasolar Terrestrial Planets,* Vol. SP-539, Heidelberg, Germany, ESA, pp. 459-464.

Kang, W. and Sparks, A. (2002), 'Coordinated Attitude and Formation Control of Multi-Satellite

Systems', *AIAA Guidance, Navigation, and Control Conference,* Monterey, California, AIAA 2002-4655.

Kang, W., Sparks, A., and Banda, S. (2000), 'Multi-Satellite Formation and Reconfiguration', *Proceedings of the American Control Conference,* Chicago, Illinois, pp. 379-383.

Kang, W., Sparks, A., and Banda, S. (2001), 'Coordinated Control of Multisatellite Systems', *Journal of Guidance, Control, and Dynamics,* Vol. 24, No. 2, pp. 360-368.

Kapila, V., Sparks, A., Buffington, J.M., and Yan, Q. (1999), 'Spacecraft Formation Flying: Dynamics and Control', *Proceedings of the American Control Conference,* San Diego, California, pp. 4137-4141.

Kapila, V., Sparks, A., Buffington, J.M., and Yan, Q. (2000), 'Spacecraft Formation Flying: Dynamics and Control', *Journal of Guidance, Control, and Dynamics,* Vol. 23, No. 3, pp. 561-563.

Kaplan, M.H. (1976), *Modern Spacecraft Dynamics and Control*, Wiley, New York, USA.

Karlsson, A. and Kaltenegger, L. (2003), 'The Technology of Darwin', *Proceedings 'Towards Other Earths': DARWIN/TPF and the Search for Extrasolar Terrestrial Planets,* Vol. SP-539, Heidelberg, Germany, ESA, pp. 41-46.

Karlsson, A., Kaltenegger, L., den Hartog, R., d'Arcio, L., Kilter, M., Erd, Ch., and Ankersen, F. (2004), *Darwin, TTN+ Mission Design Assessment*, European Space Agency, The Netherlands. Notes: Unpublished Report

Kasting, J., Whitmire, D. and Reynolds, R. (1993), 'Habitable Zones Around Main Sequence Stars', *Icarus,* Vol. 108, pp. 108.

Kasting, J.F. (1997), *Habitable Zones Around Stars and Their Relationship to CO_2, O_2, and O_3 Abundances in Planetary Atmospheres,* available at: http://astrobiology.arc.nasa.gov/workshops/1996/palebluedot/abstracts/kasting_01.html (accessed 2004).

Kazeminejad, B., Lebreton, J.P., Matson, D.L., Spilker, L., and Raulin, F. (2002), 'The Cassini/Huygens Mission to Saturn and Titan and its Relevance to Exo/Astrobiology', *Proceedings of the Second European Workshop on Exo/Astrobiology,* Vol. SP-518, Graz, Austria, ESA, pp. 261-266.

Kechichian, J.A. (2001), 'Computational Aspects of Transfer Trajectories to Halo Orbits', *Journal of Guidance, Control, and Dynamics,* Vol. 24, No. 4, pp. 796-804.

Keck Observatory Website (2004), *W.M. Keck Observatory,* available at: http://www2.keck.hawaii.edu/geninfo/about.php (accessed 2004).

Kennicutt, R.C. (1998), 'Emission-Line Diagnostics of Galaxy Evolution with NGST', *Proceedings of the 34th Liege International Astrophysics Colloquium, 'The Next Generation Space Telescope: Science Drivers and Technological Challenges',* Vol. SP-429, Liege, Belgium, ESA, pp. 81-88.

Kereszturi, A. (2002), ' The Drake Matrix and Drake Diagrams, Possible New Extensions of the Drake Formulae', *Proceedings of the Second European Workshop on Exo/Astrobiology,* Vol. SP-518, Graz, Austria, ESA, pp. 527-528.

Kiddy, A. (2002), *Rossi X-Ray Timing Explorer (RXTE) ,* available at: http://heasarc.gsfc.nasa.gov/docs/xte/xte_1st.html (accessed 2002). Notes: original website no longer available

Kilston, S. and Noecker, M.C. (2003), 'A Coronagraphic TPF: System Options and Challenges',

Proceedings 'Towards Other Earths': DARWIN/TPF and the Search for Extrasolar Terrestrial Planets, Vol. SP-539, Heidelberg, Germany, ESA, pp. 475-479.

Kim, M. and Hall, C.D. (2001), 'Lyapunov and Halo Orbits about L2', *AAS/AIAA Astrodynamics Conference,* AAS 01-324, Quebec, Canada.

King-Hele, D. (1987), *Satellite Orbits in an Atmosphere*, Blackie, Glasgow, UK.

Koch, D. (2004), *(Kepler) Mission Design: Photometer and Spacecraft,* (accessed 2004).

Kojima, H., Aoyama, S., and Yajima, K. (2004), 'Formation Flight Using Feature-Based Visual Servo Technique', *AIAA/AAS Astrodynamics Specialist Conference,* Vol. 1, Providence, Rhode Island, pp. 65-75, AIAA 2004-4738.

Kong, E. and Miller, D. (2001), 'Minimum Energy Trajectories for Techsat 21 Earth Orbiting Clusters', *AIAA Space 2001: Conference and Exposition,* Albuquerque, New Mexico, AIAA 2001-4769.

Kong, E., Miller, D., and Sedwick, R.J. (1999), 'Exploiting Orbital Dynamics for Aperture Synthesis Using Distributed Satellite Systems: Applications to a Visible Earth Imager System', *AAS/AIAA Space Flight Mechanics Conference,* Vol. 102-1, pp. 323-342, AAS 99-122.

Kong, E., Miller, D., and Sedwick, R.J. (1999b), 'Exploiting Orbital Dynamics for Interstellar Separated Spacecraft Interferometry', *Proceedings of the American Control Conference,* San Diego, California, IEEE, pp. 4153-4157.

Kong, E.M.C. and Miller, D.W. (1998), 'Optimization of Separated Spacecraft Interferometer Trajectories in the Absence of a Gravity-Well', *Astronomical Interferometry Conference,* Vol. SPIE-3350-13, Kona, Hawaii, pp. 631-643.

Koon, W.S., Lo, M.W., Masdemont, J.E., and Ross, S.D. (2000), 'Shoot the Moon', *AAS/AIAA ,* AAS 00-166.

Koon, W.S., Marsden, J.E., Murray, R.M., and Masdemont, J. (2001), 'J2 Dynamics and Formation Flight', pp. 381-387, AIAA 2001-4090.

Korablev, O.I., Bertaux, J.L., Vinogradov, I.I., Kalinnikov, Y.K., Nevejans, D., Neefs, E., Le Barbu, T., and Durry, G. (2004), 'Compact High-Resolution Echelle-AOTF NIR Spectrometer for Atmospheric Measurements', *Proceedings of the 5th International Conference on Space Optics (ICSO 2004),* Vol. SP-554, Toulouse, France, ESA, pp. 73-80.

Kormos, T. and Palmer, P. (2002), 'High Accuracy Modelling of Relative Orbits of Formation Flying Spacecraft in LEO', *International Symposium: Formation Flying Missions and Technologies,* Toulouse, France, CNES.

Kwakernaak, H. and Sivan, R. (1972), *Linear Optimal Control Systems*, John Wiley & Sons Inc, New York.

Labeyrie, A., Le Coroller, H., Dejonghe, J., and Martinache, F.e.al. (2002), *Hypertelescope Imaging: From Exo-Planets to Neutron Stars,* available at: http://www.obs-hp.fr/~coroller/spie.pdf (accessed 2004).

Labeyrie, A., Schneider, J., Boccaletti, A., Riaud, P., Moutou, C., Abe, L., and Rabou, P. (2000), 'Visible and Infra-red Imaging with Darwin: Feasibility of a Visible Precursor', *Proceedings of the Conference 'Darwin and Astronomy - The Infrared Space Interferometer',* Vol. SP-451, Stockholm, Sweden, ESA, pp. 21-26.

Lagadec, K., Lebas, J., and Ankersen, F. (2002), 'GNC System for the Control of the Darwin Free-Flying

Interferometer', *Proceedings of the International Symposium: Formation Flying Missions and Technologies,* Toulouse, France, CNES.

Lagadec, K., Lebas, J., and Ankersen, F. (2003), 'Precision Formation Flying for the Darwin Interferometer', *Proceedings of the 5th ESA International Conference on Spacecraft Guidance, Navigation and Control Systems,* Vol. SP-516, Frascati, Italy, ESA, pp. 201-207.

Lanzano, P. (1967), *Periodic Solutions for the Restricted Three-Body Problem of Celestial Mechanics*, Report no. NASA Contractor Report NASA CR-765, NASA,

Lardiere, O., Labeyrie, A., Gillet, S., and Riaud, P. (2001), *Spacebourne Hypertelescope: A Spacecraft Formation Flying Controlled by Solar Sails,* available at: http://www.obs-hp.fr/~lardiere/publi/2001-Lardiere-haifa.pdf (accessed 2004).

Larson, W.J. and Wertz, J.R. (1996), *Space Mission Analysis and Design* (Second edition), Kluwer Academic Publishers, UK.

Lau, K., Lichten, S., Young, L., and Haines, B. (1996), 'An Innovative Deep Space Application of GPS Technology for Formation Flying Spacecraft', *AIAA Guidance, Navigation, and Control Conference,* AIAA 96-3819.

Lawton, J., Beard, R.W., and Hadaegh, F.Y. (1999), 'An Adaptive Control Approach to Satellite Formation Flying with Relative Distance Constraints', *Proceedings of the American Control Conference,* San Diego, California, pp. 1545-1549.

Lawton, J., Beard, R.W., and Hadaegh, F.Y. (2000), 'Elementary Attitude Formation Maneuvers Via Leader-Following and Behaviour-Based Control', *AIAA Guidance, Navigation, and Control Conference and Exhibit,* Denver, Colorado, pp.1414-1424, AIAA 2000-4442.

Le Fevre, O. (1998), 'Deep Spectroscopic Surveys with NGST', *Proceedings of the 34th Liege International Astrophysics Colloquium: 'The Next Generation Space Telescope: Science Drivers and Technological Challenges',* Vol. SP-429, Liege, Belgium, ESA, pp. 97-102.

Leger, A., Labeque, A., Ollivier, M., Sekulic, P., and Valette, C. (2002), 'Selected Open Problems in Planetary Science', *Proceedings of the First Eddington Workshop 'Stellar Structure and Habitable Planet Finding',* Vol. SP-485, Cordoba, Spain, pp. 171-176.

Leitch, J. (1999), *Formation Flying for Assembly of Deep Space Interferometers,* (accessed 2002). Notes: Website no longer available

Leveque, S. (2004), *The Very Large Telescope Interferometer,* available at: http://www.eso.org/projects/vlti/ (accessed 2004).

Lineweaver, C.H. (2001), 'An Estimate of the Age Distribution of Terrestrial Planets in the Universe: Quantifying Metallicity as a Selection Effect', *Icarus,* Vol. 151, pp. 307-313.

Liotard, A. and Zamkotsian, F. (2004), 'Static and Dynamic Micro Deformable Mirror Characterization by Phase-Shifting and Time-Averaged Interferometry', *Proceedings of the 5th International Conference on Space Optics (ICSO 2004),* Vol. SP-554, Toulouse, France, ESA, pp. 801-808.

Lo, M.W., Anderson, R.L., Whiffen, G., and Romans, L. (2004), 'The Role of Invariant Manifolds in Low Thrust Trajectory Design', *14th AAS/AIAA Space Flight Mechanics Conference,* Maui, Hawaii, USA, AAS 04-288.

Lo, M.W., Koon, W.S., Marsden, J.E. and Murray, R.M. (2000), 'Formation Flight Near Libration Points: Survey and Recommendations', *Journal of Space Mission Architecture,* Fall 2000, pp. 35-48.

Lochner, J. (2002a), *Imagine The Universe - Regions of the Electromagnetic Spectrum,* available at: http://imagine.gsfc.nasa.gov/docs/science/know_l1/spectrum_chart.html (accessed 2002).

Lochner, J. (2002b) *Imagine The Universe - The Electromagnetic Spectrum,* available at: http://imagine.gsfc.nasa.gov/docs/science/know_l1/emspectrum.html (accessed 2002).

Lochner, J. (2004), *Imagine The Universe,* available at: http://imagine.gsfc.nasa.gov/docs/science/know_l2/emspectrum.html (accessed 2004).

Lovell, T.A., Tragesser, S.G., and Tollefson, M.V. (2004), 'A Practical Guidance Methodology for Relative Motion of LEO Spacecraft Based on the Clohessy-Wiltshire Equations', *14th AAS/AIAA Space Flight Mechanics Conference,* Maui, Hawaii, AAS 04-252.

Mallory, G.J., Jilla, C.D., and Miller, D.W. (1998), 'Optimization of Geosynchronous Satellite Constellations for Interferometric Earth Imaging', *AIAA/AAS Astrodynamics Specialist Conference,* Boston, Massachusetts, pp. 150-158, AIAA 98-4379.

Mandutianu, S., Hadaegh, F., and Elliot, P. (2001), 'Multi-Agent System for Formation Flying Missions', *IEEE Aerospace Conference,* Vol. 6, IEEE, pp. 2793-2802.

Manikonda, V., Arambel, P.O., Gopinathan, M., Mehra, R.K., and Hadaegh, F.Y. (1999), 'A Model Predictive Control-based Approach for Spacecraft Formation Keeping and Attitude Control', *Proceedings of the American Control Conference,* San Diego, California, pp. 4258-4262.

Marchal, C. (1990), *The Three-Body Problem*, Elsevier, New York.

Marchand, B.G. and Howell, K.C. (2004), 'Aspherical Formations Near the Libration Points in the Sn-Earth/Moon Ephemeris System', *14th AAS/AIAA Space Flight Mechanics Conference,* Maui, Hawaii, AAS 04-157.

Marotta (Polyflex) Website (2005), *Products: MicroNewton Proportional Thrusters,* available at: http://www.polyflexspace.com/pages/prprothrust.htm (accessed 2005).

Marr, J., Dallas, S., Laskin, R., Unwin, S., and Yu, J. (1999), 'Space Interferometry Mission: Measuring the Universe', IEEE, pp. 1117-1122.

Massari, M., Armellin, R., and Ercoli Finzi, A. (2004), 'Optimal Trajectory Generation and Control for Reconfiguration Maneuvers of Formation Flying using Low-Thrust Propulsion', *14th AAS/AIAA Space Flight Mechanics Conference,* Maui, Hawaii, AAS 04-258.

Mattson, B. (2005), *Constellation-X: Mission Design,* available at: http://constellation.gsfc.nasa.gov/science/design/description.html (accessed 2005).

Mauldin, J.R., Bettadpur, S., and Fowler, W.T. (2004), 'The Design and Development of the GRACE Mission Analysis Tool', *14th AAS/AIAA Space Flight Mechanics Conference,* Maui, Hawaii, AAS 04-303.

Mazanek, D., Kumar, R., Seywald, H., and Qu, M. (2000), 'GRACE Mission Design: Impact of Uncertainties in Disturbance Environment and Satellite Force Models', *AAS/AIAA Space Flight Mechanics Meeting,* Vol. 105, Clearwater, Florida, pp. 967-985, AAS 00-163.

McInnes, C.R. (1995), 'Autonomous Ring Formation for a Planar Constellation of Satellites', *Journal of Guidance, Control and Dynamics,* Vol. 18, No. 5, pp. 1215-1217.

McInnes, C.R. (2004), *Solar Sailing: Technology, Dynamics and Mission Applications*, Springer, Praxis, London.

McLaughlin, C.A., Alfriend, K.T., and Lovell, T.A. (2002), 'Analysis of Reconfiguration Algorithms for Formation Flying Experiments', *Proceedings of the International Symposium: Formation Flying Missions and Technologies,* Toulouse, France, CNES.

McQuade, F., Ward, R., and McInnes, C.R. (2002), 'The Autonomous Configuration of Satellite Formations Using Generic Potential Functions', *Proceedings of the International Symposium: Formation Flying Missions and Technologies,* Toulouse, France, CNES.

Megla, E., Konangi, V., and Seibert, M. (2002), 'Protocols for Inter-Satellite Communication in a Formation Flying System', *20th AIAA International Communication Satellite Systems Conference and Exhibit,* Montreal, Quebec, Canada,. AIAA 2002-1960.

Melton, R.G. (2000), ' Time-Explicit Representation of Relative Motion Between Elliptical Orbits', *Journal of Guidance, Control and Dynamics,* Vol. 23, No. 4, pp. 604-610.

Menon, S. (1995), *Insects of the Oxygeniferous - Plentiful Oxygen May Have Helped Carboniferous Insects Grow to Giant Size,* available at: http://www.findarticles.com/p/articles/mi_m1511/is_n9_v16/ai_17199031 (accessed 2004).

Mesbahi, M. and Hadaegh, F.Y. (1999), 'Formation Flying Control of Multiple Spacecraft: Graph Theoretic Properties and Switching Schemes', pp.1585-1595, AIAA 99-4268.

Mesbahi, M. and Hadaegh, F.Y. (2000), 'Mode and Logic-based Switching for the Formation Flying Control of Multiple Spacecraft', AAS 00-017.

Mesbahi, M. and Hadaegh, F.Y. (2001a), 'Mode and Logic-based Switching for the Formation Flying Control of Multiple Spacecraft', *Proceedings of the American Control Conference,* Arlington, Virginia, pp. 710-714.

Mesbahi, M. and Hadaegh, F.Y. (2001b), 'Formation Flying Control of Multiple Spacecraft via graphs, Matrix Inequalities, and Switching', *Journal of Guidance, Control and Dynamics,* Vol. 24, No. 2, pp. 369-377.

Meyer, C. (2003), *Mars Meteorite Compendium - 2003,* available at: http://curator.jsc.nasa.gov/antmet/mmc/Chap%20I.pdf (accessed 2004).

Microlensing Observations in Astrophysics Website (2004), *Microlensing Observations in Astrophysics - Extrasolar Planets,* available at: http://www.physics.auckland.ac.nz/moa/extrasolar_planets.html (accessed 2004).

Milam, M.B., Petit, N., and Murray, R.M. (2001), 'Constrained Trajectory Generation for Micro-Satellite Formation Flying', *AIAA Guidance, Navigation, and Control Conference and Exhibit,* Montreal, Canada, AIAA 2001-4030.

Morring, F. (Aug 5, 2002) Mirror Technology Push Aids Hunt for New Earths. *Aviation Week & Space Technology* 44-48. McGraw-Hill.

Mortari, D. (2003), *The Flower Constellations Group at Texas A&M University,* available at: http://flowerconstellation.tamu.edu/ (accessed 2005).

Mortari, D., Wilkins, M., and Bruccoleri, C. (2003), 'The Flower Constellations', *John L. Junkins Astrodynamics Symposium,* College Station, Texas, AAS 03-274.

Morton, B., Weininger, N., and Tierno, J.E. (1999), 'Collective Management of Satellite Clusters', AIAA 99-4267.

MOST Website (2005), *MOST: Canada's First Space Telescope,* available at: http://www.astro.ubc.ca/MOST/overview.html (accessed 2005).

Mueller, J.B. (2004), 'A Multiple-Team Organization for Decentralized Guidance and Control of Formation Flying Spacecraft', *AIAA 1st Intelligent Systems Technical Conference,* Chicago, Illinois, AIAA 2004-6249.

Mueller, J.B. and Brito, M. (2003), 'A Distributed Flight Software Design for Satellite Formation Flying Control', *AIAA Space 2003,* Long Beach, California, AIAA 2003-6373.

Mullen, L. (2002), *Salt of the Early Earth,* available at: http://zdna2.umbi.umd.edu/~dassarma/Astrobiology.html (accessed 2004).

Myers, J.D. (2004a), *About the Compton Gamma Ray Observatory,* available at: http://cossc.gsfc.nasa.gov/cgro/ (accessed 2004).
Notes: Follow links for instrument details to http://cossc.gsfc.nasa.gov/nra/appendix_g.html#II.%20OSSE%20GUEST%20INVESTIGATOR%20PROGRAM

Myers, J.D. (2004b), *GLAST Overview,* available at: http://glast.gsfc.nasa.gov/science/overview.html (accessed 2004).

Myers, J.D. (2004c), *Swift Fact Sheet,* available at: http://swift.gsfc.nasa.gov/docs/swift/about_swift/factsheet.html (accessed 2004).

Naasz, B.J., Karlgaard, C.D., and Hall, C.D. (2002), 'Application of Several Control Techniques for the Ionospheric Observation Nanosatellite Formation', *Space Flight Mechanics,* 1063-1079, AAS 02-188.

NASA Astrobiology Institute (2003), *What is Astrobiology?,* available at: http://ares.jsc.nasa.gov/astrobiology/biomarkers/whatis.html (accessed 2004).

NASA Astrobiology Roadmap (2002), *Astrobiology Roadmap,* available at: http://astrobiology.arc.nasa.gov/roadmap/roadmap.pdf (accessed 2004).

NASA Origins Programme (2004), *Origins 2003,* available at: http://origins.jpl.nasa.gov/library/roadmap03/index.html (accessed 2004).
Notes: Astrobiology

NASA Origins Website (2000), *Planet Imager Mission,* available at: http://origins.jpl.nasa.gov/missions/pi.html (accessed 2002).
Notes: Website no longer available

NASA Presentation (1997), *NASA's Interferometry Program: The Search for Life Beyond the Solar System,* available at: http://origins.jpl.nasa.gov/library/ipff/ipff.pdf (accessed 2001).

NASA Science and Technology Definition Team (2004), *The Magnetospheric Constellation: Global Dynamics of the Structured Magnetotail,* available at: http://stp.gsfc.nasa.gov/missions/mc/STDT_20050103.pdf (accessed 2005).

NASA TPF Report (1999), *TPF Terrestrial Planet Finder: Origins of Stars, Planets and Life,* available at: http://tpf.jpl.nasa.gov (accessed 2002).

NASA Website (2004a), *Mars Exploration Rover Mission: Summary,* available at: http://marsrovers.jpl.nasa.gov/overview (accessed 2004).

NASA Website (2004b), *Mission Success: The Magic of Mars Odyssey,* available at: http://marsprogram.jpl.nasa.gov/spotlight/odyssey-mission-success.html (accessed 2004).

NASA Website (2005), *ALH84001,* available at: http://www-curator.jsc.nasa.gov/curator/antmet/marsmets/ALH84001/alh84001,0.htm (accessed 2005).

Natarajan, A., Kapania, R.K., and Inman, D.J. (2001), 'Near-Exact Analytical Solutions to Linear Time-Variant Systems', *42nd AIAA/ASME/ASCE/AHS/ASC Structures, Structural Dynamics, and Materials Conference,* Seattle, WA, AIAA 2001-1295.

National Academy of Sciences (2000), *The Role of Small Satellites in NASA and NOAA Earth Observation Programs,* available at: http://www.nap.edu/html/ssb_html/small_sat_2000/smallsatch6.shtml (accessed 2001).

Nella, J., Atkinson, C., Bronowicki, A., Lynch, R., and Atcheson, P.e.al. (2004), *James Webb Space Telescope (JWST) Observatory Architecture and Performance (AIAA 2004-5986),* available at: http://www.stsci.edu/jwst/docs/presentations/JwstObservatoryArchitectureAndPerformance_3318.pdf (accessed 2004).

Nelson, E., Sparks, A., and Kang, W. (2001), 'Coordinated Nonlinear Tracking Control for Satellite Formations', AIAA 2001-4025.

Newman, P. (2001), *ASCA's X-Ray Telescopes,* available at: http://heasarc.gsfc.nasa.gov/docs/asca/ascagof.html (accessed 2002).
Notes: original website no longer available

Nisbet, E.G. and Sleep, N.H. (2001), 'The Habitat and Nature of Early Life', *Nature ,* Vol. 409, pp. 1083-1091.

Noecker, C. and Kilston, S. (1999), 'Terrestrial Planet Finder: The Search for Life Elsewhere', *IEEE Aerospace Conference,* Vol. 4, pp. 49-57.

Offenberg, J.D. (2004), *James Webb Space Telescope - L2 Orbit,* available at: http://www.jwst.nasa.gov/project/text/orbits.html (accessed 2004).

Office of Naval Research Website (2005), *The Navy and Satellites - Satellite Orbits,* available at: http://www.onr.navy.mil/focus/spacesciences/images/satellites/lagrangepoints.gif (accessed 2005).

Ollivier, M., Selsis, F., and Leger, A. (2003), 'Finding and Characterising Extrasolar Planets at (Thermal) Infrared Wavelengths', *Proceedings 'Towards Other Earths': DARWIN/TPF and the Search for Extrasolar Terrestrial Planets,* Vol. SP-539, Heidelberg, Germany, ESA, pp. 241-246.

O'Neil, J. (1999), 'Quick Ride: An Innovative Approach for Low Cost , Quick Access, Small Payload Missions', *International Astronautical Federation Specialists Symposium: Novel Concepts for Smaller, Faster, and Better Space Missions,* Redondo Beach, California,

Orbital Sciences Corporation (2005), *DART Rendezvous Vehicle,* available at: http://www.orbital.com/AdvancedSpace/DART (accessed 2005).

Owen, T. (2000), 'Planets and Life', *Proceedings of the Conference 'Darwin and Astronomy - The Infrared Space Interferometer',* Vol. SP-451, Stockholm, Sweden, ESA, pp. 163.

Park, C.-W., Olsen, E.A., and How, J.P. (2000), 'Sensing Technologies for Spacecraft Formation Flying', *Navigating Into the New Millenium: Institute of Navigation 2000 National Technical Meeting*

(ION NTM 2000), Anaheim, California,

Park, K., Wilkins, M.P., and Mortari, D. (2004), 'Uniformly Distributed Flower Constellation Design Study For Global Navigation System', *14th AAS/AIAA Space Flight Mechanics Conference,* Maui, Hawaii, AAS 04-297.

Parker, S.P. (1988), *Spectroscopy Source Book*, McGraw-Hill, Inc., New York, USA.

Parnell, J. (2002), 'Sampling of Paleo-Water and Biomolecules from Surface Deposits on Mars', *Proceedings of the Second European Workshop on Exo/Astrobiology,* Vol. SP-518, Graz, Austria, ESA, pp. 395-398.

Payload Systems Inc. (2003), *Synchronized Position Hold, Engage and Reorient Experimental Satellites (SPHERES),* available at: www.payload.com/pdfs/SPHEREShigh1.pdf (accessed 2005).

Pedretti, E., Labeyrie, A., Arnold, L., Thureau, N. and Lardiere, O.e.al. (2000), 'First Images on the Sky from a Hyper Telescope', *Astronomy and Astrophysics Supplement Series,* Vol. 147, pp. 285-290.

Penny, A., Cowan, D., Cockell, C., and Wynn-Williams, D. (2001), 'The UK Astrobiology Forum', *Proceedings of the First European Workshop on Exo/Astro-Biology,* Vol. SP-496, Frascati, Italy, pp. 13-15.

Perrins, J.A. (2002), *Satellite Formation Flying for an Interferometry Mission*, Cranfield University, Unpublished 9-Month Review PhD Report.

Perryman, M.A.C. (1999), *Hipparcos: Background Information,* available at: http://astro.estec.esa.nl/Hipparcos/further_more.html#themission (accessed 2004). Notes: Also http://astro.estec.esa.nl/Hipparcos/hipp_payload.html

Perryman, M.A.C. (2002), 'GAIA and Eddington', *Proceedings of the First Eddington Workshop 'Stellar Structure and Habitable Planet Finding',* Vol. SP-485, Cordoba, Spain, pp. 229-234.

Peslen, C. and Stoner, K. (2005a), *GOES Project: Current Status,* available at: http://goespoes.gsfc.nasa.gov/goes/project/index.html, also http://goespoes.gsfc.nasa.gov/mission.html (accessed 2005).

Peslen, C. and Stoner, K. (2005b), *POES Project: Current Status,* available at: http://goespoes.gsfc.nasa.gov/poes/project/index.html, also http://goespoes.gsfc.nasa.gov/mission.html (accessed 2005).

Phillips, A.C. (2003), *Introduction to Quantum Mechanics*, Wiley, New York, USA.

Prussing, J.E. and Conway, B.A. (1993), *Orbital Mechanics*, Oxford University Press, New York.

Psiaki, M.L. (1999), ' Autonomous Orbit Determination for Two Spacecraft from Relative Position Measurements', *Journal of Guidance, Control, and Dynamics,* Vol. 22, No. 2, pp. 305-312.

Queloz, D., Santos, N.C., and Mayor, M. (2002), 'Search for Extra-Solar Planets', *Proceedings of the First Eddington Workshop 'Stellar Structure and Habitable Planet Finding',* Vol. SP-485, Cordoba, Spain, pp. 117-121.

Quirrenbach, A. (2003), 'Astrometry as a Precursor to Darwin/TPF', *Proceedings 'Towards Other Earths': DARWIN/TPF and the Search for Extrasolar Terrestrial Planets,* Vol. SP-539, Heidelberg, Germany, ESA, pp. 19-30.

Rees, M. (2002), *Our Cosmic Habitat*, Weidenfield and Nicolson, London.

Reichbach, J.G., Sedwick, R.J., and Martinez-Sanchea, M. (2001), 'Micropropulsion System Selection for Precision Formation Flying Satellites', *37th AIAA/ASME/SAE/ASEE Joint Propulsion Conference and Exhibit,* Salt Lake City, Utah, AIAA 2001-3646.

Riaud, P., Boccaletti, A., Baudrand, J., Reess, J., and Rouan, D. (2003), 'Recent Experimental Results with the Four-Quadrant Phase-Mask Coronograph', *Proceedings 'Towards Other Earths': DARWIN/TPF and the Search for Extrasolar Terrestrial Planets,* Vol. SP-539, Heidelberg, Germany, ESA, pp. 361-366.

Riaud, P., Boccaletti, A., Gillet, S., Schneider, J. and Labeyrie, A.e.al. (2002), 'Coronagraphic Search for Exo-planets with a Hypertelescope', *Astronomy and Astrophysics,* Vol. 396, pp. 345-352.

Richards, A., Schouwenaars, T., How, J.P. and Feron, E. (2002), 'Spacecraftr Trajectory Planning with Avoidance Constraints Using Mixed-Integer Linear Programming', *Journal of Guidance, Control, and Dynamics,* Vol. 25, No. 4, pp. 755-764.

Richardson D.L. and Cary N.D. (1975), 'A Uniformly Valid Solution for Motion about the Interior Libration Point of the Perturbed Elliptic-Restricted Problem', *AIAA/AAS Astrodynamics Specialist Conference,* Nassau, Bahamas, American Astonautical Society, AAS 75-021.

Richardson, D.L. (1980a), 'Analytical Construction of Periodic Orbits about the Collinear Points', *Celestial Mechanics ,* Vol. 22 , pp. 241-253.

Richardson, D.L. (1980b), 'A Note on a Lagrangian Formulation for Motion about the Collinear Points', *Celestial Mechanics ,* Vol. 22, pp. 231-236.

Richardson, D.L. (1980c), 'Halo Orbit Formulation for the ISEE-3 Mission', *Journal of Guidance and Control,* Vol.3 No.6, pp. 543-548.

Richardson, D.L. and Mitchell, J.W. (2002), 'A Third-Order Analytical Solution for Relative Motion with a Circular Reference Orbit', *Advances in the Astronautical Sciences,* Vol. 112, No. 1, pp. 605-613.

Richmond, M. (2004), *The Chemical Composition of Stars and the Universe,* available at: http://spiff.rit.edu/classes/phys240/lectures/elements/elements.html (accessed 2004).

Ritz, S. (2004), *GLAST LAT Performance,* available at: http://www-glast.slac.stanford.edu/software/IS/glast_lat_performance.htm (accessed 2004).

Roberts, C.E. (2001), 'Long Duration Lissajous Orbit Control for the ACE Sun-Earth L1 Libration Point Mission', AAS 01-204.

Roberts, P.C.E., Bowling, T.S., and Hobbs, S.E. (2002), 'MUSTANG: A Technology Demonstrator for Formation Flying and Distributed Systems Technologies in Space', *5th Cranfield Conference on the Dynamics and Control of Systems and Structures in Space,* Cambridge, UK, Cranfield University Press, Cranfield, UK.

Roberts, J.A. (2006), Mission Design for Extrasolar Planet Observation, College of Aeronautics Report, Cranfield University.

Robertson, A., Inalhan, G., and How, J.P. (1999a), 'Spacecraft Formation Flying Control Design for the Orion Mission', AIAA 99-4266.

Robertson, A., Inalhan, G., and How, P. (1999b), 'Formation Control Strategies for a Separated Spacecraft Interferometer', *Proceedings of the American Control Conference,* San Diego, CA,

pp. 4142-4147.

Rohrbaugh, D. and Schiff, C. (2002), 'Stationkeeping Approach for the Microwave Anisotropy Probe (MAP)', *AIAA/AAS Astrodynamics Specialist Conference and Exhibit,* Vol. AIAA 2002-4429, Monterey, CA.

Roithmayr, C.M. and Kay-Burnell, L. (2004), 'Keeping a Spacecraft on the Sun-Earth Line', *AAS/AIAA Space Flight Mechanics Conference,* Maui, Hawaii, USA, AAS 04-246.

Rothschild, L.J. and Mancinelli, R.L. (2001), 'Life in Extreme Environments', *Nature,* Vol. 409, pp. 1092-1101.

Rottgering, H.J.A., D'Arcio, L., Eiroa, C., Labbe, I., and Rudnick, G. (2003), 'Astrophysical Imaging with the Darwin IR Interferometer', *Proceedings 'Towards Other Earths': DARWIN/TPF and the Search for Extrasolar Terrestrial Planets,* Vol. SP-539, Heidelberg, Germany, ESA, pp. 299-308.

Rouan, D. (2003), 'From Fractals to Exoplanets Detection: How To Reach Any Nulling Depth With An Interferometer', *Proceedings 'Towards Other Earths': DARWIN/TPF and the Search for Extrasolar Terrestrial Planets,* Vol. SP-539, Heidelberg, Germany, ESA, pp. 565-569.

Rouan, D., Baglin, A., Barge, P., Borde, P., Deleuil, M., Leger, A., Schneider, J., and Vuillemin, A. (2000), 'Detecting Earth-Uranus Class Planets with the Space Mission COROT', *Proceedings of the Conference 'Darwin and Astronomy - The Infrared Space Interferometer',* Vol. SP-451, Stockholm, Sweden, ESA, pp. 221-226.

Roy, A.E. (1988), *Orbital Motion* (3rd edition), Adam Hilger, Bristol.

Roy, A.E. and Clarke, D. (1991), *Astronomy Principles and Practice* (Third edition), Adam Hilger, Bristol, UK.

Sabol, C., Burns, R. and McLaughlin, C.A. (2001), 'Satellite Formation Flying Design and Evolution', *Journal of Spacecraft and Rockets,* Vol. 38, No. 2, pp. 270-278.

Sabol, C., Burns, R., and McLaughlin, C.A. (1999), 'Satellite Formation Flying Design and Evolution', *AAS/AIAA Spaceflight Mechanics Meeting,* Breckenridge, Colorado, pp. 265-284, AAS 99-121.

Saenz-Otero, A. (2000), The SPHERES Satellite Formation Flight Testbed. Massachusetts Institute of Technology , MIT.

Saenz-Otero, A. and Miller, D. (2003), 'The SPHERES ISS Laboratory for Rendezvous and Formation Flight', *Proceedings of the 5th ESA International Conference on Spacecraft Guidance, Navigation and Control Systems,* Vol. SP-516, Frascati, Italy, ESA, pp. 217-224.

Saenz-Otero, A., Miller, D.W., and Halstead, M. (2002), 'SPHERES: a Laboratory for Formation Flight and Docking Research', *Proceedings of the 5th Cranfield Conference on Dynamics and Control of Systems and Structures in Space,* Cambridge, UK, Cranfield University Press, Cranfield University,

Samson (2004), *Evolution of the Atmosphere: Composition, Structure and Energy,* available at: http://www.globalchange.umich.edu/globalchange1/current/lectures/samson/evolution_atm/#structure (accessed 2004).

Satellite Tool Kit (2005), *Analytical Graphics, Inc.,* available at: www.stk.com (accessed 2005).

Schaub, H. and Alfriend, K.T. (1999), 'J2 Invariant Relative Orbits for Spacecraft Formations', *Flight Mechanics Symposium,* NASA Goddard Space Flight Centre, Greenbelt, Maryland, NASA.,

Schaub, H. and Alfriend, K.T. (2000a), 'Hybrid Cartesian and Orbit Element Feedback Law for Formation Flying Spacecraft', AIAA 2000-4131.

Schaub, H. and Alfriend, K.T. (2000b), 'Impulsive Spacecraft Formation Flying Control to Establish Specific Mean Orbit Elements', *Proceedings of the AAS/AIAA Spaceflight Mechanics Meeting,* Clearwater, Florida , AAS 00-113.

Schaub, H. and Alfriend, K.T. (2001), 'Impulsive Feedback Control to Establish Specific Mean Orbit Elements of Spacecraft Formations', *Journal of Guidance, Control, and Dynamics,* Vol. 24, No. 4, pp. 739-745.

Schaub, H. and Junkins, J.L. (2003), *Analytical Mechanics of Space Systems*, AIAA, Reston, Virginia, USA.

Schaub, H., Vadali, S.R., Junkins, J.L., and Alfriend, K.T. (1999), 'Spacecraft Formation Flying Control Using Mean Orbital Elements ', *Proceedings of the Advances in the Astronautical Sciences Astrodynamics Conference,* AAS 99-310.

Scheeres, D.J. and Vinh, N.X. (2000), 'Dynamics and Control of Relative Motion in an Unstable Orbit', *AIAA/AAS Astrodynamics Specialist Conference,* Denver, Colorado, USA, AIAA 2000-4135.

Scheeres, D.J., Park, C., and Guibout, V.M. (2003), 'Solving Optimal Control Problems with Generating Functions', *AAS/AIAA Astrodynamics Conference,* Vol. 116 pt.2, Big Sky, MT, pp. 1185-1205, AAS 03-575.

Schneider, J. (2002), 'Biosignatures and Exoplanet Characterization: Visible Versus Thermal Infrared Imaging', *Proceedings of the Second European Workshop on Exo/Astrobiology,* Vol. SP-518, Graz, Austria, ESA, pp. 409-412.

Schneider, J. (2003), 'Biosignatures and Extrasolar Planet Characterization: Visible Versus Infrared', *Proceedings 'Towards Other Earths': DARWIN/TPF and the Search for Extrasolar Terrestrial Planets,* Vol. SP-539, Heidelberg, Germany, ESA, pp. 205-213.

Schneider, J. (2004), 'Multi-Planet System Detection With Eddington', *Proceedings of the 2nd Eddington Workshop 'Stellar Structure and Habitable Planet Finding',* Vol. SP-538, Palermo, Italy, ESA, pp. 407-410.

Schneider, J. (2005), *Extra-Solar Planets Catalog,* available at: http://www.obspm.fr/encycl/catalog.html (accessed 2005).

Scholler, M. and Glindemann, A. (2003), 'The VLT Interferometer', *Proceedings 'Towards Other Earths': DARWIN/TPF and the Search for Extrasolar Terrestrial Planets,* Vol. SP-539, Heidelberg, Germany, ESA, pp. 109-120.

Schulze-Makuch, D., Irwin, L.N., and Irwin, T. (2002), 'Astrobiological Relevance and feasibility of a Sample Collection Mission to the Atmosphere of Venus', *Proceedings of the Second European Workshop on Exo/Astrobiology,* Vol. SP-518, Graz, Austria, ESA, pp. 247-250.

Schwartz, J.L. and Hall, C.D. (2004), 'Comparison of System Identification Techniques for A Spherical Air-Bearing Spacecraft Simulator', *AAS/AIAA Astrodynamics Conference,* Vol. 116 pt. 2, Big Sky, Montana, pp. 1725-1741, AAS 03-611.

Schweighart, S.A. and Sedwick, R.J. (2001a), 'Development and Analysis of a High Fidelity Linearized J2 Model for Satellite Formation Flying', *AIAA Space 2001: Conference and Exposition,* Albuquerque, New Mexico, AIAA 2001-4744.,

Schweighart, S.A. and Sedwick, R.J. (2001b), 'A Perturbative Analysis of Geopotential Disturbances for Satellite Cluster Formation Flying', *IEEE Aerospace Conference,* Vol. 2, Big Sky, Montana, IEEE, pp. 1001-1019.

Schweighart, S.A. and Sedwick, R.J. (2002), 'High-Fidelity Linearized J_2 Model for Satellite Formation Flight', *Journal of Guidance, Control and Dynamics,* Vol. 25, No. 6, pp. 1073-1080.

Schweighart, S.A. and Sedwick, R.J. (2004), 'Dynamics of an Electromagnetically Flown Formation of Spacecraft within the Earth's Magnetic Field', *Proceedings of the SPIE: UV/Optical/IR Space Telescopes: Innovative Technologies and Concepts,* Vol. 5166, pp. 86-97.

Sears, F.W., Zemansky, M.W., and Young Y.D. (1987), *University Physics* (Seventh edition), Addison-Wesley Publishing Company, Massachusetts.

Sedwick, R.J., Kong, W.M.C., and Miller, D.W. (1998), 'Exploiting Orbital Dynamics and Micropropulsion for Aperture Synthesis Using Distributed Satellite Systems: Applications to Techsat21', AIAA 98-5289.

Sedwick, R.J., Miller, D., and Kong, E. (1999), 'Mitigation of Differential Perturbations in Clusters of Formation Flying Satellites', *AIAA/AAS Space Flight Mechanics Conference,* Vol. 102 - 1, Breckenridge, Colorado, pp. 323-342, AAS 99-124.

Segerman, A.M. and Zedd, M.F. (2003), 'Preliminary Planar Formation-Flight Dynamics Near Sun-Earth L2 Point', *AAS/AIAA Space Flight Mechanics Meeting,* Ponce, Puerto Rico.

Selsis, F. (2000), 'Darwin and the Atmospheres of Terrestrial Planets', *Proceedings of the Conference 'Darwin and Astronomy - The Infrared Space Interferometer',* Vol. SP-451, Stockholm, Sweden, ESA, pp. 133-140.

Selsis, F. (2002), 'Exo-/Astrobiology with a Darwin/TPF Mission', *Proceedings of the Second European Workshop on Exo/Astrobiology,* Vol. SP-518, Graz, Austria, ESA, pp. 365-370.

Sengupta, P. and Vadali, S.R. (2004), 'A Lyapunov-Based Controller for Satellite Formation Reconfiguration in the Presence of J2 Perturbations', *14th AAS/AIAA Space Flight Mechanics Conference,* Maui, Hawaii, AAS 04-253.

Serabyn, E. (2003), 'An Overview of the Keck Interferometer Nuller', *Proceedings 'Towards Other Earths': DARWIN/TPF and the Search for Extrasolar Terrestrial Planets,* Vol. SP-539, Heidelberg, Germany, ESA, pp. 91-98.

Serabyn, E. (2003), 'Experimental Confirmation of Deep Nulling', *Proceedings 'Towards Other Earths': DARWIN/TPF and the Search for Extrasolar Terrestrial Planets,* Vol. SP-539, Heidelberg, Germany, ESA, pp. 101-105.

Shaw, G. B., Yashko, G., Schwarz, R., Wickert, D., and Hastings, D. (1999), Analysis Tools and Architecture Issues for Distributed Satellite Systems. In: Helvajian, H. ed. Microengineering Aerospace Systems. El Segundo, California, The Aerospace Press.

Shen, H., Kumar, R., and Seywald, H. (2004), 'Minimum-Fuel Periodic Orbits in the Vicinity of a Fixed Point on the Sun-Earth Line: The Planar Case', *14th AAS/AIAA Space Flight Mechanics Conference,* Maui, Hawaii, USA, AAS 04-247.

Shostak, S. (2004) Listening for a Whisper. *Astronomy Magazine* **32** (9):34-39. Wisconsin, USA: Kalmbach Publishing.

Sidi, M.J. (1997), *Spacecraft Dynamics and Control A Practical Engineering Approach*, Cambridge University Press, Cambridge.

Singh, G. and Hadaegh, F.Y. (2001), 'Collision Avoidance Guidance for Formation-Flying Applications', *AIAA Guidance, Navigation and Control Conference,* Montreal, Canada, AIAA 01-4088.

Skogestad, S. and Postlethwaite, I. (2001), *Multivariable Feedback Control, Analysis and Design*, John Wiley & Sons, Chichester, UK.

Smith, D.R., Ambrosi, R.M., Holland, A.D., Hutchinson, I.B., and Wells, A. (2004), 'The Prompt Particle Background and Micrometeoroid Environment at L2 and Its Implications for Eddington', *Proceedings of the 2nd Eddington Workshop 'Stellar Structure and Habitable Planet Finding',* Vol. SP-538, Palermo, Italy, ESA , pp. 417-420.

Smith, R.S. and Hadaegh, F.Y. (2002), 'Control Topologies for Deep Space Formation Flying Spacecraft', *American Control Conference,* Anchorage, AK, USA,

Smith, R.S. and Hadaegh, F.Y. (2002b), 'Distributed Control Topologies for Deep Space Formation Flying Spacecraft', *Proceedings of the International Symposium: Formation Flying Missions and Technologies,* Toulouse, France, CNES.

Snow, P.T. (1991), *The Dynamic Universe* (4 edition), West Publishing Company, New York, USA.

Sohus, A.M. (2001), *Space Sciences: Astronomical Search for Origins and Planetary Systems,* available at: http://www2.jpl.nasa.gov/sespd/space/astro.html (accessed 2005).

Sol Company (2004), *Stars and Habitable Planets,* available at: http://www.solstation.com/habitable.htm (accessed 2004).

Space Studies Board (2000), *Evaluating the Biological Potential in Samples Returned from Planetary Satellites and Small Solar Syste Bodies,* available at: http://www7.nationalacademies.org/ssb/sssbch1.html (accessed 2004).

Space.com Website (2005), *Planetary Transit,* available at: http://www.space.com/images/040824_plane_transit_03.jpg (accessed 2005).

Sparks, A. (2000a), 'Linear Control of Spacecraft Formation Flying', *AIAA Guidance, Navigation, and Control Conference,* Denver Colorado, AIAA 2000-4438.

Sparks, A. (2000b), 'Satellite Formationkeeping Control in the Presence of Gravity Perturbations', *Proceedings of the American Control Conference,* Chicago, Illinois, pp. 844-848.

Spitzer Website (2004), *About Spitzer,* available at: http://www.spitzer.caltech.edu/about/index.shtml (accessed 2004).

Stadter, P.A., Heins, R.J., Chacos, A.A., Moore, G.T., and Kusterer, T.L. (2001), 'Enabling Distributed Spacecraft Systems with the Crosslink Transceiver', *AIAA Space 2001,* Albuquerque, New Mexico, AIAA 2001-4670.

Stam, D.M. (2003), 'Polarization Spectra of Extrasolar Planets', *Proceedings 'Towards Other Earths': DARWIN/TPF and the Search for Extrasolar Terrestrial Planets,* Vol. SP-539, Heidelberg, Germany, ESA, pp. 615-619.

Stansbery, D.T. and Cloutier, J.R. (2000), 'Nonlinear Control of Satellite Formation Flight', *AIAA Guidance, Navigation, and Control Conference and Exhibit,* Denver, Colorado, AIAA 2000-4436.

Starin, S.R., Yedavalli, R.K., and Sparks, A. (2001a), 'Design of a LQR Controller of Reduced Inputs for Multiple Spacecraft Formation Flying', *Proceedings of the American Control Conference,* Arlington, Virginia, pp. 1327-1332.

Starin, S.R., Yedavalli, R.K., and Sparks, A. (2001b), 'Spacecraft Formation Flying Maneuvers Using Linear-Quadratic Regulation with No Radial Axis Inputs', AIAA 2001-4029.

Stenmark, L. and Eriksson, A.B. (2002), 'Cold Gas Micro Thrusters', *Final Draft of AIAA Paper in Unpublished Form.*

Stevens, H.D., Rodden, J., Morton, P., and Fehrenbach, M. (2000), 'Validating a Formation Flying Control System Design: The Grace Project Experience', *AAS Guidance and Control Conference,* Breckenridge, Colorado, AAS 00-014.

Strizzi, J.D., Kutrieb, J.M., Damphouse, P.E., and Carrico, J.P. (2001), 'Sun-Mars Libration Points and Mars Mission Simulations', AAS 01-159.

Swank, A.J., McLaughlin, C.A., Sabol, C., and Burns, R.D. (2002), 'Long-Duration Analysis of the J2-Model Equations of Relative Motion for Satellite Clusters', *Proceedings of the AAS/AIAA Space Flight Mechanics Meeting,* Vol. 112, San Antonio, Texas, pp. 1005-1020, AAS 02-185.

Szebehely, V. (1967), *Theory of Orbits*, Academic Press Inc., New York and London.

Tan, Z. and Bainum, P.M. (2001), 'An Improved Strategy for Maintaining Constant Distance Between Satellites in an Elliptically Orbiting Constellation', *Proceedings of the AAS/AIAA Space Flight Mechanics Meeting,* Santa Barbara, California, pp. 1649-1663, AAS 01-219.

Tan, Z., Bainum, P.M., and Strong, A. (1999), 'A Strategy for Maintaining Distance Between Satellites in an Orbiting Constellation', *Proceedings of the AAS/AIAA Space Flight Mechanics Meeting,* Vol. 102 Pt.1, Breckenridge, Colorado, pp. 343-354, AAS 99-125.

Tan, Z., Bainum, P.M., and Strong, A. (2000), 'The Implementation of Maintaining Constant Distance Between Satellites in Elliptic Orbit', *Proceedings of the AAS/AIAA Space Flight Mechanics Conference,* Clearwater, Florida, pp. 667-683, AAS 00-141.

Tarter, J. (2003), 'SETI: Another Way to Find Habitable Worlds', *Proceedings 'Towards Other Earths': DARWIN/TPF and the Search for Extrasolar Terrestrial Planets,* Vol. SP-539, Heidelberg, Germany, ESA, pp. 31-38.

Tene, N., Richon, K., Folta, D., and Tene, K. (1998), 'Using Solar Radiation Pressure to Control L2 Orbits', *AAS International Flight Mechanics Symposium,* GSFC, AAS 98-348.

Thompson, A.R., Moran, J.M., and Swenson, G.W. (2001), *Interferometry and Synthesis in Radio Astronomy* (2nd edition), John Wiley & Sons Inc., New York.

Tierno, J.E. (2000), 'Control of LEO Satellite Clusters', *Proceedings of the 39th IEEE Conference on Decision and Control,* Sydney, Australia, IEEE, pp. 334-339.

Tillerson, M. and How, J.P. (2001), 'Formation Flying Control in Eccentric Orbits', AIAA 2001-4092.

Tollefson, M.V. (2001), 'Relative Orbit Design Tool', *IEEE Aerospace Conference,* Big Sky, MT, 10-17 Mar. 2001. pp. 3471-3478. 2001.

Toporski, J. and Steele, A. (2002), 'The Relevance of Bacterial Biomarkers in Astrobiological Research', *Proceedings of the Second European Workshop on Exo/Astrobiology,* Vol. SP-518, Graz, Austria, ESA, pp. 239-242.

Traub, W.A. (2005), *Beam Combination and Fringe Measurement*, Unpublished Communication.

Traub, W.A. (2003), 'Extrasolar Planet Characteristics in the Visible Wavelength Range ', *Proceedings 'Towards Other Earths': DARWIN/TPF and the Search for Extrasolar Terrestrial Planets,* Vol. SP-539, Heidelberg, Germany, ESA, pp. 231-239.

Turnbull, M.C. and Tarter, J.C. (2002), *Target Selection for SETI: A Catalog of Nearby Habitable Stellar Systems,* available at: http://www.nstars.arc.nasa.gov/TurnbullTarter.pdf (accessed 2004).

Turner, A.E. (2001), 'Molniya/Tundra Orbit Constellation Considerations for Commercial Applications', AAS 01-215.

Twiggs, R. and How, J. (1998), 'Orion: A Microsatellite Testbed for Formation Flying', *12th AIAA/USU Conference on Small Satellites,* Logan, Utah.

Udrea, B. (2003), *Low Earth Orbit Formation Design Tool*, Unpublished Communication and Software.

Udry, S. and Mayor, M. (2001), 'Extra-Solar Planets Around Solar-Type Stars', *Proceedings of the First European Workshop on Exo/Astro-Biology,* Vol. SP-496, Frascati, Italy, pp. 65-72.

Ulamec, S. and Biele, J. (2002), 'Rosetta Landa - Overview', *Proceedings of the Second european Workshop on Exo/Astrobiology,* Vol. SP-518, Graz, Austria, ESA, pp. 115-118.

Ulybyshev, Y. (1998), 'Long-Term Formation Keeping of Satellite Constellation Using Linear-Quadratic Controller', *Journal of Guidance, Control, and Dynamics,* Vol. 21, No. 1, pp. 109-115.

Underwood, C., Richardson, G., and Savignol, J. (2001), 'SNAP-1: A Low Cost Modular COTS-Based Nano-Satellite - Design, Construction, Launch and Early Operations Phase', *Proceedings of the 15th AIAA/USU Conference on Small Satellites,* Utah, AIAA, SSC01-VI-7.

Vadali, S.R. (2002), 'An Analytical Solution for Relative Motion of Satellites', *5th Cranfield Conference on the Dynamics and Control of Systems and Structures in Space,* Cambridge, UK, Cranfield University Press, Cranfield, UK,

Vadali, S.R. and Vaddi, S. (2000), 'Orbit Establishment for Formation Flying of Satellites', *Proceedings of the AAS/AIAA Space Flight Mechanics Conference,* Clearwater, Florida, AAS 00-111.

Vadali, S.R., Alfriend, K.T., and Vaddi, S. (2000), 'Hills Equations, Mean Orbital Elements and Formation Flying of Satellites', *Richard H. Battin Astrodynamics Symposium,* College Station, Texas, pp. 187-203, AAS 00-258.

Vadali, S.R., Bae, H.W., and Alfriend, K.T. (2004), 'Design and Control of Libration Point Satellite Formations', *14th AAS/AIAA Space Flight Mechanics Conference,* Maui, Hawaii, USA, AAS 04-161.

Vadali, S.R., Schaub, H., and Alfriend, K.T. (1999), 'Initial Conditions and Fuel-Optimal Control for Formation Flying of Satellites', *Proceedings of the AIAA Guidance, Navigation, and Control Conference,* Portland, Oregon, AIAA 99-4265.

Vadali, S.R., Vaddi, S.S., and Alfriend, K.T. (2001), 'A New Concept for Controlling Formation Flying Satellite Constellations', AAS 01-218.

Vaddi, S.S., Alfriend, K.T., and Vadali, S.R. (2003), 'Sub-Optimal Formation Establishment and Reconfiguration Using Impulsive Control', *Proceedings of the AAS/AIAA Astrodynamics Conference,* Vol. 116 Pt. 2, Big Sky, Montana, pp. 1419-1435, AAS 03-590.

Vaddi, S.S., Vadali, S.R. and Alfriend, K.T. (2003), 'Formation Flying: Accommodating Nonlinearity and Eccentricity Perturbations', *Journal of Guidance, Control, and Dynamics,* Vol. 26, No. 2, pp. 214-223.

Vaddi, S.S., Vadali, S.R., and Alfriend, K.T. (2002), 'Formation Flying: Accommodating Nonlinearity and Eccentricity Perturbations', *Proceedings of the AAS/AIAA Space Flight Mechanics Meeting,* San Antonio, Texas, pp. 985-1004, AAS 02-184.

Vallado, D.A. (2001), *Fundamentals of Astrodynamics and Applications* (2nd edition), Microcosm Press, El Segundo, California.

van der Avoort, C., D'Arcio, L., and den Herder, J. (2003), 'Numerical Simulations on Dynamical Aspects of the Darwin Constellation While Imaging', *Proceedings 'Towards Other Earths': DARWIN/TPF and the Search for Extrasolar Terrestrial Planets,* Vol. SP-539, Heidelberg, Germany, ESA, pp. 333-338.

Vassar, R.H. and Sherwood, R.B. (1985), 'Formationkeeping for a Pair of Satellites in a Circular Orbit', *Journal of Guidance, Control, and Dynamics,* Vol. 8, No. 2, pp. 235-242.

Velusamy, T. and Beichman, C.A. (2001), 'Nulling Interferometry for Extra-solar Planet Detection: Sensitivity and Image Reconstruction', Vol. 4, IEEE, pp. 2013-2025.

Vincent, M.A. and Salcedo, C. (2004), 'The Insertion of Cloudsat and CALIPSO into the A-Train Constellation', *AAS/AIAA Astrodynamics Conference,* Vol. 116 pt. 2, Big Sky, Montana, pp. 1401-1418, AAS 03-589.

Vishnivetskaya, T.A., Vorobyova, E.A., and Gilichinsky, D.A. (2002), 'Viable Green Algae and Cyanobacteria within Terrestrial Permafrost', *Proceedings of the Second European Workshop on Exo/Astrobiology,* Vol. SP-518, Graz, Austria, ESA, pp. 295-298.

VLA Website (2002), *Radio Astronomy in New Mexico: The VLA and the VLBA,* available at: http://www.aoc.nrao.edu/intro/NM_astro.html (accessed 2002).

Volonte, S. and Fridlund, C.V.M. (2003), 'The Search For Exoplanets in the ESA Science Programme', *Proceedings 'Towards Other Earths: DARWIN/TPF and the Search for Extrasolar Terrestrial Planets',* Vol. SP-539, Heidelberg, Germany, ESA, pp. 277-281.

Volwerk, M., Kivelson, M., Khurana, K., and Zimmer, C. (2002), 'Discovery of Water on the Galilean Satellites by the Galileo Magnetometer', *Proceedings of the Second European Workshop on Exo/Astrobiology,* Vol. SP-518, Graz, Austria, ESA, pp. 565-566.

von Bloh, W., Bounama, C., and Franck, S. (2002), 'The Number of Habitable Planets in the Milky Way Over Cosmological Time Scales', *Proceedings of the Second European Workshop on Exo/Astrobiology,* Vol. SP-518, Graz, Austria, ESA, pp. 503-504.

von Bloh, W., Cuntz, M., Bounama, C., and Franck, S. (2002), 'The Habitable Zone of Earth-Like Planets Around 47UMA', *Proceedings of the Second European Workshop on Exo/Astrobiology,* Vol. SP-518, Graz, Austria, ESA, pp. 413-415.

VSOP Website (1997), *VSOP Basic Information,* available at:
http://www.vsop.isas.ac.jp/general/Basics.html (accessed 2004).
Notes: http://www.vsop.isas.ac.jp for link to VSOP-2

Walker, H. (1995), *The Infra-Red Astronomical Satellite (IRAS),* available at:
http://ast.star.rl.ac.uk/isouk/iras/iras_overview.html#overview (accessed 2002).

Wang, P.K.C. and Hadaegh, F.Y. (1993), 'Modal Noninteracting Controls for Deformable Mirrors', *Second IEEE Conference on Control Applications,* Vancouver, Canada, IEEE, pp. 121-128.

Wang, P.K.C. and Hadaegh, F.Y. (1996), 'Computation of Static Shapes and Voltages for Micromachined deformable Mirrors with Nonlinear Electrostatic Actuators', *Journal of Microelectromechanical Systems,* Vol. 5, No. 3, pp. 205-219.

Wang, P.K.C. and Hadaegh, F.Y. (1999), 'Minimum-Fuel Formation Reconfiguration of Multiple Free-Flying Spacecraft', *Journal of the Astronautical Sciences,* Vol. 47, No. 1 and 2.

Wang, P.K.C. and Hadaegh, F.Y. (2000), 'Self-Organizing Control of Multiple Free-Flying Miniature Spacecraft in Formation', *AIAA Guidance, Navigation, and Control Conference and Exhibit,* Denver, Colorado, pp.1374-1383, AIAA 2000-4437.

Wang, P.K.C. and Hadaegh, F.Y. (2001), 'Control of Large Micro-Spacecraft Formations Based on Quasi-Distributed-Parameter Models ', AIAA 2001-4384.

Wang, Z. and Williams, T. (2002), 'A Study of the Steering Law of Satellite Formation Flight Using Solar Radiation Pressure', *Proceedings of the AAS/AIAA Space Flight Mechanics Meeting,* Vol. 112, San Antonio, Texas, pp. 1043-1062, AAS 02-187.

Wanner, N. (1998), *Sunspots,* available at: http://www.exploratorium.edu/sunspots/index.html (accessed 2004).

Watanabe, S. (2004), *Solar System,* available at: http://www.jpl.nasa.gov/solar_system/sun/sun_index.html (accessed 2004).

Weisstein, E.W. (2005), *Eric Weisstein's World of Scientific Biography,* available at: http://scienceworld.wolfram.com/biography/ (accessed 2005).

Westall, F., Brack, A., Barbier, B., Bertrand, M., and Chabin, A. (2002), 'Early Earth and Early Life: An Extreme Environment and Extremophiles - Application to the Search for Life on Mars', *Proceedings of the Second European Workshop on Exo/Astrobiology,* Vol. SP-518, Graz, Austria, ESA, pp. 131-136.

Westall, F., Nijman, W., Brack, A., Steele, A., and Toporski, J. (2001), 'The Oldest Fossil Life on Earth, its Geological Context and Life on Mars', *Proceedings of the First European Workshop on Exo/Astro-Biology,* Vol. SP-496, Frascati, Italy, pp. 81-90.

Whidborne, J.F. (2005), Multivariable Control Systems for Aerospace Applications, Lecture Notes, Cranfield, July 2005.

Whitehouse, D. (2003), *Hubble Sees Evaporating World,* available at: http://news.bbc.co.uk/1/hi/sci/tech/2845715.stm (accessed 2004).

Whitehouse, D. (2004a), *Hubble Probes Planet Around Star,* available at: http://news.bbc.co.uk/1/hi/sci/tech/3432629.stm (accessed 2004).

Whitehouse, D. (2004b), *Lens Effect Reveals Distant World,* available at: http://news.bbc.co.uk/1/hi/sci/tech/3631889.stm (accessed 2004).

Whitehouse, D. (2004c), *Small Planets Seen By Astronomers,* available at: http://news.bbc.co.uk/1/hi/sci/tech/3615940.stm (accessed 2004).

Whitehouse, D. (2004d), *Telescope Snaps Distant Planet,* available at:

http://news.bbc.co.uk/1/hi/sci/tech/3644410.stm (accessed 2004).

Wie, B. (1998), *Space Vehicle Dynamics and Control*, AIAA, Virginia, USA.

Wiesel, W.E. (2002), ' Relative Satellite Motion About An Oblate Plane', *Journal of Guidance, Control, and Dynamics,* Vol. 25, No. 4, pp. 776-785.

Wiesel, W.E. (2003), ' Optimal Impulsive Control of Relative Satellite Motion', *Journal of Guidance, Control, and Dynamics,* Vol. 26, No. 1, pp. 74-78.

Wiesel, W.E. (2001), 'The Dynamics of Relative Satellite Motion', *AAS/AIAA Space Flight Mechanics Meeting,* Santa Barbara, California, pp. 869-879, AAS 01-163.

Wiesel, W.E. (2003), 'Suppose A(t) Isn't Constant?', *AAS/AIAA Space Flight Mechanics Meeting,* Ponce, Puerto Rico, AAS 03-114.

Williams, D.R. (2004), *Earth Fact Sheet,* available at:
http://nssdc.gsfc.nasa.gov/planetary/factsheet/earthfact.html (accessed 2004).

Williams, D.R. (2004a), *NASA Jupiter Fact Sheet,* available at:
http://nssdc.gsfc.nasa.gov/planetary/factsheet/jupiterfact.html (accessed 2005).

Williams, D.R. (2004b), *Sun Fact Sheet,* available at:
http://nssdc.gsfc.nasa.gov/planetary/factsheet/sunfact.html (accessed 2004).

Williams, T. and Wang, Z. (2000a), 'Potential Non-Propulsive Stationkeeping Techniques for Picosatellite Formation Flight', *AIAA/AAS Astrodynamics Specialist Conference,* Denver, Colorado, AIAA 2000-4134.

Williams, T. and Wang, Z. (2000b), 'Potential Uses of Solar Radiation Pressure in Satellite Formation Flight', *AAS/AIAA Space Flight Mechanics Meeting,* Vol. 105, Clearwater, Florida, pp. 1599-1611, AAS 00-204.

Williams, T. and Wang, Z. (2001), 'Solar Radiation Pressure and Satellite Formation Flight: Analytical Results', *American Astronautical Society,* AAS 01-164.

Wilson, T.L. (2001), ' The Search for Extraterrestrial Intelligence', *Nature,* Vol. 409, pp. 1110-1114.

Woolf, N. (2003), 'Interferometers and Coronagraphs: The Potential and Realities of Looking for Other Earths', *Proceedings 'Towards Other Earths': DARWIN/TPF and the Search for Extrasolar Terrestrial Planets,* Vol. SP-539, Heidelberg, Germany, ESA, pp. 263-269.

World Heritage Web Site (2004), *Stromatolites,* available at:
http://www.sharkbay.org/terrestrial_environment/page_15.htm (accessed 2004).

Yakimov, V. (2004), *RadioAstron Mission,* available at:
http://www.asc.rssi.ru/radioastron/description/intro_eng.htm (accessed 2004).

Yamanaka, K. (2000), 'Simultaneous Translation and Rotation Control Law for Formation Flying Satellites', *AIAA Guidance, Navigation, and Control Conference and Exhibit,* Denver, Colorado, AIAA 2000-4440.

Yamanaka, K. and Ankersen, F. (2002), 'New State Transition Matrix for Relative Motion on an Arbitrary Elliptical Orbit', *Journal of Guidance, Control, and Dynamics,* Vol. 25, No. 1, pp. 60-66.

Yan, Q., Kapila, V., and Sparks, A. (2000), 'Pulse-Based Periodic Control for Spacecraft Formation

Flying', *Proceedings of the American Control Conference,* Chicago, Illinois, pp. 374-378.

Yan, Q., Yang, G., Kapila, V., and de Queiroz, M.S. (2000), 'Nonlinear Dynamics and Output Feedback Control of Multiple Spacecraft In Elliptical Orbits', *Proceedings of the American Control Conference,* Chicago, Illinois, pp. 839-843.

Yedavalli, R.K. and Sparks, A. (2000), 'Satellite Formation Flying Control Design Based on Hybrid Control System Stability Analysis', *Proceedings of the American Control Conference,* Chicago, Illinois, pp. 2210-2214.

Yedavalli, R.K. and Sparks, A. (2001), 'Satellite Formation Keeping Control Design Based on Ultimate Bounded Analysis of Switched Systems', AIAA 2001-4027.

Yeh, H. and Sparks, A. (2000), 'Geometry and Control of Satellite Formations', *Proceedings of the American Control Conference,* Chicago, Illinois, pp. 384-388.

Yeh, H., Nelson, E., and Sparks, A. (2000), 'Nonlinear Tracking Control for Satellite Formations', *Proceedings of the 39th IEEE Conference on Decision and Control,* Sydney, Australia, IEEE, pp. 328-333.

Yim, J.R., Crassidis, J.L., and Junkins, J.L. (2004), 'Autonomous Orbit Navigation of Two Spacecraft System Using Relative Line of Sight Vector Measurements', *14th AAS/AIAA Space Flight Mechanics Conference,* Maui, Hawaii, AAS 04-257.

Young, H.D. (1992), *University Physics* (8th edition), Addison-Wesley, Massachusetts, USA.

Zhang, W. and Newman, P. (2002), *Generation-X: A Future, Ultra-Large-Aperture X-Ray Telescope,* available at: http://generation-x.gsfc.nasa.gov/docs/mission/concepts.html (accessed 2005).

Appendix A - Satellite Formations and Formation Flying Missions

This section includes tabulated mission summaries and supporting references for the formation flying missions survey. The information contains acronyms, either defined in the table itself, or in section A.1, and cross-references to a supporting references section (A.3).

- Table A-1: Current Formation Flying Missions
- Table A-2: Examples of Current and Future Satellite Formations (Note: these satellites are not actually formation flying according to the definition in section 2.1.1)
- Table A-3: Future Formation Flying Missions
- Table A-4: Recent University Formation Flying Mission Studies

A.1 Acronyms

AFOSR	Air Force Office of Scientific Research (US)
AFRL	Air Force Research Laboratory (US)
CALIPSO	Cloud-Aerosol Lidar and Infrared Pathfinder Satellite Observations
DARPA	Defence Advanced Research Projects Agency (US)
DoD	Department of Defence (US)
EOS	Earth Observing System
ESA	European Space Agency
ESE	Earth Science Enterprise
ESSP	Earth System Science Pathfinder (NASA Initiative)
EUMETSAT	European Organisation for the Exploitation of Meteorological Satellites
GSFC	Goddard Space Flight Centre
JPL	Jet Propulsion Laboratory
LEO	Low Earth Orbit
LESIA	Laboratoire d'Etudes Spatiales et d'Instrumentation en Astrophysique
LPCE	Laboratoire de Physique et Chimie de l'Environement
MEO	Medium Earth Orbit
MIT	Massachusetts Institute of Technology
NOAA	National Oceanic and Atmospheric Administration
NMP	New Millennium Programme (NASA)
NPOESS	National Polar-orbiting Operational Environmental Satellite System
OCO	Orbiting Carbon Observatory
ODL	Optical Delay Line
PARASOL	Polarization and Anisotropy of Reflectances for Atmospheric Science coupled with Observations from a Lidar
R_E	Earth Radius
SEC	Sun-Earth Connection Programme (NASA)
SEM	Space Environment Monitor
STP	Solar Terrestrial Probes Missions
TBD	To Be Determined
UNP	University Nanosatellite Programme (US)

A.2 Satellite Formations and Formation Flying Mission Details

Table A-1: Current Formation Flying Missions

Mission (Programme)	Launch	Formation Type (No. Satellites)	Orbit	Objectives/ Technology Demonstrated	Main Supporting Organisations
EO-1[c,d,e,f,g] Earth Observing-1 (NMP) **Landsat 7**[h] Land Remote Sensing Satellite	2000 1999 -current	Ground-track Leader-Follower (2)	LEO r = 705km circular, sun-synchronous orbit	Demonstrate Enhanced Formation Flying (EFF) Autonomous 3-axis control for formation maintenance and inclination control (multiple-manoeuvres). EO-1 maintains ~450km separation with Landsat 7 and ±3km ground track accuracy (at the equator). Technology demonstration of Advanced Land Imager.	NASA GSFC, JPL , Stanford University, Phillips Laboratory, SPA, Microcosm, A.I.Solutions, US Geological Survey.
GRACE[a,b] Gravity Recovery and Climate Experiment (ESSP)	2002 -current	Along-track Leader-Follower (2)	LEO r = 485km i = 89^{o}	Maintain ~220km along-track separation. Achieving 170-270km separation and make gravity field measurements using micron level accuracy inter-satellite range measurements. Support oceanography and other scientific research.	NASA (ESSP Initiative) DLR (Germany) JPL (Caltech)
TechSat 21 Flight Experiment[dd, 7]	2003	Cluster (3)	LEO r = 600km	Microsatellites must accurately maintain 500m separation.	AFRL, AFOSR, University Nanosatellite Programme, MIT.

Table A-1: Current Formation Flying Missions

Table A-2: Examples of Current and Future Satellite Formations

Mission (Programme)	Launch	Formation Type (No. Satellites)	Orbit	Objectives/ Technology Demonstrated	Main Supporting Organisations
POES[n] (Polar-orbiting Operational Environmental Satellite) NOAA-11 to NOAA-17 NOAA-N METOP-2 NOAA-N' METOP-1 METOP-3	 1988 to 2002 2005 2006 2007 2010 2015	Constellation (2 currently operational, POES -16,17)	LEO r = 830-870km Polar orbits	Storm tracking. Long range weather forecasting. Global data measurement for resource management (e.g. industrial expansion, population growth) and environmental research. Monitoring ozone levels.	National Oceanic and Atmospheric Administration (NOAA), UK, France. (NPOESS and EUMETSAT)
GOES[m,o] (Geo-stationary Operational Environmental Satellites) GOES-8 GOES-10 GOES-12 GOES-N GOES-O GOES-P GOES-R GOES-S	 1995 -x 1997 2001 2005 2007 2008 2012 2014	Constellation (2 currently operational, GOES-10,12)	GEO	Weather imagery and atmospheric sounding for weather forecasting. Monitoring space weather using SEM. Measure X-rays, magnetic field primarily to detect onset of solar flares.	National Oceanic and Atmospheric Administration (NOAA), NASA.
The Afternoon 'A-Train' Constellation OCO Aqua Cloudsat CALIPSO[u] PARASOL Aura[i,,j,k] (NASA EOS, ESE, ESSP)	 ---- 2002 2005 2005 2004 2004	Leader-Follower Train Constellation (5) Aqua is lead satellite until OCO is launched.	LEO r = 705km i = 98^{o} polar sun-synchronous orbit	Individual satellites in the same orbit, with 15 minute separations between lead and trailing satellites (and 15 second separation between Cloudsat and CALIPSO). Each satellite studies different aspects of Earth atmosphere, in the order listed: Carbon dioxide concentration, the water cycle, the role of clouds in climate regulation, the role of aerosols in the atmosphere, the use of polarisation to study the surface/atmosphere, and to monitor air quality, ozone and climate change.	NASA GSFC, CNES (Centre National d'Etudes Spatiales)

COSMIC[bb,9] Constellation Observing System for Meteorology Ionosphere and Climate and **FORMOSAT-3** (Taiwan)	2005	Constellation (6)	LEO r = 400km – 800km	Atmospheric sounding using radio occultation measurements to determine atmospheric parameters. Also will make geodetic measurements	USA and Taiwan.
NPOESS[cc] National Polar-orbiting Operational Environmental Satellite System	2008	Constellation (5)	LEO Operate in 2-3 orbital planes (includes POES)	Convergence of POES and DMSP (Defence Meteorological Satellite Programme), also METOP and other specialised satellites. Provide complete global coverage of environmental conditions.	NASA, NOAA, DoD, partners with NASDA and EUMETSAT.
GPM[z] Global Precipitation Measurement Constellation **EGPM**[aa] European Contribution to Global Precipitation Measurement (Earth Watch)	TBD (was initially 2007-2012)	Constellation (~5) 1 primary satellite and an international constellation of other satellites to provide global measurements	LEO r = 510km Near polar Sun-synchronous orbit (for primary)	Determine the global rainfall distribution with improved accuracy. Improve accuracy of global and regional weather prediction models for forecasting and flood hazard prediction. (Improve storm monitoring and understanding of flash floods). Using precipitation radar and microwave radiometers.	NASA, NASDA (Japan), ESA
Fuego[y] (Earth Watch) Demonstrator	TBD 2005	Constellation	LEO	Detection and monitoring of forest fires	EC, ESA, European Companies
TWINS[zz] Two Wide-angle Imaging Neutral-atom Spectrometers	2005	Constellation (2)	2 separate Molniya Orbits i = 63.4° $r_{apogee}=7.2R_E$	Perform stereoscopic imaging of the magnetosphere	NASA SEC, Los Alamos National Laboratory, Southwest Research Institute USA.

ST-5[ee] Space Technology-5 Nanosat Constellation Trailblazer (NMP)	2005	Constellation (3)	GEO r ~ 30000km	Demonstrate new technologies: e.g. long life Li-Fe batteries, autonomous formation flying and comms. instrument, GPS relative positioning, MEMS chip for attitude control. Precursor for MagCON Mission. Measure effect of Solar activity on Earth Magnetosphere. Demonstrate ability to autonomously identify scientific events and perform cooperative data acquisition. Commanded from the ground during mission, except for one week of autonomous behaviour demonstration.	NASA New Millennium Programme. GSFC.
Magnetospheric Constellation Mission (MagCON)[v] Also named **DRACO** Dynamic Response and Coupling Observatory (STP)	---- (was 2010)	Constellation/ Swarm (50)	Nested elliptical orbits at low inclination. r = 3x7R_E to 3x40R_E and 1-2R_E satellite separation	Characterise magnetotail dynamics. Discover how magnetotail stores, transports and releases matter and energy. Understand the effects of the Solar wind on the magnetotail.	NASA SEC/ STP, GSFC, Boston University.
GPS Navstar Global Positioning System	1978-1994 continue to replace	Constellation (24)	Circular r=20200km i=55^o 6 orbit planes, each x4 satellites	Provide global navigation coverage. Signals are triangulated to determine locations on Earth of receivers. (Same as GLONASS)	US DoD (Department of Defence)
GLONASS[q] Global Navigation Satellite System	1982-1998 continue to replace	Constellation (24)	Circular r=19140km i=64.8^o 3 orbit planes separated by 120^o, each x8 equally spaced satellites	Provide global navigation coverage. Signals are triangulated to determine locations on Earth of receivers. (Same as GPS)	Russian Federation Ministry of Defence

GALILEO[r]	2005-2008	Constellation (30) 27 operational, 3 spare	MEO r=23616km i=56^o	Global navigation. Search and rescue facility.	European Commission (EC) and ESA. (involvement with EU, China, India, possibly Canada, Brazil, Korea)
Communications		Constellations		Provide global, mobile satellite voice and data relay.	
Iridium	2001	(66)	LEO		
Globalstar	2000	(48)	LEO		
Teledesic	----	(30)	MEO		
Odyssey		(12)	MEO		
Skynet 4	~1990	(3)	LEO	Military Communications	UK MoD, Portugal
Skynet 5[s,t]	2005/6				

Table A-2: Examples of Current and Future Satellite Formations

Table A-3: Future Formation Flying Missions

Mission (Programme)	**Launch**	**Formation Type (No. Satellites)**	**Orbit**	**Objectives/ Technology Demonstrated**	**Main Supporting Organisations**
XEUS[ffgghh] X-ray Evolving Universe Spectroscopy Mission (ESA Horizons 2000)	2010+	Leader-Follower (2) 1 mirror and 1 detector	L2 Halo	Detect and study black holes and dark matter. Mirror and detector will maintain a 50m separation, equal to focal length. Will achieve 1mm relative position accuracy or 100μm post observation reconstruction. Will operate with 10m^2 collecting area at 1keV and spectral resolution over large range 0.1-80keV.	ESA, ISAS (Institute of Space and Astronautical Science, Japan).
Constellation – X [ii,jj,kk] (Beyond Einstein Programme)	2011	Cluster (4)	L2 Halo	Observe and trace evolution of supermassive black holes, investigate dark matter, and how matter releases energy close to the event horizon. Measure elements dispersed by stellar explosions. Each telescope has diameter 1.6m and focal length 10m.	NASA, GSFC.

Generation-X [ll,mm] (NASA's former "Structure and Evolution of the Universe" theme).	2020+	Cluster (6)	L2	Meet a broad range of scientific objectives e.g. evolution of quasars, accretion disks, star flares. Resolution will be improved from Constellation-X. 6 telescopes have diameter 4.5m. Focal length ideally increased to 150m. Proposed Alternative by Gorenstein (2000): Formation comprises 1 large 30m diameter telescope, and a variety of smaller detectors. Focal length will be increased 300m.	NASA, GSFC ----------
LISA[nn,oo] Laser Interferometer Space Antenna The 'LISA-Pathfinder' is a single-satellite precursor to the LISA mission (and formerly the SMART-2 formation flying mission)	2012	Cluster (3)	Heliocentric (Earth trailing orbit) r_s=149.6x10km 5million km separation.	Detect and observe gravitational waves from massive black holes and galactic binaries. Element of formation flying in eliminating any external disturbance effects on proof masses inside the spacecraft (drag free control). Formation behaves as Michelson interferometer. Spacecraft control must be to micrometer precision – use FEEP μN thrusters.	ESA, NASA
Magnetospheric Multiscale Mission (MM)[w] (STP)	2010	Cluster (4)	Varying TBD	Tetrahedral formation with variable baseline from 1km to several R_E. Determine the basic small-scale plasma processes which control the structure and dynamics of Earth's magnetosphere.	NASA SEC

GEC[x] Geospace Electrodynamic Connections Mission (STP)	2011	Cluster (4)	High inclination r=200-2000km	'Dipping' satellites with 10km-1/4 orbit separation, dipping to 130km altitude in 'string-of-pearls' and 'petal' formations. Satellites will communicate and operate autonomously. Makes simultaneous measurements of energy transfer between ionosphere and thermosphere.	NASA SEC
SMART-3[pp,vv] Small Missions for Advanced Research in Technology	2010	Leader-Follower/ Cluster (3)	GTO Elliptical orbit	Formation flying demonstrator for Darwin (TPF).	ESA (possibly joint with NASA)
Darwin[qq] **(IRSI)** Infrared Space Interferometer	2015	Cluster (4) 3 telescopes and 1 beam combiner (hub)	L2 Lissajous	Perform nulling interferometry for high resolution astronomy and extra-solar planet detection and observation. All satellites will simultaneously point at the same object. Telescope mirror diameters are 3.15m. Satellite separation will be 15-50m, maintaining nanometre relative position accuracy with onboard ODL control.	ESA Science Mission (programme may be combined with NASA TPF mission).
TPF[ss,tt,uu,vv] Terrestrial Planet Finder					
Mission 1: **TPF-C**	2014	Single Satellite		**TPF-C** Single satellite visible light coronagraph with mirror size 6mx3.5m	NASA, Origins Programme, JPL.
Mission 2: **TPF-I** (NASA Origins Programme)	2018	Cluster (5)	L2 Orbit	**TPF-I** Formation flying infrared interferometer for high resolution astronomy and extra-solar planet detection and characterisation (150 stars up to 45 light years away). Formation comprises 4 telescopes each of 4m diameter operating in a 70-150m array, and a single beam combiner.	NASA Origins Programme, JPL and ESA.

Life Finder[ww]	Beyond 2020	Cluster	TBD	Array of more sensitive telescopes than TPF. Produce high resolution infrared spectra of distant planet atmospheres. Observe seasonal variations in chemical composition and identify life signs.	NASA, Origins Programme, JPL.
Planet Imager[xx,yy] (NASA Origins Programme)	Beyond 2020	Cluster	TBD	Produce pictures of single planets at much higher resolution than any preceding mission. Proposed formation comprises 5 interferometer configurations of 4 telescopes, each telescope being 8m in diameter, and each configuration being distributed along a parabola of baseline 6000km with a beam combiner at the focal point (to generate a 25x25 pixel planet image).	NASA, Origins Programme, JPL.

Table A-3: Future Formation Flying Missions

Table A-4: Recent University Formation Flying Mission Studies

Mission (Programme)	**Formation Type (No. Satellites)**	**Orbit**	**Objectives/ Technology Demonstrated**	**Main Supporting Organisations**
Orion[1]	Cluster (6)	LEO	Microsatellite testbed. Proposed formation flying demonstrator for Carrier-Phase Differential GPS (CDGPS) relative navigation.	Stanford University/MIT, GSFC, AFRL.
MUSTANG[2] Multi-University Space Technology Advanced Nanosatellite Group	Leader-Follower (2)	LEO	Microsystems Technology demonstration. Demonstration of formation flying for a large cluster.	BNSC, Cranfield University, Southampton University, Astrium UK, Oxford University, Cambridge University, Imperial College.

SNAP-1[†] **/Tsinghua-1** (launched June 2000)	Leader-Follower (2)	LEO	Rendezvous and formation flying	SSTL Surrey Satellite Technology Ltd.
University Nanosatellite Programme[3,4,5,13] **(UNP)** ***TechSat21***[7,8,10,11,12] ***(Programmes Cancelled in 2003)***	***Cluster (up to 35 clusters of 8 microsatellites)***	***LEO***	**Supporting TechSat 21 (Cancelled in 2003)** ***Precision formation flying to achieve*** *Ground Moving Target Indication (10-50m geolocation accuracy) through Synthetic Aperture Radar (SAR).*	**US DoD, AFOSR, NASA DARPA, Lockheed Martin, other companies.** *AFRL, AFOSR, UNP, MIT.*
3^Sat[4] Three Corner Sat (UNP)	Leader-follower (3)	LEO	Identical nanosatellites demonstrating stereo imaging of clouds, dust storms etc. Satellites collaborate, operating as a network and 'virtual formation' using innovative command and data handling, but do not maintaining precise spatial formation. Satellites use cellular phone constellations for communication links.	Arizona State University, University of Colorado, New Mexico State University
EMERALD[4] Electromagnetic Radiation and Lightning Detection (UNP) **Orion-Emerald**[14,15]	Leader-Follower (2) (3)	LEO	Validate formation flying technologies. Satellites deploy from stacked single entity into tethered formation, and then tether is cut to permit true formation flying. Will fly in 3-satellite formation with the Orion-1 microsatellite (See Orion project above). Demonstrate autonomous formation flying using CDGPS for relative navigation and onboard orbit determination.	Santa Clara University, Stanford University

Constellation Pathfinder[4] Programme supporting NASA's SEC Magnetospheric Constellation Project (UNP)	Cluster (3)	------	Fly 3 picosatellites (<1kg) to demonstrate the feasibility of coordinating a fleet of hundreds of small satellites to measure magnetic field strength and direction throughout the Earth's magnetosphere and magnetotail.	Boston University (also developed sensors for the Cluster mission currently flying)
ION-F[rr,4,6] Ionospheric Observation Nanosatellite Formation (UNP)	Leader-Follower (3)	LEO	Simultaneous examination of electron density of the Earth's ionosphere and ionospheric effects on communications signals. Fly in leader-follower along-track and ground-track formation at 1km separation and perform manoeuvres (to be decided).	Utah State University (USUsat), University of Washington (Dawgstar), Virginia Tech (HokieSat)

Table A-4: Recent University Formation Flying Mission Studies

A.3 Mission References

† Underwood, C., Richardson, G., and Savignol, J. (2001), 'SNAP-1: A Low Cost Modular COTS-Based Nano-Satellite - Design, Construction, Launch and Early Operations Phase', *Proceedings of the 15th AIAA/USU Conference on Small Satellites,* Utah, AIAA, pp. SSC01-VI-7.

[2] Roberts, P.C.E., Bowling, T.S., and Hobbs, S.E. (2002), 'MUSTANG: A Technology Demonstrator for Formation Flying and Distributed Systems Technologies in Space', *5th Cranfield Conference on the Dynamics and Control of Systems and Structures in Space,* Cambridge, UK, Cranfield University Press, Cranfield, UK.

[3] Agee, F.J., Janni, J.F., King, Y.J., Witt, G., and Fender, J.S. (2001), 'Research for an Innovative Approach to Satellite Technology', *AIAA Space 2001,* Albuquerque, NM, AIAA 2001-4555.

[4] University Nanosatellite Programme Website (2001), *The University Nanosatellite Program,* available at: http://www.nanosat.usu.edu (accessed 2001).

[5] Luu, K., Martin, M., and Das, A.e.al. (1999), 'Microsatellite and Formation Flying Technologies on University Nanosatellites', *AIAA Space Technology Conference,* Albuquerque, New Mexico, AIAA 99-4535.

[6] Campbell, M., Fullmer, R.R., and Hall, C.D. (2000), 'The ION-F Formation Flying Experiments', *AAS/AIAA Space Flight Mechanics Meeting,* Clearwater, Florida, AAS 00-108.

[7] Garnham, J., Wainwright, R., and Burns, R. (2001), 'Enabling Research and Development for Flight Demonstration of Sparse Aperture Sensing', *AIAA Space 2001 - Conference and Exposition,* Albuquerque, New Mexico, AIAA 2001-4552.

[8] AFRL Space Vehicles Directorate (1998), *Autonomous Control and Co-ordination of Formation-Flying Satellites,* available at: http://www.vs.afrl.af.mil/ (accessed 2001).
Notes: Website no longer available

[9] Kuo, Y.H., Chao, B.F., Cheng, M.D., Hajj, G., Kursinski, E.R., Lee, L.C., Liu, C.H., Liu, G.C., North, G.R., Rocken, C., Tsai, Y.B., and Yunck, T. (2001), *Constellation Observing System for Meteorology, Ionosphere, and Climate: A Joint Taiwan-US Space Mission for Atmospheric and Geodetic Sciences,* available at: http://genesis2.jpl.nasa.gov/archive/200212018/01/cosmic.eos.pdf (accessed 2005).

[10] Cobb, R., Das, A., and Denoyer, K. (1999), 'TechSat21: Developing Low-Cost Highly Functional Micro-Satellite Clusters for 21st Century Air Force Missions', *International Astronautical Federation Specialists Symposium: Novel Concepts for Smaller, Faster and Better Space Missions,* Redondo Beach, California,

[11] Martin, M. and Stallard, M.J. (1999), 'Distributed Satellite Missions and Technologies - The Techsat21 Programme', AIAA 99-4479.

[13] Martin, M., Cobb, R., Peffer, A., Ganley, J., Campbell, M., and Hall, C.e.al. (1999), 'University Nanosatellite Program', *International Astronautical Federation Specialists Symposium: Novel Concepts for Smaller, Faster and Better Space Missions,* Redondo Beach, California,

[14] Busse, F.D., Inalhan, G., and How, J.P. (2000), 'Project Orion: Carrier Phase Differential GPS Navigation for Formation Flying', *AAS Guidance and Control Conference,* Breckenridge, Colorado, pp. 197-212, AAS 00-016.

[15] Inalhan, G., Busse, F., and How, J.P. (2000), 'Precise Formation Flying Control of Multiple Spacecraft Using Carrier-Phase Differential GPS', *AAS/AIAA Space Flight Mechanics Meeting,* Clearwater, Florida, pp. 151-165, AAS 00-109.

[a] Mauldin, J.R., Bettadpur, S., and Fowler, W.T. (2004), 'The Design and Development of the GRACE Mission Analysis Tool', *14th AAS/AIAA Space Flight Mechanics Conference,* Maui, Hawaii, AAS 04-303.

[aa] ESA Website (2004), *EGPM,* available at: http://www.esa.int/export/esaLP/ESA6KZJE43D_egpm_0.html (accessed 2005).

[b] Mazanek, D., Kumar, R., Seywald, H., and Qu, M. (2000), 'GRACE Mission Design: Impact of Uncertainties in Disturbance Environment and Satellite Force Models', *AAS/AIAA Space Flight Mechanics Meeting,* Vol. 105, Clearwater, Florida, pp. 967-985, AAS 00-163.

[bb] COSMIC Website (2004), *Constellation Observing System for Meteorology, Ionosphere and Climate: COSMIC,* available at: http://www.cosmic.ucar.edu/about.html (accessed 2005).

[c] Folta, D. and Hawkins, A. (2002), 'Results of NASA's First Autonomous Formation Flying Experiment: Earth Observing-1 (EO-1)', *AIAA?AAS Astrodynamics Specialist Conference ,* Monterey, California, AIAA 2002-4743.

[cc] Schaeffer, J. (2005), *NPOESS: National Polar-Orbiting Operational Environmental Satellite System,* available at: http://www.npoess.noaa.gov/ and http://www.npoess.noaa.gov/About/sat_evolu.html (accessed 2005).

[d] Folta, D. and Quinn, D. (1998), 'A Universal 3-D Method for Controlling the Relative Motion of Multiple Spacecraft in Any Orbit', AIAA 98-4193.

[dd] MIT Space Systems Laboratory (2000), *Techsat21,* available at: http://ssl.mit.edu/overview/OpenHouse2001/DSS/OpenHouse2001_DSS.pdf (accessed 2005).

[e] Bauer, F., Bristow, J., Folta, D., Hartman, K., Quinn, D., and How, J.P. (1997), 'Satellite Formation Flying Using an Innovative Autonomous Control System (AUTOCON) Environment', AIAA 97-3821.

[ee] Leon, N.J. (2004), *Space Technology 5: Technology,* available at: http://nmp.jpl.nasa.gov/st5/TECHNOLOGY/tech-index.html (accessed 2005).

[f] Esper, J., Perry, M.E., and Cully, M.J. (1999), 'Opportunities for the Application of New Millenium EO-1 Concepts and Technologies', *International Astronautical Federation.*

[ff] ESA Website (2005), *XEUS - Spacecraft Design,* available at: http://www.rssd.esa.int/index.php?project=XEUS&page=Concept_01 (accessed 2005).

[g] Guinn, J.R. (1997), 'Autonomous Navigation for the New Millennium Program Earth Orbiter 1 Mission', AIAA 97-3816.

[gg] ESA Website (2004e), *XEUS Overview,* available at: http://www.esa.int/export/esaSC/120369_index_0_m.html (accessed 2004).

[h] Williams, D. (2005), *Landsat Data Continuity Mission,* available at: http://ldcm.nasa.gov/ (accessed 2005).

[hh] XEUS Steering Committee (2000), *X-ray Evolving-Universe Spectroscopy - The XEUS Mission Summary, ESA SP-1242,* available at: ftp://ftp.rssd.esa.int/pub/XEUS/BROCHURE/sp1242.pdf (accessed 2005).

[i] Schoeberl, M.R. (2001), 'The Afternoon Constellation: A Formation of Earth Observing Systems for the Atmosphere and Hydrosphere', AIAA 2001-4550.

[ii] Grady, J.F. and Gadwal, G.R. (2001), 'The Constellation X-ray Mission: Exploring the Mysteries of Matter in the Universe', *IEEE Aerospace Conference 2001,* Vol. 7, IEEE, pp. 7-3629 to 7-3635.

[j] NASA Earth Science Enterprise Series (2003), *Formation Flying: The Afternoon 'A-Train' Satellite Constellation,* available at: http://eospso.gsfc.nasa.gov/ftp_docs/A-Train_Fact_Sheet.pdf (accessed 2005).

[jj] Newman, P. (2005), *Beyond Einstein: Constellation-X,* available at: http://universe.nasa.gov/program/conx.html (accessed 2005).

[k] Vincent, M.A. and Salcedo, C. (2004), 'The Insertion of Cloudsat and CALIPSO into the A-Train Constellation', *AAS/AIAA Astrodynamics Conference,* Vol. 116 pt. 2, Big Sky, Montana, pp. 1401-1418, AAS 03-589.

[kk] Weaver, K. (2004), *Constellation-X,* available at: http://constellation.gsfc.nasa.gov/science/design/index.html (accessed 2005).

[l] Twiggs, R. and How, J. (1998), 'Orion: A Microsatellite Testbed for Formation Flying', *12th AIAA/USU Conference on Small Satellites,* Logan, Utah,

[ll] Gorenstein, P. (2000), ' A Generation-X Ultra High Throughput X-ray Astronomy Observatory With a New Mission Architecture', *IEEE Aerospace Conference 2000,* Vol. 2, IEEE, pp. 235-241.

[m] NOAA Web Page (2001), *Space Environment Monitor Mission,* available at: http://www.ngdc.noaa.gov/stp/GOES/goes_mission.htm (accessed 2001).

[mm] Zhang, W. and Newman, P. (2002), *Generation-X: A Future, Ultra-Large-Aperture X-Ray Telescope,* available at: http://generation-x.gsfc.nasa.gov/docs/mission/concepts.html (accessed 2005).

[n] Peslen, C. and Stoner, K. (2005), *POES Project: Current Status,* available at: http://goespoes.gsfc.nasa.gov/poes/project/index.html, also http://goespoes.gsfc.nasa.gov/mission.html (accessed 2005).

[nn] ESA Website (2004), *LISA Fact Sheet,* available at: http://sci.esa.int/science-e/www/object/index.cfm?fobjectid=31403 (accessed 2005).

[o] Peslen, C. and Stoner, K. (2005), *GOES Project: Current Status,* available at: http://goespoes.gsfc.nasa.gov/goes/project/index.html, also http://goespoes.gsfc.nasa.gov/mission.html (accessed 2005).

[oo] Roberts, P. C. E. Drag-Free Control and Technological Risk Assessment for the LISA Gravitational Wave Space Antenna. 2000. Cranfield University, Cranfield University.

[pp] Caramagno, A., Araujo, J., Bastante, J.C., and Penin, L.F. (2005), Unpublished Presentation at ESA-ESTEC,

[q] Husson, V. (2005), *GLONASS,* available at: http://ilrs.gsfc.nasa.gov/satellite_missions/list_of_satellites/glonass/index.html (accessed 2005).

[qq] Karlsson, A., Kaltenegger, L., den Hartog, R., d'Arcio, L., Kilter, M., Erd, Ch., and Ankersen, F. (2004), *Darwin, TTN+ Mission Design Assessment*, ESA, Notes: Unpublished Report

[r] ESA Website (2004b), *ESA Navigation: What is Galileo?,* available at: http://www.esa.int/export/esaNA/GGGMX650NDC_index_0.html (accessed 2005).

[rr] Naasz, B.J., Karlgaard, C.D., and Hall, C.D. (2002), 'Application of Several Control Techniques for the Ionospheric Observation Nanosatellite Formation', *Space Flight Mechanics* , pp. 1063-1079, AAS 02-188.

[s] Witz, S. (2003), *Satellite Constellation Survey,* available at: http://www.vla.nrao.edu/astro/rfi/surveys/satellite/ (accessed 2005).

[t] Holdaway, R. and Spalding, G. (1998), 'The Potential Use of Satellite Mobile Phone Constellations for Global Disaster Warning and Monitoring', *AIAA/AAS Astrodynamics Specialist Conference,* Boston Massachusetts.

[tt] Beichman, C.A., Coulter, D.R., Lindensmith, C.A. , and Lawson, P.R. (2002), *Summary Report on Architecture Studies for the Terrestrial Planet Finder,* available at: http://planetquest.jpl.nasa.gov/TPF/TPFrevue/FinlReps/JPL/tpfrpt1a.pdf (accessed 2005).

[u] Mailhe, L.M., Schiff, C.S., and Stadler, J.H. (2004), 'CALIPSO's Mission Design: Sun-Glint Avoidance Strategies', *14th AAS/AIAA Space Flight Mechanics Conference,* Maui, Hawaii, AAS 04-114.

[uu] Beichman, C.A. (2004), *Memo to the TPF Science Working Group,* available at: http://planetquest.jpl.nasa.gov/TPF/SWG_AnnoucementV2.pdf (accessed 2005).

[v] Ford, K. (2005a), *Magnetospheric Constellation (MagCON) Mission,* available at: http://stp.gsfc.nasa.gov/missions/mc/mc.htm (accessed 2005).

[vv] Beichman, C.A. (2004b), *New Directions for TPF,* available at: http://planetquest.jpl.nasa.gov/TPF/TPFDownselectUpdate.pdf (accessed 2005).

[w] Ford, K. (2005c), *STP Magnetospheric MultiScale Mission: Concept,* available at: http://stp.gsfc.nasa.gov/missions/mms/mms_science.htm (accessed 2005).

[ww] Jackson, R. (2004b), *Origins: Missions: Life Finder,* available at: http://planetquest.jpl.nasa.gov/science/finding_life.html (accessed 2005).
Notes: Same material as on webpage viewed in February 2002

[x] Ford, K. (2005b), *STP Geospace Electrodynamic Connections Mission: GEC Technology,* available at: http://stp.gsfc.nasa.gov/missions/gec/gec_technology.htm (accessed 2005).

[xx] NASA Origins Website (2000), *Planet Imager Mission,* available at: http://origins.jpl.nasa.gov/missions/pi.html (accessed 2002).
Notes: Website no longer available

[y] ESA Website (2004c), *Earth Watch: The Living Planet Programme,* available at: http://www.esa.int/export/esaLP/M0HVCKSC_earthwatch_0.html#subhead6 (accessed 2005).

[yy] Jackson, R. (2004c), *Origins: Missions: Planet Imager,* available at: http://planetquest.jpl.nasa.gov/science/finding_life.html (accessed 2005).

[z] Morris, C. (2004), *Global Precipitation Measurement,* available at: http://gpm.gsfc.nasa.gov/mission.html (accessed 2005).

[zz] TWINS Websites (2004), *TWINS: Two Wide-Angle Imaging Neutral-Atom Spectrometers,* available at: http://twins.swri.edu and http://nis-www.lanl.gov/nis-projects/twins/ (accessed 2005).

Appendix B – The Darwin Mission: Technical Requirements

This section provides a summary of the technical requirements and specifications for the ESA Darwin mission, representing a snapshot of the mission status in the 2002-2003 timeframe. This information is used in chapter 2 (sections 2.2.4 and section 2.3) to support the formation manoeuvres design and Planet Imager formation design. The contents of the following tables are referenced in full in the thesis 'References' section.

- Table B-1: Planet Detection and Characterisation Phase
- Table B-2: Astrophysical Imaging Phase
- Table B-3: Darwin Subsystems and Mass

B.1 Formation and Spacecraft Mission Level Design Requirements

Table B-1: Planet Detection and Characterisation Phase

Specification	Target Mission Parameters	Comments
Observation Distance[a]	Minimum 10pc, desired 25pc	For direct detection of an Earth-like planet at a black body temperature of ~300K, circling a G2 (Solar-type) star. Upper limit is preferable to enable a significant number of targets to be detected and observed.
Operating Wavelength[b]	Infrared 6μm to 18μm band.	Maximum emitted radiation intensity for Earth (254.3K-300K, refer to Figure 3-16, chapter 3) is at ~10μm and the biosignatures O_3, H_2O, CO_2 have strong spectral signature in this range. Also other compounds (probably to faint to detect) that have transition bands in this range include CH_4, NH_3, N_2O, NO_2, SO_2.[c]
Null Depth[a]	10^{-5}-10^{-6}	To detect a planet signal from the habitable zone, the starlight must be nulled to one part in 100,000.
Angular Resolution[a]	100mas for planet at 10pc 40mas for planet at 25pc	Angular resolution corresponding to distance away for an Earth-like planet around a Solar-type star. (Note: 1AU/25pc = 40mas) This requirement may reduce further for cooler/dimmer K or M-type stars.
Observation Direction[a,b]	Within a ±45° cone in the anti-Sun direction	Avoids scattered light and maintains thermal stability.
Number of Targets[b]	Minimum 150 stars, ideally >500 (requires minimum 20pc observation distance)	Detect and study Earth-like planets in the HZ around a large enough sample of F,G,K and M type stars to give statistical significance, and to cover different evolutionary phases and different physical properties of the star.
Integration Time[b,d,e,f]	t≈30 hrs	For detection of an Earth-like planet orbiting a Sun-like star at 1AU, 10pc away with SNR =5.
Spectral Resolution[b,g]	Minimum $R=\Delta\lambda/\lambda$=20-40	To observe thermal spectrum and simultaneously detect H_2O, O_3, and CO_2 (and CH_4) on an Earth-like planet out to 20 pc.
Spectroscopy Integration Time (estimated)	~600 hrs for spectral analysis at R=20 of Earth-like planetary atmosphere (orbiting a Sun, 10pc away).	For a constant SNR being inversely proportional to √R, and proportional to √t.
Signal-To-Noise Ratio (SNR)[d]	≥5-10	Values specified in all the calculations leading to the Darwin baseline estimates above.
Frequency of Revisit to Target	3 Revisits. The duration over which this occurs will depend on optimisation of global coverage strategy	In the infrared, 3 revisits are necessary to determine the orbit and confirm the detection of a planet (refer to Table 4-8 in chapter 4).

Table B-1: Planet Detection and Characterisation Phase ([a]Karlsson and Kaltenegger (2003), [b]Fridlund (2004), [c]Selsis (2000), [d]Fridlund (2002), [e]Fridlund (2001), [f]Fridlund (1999), [g]Fridlund and Kaltenegger (2002))

Table B-2: Astrophysical Imaging Phase Requirements

Specification	Target Mission Parameters	Comments
Imaging Resolution[a]	2.5mas at 6μm. 4mas maximum resolution at 10μm with 500m baseline.	Spatial resolution 1-2 orders of magnitude higher than the JWST (James Webb Space Telescope)
Imaging Field of View (FOV)[a,b]	1 arcsec FOV desireable. 0.3arcsec achievable with current nulling Michelson interferometer. 1.4arcsec achievable with Fizeau interferometer at 10μm.	Alternative Fizeau 'variable-magnification' interferometer design may be required (alternative hub) to achieve target.
Imaging Integration Time[a]	Source can be mapped in 1hr if the total flux within 1arcsec is more than 25-50μJy (and SNR=5).	Using the 6-telescope configuration.
Imaging Spectral Resolution[c]	R=300 $R = \Delta\lambda/\lambda$ (smallest resolvable wavelength range/observation wavelength)	Much greater than that required for the nulling phase to provide image contrast.
Operating Wavelength[b]	Infrared 6μm to 18μm band.	Same band as the planet detection phase.

Table B-2: Astrophysical Imaging Phase ([a]Rottgering et al. (2003), [b]D'Arcio and Le Poole (2003), [c]d'Arcio and Karlsson (2004))

B.2 Formation and Spacecraft Technical Description

(a) **(b)**

Figure B-1: The Darwin Configuration (a) Planet Detection (formation is split into subgroups for signal modulation) (b) Imaging (edited from ESA Report (2000))

Table B-3: Darwin Subsystems and Mass

Sub-System	Characteristics
Mass Budget and Launch	• Telescope mass = 493kg. • Hub mass = 396kg. • Master satellite = 179kg. • Launch vehicle – Ariane 5, simultaneous launch of all satellites. • Propellant (total for 5 year mission) ≈ 33.5kg for I_{SP}=1500 FEEP.
Power	• Each satellite in the formation has an independent solar array, power conditioning unit and power distribution unit. • Solar cells: GaAs 16% efficiency.
Thermal	• All payload optics must be <40K to achieve desired sensitivity in IR. - Passive cooling is achieved using Sun shields. - Sun shield area/Spacecraft mass is the same for all spacecraft in the formation for balanced Solar Radiation Pressure effects. - Sunshield diameters = 7.4m for telescopes, 5.0m for the hub. - Sunshield is a deployable structure, carrying the RF metrology antennae and solar arrays. • Temperature differences between components in the arms of the interferometer <30mK. • Detector must be cooled to 6-8K (active cooling - cryogenics). • All non-optics modules will operate at 300K, and be isolated from the optical payload.
Communications • Intersatellite • Ground	• Master satellite is responsible for all communications with Earth, with a main X-band high gain antenna, and a backup S-band low gain antenna. • Preliminary link budget analyses have shown that: - Direct communications to all satellites are possible from Perth (X-band at 1kbit/s). - Medium gain antenna is required to communicate between L2 and Kourou or Perth. - Deep Space Network can provide up-link to low gain antenna. • Telecommands from the master satellite to the formation can transmit over 30.5km and return 19.5km for 10W power output using S-band link. • Intersatellite communications will be combined with the RF metrology system.

Table B-3: Darwin Core System Characteristics (ESA Report (2000), Karlsson and Kaltenegger (2003))

Appendix C – GNC Systems: Metrology and Propulsion

This section provides supporting material for section 2.2.5 of chapter 2. Table contents are cross-referenced to literature listed in the 'References' section of the thesis.

- Table C-1: Formation Flying Metrology Systems
- Table C-2: Formation Flying Propulsion Systems

Table C-1: Formation Flying Metrology Systems

Sensor/ Sensing Technique	Parameter Measured	Accuracy	Comments
GPS[a]	- Absolute position and velocity - Time	~1 m	• Robust, reliable, low-mass, low-power, relatively cheap sensors. • Deliberately accuracy-limited. • Require 4 satellites for position/velocity data. • Satellites are rapidly acquired and lost during formation orbit. • Accuracy degrades rapidly at altitudes above the GPS constellation (r=20200km).
CDGPS[a,b,c] (Carrier Phase Differential GPS)	- Relative position and velocity - Relative attitude (in addition to standard GPS capabilities)	~2-5 cm 1 cm/s in real time	• By monitoring signal over a period of time (as GPS satellites move) or while moving the receiver, it is possible to determine the integer biases. • High sub-carrier-phase-wavelength relative position accuracy is achieved using extended Kalman filtering techniques. • Satellites are rapidly acquired and lost during formation orbit – potentially overcome by use of pseudolite within formation. • Accuracy degrades rapidly at altitudes above the GPS constellation (r=20200km).
CLT[d] Cross Link Transceiver	- Absolute position and velocity - Relative navigation - Inter-satellite communications	~2-5cm	• Integrates standard GPS navigation receivers with the benefits of onboard pseudolites to extend CDGPS relative navigation beyond LEO.
Radar (RF) Ranging[a] - Pulse modulated/ continuous signal - Doppler Shift - Narrow beam antenna pointing/ amplitude and rotation	- Range - Range Rate - Line-of-sight direction - Relative attitude	Coarse range precision (cm)	• Determine range between two objects by measuring the signal time of travel between the two objects, or the phase shift between an incident and reflected signal at both the transmitter and receiver. • Determine the range rate by measuring the shift of the incident wave frequency arriving at the receiver due to relative motion between transmitter and receiver. • Limited operational range (power α range^{-4}) so increase the power of the return signal by placing a transponder on the target. • Relatively bulky hardware (antennae, electronics).
Laser Ranging[a] - Pulse modulated/ continuous signal	- Range - Range Rate - Line-of-sight direction	Fine range precision 5-50mm over most range Sub-mm in close proximity	• Generally operate in the near-infrared range. • Achieve much higher measurement accuracy due to small wavelength of signal. • Range rate information is obtained by differentiation of the range signal or by Doppler shift measurement using heterodyning. • Operating range varies from sub-metre to a few km, depending on transmitter power and signal type (pulse/continuous). • Less sensitive to disturbances than other sensors (due to narrow beam and small field of view).

Camera[a,e] (Imaging Sensor)	- Range - Line-of-sight direction - Relative Attitude	~1cm @10m range, ~10cm @30m range, ~1m@ 100m range	• Different size reflector patterns are required for sensor to operate over different ranges (pattern size must be increased with range, and sensor mode must be switched to observe correct pattern). • Achieve increasing accuracy with decreasing range. • System are sensitive to external light sources, therefore field of view limited.
Intelligent Vision-Based Relative Navigation[f,g] - Electro-optical measurement of line-of-sight vector	- Range - Relative attitude		• Uses Position Sensing Diodes and cameras to monitor variation in incident light which can be intelligently converted into line-of-sight range and relative attitude.

Table C-1: Summary of Sensors for On-Orbit Relative Parameter Measurements ([a]Fehse (2003), [b]Park, Olsen and How (2000), [c]Ferguson, Busse et al. (2001), [d]Stadter et al. (2001), [e]Kojima et al. (2004), [f]Alonso, Crassidis and Junkins (2000), [g]Yim, Crassidis and Junkins (2004))

Table C-2: Formation Flying Propulsion Systems

Propulsion System	Thrust Range (N)	I_{SP} (s)	Comments
Cold Gas (N_2, NH_3, Freon, He)	0.05-200	50-75	• Simple, reliable, low cost. • Clean, low noise. • Recent miniaturisation to Micro-Thrusters (mass reduction to 15g per thruster, reduction in minimum impulse bit). • Avoid hot gas exhaust. • High fuel consumption with associated significant mass distribution change. • Isp low, but improved by heating gas before it exits through the nozzle. • Contains precision (proportional) flow control but valve open/closure rates may limit achievable thrust.
Cold Gas Micro Thrusters (N_2 or C_4H_{10}, C_3H_8, or use propellant gas stored in solid phase e.g. CO_2)	0.0005-0.01	Min. 120 (min. 70*)	
Liquid Chemical Monopropellant (MMH monomethyl hydrazine)	5-5x10^6	300-340	• Standard use for attitude control and orbit maintenance. • Thrust too large for precision formation flying, but sufficient for some formation-keeping tasks. • Liquid fuel storage (sloshing) and mass distribution changes during consumption adversely affect ability to perform accurate formation flying.
Electrostatic **FEEP** (Field Emission Electric Propulsion)	~5x10^{-6}	2000-6000	• Caesium or Indium ion emission through a slit or needle emitter provides continuous, variable, precision (μN) thrust ideal for formation-keeping. • Controlled by voltage. • Very high I_{SP} and low noise. • Capacity for very high exhaust velocity (limited by power available to thruster system). • Not proven technology in space.
Colloid **Micro-Colloid** (Glycerine)	5x10^{-6} to 0.05	1200	• Array of needles emit charged droplets. • Array can be throttled. • Provides very small amounts of thrust to counteract disturbance forces. • Efficiency remains unaffected by thrust variation.
Electromagnetic Pulsed Plasma Thrusters (PPT)	5x10^{-6} to 0.005	1500	• Fixed thrust magnitude and pulse width means hardware operates with deadband • Larger impulse means fewer pulses required, but if too large, opposing corrective pulses may also be required to perform desired manoeuvre/counteract disturbances, and more fuel may be used. • More noisy due to pulsed operation • Proven technology in space.

Table C-2: Formation Flying Propulsion Systems (Larson and Wertz (1996), Stenmark and Eriksson (2002), Reichbach, Sedwick and Martinez-Sanchez (2001), *Marotta (Polyflex) Website (2005))

Appendix D - Low Earth Orbit Model Development

This section contains supporting material for chapter 4:

- Summary of the Hill equations derivation and solutions (Wie, 1998)
- Summary of cross-track model derivation for LEO formation flying in the presence of the J_2 perturbation (Schweighart and Sedwick, 2002)

D.1 Hill Equations Summary

Derivation of the Hill equations in the Circular Orbit Reference Frame

Originally developed for orbital rendezvous, the Hill (1878) or Clohessy-Wiltshire (1960) equations of relative motion are based on a relative coordinate frame which is a right handed set, travelling around a circular orbit with an angular velocity, ω (equal to n). These equations can be derived for two satellites in circular orbits using either an Earth-centred-fixed (ECF) or 'inertial' coordinate frame (I, J, K), or a moving coordinate frame (i, j, k). The 'non-inertial' or 'Hill' reference frame is also illustrated in Figure B-1, rotating with P_0 around a circular orbit. The relative acceleration of P_1 with respect to P_0 can be derived or transformed between the two coordinate systems.

If P_0 and P_1 are travelling in near-circular orbits at slightly different altitudes ($\underline{\delta r}_{1ECF}, \underline{\delta r}_1 << \underline{r}_0, \underline{r}_1$), the accelerations of each satellite are $\underline{\ddot{r}}_0$ and $\underline{\ddot{r}}_1$ respectively. It is assumed that these accelerations are only affected by point mass gravity.

$$\underline{\ddot{r}}_0 = \underline{g}(\underline{r}_0) \text{ and } \underline{g}(\underline{r}_0) = \frac{-\mu}{r_0^3}\underline{r}_0 \qquad \text{(D-1)}$$

$$\underline{\ddot{r}}_1 = \underline{g}(\underline{r}_1) \text{ and } \underline{g}(\underline{r}_1) = \frac{-\mu}{r_1^3}\underline{r}_1 \qquad \text{(D-2)}$$

The Hill equations can be derived purely in terms of the moving reference frame by converting the expressions for point mass gravity acting on each satellite to the relative coordinate system.

The definition of the Hill frame in Figure B-2, with the x axis in the direction of the radius vector, means that the absolute acceleration of P_1 in Figure D-1 can be expressed as

$$\underline{r}_1 = (r_0 + x_1)\underline{i} + y_1\underline{j} + z_1\underline{k} \qquad \text{(D-3)}$$

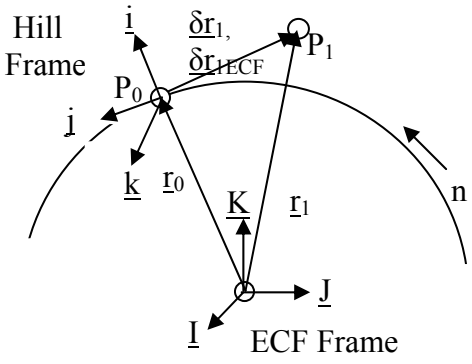

$\underline{r}_0$ = vector to satellite P_0 in ECF frame
$\underline{r}_1$ = vector to satellite P_1 in ECF frame
$\underline{\delta r}_1$ = relative position vector in Hill frame
$\underline{\delta r}_{1ECF}$ = relative position vector in ECF frame

Figure D-1: Axis systems defining the motion of two satellites in LEO

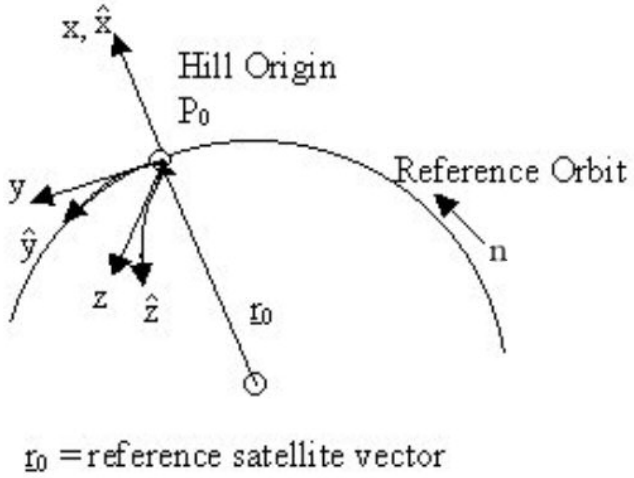

Figure D-2: The Hill coordinate frame

The absolute velocity and acceleration of the satellite at P_1 in terms of its relative position to the Hill origin at P_0 are easily derived using the relationships in equations (D-4) to (D-9).

$$n^2 = \frac{\mu}{r_o^3} \tag{D-4}$$

$$\underline{\delta r}_{1ECF} = x_1\underline{i} + y_1\underline{j} + z_1\underline{k} \tag{D-5}$$

$$\begin{aligned} \underline{\delta r}_1 &= x_1\underline{i} + y_1\underline{j} + z_1\underline{k} \\ \underline{\delta \dot{r}}_1 &= \dot{x}_1\underline{i} + \dot{y}_1\underline{j} + \dot{z}_1\underline{k} \\ \underline{\delta \ddot{r}}_1 &= \ddot{x}_1\underline{i} + \ddot{y}_1\underline{j} + \ddot{z}_1\underline{k} \end{aligned} \tag{D-6}$$

$$\underline{\omega} = n\underline{k} \tag{D-7}$$

$$\underline{r}_0 = r_0\underline{i} \tag{D-8}$$

$$\begin{aligned}\dot{\underline{i}} &= \underline{\omega}\times\underline{i} = n\underline{k}\times\underline{i} = n\underline{j}\\ \dot{\underline{j}} &= \underline{\omega}\times\underline{j} = n\underline{k}\times\underline{j} = -n\underline{i}\\ \dot{\underline{k}} &= \underline{\omega}\times\underline{k} = n\underline{k}\times\underline{k} = 0\end{aligned} \tag{D-9}$$

The velocity is given by

$$\dot{\underline{r}}_1 = \left(\dot{r}_0 + \dot{x}_1\right)\underline{i} + \dot{y}_1\underline{j} + \dot{z}_1\underline{k} + \left(r_0 + x_1\right)\dot{\underline{i}} + y_1\dot{\underline{j}} + z_1\dot{\underline{k}} \tag{D-10}$$

and therefore,

$$\dot{\underline{r}}_1 = \left(\dot{r}_0 + \dot{x}_1 - ny_1\right)\underline{i} + \left(\dot{y}_1 + n\left(r_0 + x_1\right)\right)\underline{j} + \dot{z}_1\underline{k} \tag{D-11}$$

The absolute acceleration of P_1 in the Hill frame is

$$\ddot{\underline{r}}_1 = \left(\ddot{x}_1 - 2n\dot{y}_1 - n^2\left(r_0 + x_1\right)\right)\underline{i} + \left(\ddot{y}_1 + 2n\dot{x}_1 - n^2 y_1\right)\underline{j} + \ddot{z}_1\underline{k} \tag{D-12}$$

The equation of motion of P_1 in terms of the gravitational force due to a spherical Earth (zeroth order gravitational force) is

$$\ddot{\underline{r}}_1 = g(r_1) \tag{D-13}$$

where

$$\underline{g}\left(\underline{r}_1\right) = \frac{-\mu}{r_1^{\,3}}\underline{r}_1 = \frac{-\mu\left[\left(r_0 + x_1\right)\underline{i} + y_1\underline{j} + z_1\underline{k}\right]}{\left[\left(r_0 + x_1\right)^2 + y_1^{\,2} + z_1^{\,2}\right]^{\frac{3}{2}}} \tag{D-14}$$

By assuming that the relative motion between P_1 and P_0 is small compared to the radius of the perturbed orbit, and neglecting higher order terms, this can be simplified to

$$\underline{g}\left(\underline{r}_1\right) \approx -n^2\left[\left(r_0 - 2x\right)\underline{i} + y\underline{j} + z\underline{k}\right] \tag{D-15}$$

Note again,

$$n = \sqrt{\frac{\mu}{r_0^{\,3}}} \tag{D-16}$$

By equating equations (D-12) and (D-15) (referring to (D-13)) the r_0 terms cancel out and the linear differential equations of relative motion in the curvilinear Hill frame result.

$$\begin{aligned} &\ddot{x}_1 - 2n\dot{y}_1 - 3n^2 x_1 = 0 \\ &\ddot{y}_1 + 2n\dot{x}_1 = 0 \\ &\ddot{z}_1 + n^2 z_1 = 0 \end{aligned} \qquad \text{(D-17)}$$

These equations can be easily solved analytically, and form the basis for the development of expressions for relative satellite motions in a perturbed environment. They also provide a baseline with which to compare higher fidelity analytical solutions for relative motion in LEO.

$$\begin{bmatrix} x(t) \\ y(t) \\ \dot{x}(t) \\ \dot{y}(t) \end{bmatrix} = \begin{bmatrix} 4-3\cos nt & 0 & \sin nt/n & 2(1-\cos nt)/n \\ 6\sin nt - 6nt & 1 & 2(-1+\cos nt)/n & 4\sin nt/n - 3t \\ 3n\sin nt & 0 & \cos nt & 2\sin nt \\ 6n(-1+\cos nt) & 0 & -2\sin nt & -3+4\cos nt \end{bmatrix} \begin{bmatrix} x_0 \\ y_0 \\ \dot{x}_0 \\ \dot{y}_0 \end{bmatrix} \qquad \text{(D-18)}$$

$$\begin{aligned} z(t) &= z_0 \cos nt + \frac{z_0}{n} \sin nt \\ \dot{z}(t) &= -z_0 n \sin nt + \dot{z}_0 \cos nt \end{aligned} \qquad \text{(D-19)}$$

D.2 Cross-Track Model Summary

This overview of the relative cross-track dynamics model derivation is summarised from Schweighart and Sedwick (2002). Further details can be obtained from this reference.

In the presence of the J_2 perturbation, the perturbed satellite orbit and the reference orbit are not coplanar, and the relative motion between the satellites ranges from zero when the planes intersect to a maximum after one quarter of a period. The location of the intersection of the planes will vary with time, as will the maximum satellite separation. Schweighart and Sedwick (2002) deduce that the relative motion can be expressed in the following form.

$$z = A(t)\{\sin[B(t)t + \varphi]\} \qquad \text{(D-20)}$$

Initial relative cross-track position and velocity conditions are defined at the outset as z_0 and $\dot{z}_0$. This enables the calculation of the inclination of the perturbed orbit relative to the reference (equation (D-21)) at these conditions.

$$i_{sat} = \frac{\dot{z}_o}{k r_{ref}} + i_{ref} \qquad \text{(D-21)}$$

After one orbit, the 'initial' separation in the longitude of ascending nodes is given by equation (D-22).

$$\Delta\Omega_0 \approx \frac{z_0}{r_{ref} \sin i_{ref}} \tag{D-22}$$

Spherical trigonometry can be used to calculate the location of the intersection of the orbit planes, based on the reference orbit inclination, the change in longitude of ascending node (which varies with time), and the inclination of the perturbed satellite, based on the initial relative position and velocity conditions (i_{sat}). Figure D-3 illustrates the moving intersection of the orbital planes and the associated parameters.

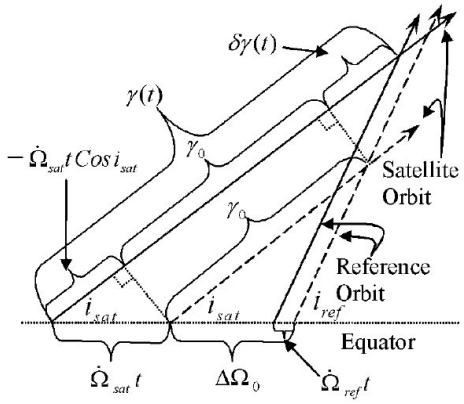

Figure D-3: Moving Intersection of the Orbital Planes (Schweighart and Sedwick (2002))

The argument of the cross-track motion (B) in equation (D-20) is given by

$$q = nc - \delta\dot{\gamma} \tag{D-23}$$

where

$$\delta\dot{\gamma}(t) = \dot{\gamma}(t) + \dot{\Omega}_{sat} \cos i_{sat} \tag{D-24}$$

The amplitude A(t) of the cross-track motion describes the maximum separation between the perturbed satellite and reference orbit planes. The spherical trigonometry which leads to the derivation for the expressions for the amplitude of the relative cross-track motion is illustrated in Figure D-4.

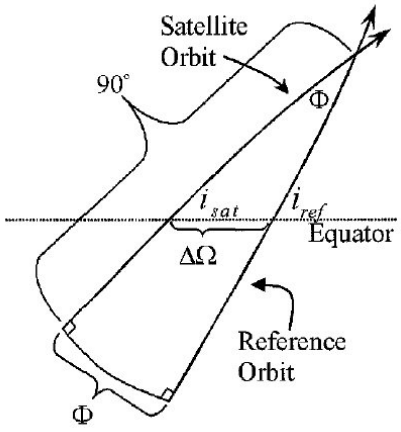

Figure D-4: Determining the amplitude (Schweighart and Sedwick (2002))

The amplitude is given by

$$A(t) = r_{ref}\Phi(t) = lt + m \tag{D-25}$$

where m is defined in equation (4-64) through the cross-track initial conditions and also

$$l \equiv r_{ref}\dot{\Phi} \text{ and } m \approx r_{ref}\Phi_0 \tag{D-26}$$

The final expression for the cross-track motion of one perturbed satellite relative to the reference orbit (with orbit period corrected and nodal drift corrected) is

$$z = (lt + m)\sin(qt + \phi) \tag{D-27}$$

The final equation of relative cross-track motion to replace those of previous models for one perturbed and one reference satellite is obtained below (where q is given by equation (D-23)). Terms are also defined in the main thesis text (section 4.3.5).

$$\ddot{z} + q^2 z = 2lq\cos(qt + \varphi) \tag{D-28}$$

Appendix E - L2 Formation Flying Model Development

Supporting material for the Lagrange point formation flying model development work, reported in chapter 6, is included below. The expressions summarised in the following subsections were implemented as part of the model (section E.1) or for comparison with the linear model (section E.2). Further detail of the analyses summarised here can be found in:

- Richardson (1980a) for section E.1
- Segerman and Zedd (2003) for section E.2

E.1 Third Order Analytical Description of a Halo Orbit

The analytical solutions to non-dimensionalised equations of motion for a single satellite on a halo orbit around L2 are:

$$x = a_{21}A_x^2 + a_{22}A_z^2 - A_x\cos\tau_1 + \left(a_{23}A_x^2 - a_{24}A_z^2\right)\cos2\tau_1 + \left(a_{31}A_x^3 - a_{32}A_xA_z^2\right)\cos3\tau_1 \quad \text{(E-1)}$$

$$y = kA_x\sin\tau_1 + \left(b_{21}A_x^2 - b_{22}A_z^2\right)\sin2\tau_1 + \left(b_{31}A_x^3 - b_{32}A_xA_z^2\right)\sin3\tau_1 \quad \text{(E-2)}$$

$$z = \delta_n A_z\cos\tau_1 + \delta_n d_{21}A_xA_z\left(\cos2\tau_1 - 3\right) + \delta_n\left(d_{32}A_zA_x^2 - d_{31}A_z^3\right)\cos3\tau_1 \quad \text{(E-3)}$$

Linear solutions are:

$$\begin{aligned} x &= -A_x\cos(\lambda t + \phi) \\ y &= kA_x\sin(\lambda t + \phi) \\ z &= A_z\sin(\lambda t + \psi) \end{aligned} \quad \text{(E-4)}$$

where

$$\psi = \phi + \frac{n\pi}{2}, \quad n = 1,\ 3 \quad \text{(E-5)}$$

$$k = \frac{1}{2\lambda}\left(\lambda^2 + 1 + 2c_2\right) = \frac{2\lambda}{\lambda^2 + 1 - c_2} \quad \text{(E-6)}$$

and the cross-track frequency, λ, is matched to the in-plane frequency (and a correction term is included in the nonlinear equations of motion)

$$\lambda^4 + \left(c_2 - 2\right)\lambda^2 - \left(c_2 - 1\right)\left(1 + 2c_2\right) = 0 \quad \text{(E-7)}$$

Define

$$s = n_1 t \tag{E-8}$$

where n_1 is orbital mean motion, t is time, and

$$\tau = \omega s \tag{E-9}$$

where ω is a frequency correction

$$\omega = \omega_1 + \omega_2 ..... \tag{E-10}$$

In the solution process it is found that (to remove secular terms):

$$\begin{aligned} \omega_1 &= 0 \\ \omega_2 &= s_1 A_x^2 + s_2 A_z^2 \end{aligned} \tag{E-11}$$

where

$$\begin{aligned} s_1 &= \frac{1}{2\lambda\left[\lambda\left(1+k^2\right)-2k\right]}\left\{\tfrac{3}{2}c_3\left[2a_{21}\left(k^2-2\right)-a_{23}\left(k^2+2\right)-2kb_{21}\right]-\tfrac{3}{8}c_4\left(3k^4-8k^2+8\right)\right\} \\ s_2 &= \frac{1}{2\lambda\left[\lambda\left(1+k^2\right)-2k\right]}\left\{\tfrac{3}{2}c_3\left[2a_{22}\left(k^2-2\right)+a_{24}\left(k^2+2\right)+2kb_{22}+5d_{21}\right]-\tfrac{3}{8}c_4\left(12-k^2\right)\right\} \end{aligned} \tag{E-12}$$

The amplitude relationship is given by:

$$l_1 A_x^2 + l_2 A_z^2 + \Delta = 0$$

where Δ is the cross-track frequency correction and

$$\begin{aligned} l_1 &= a_1 + 2\lambda^2 s_1 \\ l_2 &= a_2 + 2\lambda^2 s_2 \\ a_1 &= -\tfrac{3}{2}c_3\left(2a_{21}+a_{23}+5d_{21}\right)-\tfrac{3}{8}c_4\left(12-k^2\right) \\ a_2 &= \tfrac{3}{2}c_3\left(a_{24}-2a_{22}\right)+\tfrac{9}{8}c_4 \end{aligned} \tag{E-13}$$

Note:

$$\begin{aligned} A_x &> 0 \\ A_z &\geq 0 \\ A_{x\ \text{minimum}} &= \sqrt{\left|\frac{\Delta}{l_1}\right|} \end{aligned} \tag{E-14}$$

Other terms in the solutions are the time variable

$$\tau_1 \overset{\Delta}{=} \lambda\tau + \varphi \tag{E-15}$$

and remaining constant terms:

$$\delta_n = 2 - n, \quad n = 1,\ 3 \tag{E-16}$$

$$a_{21} = \frac{3c_3\left(k^2 - 2\right)}{4\left(1 + 2c_2\right)} \tag{E -17}$$

$$a_{22} = \frac{3c_3}{4\left(1 + 2c_2\right)} \tag{E -18}$$

$$a_{23} = -\frac{3c_3\lambda}{4kd_1}\left[3k^3\lambda - 6k\left(k - \lambda\right) + 4\right] \tag{E -19}$$

$$a_{24} = -\frac{3c_3\lambda}{4kd_1}\left(2 + 3k\lambda\right) \tag{E -20}$$

$$a_{31} = -\frac{9\lambda}{4d_2}\left[4c_3\left(ka_{23} - b_{21}\right) + kc_4\left(4 + k^2\right)\right] + \left(\frac{9\lambda^2 + 1 - c_2}{2d_2}\right)\left[3c_3\left(2a_{23} - kb_{21}\right) + c_4\left(2 + 3k^2\right)\right] \tag{E -21}$$

$$a_{32} = -\frac{1}{d_2}\left\{\frac{9\lambda}{4}\left[4c_3\left(ka_{24} - b_{22}\right) + kc_4\right] + \tfrac{3}{2}\left(9\lambda^2 + 1 - c_2\right)\left[c_3\left(kb_{22} + d_{21} - 2a_{24}\right) - c_4\right]\right\} \tag{E-22}$$

$$b_{21} = -\frac{3c_3\lambda}{d_1}\left(3k\lambda - 4\right) \tag{E-23}$$

$$b_{22} = \frac{3c_3\lambda}{d_1} \tag{E-24}$$

$$b_{31} = \frac{3}{8d_2}\left\{8\lambda\left[3c_3\left(kb_{21} - 2a_{23}\right) - c_4\left(2 + 3k^2\right)\right] + \left(9\lambda^2 + 1 + 2c_2\right)\left[4c_3\left(ka_{23} - b_{21}\right) + kc_4\left(4 + k^2\right)\right]\right\} \tag{E-25}$$

$$b_{32} = \frac{1}{d_2}\left\{9\lambda\left[c_3\left(kb_{22} + d_{21} - 2a_{24}\right) - c_4\right] + \tfrac{3}{8}\left(9\lambda^2 + 1 + 2c_2\right)\left[4c_3\left(ka_{24} - b_{22}\right) + kc_4\right]\right\} \tag{E-26}$$

$$d_{21} = -\frac{c_3}{2\lambda^2} \tag{E-27}$$

$$d_{31} = \frac{3}{64\lambda^2}\left(4c_3a_{24} + c_4\right) \tag{E-28}$$

$$d_{32} = \frac{3}{64\lambda^2}\left[4c_3\left(a_{23} - d_{21}\right) + c_4\left(4 + k^2\right)\right] \tag{E-29}$$

$$d_1 = \frac{3\lambda^2}{k}\left[k\left(6\lambda^2 - 1\right) - 2\lambda\right] \tag{E-30}$$

$$d_2 = \frac{8\lambda^2}{k}\left[k\left(11\lambda^2 - 1\right) - 2\lambda\right] \tag{E-31}$$

E.2 High Order Relative Motion Model

The full nonlinear equations of relative motion of one satellite relative to the hub are

$$\Delta\underline{\ddot{r}} = \underline{\ddot{r}}_t - \underline{\ddot{r}}_h \tag{E -32}$$

where $\underline{\ddot{r}}_{h/t}$ are each individually described by equations of motion of the dimensional form given in equations (6-9) to (6-11) (refer to section 6.2.2, chapter 6 for terms). μ terms are gravitational constants of the Sun/Earth.

$$\delta\ddot{x}_{dim} = -\left(\frac{\mu_s \delta x}{\rho_s^3} + \frac{\mu_e \delta x}{\rho_e^3}\right) - \left(\frac{\mu_s\left(x_o - x_s\right)}{\rho_s^3} + \frac{\mu_e\left(x_o - x_e\right)}{\rho_e^3}\right) + n^2 x_o \tag{E-33}$$

$$\delta\ddot{y}_{dim} = -\left(\frac{\mu_s \delta y}{\rho_s^3} + \frac{\mu_e \delta y}{\rho_e^3}\right) \tag{E-34}$$

$$\delta\ddot{z}_{dim} = -\left(\frac{\mu_s \delta z}{\rho_s^3} + \frac{\mu_e \delta z}{\rho_e^3}\right) \tag{E-35}$$

Note $\underline{\ddot{r}} = \left[\delta\ddot{x} \quad \delta\ddot{y} \quad \delta\ddot{z}\right]$ (E-36)

Magnitude ordering gives the following truncated equations of relative motion:

$$\Delta\underline{\ddot{r}} = A\left[-\Delta\underline{r} + 3\Delta x\Delta\hat{\underline{x}}\right] + B\left[3\Delta x\underline{r}_h + 3x_h\Delta\underline{r} + \left(3\underline{r}_h \cdot \Delta\underline{r} - 15\Delta x x_h\right)\Delta\hat{\underline{x}}\right].. \tag{E-37}$$
$$... + C\left[\left(3\underline{r}_h \cdot \Delta\underline{r} - 15\Delta x x_h\right)\underline{r}_h + \tfrac{3}{2}\left(r_h^2 - 5x_h^2\right)\Delta\underline{r} - \tfrac{15}{2}\left(2x_h\underline{r}_h \cdot \Delta\underline{r} - 7\Delta x x_h^2 + \Delta x r_h^2\right)\Delta\hat{\underline{x}}\right]$$

where terms in Δ denote 'relative' and subscripts h denote the reference or 'hub', also

$$A = \frac{\mu_1}{\left(x_e + D_1\right)^3} + \frac{\mu_2}{\left(x_e - D_2\right)^3} \qquad B = \frac{\mu_1}{\left(x_e + D_1\right)^4} + \frac{\mu_2}{\left(x_e - D_2\right)^4} \qquad C = \frac{\mu_1}{\left(x_e + D_1\right)^5} + \frac{\mu_2}{\left(x_e - D_2\right)^5} \tag{E-38}$$

where D_1 is the distance between the barycentre and Sun, D_2 is the distance between the Earth-Moon barycentre and Sun-Earth/Moon barycentre, and x_e is the distance from the barycentre to L2.

In the rotating frame

$$\Delta\underline{\ddot{r}} = \begin{bmatrix} \Delta\ddot{x} - 2n\Delta\dot{y} - n^2\Delta x \\ \Delta\ddot{y} + 2n\Delta\dot{x} - n^2\Delta y \\ \Delta\ddot{z} \end{bmatrix} \tag{E-39}$$

The solutions are of the form:

$$\begin{aligned} x &= -A_x \cos(\lambda\tau + \phi)... \\ &...+ \left(\rho_{21}A_xA_{xh} - \rho_{24}A_zA_{zh}(-1)^l\right)\cos(\lambda(2+\Delta\omega_2)\tau + \phi_h + \phi)... \\ &...+ \left(\rho_{22}A_xA_{xh} + \rho_{23}A_zA_{zh}(-1)^l\right)\cos(\lambda\Delta\omega_2\tau + \phi_h - \phi) \end{aligned} \tag{E-40}$$

$$\begin{aligned} y &= kA_x \sin(\lambda\tau + \phi)... \\ &...+ \left(\sigma_{21}A_xA_{xh} - \sigma_{24}A_zA_{zh}(-1)^l\right)\sin(\lambda(2+\Delta\omega_2)\tau + \phi_h + \phi)... \\ &...+ \left(\sigma_{22}A_xA_{xh} - \sigma_{23}A_zA_{zh}(-1)^l\right)\sin(\lambda\Delta\omega_2\tau + \phi_h - \phi) \end{aligned} \tag{E-41}$$

$$\begin{aligned} z &= \left[(-1)^l A_x \cos(\lambda\tau + \phi)...\right. \\ &...+ \left(\kappa_{21}A_xA_{zh} + \kappa_{23}A_zA_{xh}(-1)^l\right)\cos(\lambda(2+\Delta\omega_2)\tau + \phi_h + \phi)... \\ &...+ \left.\left(\kappa_{22}A_xA_{zh} + \kappa_{24}A_zA_{xh}(-1)^l\right)\cos(\lambda\Delta\omega_2\tau + \phi_h - \phi)\right](2-j) \end{aligned} \tag{E-42}$$

where $\tau = (1+\omega_2 t)$. Also, A_x, A_y, A_z are relative amplitudes of bounded relative motion, and A_{xh}, A_{yh}, A_{zh} represent the reference halo amplitudes. The remaining terms are frequencies, frequency corrections and constants arising from the solution method (Segerman and Zedd, 2003).